

CR-171724  
c.1



# Axiomatix

(NASA-CR-171724) ENGINEERING EVALUATIONS  
AND STUDIES. / VOLUME 1: EXHIBIT A Final  
Report (Axiomatix, Los Angeles, Calif.)

N84-15174

481 p HC A21/MF A01

CSSL 22B

Unclas

G3/16

43325



ENGINEERING EVALUATIONS AND STUDIES  
FINAL REPORT FOR CONTRACT NAS 9-16067  
VOLUME I, EXHIBIT A

Technical Monitor: William Teasdale

Prepared for

NASA Lyndon B. Johnson Space Center  
Houston, Texas 77058

Prepared by

Unjeng Cheng  
James G. Dodds  
Gaylord K. Huth  
Jack K. Holmes  
Richard S. Iwasaki  
Robert G. Maronde  
Peter W. Nilsen  
Andreas Polydoros  
Don Roberts  
Sergei Udalov  
Charles L. Weber

Axiomatix  
9841 Airport Blvd., Suite 912  
Los Angeles, California 90045

Axiomatix Report No. R8310-6  
October 31, 1983

TABLE OF CONTENTS

Page

Volume I, Exhibit A

1.0	EXECUTIVE SUMMARY . . . . .	1
1.1	Contract Tasks . . . . .	2
1.1.1	Exhibit A Contract Tasks . . . . .	2
1.1.2	Exhibit B Contract Tasks . . . . .	7
1.1.3	Exhibit C Contract Tasks . . . . .	11
1.2	Performance of the Contract Tasks . . . . .	12
2.0	ORBITER INERTIAL UPPER-STAGE STUDIES . . . . .	16
3.0	KU-BAND HARDWARE STUDIES . . . . .	19
4.0	S-BAND HARDWARE INVESTIGATIONS . . . . .	21
5.0	SHUTTLE/CENTAUR COMMUNICATION SYSTEM ENGINEERING INVESTIGATIONS.	22

Volume II, Exhibit B, Part 1

6.0	KU-BAND COMMUNICATION SYSTEM ANALYSIS . . . . .	23
6.1	Shuttle/TDRSS Sidelobe Avoidance . . . . .	25
6.1.1	Introduction . . . . .	25
6.1.2	Derivation of Sidelobe Discrimination Budgets . . . . .	26
6.1.3	Conclusions . . . . .	26
6.2	Shuttle/TDRSS Acquisition and Tracking Performance . . . . .	30
6.2.1	Introduction . . . . .	30
6.2.2	Dynamic-Rate Limitations . . . . .	30
6.2.3	Flux-Density Specification Considerations . . . . .	31
6.2.4	Summary and Conclusions . . . . .	32
7.0	S-BAND SYSTEM INVESTIGATIONS . . . . .	33
8.0	ORBITER ANTENNA STUDIES AND INVESTIGATIONS . . . . .	34
9.0	PAYLOAD COMMUNICATION INVESTIGATIONS . . . . .	36
10.0	SHUTTLE/TDRSS AND GSTDN COMPATIBILITY ANALYSIS . . . . .	37
10.1	TDRSS Antenna Scan for Shuttle Acquisition . . . . .	37
10.2	PSD of Staggered Quadrature PN with Identical Sequences . . . . .	38

TABLE OF CONTENTS (CONTINUED)

		<u>Page</u>
<u>Volume II, Exhibit B, Part 2</u>		
11.0	PRELIMINARY SHUTTLE/CENTAUR COMMUNICATION SYSTEM ANALYSIS . . .	39
12.0	SHUTTLE GLOBAL-POSITIONING SYSTEM INVESTIGATIONS . . . . .	40
13.0	TELEVISION DIGITIZER DEVELOPMENT . . . . .	41
13.1	Background . . . . .	43
13.2	Principles of Delta Modulation . . . . .	44
13.2.1	Conventional Bistate Delta Modulation . . . . .	44
13.2.2	Tri-State Delta Modulation . . . . .	47
13.2.3	Application of TSDM to NTSC Color TV . . . . .	50
13.3	Breadboard System Description . . . . .	52
13.3.1	Overall Test Setup . . . . .	52
13.3.2	Transmitter Functional Block Diagram Description . . . . .	55
13.3.3	Receiver Functional Block Diagram Discussion . . . . .	57
13.3.4	TSDM Digitizer/Reconstructor Implementation . . . . .	59
13.3.5	Run-Length Encoder Implementation . . . . .	63
13.3.6	Implementation of the Run-Length Decoder . . . . .	66
13.4	Summary and Conclusions . . . . .	66

Volume III, Exhibit C

14.0	ORBITER/PAYLOAD INTERFACE INVESTIGATIONS . . . . .	69
14.1	Spacelab ICD Revision . . . . .	70
14.1.1	HRM Asymmetry and Jitter . . . . .	70
14.1.2	Data-Dependent Amplitude Variations . . . . .	76
14.1.3	Transition Density . . . . .	76
15.0	PAYLOAD/SHUTTLE DATA-COMMUNICATION-LINK HANDBOOK . . . . .	77
REFERENCES	. . . . .	78

APPENDIX A - MONTHLY PROGRESS REPORTS

## 1.0 EXECUTIVE SUMMARY

The engineering and evaluation studies of Contract NAS 9-16067 began on May 1, 1980. During this time, the Shuttle communication and tracking systems went through their major development phases; only in the last few months have the flight units been tested on orbit. Because of the fairly large number of subsystems comprising the communication and tracking systems, a significant number of analysis areas were required during the development effort in order to resolve problems as they occurred so as to meet the Shuttle performance requirements in a cost-effective manner. This final report presents the significant analyses in the form of memoranda and reports which were produced over the contract period from May 1, 1980 to September 30, 1983. Numerous small analyses performed to solve problems that occurred on a daily basis were not documented in formal memoranda and reports but, to some extent, appeared in monthly status reports. The most pertinent monthly reports are included in Appendix A.

## 1.1 Contract Tasks

The contract tasks were divided into three exhibits. Exhibit A contained tasks related to the hardware development of the Shuttle communication and tracking systems. Exhibit B included tasks related to the overall system performance of the Shuttle communication and tracking systems in the Tracking and Data-Relay Satellite System (TDRSS) and Ground Spaceflight Tracking and Data Network (GSTDN). The tasks of Exhibit C were to provide analyses of the Shuttle/payload communication and data-system interfaces. The detailed tasks follow.

### 1.1.1 Exhibit A Contract Tasks

#### Task 1: GPS Requirements Analysis

During the preaward phase of the Orbiter GPS (Global Positioning System) project, the contractor shall participate in the review and development of GPS procurement specifications and other GPS definition documents. As part of his participation in this effort, the contractor shall attend GPS program reviews and working group meetings and shall provide recommendations as to the validity and achievability of proposed GPS subsystem requirements.

Following award of the GPS subsystem contract, the contractor shall perform engineering studies to assess the GPS vendor's technical approach toward meeting baselined GPS requirements. The contractor shall carry this effort through to the Orbiter GPS CDR (critical design review) and shall document his findings in accordance with instructions contained in the Data Requirements List. During this effort, primary emphasis shall be placed on the vendor's approach to the design of the signal processing segment of the GPS receiver/processor assembly.

As baseline GPS performance and interface requirements are adjusted during the GPS development effort, the contractor shall provide technical support by examining proposed baseline changes, assessing the advisability of implementing such changes, and recommending methods by which proposed changes can be implemented.

During the course of the study contract, the contractor shall provide periodic written assessments as to the Orbiter GPS equipment's ability to meet subsystem performance requirements. The assessment shall be submitted in accordance with instructions contained in the Data Requirements List.

#### Task 2: GPS Problem Identification

During the preaward phase of the Orbiter GPS project, the contractor shall begin a study directed toward the identification and resolution of GPS technical problems and shall carry this study through to the completion of the engineering studies contract. As part of this effort, the contractor shall attend GPS program reviews and working group meetings and shall accept problem identification and problem resolution action items as approved by the contract technical monitor.

In the event that problem resolution recommendations require the coordinated support of several organizations involved in the GPS program, the contractor shall, through the preparation of briefing material, background papers, and other documentation, assist in obtaining the required coordination.

The contractor shall maintain informal liaison with members of the GPS technical community and shall maintain a knowledge of the various GPS segments sufficient for a broad understanding of existing or potential GPS problems.

Reports, documenting specific problems and their resolution, shall be submitted in accordance with the Data Requirements List.

### Task 3: GPS Design Assessment

Following award of the GPS subsystem contract and continuing through the completion of the engineering studies contract, the contractor shall actively assess the technical progress of the GPS subsystem vendor in meeting baseline design requirements and design goals. The contractor shall review the GPS vendor's initial design concept, intermediate design, and final design and shall evaluate the progress of these iterations to determine if performance requirements will be achieved.

The contractor shall make formal assessments of the vendor's progress based on material presented at the Orbiter GPS PDR (preliminary design review) and CDR (critical design review). At the invitation of the contract technical monitor, the contractor shall provide representatives to attend the Orbiter GPS PDR and CDR.

The contractor shall provide written assessments of the progress of the GPS design. Such assessments shall be included in the monthly activity report provided in accordance with the Data Requirements List.

As GPS software development proceeds, the contractor shall review software products and participate in software design reviews.

### Task 4: GPS Change Proposal Evaluation

Following award of the GPS subsystem contract and continuing through the completion of the engineering studies contract, the contractor shall provide the TCDD with independent assessments of change proposals received from the GPS subsystem vendor or from the Orbiter/GPS integrator.

As may be required to assess the merits of engineering change proposals, the contractor shall recommend methods by which the proposed change can be independently evaluated in JSC facilities.

Assessments provided by the contractor shall include as a minimum an analysis of the effect which the proposed change will have on subsystem interfaces, internal subsystem software, subsystem reliability, subsystem test requirements, and baselined subsystem performance requirements.

#### Task 5. GPS Subsystem Test Evaluation

Using the results of work previously accomplished in the definition of generic test objectives and test methods, the contractor shall add further definition of the test concepts to be used in the ESTL (Electronic Systems Test Laboratory) for GPS subsystem testing. In accomplishing this task, the contractor shall review existing and programmed ESTL tests and shall propose a prioritized list of test objectives recommended for the ESTL. Such objectives shall take into consideration other testing planned as part of the vendor or integrator qualification and acceptance tests and those tests to be performed by other JSC laboratories.

As ESTL test objectives are solidified, the contractor shall assist the ESTL in developing specific test procedures to be following during GPS ESTL certification testing. Such procedures shall take into account the capabilities and limitations of the GPS RF simulator discussed in Task 6.

As GPS development testing progresses, the contractor shall perform evaluations of the resulting test data to determine if problems exist in the GPS design or if test objectives are not being met.

#### Task 6. GPS Simulator Evaluation

The contractor shall provide technical assistance to the ESTL in establishing a GPS simulation system. The contractor shall review ESTL simulation plans and concepts and shall make recommendations for detailed design of simulator hardware and software and for the integration of vendor-supplied equipment with existing ESTL facilities.

The contractor shall investigate and recommend methods by which ESTL GPS simulations could be enhanced or conducted in a more cost-effective manner through the use of actual GPS signals transmitted from orbiting Navigation Data Satellites.

#### Task 7. GPS Data Critiques

Upon request by the contract technical monitor, the contractor shall provide written critiques of technical data received from the GPS vendor or Orbiter/GPS integrator. Such data shall include, but not be limited to, specifications, qualification and acceptance test plans/procedures/reports, failure analysis reports, reliability analyses, interface control documents, and progress reports.

The contractor shall assist in interpreting detailed Orbiter GPS design information such that equipment functionally equivalent to the GPS vendor's design can be fabricated and evaluated by NASA laboratories.

#### Task 8. Orbiter/IUS ICD Review

The contractor shall continue the Orbiter/IUS ICD (Interface Control Document) review begun during the performance of Contract NAS 9-15409. As the Orbiter/IUS definition further materializes, the contractor shall expand the ICD review effort to all those Orbiter subsystems affected by IUS



compatibility requirements. For this effort, the contractor shall seek to identify all pertinent Orbiter/IUS interfaces and to assess the effects which such interfaces will have on Orbiter subsystems.

As the Orbiter/IUS interface definition continues, the contractor shall investigate interface incompatibilities and shall propose methods for resolving those incompatibilities. Investigations and recommendations for resolving incompatibilities shall be documented in reports provided by the contractor in accordance with the Data Requirements List.

#### Task 9: Orbiter/IUS Problem Identification

The contractor shall perform an investigative effort aimed at the identification and resolution of technical problems associated with the Orbiter/IUS communications system. The contractor shall participate in design reviews and shall accept action items to be undertaken for the resolution of review item dispositions. Equipment involved will include the NASA and DOD IUS transponders and the DOD communications interface unit and the interfaces between these units and the Orbiter payload/operational communications equipment.

The contractor shall document his problem resolution actions in reports to be provided in accordance with the Data Requirements List.

#### Task 10: COMSEC Evaluations

The contractor shall provide technical assistance in the interfacing of DOD COMSEC (Communications Security) equipment with IUS and Orbiter electronics. Such assistance will be provided through the contractor's participation in COMSEC design reviews, the evaluation of COMSEC-related interface control documents, and the review of COMSEC-related specifications and test data.

The contractor shall document his COMSEC-related efforts in reports to be provided in accordance with the Data Requirements List.

#### Task 11: IUS/Orbiter Testing

Using the results of work previously accomplished, the contractor shall add further definition to the set of ESTL test objectives for IUS-related hardware and shall update the ESTL testing concept as hardware and software designs mature.

The contractor shall evaluate test documentation associated with IUS-related equipment and will assess the degree to which development test objectives have been achieved.

The contractor shall document his test-related activities in reports prepared in accordance with the Data Requirements List.

#### Task 12: Ku-Band Problem Resolution

The contractor shall provide an independent technical assessment of problems revealed during all phases of Ku-band testing. This assessment shall include an analytical treatment of the effects on overall system performance, recommendations for design changes to correct the problem, and identification of possible alternatives to design changes that would still satisfy overall systems requirements. The contractor shall provide a thorough analysis of

any recommended design changes, including those recommended by the hardware contractor, the Orbiter contractor or NASA. The contractor shall participate in design reviews and technical meetings dealing with these problem areas.

The contractor shall document these efforts in reports to be provided in accordance with the Data Requirements List.

#### Task 13: Radar Range Test Evaluation

The contractor shall provide support to NASA in preparation for the radar tests to be conducted at the White Sands Test Facility. This shall include analysis to support performance predictions for radar operation at that location; for example, the effects of backscatter, etc. In addition, the contractor shall provide analysis to support evaluation of the data obtained during testing of the radar at the White Sands Missile Range. These tests will involve operation of the radar against moving targets and will be the only such tests performed prior to an actual mission. Data obtained from the radar will be compared to that obtained from the instrumentation standards. The contractor shall identify any areas in which the measured performance does not meet the specified requirements and shall provide an assessment of the impact to overall system performance.

The contractor shall document these efforts in reports to be provided in accordance with the Data Requirements List.

This task will require approximately three weeks of effort at the White Sands Missile Range, New Mexico, consisting of three one-week intervals.

#### Task 14. Mission Support/Post-Flight Evaluation for OFT

The contractor shall provide analysis to support the data reduction and performance evaluation of the Ku-band Radar/Communications System during Space Transportation System mission operations. This analysis shall be performed on data that is transmitted to the MCC during mission operation. Special attention will be given to any apparent anomalies in the data obtained.

The contractor shall document these efforts in reports to be provided in accordance with the Data Requirements List.

#### Task 15: S-Band Payload Communications

The contractor shall continue the review and evaluation of S-band test requirements and verification plans begun on Contract NAS 9-15792 and shall make recommendations for improvement of the S-band test program. During the verification effort, the contractor shall monitor the progress of testing conducted at ADL (Avionics Development Laboratory), ESTL, SAIL (Shuttle Avionics Integration Laboratory) and KSC and shall identify inconsistencies or omissions in the verification tests. Results of the contractor's evaluation of the test effort shall be documented in accordance with the Data Requirements List.

The contractor shall continue the evaluation of the baselined S-band design developed by the system vendor, assess the ability of this design to meet established NASA requirements, and shall report on the results of this assessment with the Data Requirements List. As part of the design evaluation, the

contractor shall participate in S-band payload communications equipment design reviews and shall accept action items to be undertaken for the resolution of review item dispositions.

During the period of operational flight testing, the contractor shall conduct pre- and post-mission, S-band equipment performance evaluations. Such evaluations will include detailed assessments.

### 1.1.2 Exhibit B Contract Tasks

#### Task 1: Ku-Band Radar/Communications System Analysis

##### Subtask 1--System Implementation Assessment

The contractor shall provide technical support of the Ku-band system implementation as it progresses from development status into system tests, flight tests, Orbiter integration, KSC checkout, OFT and SSP operations. The contractor shall analyze the system implementation, including proposed design changes, test plans and test data to provide an independent assessment of the Ku-band system capability and its interface compatibility. The contractor shall recommend design changes and/or tests as required to assure Ku-band system compliance with the SSP operational requirements and to resolve areas of incompatibility. The contractor shall participate in designated Ku-band reviews and briefings and respond to assigned action items within the scope of this SOW.

##### Subtask 2-- System Performance Evaluation

The contractor shall evaluate the overall Ku-band system performance using updated system parameters, analytical models and designated mission profiles. The contractor shall generate and maintain an updated list of system parameters supported by test data. The radar performance evaluation shall quantify nominal system operation, deviations due to variations in system parameters and deviations due to target effects, and shall determine operational limitations. The communication performance evaluation shall quantify nominal system operation, deviations due to variations in system parameters and deviations due to TDRSS user constraints, and shall determine operational limitations. The contractor shall identify marginal system performance measures and recommend judicious changes to the Ku-band system, its RF interfaces and/or SSP operational limitations.

#### Task 2: S-Band Communication System Analysis

##### Subtask 1--System Implementation Assessment

The contractor shall provide technical support of the S-band PM and FM systems implementation as it progresses from systems tests to Orbiter integration, KSC checkout, OFT and SSP operations. The contractor shall analyze the system implementation, including proposed design changes, test plans and test data to provide an independent assessment of the S-band system capability and its interface compatibility. The contractor shall recommend design changes and/or tests as required to assure compliance of the S-band PM and FM systems with the SSP operational requirements and to resolve areas of incompatibility. The contractor shall participate in designated reviews and briefings and respond to assigned action items.

### Subtask 2--System Performance Evaluation

The contractor shall evaluate the overall S-band PM and FM system performance in operations with the TDRSS, GSTDN and SGLS networks. The contractor shall generate and maintain an updated list of S-band system parameters supported by test data. The performance evaluation shall quantify the nominal system operation, deviations due to variations in system parameters and deviations due to TDRSS, GSTDN and SGLS network constraints and shall identify any marginal system performance areas and recommend judicious changes to the S-band system, operations of the interfacing space network and/or SSP operational limitations.

### Task 3. Orbiter Antenna Patterns

The signal margins of certain communication links are critically dependent upon the spacecraft antenna gain realized. Uncertainties and limitations of the one-tenth scale model and Orbiter section mockups preclude obtaining antenna pattern data of sufficient accuracy and extent from ground tests. The contractor shall study and recommend a method for generating refined antenna pattern estimates from operational flight data recordings. The contractor shall identify and recommend specific inflight signals to be measured and recorded, including the record rate and length of each signal. The contractor shall also recommend and detail the post-flight processing required to generate refined antenna-pattern estimates from the inflight recordings. The specific antennas to be considered are the S-band quads, S-band hemis and UHF antennas.

### Task 4 S-Band Payload Communication System

#### Subtask 1--System Implementation Assessment

The contractor shall provide technical support for the S-band payload communication system as it progresses from development status into system tests, Orbiter integration, payload integration, KSC checkout, OFT and SSP operations. The contractor shall provide an independent assessment of the system implementation and the interface compatibility of the payload interrogator, the payload signal processor, the DOD communication interface unit, the payload data interleaver, the network signal processor and the Ku-band signal processor. The contractor shall recommend design changes and/or tests as required to assure compliance with system requirements and interface compatibility and to resolve areas of incompatibility.

#### Subtask 2--System Performance Evaluation

The contractor shall evaluate the overall performance of the payload communication system and, where required, its interfaces. The performance evaluation shall quantify nominal system operation and deviations due to variations in system parameters. The contractor shall determine operational limitations of the payload communication system. The contractor shall identify areas of marginal system performance and recommend judicious changes to the Shuttle payload communication system, specific interfaces and/or operational limitations.

### Task 5: Space Shuttle/TDRSS and GSTDN Compatibility Analysis

The contractor shall analyze the Space Shuttle/TDRSS and GSTDN communication links and systems to ensure compatibility, to evaluate the effects of user constraints, and to predict nominal system performance and expected deviations. The contractor shall review the pertinent RF ICD's to identify potential problem areas. The contractor shall analyze and recommend design changes, user constraints, and/or tests as required to assure compliance with SSP requirements and to resolve areas of incompatibility.

### Task 6: Global-Positioning System Analysis

#### Subtask 1--SSP/GPS Requirements Definition

The contractor shall define technical requirements for the SSP/GPS. The requirements shall be derived from studies, analyses and SSP plans coordinated with the conclusions and recommendations of the Space Shuttle GPS Panel. The contractor shall prepare a Level-II ICD to formalize the NASA requirements with GPS Program Management. The contractor shall provide technical information for SSP/GPS definition documents and shall conduct a thorough technical review of all documentation pertinent to the RF link, the SSP hardware, and all associated interfaces to ensure compatibility and performance commensurate with SSP requirements.

#### Subtask 2--System Implementation Assessment

The contractor shall provide technical support of the SSP/GPS implementation from initial design, into test, integration, checkout and operational use. The contractor shall provide an independent assessment of the system implementation, technical alternatives and deviations from specifications by vendors. The contractor shall analyze test plans and test data to assess the GPS capability and its interface compatibility. The contractor shall recommend design changes and/or tests as required to assure compliance with SSP operational requirements and to resolve areas of incompatibility.

#### Subtask 3--System Performance Evaluation

The contractor shall evaluate the overall GPS performance using updated system parameters, analytical models and designated mission profiles. The contractor shall generate and maintain an updated list of system parameters supported by test data. The contractor shall identify areas of marginal system performance and recommend judicious changes to the GPS system and/or SSP operational limitations.

### Task 7. TV Digitizer Development

#### Subtask 1--Engineering Breadboard Implementation

The contractor shall design, fabricate and test an engineering breadboard of a digital NTSC color-TV processing system. The system design shall use a tri-state modulator/demodulator and a run-length encoder/decoder and shall be capable of being implemented for spaceflight use. The contractor shall test the breadboard to verify system operation, to obtain performance data and to determine the sensitivity of key parameters to system variables. The contractor shall deliver the breadboard to NASA/JSC and demonstrate its operation. The contractor shall document the design, test data and conclusion of this task activity.

### Subtask 2--Space Shuttle Digital TV Specification

The contractor shall prepare a technical requirements specification of a digital TV system for operational use on the Space Shuttle Orbiter. The specification shall incorporate the NASA and DOD requirements for a digital TV system that is compatible with existing Orbiter avionics.

In addition to the original tasks of Exhibit B listed above, technical direction from William E. Teasdale on June 1, 1981, transmitted to Axiomatix through John E. Jones, the Contracting Officer, redefined Tasks 2 - 5 to support the Centaur project as a newly defined Level-III element of the Shuttle program. Also, Axiomatix was directed to terminate all present analysis efforts relative to refinement of Shuttle antenna-pattern estimation using calibrated flight-measurement data defined in Task 3, Orbiter Antenna Patterns. All antenna analyses to be performed under Task 3 after June 1, 1981 were to be directed toward Shuttle antenna design and performance evaluations and problem-area resolution. The Centaur tasks to be performed under the broad scope of Tasks 2 - 5 were defined as follows

Task 1: The contractor shall support Level-II Centaur requirements and design reviews and Centaur communication and data systems panel meetings and activities.

Task 2. The contractor shall perform Centaur communication and tracking system performance and compatibility analyses in support of the Centaur communication and tracking system design.

Task 3. The contractor shall perform a Centaur transponder design trade-off study and evaluation for application to Shuttle/Centaur and Centaur/ground network links. The results of the transponder study shall be used as a data base for transponder vendor selection, specification requirements and interface control documents.

Task 4. The contractor shall generate preliminary specifications and interface design characteristics for the Shuttle/Centaur and Centaur/ground network interface control documents.

### 1.1.3 Exhibit C Contract Tasks

#### Task 1: Payload Interface-Compatibility Analysis

The contractor shall, through analysis and/or simulation, continue identification of possible hardware design weaknesses and potential interface compatibility problems (associated with interfacing payload elements such as the IUS, CIU, TDRS and PAM with Orbiter communications and data-handling elements, i.e., the Ku-band signal processor, payload signal processor, payload interrogator, payload data interleaver, payload recorders) that would result from payload or Orbiter failure to meet agreed-to interface requirements contained in the Orbiter/cargo standard interface specification (NASA JSC ICD No. 2-19001) and payload-unique ICD's. The contractor shall review updated Orbiter hardware documentation (procurement specifications, test documentation, etc.) pertaining to the above-listed Orbiter elements, and existing payload interface hardware-system design documentation as provided by NASA for compatibility with the standard interface specification and payload ICD's.

The contractor shall perform analyses of specific interface issues involving IUS, CIU, TDRS and PAM which result from continuing technical interface discussions with the candidate payloads during the performance period of the contract. The contractor shall perform trade-off analyses and end-to-end data-link performance optimization. The result of these analyses will be used by JSC as a data base to support future negotiations of interface agreements and ICD's with the subject payloads.

#### Task 2: Problem-Area Analyses and Resolution

The contractor shall determine and assess viable alternatives to payload system design, operational requirements (especially those affecting signal acquisition) and/or interface configurations which will allow resolution or workarounds of problems identified under Task 1. Problems identified which are due to Orbiter failure to meet interface specifications shall be assessed and viable solutions shall be proposed.

## 1.2 Performance of the Contract Tasks

During the contract period from May 1, 1980 to October 31, 1983, the development and flight schedules for the communication and tracking systems were changed several times. Also, some systems such as GPS have yet to be implemented on the Shuttle, while others such as Centaur have been added and are in the middle of development. Therefore, Tasks 1 - 7 of Exhibit A, dealing with the implementation of GPS, were not funded.

The primary emphasis in performing IUS Tasks 8 - 11 was the analysis of the IUS STDN/TDRS transponder performance. The analysis included augmenting and, in some instances, correcting the CDR data, analyses and investigations provided by TRW (the IUS STDN/TDRS transponder vendor). Other areas of investigation of the IUS system and its interface with the Shuttle payload communication system were. (1) determination of the allowable phase noise that could be transmitted by the IUS to the PI, (2) determination that the IUS transmitted adequate residual carrier for PI signal-acquisition and tracking, (3) determination of the cable-loss degradation between the PI and CIU, and (4) evaluation of the IUS STDN/TDRS receiver-frequency acquisition using an automatic frequency control (AFC) loop. However, Task 10, COMSEC Evaluations, was not performed since the COMSEC development was so far along before the contract started that no useful areas existed in which Axionix could provide technical assistance. The analyses performed under IUS Tasks 8 - 11 are presented in Section 2 of this report.

The Ku-band system encountered many delays in its development schedule, as did the Shuttle program in general. Therefore, of Ku-band Tasks 12 - 14, only Task 12, Ku-Band Problem Resolution, was completed under this contract. Task 13, Radar-Range Test Evaluation, is now scheduled for early 1984 and will have to be part of some other contract effort. Similarly, Task 14, Mission Support/Post-Flight Evaluation for OFT, is just beginning and will be part of some other contract effort. However, extensive analyses, investigations and evaluations of the Ku-band problems which occurred during development were performed and are presented in Section 3 of this report.

Two major efforts were performed under Task 15, S-Band Payload Communications. First, the S-band network equipment was investigated to understand problems which occurred during ESTL and KSC tests. The problems involved false lock of the PN code in the S-Band Spread-Spectrum Processor and increased forward-link doppler rates encountered during launch. The results of these investigations are presented in Section 4 of this report.



The second major effort under Task 15 was Shuttle/Centaur communication systems engineering investigations. These investigations became part of Task 15 as the Centaur communication system progressed further into the hardware development stages. These investigations occurred during the period from October 1, 1982 to September 30, 1983. The results of these investigations are presented in Section 5 of this report.

The Exhibit B tasks were oriented more toward the overall Shuttle/TDRSS and Shuttle/GSTDN links than the individual communication subsystem development implementation. Therefore, the Exhibit B tasks tend to address the overall communication system performance and were concerned with the subsystem implementation details only when the overall system performance was affected. Section 6 addresses the analyses of the Ku-band system as part of Task 1 of Exhibit B which were documented in memoranda and reports. Many other analyses were performed to answer daily problems that developed, and were not documented. As was pointed out earlier, the Ku-band development schedule as well as the Shuttle schedule in general slipped such that there is now a lot of analysis activity since the Ku-band system has been tested on orbit with the TDRSS. This current analysis activity, however, is being performed under a new contract, NAS 9-16893.

Task 2 of Exhibit B was oriented toward the S-band network communication equipment which was through the major stages of development before this contract effort started, but on-orbit tests with the TDRSS have taken place only in the last few months due to the delayed launch of the TDRS and the initial problems of the satellite achieving synchronous orbit. Therefore, the analyses of the S-band network overall system performance were limited to acquisition times with the wide data filter and the data off, and the Shuttle G/T and EIRP calculations. These analyses are presented in Section 7. It should be pointed out that additional analyses related to problems which developed in ESTL and KSC tests are documented as part of Task 15 of Exhibit A.

Task 3, Orbiter Antenna Patterns, was composed of two separate areas of investigation. First, were the analyses to improve the S-band quad antennas performance. Axionix was heavily involved in this effort and provided many significant contributions to the improvement of coverage performance. The second area of investigation under this task was to develop techniques to determine the actual Orbiter antenna gain and coverage from on-orbit measurements. After an initial investigation, Axionix presented its findings in a report and was directed on June 1, 1981 to terminate further analysis in this area because

little could be gained by on-orbit measurements from several ground stations that were calibrated differently. The analyses from these two areas of investigation are presented in Section 8.

The major emphasis of the Axiomatix investigation of the payload communication system as part of Task 4 centered on the payload signal processor (PSP) bit-synchronizer false-lock problem found during ESTL tests. Extensive analyses were performed to understand and to solve this problem. Axiomatix made several recommendations that were incorporated into the design changes to the PSP bit synchronizer. The results of these analyses, investigations and recommendations are presented in Section 9.

While Task 5, Space Shuttle/TDRSS and GSTDN compatibility analysis, was directed at the overall system compatibility, many of the analyses were performed as part of the individual communication subsystems such as the S-band network equipment and the Ku-band communication system. Under this task, Axiomatix attended all the TDRSS design reviews and evaluated review material and, along with NASA/JSC personnel, generated Review Item Dispositions (RID's). The last TDRSS design review which Axiomatix attended was the TDRSS Ground Segment Final Design Review at TRW September 22-24, 1981. Section 10 discusses two of the analyses performed to establish compatibility between the Shuttle Ku-band communication system and the TDRSS. These two analyses are: TDRSS antenna scan for Shuttle acquisition, and the power-spectral density of staggered quadriphase PN with identical sequences. For additional analyses concerning Shuttle/TDRSS and GSTDN compatibility, refer to the sections of this report dealing with the individual communication subsystems.

In response to the June 1, 1981 technical direction, Axiomatix began the preliminary Centaur system analysis. This analysis was performed under the broad scope of Tasks 2 - 5 and is presented in Section 11. The preliminary effort was concluded toward the end of 1981 when the Centaur development as part of the Shuttle was not funded by Congress. Because the Centaur communication system was now on a tight schedule, system implementation became the most important task. Therefore, further analyses of the Centaur communication system was performed under Task 15 of Exhibit A and is presented in Section 5.

The GPS was investigated to determine if it could be a cost-effective alternative to TACAN for navigation of the Shuttle. Axiomatix provided the analyses to establish the viability of GPS under Task 6. While the Axiomatix

analyses presented in Section 12 shows that GPS could provide very accurate navigation, the schedule for deployment of the satellites and the development of the user equipment was well behind that of the flight schedules of the Shuttle Orbiter. Therefore, the GPS has yet to be implemented on the Shuttle.

The final task of Exhibit B was Task 7, TV Digitizer Development. This task was to design, fabricate and test an engineering breadboard of a digital NTSC color-TV processing system based on the tri-state modulator/demodulator and run-length (R/L) encoder/decoder that Axiomatix had studied under a previous contract. Section 13 presents the results of this breadboard activity and describes the desirability of this technique to produce digital NTSC color TV. Because of the decreased need of DOD for NTSC color TV in favor of slow-scan TV, the subtask to develop the Space Shuttle digital-TV specification was not funded.

Exhibit C has two major tasks. Task 1 was to provide payload compatibility analyses to identify possible hardware design weakness and potential interface compatibility problems. Task 2 was for problem-area analyses and resolution. In accomplishing these tasks, Axiomatix generated a Spacelab Interface Control Document (ICD) revision, a PSP command specification review, payload nonstandard modulation constraints to become part of the Shuttle/payload ICD, and an analysis of the performance of the Spacelab High-Rate Multiplexer address coding using the Shuttle Ku-band communication system. These analyses and revisions to ICD's are presented in Section 14. In addition to these analyses, Axiomatix generated a Payload/Shuttle Data Communication Link Handbook to provide the payload user with the technical performance information necessary to independently assess which aspect of the Shuttle communication systems capability can best be employed to satisfy his requirements. The handbook is found in Section 15 of this report.

## 2.0 ORBITER INERTIAL UPPER-STAGE STUDIES

When performing Orbiter Inertial Upper-Stage (IUS) Tasks 8 - 11, the primary emphasis was the IUS STDN/TDRS transponder performance analysis. This analysis included augmenting and, in some instances, correcting the CDR data and analyses as well as investigations provided by TRW (the IUS STDN/TDRS transponder vendor). The IUS STDN/TDRS transponder performance analysis is included in Axiomatix Report No. R8110-3, "Annual Final Report for IUS Studies," which is a part of this section. Other areas of investigation of the IUS system and its interface with the Shuttle payload-communication system were: (1) determination of the allowable phase noise that could be transmitted by the IUS to the PI, (2) determination that the IUS transmitted adequate residual carrier for the PI signal acquisition and tracking, (3) determination of the cable-loss degradation between the PI and CIU, and (4) evaluation of the IUS STDN/TDRS receiver frequency acquisition using an automatic-frequency-control (AFC) loop.

Under NASA Contract NAS 9-15240, Exhibits E, F and G, Axiomatix made extensive analyses on the theory of mean-square phase-noise performance of one-/two-way coherent communication links. Using the result of these analyses and the measured performance of the Orbiter PI, Axiomatix determined that the maximum-allowed phase noise from the IUS to the PI was  $5^\circ$  RMS measured in a bandwidth from 100 Hz to 10 MHz.

The PI procurement specification requires the maximum carrier suppression to be -10 dB in order for the PI to meet its acquisition and tracking performance requirements. However, the payload ICD allows the modulation index of the 1.024-MHz subcarrier to be 1.7 radians  $\pm$  15%. Axiomatix calculated that the maximum -10 dB carrier suppression occurred at a modulation index of 1.84 radians, which relates to the nominal value of 1.7 radians + 8%. A carrier suppression of -12 dB occurs for 1.7 radians + 15% (i.e., 1.96 radians), which exceeds the allowed maximum-carrier suppression, while 1.7 radians - 15% (i.e., 1.45 radians) gives a carrier suppression of -5.3 dB. It was therefore recommended that the tolerance of the modulation index be changed to make it consistent with the PI carrier-suppression specification.

From a more practical standpoint, the PI Engineering Model was tested on May 6, 1983 to determine performance with a modulation index of 2 radians for BER's ranging from  $10^{-3}$  to  $10^{-6}$ . No performance degradation was apparent, so a carrier suppression of -12 dB did not appear to be a problem. It should

be noted that acquisition and tracking-level specifications remain fixed -125 dBm and -124 dBm, respectively, for the modulation index case of 1.7 radians  $\pm 15\%$ , so that more transmitter power is required for larger carrier suppression.

In the ICD between the Orbiter and the DOD IUS, it was found that no allocation existed for the voltage drop between the PI and CIU. Specifically, the PI minimum output is specified at 1.6 V RMS, i.e., the same as the CIU input. But, because of the 0.5-dB cable loss, the actual level at the CIU input is 1.5 V RMS. Axiomatix reviewed this problem with Rockwell; Rockwell's Mike Zelon stated that, if required, he believed that the signal-level output of the PI could be increased by modifying the PI.

Upon request from Rockwell, Axiomatix discussed this discrepancy with the Boeing personnel responsible for the CIU. The Boeing engineers stated informally that they did not expect the small loss to be a problem if the CIU input receivers were designed properly. However, they did not officially agree to a possible CIU specification change. Instead, they suggested that the PI/CIU interface be evaluated properly at ESTL and SAIL. Only following such an evaluation should the final decision be made regarding changes to the CIU specification or PI output increase. The initial evaluation of the PI/CIU interface at ESTL was confused because a buffer amplifier was used between the PI output and the CIU in order to obtain the expected performance. However, subsequent tests at SAIL showed that the buffer amplifier was not required and the current specifications on the PI and CIU were adequate.

Determining the carrier-acquisition performance and limitations of a generic IUS receiver using an AFC loop were the final areas of investigation. The use of an AFC loop is the determining factor in the carrier acquisition because, for large doppler offsets and/or oscillator drifts, a narrowband Costas loop typically requires a relatively slow sweep across the frequency uncertainty, thus causing slow carrier-acquisition performance. However, a frequency-lock-loop, on the other hand, can have a narrow bandwidth but still pull in from a large frequency offset relatively quickly. Since noise can affect the speed at which the AFC loop will pull in, as well as the probability of staying locked, it is important to analyze the performance of the AFC in noise. Pursuant to this, several AFC analyses conducted as part of this task are presented in this section.

As can be seen from Axiomatic Technical Memoranda M8112-1 and M8201-3, the analyses are very complicated. Due to the analytical complexity, computer simulations of the AFC loop were developed. Actually, several AFC loop types were simulated and several types of lock detectors were studied. It was found that developing a meaningful criterion for "in lock" is a difficult problem. Unfortunately, the simulation effort was not completed due to funding limitations. Some of the preliminary results, however, are given in this section.

ENGINEERING EVALUATIONS AND STUDIES  
ANNUAL FINAL REPORT FOR IUS STUDIES

Contract No. NAS 9-16067, Exhibit A

Prepared for

Lyndon B. Johnson Space Center  
Houston, Texas 77058

Prepared by

AXIOMATIX  
9841 Airport Blvd., Suite 912  
Los Angeles, California 90045

AXIOMATIX Report No. R8110-3  
October 20, 1981

## TABLE OF CONTENTS

	<u>Page</u>
1.0 INTRODUCTION . . . . .	1
1.1 Statement of Work . . . . .	1
1.1.1 Objectives . . . . .	1
1.1.2 Stipulated Tasks . . . . .	1
2.0 GENERAL APPROACH . . . . .	2
3.0 TECHNICAL INVESTIGATION . . . . .	3
3.1 Analysis of IUS STDN/TDRS Transponder Performance . .	3
3.1.1 IUS Memo No. 125 . . . . .	9
3.1.2 IUS Memos No. 112 and 118 . . . . .	10
3.1.3 IUS Memos No. 114 and 116 . . . . .	11
3.1.4 IUS Memo No. 115 . . . . .	13
3.1.5 IUS Memo No. 117 . . . . .	16
3.1.6 IUS Memo No. 123 . . . . .	18
3.1.7 IUS Memo No. 110 . . . . .	20
3.1.8 IUS Memo No. 124 . . . . .	21
3.1.9 IUS Memos No. 122 . . . . .	24
3.1.10 IUS Memos No. 119 and 120 . . . . .	26
3.1.11 IUS Memo No. 121 . . . . .	28
4.0 CDR ACTIVITY . . . . .	37
5.0 SUMMARY AND CONCLUSIONS . . . . .	40
REFERENCES . . . . .	41



1.0 INTRODUCTION

1.1 Statement of Work

1.1.1 Objectives

The objectives of this contract were to identify and resolve problems associated with the Orbiter/IUS communications systems.

1.1.2 Stipulated Tasks

The tasks associated with this contract include participation in design reviews, coupled with acceptance of action items to be undertaken for the resolution of review item dispositions (RID's). This includes reviewing all performance analyses submitted by the transponder contractor.

## 2.0 GENERAL APPROACH

In the process of carrying out the required tasks, Axionatix has worked closely with the cognizant NASA personnel, the Orbiter prime contractor (Rockwell International), the IUS prime contractor (Boeing Aerospace Co.), and the IUS and Orbiter payload communication equipment subcontractor (TRW Defense and Space Group). This activity included attending the Critical Design Review (CDR) and reviewing in detail all communication-related performance analyses submitted by TRW.

While Axionatix was engaged in these contractual activities, TRW, the IUS STDN/TDRS transponder contractor, received a stop-work order since the Centaur is to be used as an upper stage for NASA missions, and the NASA TDRS/GSTDN standard transponder built by Motorola was chosen for use on the Centaur. Therefore, the remainder of this report documented the analyses and investigations undertaken by Axionatix and completed at the time of the stop-work order.

### 3.0 TECHNICAL INVESTIGATION

This section documents the reviews, investigations and analyses of the TRW IUS STDN/TDRS transponder performed by Axiomatix. First, it is appropriate to discuss where this equipment or subsystem fits into the overall Orbiter/Payload communication link. Figure 1 shows the top-level IUS STDN/TDRS transponder interfaces with the payload IUS and the Orbiter. As can be seen in this figure, the transponder receives telemetry from the IUS and passes commands to the IUS. The interface with the Orbiter is via an S-band RF link with the Payload Interrogator (PI). Thus, the IUS STDN/TDRS transponder must perform all the typical communication functions of acquisition, tracking, data demodulation and data modulation. These functions will be addressed in subsequent sections.

Before analyzing these communication functions, however, it is helpful to gain some perspective as to where and how these functions relate to the overall transponder. This perspective is afforded by the transponder block diagram shown in Figure 2. The specific detailed areas of the transponder involved in the Axiomatix investigation are indicated by the cross-hatch lines in the transponder block diagram given in Figure 3.

#### 3.1 Analysis of IUS STDN/TDRS Transponder Performance

Volume I (Analysis) of the STDN/TDRS Transponder, S-Band Critical Design Review (CDR) data package contains a series of detailed electrical design analyses performed by TRW for Boeing that pertain to the manner in which the STDN/TDRS transponder meets the performance specifications imposed by NASA for its use in IUS missions. Many of these analyses previously appeared in the Preliminary Design Review (PDR) data package delivered to Boeing on June 11, 1979. To the extent that these analyses (IUS memos) were complete at that time, Axiomatix reviewed and critiqued their contents and reported its findings shortly thereafter in Axiomatix Report No. R7911-5, November 30, 1979. Also included in that report were three appendices (C, E and F) which augmented and, in some instances, corrected several of the TRW analyses.

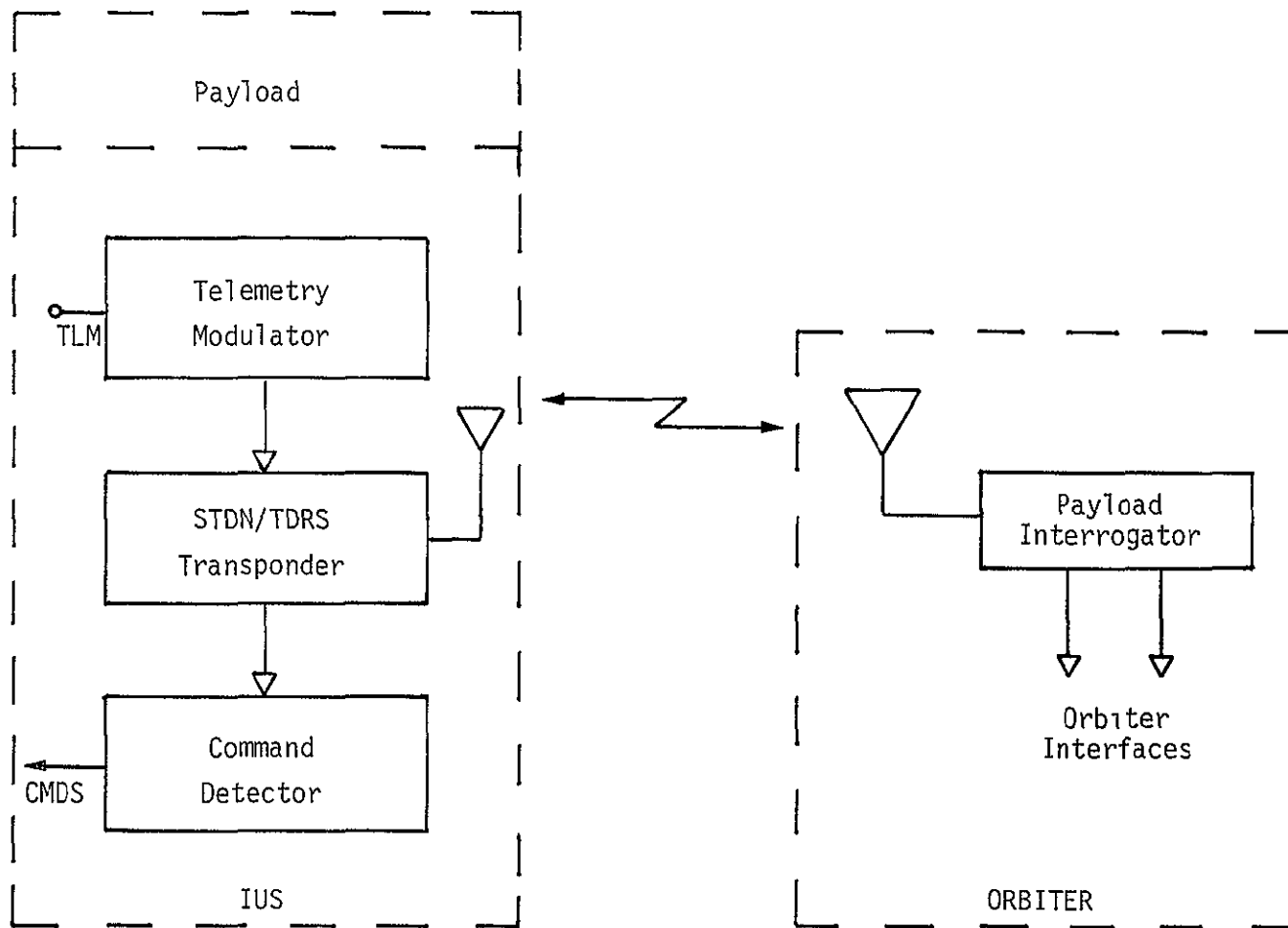
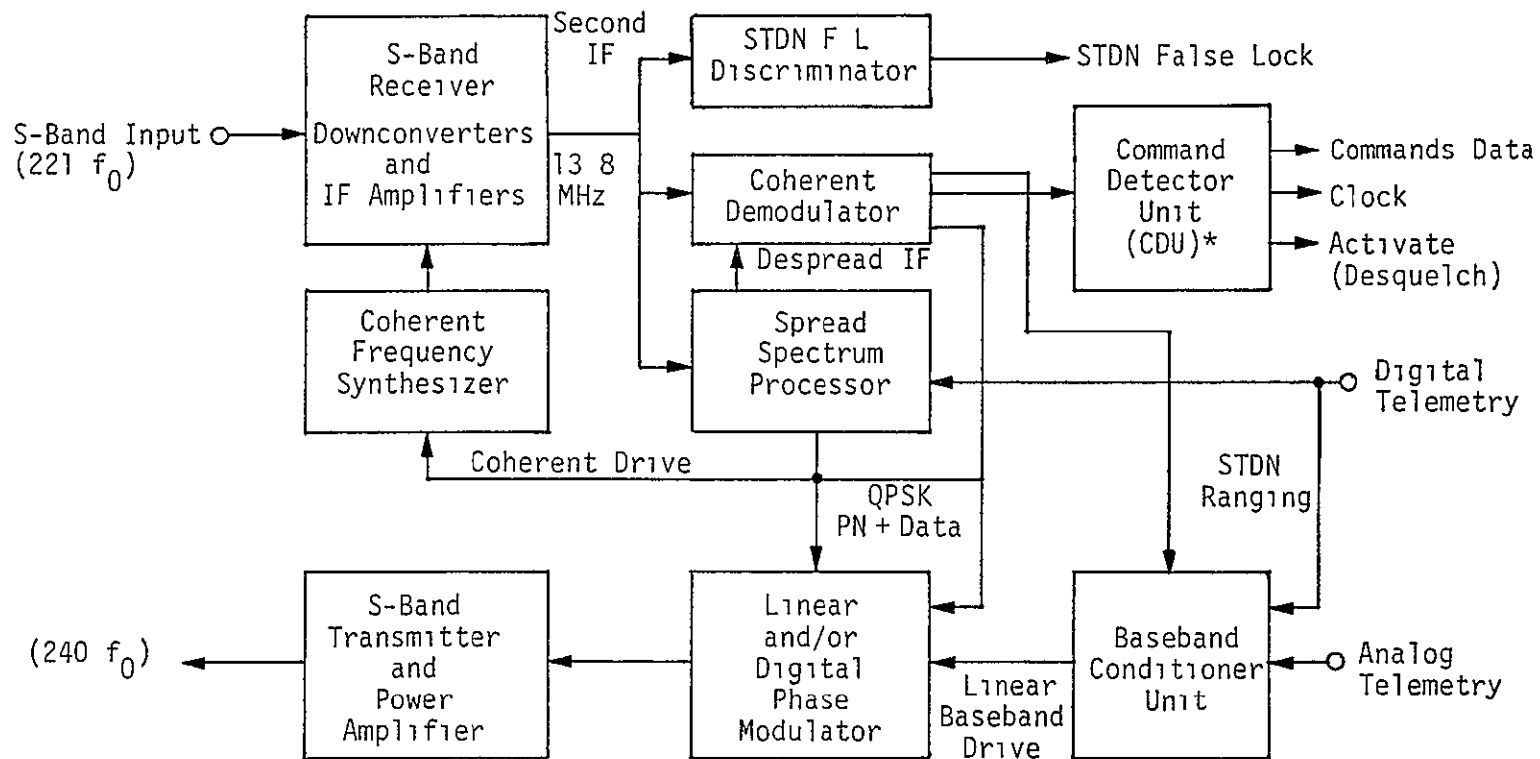
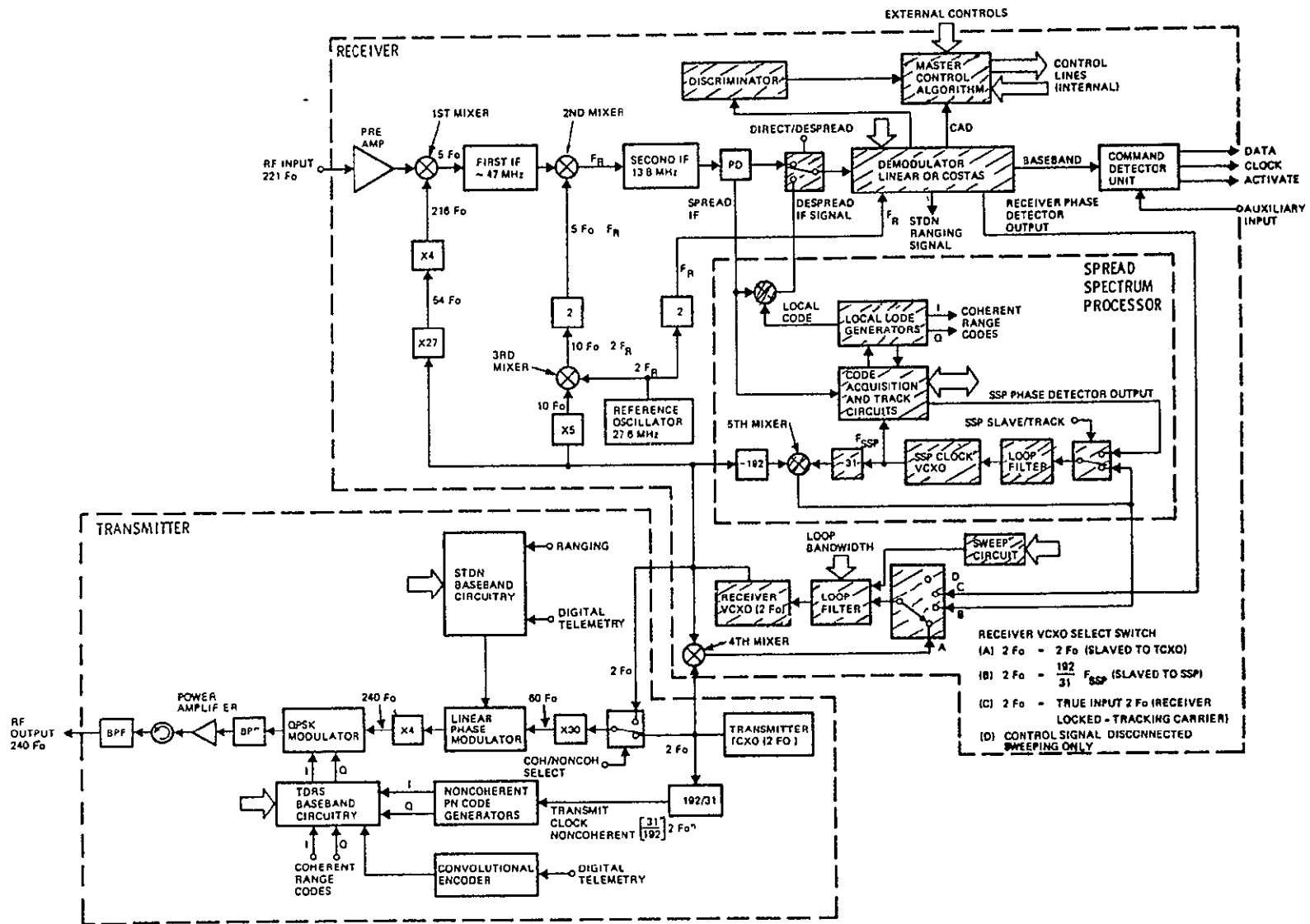


Figure 1. Top-Level IUS STDN/TDRS Transponder Interfaces



\*Includes bit synchronizer

Figure 2. IUS STDN/TDRS Transponder Functional Block Diagram



ORIGINAL PAGE IS  
OF POOR QUALITY

Figure 3 IUS STDN/TDRS Transponder Simplified Block Diagram with Shading of Functional Areas Analyzed and Reviewed

Since these same IUS memos are contained in the CDR data package, Axiomatix shall avoid duplication of effort by reviewing and critiquing only those memos which were not contained in the PDR package. In dealing with each of these analyses one by one, we shall simply refer to them by their IUS memo numbers, as per the entries in Table 1. It should also be pointed out that most of the analyses were performed by a single individual\* (namely, Dr Jack K. Holmes, Consultant to TRW) and thus it should not be surprising that comments made on one particular analysis might apply equally to many of the others. Such similarities in approach, style, etc., will be indicated in our discussion so as to avoid unnecessary redundancies.

---

\*The remainder were performed by Dr. H. C Osborne of TRW.

Table 1. IUS Memos Reviewed and Analyzed

Section	IUS Memo No.	Title
2. TDRS Mode--General	125	TDRSS Lock Detector Parameters, Structure and Performance for IUS
3. TDRS--Carrier Acquisition Analysis and Experiment	112	A Possible Problem in the IUS Code-Aided Carrier Acquisition Approach
	118	Improved Estimate of the Code-Multiplied Spectral Density
	114	Instantaneous Frequency Error of the Carrier Loop Reference (at the Moment of Code VCXO Disconnect)
	116	Instantaneous Frequency Error of the Carrier Loop Reference at the Moment of Code Loop Disconnect--Revisited
4. Costas Loop Performance--Analysis	115	Revision A--IUS Phase Detector Biases Due to Hybrid and Arm Filter Imperfections in the Costas Loop
	117	IUS Slip Time
	123	Influence of Arm Filter Delay on Tracking Performance of the IUS Costas Loop
5. SSP Analysis	110	Code Tracking Lock Detector Mean Time to Declare Out-of-Lock
6. STDN Dual Mode	122	STDN Dual Acquisition and Tracking Analysis
	124	Open-Loop Frequency Acquisition
7. STDN Only Mode	119	STDN Acquisition and Tracking Logic
	120	STDN Acquisition and Tracking Analysis
	121	IUS STDN-Only Discriminator Analysis for False Lock Avoidance



### 3.1.1 IUS Memo No. 125

This memo discusses the design and analyses of carrier lock detector performance for TDRSS dual-mode operation. In this mode, 2 kbps (125 bps in the low rate mode) data is modulated on the I-channel and modulo-two added to the command spreading PN (Gold) code while the ranging mode spread spectrum (truncated PN code) signal is modulated on the Q-channel. The power ratio of the I- and Q-channels is 10 dB.

The lock detector, in conjunction with the AGC amplifier, derives its error signal in the conventional manner from the  $I^2 - Q^2$  output of a Costas loop. This error signal, which has the identical  $SxS^*$ ,  $SxN$  and  $NxN$  components of the Costas loop tracking error signal, is filtered by a narrowband (with respect to the arm filter bandwidth) lowpass filter and the output is compared to a fixed threshold which is set at one-half the threshold (minimum  $C/N_0$ ) signal level corresponding to the low data rate (125 bps) mode. The threshold outputs are used in a verification-type algorithm to decide whether or not the loop is in lock. In particular, two successive below-threshold indications must occur to assure that the lock detector declares the loop to be out of lock. If the loop is indeed in lock when this occurs, a false dismissal then occurs. One is interested in designing the mean false dismissal time to be quite long (perhaps on the order of years).

On the other hand, when the loop is out of lock and a given lowpass filter output sample exceeds the threshold, we have a false alarm. Here one is interested in keeping the probability of such an occurrence small so that the loop is not captured by frequent false alarms which then require the verification algorithm to produce two successive below-threshold indications in order to finally declare the loop truly out of lock.

In characterizing the performance of lock detection algorithms as described above, the theory of finite Markov chains is particularly useful. In this application, a three-state diagram is sufficient, with the transition probabilities determined from the lowpass filter output statistics. Since, as previously mentioned, the lowpass filter has a bandwidth which is narrow compared to that of the Costas loop arm filters,

---

\* For this component, we must replace  $\sin 2\phi$  by  $\cos 2\phi$ .

the filter output may then be assumed to have Gaussian statistics, in which case, the transition probabilities take on the form of complementary error functions of a threshold-to-noise ratio. The effective amount of time one remains (dwells) in each state is determined by the time constant (correlation time) of the lowpass filter (for state 1) and the specified wait time after a below-threshold indication (for state 2).

Appendix I of this memo derives the mean and variance of the false dismissal time (the time to reach the absorbing state (#3) in the Markov chain). For a small probability of missed detection, the variance is shown to be approximately equal to the square of the mean, which is the same relation between the first two moments of an exponential distribution. Assuming such a distribution for false dismissal time, the author easily shows that the probability of falsely dismissing in  $t$  seconds or less is  $1 - \exp(-t/\bar{T}_{FD})$ , where  $\bar{T}_{FD}$  is the mean false dismissal time.

Computations made from the above theoretical discussions reveal a mean-time-to-false-dismissal of greater than seven years (for either data rate) and a mean-time-to-dismiss a false alarm once the algorithm has been put in the tracking mode of 175 ms (for either data rate)

Based on the foregoing, the memo correctly concludes that false alarms will not "capture" the system (since their probability of occurrence is only 0.0016 and they are quickly dismissed) and false dismissals of true lock occur, on the average, infrequently enough (every seven years) so as to "never" cause a problem.

### 3.1.2 IUS Memos No. 112 and 118

The TDRS carrier acquisition analysis and experiment section of the CDR data package contains four\* memos which can be arranged in two pairs, namely, 112 and 118, and 114 and 116. The second memo of each pair represents a revision of the first and, as such, contains the more meaningful results. Thus, we shall, in actuality, discuss only these second memos (118 and 116) while, at the same time, pointing out the changes made in the assumptions as given in the first memos (112 and 114).

IUS memo #112 calls attention to a possible problem (potential malfunction of the code loop and carrier lock detector during code loop loss of lock) in the IUS code-aided carrier acquisition approach. This

---

\* Actually, there are five memos in this section, but one (#107) was included in the PDR and, as such, was previously critiqued.

approach consists of locking the receiver VCXO to a multiple (192/31) of the code loop VCXO with a CW loop, then multiplying this receiver VCXO output signal up to S-band (a factor of 110.5) to serve as the code loop input. The assumptions made in this memo are a 2-Hz single-sided code loop noise bandwidth at threshold ( $C/N_0 = 34$  dB-Hz) and a carrier loop bandwidth much wider than the code loop bandwidth. As such, the interaction (cascading) of the carrier loop with the code loop was ignored and, thus, the carrier loop was assumed to do no more than scale the code loop phase noise process by the factor 192/31. Because of these oversimplifying assumptions, the results of memo #112 led to the conclusion that the code loop would potentially drop out in this mode and the carrier lock detector would not detect the presence of signal.

IUS memo #118 reconsidered the code-multiplied carrier acquisition problem under the assumptions of a 1-Hz (half as wide) code loop threshold bandwidth and an identical carrier loop threshold bandwidth. Certainly now the cascade of the code and carrier loop transfer functions further reduces the spreading of the code clock multiplied carrier produced by the multiplied-up phase noise of the code loop VCXO. Thus, despite the fact that the line component of the carrier power spectral density is essentially suppressed by the large phase noise obtained from the multiplied-up code clock, all the spread component (although much wider than the original phase noise process) is virtually contained within a  $\pm 100$  Hz bandwidth. In conclusion, then, the very wideband estimates of the code-multiplied carrier power spectral density made in IUS memo #112 which could potentially cause the code loop to drop out in this mode were, in IUS memo #118, refined to the point where it may be safely concluded that the IUS code-aided carrier acquisition technique is viable.

AXIOMATIX has carefully reviewed the analyses performed in these two memos and agrees with the conclusions drawn therein.

### 3.1.3 IUS Memos No. 114 and 116

This second pair of memos in the TDRS carrier acquisition analysis and experiment section addresses the problem of predicting the instantaneous frequency error in the carrier loop just after disconnecting the code loop VCXO when, prior to that time, the carrier loop was configured to track a scaled version of the code loop clock. Indeed, an accurate

estimate of this instantaneous frequency error is essential in deciding whether or not the carrier loop bandwidth is sufficient to pull in this frequency offset during acquisition.

Clearly, when the carrier loop is connected to the code loop VCXO, an instantaneous frequency error  $\Delta f$  in the code loop would produce a carrier frequency offset equal to  $(192/31) \times (110.5) \Delta f = 684.4 \Delta f$ . Here the first factor represents the scaling of the PN code clock at the receiver VCXO input, and the second factor is the multiplication required to bring this reference up to S-band. Thus, a one-sigma code loop frequency error at threshold ( $C/N_0 = 33$  dB-Hz) on the order of 13 Hz (see IUS memo #117) would produce, before disconnect, a carrier frequency offset of  $(684.4)(13) = 8897.2$  Hz, which is so large that the carrier loop could never acquire with any reliability. When the code loop VCXO is disconnected, however, the action of the code loop and carrier loop filters reduce this frequency offset considerably, in particular, to a value well within the frequency acquisition range of the carrier loop.

In IUS memo #114, the assumption is again (as in IUS memo #112) that the carrier loop is wide compared to the code loop. Thus, the approach taken in memo #112 was to compute (approximately) the standard deviation of the voltage on the capacitor in the code loop filter, then simply scale this quantity by the factor  $(192/31)(110.5) = 684.4$  to arrive at the carrier (one-sigma) frequency offset at S-band\*. Multiplication of this result by three (to give a three-sigma value) was then used to give a rough estimate of the required carrier loop bandwidth during acquisition.

Interestingly enough, the computed value of carrier frequency offset, namely,  $(192/31)(110.5/4) \times (0.155 \text{ Hz}) = 26.5$  Hz (0.155 Hz was the computed one-sigma value of code loop filter capacitor voltage) was in excellent agreement with a measured value in the laboratory of 25 Hz. Unfortunately, however, this was just a coincidence apparently caused by nullifying errors in the assumptions made in the analysis. In particular, the variance of the capacitor voltage as given by equation (115) of this memo is in  $(\text{rad/sec})^2$ , not  $(\text{Hz})^2$ , since the code loop VCXO gain,  $K_V$ , is

---

\* Actually, the laboratory measurements were made at 25% of the final S-band frequency, thus, the appropriate multiplication factor for comparison of theory and experiment is  $(192/31)(110.5/4) = 171.1$ .

in rad/sec/V. Thus, the calculated value of carrier frequency offset given previously, namely, 26.5 Hz, should be divided by  $2\pi$ , which results in 4.2 Hz. Furthermore, as discussed in IUS memo #116, the wideband carrier loop assumption must be revoked in favor of a loop whose bandwidth is identical to that of the PN code loop. When the two loops are now considered in cascade, the problem must be reformulated to directly compute the RMS voltage (due to frequency offset) on the capacitor in the carrier loop filter. When this is done (as in memo #116), along with the  $2\pi$ -factor correction previously discussed, then the one-sigma (RMS) frequency error at S-band becomes  $(192/31)(110.5)(0.01 \text{ Hz}) = 6.84 \text{ Hz}$  or, at the laboratory measurement frequency,  $(192/31)(110.5/4)(0.01 \text{ Hz}) = 1.71 \text{ Hz}$ . These numbers correspond to threshold loop conditions, namely, both loop dampings are at 0.707 and both loops have a bandwidth of 1 Hz.

Now since the theoretical values of frequency offset error are considerably less than laboratory measurement values, the author points out that this may be true because the analysis ignores the effects of logic noise and oscillator noises. Indeed, since a large discrepancy exists between measured and theoretical values, one might suggest that these other unaccounted for effects tend to dominate. We hasten to add, however, that estimates of oscillator noise and, in particular, logic noise are difficult to come by, which makes accounting for these effects analytically all the more difficult.

#### 3.1.4 IUS Memo No. 115

This is the first memo in the Costas loop performance analysis section of the CDR to be critiqued and discusses the static tracking phase error induced by thermal noise biases at the output of the loop's third multiplier. The two sources of bias discussed are an imperfect (other than  $90^\circ$ ) input hybrid and a combination of arm filter mismatch and input bandpass filter asymmetry. Their effects in producing static phase errors are treated independently.

In the hybrid misalignment analysis, the hybrid is modeled as producing a pair of "quadrature" demodulation reference signals which are separated in phase by  $90^\circ + \delta\theta$ , the quantity  $\delta\theta$  representing the hybrid angle error. When computing the phase detector outputs due to signal only

(as in eq. (10)), the author commits an error in that he ignores the hybrid angle error. Thus, his final result for static phase error (eq. (14)) includes only the effect of hybrid angle error on the noise component at the third multiplier output, which indeed turns out to be the less dominant effect. To correct this error, we suggest that equations (10), (11), (12) and (14) read as follows:

$$e_c(t) = \sqrt{P} \tilde{d}(t) \cos\phi ; e_s(t) = \sqrt{P} \tilde{d}(t) \sin(\phi - \delta\theta) , \quad (10)$$

$$\begin{aligned} \bar{e} &= \alpha P \sin(\phi - \delta\theta) \cos\phi \\ &= \alpha P \left[ \frac{\sin(2\phi - \delta\theta)}{2} - \frac{\sin(\delta\theta)}{2} \right] , \end{aligned} \quad (11)$$

$$\left( \frac{\tilde{n}_c^2}{\alpha P} + 1 \right) \delta\theta = \phi_{SS} , \quad (12)$$

and

$$\phi_{SS} = \left( \frac{N_0 \pi f_0}{2\alpha P} + 1 \right) \delta\theta . \quad (14)$$

Then, for the case where  $R_b = 2000$  bps,  $f_0 = 2000$  Hz,  $\alpha = 0.84$ , and  $P/N_0 = 43$  dB-Hz (includes 1-dB despreader loss), Table I of the memo, which tabulates static phase error versus hybrid angle error, should be modified as follows.

$\delta\theta(^{\circ})$	$\phi_{SS}(^{\circ})$
1	1.187
2	2.375
3	3.56
4	4.75
5	5.94

Thus, the statement made in the summary of the memo, namely, that "the steady-state error is about 1/5 of the hybrid angle error" should be changed to read "the steady-state error is slightly greater than the hybrid angle error."

The second part of this memo assumes a perfect (90°) input hybrid and examines the effects of mismatched arm filters and an input bandpass filter (BPF) with an asymmetric frequency response around its center frequency. In particular, the two lowpass arm filters are assumed to be one-pole RC filters with different 3-dB cutoff frequencies, namely,  $f_1$  and  $f_2$ , and the asymmetry in the equivalent lowpass version of the input BPF is modeled as a linear "tilt" in the corresponding power spectral density, namely,

$$S_L(f) = \frac{N_0}{2} (1 + af); |f| \leq 5 \text{ kHz.}$$

The author then shows that the static phase error produced by these two sources of filter imperfection is given by

$$\phi_{SS} = \frac{\pi}{4} \left( \frac{aN_0}{\alpha P} \right) (f_2 - f_1) f' ,$$

where many simplifications in the analysis were made by letting  $f'$  equal  $f_1$  or  $f_2$  in some of the manipulations.

For a 0.1 dB tilt at  $f = 5$  kHz, ( $10 \log_{10}(1 + a \times 5 \times 10^3) = 0.1$ , or  $a = 4.88 \times 10^{-6}$ ),  $\alpha = -0.5$  dB,  $P/N_0 = 43$  dB-Hz,  $f_1 = 1948.3$  Hz and  $f_2 = 2096.6$  Hz, the computed value of  $\phi_{SS}$  (assuming  $f' = f_2$ ) is  $0.0038^\circ$ . The memo follows with a table which computes  $\phi_{SS}$  for larger values of tilts. The latter three values of  $\phi_{SS}$  in this table, corresponding to respective tilts of 0.3, 0.5 and 1.0 dB, should be corrected to read 0.0108, 0.018 and 0.0392°.

One further point of correction, although probably of second-order importance, deserves mention at this time. The parameter  $\alpha$  in the above equation which ordinarily characterizes the arm filtering degradation on the SxS term in the loop when both arm filters are identical should be modified for the case where the arm filters are different. In particular, we would now have (analogous to eq. (42)) for the noise effects

$$\alpha = \frac{1}{2} \int_{-\infty}^{\infty} \left[ H_1(\omega) H_2^*(\omega) + H_1^*(\omega) H_2(\omega) \right] S_d(\omega) \frac{d\omega}{2\pi}$$

where  $S_d(\omega)$  is the data modulation spectrum and  $H_1(\omega)$ ,  $H_2(\omega)$  are the arm filter transfer functions, i.e.,

$$H_i(\omega) = \frac{1}{1 + j \frac{f}{f_i}} ; \quad i=1,2$$

Substitution of  $H_1(\omega)$  into the above expression for  $\alpha$  and simplifying yields

$$\alpha = \int_{-\infty}^{\infty} \frac{\left(1 + \frac{\omega}{\omega_1}\right)\left(1 + \frac{\omega}{\omega_2}\right)}{\left(1 + \left(\frac{\omega}{\omega_1}\right)^2\right)\left(1 + \left(\frac{\omega}{\omega_2}\right)^2\right)} S_d(\omega) \frac{d\omega}{2\pi}$$

which, for a small 3-dB cutoff frequency difference, is approximately  $\alpha$ , as previously computed for identical arm filters.

Thus, in conclusion, the hybrid imperfection effect dominates over the imperfect filtering effects, and the static phase error induced is on the order of the hybrid angle error.

### 3.1.5 IUS Memo No. 117

The mean slip time of the carrier-tracking loop in the IUS-TDRS transponder is computed at both threshold conditions ( $C/N_0 = 33.7$  dB-Hz,  $R_B = 125$  bps) and strong signal conditions ( $C/N_0 = 43.7$  dB-Hz,  $R_B = 2000$  bps). The loop is configured as a standard Costas loop with an input signal having an unbalanced QPSK format characterized as follows. The received signal has a PN spread data modulation on the strong (I) channel and PN only on the weak (Q) channel. The power ratio is fixed at 10:1. After being despread by the I-channel PN code, the signal retains an unbalanced QPSK format with data modulation only (assuming "perfect" despreading with a fixed despreading loss) on the I-channel, and PN only (the product of the in-phase and quadrature PN codes) on the Q-channel. This signal serves as the Costas loop input. As such, the evaluation of the loop's phase error variance due to thermal noise follows along the lines of previous analyses of biphase Costas loops with passive arm filters and unbalanced QPSK inputs. In making this statement, we tacitly make the assumption that the



PN code on the Q-channel behaves as a random data modulation of rate  $R_c = f_c$ , where  $f_c$  is the PN chip rate (i.e.,  $3 \times 10^6$  Mchips/s). Thus, it is not surprising that eq. (22) of the memo agrees with [1, eqs. (28) and (30)] after the appropriate changes in notation.

Next, the memo evaluates the phase error variance component due to oscillator phase noise. The phase noise model, based on IUS phase noise specifications, was assumed to have a power spectral density which varied as  $K/f^6$ . For simplicity of computation of the phase error variance due to phase noise, the out-of-band loop transfer function  $1-H(f)$  was assumed to behave like a "brick wall" filter having zero value below the loop natural frequency and unity value above this frequency. Finally, the two phase error variance components (that due to thermal noise and that due to oscillator phase noise) are added to give the total phase error variance  $\sigma_{2\phi}^2$ .

Before determining the mean slip time of the Costas loop, one needs, in addition to the total phase error variance, the steady-state phase error due to dynamics such as a residual carrier frequency rate of  $\Delta f$  Hz/sec. For a second-order Costas loop, these two parameters are related by

$$2\phi_{SS} = 2 \left( \frac{2\pi\Delta f}{\omega_n} \right) \quad (1)$$

where  $\omega_n$  is the loop's radian natural frequency which, for a 0.707 loop damping, is related to the loop bandwidth  $B_L$  by  $\omega_n = 1.89 B_L$ . Having now determined  $\sigma_{2\phi}^2$  and  $\phi_{SS}$ , the author computes mean slip time  $\bar{T}$  (normalized by the loop bandwidth) from the formula

$$\begin{aligned} B_L \bar{T} &= 1.5 \exp \left[ \frac{1.2}{\sigma_{2\phi}} \left( 1 - \sin 2\phi_{SS} \right) \right] \\ &= 1.5 \exp \left\{ \frac{1.2}{\sigma_{2\phi}} \left[ 1 - \sin \left( \frac{4\pi\Delta f}{(1.89)^2 B_L^2} \right) \right] \right\} \quad (2) \end{aligned}$$

This relation is valid for a second-order Costas loop with an active loop filter and was originally obtained from simulation results on an analogous phase-locked loop.

The author concludes with an evaluation of (2) for threshold and strong signal conditions, and  $\Delta\dot{f} = 70$  Hz/sec. At threshold, a value of  $B_L = 25$  Hz maximizes  $\bar{T}$ , whose value is 6000 sec (10 min). In the absence of phase noise and loop dynamics ( $\Delta\dot{f}$ ),  $\bar{T}$  is monotonically decreasing with increasing  $B_L$ . At strong signals, the same  $B_L = 25$  Hz produces  $\bar{T} \gg 10^4$  min.

The results given in this memo are obtained by straightforward application of previously derived results and, as such, need no further investigation.

### 3.1.6 IUS Memo No. 123

The effect of the delay induced by the arm filters in the IUS-TDRS Costas loop on loop bandwidth and, hence, the phase error variance, is investigated. The key step in the analysis is the approximation made with respect to the signal  $e_u(t)$  appearing at the upper arm filter output, namely, that the effect of this filter on the data modulation and the loop phase error are separable. More specifically, letting  $H(s)$  denote the arm filter transfer function, then

$$e_u(t) = \sqrt{P} H(p)[d(t) \sin \phi(t)] \quad (1)$$

which, for small  $\phi$ , becomes

$$e_u(t) \cong \sqrt{P} H(p)[d(t) \phi(t)] \quad (2)$$

is approximated by

$$e_u(t) \cong \sqrt{P} (H(p) d(t))(H(p) \phi(t)) \quad (3)$$

where  $p$  has been used to denote the Heaviside operator. It is argued that (3) follows from (2), provided that "the lowpass arm filter  $H(s)$  does not seriously distort the baseband data stream " Although there appears to be no approximate mathematics that can lead one from (2) to (3), there is a

reasonable plausibility argument that one can use to make this step somewhat believable. Typically, the  $\phi(t)$  process being slowly varying with respect to  $d(t)$  appears as an envelope modulation on  $d(t)$  which, when passed through the arm filter, is essentially unaffected in amplitude but is shifted (delayed) by the arm filter group delay. Thus, if we approximate  $\phi(t)$  as a single-frequency (say,  $\omega_0$ ) beat note, then  $H(t) \phi(t) \approx \phi(t - t_0)$ , where  $t_0 = \arg H(j\omega_0)/\omega_0$  is a good approximation to the envelope modulation on the filtered data stream.

Making the above approximation, the author proceeds to find a simple relation between the loop bandwidth (including the arm filter delay effect), say  $B_L(D)$ , and the zero-delay loop bandwidth  $B_{L0}$ , namely,

$$\frac{B_L(D)}{B_{L0}} = \frac{1}{1 - \frac{D}{2\zeta}} = \frac{\sigma_{\phi}^2(D)}{\sigma_{\phi 0}^2} \quad (4)$$

where  $\zeta$  is the loop damping and  $D = \omega_{n0} \tau$ , with  $\omega_{n0}$  the zero-delay radian natural frequency and  $\tau$  the time constant of the single-pole arm filter  $H(s)$ . Since  $\omega_{n0}$  and  $B_{L0}$  are related by

$$\omega_{n0} = 2B_{L0} \left( \frac{4\zeta}{1 + 4\zeta^2} \right) \quad (5)$$

then (4) can be alternately be written as

$$\frac{B_L(D)}{B_{L0}} = \frac{1}{1 - \frac{4B_{L0}\tau}{1+4\zeta^2}} = \frac{\sigma_{\phi}^2(D)}{\sigma_{\phi 0}^2} \quad (6)$$

Clearly, the mean-square phase jitter with delay becomes unbounded when

$$B_{L0}\tau = (1 + 4\zeta^2)/4 \quad (7)$$

For  $\zeta = 0.707$ ,  $B_{L0} = 75$  Hz and a 100-Hz 3-dB cutoff frequency (i.e.,  $\tau = 1/2\tau(100) = 0.00159$ ), the increase in RMS phase jitter is only 9% ( $\sigma_{\phi}(0)/\sigma_{\phi 0} = 1.09$ ).

The author follows the computation of mean-square phase jitter with a discussion of the effect of the arm filter delay on loop stability, as determined by Routh's stability criterion, and the root locus plot. The interesting (but not too surprising) result is that the loop bandwidth at which the loop becomes unstable is also determined from (7), namely, the same value at which the mean-square phase error variance becomes unbounded.

Finally, we wish to call attention to a similar study [2] with similar results in which the effect of delay on the loop bandwidth and stability of a data-aided loop (DAL) were investigated, thus lending more credibility to the analysis performed in this memo. The DAL, which is also used for tracking suppressed carrier signals, has much similarity to the conventional Costas loop.

### 3.1.7 IUS Memo No. 110

This memo is the only one in the SSP analysis section which was not previously critiqued by AXIOMATIX. In particular, it addresses the mean time to declare out-of-lock for the code-tracking loop, both when the signal is present and when it is absent. The lock detector algorithm is of the "n-out-of-n" type wherein n (typically, 16) successive below-threshold events are required to declare an out-of-lock condition. If an above threshold event occurs anywhere along the way, the algorithm returns the system to its initial state and resets the below-threshold count to zero.

The mean time to out-of-lock performance of such a discrete time lock detector algorithm is best determined by modeling the algorithm as a 17-state Markov chain (the 17th state being the absorbing state, namely, an out-of-lock declaration) and applying the well-known theory for such chains to this particular case. Actually, for  $n \leq 5$ , a formula for this mean-time performance was determined by brute force (direct) calculation in a previous memo by the author (see TRW IOC No. SCTE-50-76-275/JKH). Thus, this memo serves to merely formalize the

validity of this result for all values of  $n$ . In particular, the mean time to out-of-lock,  $\bar{T}$ , is simply given by

$$\bar{T} = \frac{q^{-n}-1}{1-q} T_{\text{DWELL}}$$

where  $T_{\text{DWELL}}$  is the dwell time per state (assumed equal for all states), i.e., the time between threshold tests of the integrator output, and  $q$  is the probability of a below-threshold event for any given threshold test.

Since, when signal is absent,  $q = 0.95$  and, when signal is present,  $q = 0.5$ , then for  $n = 16$  and a 50-ms dwell time, the corresponding values of  $T$  are found to be 1.27 seconds and 109.2 minutes, respectively.

The straightforward nature of these results and the absence of complicating assumptions requires that no further investigation be performed.

In the STDN dual mode section of the CDR package, two memos were written which pertain to the analysis and design of the lock detector, noncoherent, AGC and open-loop frequency acquisition circuits associated with the carrier-tracking loop of the IUS transponder. Since the first of these two memos (#122) assumes knowledge of the second (#124), we shall start by critiquing the second.

### 3 1 8 IUS Memo No. 124

In the STDN dual mode of the IUS transponder, an open-loop frequency acquisition scheme is used which involves linear sweeping of the VCO frequency to bring the initial frequency uncertainty within the pull-in range of the loop (typically on the order of the loop bandwidth). Since the loop is open during this sweep interval, an auxiliary detection circuit must be used to determine when to remove the sweep and simultaneously\* close the loop. This auxiliary detector consists of a coherent amplitude detector (CAD) followed by a lowpass filter and threshold device.

---

\* In the actual frequency acquisition scheme used in the STDN mode, the sweep continues for an additional 4 ms after the detector indicates acquisition has been achieved to allow for the processing time of the microprocessor which controls the closing of the loop.

An instantaneous crossing\* of the threshold by a signal at the input to this device indicates acquisition whereupon the sweep is terminated and the loop closed.

Such a half-wave rectifier type of open-loop frequency search circuit has been previously described in [3]. This memo discusses its application to the IUS transponder in the STDN dual mode. In particular, computer simulation and laboratory test results are obtained for the waveforms at the output of the lowpass RC decision filter (in the absence of noise) so as to enable selection of this filter's 3-dB cutoff frequency  $\beta$  for a given sweep rate  $R$  (Hz/sec), normalized (to the peak signal amplitude) threshold level  $\delta$ , and closed-loop bandwidth  $f_1$ . Indeed, it is shown that if, for a given initial frequency offset outside the loop's pull-in range,  $\beta$  is too small, then, depending on the initial phase difference  $\phi_0$  between the input signal and the swept VCO, the threshold may or may not be exceeded as the VCO is swept through the pull-in range. Increasing  $\beta$  helps this situation, however, if  $\beta$  is too large, then the threshold is exceeded while the loop is still outside its pull-in range. Hence, the sweep will be terminated and, consequently, the loop closed prematurely.

The author provides what appears to be a reasonable rule of thumb for the selection of  $\beta$ , namely, the peak value of the normalized detector output frequency response  $H(f)$ , evaluated at the edge of the pull-in range (assumed equal to the loop bandwidth  $f_1$ ) should be less than the normalized threshold  $\delta$ . For a single-pole decision filter ( $\beta = 3$ -dB frequency), it is straightforward to show that the above is equivalent to the condition†

$$\beta < \frac{f_1 \delta}{\sqrt{1-\delta^2}}$$

---

\* Again, because of the 4-ms processing time of the microprocessor, a "stretching" or hold circuit follows the threshold detector to prevent situations where the input signal reverses and falls below threshold in less than 4 ms, i.e., sharp peaks.

† The author does not actually write this inequality in this form although it is obtained by obvious steps from the results given therein. Also note that this result is independent of the sweep rate  $R$  although the actual simulation results were performed for  $R=40 \times 10^3$  Hz/s.

Thus, for  $\delta = 0.5$  and  $f_1 = 400$  Hz (STDN parameters), we obtain  $\beta < 400/\sqrt{3} = 231$  Hz (the author uses the approximate value 250 Hz).

The next area of investigation was the calculation of acquisition probabilities which were performed by computer simulation (in the absence of noise) in view of the difficulty of obtaining these results analytically. Note again that, although the additive noise was assumed to be absent, the probability of acquisition is, in general, less than one due to dependence of the acquisition process on the initial phase difference  $\phi_0$ . The author compares the acquisition probability results obtained by the above-mentioned simulation with experimental results obtained in [3]. In some cases, there appears to be reasonable agreement whereas, in other cases, there seems to be no match at all. Since, for the latter situation, the author of [3] does not state to which of the three possible open-loop implementations (one mixer and one half-wave rectifier, one mixer and one full-wave rectifier, or two mixers and two full-wave rectifiers) his results apply, one is unable to resolve the discrepancy. Herein lies one of the principal reasons for issuing IUS Memo #124 in the first place, namely, to point out the lack of agreement between the previously published experimental results and the computer simulation results obtained by the author of the memo

Finally, this memo concludes with a discussion of how the results might be extended to account (in a very rough sense) for the effects of additive noise.

In the opinion of AXIOMATIX, the results documented in this memo represent a significant contribution to the understanding of the performance and behavior of open-loop frequency acquisition techniques of the type described therein. As such, the results are given in a sufficiently general parametric form as to be useful in applications outside of the IUS transponder. Perhaps the only area which would require further investigation would be the noise-present case, where computer simulation could again be used (although with more difficulty) rather than the rough extension (valid only for high SNR) approach given in the memo. Indeed, the entire subject of frequency acquisition in noise is an area of research where much needs to be done

## 3.1.9 IUS Memo No. 122

Associated with the open-loop frequency acquisition technique described in IUS Memo #124 is the lock detector of the STDN dual mode whose functions are to close the tracking loop and stop and sweep\* when frequency acquisition has been completed. The indication that frequency acquisition is complete is a high (above threshold) signal from the sampled-and-held output of the threshold device in the frequency acquisition circuit. Thus, this signal serves as the input to the lock detector whose control algorithm is as follows: When the loop is initially open, a single high sampled-threshold output shall close the loop. Two successive high-threshold outputs are required to terminate the sweep. Also, when the loop is initially closed and in lock, two successive low-threshold outputs are required to open the loop and reinstate the sweep.

The purpose of this memo is to determine decision filter bandwidth and threshold settings for the above circuit, taking into account both the hold circuit at the sampled-threshold output and the noncoherent AGC (NAGC) which accompanies the loop. As in the previous lock detector analyses (see IUS Memos #125 and 110), the theory of finite Markov chains is used to determine the mean time to false alarm (falsely close the loop and falsely disable the sweep) performance. Other computations include probability of false alarm (falsely closing the loop and falsely disabling the sweep) and accidental restart (falsely open the loop).

For the NAGC effects, the author assesses the increase in AGC gain in going from acquisition ( $S/N_0 = 46$  dB-Hz) to tracking (effective<sup>†</sup>  $S/N_0 = 40$  dB-Hz) as a function of the AGC filter bandwidth. Also determined is the further increase in gain (up to a practical limit) when only noise is present. The analyses performed here is similar to that done in IUS Memo #125 and, as such, requires no further explanation. Similarly, the false alarm and accidental restart probability calculations parallel those performed in IUS Memo #125 (except for the effect of holding the threshold output sample for 4 ms, which is shown to roughly double the false alarm probabilities which would be calculated for an instantaneous

---

\* Actually, the lock detector telemeters a message to the ground and the ground stops the sweep

† The actual  $S/N_0$  during tracking is 43 dB-Hz; however, the additional suppression caused by the presence of command modulation and, possibly, two ranging tones, both phase-modulated on the carrier, is 3 dB.



sampling operation). Since the loop is closed after the first threshold crossing and the sweep disabled after the second threshold crossing, the author computes the "instantaneous" probability of falsely disabling the sweep as the square of the probability of falsely closing the loop. This is only approximately correct since the probability of exceeding the threshold the second time must be computed with the loop closed, while the probability of exceeding the threshold the first time is computed with the loop open. In general, these two threshold crossing probabilities will be different, depending on how far out of lock (amount of frequency offset relative to the loop's pull-in range) the loop is by the time of the second threshold crossing.

Analogous to the difference in the false alarm probabilities for closing the loop and disabling the sweep, the mean time to occurrence of these false alarm events must be computed from different Markov state models. For the former, the mean time is simply

$$\bar{T}_{\text{close}} = \frac{T_0}{p}$$

where  $T_0$  is the threshold sampling time interval (i.e., 4 ms) and  $p$  is the threshold crossing probability when the loop is out of lock. For the latter, the mean time is\*

$$\bar{T}_{\text{disable}} = \frac{T_0 + (1-q) T_1}{(1-q)^2}$$

where  $T_1$  is the time the loop remains closed after the initial closure before the threshold is again sampled, and  $1-q$  is the probability of exceeding the threshold when the loop is in lock. Here again, the above result is only approximately correct since it assumes that the transition probabilities from state 1 (loop closed) to state 2 (sweep disabled) are the same as those from state 0 (loop open) to state 1.

---

\*The author's result for this quantity, namely,

$$\bar{T}_{\text{disable}} = \frac{T_0 (1-q) T_1}{(1-q) T_1^2}$$

is incorrect although the numerical evaluation appears to be correct

To compute the probability of accidental reopening of the loop, the author points out that three cases can occur. For the first case, the assumption is that the loop has locked but the sweep is still on; hence, the loop is tracking the sweep with a steady-state phase error equal to the arc sine of the ratio of the sweep rate to the square of the loop's natural frequency. For the second case, the loop is tracking, but the NAGC has not yet had time to act. Finally, the third case is the same as the second except that the NAGC has now had time to act. This last case yields the largest restart (reopening of the loop) probability and, hence, represents the worst case.

The memo concludes with the corresponding mean-time-to-loss-of-lock calculations which employ a Markov state model analogous to that used in computing mean time to disable the sweep, the difference being that the above-threshold probabilities are switched with below-threshold probabilities and the latter computed assuming an in-lock condition, i.e., tracking.

In summary, the computations are straightforward applications of the Markov chain approach, the theory of which was documented in previous IUS memos. Thus, other than the modifications to include such effects as sample-and-hold time, the results are analogous to those previously obtained for the TDRS carrier and PN code loops.

### 3.1.10 IUS Memos No. 119 and 120

These two memos are for the STDN-only mode, the companions to IUS memos 124 and 122 for the STDN dual mode of operation. Again, the purpose of the documentation is to characterize the behavior and analyze the performance of the acquisition and lock detector schemes, along with a determination of the necessary threshold settings. Although, in principle, three possible frequency acquisition schemes are under consideration, namely, (1) an open-loop scheme similar to that for the STDN dual mode, (2) an existing digital hardware version of a closed-loop scheme and (3) a software implementation of (2), only the second scheme (also referred to as the DOD version) is discussed in these memos. Since this scheme is referred to as a "closed" loop frequency acquisition technique, it implies that the VCO is swept with the loop closed and, thus, a high

(greater than threshold) signal out of the lock detector is used only to stop the sweep. In reality, the VCO is initially swept open-loop and can be immediately (with no delay) closed by a low (less than threshold) output from an auxiliary discriminator circuit prior to a lock detector threshold crossing, or subsequently (after a short delay) by a lock detector (high) signal\* itself, with the former being the more likely to occur. Once the loop is closed, however, only the lock detector output signal both stops the sweep and maintains the closed loop after the sweep has stopped. It is in this sense that the behavior of the lock detector is analogous to that of the STDN dual mode of operation

The behavior of the actual closed-loop frequency-searching circuit employed closely parallels that previously described in [3], the main difference being that, during the initial part of the sweep, the loop is open until closed by the discriminator. In addition, after the loop is closed and the sweep has been stopped, the loop bandwidth is narrowed for the tracking mode of operation

Assuming that the loop has locked and reached the steady state (the discriminator has previously indicated that the loop be closed), but the sweep has not yet been removed. The DC output of the coherent amplitude detector (CAD) is then simply given by

$$u_0 = \sqrt{S_1} J_0(1.1) \sqrt{1 - (R/\omega_n^2)^2} \quad (1)$$

where  $S_1$  is the signal power at this point,  $R/2\pi = 10^6$  Hz/sec is the sweep rate, and  $\omega_n = 1.89 B_L = 3780$  rad/sec is the natural frequency of the loop, with  $B_L = 2000$  Hz the loop noise bandwidth. The  $J_0(1.1)$  factor occurs because the input carrier is phase modulated by a data-modulated 16 kHz sinusoidal subcarrier with modulation index 1.1 radians. Thus, once  $S_1$  is determined (depending on the action of the noncoherent AGC),  $u_0$  is specified. Furthermore, the variance of the noise at the CAD filter output also depends on the NAGC action, i.e., whether or not signal is

---

\* Actually, two possibilities exist here, namely, a single high pulse of greater than 3-ms duration, or two or more short (less than 3-ms duration) pulses within 33 ms (but greater than 3 ms apart) will close the loop after a total delay of 36 ms after the leading edge of the first pulse.

present. The AGC gain is normalized such that it has value unity when signal is present and  $S/N_0 = 52$  dB-Hz. Thus, when signal is present, the CAD decision filter output has a DC value given by (1) with  $S_1 = S$  and a noise variance  $\sigma_{u_1}^2 = N_0 B$ , where  $B$  is the noise bandwidth of this filter (a single-pole RC filter). When signal is absent, the DC output is zero and the noise variance is

$$\sigma_1^2 = \left(1 + \frac{S}{N_0 B_{AGC}}\right) N_0 B \quad (2)$$

where  $B_{AGC}$  is the noise bandwidth of the AGC input filter [also, a single-pole RC with 3-dB cutoff frequency of 1600 Hz, i.e.,  $B_{AGC} = (\pi/2)(1600)$ ]. Using these relations and some additional results given in [3] for probability of successful acquisition, it is a relatively straightforward matter to compute the false alarm and detection probabilities associated with the action of the lock detector in stopping the sweep. One further assumption is made that the threshold  $\delta$  is chosen equal to half the DC value of the decision filter output corresponding to signal present, i.e.,  $\delta = 1/2 u_0$ , where  $u_0$  is given by (1). This yields (for a decision filter bandwidth of 200 Hz) a false-alarm probability\* of  $10^{-3}$ .

3 1.11 IUS Memo No. 121

(a) Introduction

The purpose of this memo is to give an approximate analysis of a discriminator used to avoid false locks and to specify the filter bandwidths and number of poles needed for these filters. The two latter tasks seem to be rather straightforward, and no major objections arise, at least insofar as the resulting SNR is the dominant measure of performance for the last case

The analysis of the discriminator is basically composed of two similar parts: Case A/B and Case C. The first part (A/B) tries to estimate the probability that, as it sweeps through the subcarrier component

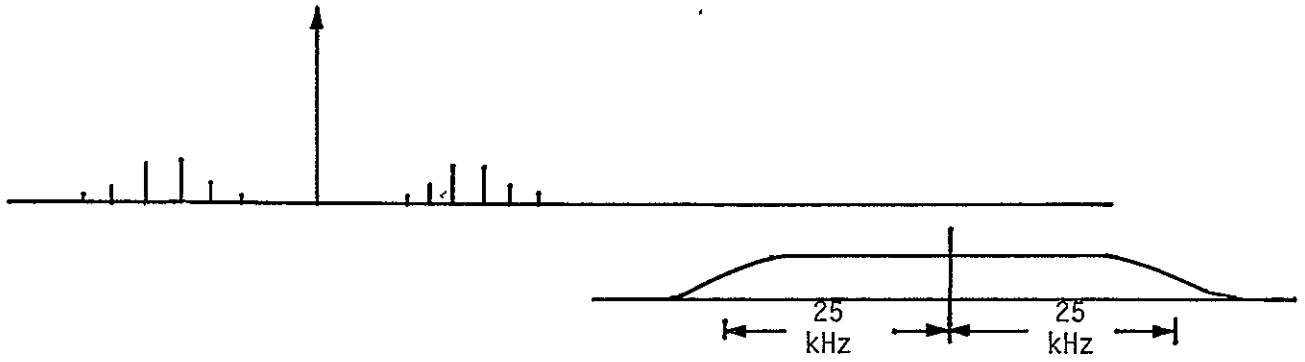
---

\* Actually, this false alarm probability is the probability that two or more samples of the CAD decision filter output exceed the threshold  $\delta$  in a 65-ms interval

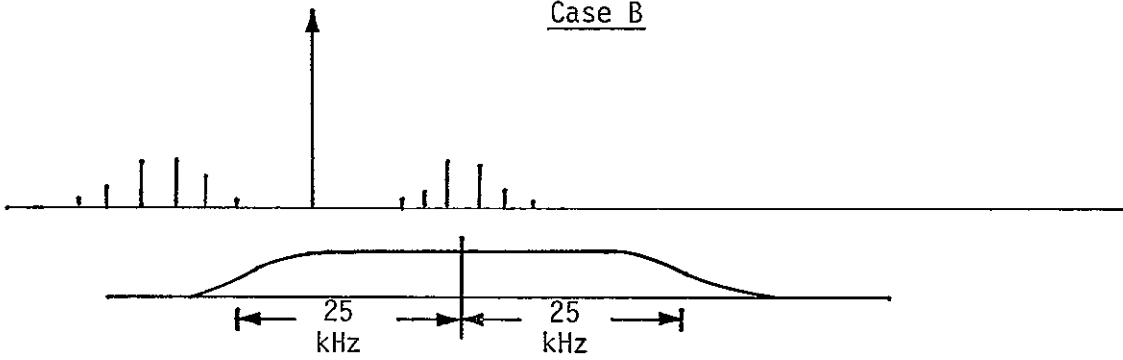
of the spectrum (as shown in Figure 4), the discriminator will indicate a voltage below threshold which would imply a false-lock case. In other words, the phase-lock loop would track that component, while the discriminator would falsely indicate (by being below threshold) that this is actually the carrier component. Ideally, this would not occur if noise were not present because the discriminator window centered at the first subcarrier harmonic would "see" an asymmetric spectrum, consisting mainly of the carrier component at the edge, and would thus produce an output above the threshold. Note that the distance between the carrier and the first subcarrier is 16 kHz, while the discriminator window is 25-kHz wide (one-sided). Hence, the carrier is well within its reach when the window's center is at  $f_{\text{carrier}} + f_{\text{subcarrier}}$ . Therefore, it is the noise which might cause a false indication. Hence, the analysis of section C has a similar objective and it addresses the case where the discriminator is centered at the carrier which should, ideally, provide an indication below threshold. The analysis then aims at the probability of false rejection. Since the analytical tools are identical in both cases, we examine in detail only the first. It should be stated that the overall system is highly complicated (nonlinear/time-varying/stochastic), and thus, it is possible that both the original analysis and our critique can be subjected to further questions regarding the accuracy of some of the approximations and analytical techniques. In all fairness, however, we should recognize that the analysis is very close to the limits of analytical techniques, exempting, of course, any numerical mistakes and, possibly, some minor theoretical improvements. We note at the very onset of the analysis however, that there is a fundamental question concerning the validity of the approach. The question is: since the system is time varying (because of the sweeping process), can steady-state analysis provide credible results, especially when calculating noise variances? Assuming that the above is answered positively (otherwise, the whole analysis collapses), we will proceed with side observations/corrections/improvements, as listed below, further indicating which ones might bear significance to the final results.

ORIGINAL PAGE IS  
OF POOR QUALITY

Case A



Case B



Case C

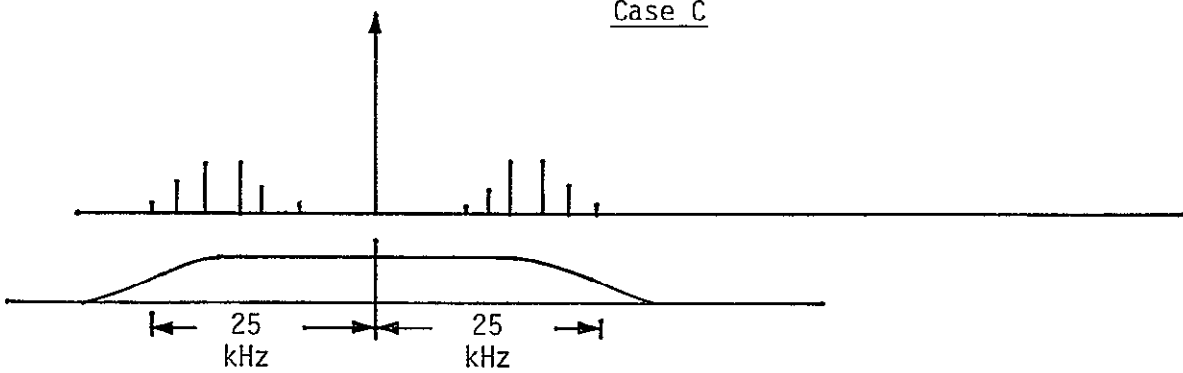


Figure 4. The Three Cases of Discriminator Detection of Interest

(b) Specific Comments

Since the carrier-tracking loop is a phase-lock loop, it should not lock to the subcarrier if the subcarrier is biphase modulated by completely random data. This modulation, of course, results in a  $(\sin x/x)^2$  spectrum. If there is a periodic component or long string of all zeros or all ones, however, in this data, then the carrier loop can lock. Thus, the analysis performed by the author is a worst-case analysis since it assumes no data modulation on the subcarrier.

The author's expression for sweep rate as determined by Viterbi (7) has an extra factor of  $10^6$  in it and should be stated as

$$R_{NF} = \frac{1}{2} \pi \frac{\omega_1^2}{2} = 1.14 \text{ MHz/sec}$$

Likewise, the sweep rate for the STDN-only mode (8) has an extra factor of  $10^6$  and should be stated as

$$R = 1 \text{ MHz/sec.}$$

Also, the expression for the outputs of the in-phase and quadrature multiplexers, (19) and (20), erroneously have  $\omega_1$  rather than  $\omega_0$ , and the expressions for the arm filter outputs of these signals,  $\tilde{e}_c(t)$  and  $\tilde{e}_s(t)$  ((24) and (28)), should have  $\tilde{n}_1(t)$  and  $\tilde{n}_2(t)$  for the noise terms rather than  $n_1(t)$  and  $n_2(t)$ . We also note that, by introducing a  $\Delta\omega$  parameter ( $\Delta\omega = \text{frequency from } f_{\text{carrier}} + f_{\text{subcarrier}}$ ) and proceeding with the analysis, one assumes that  $\Delta\omega$  is fixed, a contradiction to the very fact of the sweeping mechanism. Pursuing this, we see that the factor  $H_1^2(\Delta\omega)$  has been omitted from the expression for the input SNR,  $\rho_1$ , for the limiter (48). Correctly stated,  $\rho_1$  is given by

$$\rho_1 = \frac{P J_1^2(1.1) H_1^2(\Delta\omega)}{2 N_0 B_1}$$

The significance of that is rather minor if  $\Delta\omega$  is assumed to be well within the flat portion of the filter. However,  $\Delta\omega$  is variable with time. Furthermore, in the expression for  $\rho_1$ , the author has used  $J_1^2(1.1)$  incorrectly, instead of  $J_0^2(1.1)$ . This means that the numerical evaluation of  $\rho_1$  should be corrected accordingly. Thus,  $\rho_1$  should be -3.48 dB

(not 0.24 dB), or a factor of 0.4468 (not 1.06). Since the SNR  $\rho_1$  is used to evaluate the noise variance, the error might be important in the sense that the noise is underestimated.

The noise spectra calculated by the author and shown in Figure 5 are confusing. The sum bound comes from a calculation which is not shown and is of questionable value since it is not used anywhere in the following text. Furthermore, the values of  $A_L$  (hard-limiter voltage gain) and  $\Delta\omega$  are not indicated anywhere. Spectrum  $S_{N_2}(f)$  has been plotted for some value of  $\Delta\omega$ , but the sum of  $S_{N_1}(f) + S_{N_2}(f)$  does not match the sum spectrum. The purpose of the overall argument is to substitute (or upper bound) the sum of noises

$$\frac{\sqrt{2} A_L}{\sqrt{\pi} \sigma} e^{-\rho_1/2} I_0\left(\frac{\rho_1}{2}\right) \tilde{n}_1(t) + \frac{2\sqrt{2} A_L}{\sqrt{\pi} \sigma} e^{-\rho_1/2} I_1\left(\frac{\rho_1}{2}\right) \tilde{n}_1(t) \sin(2\Delta\omega t + 2\theta)$$

with a single noise process  $\tilde{n}_1(t)$  with an appropriate gain. The simplest way to do it would be to neglect  $\sin(\cdot)$  since  $|\sin(\cdot)| \leq 1$ , then upper bound the sum as

$$\frac{\sqrt{2} A_L}{\sqrt{\pi} \sigma} e^{-\rho_1/2} I_0\left(\frac{\rho_1}{2}\right) \tilde{n}_1(t) \left[ 1 + \frac{I_1\left(\frac{\rho_1}{2}\right)}{I_0\left(\frac{\rho_1}{2}\right)} \right]$$

Then, for the range of  $\rho_1$  of interest, substitute the ratio  $(I_1(\cdot))/I_0(\cdot)$  with an appropriate number of the order of 0.2 - 0.5. Instead, the analysis uses the factor  $\sqrt{1.2}$  without further justification. Also, the author states that the resulting noise is essentially flat up to 30 kHz. That is obviously a pessimistic assumption since  $\tilde{n}_1(t)$  is simple white band-pass noise filtered by  $LPF_1$ , which is a one-pole filter with cut-off frequency of 25 kHz. However, this is not a bad assumption from the point of view that it upper bounds the noise contribution and simplifies the following analysis.

We should point out the following: In the numerical results, it seems that the author uses the value  $\Delta f = 0$  since he is interested in the case where the discriminator is centered exactly at  $f_c + f_{sc}$ . If that



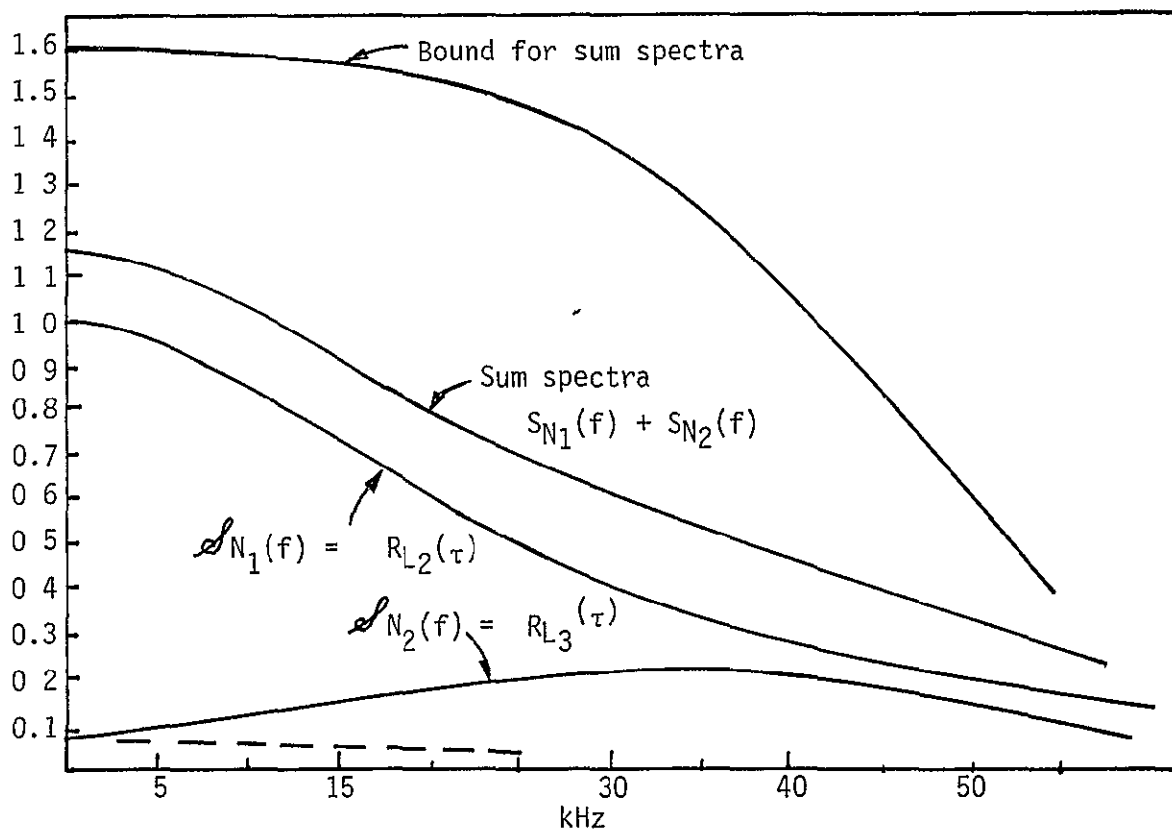


Figure 5 Individual, Composite and Upper-Bound Noise Spectra

is indeed the case (and there is no contrary evidence since the value of  $\Delta f$  does not appear anywhere), all the calculations for  $S_{e_3}(0)$  and  $S_{e_2}(0)$  are useless because they will be zero for  $\Delta f = 0$  ((68) and (70)).

In a very heuristic coupling of transient to steady-state concepts, the author models a time-varying input to  $LPF_3$ , as shown in Figure 6. The signal level at the output of  $LPF_3$  is calculated based on that input and, from that, the resulting probabilities are calculated. Therefore, such an assumption really affects the overall conclusions of the analysis. This statement is made in light of our lack of faith in using steady-state analysis techniques to calculate the performance of essentially time-varying phenomena. However, an exact assessment of the appropriateness of this assumption is beyond the scope of this review.

For the case of only two signals and noise into a hard limiter, as is the case here, the results of Jones [4] will yield a more accurate answer than Shaft's [5] expression used by the author.

Thus, using Jones' results, we have the carrier and subcarrier components, respectively given by

$$b_{010} = \frac{1}{\pi} \left( \frac{S_1}{N} \right)^{1/2} \sum_{i=0}^{\infty} \frac{(-1)^i \left( \frac{S_1}{N} \right)^i}{i!(i+1)!} \Gamma\left(i + \frac{1}{2}\right) {}_2F_1\left(-i, -1, -1; 1; \frac{S_2}{S_1}\right)$$

and

$$b_{001} = \frac{1}{\pi} \left( \frac{S_2}{N} \right)^{1/2} \sum_{i=0}^{\infty} \frac{(-1)^i \left( \frac{S_1}{N} \right)^i}{(i!)^2} \Gamma\left(i + \frac{1}{2}\right) {}_2F_1\left(-i; -1, 2, \frac{S_2}{S_1}\right)$$

where

$$S_1 = \frac{A_1^2}{2}, \quad S_2 = \frac{A_2^2}{2}, \quad N = \sigma^2.$$

We also note that the author's expression for the discriminator dynamic DC output voltage ((95))

$$S = \frac{8 \alpha_c^2 A_L^2 (75)}{\pi^2} \tau (2\pi) (16 \times 10^3)$$

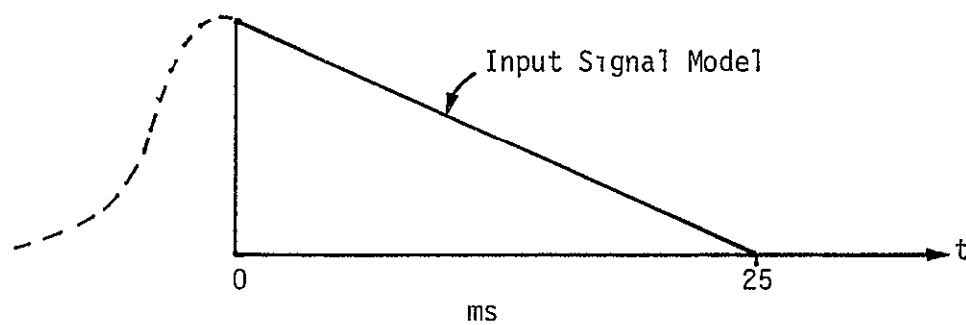


Figure 6. Model of  $LPF_3$  Input Signal Due to Subcarrier

is calculated for  $\Delta\omega = 0$ ; in which case, the second term in his expression for the noise variance

$$\sigma^2 = 3.9 A_L^2 f_0^3 N_0^2 e^{-2\rho} I_0^4\left(\frac{\rho}{2}\right) 2B_{LP} + \frac{76.8 N_0 \alpha A_L^4 \tau^2}{\pi\sigma^2} e^{-\rho} I_0^2\left(\frac{\rho}{2}\right) \times \frac{(\Delta f)^2 |H_2(\Delta f)|^2}{\left[1 + \left(\frac{\Delta f}{f_0}\right)^4\right]} 2B_{LP}$$

should be zero. Finally, the rationale for the selection of the threshold as  $T_h = 1/2 S$  is not provided.

In summary, we have found some minor flaws in the author's analysis; we also question the appropriateness of using steady-state analytical techniques to analyze time-varying phenomena. However, we do not believe that the minor flaws significantly change the conclusions reached by the author, nor do we have any alternate analytical techniques to suggest. This type of system is difficult to analyze, and the author's efforts probably represent the best that can be done in a reasonable amount of time and at a reasonable cost.

#### 4.0 CDR ACTIVITY

As part of its contractual activity, Axiomatix attended the STDN/TDRS CDR. There were 21 action items and 26 RID's. The action items and RID's primarily concerned the lack of test data to establish the communication performance of the transponder over the link. Tables 2 and 3 present descriptions of the key action items and RID's, respectively. It should be noted that the action items and RID's correspond in most cases to the areas of analysis that Axiomatix is engaged in and documented in Section 3 of this report. Action items that addressed new areas were AI-5, AI-9, AI-10 and AI-21. These new areas were scheduled into the Axiomatix analysis effort but, due to cancellation of the STDN/TDRS transponder effort, were not completed.

Table 2. Key IUS TDRS/STDN Transponder CDR Action Item Descriptions

Item	Title	Description
AI-2	TDRS Command Detection Test Data	Command detection performance needs to be tested over temperature range
AI-3	TDRS Acquisition and Tracking Test Data	Testing of acquisition and tracking of a TDRS signal with $\pm 70$ Hz/s doppler rates with a dynamic phase error of $< 15^\circ$ peak.
AI-4	Performance Evaluation with Integrated Tests	The test data presented at the CDR did not include the SSP integrated with the receiver.
AI-5	STE Carrier-Interrupt Time Discrepancy	The transponder, as built, has a 21-ms carrier interrupt time but the allowed carrier drop-out time is 43 ms.
AI-8	Enumeration of Performance Degradations	The performance degradations due to TDRSS user constraint noncompliance needs to be determined.
AI-9	Downconverter #1 In-Band Spurs	In-band spurs are listed as less than -80 dBm, but the requirement is for -100 dBm.
AI-10	Demodulator AGC Worst-Case Analysis	AGC gain is shown to be deficient at end-of-life.
AI-11	Demodulator 2 Spurious Output	The requirement for spurious output is $> 136$ dBm but the capability is only $> 90$ dBm. Also, linearity is only 13% rather than 10%
AI-12	RF Filter Description	No data is given for the new preselector and image filters.
AI-21	Decoder Activate/Deactivate Time Constant	There is a defined requirement for the 90% probability decoder deactivate level.

Table 3. Key IUS TDRS/STDN Transponder RID Descriptions

Item	Title	Description
RID-2	QPSK Modulator Data Rate	The QPSK modulator must handle the 3-Mchips/second PN rate, but the test data shows a capability for only 2 Mbps.
RID-12	Carrier-Suppression Discrepancy	The test data shows only 27 dB of carrier suppression rather than the required $\geq 30$ dB.
RID-14	Transmitter Output Power Discrepancy	The test data shows that the output power is less than the required 2.5 W at 160°F when the voltages are at low tolerances.
RID-15	Static Phase Error	Analysis shows that the static phase error may exceed the required $\leq \pm 5^\circ$ in the tracking range of $\pm 100$ kHz.
RID-22	Telemetry Data/Clock Skew	The transponder is required to handle data/skew from 250 - 3.5 $\mu$ s, but the CDR data shows only 50 - 1.9 $\mu$ s.
RID-23	Receiver Phase Noise Discrepancy	The phase noise in the data bandwidth is required to be less than 3° RMS, but the only data is for less than 15° RMS during vibration.
RID-24	Biphase-L Waveform Symmetry Deficiency	The transmitter is required to reformat the input telemetry so that a waveform symmetry equal to or better than 2% is achieved. The data package states that the output symmetry will be whatever the clock input provides.

## 5.0 SUMMARY AND CONCLUSIONS

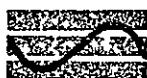
The analyses, reviews and investigations conducted by Axiomatix prior to cancellation of the TRW IUS STDN/TDRS transponder effort uncovered no basic reasons to believe that the transponder would not work satisfactorily with the Orbiter. However, Axiomatix did uncover several minor flaws in some of the analyses performed by TRW. It is doubtful that these flaws would significantly change the conclusion stated above. Had the effort continued, however, Axiomatix would have refined or reanalyzed the areas in question. Furthermore, where some of the analyses for performance in noise were very approximate by necessity, Axiomatix would have conducted computer simulations to verify parameter values and performance.

As a result of its participation in the IUS STDN/TDRS transponder CDR, Axiomatix undertook several new analyses. Due to cancellation of the transponder effort, however, only several of these were completed. These are documented in Section 3 of this final report.



## REFERENCES

1. M. K. Simon and W. K. Aled, "Tracking Performance of Unbalanced QPSK Demodulators: Part I--Biphase Costas Loop with Passive Arm Filters," IEEE Transactions on Communications, Vol. COM-26, No. 8, August 1978, pp 1147-1156.
2. M. K. Simon and J. C. Springett, "The Theory, Design and Operation of the Suppressed Carrier Data-Aided Tracking Receiver," JPL Technical Report #32-1583, June 15, 1973.
3. A. Blanchard, Phase-Locked Loops: Application to Coherent Receiver Design, J. Wiley and Sons, 1976, Chapter 11.
4. P. Shaft, "Limiting of Several Signals and Its Effect on Communication System Performance," IEEE Transactions on Communications Technology, Vol. COM-13, No. 4, December 1965.



# Axiomatix

9841 Airport Boulevard • Suite 912 • Los Angeles, California 90045 • Phone (213) 641 8600

TECHNICAL MEMORANDUM NO. M8109-3

TO:	P. Nilsen	DATE:	September 30, 1981
FROM:	J. K. Holmes	COPIES:	J. Pawłowski M. Simon 16067"A" File
SUBJECT:	Mean Discriminator Output Due to a Tone-Plus-Noise Input		

-----

## 1.0 SUMMARY

The output of a particular frequency error detector was considered and shown to have the same ensemble average error output with or without noise present. As a consequence, the mean error output does not appear to be a sufficient measure of pull-in or acquisition performance.

## 2.0 ANALYSIS

Consider the frequency detector shown in Figure 1. We shall determine the mean error output ( $\bar{e}_0$ ) in a noise environment.

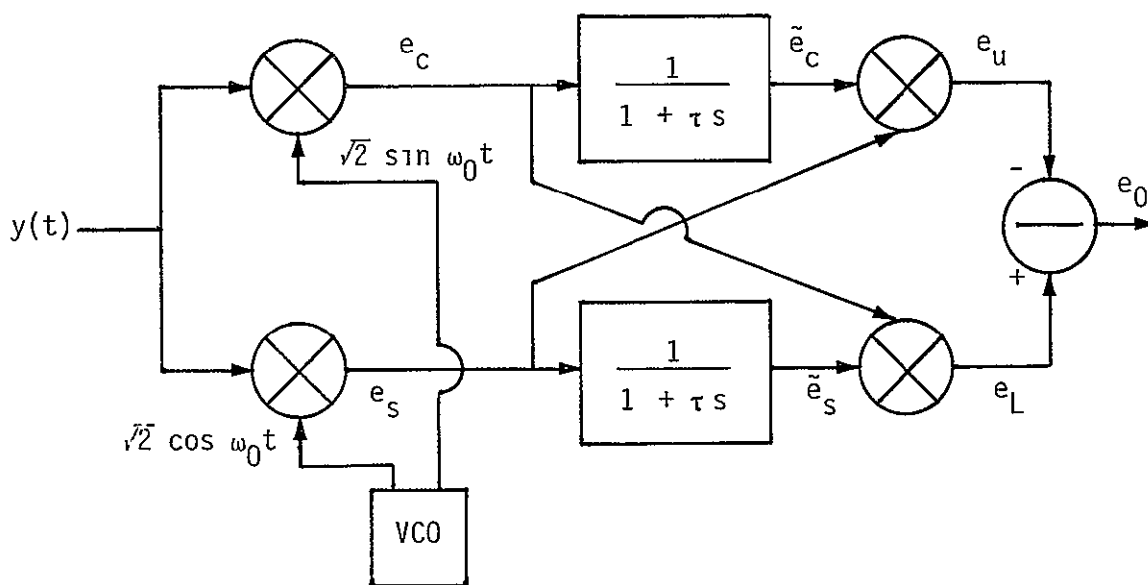


Figure 1. Frequency Error Detector

**ORIGINAL PAGE IS  
OF POOR QUALITY**

Let the received signal frequency be  $\lambda$  rads/s in error from the VCO center frequency,  $\omega_0$ . Assume that the additive noise process is white Gaussian noise. Let

$$y(t) = \sqrt{2} A \sin \left[ (\omega_0 + \lambda) t \right] + \sqrt{2} N_c(t) \cos \omega_0 t + \sqrt{2} N_s(t) \sin \omega_0 t \quad (1)$$

where  $\omega_0$  is the VCO rest frequency and  $\lambda$  is the frequency difference between the received signal and the local signal. The in-phase and quadrature signals, neglecting the double-frequency terms, are

$$e_c(t) = A \cos \lambda t + N_s(t) \quad (2)$$

and

$$e_s(t) = A \sin \lambda t + N_c(t) \quad (3)$$

where  $N_s(t)$  and  $N_c(t)$  are the in-phase and quadrature baseband noise terms. Out of the lowpass filters, we have

$$\tilde{e}_c(t) = \frac{A}{\sqrt{1 + (\lambda\tau)^2}} \cos(\lambda t + \phi) + \tilde{N}_s \quad (4)$$

and

$$\tilde{e}_s(t) = \frac{A}{\sqrt{1 + (\lambda\tau)^2}} \sin(\lambda t + \phi) + \tilde{N}_c \quad (5)$$

where  $\tau$  is the RC time constant of the lowpass filter and  $\tilde{N}_c(t)$  and  $\tilde{N}_s(t)$  are the lowpass filtered versions of  $N_c(t)$  and  $N_s(t)$ .

The phase angle  $\phi$  is given by

$$\phi = \tan^{-1}(\lambda\tau) \quad (6)$$

Out of the upper multiplier, we obtain

$$\begin{aligned} -e_u &= -e_s \tilde{e}_c = \frac{-A^2}{2\sqrt{1 + (\lambda\tau)^2}} \left[ \sin(2\lambda t + \phi) + \sin(-\phi) \right] - N_c(t) \tilde{N}_s(t) \\ &\quad - \frac{A N_c(t)}{\sqrt{1 + (\lambda\tau)^2}} \cos(\lambda t + \phi) - A \sin \lambda t \tilde{N}_s \end{aligned} \quad (7)$$

ORIGINAL PAGE IS  
OF POOR QUALITY

and, out of the lower arm, we have

$$e_L = \tilde{e}_s e_c = \frac{A^2}{2\sqrt{1+(\lambda\tau)^2}} \left[ \sin(2\lambda t + \phi) + \sin\phi \right] + \tilde{N}_c(t) N_s(t) \\ + \tilde{N}_c(t) A \cos(\lambda t) + \frac{A \sin(\lambda t + \phi)}{\sqrt{1+(\lambda\tau)^2}} N_s(t) \quad (8)$$

The frequency detector output is given by the difference between  $e_L$  and  $e_u$ , so that

$$e_0(\lambda) = \frac{A^2 \lambda \tau}{1 + (\lambda \tau)^2} + \tilde{N}_c(t) N_s(t) - N_c(t) \tilde{N}_s(t) \\ + A \tilde{N}_c(t) \cos(\lambda t) - A \tilde{N}_s(t) \sin \lambda t \\ + \frac{A \sin(\lambda t + \phi)}{\sqrt{1 + (\lambda \tau)^2}} N_s(t) - \frac{A \cos(\lambda t + \phi)}{\sqrt{1 + (\lambda \tau)^2}} N_c(t) \quad (9)$$

Since  $N_s(t)$  and  $N_c(t)$  are statistically independent processes, we now see that the statistical average of  $e_0(t)$  denoted by  $\bar{e}_0(t)$  is given by

$$\bar{e}_0(\lambda) = \frac{A^2 \lambda \tau}{[1 + (\lambda \tau)^2]} \quad (10)$$

Clearly, noise does not degrade the mean error control signal, which was the question to be answered by this memorandum. We have used the fact that

$$\sin\phi = \frac{\lambda\tau}{\sqrt{1+(\lambda\tau)^2}} \quad (11)$$

in going from (9) to (10).



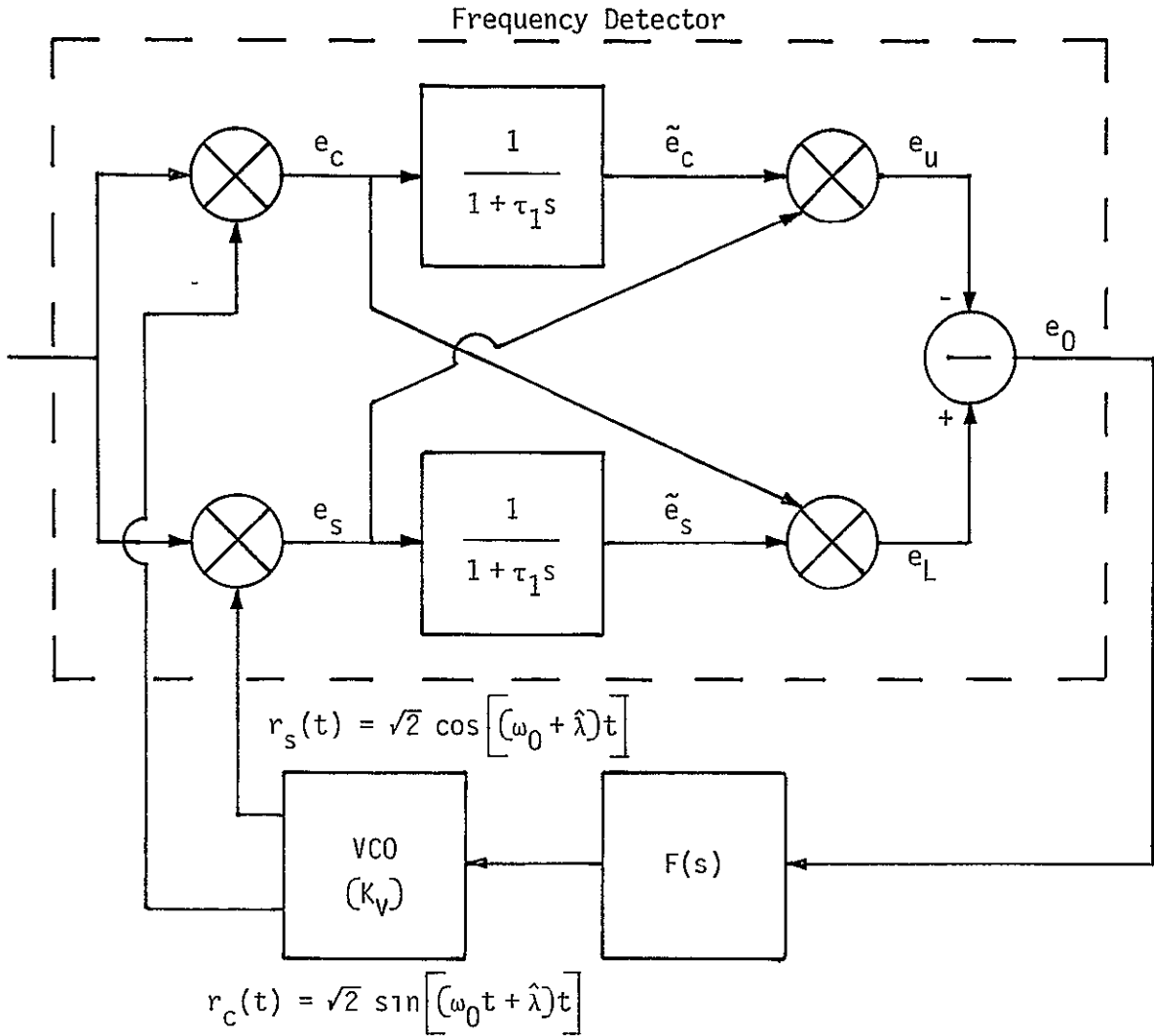


Figure 1. Frequency Lock Loop Utilizing a Delay and Multiply Type of Frequency Detector

Let the received signal frequency be  $\lambda$  rads/s in error from the VCO center frequency,  $\omega_0$ . Assume that the additive noise process is white Gaussian noise. Let the input be  $y(t)$ , then

$$y(t) = \sqrt{2} A \sin \left[ (\omega_0 + \lambda)t \right] + \sqrt{2} n_c(t) \cos \omega_0 t + \sqrt{2} n_s(t) \sin \omega_0 t \quad (2)$$

where  $\omega_0$  is the VCO rest frequency. The reference signals are given by

$$r_c(t) = \sqrt{2} \sin \left[ (\omega_0 + \hat{\lambda})t \right] \quad (3)$$

and

$$r_s(t) = \sqrt{2} \cos \left[ (\omega_0 + \hat{\lambda})t \right] \quad (4)$$

The in-phase and quadrature signals, neglecting the double-frequency terms, are

$$e_c(t) = A \cos (\lambda - \hat{\lambda})t + n_s(t) \quad (5)$$

and

$$e_s(t) = A \sin (\lambda - \hat{\lambda})t + n_c(t) \quad (6)$$

where  $n_s(t)$  and  $n_c(t)$  are the in-phase and quadrature baseband noise terms. Out of the lowpass filters, we have (the tilde denotes filtering)

$$\tilde{e}_c(t) = \frac{A}{\sqrt{1 + (\lambda\tau_1)^2}} \cos \left( (\lambda - \hat{\lambda})t + \phi \right) + \tilde{n}_s \quad (7)$$

and

$$\tilde{e}_s(t) = \frac{A}{\sqrt{1 + (\lambda\tau_1)^2}} \sin \left( (\lambda - \hat{\lambda})t + \phi \right) + \tilde{n}_c \quad (8)$$

where  $\lambda - \hat{\lambda}$  is the frequency error in the loop,  $\tau_1$  is the RC time constant of the lowpass filter, and  $\tilde{n}_c(t)$  and  $\tilde{n}_s(t)$  are the lowpass filtered versions of  $n_c(t)$  and  $n_s(t)$ .

The phase angle  $\phi$  is given by

$$\phi = \tan^{-1}((\lambda - \hat{\lambda})\tau_1) \quad (9)$$

Out of the upper multiplier, we obtain

$$\begin{aligned} -e_u = -e_s \tilde{e}_c &= \frac{-A^2}{2\sqrt{1 + (\lambda\tau_1)^2}} \left[ \sin\{2(\lambda - \hat{\lambda})t + \phi\} + \sin(-\phi) \right] - n_c(t) \tilde{n}_s(t) \\ &\quad - \frac{A n_c(t)}{\sqrt{1 + (\lambda\tau_1)^2}} \cos(\lambda - \hat{\lambda})t - A \tilde{n}_s(\sin \lambda - \hat{\lambda})t \end{aligned} \quad (10)$$

and, out of the lower arm, we have

$$\begin{aligned} e_L = \tilde{e}_s e_c &= \frac{A^2}{2\sqrt{1 + (\lambda\tau_1)^2}} \left[ \sin\{2(\lambda - \hat{\lambda})t + \phi\} + \sin\phi \right] + \tilde{n}_c(t) n_s(t) \\ &\quad + \tilde{n}_c(t) A \cos(\lambda - \hat{\lambda})t + \frac{A \sin(\lambda - \hat{\lambda})t + \phi}{\sqrt{1 + (\lambda - \hat{\lambda})\tau_1^2}} n_s(t) \end{aligned} \quad (11)$$

The frequency detector output is given by the difference between  $e_L$  and  $e_u$ , so that

$$\begin{aligned} e_0(\lambda) &= \frac{A^2(\lambda - \hat{\lambda})\tau_1}{1 + ((\lambda - \hat{\lambda})\tau_1)^2} + \tilde{n}_c(t) n_s(t) - n_c(t) \tilde{n}_s(t) \\ &\quad + A \tilde{n}_c(t) \cos(\lambda - \hat{\lambda})t - A \tilde{n}_s(t) \sin(\lambda - \hat{\lambda})t \\ &\quad + \frac{A \sin((\lambda - \hat{\lambda})t + \phi)}{\sqrt{1 + ((\lambda - \hat{\lambda})\tau_1)^2}} n_s(t) - \frac{A \cos((\lambda - \hat{\lambda})t + \phi)}{\sqrt{1 + ((\lambda - \hat{\lambda})\tau_1)^2}} n_c(t) \end{aligned} \quad (12)$$



Since  $n_s(t)$  and  $n_c(t)$  are statistically independent processes, we now see that the statistical average of  $e_0(t)$  denoted by  $\bar{e}_0(t)$  is given by

$$\bar{e}_0(\lambda) = \frac{A^2(\lambda - \hat{\lambda})\tau_1}{\left[1 + (\lambda - \hat{\lambda})\tau_1\right]^2} \quad (13)$$

which is odd symmetric in the frequency error,  $\lambda - \hat{\lambda}$ . In going from (10) to (13), we have used the fact that

$$\sin\phi = \frac{(\lambda - \hat{\lambda})\tau_1}{\sqrt{1 + (\lambda - \hat{\lambda})\tau_1\right]^2}} \quad (14)$$

Now denote all the terms of (10), except the first, as noise,  $n(t)$ . We will initially assume that  $n(t)$  can be modeled as a white Gaussian noise process for values of  $\omega$  and  $\lambda$  of interest. In a later memorandum, we will show the conditions under which this assumption is valid. The VCO output frequency estimate is given by

$$\hat{\lambda} = K_V F(s) \left[ \frac{A^2(\lambda - \hat{\lambda})\tau_1}{1 + (\lambda - \hat{\lambda})\tau_1\right]^2} + n(t) \right] \quad (15)$$

where  $K_V$  is the VCO parameter relating input voltage of output frequency in radians/second and  $F(s)$  is the loop filter transfer function. Since we want to consider a first-order FLL, we shall let  $F(s) = 1/s$ . Since the frequency estimate  $\hat{\lambda}$  can be written in terms of the frequency error  $\Omega = \lambda - \hat{\lambda}$ , we can write

$$\hat{\lambda} = \lambda - \Omega \quad (16)$$

so that

$$\lambda - \Omega = K_V \frac{1}{s} \left[ \frac{A^2 \Omega \tau_1}{1 + (\Omega \tau_1)^2} + n(t) \right] \quad (17)$$

ORIGINAL PAGE IS  
OF POOR QUALITY

or

$$\dot{\omega}(t) + \frac{A^2 K_V \tau_1}{1 + (\omega \tau_1)^2} \omega(t) = -K_V n(t) + \dot{\lambda}(t) \quad (18)$$

If we assume that the loop bandwidth of the FLL is small compared to the arm filter bandwidths,  $(2\pi\tau_1)^{-1}$ , then, under certain conditions to be discussed in a later memorandum, the noise process,  $n(t)$ , will be essentially white and approximately Gaussian. Under the assumption of white Gaussian noise, the frequency error  $\omega(t)$  is a Markov process. Our main interest here is in the mean time it takes the FLL to acquire frequency.

To model this phenomena analytically, we artificially terminate the process whenever the frequency error that starts from an initial error of  $\lambda_I$  rads/s decreases to some small positive frequency offset  $\lambda_F$  rad/s. In other words,  $\lambda_F$  becomes an absorbing boundary. As long as the error has not "punctured" the boundary  $\lambda_F$ , the frequency error process satisfies the Fokker-Planck equation.

We now derive the Fokker-Planck equation for the first-order FLL. Since we are concerned with acquisition, we will assume that a step in frequency of magnitude  $\lambda_I$  occurs at  $t=0$  and for all  $t > 0$   $\dot{\lambda}(t) = 0$ , hence, (18) can be written as

$$\dot{\omega}(t) + \frac{A^2 K_V \tau_1}{1 + (\omega \tau_1)^2} \omega(t) = -K_V n(t) \quad (19)$$

### 3.0 MEAN TIME TO ACQUIRE

The Fokker-Planck equation becomes ( $t > 0$ )

$$\frac{\partial P}{\partial t}(\omega, t) = -\frac{\partial}{\partial \omega} \left[ A_1(\omega) p(\omega, t) \right] + \frac{1}{2} \frac{\partial^2}{\partial \omega^2} \left[ A_2(\omega) p(\omega, t) \right] \quad (20)$$

with the condition

$$p(\omega, 0) = \delta(\omega - \lambda_I) \quad (21)$$

where  $p(\Omega, t)$  is the probability density of the frequency error  $\Omega$  and time  $t$ . If we integrate (19) from  $t$  to  $t + \Delta t$ , we obtain

$$\Delta\Omega(t) = \Omega(t + \Delta t) - \Omega(t) = \frac{-K\Omega}{1 + (\tau_1\Omega)^2} \Delta t - K_V \int_t^{t+\Delta t} n(u) du \quad (22)$$

where  $K = A^2 K_V \tau_1$ . Therefore, the two coefficients are given by

$$A_1(\Omega) = \lim_{\Delta t \rightarrow 0} \frac{E[\Delta\Omega | \Omega]}{\Delta t} = \frac{-K\Omega}{1 + (\tau_1\Omega)^2} \quad (23)$$

and

$$A_2(\Omega) = \lim_{\Delta t \rightarrow 0} \frac{E[\Delta\Omega^2 | \Omega]}{\Delta t} = \lim_{\Delta t \rightarrow 0} K_V^2 \int_t^{t+\Delta t} \int_t^{t+\Delta t} E[n(u)n(v)] du dv \quad (24)$$

or

$$A_2(\Omega) = \frac{K_V^2 N_0'}{2} \quad (25)$$

where  $N_0'$  is the one-sided effective noise spectral density of the noise process,  $n(t)$ , and is assumed to be independent of  $\Omega$  and  $\omega$ . Therefore, the Fokker-Planck equation becomes

$$\frac{\partial p}{\partial t}(\Omega, t) = \frac{\partial}{\partial \Omega} \left[ \frac{K\Omega}{1 + (\tau_1\Omega)^2} p(\Omega, t) \right] + \frac{1}{2} \frac{\partial^2}{\partial \Omega^2} \left[ \frac{K_V^2 N_0'}{2} p(\Omega, t) \right] \quad (26)$$

We denote  $q(\Omega, t)$  as the solution to our Fokker-Planck equation with the condition that, at  $t=0$ ,  $q(\Omega, 0)$  satisfies

$$q(\Omega, 0) = \delta(\Omega - \lambda_1) \quad (27)$$

and the condition that

$$q(\lambda_1, t) = 0 \quad , \quad \forall t \quad (28)$$

The probability that lock has not yet been achieved at time  $t$  is given by

$$\psi(t) = \int_{\lambda_F}^{\infty} q(\Omega, t) d\Omega \quad (29)$$

and the probability density of the time to reach  $\lambda_F$  is given by

$$\frac{-\partial\psi}{\partial t} \quad (30)$$

Therefore, the mean time to reach  $\lambda_F$  is given by

$$T_{ACQ} = \int_0^{\infty} t \frac{-\partial\psi}{\partial t} dt = -t \psi(t) \Big|_0^{\infty} + \int_0^{\infty} \psi(t) dt \quad (31)$$

It follows that

$$T_{ACQ} = \int_0^{\infty} \int_{\lambda_F}^{\infty} q(\Omega, t) d\Omega dt - t\psi(t) \Big|_0^{\infty} \quad (32)$$

In order that the function  $\psi(t)$  exists, we require  $\psi(t)$  to decrease faster than  $1/t$  for  $t$  large and we also assume that  $\psi(0)$  is bounded by one in order to be a well-defined probability. Therefore, (32) becomes

$$T_{ACQ} = \int_0^{\infty} \int_{\lambda_F}^{\infty} q(\Omega, t) d\Omega dt \quad (33)$$

Define  $Q(\Omega)$  by

$$Q(\Omega) = \int_0^{\infty} q(\Omega, t) dt \quad (34)$$

ORIGINAL PAGE IS  
OF POOR QUALITY

so that

$$T_{ACQ} = \int_{\lambda_F}^{\infty} Q(\Omega) d\Omega \quad (35)$$

Let us now determine the differential equation that  $Q(\Omega)$  satisfies. Integrating (26) from zero to infinity and using  $q(\Omega, t)$  to denote the solution to our first passage time problem yields

$$q(\Omega, t) \Big|_0^{\infty} = \frac{\partial}{\partial \Omega} \left[ \frac{K\Omega}{1 + (\tau_1 \Omega)^2} Q(\Omega) \right] + \frac{1}{2} \frac{\partial^2}{\partial \Omega^2} \left[ \frac{K_V^2 N_0}{2} Q(\Omega) \right] \quad (36)$$

We assume that  $q(\Omega, \infty)$  is zero so that  $Q(\omega)$  is finite. Furthermore, at  $t=0$ , we have

$$q(\Omega, 0) = \delta(\Omega - \lambda_I) \quad (37)$$

where  $\lambda_I$  is the initial frequency offset expressed in units of radians per second. Using these two facts, (36) becomes

$$-\delta(\Omega - \lambda_I) = \frac{d}{d\Omega} \left[ \frac{K\Omega}{1 + (\tau_1 \Omega)^2} Q(\Omega) \right] + \frac{K_V^2 N_0}{4} \frac{d^2 Q(\Omega)}{d\Omega^2} \quad (38)$$

with the boundary condition

$$Q(\lambda_F) = \int_0^{\infty} q(\lambda_F, t) dt = 0 \quad (39)$$

Integrating (38) once yields

$$C - U(\Omega - \lambda_I) = \frac{K\Omega}{1 + (\tau_1 \Omega)^2} Q(\Omega) + \frac{K_V^2 N_0}{4} \frac{dQ(\Omega)}{d\Omega} \quad (40)$$

The solution to (40) can be written as

$$Q(\Omega) = e^{-\int^{\Omega} M(u) du} \int_0^{\Omega} N(u) e^{\int^u M(v) dv} du + B e^{-\int^{\Omega} M(u) du} \quad (41)$$

where

$$M(\Omega) = \frac{4K}{N_0' K_V^2} \frac{\Omega}{1 + (\tau_1 \Omega)^2} \quad (42)$$

and

$$N(\Omega) = \frac{C - U(\Omega - \lambda_T)}{\left( \frac{K_V^2 N_0'}{4} \right)} \quad (43)$$

with both C and B to be determined. First consider

$$\int^{\Omega} M(u) du = \frac{2K}{\tau_1^2 N_0' K_V^2} \int^{\Omega} \frac{u \tau_1^2}{1 + (\tau_1 u)^2} du \quad (44)$$

$$\int^{\Omega} M(u) du = \frac{2K}{N_0' \tau_1^2 K_V^2} \ln \left[ 1 + (\tau_1 \Omega)^2 \right] \quad (45)$$

Hence,

$$e^{-\int^{\Omega} M(u) du} = \left[ 1 + (\tau_1 \Omega)^2 \right]^{-\alpha} \quad (46)$$

where

$$\alpha = \frac{2K}{N_0' K_V^2 \tau_1^2} \quad (47)$$

Therefore,  $Q(\Omega)$  becomes

ORIGINAL PAGE IS  
OF POOR QUALITY

$$Q(\Omega) = \left[ \frac{1}{1 + (\tau_1 \Omega)^2} \right]^\alpha \int_0^\omega \frac{[C - U(\Omega - \lambda_I)]}{\left( \frac{K_V^2 N_0'}{4} \right)} \left[ 1 + (\tau_1 \Omega)^2 \right]^\alpha d\Omega$$

$$+ \frac{B}{\left[ 1 + (\tau_1 \Omega)^2 \right]^\alpha} \quad (48)$$

Now  $C=1$  implies that  $Q(\infty)=0$ , which implies that  $T_{ACQ} < \infty$ , which follows directly from (35) and (48). Furthermore, if  $C \neq 1$ , then  $T_{ACQ} = \infty$ , which is not physically possible for the system under study. From (35), we have

$$T_{ACQ} = \int_{\lambda_F}^{\infty} \frac{1}{\left[ 1 + (\tau_1 \Omega)^2 \right]^\alpha} \left\{ \int_0^\Omega \frac{[1 - U(u - \lambda_I)]}{\left( \frac{K_V^2 N_0'}{4} \right)} \left[ 1 + (\tau_1 u)^2 \right]^\alpha du \right\} d\Omega$$

$$+ \int_{\lambda_F}^{\infty} \frac{B}{\left[ 1 + (\tau_1 \Omega)^2 \right]^\alpha} d\Omega \quad (49)$$

By virtue of the definition of the step function, we can break the integral of (49) into two terms to yield

$$T_{ACQ} = \int_{\lambda_F}^{\lambda_I} \frac{1}{\left[ 1 + (\tau_1 \Omega)^2 \right]^\alpha} \int_0^\Omega \beta \left[ 1 + (\tau_1 u)^2 \right]^\alpha du d\Omega$$

$$+ \int_{\lambda_I}^{\infty} \frac{1}{\left[ 1 + (\tau_1 \Omega)^2 \right]^\alpha} \int_0^{\lambda_I} \beta \left[ 1 + (\tau_1 u)^2 \right]^\alpha du d\Omega$$

$$+ \int_{\lambda_F}^{\infty} \frac{B}{\left[ 1 + (\tau_1 \Omega)^2 \right]^\alpha} d\Omega \quad (50)$$

where

$$\beta = \frac{4}{K_V^2 N_0'} \quad (51)$$

Now, from (39) and (48), we obtain

$$0 = \left[ \frac{1}{1 + (\tau_1 \lambda_F)^2} \right]^\alpha \int_0^{\lambda_F} \beta \left[ 1 + (\tau_1 \Omega)^2 \right]^\alpha d\Omega + \frac{B}{\left[ 1 + (\tau_1 \lambda_F)^2 \right]^\alpha} \quad (52)$$

We conclude from (49) that

$$B = - \int_0^{\lambda_F} \beta \left[ 1 + (\tau_1 \Omega)^2 \right]^\alpha d\Omega \quad (53)$$

Therefore, from (50) and (53), we obtain

$$\begin{aligned} T_{ACQ} &= \int_{\lambda_F}^{\lambda_I} \frac{1}{\left[ 1 + (\tau_1 \Omega)^2 \right]^\alpha} \int_0^{\Omega} \beta \left[ 1 + (\tau_1 u)^2 \right]^\alpha du d\Omega \\ &+ \int_{\lambda_I}^{\infty} \frac{1}{\left[ 1 + (\tau_1 \Omega)^2 \right]^\alpha} \int_0^{\lambda_I} \beta \left[ 1 + (\tau_1 u)^2 \right]^\alpha du d\Omega \\ &- \int_{\lambda_F}^{\infty} \int_0^{\lambda_F} \beta \left[ 1 + (\tau_1 u)^2 \right]^\alpha du \frac{1}{\left[ 1 + (\tau_1 \Omega)^2 \right]^\alpha} d\Omega \quad (54) \end{aligned}$$

Since the third term cancels a portion of the first and second terms, we obtain

$$\begin{aligned} T_{ACQ} &= \int_{\lambda_F}^{\lambda_I} \frac{1}{\left[ 1 + (\tau_1 \Omega)^2 \right]^\alpha} \int_{\lambda_F}^{\Omega} \beta \left[ 1 + (\tau_1 u)^2 \right]^\alpha du d\Omega \\ &+ \int_{\lambda_I}^{\infty} \frac{1}{\left[ 1 + (\tau_1 \Omega)^2 \right]^\alpha} \int_{\lambda_F}^{\lambda_I} \beta \left[ 1 + (\tau_1 u)^2 \right]^\alpha du d\Omega \quad (55) \end{aligned}$$

which is our final result for the mean FLL acquisition time. Notice that that, when the initial frequency offset  $\lambda_I$  equals the final frequency offset,  $T_{ACQ} = 0$ , as it should.



For integer values of  $\alpha$ ,  $T_{ACQ}$  can be evaluated.

#### 4.0 EVALUATION OF $\alpha$ AND $\beta$

Now we consider the evaluation of the parameters  $\alpha$  and  $\beta$ . From (47), we have

$$\alpha = \frac{2K}{N_0' K_V^2 \tau_1^2} \quad (56)$$

and, from the line below (22), we obtain

$$K = K_V A^2 \tau_1 \quad (57)$$

Using (57) in (56) produces

$$\alpha = \frac{2A^4}{N_0' K}$$

Since it is well known that the loop gain of a first-order servo loop is four times the one-sided closed-loop bandwidth, we obtain

$$\alpha = \frac{A^4}{2N_0' B_L} \quad (58)$$

In a later memorandum, we will show that, under certain conditions, the linearized frequency-tracking error is given by

$$\sigma_\lambda^2 = \frac{N_0'^2 B_L^2}{2A^4 \tau_1^3} \quad (59)$$

This calculation used the fact that the effective noise spectral density is given by

$$N_0' = \frac{N_0^2}{4\tau_1} \quad (60)$$

Consequently, using (59) and (60) in (58) produces the result

$$\alpha = \frac{1}{\sigma_\lambda^2 \tau_1^2} \quad (61)$$

which is the inverse of a normalized frequency mean-squared error. Now consider expressing  $\beta$  in terms of useful parameters. From (51), we have

$$\beta = \frac{4}{K_V^2 N_0} \quad (62)$$

Using (57) in (62) yields

$$\beta = \frac{16 A^4 \tau_1^3}{N_0^2 K^2} \quad (63)$$

Using  $K = 4B_L$  and (59) in (63) yields

$$\beta = \frac{1}{2\sigma_\lambda^2 B_L} \quad (64)$$

Finally, using (61) and (62) in (55) produces

$$\begin{aligned} 2 B_L T_{ACQ} &= \frac{1}{\sigma_\lambda^2} \int_{\lambda_F}^{\lambda_I} \frac{1}{[1 + (\tau_1 \chi)^2]^\alpha} \int_{\lambda_F}^{\chi} [1 + (\tau_1 u)^2]^\alpha du d\chi \\ &+ \frac{1}{\sigma_\lambda^2} \int_{\lambda_I}^{\infty} \frac{1}{[1 + (\tau_1 \chi)^2]^\alpha} d\chi \int_{\lambda_F}^{\lambda_I} [1 + (\tau_1 u)^2]^\alpha du \\ \alpha &= \frac{1}{\sigma_\lambda^2 \tau_1^2} \quad (65) \end{aligned}$$

In a later memo, we shall evaluate this expression for various values of  $\alpha$ .



ORIGINAL PAGE IS  
OF POOR QUALITY

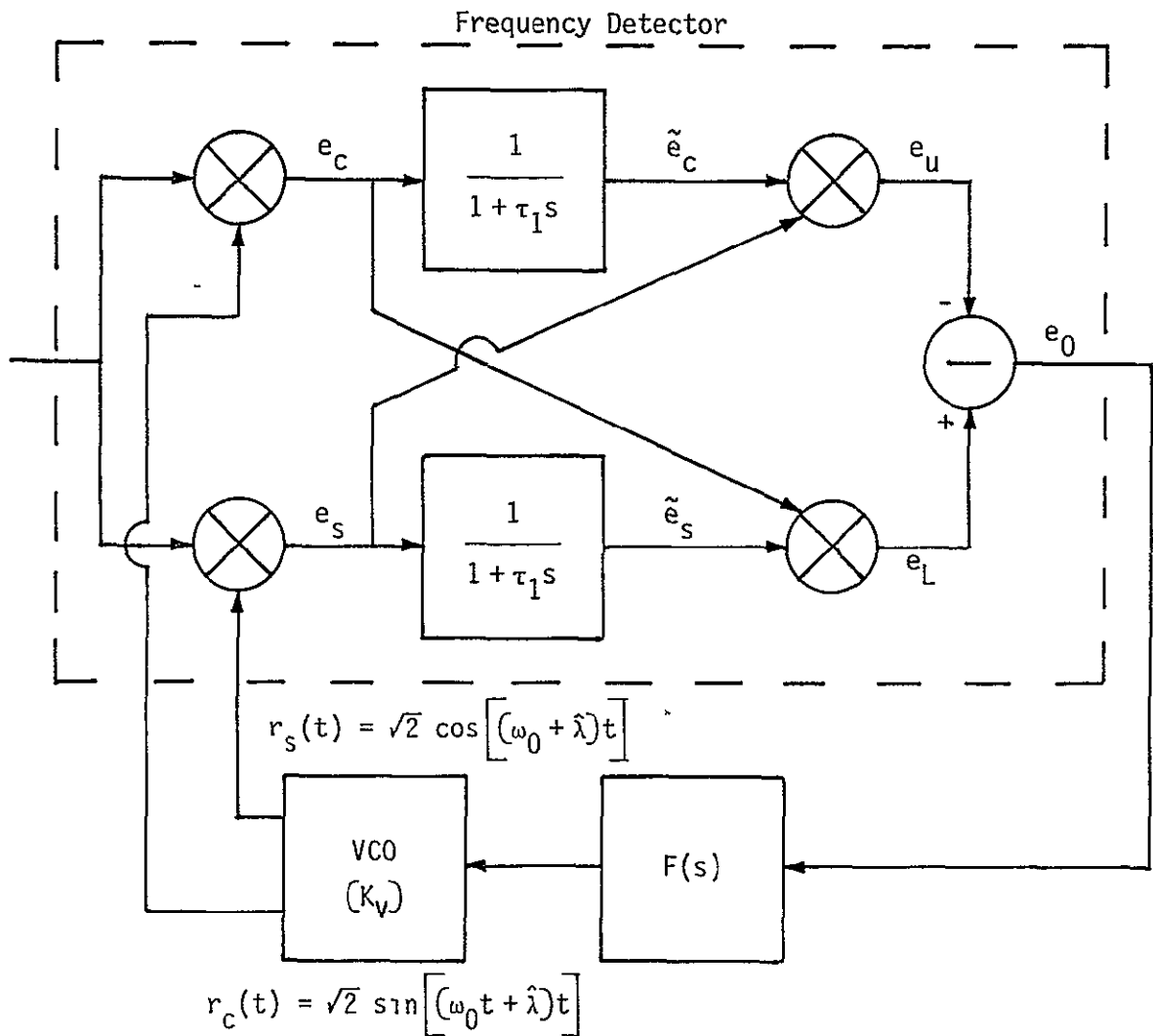


Figure 1. Frequency Lock Loop Utilizing a Delay and Multiply Type of Frequency Detector

ORIGINAL PAGE IS  
OF POOR QUALITY

$$\hat{\lambda} \cong \frac{I(t - \Delta t) Q(t) - I(t) Q(t - \Delta t)}{\Delta t} \quad (1)$$

Now we consider the FLL analysis of the block diagram. Let the received signal frequency be  $\lambda$  rads/s in error from the VCO center frequency,  $\omega_0$ . Assume that the additive noise process is white Gaussian noise. Let the input be  $y(t)$ , then

$$y(t) = \sqrt{2} A \sin[(\omega_0 + \lambda)t] + \sqrt{2} n_c(t) \cos \omega_0 t + \sqrt{2} n_s(t) \sin \omega_0 t \quad (2)$$

where  $\omega_0$  is the VCO rest frequency. The reference signals are given by

$$r_c(t) = \sqrt{2} \sin[(\omega_0 + \hat{\lambda})t] \quad (3)$$

and

$$r_s(t) = \sqrt{2} \cos[(\omega_0 + \hat{\lambda})t] \quad (4)$$

The in-phase and quadrature signals, neglecting the double-frequency terms, are

$$e_c(t) = A \cos(\lambda - \hat{\lambda})t + n_s(t) \quad (5)$$

and

$$e_s(t) = A \sin(\lambda - \hat{\lambda})t + n_c(t) \quad (6)$$

where  $n_s(t)$  and  $n_c(t)$  are the in-phase and quadrature baseband noise terms. Out of the lowpass filters, we have (the tilde denotes filtering)

$$\tilde{e}_c(t) = \frac{A}{\sqrt{1 + (\lambda\tau_1)^2}} \cos((\lambda - \hat{\lambda})t + \phi) + \tilde{n}_s \quad (7)$$

and

$$\tilde{e}_s(t) = \frac{A}{\sqrt{1 + (\lambda\tau_1)^2}} \sin((\lambda - \hat{\lambda})t + \phi) + \tilde{n}_c \quad (8)$$

where  $\lambda - \hat{\lambda}$  is the frequency error in the loop,  $\tau_1$  is the RC time constant of the lowpass filter, and  $\tilde{n}_c(t)$  and  $\tilde{n}_s(t)$  are the lowpass filtered versions of  $n_c(t)$  and  $n_s(t)$ .

The phase angle  $\phi$  is given by

$$\phi = \tan^{-1}((\lambda - \hat{\lambda})\tau_1) \quad (9)$$

Out of the upper multiplier, we obtain

$$\begin{aligned} -e_u = -e_s \tilde{e}'_c &= \frac{-A^2}{2\sqrt{1 + (\lambda\tau_1)^2}} \left[ \sin\{2(\lambda - \hat{\lambda})t + \phi\} + \sin(-\phi) \right] - n_c(t)\tilde{n}_s(t) \\ &\quad - \frac{A n_c(t)}{\sqrt{1 + (\lambda\tau_1)^2}} \cos(\lambda - \hat{\lambda})t - A \tilde{n}_s \sin(\lambda - \hat{\lambda})t \end{aligned} \quad (10)$$

and, out of the lower arm, we have

$$\begin{aligned} e_L = \tilde{e}_s e_c &= \frac{A^2}{2\sqrt{1 + (\lambda\tau_1)^2}} \left[ \sin\{2(\lambda - \hat{\lambda})t + \phi\} + \sin\phi \right] + \tilde{n}_c(t)n_s(t) \\ &\quad + \tilde{n}_c(t) A \cos(\lambda - \hat{\lambda})t + \frac{A \sin(\lambda - \hat{\lambda})t + \phi}{\sqrt{1 + (\lambda - \hat{\lambda})\tau_1)^2}} n_s(t) \end{aligned} \quad (11)$$

The frequency detector output is given by the difference between  $e_L$  and  $e_u$ ,  $e_0 = e_L - e_u$ , so that

$$\begin{aligned} e_0(\lambda) &= \frac{A^2(\lambda - \hat{\lambda})\tau_1}{1 + ((\lambda - \hat{\lambda})\tau_1)^2} + \tilde{n}_c(t)n_s(t) - n_c(t)\tilde{n}_s(t) \\ &\quad + A \tilde{n}_c(t) \cos(\lambda - \hat{\lambda})t - A \tilde{n}_s(t) \sin(\lambda - \hat{\lambda})t \\ &\quad + \frac{A \sin((\lambda - \hat{\lambda})t + \phi)}{\sqrt{1 + ((\lambda - \hat{\lambda})\tau_1)^2}} n_s(t) - \frac{A \cos((\lambda - \hat{\lambda})t + \phi)}{\sqrt{1 + ((\lambda - \hat{\lambda})\tau_1)^2}} n_c(t) \end{aligned} \quad (12)$$

In going from (10) to (12), we have used the fact that

$$\sin\phi = \frac{(\lambda - \hat{\lambda})\tau_1}{\sqrt{1 + ((\lambda - \hat{\lambda})\tau_1)^2}} \quad (13)$$

Now denote all the terms of (10), except the first, as noise,  $n(t)$ . The VCO output frequency estimate is given by

$$\lambda = K_V F(s) \left[ \frac{A^2 (\lambda - \hat{\lambda}) \tau_1}{1 + (\lambda - \hat{\lambda})^2 \tau_1^2} + N(t) \right] \quad (14)$$

where  $K_V$  is the VCO parameter relating input voltage of output frequency in radians/second,  $F(s)$  is the loop filter transfer function and  $N(t)$  is given by all the terms of (12) except the first term. Since we want to consider a first-order FLL, we shall let  $F(s) = 1/s$ . Since the frequency estimate  $\hat{\lambda}$  can be written in terms of the frequency error  $\Omega = \lambda - \hat{\lambda}$ , we can write

$$\hat{\lambda} = \lambda - \Omega \quad (15)$$

so that

$$\lambda - \Omega = K_V \frac{1}{s} \left[ \frac{A^2 \Omega \tau_1}{1 + (\Omega \tau_1)^2} + N(t) \right] \quad (16)$$

or

$$\dot{\Omega}(t) + \frac{A^2 K_V \tau_1}{1 + (\tau_1 \Omega(t))^2} \Omega(t) = -K_V N(t) + \dot{\lambda}(t) \quad (17)$$

3.0 SPECTRAL DENSITY OF THE NOISE PROCESS

We can now compute the spectral density of the noise term as a function of both the input frequency error and Fourier transform variable  $\omega$ . From (12), we have for all terms but the first, letting  $\Omega = \lambda - \hat{\lambda}$ ,

$$N(t) = n_c(t) n_s(t) - n_c(t) \tilde{n}_s(t) + A \tilde{n}_c(t) \cos \Omega t - A \tilde{n}_s(t) \sin \Omega t + \frac{n_s(t) \sin(\Omega t + \phi)}{1 + (\Omega \tau_1)^2} - \frac{A n_c(t) \cos(\Omega t + \phi)}{1 + (\Omega \tau_1)^2} \quad (18)$$

Expanding the last two terms and using (13) produces

$$N(t) = \overbrace{n_c(t) n_s(t) - n_c(t) \tilde{n}_s(t)}^{T_1} + \overbrace{-A \tilde{n}_s(t) \sin \Omega t + \frac{A n_s(t) \sin \Omega t}{1 + (\Omega \tau_1)^2} + \frac{A n_s(t) (\Omega \tau_1) \cos \Omega t}{1 + (\Omega \tau_1)^2}}^{T_2} + \overbrace{+A \tilde{n}_c(t) \cos \Omega t - \frac{A n_c(t) \cos \Omega t}{\sqrt{1 + (\Omega \tau_1)^2}} + \frac{A n_c(t) (\Omega \tau_1) \sin \Omega t}{\sqrt{1 + (\Omega \tau_1)^2}}}_{T_3} \quad (19)$$

Note that all three terms  $T_1$ ,  $T_2$  and  $T_3$  are statistically independent. Now consider  $T_1$

$$T_1 = \tilde{n}_c(t) n_s(t) - n_c(t) \tilde{n}_s(t) \quad (20)$$

The autocorrelation function is given by

$$\begin{aligned} R_{T_1}(\tau) &= E\left[T_1(t) T_1(t+\tau)\right] = E\left[\left(\tilde{n}_c(t) n_s(t) - n_c(t) \tilde{n}_s(t)\right) \right. \\ &\quad \left. \times \left(\tilde{n}_c(t+\tau) n_s(t+\tau) - n_c(t+\tau) \tilde{n}_s(t+\tau)\right)\right] \\ &= R_{\tilde{n}_c}(\tau) R_{n_s}(\tau) + R_{n_c}(\tau) R_{\tilde{n}_s}(\tau) - R_{n_c \tilde{n}_c}(\tau) R_{\tilde{n}_s n_s}(\tau) \\ &\quad - R_{\tilde{n}_c n_c}(\tau) R_{n_s \tilde{n}_s}(\tau) \quad (21) \end{aligned}$$



The spectral density is therefore given by

$$\begin{aligned} \mathcal{L}_{T_1}(\omega) = & \int_{-\infty}^{\infty} \overbrace{R_{\tilde{n}_c}(\tau) R_{n_s}(\tau) e^{-i\omega\tau} d\tau}^{T_{11}} + \int_{-\infty}^{\infty} \overbrace{R_{n_c}(\tau) R_{\tilde{n}_s}(\tau) e^{-i\omega\tau} d\tau}^{T_{12}} \\ & - \int_{-\infty}^{\infty} \overbrace{R_{n_c \tilde{n}_c}(\tau) R_{\tilde{n}_s n_s}(\tau) e^{-i\omega\tau} d\tau}^{T_{13}} - \int_{-\infty}^{\infty} \overbrace{R_{\tilde{n}_c n_c}(\tau) R_{n_s \tilde{n}_s}(\tau) e^{-i\omega\tau} d\tau}^{T_{14}} \end{aligned} \quad (22)$$

Consider the term  $T_{11}$  defined in (22)

$$T_{11} = \int_{-\infty}^{\infty} R_{\tilde{n}_c}(\tau) R_{n_s}(\tau) e^{-i\omega\tau} d\tau \quad (23)$$

where

$$R_{\tilde{n}_c}(\tau) = \int_{-\infty}^{\infty} \mathcal{L}_{\tilde{n}_c}(\omega) e^{i\omega\tau} \frac{d\omega}{2\pi} \quad (24)$$

$T_{11}$  can be written as

$$T_{11} = \int_{-\infty}^{\infty} \int_{-\infty}^{\infty} \int_{-\infty}^{\infty} \mathcal{L}_{\tilde{n}_c}(\omega'') \mathcal{L}_{n_s}(\omega') e^{-i\omega\tau} e^{i\omega'\tau} e^{i\omega''\tau} d\tau \frac{d\omega'}{2\pi} \frac{d\omega''}{2\pi} \quad (25)$$

Now we integrate on  $\tau$  using the fact that

$$\frac{1}{2\pi} \int_{-\infty}^{\infty} e^{i u(x-x_0)} du = \delta(x-x_0) \quad (26)$$

we obtain

$$T_{11} = \iint_{-\infty}^{\infty} \mathcal{L}_{\tilde{n}_c}(\omega'') \mathcal{L}_{n_s}(\omega') \delta(\omega' + \omega'' - \omega) \frac{d\omega'}{2\pi} d\omega'' \quad (27)$$

or finally

$$T_{11} = \int_{-\infty}^{\infty} \mathcal{L}_{\tilde{n}_c}(\omega'') \mathcal{L}_{n_s}(\omega - \omega'') \frac{d\omega''}{2\pi} \quad (28)$$

In the same manner, it can be shown that

$$T_{12} = \int_{-\infty}^{\infty} \mathcal{L}_n(\omega'') \mathcal{L}_{\tilde{n}_s}(\omega - \omega'') \frac{d\omega''}{2\pi} \quad (29)$$

Assuming a one-pole arm filter of the form

$$H(\omega) = \frac{1}{1 + (\tau_1 \omega)^2} \quad (30)$$

we obtain

$$T_{11} = \left(\frac{N_0}{2}\right)^2 \int_{-\infty}^{\infty} \frac{1}{1 + \tau_1^2 (\omega'')^2} \frac{d\omega''}{2\pi} \quad (31)$$

which can be evaluated to be

$$T_{11} = \frac{1}{2\tau_1} \left(\frac{N_0}{2}\right)^2 \quad (32)$$

It follows that

$$T_{12} = \frac{1}{2\tau_1} \left(\frac{N_0}{2}\right)^2 \quad (33)$$

Now consider  $T_{13}$  of (22); recall

$$-T_{13} = \int_{-\infty}^{\infty} E \left[ \tilde{n}_c(t) \tilde{n}_c(t + \tau) \right] E \left[ \tilde{n}_s(t) n_s(t + \tau) \right] e^{1\omega\tau} d\tau \quad (34)$$

Using

$$E[n_c(t)\tilde{n}_c(t+\tau)] = E\left[n_c(t) \int_{-\infty}^{\infty} h(t+\tau-u)n_c(u)du\right] \quad (35)$$

or

$$E[n_c(t)\tilde{n}_c(t+\tau)] = \frac{N_0}{2} \int_{-\infty}^{\infty} h(t+\tau-u) \delta(t-u) du = \frac{N_0}{2} h(\tau) \quad (36)$$

$$E[\tilde{n}_s(t)n_s(t+\tau)] = E\left[n_s(t+\tau) \int_{-\infty}^{\infty} h(t-u)n_s(u)du\right] = \frac{N_0}{2} \int_{-\infty}^{\infty} h(t-u)\delta(u-(t+\tau)) du \quad (37)$$

or

$$E[\tilde{n}_s(t)n_s(t+\tau)] = \frac{N_0}{2} \int_{-\infty}^{\infty} h(t-u) \delta(u-t-\tau) du = \frac{N_0}{2} h(-\tau) \quad (38)$$

Hence, using (36) and (38) in (34) produces

$$-T_{13} = \int_{-\infty}^{\infty} \frac{N_0}{2} h(\tau) \frac{N_0}{2} h(-\tau) e^{-j\omega\tau} d\tau = 0, \quad |h(\tau)| < \infty \quad (39)$$

since

$$\begin{aligned} h(\tau) &= \frac{1}{\tau_1} e^{-t/\tau_1} & \tau \geq 0 \\ &= 0 & \tau < 0 \end{aligned} \quad (40)$$

for the one-pole lowpass filter.

Consider  $T_{14}$ :

$$-T_{14} = \int_{-\infty}^{\infty} \overline{\tilde{n}_c(t)n_c(t+\tau)} \overline{n_s(t)\tilde{n}_s(t+\tau)} e^{-j\omega\tau} d\tau \quad (41)$$

Now

$$E[\tilde{n}_c(t)n_c(t+\tau)] = E\left[n(t+\tau) \int_{-\infty}^{\infty} n_c(u)h(t-u)du\right] \quad (42)$$

or

$$E[\tilde{n}_c(t)n_c(t+\tau)] = \frac{N_0}{2} \int_{-\infty}^{\infty} h(t-u) \delta(u-t-\tau)du = \frac{N_0}{2} h(-\tau) = 0, \quad \tau > 0 \quad (43)$$

Similarly,

$$E[n_s(t)\tilde{n}_s(t+\tau)] = E\left[n_s(t) \int_{-\infty}^{\infty} h(t+\tau-u)n_s(u) du\right] \quad (44)$$

or

$$E[n_s(t)\tilde{n}_s(t+\tau)] = \frac{N_0}{2} \int_{-\infty}^{\infty} h(t+\tau-u) \delta(t-u) du = \frac{N_0}{2} h(\tau) = 0, \quad \tau < 0 \quad (45)$$

Hence, we find that

$$-T_{14} = \int_{-\infty}^{\infty} \left(\frac{N_0}{2}\right)^2 h(\tau)h(-\tau) e^{i\omega\tau} d\tau = 0 \quad (46)$$

It follows from (32), (33), (40) and (45) that

$$S_{T_1}(\omega) = \frac{1}{\tau_1} \left(\frac{N_0}{2}\right)^2, \quad \forall \omega \quad (47)$$

The two remaining terms from (19) are

$$T_2 = \frac{A n_s(t) \sin \Omega t}{1 + (\Omega\tau_1)^2} + \frac{A n_s(t)(\Omega\tau_1) \cos \Omega t}{[1 + (\Omega\tau_1)^2]} - A \tilde{n}_s(t) \sin \Omega t \quad (48)$$

$$T_3 = A\tilde{n}_c(t) \cos \Omega t + \frac{A n_c(t)(\Omega\tau_1) \sin \Omega t}{[1 + (\Omega\tau_1)^2]} - \frac{A n_c(t) \cos \Omega t}{[1 + (\Omega\tau_1)^2]} \quad (49)$$

We consider  $T_2$  by determining the autocorrelation of  $T_2$ . In order to evaluate the noise times tone terms, we shall assume that the carrier has an additional unknown phase angle,  $\theta$ , uniform on  $(0, 2\pi)$ . We have

$$R_{T_2}(\tau, t) = E \left\{ \left[ \frac{A n_s(t) \sin(\Omega t + \theta)}{[1 + (\Omega\tau_1)^2]} + \frac{A n_s(t)(\Omega\tau_1) \cos(\Omega t + \theta)}{[1 + (\Omega\tau_1)^2]} - A\tilde{n}_s(t) \sin(\Omega t + \theta) \right] \right. \\ \left. \times \left[ \frac{A n_s(t+\tau) \sin[\Omega(t+\tau) + \theta]}{[1 + (\Omega\tau_1)^2]} + \frac{A n_s(t+\tau)(\Omega\tau_1) \cos[\Omega(t+\tau) + \theta]}{[1 + (\Omega\tau_1)^2]} - A\tilde{n}_s(t+\tau) \sin[\Omega(t+\tau) + \theta] \right] \right\} \quad (50)$$

$$\begin{aligned}
 R_{T_2}(\tau, t) = & \frac{\overbrace{E\{A^2 n_s(t)n_s(t+\tau) \sin \Omega(t+\theta) \sin[\Omega(t+\tau) + \theta]\}}^{T_{21}}}{[1 + (\Omega\tau_1)^2]^2} \quad \theta \in (0, 2\pi) \\
 & + \frac{\overbrace{E\{A^2 n_s(t)n_s(t+\tau)(\Omega\tau_1) \sin(\Omega t + \theta) \cos[\Omega(t+\tau) + \theta]\}}^{T_{22}}}{[1 + (\Omega\tau_1)^2]^2} \\
 & - \frac{\overbrace{E\{A^2 n_s(t)\tilde{n}_s(t+\tau) \sin(\Omega t + \theta) \sin[\Omega(t+\tau) + \theta]\}}^{T_{23}}}{[1 + (\Omega\tau_1)^2]} \\
 & + \frac{\overbrace{E\{A^2 n_s(t)n_s(t+\tau)(\Omega\tau_1) \cos(\Omega t + \theta) \sin[\Omega(t+\tau) + \theta]\}}^{T_{24}}}{[1 + (\Omega\tau_1)^2]^2} \\
 & + \frac{\overbrace{E\{A^2 n_s(t)n_s(t+\tau)(\Omega\tau_1)^2 \cos(\Omega t + \theta) \cos[\Omega(t+\tau) + \theta]\}}^{T_{25}}}{[1 + (\Omega\tau_1)^2]^2} \\
 & - \frac{\overbrace{E\{A^2 n_s(t)\tilde{n}_s(t+\tau)(\Omega\tau_1) \cos(\Omega t + \theta) \sin[\Omega(t+\tau) + \theta]\}}^{T_{26}}}{[1 + (\Omega\tau_1)^2]} \\
 & - \frac{\overbrace{E\{A^2 n_s(t+\tau)\tilde{n}_s(t) \sin(\Omega t + \theta) \sin[\Omega(t+\tau) + \theta]\}}^{T_{27}}}{[1 + (\Omega\tau_1)^2]} \\
 & - \frac{\overbrace{E\{A^2 \tilde{n}_s(t+\tau)n_s(t) \sin(\Omega t + \theta) \cos[\Omega(t+\tau) + \theta]\}}^{T_{28}}}{[1 + (\Omega\tau_1)^2]} \\
 & + \frac{\overbrace{E\{A^2 \tilde{n}_s(t)\tilde{n}_s(t+\tau) \sin(\Omega t + \theta) \sin[\Omega(t+\tau) + \theta]\}}^{T_{29}}
 \end{aligned} \tag{51}$$

Now evaluate  $T_{21}$  through  $T_{29}$ . Using the overbar to denote the ensemble average, we have

$$T_{21} = \frac{A^2 R_{n_S}(\tau)}{\left[1 + (\Omega\tau_1)^2\right]^2} \overline{\sin(\Omega t + \theta) \sin(\Omega t + \Omega\tau + \theta)} \quad (52)$$

$$T_{21} = \frac{A^2 R_{n_S}(\tau)}{\left[1 + (\Omega\tau_1)^2\right]^2} \left\{ \frac{1}{2} \cos(\Omega\tau) - \overline{\cos(2\Omega t + \Omega\tau + 2\theta)} \right\} \quad (53)$$

so that

$$T_{21} = \frac{1}{2} \frac{A^2 R_{n_S}(\tau)}{\left[1 + (\Omega\tau_1)^2\right]^2} \cos \Omega\tau \quad (54)$$

Consider  $T_{22}$ :

$$T_{22} = \frac{A^2 R_{n_S}(\tau)(\Omega\tau_1)}{\left[1 + (\Omega\tau_1)^2\right]^2} \left\{ \frac{1}{2} \overline{\sin(2\theta + 2\Omega t + \Omega\tau)} + \frac{1}{2} \overline{\sin(-\Omega\tau)} \right\}$$

or

$$T_{22} = \frac{-A^2 R_{n_S}(\tau)(\Omega\tau_1)}{2\left[1 + (\Omega\tau_1)^2\right]^2} \sin \Omega\tau \quad (55)$$

Consider  $T_{23}$ :

$$T_{23} = - \frac{A^2 \overline{n_S(t) \tilde{n}_S(t+\tau)}}{2\left[1 + (\Omega\tau_1)^2\right]} \cos \Omega\tau \quad (56)$$

or

$$T_{23} = - \frac{A^2 N_0}{2} \frac{h(\tau)}{\left[1 + (\Omega\tau_1)^2\right]} \cos \Omega\tau \quad (57)$$

Consider  $T_{24}$ :

$$T_{24} = \frac{A^2 R_{n_S}(\tau)(\Omega\tau_1)}{[1 + (\Omega\tau_1)^2]^2} \frac{\cos(\Omega t + \theta) \sin[\Omega(t + \tau) + \theta]}{2} \quad (58)$$

or

$$T_{24} = \frac{A^2 R_{n_S}(\tau)(\Omega\tau_1)}{2[1 + (\Omega\tau_1)^2]^2} \sin \Omega\tau \quad (59)$$

which, we notice, cancels  $T_{22}$ . Now consider  $T_{25}$ , which can be evaluated to the value

$$T_{25} = \frac{A^2 R_{n_S}(\tau)(\Omega\tau_1)^2}{2[1 + (\Omega\tau_1)^2]^2} \sin \Omega\tau \quad (60)$$

Similarly, for  $T_{26}$ , we have

$$T_{26} = \frac{-A^2 n_S(t)\tilde{n}_S(t+\tau)(\Omega\tau_1)}{2[1 + (\Omega\tau_1)^2]} \sin \Omega\tau \quad (61)$$

or, finally,

$$T_{26} = \frac{-A^2 \frac{N_0}{2} h(\tau)(\Omega\tau_1)}{2[1 + (\Omega\tau_1)^2]} \sin \Omega\tau \quad (62)$$

Now consider  $T_{27}$ .

$$T_{27} = \frac{-A^2 E[n_S(t+\tau)\tilde{n}_S(t)]}{[1 + (\Omega\tau_1)^2]} \frac{\sin(\Omega t + \theta) \sin[\Omega(t + \tau) + \theta]}{2} \quad (63)$$



ORIGINAL PAGE IS  
OF POOR QUALITY

or

$$T_{27} = \frac{-A^2 \frac{N_0}{2} h(-\tau) \cos \Omega \tau}{2 [1 + (\Omega \tau_1)^2]} \quad (64)$$

Now consider  $T_{28}$ .

$$T_{28} = \frac{-A^2 \tilde{n}_s(t) \tilde{n}_s(t+\tau) (\Omega \tau_1) \sin(\Omega t + \theta) \cos[\Omega(t+\tau) + \theta]}{[1 + (\Omega \tau_1)^2]} \quad (65)$$

therefore, we obtain,

$$T_{28} = \frac{A^2 \frac{N_0}{2} h(-\tau) (\Omega \tau_1)}{2 [1 + (\Omega \tau_1)^2]} \sin(\Omega \tau) \quad (66)$$

Consider  $T_{29}$ .

$$A^2 \tilde{n}_s(t) \tilde{n}_s(t+\tau) \sin(\Omega t + \theta) \sin[\Omega(t+\tau) + \theta] \quad (67)$$

so that we obtain

$$T_{29} = \frac{A^2 R_{\tilde{n}_s}(\tau) \cos(\Omega \tau)}{2} \quad (68)$$

Now consider  $T_3$  ((50)).

$$T_3(t) = A \tilde{n}_c(t) \cos(\Omega t + \theta) + \frac{A n_c(t) (\Omega \tau_1) \sin(\Omega t + \theta)}{[1 + (\Omega \tau_1)^2]} - \frac{A n_c(t) \cos(\Omega t + \theta)}{[1 + (\Omega \tau_1)^2]} \quad (69)$$

ORIGINAL PAGE IS  
OF POOR QUALITY

Determine  $R_{T_3}(\tau)$ :

$$R_{T_3}(\tau) = E \left\{ \left[ \begin{aligned} & A\tilde{n}_c(t) \cos(\Omega t + \theta) + \frac{A n_c(t) (\Omega \tau_1) \sin(\Omega t + \theta)}{[1 + (\Omega \tau_1)^2]} - \frac{A n_c(t) \cos(\Omega t + \theta)}{[1 + (\Omega \tau_1)^2]} \\ & \times \left[ \begin{aligned} & A\tilde{n}_c(t+\tau) \cos[\Omega(t+\tau) + \theta] + \frac{A n_c(t+\tau) (\Omega \tau_1) \sin[\Omega(t+\tau) + \theta]}{[1 + (\Omega \tau_1)^2]} \\ & - \frac{A n_c(t+\tau) \cos[\Omega(t+\tau) + \theta]}{[1 + (\Omega \tau_1)^2]} \end{aligned} \right] \end{aligned} \right\} \quad (70)$$

Expanding, we have

c-2

ORIGINAL PAGE IS  
OF POOR QUALITY

$$\begin{aligned}
 R_{T_3}(\tau) = & \overbrace{A^2 R_{\tilde{n}_c}(\tau) \cos(\Omega t + \theta) \cos[\Omega t + \Omega \tau + \theta]}^{T_{31}} \\
 & + \frac{\overbrace{A^2 \tilde{n}_c(t) n_c(t + \tau) (\Omega \tau_1) \cos(\Omega t + \theta) \sin[\Omega(t + \theta) + \theta]}^{T_{32}}}{[1 + (\Omega \tau_1)^2]} \\
 & - \frac{\overbrace{A^2 \tilde{n}_c(t) n_c(t + \tau) \cos(\Omega t + \theta) \cos[\Omega(t + \tau) + \theta]}^{T_{33}}}{[1 + (\Omega \tau_1)^2]} \\
 & + \frac{\overbrace{A^2 \tilde{n}_c(t) \tilde{n}_c(t + \tau) (\Omega \tau_1) \sin(\Omega t + \theta) \cos[\Omega(t + \tau) + \theta]}^{T_{34}}}{[1 + (\Omega \tau_1)^2]} \\
 & + \frac{\overbrace{A^2 \tilde{n}_c(t) n_c(t + \tau) (\Omega \tau_1)^2 \sin(\Omega t + \theta) \sin[\Omega(t + \tau) + \theta]}^{T_{35}}}{[1 + (\Omega \tau_1)^2]^2} \\
 & - \frac{\overbrace{A^2 \tilde{n}_c(t) n_c(t + \tau) (\Omega \tau_1) \sin(\Omega t + \theta) \cos[\Omega(t + \theta) + \theta]}^{T_{36}}}{[1 + (\Omega \tau_1)^2]^2} \\
 & - \frac{\overbrace{A^2 \tilde{n}_c(t + \tau) n_c(t) \cos(\Omega t + \theta) \cos[\Omega(t + \tau) + \theta]}^{T_{37}}}{[1 + (\Omega \tau_1)^2]} \\
 & - \frac{\overbrace{A^2 \tilde{n}_c(t) n_c(t + \tau) (\Omega \tau_1) \cos(\Omega t + \theta) \sin[\Omega(t + \tau) + \theta]}^{T_{38}}}{[1 + (\Omega \tau_1)^2]^2} \\
 & + \frac{\overbrace{A^2 \tilde{n}_c(t) n_c(t + \tau) \cos(\Omega t + \theta) \cos[\Omega(t + \tau) + \theta]}^{T_{39}}}{[1 + (\Omega \tau_1)^2]^2}
 \end{aligned} \tag{71}$$

Evaluating each term, we obtain

$$T_{31} = \frac{A^2 R_{\tilde{n}_C}(\tau)}{2} \cos \Omega\tau \quad (72)$$

$$T_{32} = \frac{A^2 \frac{N_0}{2} h(-\tau)(\Omega\tau_1)}{2 \left[ 1 + (\Omega\tau_1)^2 \right]} \sin \Omega\tau \quad (73)$$

$$T_{33} = - \frac{A^2 \frac{N_0}{2} h(-\tau)}{2 \left[ 1 + (\Omega\tau_1)^2 \right]} \cos \Omega\tau \quad (74)$$

$$T_{34} = \frac{A^2 \left( \frac{N_0}{2} \right) h(\tau)(\Omega\tau_1)}{2 \left[ 1 + (\Omega\tau_1)^2 \right]} \sin(-\Omega\tau) \quad (75)$$

$$T_{35} = \frac{A^2 R_{n_C}(\tau)(\Omega\tau_1)^2}{2 \left[ 1 + (\Omega\tau_1)^2 \right]^2} \cos \Omega\tau \quad (76)$$

$$T_{36} = - \frac{A^2 R_{n_C}(\tau)(\Omega\tau_1)}{2 \left[ 1 + (\Omega\tau_1)^2 \right]^2} \sin(-\Omega\tau) \quad (77)$$

$$T_{37} = - \frac{A^2 \frac{N_0}{2} h(\tau)}{2 \left[ 1 + (\Omega\tau_1)^2 \right]} \cos(\Omega\tau) \quad (78)$$

$$T_{38} = - \frac{A^2 R_{n_C}(\tau)(\Omega\tau_1)}{2 \left[ 1 + (\Omega\tau_1)^2 \right]^2} \sin(\Omega\tau) \quad (79)$$

$$T_{39} = \frac{A^2 R_{n_C}(\tau)}{2 \left[ 1 + (\Omega\tau_1)^2 \right]^2} \cos(\Omega\tau) \quad (80)$$

It follows that the autocorrelation function of the noise is given by\*

$$\begin{aligned}
 R_N(\tau) = & \mathcal{F}^{-1} \left\{ \frac{1}{\tau_1} \frac{N_0^2}{4} \right\} + \frac{1}{2} \frac{A^2 R(\tau)}{[1+(\Omega\tau_1)^2]^2} \cos \Omega\tau - \frac{A^2}{2} \frac{R(\tau)(\Omega\tau_1)}{[1+(\Omega\tau_1)^2]^2} \sin \Omega\tau \\
 & - \frac{A^2}{2} \frac{N_0}{2} \frac{h(\tau) \cos \Omega\tau}{[1+(\Omega\tau_1)^2]} + \frac{A^2}{2} \frac{R(\tau)(\Omega\tau_1)}{[1+(\Omega\tau_1)^2]^2} \sin \Omega\tau \\
 & + \frac{A^2}{2} \frac{R(\tau) (\Omega\tau_1)^2}{[1+(\Omega\tau_1)^2]^2} \cos \Omega\tau - \frac{A^2}{2} \frac{N_0}{2} \frac{h(\tau) (\Omega\tau_1)}{[1+(\Omega\tau_1)^2]} \sin \Omega\tau \\
 & - \frac{A^2}{2} \frac{N_0}{2} \frac{h(-\tau) \cos \Omega\tau}{[1+(\Omega\tau_1)^2]} + \frac{A^2}{2} \frac{N_0}{2} \frac{h(-\tau)(\Omega\tau_1)}{[1+(\Omega\tau_1)^2]} \sin(\Omega\tau) + \frac{A^2}{2} R_{\tilde{n}}(\tau) \cos(\Omega\tau) \\
 & + \frac{A^2}{2} R_{\tilde{n}}(\tau) \cos \Omega\tau + \frac{A^2}{2} \frac{N_0}{2} \frac{h(-\tau)(\Omega\tau_1)}{[1+(\Omega\tau_1)^2]} \sin \Omega\tau \\
 & - \frac{A^2}{2} \frac{N_0}{2} \frac{h(-\tau) \cos \Omega\tau}{[1+(\Omega\tau_1)^2]} - \frac{A^2}{2} \frac{N_0}{2} \frac{h(\tau)(\Omega\tau_1)}{[1+(\Omega\tau_1)^2]} \sin(\Omega\tau) \\
 & + \frac{A^2}{2} \frac{R(\tau) (\Omega\tau_1)^2}{[1+(\Omega\tau_1)^2]^2} \cos \Omega\tau + \frac{A^2}{2} \frac{(\Omega\tau_1) R(\tau)}{[1+(\Omega\tau_1)^2]^2} \sin \Omega\tau \\
 & - \frac{A^2}{2} \frac{N_0}{2} \frac{h(\tau)}{[1+(\Omega\tau_1)^2]} \cos \Omega\tau - \frac{A^2}{2} \frac{R(\tau) (\Omega\tau_1)}{[1+(\Omega\tau_1)^2]^2} \sin(\Omega\tau) \\
 & + \frac{A^2}{2} \frac{R(\tau)}{[1+(\Omega\tau_1)^2]^2} \cos(\Omega\tau)
 \end{aligned} \tag{81}$$

\* Since the statistics of  $n_C(t)$  and  $n_S(t)$  are identical, we let  $n_C(t) = n(t)$ ,  $n_S(t) = n(t)$ , and  $R_{n_S}(\tau) = R_{n_C}(\tau) = R(\tau)$ .

Simplifying and collecting all the terms yields

$$R_N(\tau) = \mathcal{F}^{-1} \left\{ \frac{1}{\tau_1} \frac{N_0^2}{4} \right\} + \frac{A^2 R(\tau)}{[1 + (\Omega\tau_1)^2]} \cos \Omega\tau - \frac{A^2 N_0}{2} \frac{[h(\tau) + h(-\tau)]}{[1 + (\Omega\tau_1)^2]} \cos \Omega\tau \\ - \frac{A^2 N_0}{2} \frac{(\Omega\tau_1)(h(\tau) - h(-\tau))}{[1 + (\Omega\tau_1)^2]} \sin \Omega\tau + A^2 R_{\tilde{h}}(\tau) \cos \Omega\tau \quad (82)$$

Now determine the spectral density of  $N(t)$  by taking the Fourier transform of each term of  $R_N(\tau)$  given by (82):

$$\mathcal{S}_N(\omega, \Omega) = \underbrace{\frac{1}{\tau_1} \frac{N_0^2}{4}}_{\mathcal{S}_1} + \underbrace{\frac{A^2}{[1 + (\Omega\tau_1)^2]} \int_{-\infty}^{\infty} R(\tau) \left[ \frac{e^{j\Omega\tau} + e^{-j\Omega\tau}}{2} \right] e^{j\omega\tau} d\tau}_{\mathcal{S}_2} \\ - \underbrace{\frac{A^2 N_0}{2} \frac{1}{[1 + (\Omega\tau_1)^2]} \int_{-\infty}^{\infty} [h(\tau) + h(-\tau)] \left[ \frac{e^{j\Omega\tau} + e^{-j\Omega\tau}}{2} \right] e^{j\omega\tau} d\tau}_{\mathcal{S}_3} \\ - \underbrace{\frac{A^2 N_0}{2} \frac{(\Omega\tau_1)}{[1 + (\Omega\tau_1)^2]} \int_{-\infty}^{\infty} [h(\tau) - h(-\tau)] \left[ \frac{e^{j\Omega\tau} - e^{-j\Omega\tau}}{2j} \right] e^{j\omega\tau} d\tau}_{\mathcal{S}_4} \\ + \underbrace{A^2 \int_{-\infty}^{\infty} R_{\tilde{h}}(\tau) \left[ \frac{e^{j\Omega\tau} + e^{-j\Omega\tau}}{2} \right] e^{j\omega\tau} d\tau}_{\mathcal{S}_5} \quad (83)$$

Consider  $\mathcal{S}_2$  defined in (83)

$$\mathcal{S}_2 = \frac{A^2}{[1 + (\Omega\tau_1)^2]} \left[ \int_{-\infty}^{\infty} \frac{R(\tau)}{2} e^{j(\omega-\Omega)\tau} d\tau + \int_{-\infty}^{\infty} \frac{R(\tau)}{2} e^{j(\Omega+\omega)\tau} d\tau \right]$$

or

$$\mathcal{S}_2 = \frac{A^2}{[1 + (\Omega\tau_1)^2]} \left( \frac{N_0}{2} \right) \quad (84)$$

since the thermal noise is assumed to be flat out to  $\omega_0 \gg \Omega$ .

Now consider  $\mathcal{S}_3$ :

$$\mathcal{S}_3 = \frac{-A^2 N_0}{2} \frac{1}{[1 + (\Omega \tau_1)^2]} \int_{-\infty}^{\infty} \left\{ \frac{h(\tau)}{2} e^{-j(\omega - \Omega)\tau} + \frac{h(\tau)}{2} e^{-j(\omega + \Omega)\tau} + \frac{h(-\tau)}{2} e^{-j(\omega - \Omega)\tau} + \frac{h(-\tau)}{2} e^{-j(\omega + \Omega)\tau} \right\} d\tau \quad (85)$$

or

$$\mathcal{S}_3 = \frac{-A^2 N_0}{2} \frac{1}{[1 + (\Omega \tau_1)^2]} \int_{-\infty}^{\infty} \left[ \frac{h(\tau)}{2} e^{-j(\omega - \Omega)\tau} + \frac{h(\tau)}{2} e^{-j(\omega + \Omega)\tau} + \frac{h(\tau)}{2} e^{j(\omega - \Omega)\tau} + \frac{h(\tau)}{2} e^{j(\omega + \Omega)\tau} \right] d\tau \quad (86)$$

or

$$\mathcal{S}_3 = \frac{-A^2 N_0}{2} \frac{1}{[1 + (\Omega \tau_1)^2]} \int_{-\infty}^{\infty} [h(\tau) \cos(\omega - \Omega)\tau + h(\tau) \cos(\omega + \Omega)\tau] d\tau \quad (87)$$

which can be written as

$$\mathcal{S}_3 = \frac{-A^2 N_0}{2} \frac{1}{[1 + (\Omega \tau_1)^2]} \operatorname{Re} \left\{ \int_{-\infty}^{\infty} [h(\tau) e^{-j(\omega - \Omega)\tau} + h(\tau) e^{-j(\omega + \Omega)\tau}] d\tau \right\} \quad (88)$$

Equation (88) can be written as

$$\mathcal{S}_3 = \frac{A^2 N_0}{2} \frac{1}{[1 + (\Omega \tau_1)^2]} \operatorname{Re} \left[ H[j(\omega - \Omega)] + H[j(\omega + \Omega)] \right] \quad (89)$$

Using one-pole filters, we have

$$\mathcal{S}_3 = \frac{-A^2 N_0}{2} \frac{1}{[1 + (\Omega \tau_1)^2]} \operatorname{Re} \left[ \frac{1}{1 + j\tau_1(\omega - \Omega)} + \frac{1}{1 + j\tau_1(\omega + \Omega)} \right] \quad (90)$$

so that we obtain

$$S_3 = \frac{-A^2 N_0}{2} \frac{1}{[1 + (\Omega \tau_1)^2]} \left[ \frac{1}{1 + \tau_1^2 (\omega - \Omega)^2} + \frac{1}{1 + \tau_1^2 (\omega + \Omega)^2} \right] \quad (91)$$

Consider  $S_4$ :

$$S_4 = -\frac{A_2 N_0}{4} \frac{(\Omega \tau_1)}{[1 + (\Omega \tau_1)^2]} \int_{-\infty}^{\infty} [h(\tau) - h(-\tau)] \left[ \frac{e^{i\Omega\tau} - e^{-i\Omega\tau}}{2i} \right] e^{i\omega\tau} d\tau \quad (92)$$

Equation (92) can be written as

$$S_4 = -\frac{A^2 N_0}{4} \frac{\Omega \tau_1}{[1 + (\Omega \tau_1)^2]} \int_{-\infty}^{\infty} \left[ \frac{h(\tau)}{2i} e^{-i(\omega - \Omega)\tau} - \frac{h(\tau)}{2i} e^{i(\Omega + \omega)\tau} - \frac{h(-\tau)}{2i} e^{i(\omega - \Omega)\tau} + \frac{h(-\tau)}{2i} e^{i(\omega + \Omega)\tau} \right] d\tau \quad (93)$$

or

$$S_4 = -\frac{A^2 N_0}{4} \frac{\Omega \tau_1}{[1 + (\Omega \tau_1)^2]} \int_{-\infty}^{\infty} [h(\tau) \sin(\omega - \Omega)\tau + h(\tau) \sin(\omega + \Omega)\tau] d\tau \quad (94)$$

Therefore,

$$S_4 = \frac{A^2 N_0}{4} \frac{\Omega \tau_1}{[1 + (\Omega \tau_1)^2]} \mathcal{I}_m \int_{-\infty}^{\infty} [h(\tau) e^{-i(\omega - \Omega)\tau} - h(\tau) e^{i(\omega + \Omega)\tau}] d\tau \quad (95)$$

or

$$S_4 = \frac{A^2 N_0}{4} \frac{\Omega \tau_1}{[1 + (\Omega \tau_1)^2]} \mathcal{I}_m [H[i(\omega - \Omega)] - H[i(\omega + \Omega)]] \quad (96)$$

Using a one-pole filter for  $H(\omega)$  yields

$$S_4(\omega, \Omega) = \frac{A^2 N_0 (\Omega \tau_1)}{[1 + (\Omega \tau_1)^2]} \left[ \frac{\tau_1 (\omega + \Omega)}{1 + \tau_1^2 (\omega + \Omega)^2} + \frac{\tau_1 (\Omega - \omega)}{1 + \tau_1^2 (\Omega - \omega)^2} \right] \quad (97)$$



Consider  $\mathcal{S}_5$  in more detail. We have

$$\mathcal{S}_5 = A^2 \int_{-\infty}^{\infty} R_{\tilde{n}}(\tau) \left[ \frac{e^{-i(\omega - \Omega)\tau}}{2} + \frac{e^{-i(\omega + \Omega)\tau}}{2} \right] d\tau \quad (98)$$

or

$$\mathcal{S}_5 = \frac{A^2}{2} \left[ \frac{N_0}{2} |H(\omega - \Omega)|^2 + \frac{N_0}{2} |H(\omega + \Omega)|^2 \right] \quad (99)$$

which, for one-pole filters, we have

$$\mathcal{S}_5(\omega, \Omega) = \frac{A^2 N_0}{4} \left[ \frac{1}{1 + \tau_1^2 (\omega - \Omega)^2} + \frac{1}{1 + \tau_1^2 (\omega + \Omega)^2} \right] \quad (100)$$

Therefore, summing  $\mathcal{S}_1$  in (83) plus (84), (91), (97) and (100), we have

$$\begin{aligned} \mathcal{S}(\omega, \Omega) = & \frac{1}{\tau_1} \frac{N_0^2}{4} + \frac{A^2}{[1 + (\Omega \tau_1)^2]} \frac{N_0}{2} - \frac{A^2 N_0}{2 [1 + (\Omega \tau_1)^2]} \left[ \frac{1}{1 + \tau_1^2 (\omega - \Omega)^2} + \frac{1}{1 + \tau_1^2 (\omega + \Omega)^2} \right] \\ & + \frac{A^2 N_0}{4} \frac{(\Omega \tau_1)}{[1 + (\Omega \tau_1)^2]} \left[ \frac{-\tau_1 (\omega - \Omega)}{1 + \tau_1^2 (\omega - \Omega)^2} + \frac{\tau_1 (\omega + \Omega)}{1 + \tau_1^2 (\omega + \Omega)^2} \right] \\ & + \frac{A^2 N_0}{4} \left[ \frac{1}{1 + \tau_1^2 (\omega - \Omega)^2} + \frac{1}{1 + \tau_1^2 (\omega + \Omega)^2} \right] \end{aligned} \quad (101)$$

which is the noise spectral density as a function of the Fourier frequency variable  $\omega$  and the frequency error variable  $\Omega$ .

Let  $\Omega = 0$ , corresponding to the tracking case\* From (101), we obtain

$$\mathcal{S}(\omega, 0) = \frac{1}{\tau_1} \frac{N_0^2}{4} + \frac{A^2 N_0}{2} \frac{\tau_1^2 \omega^2}{1 + \tau_1^2 \omega^2} \quad (102)$$

\* Note: If we start at (19) and let  $\Omega = 0$  and do not use the uniform random variable  $\theta$ , we still get (102) when  $\Omega = 0$ .

Hence, we see that there is a flat component,  $1/\tau_1 N_0^2/4$ , plus a squared frequency component (corresponding to the derivative of white noise).

Now let  $\omega = 0$  and determine  $\mathcal{S}(0, \Omega)$  from (101):

$$\begin{aligned} \mathcal{S}(0, \Omega) &= \frac{N_0^2}{4\tau_1} + \frac{A^2 N_0}{2[1 + (\Omega\tau_1)^2]} - \frac{A^2 N_0}{2[1 + (\Omega\tau_1)^2]} \left[ \frac{2}{1 + \tau_1^2 \Omega^2} \right] \\ &+ \frac{A^2 N_0}{4} \frac{\Omega\tau_1}{[1 + (\Omega\tau_1)^2]} \left[ \frac{\Omega\tau_1}{1 + \tau_1^2 \Omega^2} + \frac{\tau_1 \Omega}{1 + \tau_1^2 \Omega^2} \right] \\ &+ \frac{A^2 N_0}{4} \left[ \frac{2}{1 + \tau_1^2 \Omega^2} \right] \end{aligned} \quad (103)$$

After some algebra, we obtain

$$\mathcal{S}(0, \Omega) = \frac{N_0^2}{4\tau_1} + \frac{2 A_2 N_0 (\Omega\tau_1)^2}{[1 + (\tau_1 \Omega)^2]^2} \quad (104)$$

which can alternatively be written as

$$\mathcal{S}(0, \Omega) = \frac{N_0^2}{4\tau_1} \left[ 1 + \frac{A^2}{N_0 \left(\frac{1}{\tau_1}\right)} \frac{8(\Omega\tau_1)^2}{[1 + (\Omega\tau_1)^2]^2} \right] \quad (105)$$

Using (105) with the parameters  $\tau_1 = 0.01$  and  $\Omega\tau_1 = 0.3$ , we find that  $A_2/N_0$  can be no larger than 12.2 dB in order that the second term in brackets does not exceed 0.1, so that the spectral density does not increase by more than 0.4 dB when  $\Omega\tau_1 = 0.3$ . Obviously, this allowable value of  $A^2/N_0$  is too small to include the case  $\Omega \neq 0$  ( $\Omega\tau_1 = 0.3$ ). Therefore, (104) should be used during acquisition, whereas (102) should be used in tracking.

Because, in acquisition, (105) is a function  $\Omega$  (the frequency error), we see that the results in [2] apply only to  $C/N_0$ 's less than or equal to 12.2 dB.

## 4.0 ROOT MEAN-SQUARE FREQUENCY ERROR IN TRACKING

From (15), we obtain, assuming that the input frequency is zero ( $\Omega = 0$ ), so that

$$-\Omega = K_V \frac{1}{S} \left[ A^2 \Omega \tau_1 + N(t) \right] \quad (106)$$

or

$$\Omega = \frac{A^2 K_V \frac{\tau_1}{S} \left\{ \frac{N(t)}{A^2 \tau_1} \right\}}{\left[ 1 + \frac{A^2 K_V \tau_1}{S} \right]} \quad (107)$$

From (102), we have

$$\mathcal{S}(0, \omega) = \frac{1}{\tau_1} \frac{N_0^2}{4} + \frac{A^2 N_0}{2} \frac{\tau_1^2 \omega^2}{1 + \tau_1^2 \omega^2} \quad (108)$$

So that, using (108) and (107), we arrive at

$$\sigma_{\Omega}^2 = \frac{2B_L \left( \frac{N_0'}{2} \right)}{A^4 \tau_1^2} + \frac{\int_{-\infty}^{\infty} \frac{A^2 N_0}{2} \frac{\tau_1^2 \omega^2}{1 + \tau_1^2 \omega^2} |H(f)|^2 df}{A^4 \tau_1^2} \quad (109)$$

Now

$$\frac{N_0'}{2} = \frac{N_0^2}{4\tau_1} \quad (110)$$

so that

$$\sigma_{\Omega}^2 = \frac{\overbrace{\frac{2B_L N_0^2}{4 A^4 \tau_1^3}}^{\sigma_{\Omega_1}^2} + \overbrace{\frac{\int_{-\infty}^{\infty} \frac{A^2 N_0}{2} \frac{\tau_1^2 \omega^2}{1 + \tau_1^2 \omega^2} |H(f)|^2 df}{A^4 \tau_1^2}}^{\sigma_{\Omega_2}^2}}{\quad} \quad (111)$$

ORIGINAL PAGE IS  
OF POOR QUALITY

$$H(f) = \frac{K \left(\frac{1}{S}\right)}{1 + \frac{K}{S}} = \frac{K}{S + K} \quad (K = 4B_L) \quad (112)$$

$$H(f) = \frac{K}{j2\pi f + K} = \frac{4B_L}{j2\pi f + 4B_L} \quad (113)$$

and

$$|H(f)|^2 = \frac{16 B_L^2}{(2\pi)^2 f^2 + 16 B_L^2} \quad (114)$$

Now we evaluate  $\sigma_{\Omega}^2$ ; we have

$$\sigma_{\Omega}^2 = \frac{A^2 N_0}{A^4 \tau_1^2} \int_{-\infty}^{\infty} \frac{\tau_1^2 \omega^2}{1 + \tau_1^2 \omega^2} \frac{16 B_L^2}{16 B_L^2 + 4\pi^2 f^2} df \quad (115)$$

$$\sigma_{\Omega}^2 = \frac{A^2 N_0}{A^4 \tau_1^2} \int_{-\infty}^{\infty} \frac{\tau_1^2 4\pi^2 f^2}{1 + \tau_1^2 4\pi^2 f^2} \frac{16 B_L^2}{16 B_L^2 + 4\pi^2 f^2} df \quad (116)$$

This can be evaluated as

$$\sigma_{\Omega}^2 = \frac{2N_0 B_L}{A^2 \tau_1} \left[ \frac{2B_L \tau_1 - 8(B_L \tau_1)^2}{1 - 16(B_L \tau_1)^2} \right] \quad (117)$$

Hence, for the total mean-squared frequency error, we obtain

$$\sigma_{\Omega}^2 = \frac{B_L N_0^2}{4A^4 \tau_1^3} + \frac{2N_0 B_L}{A^2 \tau_1} \left[ \frac{2B_L \tau_1 - 8(B_L \tau_1)^2}{1 - 16(B_L \tau_1)^2} \right] \quad (118)$$

When  $B_L \tau_1 \ll 1$ , we can write

$$\sigma_{\Omega}^2 \approx \frac{B_L N_0^2}{2A^4 \tau_1^3} + \frac{4N_0 B_L^2}{A^2 \tau_1} \quad (119)$$

or

$$\sigma_{\Omega}^2 \approx \frac{\left(N_0 \frac{1}{\tau_1}\right)^2}{2(A^2)^2} \left(\frac{B_L}{\tau_1}\right) + \frac{4N_0 B_L}{A^2} \left(\frac{B_L}{\tau_1}\right) \quad (120)$$

Note that, at high SNR, the mean-squared frequency error is proportional to  $B_L^2$ , not  $B_L$ ! We have defined the two-closed-loop, frequency-lock-loop bandwidth by

$$2B_L = \int_{-\infty}^{\infty} |H(\omega)|^2 \frac{d\omega}{2\pi} \quad (\text{Hz}) \quad (121)$$

with

$$H(s) = \frac{\left[ \frac{A^2 \tau_1 \frac{K_V}{s}}{1 + \frac{A^2 K_V \tau_1}{s}} \right]}{\quad} \quad (122)$$

### References

1. J. K. Holmes, "Frequency-Lock-Loop Mean Time to Acquire," Axiomatix Technical Memorandum No. M8112-1, December 3, 1981.
2. W. B. Davenport and W. L. Root, Random Signals and Noise, Axiomatix Technical Memorandum No. M8112-1, December 3, 1981.

### 3.0 KU-BAND HARDWARE STUDIES

During the course of this contract, Axiomatix was closely involved in several aspects of the Ku-band hardware development and performed several studies to determine hardware performance. These studies include a review of the Hughes (the Ku-band hardware vendor) test plan to establish that all parameters of the system performance required by NASA were being tested by Hughes. The first review of the Hughes test plan is presented in an Axiomatix Technical Memorandum, "HAC Test Plan for Ku-Band System," dated September 19, 1980. Further review is presented in Axiomatix Report No. R8107-1, "Engineering Evaluations and Studies, Annual Final Report for Ku-Band Studies, Contract No. NAS 9-16067, Exhibit A," dated July 10, 1981; both of which are included in this section. Additional studies included in the final report are: determination of the communication-tracking performance, evaluation of the Management Hand-over Logic, analysis of the Signal Processor Assembly (SPA) Mid-Bit Detector frequency stability, critical design review test data evaluation, determination of the cross-coupling effects on antenna servo stability, and Axiomatix coverage of the Deployed Assembly (DA) Acceptance Test Plan (ATP).

An important study presented as part of this section is Axiomatix Technical Memorandum No. M8201-1, "Suggested ADL Fixes for KSC," dated January 8, 1982, which presents a review of the liens against the Ku-band system delivered to the Avionics Development Laboratory (ADL) at Rockwell and the liens against the Ku-band system delivered to ESTL at NASA/JSC. The purpose of this review was to determine if the ADL system could be suitably fixed for use at NASA/KSC CITE and SPIF. The lien review on the ESTL system, which was more current, was to determine which deficiencies found in the ESTL system (if any) would require correction in the ADL system. This memorandum includes Axiomatix recommendations for fixes to the ADL system.

The final technical memorandum (M8209-3, dated September 30, 1982) consists of a more detailed analysis of the cross-coupling effects on the stability and tracking performance of the antenna's alpha and beta servo loops than was included in the final report. The Ku-band communication antenna autotrack system contains alpha and beta servo loops whose purpose is to acquire and track the difference azimuth and elevation-error angles, respectively. Cross coupling between the difference azimuth and elevation channels that feed these loops, originating from the monopulse feeds and comparator network, has

the potential to cause stability problems during acquisition and tracking operations. Furthermore, even if stable operation is assumed, cross-coupling produces a degrading effect on each loop's tracking performance in noise. This memo derives the conditions necessary for stability and mean-squared phase jitter as a measure of tracking performance is used to assess the degradation caused by cross coupling in terms of such parameters as the servo noise bandwidth and the damping factor for each of the loops, as well as the pair of cross-coupling gains.

It is important to note that, during this contract, much of the activity by Axiomatix involved attending meetings and reviews on the Ku-band hardware development. For the most part, Axiomatix participation in these meetings and reviews is documented in monthly progress reports included in Appendix A. In addition, during this contract, Axiomatix was asked by NASA/JSC to provide expertise to help solve problems on an immediate basis. The results of these efforts sometimes did not warrant a formal report or technical memorandum and could easily be covered by a brief telephone call. These issues are not covered in this report.





The second area of concern deals with the adequacy of the system test. The reader should refer to Axiomatix Report No. R8008-1, "Shuttle Orbiter Ku-Band Radar/Communications System Design Evaluation, System Test Evaluation," dated August 26, 1980. This report evaluated the system tests conducted with the ADL Ku-band system and, as an addendum, discussed the test modules used with the DSTE along with the DSTE sell-off procedure.

Axiomatix concluded that the test modules used for system verification were inadequate in demonstrating compliance to the Rockwell specification. In addition, selling off the DSTE on the basis that, if the Ku-band system functions properly with the DSTE, then the DSTE must be functioning properly, is also an inadequate demonstration of the DSTE performance.

The third area of concern is that there are three types of tests listed in the Hughes ESTL test plan verification matrix development, qualification and acceptance. The majority of the test to be used to verify the ESTL system are development tests.

From a theoretical viewpoint, development tests would be conducted on only one set of prototype LRU's in order to have design confidence, and the qualification tests would be conducted on another set of flight quality LRU's to substantiate the design. Subsequent flight LRU's would be subjected to acceptance tests to verify that the LRU's were properly manufactured. The question is: Will the development tests listed in the ESTL test plan in fact be conducted with the ESTL LRU's or will the requirements of a specific paragraph be deemed to have been met because of tests already conducted on the ADL LRU's?

Even if the development tests are conducted with the ESTL LRU's, not all the paragraphs which Hughes has marked as being verified will be verified. For example, paragraph 3.2 3.3 6, "Data Asymmetry," listed in the ESTL test plan, is partially demonstrated by Hughes test module Communications Return Link Functional Test (RLFT), but this module will not be used during the ESTL system tests. Many other examples may be cited showing that the system tests that Hughes intends to conduct will not even verify all the paragraphs which are checked to be verified in the Hughes ESTL test plan.

### 3.0 QUALIFICATION TEST PLAN, QTP

Each of the four LRU's is defined in a separate section within the Rockwell specification. Section 3.0 defines the overall Ku-band system, Section 10.0 defines the SPA LRU, Section 20.0 defines the EA-1 LRU, Section 30.0 defines the DA LRU and Section 40.0 defines the EA-2 LRU.

Since each section defines an individual LRU performance, it would seem appropriate to base the LRU QTP design verification matrices on the respective paragraphs. Hughes initially did this in the Rockwell required document "Verification Plan Ku-Band Integrated Radar and Communications Equipment," HS237-528, dated September 14, 1979, or what is commonly referred to as "TMO1." In fact, when TMO1 was initially submitted, Rockwell noted that the matrices had a number of check marks in the wrong columns. Rockwell therefore made the appropriate comments and returned TMO1 to Hughes for the corrections. To date, TMO1 has not been resubmitted to Rockwell.

Except for the delta qualification test, TMO1 was a good start on a qualification test plan. In fact, TMO1 should be used to provide the basis for any future test plans.

The Hughes qualification test plan currently being reviewed does not seem to be based on TMO1, but on an entirely new plan. As previously stated, TMO1 verified the individual LRU's by testing specific paragraphs within the respective LRU specification sections.

The new test plan refers a majority of the LRU tests to Section 3.0, the system requirements, instead of the appropriate Section 10.0, 20.0, 30.0 or 40.0 paragraphs. For example, the DA qualification tests are based entirely on Section 3.0, and no tests are listed to verify DA LRU performance parameters as outlined in Section 30.0.

Axiomatix feels that the LRU qualification tests should be based upon the appropriate Rockwell sections and should be supplemented with the tests based on Section 3.0, the system requirements. The current test plan is based primarily on Section 3.0, not the respective LRU sections.

#### 4.0 CONCLUSIONS/RECOMMENDATIONS

For the ESTL test plan, Axiomatix recommends that the design verification matrix used be derived from the Rockwell Revision B specification, not from the Hughes internal system requirements. Since there is no document to correlate the Rockwell document with the Hughes document, basing the verification matrix on the Hughes document will only lead to confusion.

Axiomatix feels that the tests to be used to verify the ESTL system performance are inadequate to demonstrate specification compliance. Axiomatix recommends that additional test modules be generated to enhance the DSTE capability to perform system verification as per the Revision B requirements.

For the qualification test plan, Axiomatix recommends that the plan be based on TM01. Except for delta qualification tests, the latest version of TM01, which Hughes still has not resubmitted, is a good plan and most of the work has already been accomplished. Axiomatix feels that qualification test plans should be based on the individual LRU sections in the Rockwell specification, not on the system section

  
Robert Maronde

RM/1p

ENGINEERING EVALUATIONS AND STUDIES  
ANNUAL FINAL REPORT FOR KU-BAND STUDIES  
CONTRACT NAS 9-16067, EXHIBIT A

Prepared for  
NASA Lyndon B. Johnson Space Center  
Houston, Texas 77058

Prepared by  
James G. Dodds  
Gaylord K. Huth  
Robert G. Maronde  
Don Roberts

AXIOMATIX  
9841 Airport Blvd., Suite 912  
Los Angeles, California 90045

AXIOMATIX Report No. R8107-1  
July 10, 1981

## TABLE OF CONTENTS

	Page
LIST OF TABLES AND FIGURES . . . . .	iii
1.0 EXECUTIVE SUMMARY . . . . .	1
1.1 Introduction . . . . .	
1.2 Contents of the Final Report . . . . .	1
1.3 Conclusions and Recommendations . . . . .	1
1.3.1 Communications Tracking Performance . . . . .	2
1.3.2 Management Handover Logic . . . . .	2
1.3.3 SPA Mid-Bit Detector Frequency Stability . . . . .	3
1.3.4 Critical Design Review Test Data Evaluation . . . . .	3
1.3.5 Cross-Coupling Effects on Antenna Servo Stability . . . . .	3
1.3.6 Axiomatic Coverage of the DA ATP Reviews . . . . .	3
2.0 INTRODUCTION . . . . .	4
2.1 Objectives . . . . .	4
2.2 General Approach . . . . .	4
2.3 Relationship to Other Tasks . . . . .	4
2.4 Contents of this Annual Final Report . . . . .	5
2.4.1 Issues Not Covered in Major Sections . . . . .	6
2.5 Conclusions and Recommendations . . . . .	7
2.5.1 Communications Tracking Performance . . . . .	7
2.5.2 Management Handover Logic . . . . .	7
2.5.3 SPA Mid-Bit Detector Frequency Stability . . . . .	7
2.5.4 Critical Design Review Test Data Evaluation . . . . .	7
2.5.5 Cross-Coupling Effects on Antenna Servo Stability . . . . .	8
2.5.6 Axiomatic Coverage of the DA ATP Reviews . . . . .	8
3.0 COMMUNICATIONS TRACKING PERFORMANCE . . . . .	9
3.1 Introduction . . . . .	9
3.2 Ku-Band Dynamic Range Limitations . . . . .	9
3.3 Conclusions . . . . .	11
4.0 MANAGEMENT HANDOVER LOGIC SIMPLIFICATION . . . . .	12
4.1 Introduction . . . . .	12
4.2 Derivation of Simplified Transmit Enable Logic . . . . .	12

	Page
5.0 SPA MID-BIT DETECTOR FREQUENCY STABILITY . . . . .	17
5.1 Introduction . . . . .	17
5.2 Mid-Bit Detector VCO Noise . . . . .	17
5.3 Recommendations . . . . .	20
6.0 CRITICAL DESIGN REVIEW TEST DATA EVALUATION . . . . .	21
6.1 Introduction . . . . .	21
6.2 ADL and ESTL DA LRU CDR Test Data . . . . .	21
6.2.1 DA Findings . . . . .	21
6.2.2 DA Conclusions/Recommendations . . . . .	36
6.3 ADL EA-2 LRU Test DATA . . . . .	36
6.3.1 EA-2 Findings . . . . .	36
6.3.2 EA-2 Conclusions/Recommendations . . . . .	50
7.0 EFFECTS OF CROSS-COUPLING ON THE STABILITY AND TRACKING PERFORMANCE OF $\alpha/\beta$ SERVO LOOPS . . . . .	51
7.1 Introduction . . . . .	51
7.2 Noise-Free Model of Coupled Loops . . . . .	51
7.3 Noise Model of Coupled Loops . . . . .	57
8.0 AXIOMATIX COVERAGE OF THE DA ATP REVIEW MEETING . . . . .	65
8.1 Introduction . . . . .	65
8.2 Findings . . . . .	65
8.3 Conclusions/Recommendations . . . . .	66
REFERENCES . . . . .	67

APPENDICES

- A - HUGHES DEPLOYED ASSEMBLY ATP, AXIOMATIX MEMO DATED SEPTEMBER 11, 1980
- B - ROCKWELL COMMENTS ON HUGHES DA ATP TS 32012-042B
- C - ACTION ITEMS TO ADDRESS ROCKWELL COMMENTS ON HUGHES DA ATP TS 32012-042B

## LIST OF TABLES

	Page
1. DA ATP versus DA LRU Tests (ADL/CDR) . . . . .	22
2. DA ATP versus DA LRU Tests (ESTL/CDR) . . . . .	26
3. DA ATP versus DA LRU Tests (ESTL/ATP) . . . . .	30
4. ADL and ESTL DA Test Summary . . . . .	33
5. Examples of Differences Between HAC and RI Requirements . . . . .	35
6. EA-2 LRU . . . . .	38
7. Timing Synchronization Signals . . . . .	44
8. Deployed Assembly Gates . . . . .	45
9. Acquisition Program Verification . . . . .	47
10. False Alarm Rate . . . . .	48
11. Summary of Untested EA-2 Rockwell Specification Paragraphs . . . . .	49

## LIST OF FIGURES

	Page
1. Communications System Tracking Degradations . . . . .	10
2. RMS Noise Deviation versus Frequency, Motorola MC1648 . . . . .	18
3. RMS Noise Deviation versus Frequency, Motorola MC1658 . . . . .	19
4. A Simple Block Diagram for the Cross-Coupled $\alpha$ and $\beta$ Servo Loops in the Absence of Noise . . . . .	52
5. A Simple Block Diagram for the Cross-Coupled $\alpha$ and $\beta$ Servo Loops in the Presence of Noise . . . . .	58

## 1.0 EXECUTIVE SUMMARY

### 1.1 Introduction

Axiomatix was tasked by NASA/JSC under Contract NAS 9-16067, Exhibit A, to investigate specified problem areas and concerns with respect to the Hughes Aircraft Company (HAC) Ku-band radar/communications system hardware. This final report presents results of the first 13 months of effort under this contract. The purposes of this effort were to provide fast-response evaluation and analysis of Ku-band areas of difficulty as well as to provide or suggest solutions, where appropriate. This effort is related to those Exhibit B tasks concerned with system performance aspects of the Ku-band hardware and those Exhibit C tasks concerning the Ku-band/payload interfaces.

### 1.2 Contents of the Final Report

Section 2 of this report is an introduction which describes the contents of this report in greater detail and summarizes the conclusions and recommendations reached by Axiomatix. Section 3 discusses the communications track problem caused by the excessive signal dynamic range at the servo input. Actual performance of the communications track servo over the hypothesized wide dynamic range of error signals is not yet known, however, initial estimates indicated that there will be a tracking problem if the dynamic range is indeed as large as anticipated.

Section 4 discusses the management/handover logic and presents a simplified description of the logic function. The HAC "truth tables" which describe the transmitter enable logic are shown to be equivalent to a single, rather simple, logic equation. This result makes it much easier to relate the effects of Ku-band commands on the transmitter status.

In Section 5, we discuss our concern with a specific component used in the SPA return-link channel 3 mid-bit detector. This component, a Motorola voltage-controlled oscillator chip, may have excessive output noise which could degrade the return link.

In Section 6, we evaluate the DA and the EA-2 Critical Design Review (CDR) data. Section 6.2 is devoted to the DA and section 6.3 is devoted to the EA-2. The SPA and EA-1 CDR data were evaluated in a prior report [1]. In both cases, the test data was evaluated by comparing the



data with the acceptance criteria listed in the appropriate test procedure. Results of the evaluation are presented in tabular form and untested items from the test procedure are flagged. Appendix A is included as part of section 6.2. This appendix is a copy of an Axiomatix memorandum to NASA/JSC which documents our position that the DA ATP is not adequate to demonstrate conformance to the Rockwell Rev. B specification.

In Section 7, we analyze the effects of  $\alpha/\beta$  cross-coupling on the stability and communications tracking performance of the Ku-band servo. An expression for the mean-square phase jitter of the angular error is derived as a measure of servo performance.

Finally, in Section 8, we discuss the results of a series of meetings at HAC to review the DA ATP. Rockwell had submitted 123 comments concerning the ATP which were discussed and dispositioned at the meetings. Appendix B is a list of the Rockwell comments and Appendix C gives the disposition of the Rockwell comments.

### 1.3 Conclusions and Recommendations

#### 1.3.1 Communications Tracking Performance

Fixes to the DA and EA-1 required to provide adequate communications tracking capability may take as long as eight months to implement. This excessive time, plus the probable cost, dictate an alternate solution. Axiomatix has evaluated TDRSS specifications and concluded that incident flux density specification relief will permit the Ku-band system to autotrack without major LRU modifications. This analysis will be discussed in detail in the system portion of this contract's final report, Exhibit B.

#### 1.3.2 Management Handover Logic

The cumbersome description of the transmitter enable logic in HAC documentation has been reduced to a simple logic equation. The result is that, with A side selected and communications on, the transmitter is enabled if any one of the following conditions is true:

- (1) The system is in a nontracking mode (GPCDES or MANUAL)
- (2) "Primary" acquisition mode is selected (wide-beam horn)
- (3) Modulation control is nonautomatic, e.g., ON or OFF
- (4) There is a signal present on the forward link

### 1.3.3 SPA Mid-Bit Detector Frequency Stability

Based on our experience with the VCO used in the mid-bit detector, as well as manufacturers' literature, Axiomatix concludes that great care must be exercised when this device is used. Circuit layout and power supply stability are critical. The frequency stability/noise of the HAC mid-bit detector 2X clock should be measured to provide assurance that channel 3 data is not compromised by a noisy clock.

### 1.3.4 Critical Design Review Test Data Evaluation

Axiomatix has highlighted areas of testing oversights for both the DA and EA-2. A recurrent theme during the test data evaluation is the lack of correlation between the ATP's and the Rockwell specification.

### 1.3.5 Cross-Coupling Effects on Antenna Servo Stability

An analytical expression is derived which relates the mean-square phase jitter, as a measure of tracking performance, to the servo noise bandwidth, damping factor and cross-coupling gain. A necessary, but insufficient, condition for servo stability is derived. The product of cross-coupling gains must be less than unity.

### 1.3.6 Axiomatix Coverage of the DA ATP Reviews

Axiomatix feels that this series of meetings provided an excellent start in the attempt to correlate the DA ATP with the Rockwell specification.

## 2.0 INTRODUCTION

This report describes AXIOMATIX efforts on Ku-band problem resolution, Exhibit A of NASA/JSC Contract NAS 9-16067, entitled "Engineering Evaluations and Studies." The report period covers the first 13 months of the contract from May 1, 1980 to May 31, 1981.

### 2.1 Objectives

This contract provides AXIOMATIX an instrument with which to assist NASA/JSC with rapid-response capability to evaluate and solve unanticipated Ku-band problems. In lieu of a set of preordained tasks, AXIOMATIX reacts to solve problems as they occur.

### 2.2 General Approach

In order to keep abreast of current problems and Ku-band status, AXIOMATIX personnel have attended all regularly scheduled reviews, numerous special meetings called to discuss specific topics and problem areas, and participated in weekly conference calls. Specific times and places of these events are documented in the AXIOMATIX monthly reports submitted under this contract. AXIOMATIX has also obtained appropriate HAC documentation, when available, to assist in the evaluation of Ku-band development progress. This documentation consists of various HAC reports, memoranda, handouts and test data.

Where deficiencies have been found, modifications and improvements to the Ku-band system have been suggested.

### 2.3 Relationship to Other Tasks

The work described in this report represents an extension of prior AXIOMATIX work under NASA/JSC contracts as well as an adjunct to Exhibits B and C of this contract. Test data from the EA-2 and DA Critical Design Reviews (CDR) were originally intended to be covered in a prior final report under NASA/JSC contract NAS 9-15795. However, the CDR's were delayed and the test data was evaluated under this contract. Since this is an on-going contract, AXIOMATIX will continue to follow the progress of the Ku-band system and provide expertise as required.

## 2.4 Contents of this Annual Final Report

Areas of concern include hardware performance and implementation, and CDR test data evaluation. Specific topics covered are the communications tracking problem, mechanization of the management/handover logic, hardware concerns in the SPA mid-bit detector, evaluation of the DA and EA-2 test data, Block III servo performance, and a discussion of the DA ATP review meetings.

Axiomatix has investigated the communication tracking problem which is caused by wide dynamic range inputs to the tracking servo. This wide dynamic range stems from the input flux density variation, unit-to-unit variation, thermal effects, and the poor AGC performance of the track channel in the Ku-band system. The antenna servo cannot accommodate the wide dynamic range postulated. HAC has proposed a series of fixes to the DA and/or EA-1 which, with varying degrees of flux density specification relief, could provide the required tracking performance. Axiomatix has reviewed the proposed fixes and, in Section 3, we discuss the nature of the problem in more detail as well as the implications of implementing a hardware change to provide adequate performance.

In Section 4, we discuss the management/handover logic. Specifically, we evaluate the functional dependence of the transmitter enable signal on the controlling variables and commands. A minor documentation discrepancy in the HAC SPA specification has been discovered. HAC has been alerted and, after review with Rockwell, agreement was reached to accept the SPA with the transmitter enable logic as implemented.

In Section 5, we discuss our concern with the frequency stability of the mid-bit detector at the SPA high-data rate digital input port. The concern is that noise in the mid-bit circuit may affect the return link quality. Axiomatix experience with similar circuits used to generate a two-times clock, phase locked to the high-data rate clock, indicate excessive noise at the VCO output which, in turn, clocks out the encoded channel 3 data. Characteristics of this circuit and a possible alternative are described in this section.

Axiomatix attended the DA and EA-1 CDR's during this reporting period. Test data presented at the CDR's has been evaluated by Axiomatix and the results of this evaluation are presented in Section 6. The DA

test data is covered in section 6.2 and the EA-2 is covered in section 6.3. The DA test data evaluation is presented in tabular form and the test data is compared with the applicable ATP paragraphs. ATP paragraphs which are not verified during testing are flagged, and a summary table of unverified items is included. For the EA-2, a verification matrix is given which correlates the Rockwell specification with the HAC ATP. Additionally, a series of tables is given which correlate the parameters being measured and the radar modes. Again, a summary table is presented which lists the untested specification paragraphs

Block III servo performance is still a matter of concern. In Section 7, we describe Axiomatix efforts to date to characterize the angle-tracking loop, with emphasis on stability and tracking performance with  $\alpha/\beta$  cross-coupling. A necessary, but insufficient, criterion for stability is derived which is independent of the order of the tracking loop, and an expression for the mean-square phase jitter of the antenna as a function of the servo noise bandwidth and damping factor is derived.

Axiomatix personnel attended a series of review meetings to discuss the DA ATP in which an attempt was made to correlate the ATP with the Rockwell requirements. In Section 8, we discuss the results of these meetings. Appendices B and C are adjuncts to this section, Appendix B shows a list of Rockwell comments presented at the meeting and Appendix C describes the disposition of the comments

#### 2.4 1 Issues Not Covered in Major Sections

During this contract, Axiomatix was asked by NASA/JSC to provide expertise to help solve problems on an immediate basis. The results of these efforts sometimes did not warrant a formal report, and could easily be covered with a brief telephone call or informal memorandum. These issues are not covered in this report. One topic not covered is Axiomatix attendance at the Deliverable System Test Equipment (DSTE) seminar at HAC in July 1980. The seminar was attended so that Axiomatix could easily become familiar with the hardware/software in the event NASA needed assistance with the DSTE. The seminar was useful in giving potential DSTE users an overview, however, it could have been compressed to about one-half the time. While the seminar was a start, Axiomatix feels that the only effective method to gain familiarity with the DSTE will be by "hands-on" experience.

## 2.5 Conclusions and Recommendations

### 2.5.1 Communications Tracking Performance

Fixes to the DA and EA-1 required to provide adequate communications tracking capability may take as long as eight months to implement. This excessive time, plus the probable cost, dictate an alternate solution. Axiomatix has evaluated TDRSS specifications and concluded that incident flux density specification relief will permit the Ku-band system to auto-track without major LRU modifications. This analysis will be discussed in detail in the system portion of this contract's final report, Exhibit B.

### 2.5.2 Management Handover Logic

The cumbersome description of the transmitter enable logic in HAC documentation has been reduced to a simple logic equation. The result is that, with the A side selected and communications on, the transmitter is enabled if any one of the following conditions is true

- (1) The system is in a nontracking mode (GPCDES or MANUAL)
- (2) "Primary" acquisition mode is selected (wide-beam horn)
- (3) Modulation control is nonautomatic, e.g , ON or OFF
- (4) A signal is present on the forward link.

### 2.5.3 SPA Mid-Bit Detector Frequency Stability

Based on our experience with the VCO used in the mid-bit detector, as well as manufacturers' literature, Axiomatix concludes that great care must be exercised when this device is used. Circuit layout and power supply stability are critical. The frequency stability/noise of the HAC mid-bit detector two-times clock should be measured to provide assurance that channel 3 data is not compromised by a noisy clock.

### 2.5.4 Critical Design Review Test Data Evaluation

Axiomatix has highlighted areas of testing oversights for both the DA and EA-2. A recurrent theme during the test data evaluation is the lack of correlation between the ATP's and the Rockwell specification. Appendix A of this report is a copy of an Axiomatix memorandum to NASA/JSC which documents our position that the DA ATP is inadequate to demonstrate conformance to the Rockwell specification.

### 2.5.5 Cross-Coupling Effects on Antenna Servo Stability

An analytical expression is derived which relates the mean-square phase jitter, as a measure of tracking performance, to the servo noise bandwidth, damping factor and cross-coupling gain. A necessary, but insufficient, condition for servo stability is derived the product of cross-coupling gains must be less than unity. The expression for phase jitter is currently being evaluated in terms of the Ku-band rate stabilization loop parameters

### 2.5.6 Axiomatix Coverage of the DA ATP Reviews

Axiomatix feels that this series of meetings provided an excellent start in the attempt to correlate the DA ATP with the Rockwell specification.

### 3.0 COMMUNICATIONS TRACKING PERFORMANCE

#### 3.1 Introduction

The Ku-band communications system employs monopulse steering to closed-loop angle-track the TDRS forward link signal. The communications tracking system consists of a four-element difference channel feed and a sum feed on the high-gain dish, a monopulse comparator, and RF down-conversion and tracking electronics in the EA-1 LRU. HAC has analyzed the angle-track subsystem performance as it is currently implemented and has concluded that this subsystem cannot tolerate the wide variation in received signal strength of the Rockwell specification.

In this section, we describe the implications of trying to resolve this problem with hardware changes via resolution with specification changes. In the final report of Exhibit B of this contract, we will describe a solution based solely on specification relief.

In addition to the dynamic range problem, some crosstalk has been measured between the  $\alpha$  and  $\beta$  channels. In Section 7 of this report, we analyze the servo-tracking degradation due to noise cross-coupling as well as self-coupling, both with and without crosstalk

#### 3.2 Ku-Band Dynamic Range Limitations

The genesis of the dynamic range problem lies in the stringent tracking requirements during severe Orbiter motion with a wide dynamic range signal. In addition, the Ku-band autotrack subsystem has several deficiencies which contribute to the problem. One of the more significant degradations is due to the AGC envelope suppression at low SNR levels. At negative C/N (dB) into the AGC, the output-to-input power ratio is 2:1. Unfortunately, the negative C/N region is within the expected operating range of the AGC circuit. The cumulative effect of signal strength variation, thermal and unit variation, and AGC envelope suppression results in a detector output/servo input variation of 39 dB. This result is from data presented by HAC during a splinter session on March 17, 1981. Figure 1 depicts the communications-tracking system and degradations at the various points. Some DA losses, or degradations, have a compound effect in that they influence both the signal amplitude into the detector as well as the percentage AM versus angle at the detector input.



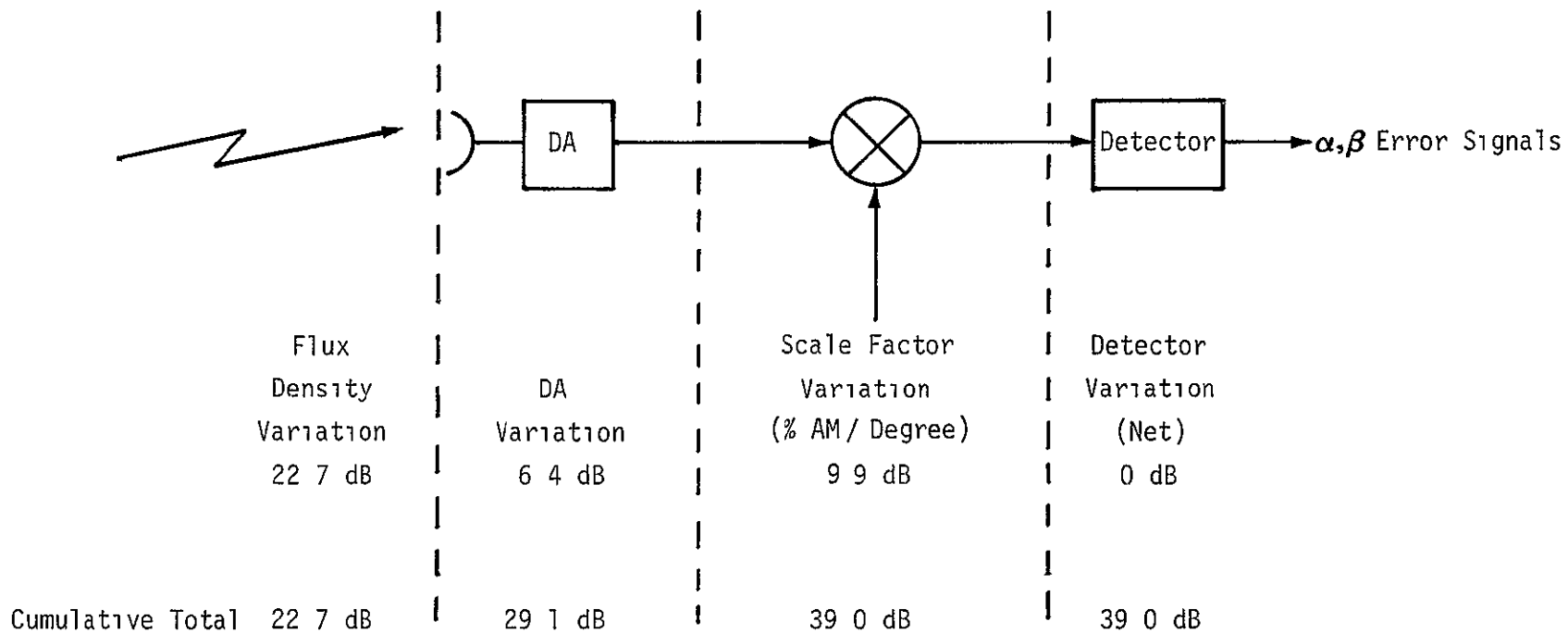


Figure 1 Communications System Tracking Degradations  
(Based on HAC-supplied data, March 1981)

### 3.3 Conclusions

The effect of the 39 dB dynamic range at the servo input is not explicitly known at this time; however, it is safe to assume that the servo is not remotely capable of accommodating this range. HAC has partitioned the dynamic range problem between the servo and the systems preceding the servo: an assumption is made that the servo can accommodate a dynamic range of 15 dB and various "fixes" have been proposed to bring the detector output/servo input dynamic range down to 15 dB. Most fixes entail a combination of EA-1 and DA modifications plus flux density specification relief. Unfortunately, the proposed modifications which provide adequate performance gain require an estimated eight months to be implemented. Axiomatix has concluded that the schedule impact of hardware fixes is not acceptable, and significant specification relief will be required to accommodate the existing hardware, as will be discussed in the Exhibit B report.

#### 4.0 MANAGEMENT HANDOVER LOGIC SIMPLIFICATION

##### 4.1 Introduction

In this section, we discuss aspects of the management/handover logic which concern transmitter enable logic. Discussions of this logic in [2] and [3] are rather difficult to follow, particularly since the function of the logic is intertwined with A-side/B-side selection. Our understanding of the functional dependence of transmitter enable on the controlling variables (e.g., tracking mode, acquisition mode, modulation control and signal present) is facilitated by considering the A-side only. The series of "truth tables" in [3] can be replaced by one simple logic equation. Alternatively, the process can be described simply by noting that, with communications on, the only configuration that disables the transmitter consists of being in a tracking mode with the high-gain antenna selected for acquisition, no signal present on the forward link, and in automatic modulation control. All other conditions with communications on enable the transmitter. In the following section, we derive these results based on information from [2] and [3].

##### 4.2 Derivation of Simplified Transmit Enable Logic

The logic equation which defines the transmit enable state is derived below. From Table 3.2.1.4-11 of [3], transmit enable logic is defined in terms of three intermediate variables, this table is shown below

HANDOVER LOGIC	0	1	1	1	1
OVER RIDE LOGIC	0	1	X	X	X
ACQUISITION LOGIC	0	0	0	1	X
TRANSMIT ENABLE	0	1	0	1	1

The X's represent a third logic state. In order to define the output in terms of Orbiter and Ku-band inputs, the tri-state logic can be defined in terms of additional auxiliary variables, as shown below

Let OVER RIDE LOGIC = 0 be defined as  
 ORL = 0, ORLX = 0

Let OVER RIDE LOGIC = 1 be defined as  
 ORL = 1, ORLX = 1

Let OVER RIDE LOGIC = X be defined as  
 ORL = 0, ORLX = 1.

Similarly, we can define two auxiliary variables for ACQUISITION LOGIC, AL and ALX. A new transmit enable table is shown below.

HL	0	0	0	0	1	1	1	1	1
ORL	0	0	1	1	1	1	0	0	0
ORLX	0	0	1	1	1	1	1	1	1
AL	0	1	0	1	0	1	0	1	0
ALX	0	1	0	1	0	1	0	1	1
TE	0	0	0	0	1	1	0	1	1

TE represents TRANSMIT ENABLE and HL represents HANDOVER LOGIC.

From the above table, we see that  $TE = HL (ORL \cdot ORLX + \overline{ORL} \cdot ORLX \cdot ALX)$ . The first of the intermediate variables, HL, is defined in Table 3 2.1 4-8 of [3] and is shown below with the names of the variables compressed to permit a more compact notation. Only the A side commands are given.

		HANDOVER LOGIC									
A SIDE COMMANDS	COMMON	0	1	1	1	1	1	1	1	1	1
	TDRSEAST	0	0	0	0	1	0	1	1	0	0
	TDRSWEST	0	0	0	0	0	1	0	0	1	1
	ENCODEMODE2	0	0	0	0	1	1	1	1	1	1
	SELECTA	0	0	0	0	0	0	1	0	1	0
TRANSMITTER A (HL)		0	1	1	1	1	1	1	0	1	0

From the previous table,

$$\overline{HL} = \overline{COMMON} + COMMON \cdot ENCODEDMODE2 \cdot \overline{SELECTA}.$$

However, A side is always selected; hence,  $\overline{SELECTA} = 0$  and  $HL = COMMON$ .

The second two intermediate variables, ORL and ORLX, are derived from Table 3.2.4-9 (sic) of [3], as shown below.

MODULATION CONTROL 1	1	0	∅	∅
MODULATION CONTROL 2	1	1	0	0
SIGNAL PRESENT	∅	∅	0	1

OVER RIDE LOGIC	1	1	X	1
-----------------	---	---	---	---

This table is modified to define the auxiliary variables

MODCON1	1	0	∅	∅
MODCON2	1	1	0	0
SIGPRES	∅	∅	0	1
ORL	1	1	0	1
ORLX	1	1	1	1

Thus,  $ORL = MODCON2 + SIGPRES$  and  $ORLX = 1$ .

The acquisition logic is given in development specification Table 3.2 1.4-10, shown below.

ENCODED MODE 1	1	0	0	0
SIGNAL PRESENT	∅	1	0	0
PRIMARY ACQ MODE ON/OFF	∅	∅	0	1

ACQUISITION LOGIC	X	X	1	0
-------------------	---	---	---	---

Thus, the final two auxiliary variables are defined below in the modified table.

ENCMOD1	1	0	0	0
SIGPRES	0	1	0	0
PRIACQOFF	0	0	0	1
AL	0	0	1	0
ALX	1	1	1	0

From the above table,  $AL = \overline{ENCMOD1} \cdot \overline{SIGPRES} \cdot \overline{PRIACQOFF}$ , and  $ALX = ENCMOD1 + SIGPRES + \overline{PRIACQOFF}$ .

The defining equation of the transmit enable logic was shown to be  $TE = HL \cdot (ORL \cdot ORLX + \overline{ORL} \cdot ORLX \cdot ALX)$ . Since  $ORLX = 1$ , this reduces to  $TE = HL \cdot (ORL + \overline{ORL} \cdot ALX)$ . This is logically equivalent to  $TE = HL \cdot (ORL + ALX)$ , as can be shown using a Karnaugh map, truth table and error, or whatever.

The next step is to substitute the independent variables for the intermediate variables, which gives:

$$TE = COMMON \cdot (MODCON2 + SIGPRES + ENCMOD1 + \overline{PRIACQOFF})$$

The modulation control bits MODCON1 and MODCON2 are defined as follows:

MODCON1	MODCON2	MODULATION MODE
0	0	AUTO
0	1	OFF
1	1	ON
1	0	AUTO

These two bits provide the logic to unconditionally turn the modulation on or off or enable modulation in the presence of a forward link signal only (AUTO)

SIGPRES should be self-explanatory, e.g.,  $SIGPRES = 1$  if a forward link signal is detected

The encoded mode bits are defined as follows from information given at the SPA CDR:

ENCMOD1	ENCMOD2	STEERING MODE
0	0	AUTO
0	1	GPCACQ
1	0	MANUAL
1	1	GPCDES

PRIACQOFF = 1 when in alternate acquisition mode, e.g., when using the high gain antenna. Thus,  $\overline{\text{PRIACQOFF}} = 1$  in primary (wide-beam horn) mode. Returning to the defining equation, the transmitter is enabled with  $\text{COMMON} = 1$  and any one or more of the variables MODCON2, SIGPRES, ENCMOD1 or  $\overline{\text{PRIACQOFF}} = 1$ . From the defining tables, MODCON2 = 1 in a nonautomatic mode, e.g., OFF or ON, and ENCMOD = 1 in any nontracking mode, MANUAL or GPCDES.

Thus, the transmitter is enabled if the communications-on bit is one and any one of the following conditions is true:

- (1) The system is in a nontracking mode (GPCDES or MANUAL)
- (2) "Primary" acquisition mode is selected (wide-beam horn)
- (3) Modulation control is nonautomatic, e.g., ON or OFF
- (4) A signal is present on the forward link

Condition (3) is at variance with Paragraph 3.2.3.1.5 of [3], which states that, in the alternate acquisition mode, the transmitter is inhibited except when modulation is commanded on. The transmitter will be enabled if the modulation control switch is in either the OFF or ON position, regardless of acquisition mode. This is not a serious problem, and Rockwell has agreed to accept the logic as is.

## 5.0 SPA MID-BIT DETECTOR FREQUENCY STABILITY

### 5.1 Introduction

The SPA has an adaptive threshold mid-bit detector at the channel 3 mode 1 input port. This port accepts high-rate data and clock at the rate of 2 - 50 Mbps, positions a sampling clock at the data mid-bit, and rate one-half convolutionally encodes the sampled data stream. The sample clock is derived from a two-times clock which, in turn, is locked to the input clock. The two-times clock is a voltage-controlled oscillator based on a Motorola MC1658. Axiomatix has experienced problems with this chip generating considerable noise and has supplanted it with an MC1648. Our concern, discussed in the next section, is that this noise could be added to the return link.

### 5.2 Mid-Bit Detector VCO Noise

The design of a phase-lock-loop with a VCO output covering the 4 - 100 MHz range presents some problems. Not many VCO's operate over a 25:1 frequency range. In this regard, the use of an RC-type of oscillator, where the frequency varies inversely with the value of capacity, is advantageous. An LC oscillator will vary its frequency inversely as the square root of the value of capacity.

The price paid for the greater frequency deviation available from an RC oscillator is the lack of a tuned circuit which will reduce noise sidebands around the operating frequency. The point about VCO noise is graphically illustrated by curves published by Motorola. In addition to the MC1658, which is an RC-type oscillator manufactured by Motorola, they make the MC1648. This device uses an LC-tuned circuit to determine the operating frequency.

Figure 2, which is taken from Motorola's MECL Integrated Circuit Data Book, shows an RMS noise frequency deviation of less than 60 Hz and an operating frequency of 100 MHz for an MC1648. Figure 3 is the comparable curve for the MC1658, and it was taken from the same source. It shows an RMS noise frequency deviation of 5000 Hz at an operating frequency of less than 70 MHz. It also shows a sharp increase in slope, starting at about 40 MHz, so the noise at an operating frequency of 100 MHz may be very high.



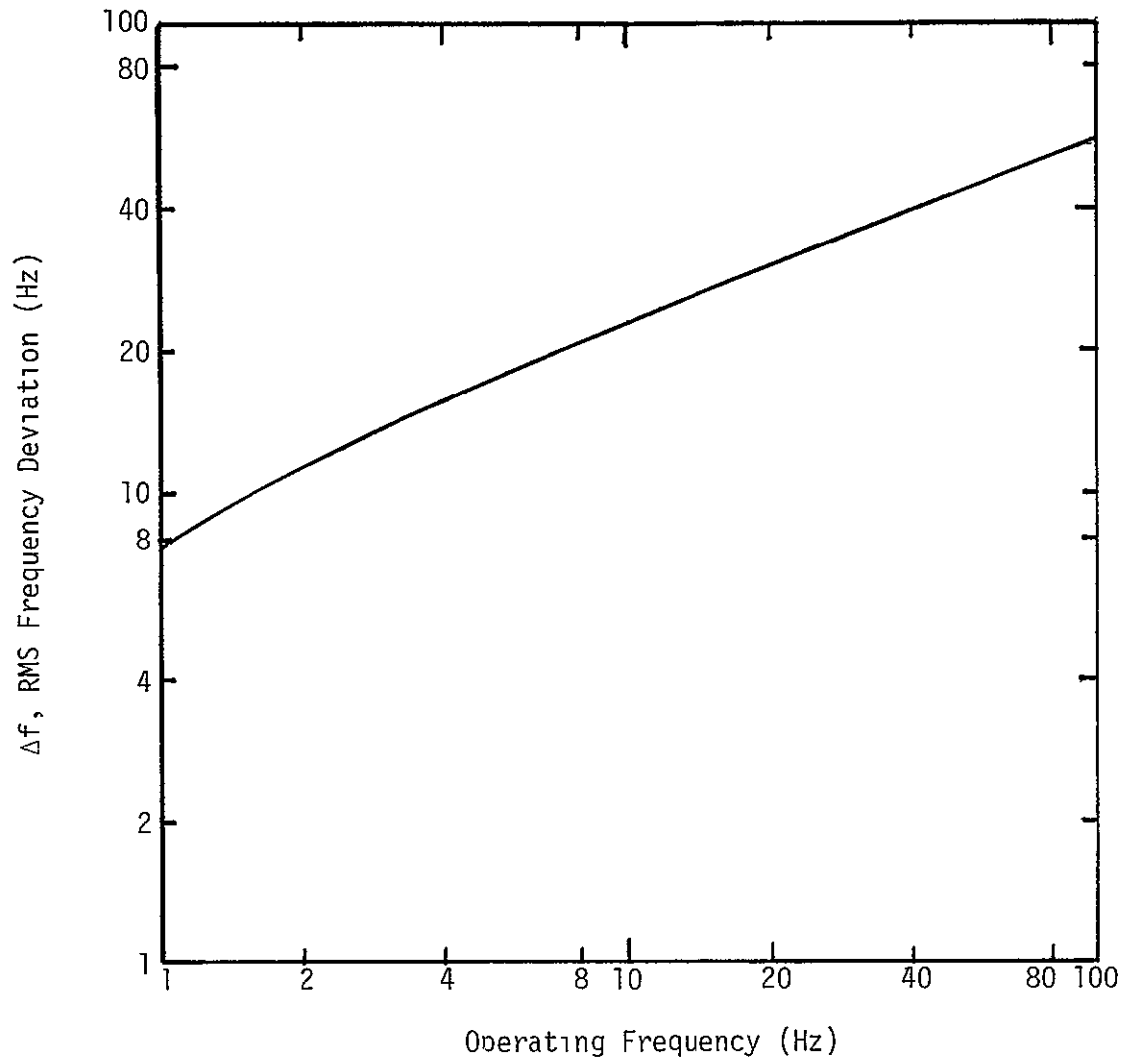


Figure 2 RMS Noise Deviation versus Frequency,  
Motorola MC1648

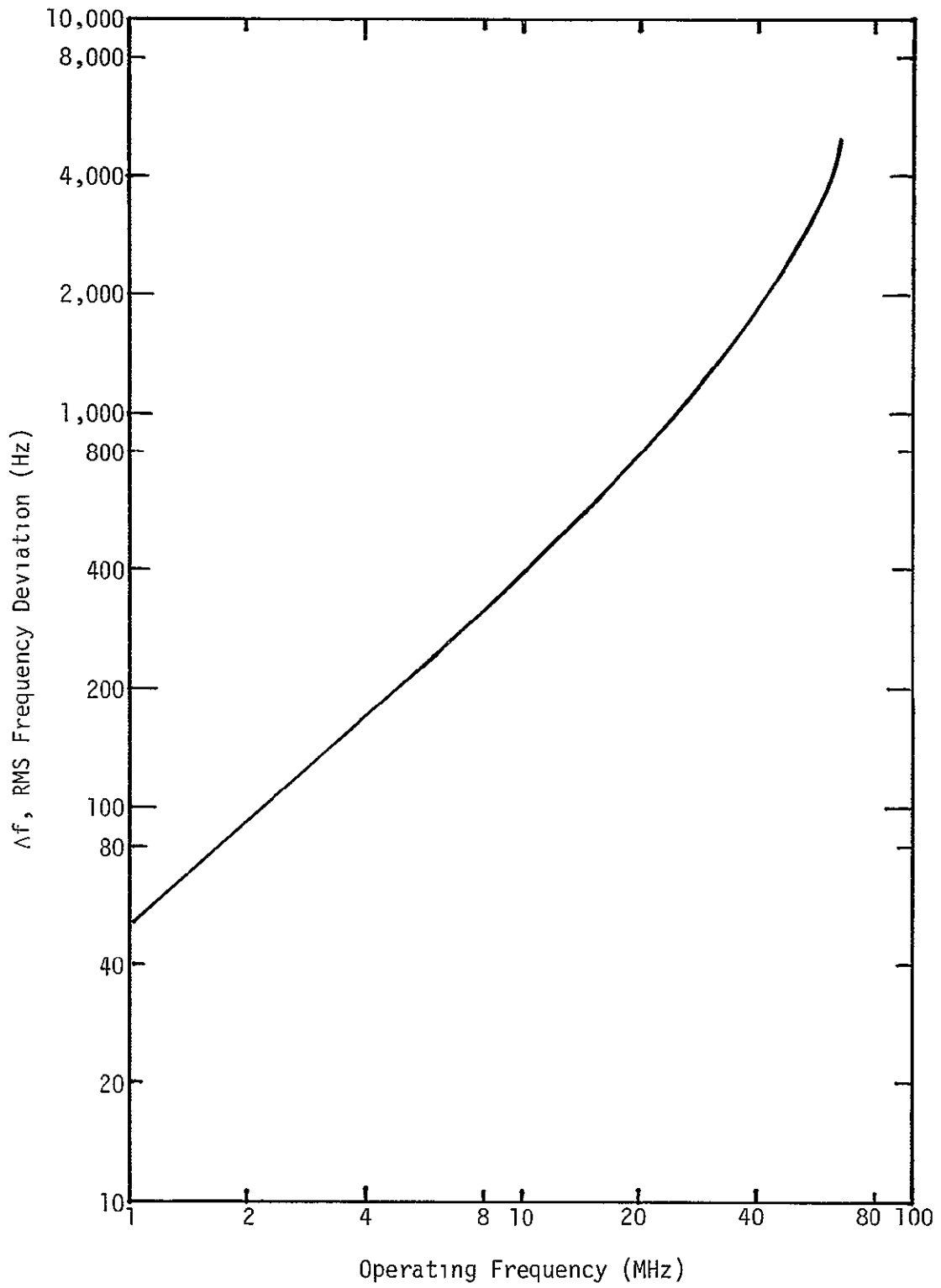


Figure 3 RMS Noise Deviation versus Frequency,  
Motorola MC1658

The problem introduced into a phase-lock-loop by VCO noise is that the only way to reduce the noise is to build a wide bandwidth loop in order to suppress the noise produced by the VCO. The wide bandwidth loop is not capable of smoothing the carrier input which it is tracking. Therefore, a compromise in loop bandwidth will probably be required to provide reasonable smoothing of the input signal tracked, and extreme measures may be necessary to reduce VCO noise. These measures, in addition to very careful filtering of power supplies, interface signals, layout, etc., might include custom selection of the MC1658's for optimum noise characteristics.

### 5.3 Recommendations

The current HAC test procedures do not include a clock noise measurement. Since this noise could affect the return link signal, the noise characteristics of the derived clock should be measured to determine the input on the return link signal.

## 6.0 CRITICAL DESIGN REVIEW TEST DATA EVALUATION

### 6.1 Introduction

In this section, we evaluate the CDR test data. Section 6.2 covers the ADL and ESTL DA LRU test data, and section 6.3 describes the ADL EA-2 test data

### 6.2 ADL and ESTL DA LRU CDR Test Data

This section covers the ADL and ESTL DA LRU CDR test data presented by Hughes Aircraft Company (HAC) on May 27-28, 1980, and the ESTL DA acceptance test data compiled by HAC during December 1980. Both ADL and ESTL DA LRU CDR test data are contained in HAC Report #HS237-2665, and the ESTL DA LRU acceptance data data are contained in HAC Report #HS318-J161, dated December 4, 1980. All three sets of DA test data were compiled using HAC Procedure #TS32012-042, Rev. A, "Ku-Band Acceptance and Qualification Test Specification "

#### 6.2.1 DA Findings

Axiomatix has reviewed more than 538 pages of HAC DA test data by comparing the data with the acceptance criteria listed in the test procedure. Tables 1-3 compare the three sets of test data with the applicable ATP paragraphs and indicates whether or not the specific ATP paragraphs were verified during testing. By reviewing Table 4, it is noted that a number of items were unverified for the ADL DA, such as no  $\alpha/\beta$  lobing tests, no power monitor tests and no monopulse phase verification. It is further noted that the ESTL CDR tests also involved a number of unverified items, such as no  $\alpha/\beta$  lobing tests and no self-tests

Table 4 summarizes those tests listed in the ATP which were not performed on either the ADL or ESTL DA LRU's. Notice that the ESTL DA was more thoroughly tested per the ATP at the LRU level.

In reviewing the test data as indicated in Tables 1-3, a number of tests were not performed due to hardware problems and, in some cases, the tests produced results which were out of specification. We feel that it is not necessary to restate all the ADL and ESTL DA performance problems discovered during the tests simply because Rockwell, NASA, Hughes and Axiomatix are well aware of the problems. For example, it is

HUGHES DA ACCEPTANCE AND QUALIFICATION  
TEST PROCEDURE TS32012-042

Table 1 DA ATP versus DA LRU Tests (ADL/CDR)

Paragraph	Title or Subsections	ADL DA (CDR Test Data)
3.2 3 1 2	Inspection	Verified
3 2.3.1.5	Continuity	Anomalies. J1-C to J1-D, 11K S/B open J1-D to J1-E, 11K S/B open J1-G to J1-H, 45b S/B open J1-A to J1-B not measured J2-A to J2-F, 53 $\Omega$ , S/B ~ 80 $\Omega$ J4-41 to J4-60, 1.8 $\Omega$ S/B open J4-41 to J4-63, 1.8 $\Omega$ S/B open J4-1 to J4-2, open, S/B ~ 110 $\Omega$ J4-4 to J4-5, open, S/B ~ 110 $\Omega$
3.2.3 1.6	Coax cable insertion loss	Not measured
3.2 3.2	Leak (DEA pressure)	Not measured
3.2 3.3	Gimbal assembly functions	N/A (note following gimbal tests conducted at $V_{BUS} = +28$ VDC only)
3.2 3 3 1.3	DEA +15, DEA -15 Boom stow enable II on	Not measured Not verified
3 2.3.3.1.4	Antenna lock Encoder initialization Mechanical limits Obscuration zone Motor shutoff limits	Verified Verified Verified Not verified Reference data only
3.2 3.3.1 5	Antenna deployment Boom stow enable II off	Verified
3.2.3 3.1 6	Antenna stow Boom stow enable II on	Verified
3 2.3 3 2	Gimbal motor torques (deleted from latest test procedure)	Verified
3.2.3 3.3	Rate sensor assembly	N/A
3.2.3 3.3.1	Gimbal drift	Data illegible

HUGHES DA ACCEPTANCE AND QUALIFICATION  
TEST PROCEDURE TS32012-042

Table 1 DA ATP versus DA LRU Tests (ADL/CDR) (Cont'd)

Paragraph	Title or Subsection	ADL DA (CDR Test Data)
3.2.3 3.3 2	Gyro scale factor	Data illegible
3.2 3.3 4	Table D2 gimbal angle encoder	Verified
3 2.3 3 5	Antenna misalignment	Verified
3 2.3 3.6.1	Radar search	Not verified (reference data only)
3 2 3 3.6.3	Table D3 miniscan	Not verified (reference data only)
3.2.3 3 7	Gyro & gimbal noise	Not measured
3 2.3 3.7 2	Gimbal friction	Not measured
3 2.3 3 8	Table D5, $\alpha$ & $\beta$ sig. gen	Not measured
3.2 3.4	DEA functions	N/A
3 2.3 4 1 2	Motor shutoff limits	Not measured (reference data only)
3 2 3 4 1 4	Coax insertion loss	Not measured
3.2.3.4 2	Radar mode power-up sequence	N/A
3.2.3.4.2.1	DEA bus current/LVPS fault off	Verified
3.2 3.4 2 2	DMA narrowbeam	Not measured
3 2.3.4 2 4	Operate status	Verified
3.2.3.4 2.5	Disable transmit enable	Not measured
3.2 3.4 2 6	Transmit enable (30° deploy)	Verified
3 2 3 4.2.7	Transmit off	Not measured
3 2.3.4.2.8	DEA off	Not measured
3.2.3.4.2 9	DEA on	Not measured
3.2.3.4.3	Radar mode frequencies	Verified
3 2.3 4.4	RF power (radar mode)	Verified except for RF power monitor
3 2 3.4 6	Comm. power-up sequence	Verified except that filament timeout not measured
3.2.3.4 8	Radar mode transmit time delay	TWT bypass mode not verified (polaroids illegible)

HUGHES DA ACCEPTANCE AND QUALIFICATION  
TEST PROCEDURE TS32012-042

Table 1. DA ATP versus DA LRU Tests (ADL/CDR) (Cont'd)

Paragraph	Title or Subsection	ADL DA (CDR Test Data)
3 2.3.4 9	Radar Mode Channel Change Time	Verified except that 1 - 4 is 154 $\mu$ s, but S/B < 100 $\mu$ s
3.2 3.4 10	Comm. Mode -- Widebeam	Verified except that power monitor not measured (polaroids illegible)
3 2 3 4 11	Comm Mode -- Narrowbeam	Verified except that power monitor not measured (polaroids illegible)
3.2 3.4 12 2	Self-test -- $\alpha$	Not measured
3.2 3 4 12 3	Transmitter off	Verified
3.2.3.4.12.4	$\alpha$ -track IF amp and phase	Not measured
3.2.3 4.12 5	$\alpha$ -track tests (Cont'd)	Not measured
3 2 3.4 12 6	Self-test -- $\beta/\beta$ track track IF	Not measured
3.2.3.4 12 8	$\beta$ -track tests (Cont'd)	Not measured
3 2 3 4 12 10	Comm mode first LO sample	Verified
3.2 3 4 13	Radar input bandwidth & gain	N/A
3.2 3 4.13.3	Radar diff. input passband	Verified (polaroid print data cards illegible)
3.2.3.4.13.4	Comm. diff input passband	Amplitude not verified (polaroid print data cards illegible)
3.2.3.4.13.5	Radar second IF (10 MHz BW)	Verified (polaroid print data cards illegible)
3.2 3.4.13.6	Radar/comm sum input passband	Verified (polaroid print data cards illegible)
3 2 3 4.13 7	Data IF	Verified (polaroid print data cards illegible)
3 2 3.4.14	AGC	Verified
3.2 3 4.15.2	Radar sum-signal rejection	Verified
3 2 3.4.15.3	Image frequency	Verified
3 2 3.4.15.4	Spur rejection -- track IF	Verified
3 2.3.4 15.5	Comm sum signal rejection	Verified
3.2.3.4.15 6	Radar spur rejection	Verified

HUGHES DA ACCEPTANCE AND QUALIFICATION  
TEST PROCEDURE TS32012-042

Table 1. DA ATP versus DA LRU Tests (ADL/CDR) (Cont'd)

Paragraph	Title or Subsection	ADL DA (CDR Test Data)
3.2.3.4 15.11	Main bang leakage	Verified
3.2.3.4.15 12	TWT bypass--10 MHz bandwidth	Not verified
3 2.3.4 15 13	High power--3 MHz bandwidth	Verified
3.2 3.4 16 1	Enable sum channel	Not verified
3.2.3.4.16 2	Sum long pulse	Verified
3 2 3 4.16 3	Diff long pulse	Verified
3 2.4	Monopulse phase verification	Not verified



HUGHES DA ACCEPTANCE AND QUALIFICATION  
TEST PROCEDURE TS32012-042

Table 2. DA ATP versus DA LRU Tests (ESTL/CDR)

Paragraph	Title or Subsections	ESTL DA (CDR Test Data)
3 2.3 1.2	Inspection	Verified
3 2 3 1.5	Continuity	Anomalies. CP12-S to CP12-T, 71 1K S/B ~ 11K CP12-W to CP12-X, 22.7K S/B ~ 40K CP12-P to CP12-R, 6.86K S/B ~ 450Ω CP12-G to CP12-H, 50 S/B ~ 80Ω CP40B-P to CP40B-R, 118Ω S/B ~ 110Ω
3 2 3.1.6	Coax cable insertion loss	Not measured
3 2 3.2	Leak (DEA pressure)	Not measured
3.2.3 3.1.3	Gimbal assembly functions	N/A (Note: following gimbal tests conducted at $V_{BUS} = +28$ VDC only)
3 2.3.3 1 4	DEA +15, DEA -15 Boom stow enable II on	OK Verified
3.2.3 3 1.4	Antenna lock Encoder initialization Mechanical limits Obscuration zone Motor shutoff limits	Not verified Verified Not verified Not verified Reference data only
3.2.3 3.1 5	Antenna deployment Boom stow enable II off	Verified
3.2 3.3 1 6	Antenna stow Boom stow enable II on	Verified
3.2 3 3.2	Gimbal motor torques (Deleted from latest test procedure)	Verified
3 2.3 3.3	Rate sensor assembly	N/A
3 2.3.3 3 1	Gimbal drift	Measured, but no pass/fail criteria listed
3 2.3.3.3.2	Gyro scale factor	Verified
3 2 3 3 4	Table D2 gimbal angle encoder	Verified

HUGHES DA ACCEPTANCE AND QUALIFICATION  
TEST PROCEDURE TS32012-042

Table 2. DA ATP versus DA LRU Tests (ESTL/CDR) (Cont'd)

Paragraph	Title or Subsections	ESTL DA (CDR Test Data)
3.2 3.3 5	Antenna misalignment	Verified
3 2 3 3.6.1	Radar search	Verified (reference data only)
3.2.3.3 6 3	Table D3 miniscan	Verified (reference data only)
3 2 3.3 7	Gyro and gimbal noise	Verified
3 2.3.3 7 2	Gimbal friction	Not measured
3 2.3.3.8	Table D5, $\alpha$ & $\beta$ sig. gen.	Verified
3 2.3 4	DEA functions	N/A
3 2.3.4.1 2	Motor shutoff limits	Verified
3.2 3.4.1 4	Coax insertion loss	Verified
3.2.3 4 2	Radar mode power-up sequence	N/A
3 2.3.4 2.1	DEA bus current/LVPS fault off	Verified
3 2.3.4.2.2	DMA narrowbeam	Verified
3.2.3 4.2.4	Operate status	Verified
3.2.3.4.2.5	Disable transmit enable	Verified
3 2 3.4.2.6	Transmit enable (30° deploy)	Verified
3.2.3 4 2.7	Transmit off	Verified
3 2.3.4 2 8	DEA off	Not measured
3.2.3 4.2 9	DEA on	Not measured
3.2.3 4.3	Radar mode frequencies	Verified
3 2.3 4 4	RF power (radar mode)	Medium & low RF power outputs below specification
3 2.3 4.6	Comm power-up sequence	Verified except that filament timeout 10 seconds too long
3.2.3.4.8	Radar mode transmit time delay	Verified (polaroid print data cards illegible)
3.2.3.4.9	Radar mode channel change time	Verified

HUGHES DA ACCEPTANCE AND QUALIFICATION  
TEST PROCEDURE TS32012-042

Table 2. DA ATP versus DA LRU Tests (ESTL/CDR) (Cont'd)

Paragraph	Title or Subsections	ESTL DA (CDR Test Data)
3.2.3.4 10	Comm. mode--widebeam	Verified except RF power output below specification by 1 39 dBm (polaroid illegible)
3.2.3 4 11	Comm. mode--narrowbeam	Verified (polaroid print data card illegible)
3.2 3 4.12.2	Self-test-- $\alpha$	Verified
3.2.3 4 12.3	Transmitter off	Verified
3 2.3.4 12 4	$\alpha$ -track IF amp. and phase	Not measured ( $\alpha$ -track nonoperative)
3.2 3 4 12.5	$\alpha$ -track tests (cont'd)	Not measured ( $\alpha$ -track nonoperative)
3.2.3.4 12 6	Self-test-- $\beta/\beta$ track track IF	Not measured except for $\beta$ lobing current ( $\beta$ -track nonoperational)
3.2.3 4.12.8	$\beta$ -track tests (cont'd)	Not measured ( $\beta$ -track nonoperative)
3.2.3.4.12.10	Comm. mode first LO sample	Verified
3.2.3.4 13	Radar input bandwidth & gain	N/A
3 2.3.4 13.3	Radar diff. input passband	Verified (polaroid print data cards illegible)
3 2.3 4.13 4	Comm. diff. input passband	Verified (polaroid print data card illegible)
3.2.3.4.13 5	Radar second IF (10 MHz BW)	Verified (polaroid print data cards illegible)
3 2 3.4.13 6	Radar/Comm sum input passband	Verified (polaroid print data cards illegible)
3 2.3.4 13.7	Data IF	Verified (polaroid print data card illegible)
3.2.3 4.14	AGC	Verified
3 2.3.4.15.2	Radar sum-signal rejection	Verified
3.2 3.4 15.3	Image frequency	Verified
3.2 3.4.15.4	Spur rejection--track IF	Verified
3.2.3.4 15.5	Comm sum signal rejection	Verified
3.2.3.4.15.6	Radar spur rejection	Verified
3 2.3.4.15 11	Main bang leakage	Verified

HUGHES DA ACCEPTANCE AND QUALIFICATION  
TEST PROCEDURE TS32012-042

Table 2. DA ATP versus DA LRU Tests (ESTL/CDR) (Cont'd)

Paragraph	Title or Subsections	ESTL DA (CDR Test Data)
3.2 3 4 15.12	TWT bypass--10 MHz bandwidth	Verified
3.2 3 4.15.13	High power--3 MHz bandwidth	Verified (polaroid print data card illegible)
3.2.3.4.16.1	Enable sum channel	Not verified
3 2 3 4 16.2	Sum long pulse	Verified (polaroid print data cards illegible)
3.2.3 4.16.3	Diff. long pulse	Verified (polaroid print data cards illegible)
3 2.4	Monopulse phase verification	Not verified

HUGHES DA ACCEPTANCE AND QUALIFICATION  
TEST PROCEDURE TS32012-042

Table 3. DA ATP versus DA LRU Tests (ESTL/ATP)

Paragraph	Title or Subsections	ESTL DA (ATP Test Data)
3.2 3.1 2	Inspection	Verified
3 2 3.1.5	Continuity	Verified
3.2 3.1.6	Coax cable insertion loss	Not measured
3 2 3 2	Leak (DEA pressure)	Out of specification
3.2.3.3	Gimbal assembly functions	N/A (Note: Following gimbal tests conducted at $V_{BUS} = +28$ VDC only)
3.2 3 3.1 3	DEA +15, DEA -15 Boom stow enable II on	OK Verified
3.2 3 3.1 4	Antenna lock Encoder initialization Mechanical limits Obscuration zone Motor shutoff limits	Deleted Deleted Deleted Deleted Reference data only
3.2.3.3.1.5	Antenna Deployment Boom stow enable II off	Verified
3 2 3 3 1 6	Antenna stow Boom stow enable II on	Verified
3.2 3.3.2	Gimbal motor torques (Deleted from latest test procedure)	Deleted
3.2 3 3 3	Rate sensor assembly	N/A
3.2 3.3 3.1	Gimbal drift	Verified
3.2.3.3.3.2	Gyro scale factor	Verified
3.2.3 3 4	Table D2 gimbal angle encoder	Verified, but criteria is less than $\pm 3$ counts and some points were -3
3.2.3 3 5	Antenna misalignment	Verified
3.2.3.3.6.1	Radar search	Not measured (reference data only)

HUGHES DA ACCEPTANCE AND QUALIFICATION  
TEST PROCEDURE TS32012-042

Table 3 DA ATP versus DA LRU Tests (ESTL/ATP) (Cont'd)

Paragraph	Title or Subsections	ESTL DA (ATP Test Data)
3 2.3 3 6.3	Table D3 miniscan	Verified (reference data only)
3.2.3 3 7	Gyro and gimbal noise	Deleted
3.2.3 3 7 2	Gimbal friction	Verified
3 2 3 3 8	Table D5, $\alpha$ & $\beta$ sig gen	Verified
3.2 3 4	DEA functions	N/A
3 2.3.4 1.2	Motor shutoff limits	Not measured (reference data only)
3 2 3 4 1 4	Coax insertion loss	Verified
3 2.3.4 2	Radar mode power-up sequence	N/A
3 2 3 4 2.1	DEA bus current/LVPS fault off	Verified (filament timeout out of specification)
3 2 3 4 2.2	DMA narrowbeam	Verified
3 2.3 4 2.4	Operate status	Verified
3 2.3 4 2.5	Disable transmit enable	Verified
3.2.3 4.2.6	Transmit enable (30° deploy)	Verified
3 2.3 4 2 7	Transmit off	Verified
3.2.3 4 2.8	DEA off	Out of specification
3.2 3.4.2.9	DEA on	Verified
3.2 3.4.3	Radar mode frequencies	Verified
3.2 3 4.4	RF power (radar mode)	Verified except low RF power output out of spec by 0.18 dB
3.2.3.4.6	Comm power-up sequence	Verified except filament timeout out of spec by 2 seconds
3.2.3 4 8	Radar mode transmit time delay	Verified
3 2.3 4 9	Radar mode channel change time	Verified
3.2 3.4 10	Comm. mode--widebeam	Verified
3.2.3.4.11	Comm. mode--narrowbeam	verified
3.2.3 4 12 2	Self-test-- $\alpha$	Verified

HUGHES DA ACCEPTANCE AND QUALIFICATION  
TEST PROCEDURE TS32012-042

Table 3. DA ATP versus DA LRU Tests (ESTL/ATP) (Cont'd)

Paragraph	Title or Subsections	ESTL DA (ATP Test Data)
3.2.3.4.12.3	Transmitter off	Verified
3 2 3 4 12 4	$\alpha$ -track IF amp and phase	Not measured
3.2 3 4 12 5	$\alpha$ -track tests (cont'd)	Not measured
3 2.3.4 12.6	Self-test - $\beta$ / $\beta$ track track IF	Not measured
3 2 3.4.12.8	$\beta$ -track tests (cont'd)	Not measured
3 2.3.4.12 10	Comm. mode first LO sample	Verified
3 2.3 4.13	Radar input bandwidth & gain	N/A
3 2.3 4 13 3	Radar diff input passband	Verified
3 2.3 4 13.4	Comm. diff input passband	Verified
3 2.3 4 13.5	Radar second IF (10 MHz BW)	Verified
3.2.3.4.13 6	Radar/comm sum input passband	Verified
3.2 3.4 13.7	Data IF	Verified
3.2 3 4.14	AGC	Verified
3.2.3.4.15 2	Radar sum-signal rejection	Verified
3.2.3 4 15 3	Image frequency	Verified
3.2 3.4.15 4	Spur rejection--track	Verified
3.2.3 4.15 5	Comm sum signal rejection	Verified
3.2 3 4.15 6	Radar spur rejection	Verified
3.2 3 4.15 11	Main bang leakage	Verified
3.2.3.4.15 12	TWT bypass--10 MHz bandwidth	Verified
3 2 3.4.15.13	High power--3 MHz bandwidth	Verified
3 2 3 4 16.1	Enable sum channel	Verified
3.2 3.4.16.2	Sum long pulse	Verified
3 2 3.4.16.3	Diff long pulse	Verified
3.2 4	Monopulse phase verification	Verified, but no pass/fail criteria listed.

Table 4. ADL and ESTL DA Test Summary

ADL DA (CDR Test Data)	ESTL DA (CDR Test Data)	ESTL DA (ATP Test Data)
No $\alpha/\beta$ lobing tests	No $\alpha/\beta$ lobing tests	No self-tests
No power monitor tests	No self-tests	No tests as a function of bus voltage
No self-tests	No environmental tests	
No environmental tests	No monopulse verification tests	
No scanning tests	No tests as a function of bus voltage	
No monopulse verification tests		
No tests as a function of bus voltage		

well known that (1) there is no self-test at this time, (2) a problem exists with the RF power monitor, (3) the ADL antenna has poor performance compared to the ESTL antenna, (4) the ADL has a  $4^\circ$  gimbal clocking error, and (5) the monopulse phase tests were not performed on the ADL unit

However, other problems surfaced during testing. For example, the gimbal angle encoder stability requirements are less than  $\pm 3$  counts, but the ESTL ATP data has seven out of 15 angle settings where the count was either +3 or -3, which corresponds to a  $\pm 0.264^\circ$  error. The requirements specify a maximum error of  $\pm 0.166^\circ$ .

The initial ESTL DA CDR test data indicated that the medium and low RF power level outputs were below specification. This problem has been addressed, but when retested with the ATP, the ESTL DA still is out of specification by 0.18 dB at the low RF power level.

The ATP lists a very detailed procedure for verifying the monopulse phase, except that the ATP fails to list any accept/reject criteria. One area of concern is that no monopulse phase verification tests were conducted on the ADL DA and, since there is no accept/reject criteria listed in the ATP, one cannot draw any conclusions from the ESTL DA phase verification tests either.

A major area of concern is that the ATP was conducted at the nominal bus voltage of 28 VDC--not over the range of 24 - 32 VDC. Many LRU problems are discovered when acceptance testing is conducted as a function of bus voltage, and it is possible that all the DA problems have not yet surfaced.



The greatest area of concern deals with the ATP itself. As compared to the more than 538 pages of the HAC DA test data to the HAC ATP, the test data review has not produced any significant surprises. However, before one concludes that successfully passing the HAC DA ATP guarantees a properly functioning DA, Axiomatix will reemphasize a fundamental flaw in the HAC test program.

The Hughes DA ATP, #TS32012-042, Rev. A, was designed to verify Hughes Document #DS32012-031, "Development Specification Deployed Assembly for the Ku-Band Integrated Radar and Communications Equipment," but was not designed to verify Rockwell Specification #MC409-0025, Rev B, "Integrated Communications and Radar Equipment, Ku-Band." Axiomatix previously commented on this situation per a memo to Jim Kelly of NASA, dated September 11, 1980, as shown in Appendix A.

The basic problem is that the Rockwell specification is the baseline document and there is a very low degree of correlation between the Hughes ATP and the Rockwell specification. Eventually, through a very tedious examination of the HAC ATP and the Rockwell requirements, some correlation would exist but, at this time, no such comparison has been performed. Table 5 gives some examples of the different requirements listed in each document and how specific ATP paragraphs address only portions of the applicable Rockwell paragraphs.

The purpose of Table 5 is to give the reader a flavor of the problems faced when comparing both documents. Ideally, if a one-to-one correspondence existed between the requirements, it would be very straightforward to determine the adequacy of the acceptance testing. As it now stands, Axiomatix can state that the ESTL DA passed most of the HAC ATP but without an exhaustive paragraph-by-paragraph comparison, it is unknown at this time whether or not the DA LRU really meets the requirements listed in the Rockwell documentation.

Both Axiomatix and Rockwell have repeatedly brought up this problem, plans have been formulated to address this situation, yet nothing has happened to change it. One of the purposes of the TM01 document that is now two years late in being issued by HAC is to address the testing program and provide a means with which to have some confidence that the hardware is meeting Rockwell requirements.

Table 5 Examples of Differences Between HAC and RI Requirements

Item	HAC ATP Paragraph HS32012-Q42	HAC-Specified Requirements DS32012-031	Rockwell Specification Paragraph MC409-0025, Rev. B	Rockwell-Specified Requirements MC409-0025, Rev. B
RF power--high	3 2 3 4 4	18 ± 3.5 dBm	30 3 2.1.2.2.3b	16.99 to 18.75 dBm
RF power--med.	3 2 3 4.4	-12 ± 3 dB from high	30 3.2.1 2.2.3b Paragraphs 30.3.2 1 2.2.3a, c-k spread throughout ATP	-12 ± 2 dB from high
Radar mode transmit-TWT bypass	3.2.3.4.8	51 ± 17 ns	30.3.1.2.4.8.1m Paragraphs 30.3.1.2.4.8.1a-l spread throughout ATP	55.5 ± 12 ns
AGC dynamic range radar mode 3	3 2 3 4 14	-	-	-
• Step IF AGC Atten.	-	-30 ± 2.5 dB	30.3.2 1.2 2.5s	-30 ± 2 dB
• Transmitter Limiter AGC	-	-30 ± 1.5 dB	30.3.2.1.2 2 5r	-30 ± 1 dB
• Linear AGC-5	-	-42 ± 4 dB	30 3.2.1.2 2.5t Paragraphs 30.3.2.1.2.2.5a-q u,v spread throughout ATP	-42 ± 2 dB

### 6.2.2 DA Conclusions/Recommendations

As per Table 4, a number of tests were not performed for both the ADL DA and the ESTL DA. However, since the ADL unit is being used by Rockwell to verify the Shuttle interfaces only, the testing performed by HAC on the ADL DA has been adequate. Since the ESTL DA will be used primarily at the ESTL to verify link performance, again, HAC testing has been sufficient.

The major issue of correlating the HAC ATP to the RI specification still remains, however, and it is Axiomatix's position that this issue must be aggressively addressed. Without the TMOI or an equivalent document to tie the HAC ATP to the Rockwell requirements, there is no confidence that HAC is delivering properly functioning DA's. As Axiomatix has repeatedly stated, the longer this issue remains unresolved, the greater the probability that future DA's may have problems which will not be discovered until late in the Ku-band program. Axiomatix therefore recommends that either Rockwell, Hughes or Axiomatix perform the task of correlating the Hughes ATP with the Rockwell requirements, and that this task should be performed as soon as possible.

### 6.3 ADL EA-2 LRU Test Data

This section covers the ADL EA-2 LRU CDR test data presented by Hughes on September 25, 1980. The tests were conducted during June 1980 to a preliminary copy of HAC ATP #TP32012-076 with the test results contained in HAC Report #HS237-3031-1, dated September 29, 1980.

#### 6.3.1 EA-2 Findings

Axiomatix has reviewed the HAC ADL EA-2 LRU CDR test data by comparing the data with the acceptance criteria listed in the ATP. For a first cut, the prerelease version of the ATP is very complete, with the functional tests divided into the following categories:

- Power
- Timing
- Detection Sensitivity
- Sidelobe Test
- Velocity Processing
- Acquisition Program
- Serial Data
- False Alarm Rate
- Automatic Gain Control
- Range Processor
- Angle Processing
- Track Program Timing

The ATP exercised all of the EA-2 functions and, for the most part, the ADL EA-2 performed within specification tolerances. However, some anomalies such as a high false alarm rate did occur. All of the out-of-specification test data are the result of EA-2 problems which were fully documented by either Axiomatix, Hughes and/or Rockwell previously. Since the EA-2 problems are known to all parties, Axiomatix feels that it is not necessary to restate them in this report.

Even though the ADL EA-2 LRU CDR test data review did not uncover any new EA-2 problems, the review has given Axiomatix an opportunity to study the EA-2 ATP in greater detail. As mentioned in the DA section, the major Axiomatix concern deals with the low degree of correlation between the Hughes DA specification and the Rockwell DA requirements. On the other hand, with the EA-2 ATP, the procedure is written in a different format than the DA ATP, and the different EA-2 format contributes to a very high degree of correlation with the Rockwell specification. Each of the EA-2 ATP functional test sections, as listed above, deals with a major requirement or a significant portion of a major requirement within the Rockwell specification, making cross-correlation much easier.

Table 6 is the Rockwell specification/Hughes EA-2 ATP verification matrix. Note that, for the most part, the Hughes ATP verifies the applicable Rockwell paragraphs.

Tables 7-10 are also matrices of the three radar operating phases (search, acquisition and track) versus designated ranges, and each table indicates in which mode (GPC acquisition, GPC designate, autotrack and manual) and target type (active and passive) given parameters, such as timing synchronization signals, are measured and verified. The active modes and the passive autotrack and passive manual modes are not shown as a function of designated range because range designates are not used in these radar modes. By studying Tables 7-10, it is noted that a fairly comprehensive number of tests are being conducted.

On the other hand, Table 11 is the summary of untested Rockwell specification paragraphs. The first two items listed in Table 11 require verification of the interface signals only, and item 3 cannot be addressed until Rockwell defines the GPC designate, passive mode, operation. The last four items in Table 11 are testing oversights which must be addressed since verification is required per the Rockwell ATP requirements.

Table 6. EA-2 LRU

Rockwell Specification MC 409-0025, Rev B		Req'd per Table 40-IX Acceptance Tests	N/A	Hughes Acceptance Test Procedure TP 32012-076
Paragraph Number	Paragraph Title			Paragraph Number
40	Electronic Assembly EA-2		X	Signals supplied by test equipment; therefore, EA-2 implicitly tested.
40.1	Scope		X	
40.2	Applicable Documents		X	
40.3	Requirements		X	
40 3.1	Item Definition		X	
40.3.1 1	Item Diagram		X	
40 3.1.2	Interface Definition		X	
40.3 1.2.1	Electrical Power		X	
40.3 1 2 2	Mechanical		X	
40.3.1.2 2.1	Connector Location and Pin Alignment		X	
40.3 1 2 3	Cooling		X	
40 3.1.2 4	Signal Interface Definition		X	
40.3.1.2 4.1	EA-1A Interface		X	
40.3.1.2.4 1 1	Serial Digital I/O Characteristics	X		
40.3.1.2.4.1.1.1	EA-2A Serial Input Data Characteristics	X		
40.3 1.2.4.1 1.2	EA-2A Clock Characteristics	X		
40.3.1.2.4.1.1.3	EA-2A Data Cover Pulse Characteristics	X		
40.3.1.2.4.1.1.4	EA-2A Status Cover Pulse Characteristics	X		

Table 6. EA-2 LRU (Cont'd)

Rockwell Specification MC 409-0025, Rev B		Req'd per Table 40-IX Acceptance Tests	N/A	Hughes Acceptance Test Procedure TP 32012-076
Paragraph Number	Paragraph Title			Paragraph Number
40.3.1.2 4.1.2	Controls and Status Discrettes		X	
Input a	Radar On	X		2.2.1
b	Radar Standby		X	
c.	Radar Power Low	X		2.7.15
d.	Radar Power Medium	X		2.7.15
Output a.	Target Present	X		2.12
b	Lobing Enable	X		<u>Not verified</u>
c.	Lobing Alpha/Beta	X		<u>Not verified</u>
d.	Lobing Phase 0 - 180°	X		<u>Not verified</u>
40.3.1 2.4.1.3	Analog Signal Characteristics		X	
40.3.1.2 4 1.3.1	Radar Signal Strength	X		2 7 12
40.3.1.2.4.1.3.2	Alpha Error/Beta Error	X		2.11
40 3 1.2 4.1.3.3	156 MHz Reference Frequency	X		Signal supplied by test equipment; therefore, EA-2 implicitly tested.
40.3.1.2.4.2	DA-A Interface		X	
40 3.1.2 4.2.1	Controls and Status Discrettes		X	
a	Radar Power Low	X		2.7.15
b.	Radar Power Medium	X		2.7.15
c.	Frequency Select A, B, C	X		2 4.2.1, 2.4.2.2, 2.4.2.3

Table 6 EA-2 LRU (Cont'd)

Rockwell Specification MC 409-0025, Rev B		Req'd per Table 40-IX Acceptance Tests	N/A	Hughes Acceptance Test Procedure TP 32012-076
Paragraph Number	Paragraph Title			Paragraph Number
d.	High Sample Rate Select	X		Verified throughout ATP
e	Radar Sum Enable	X		<u>Not verified</u>
f	Radar Difference Enable	X		<u>Not verified</u>
g.	TWT Bypass Enable	X		Verified throughout ATP
h	Transmitter Limiter AGC	X		<u>Not verified</u>
i.	First IF Step AGC	X		<u>Not verified</u>
40.3.1.2.4 2.2	Analog Signal Characteristics		X	
40.3.1.2.4.2.2 1	Linear AGC	X		2.7
40.3.1.2.4.2.3	Timing Pulses I/O Characteristics		X	
40.3.1.2.4.2.3 1	Transmit Gate	X		2.4
40.3.1.2.4.2.3 2	Receiver Gate	X		2.4
40.3.1.2.4.2.3 3	Exciter Gate	X		2.4
40.3.1.2.4.2.4	Radar Second IF	X		Signal supplied by test equipment, therefore, EA-2 implicitly tested.
40.3.1.2.4.3	LRU Test Connector		X	
40.3.1.2.4.3 1	GSE Checkout	X		} Verified by conducting ATP
40.3.1.2.4.3.2	SRU Checkout	X		
40.3.1.2.5	Instrumentation	X		
40.3.1.3	Item Identification		X	

Table 6 EA-2 LRU (Cont'd)

Rockwell Specification MC 409-0025, Rev B		Req'd per Table 40-IX Acceptance Tests	N/A	Hughes Acceptance Test Procedure TP 32012-076
Paragraph Number	Paragraph Title			Paragraph Number
40 3 2	Characteristics		X	
40.3.2 1	Performance		X	
40.3.2.1.1	Life Requirements		X	
40 3 2.1.1 1	Operating Life		X	
40.3.2.1 1.2	Useful Life		X	
40.3.2.1.1.3	Shelf Life		X	
40 3.2 1 2	Functional Performance Requirements		X	
40 3.2 1.2.1	Primary Power Consumption	X		2.2.1
40 3 2 1.2 1.1	Duty Cycle		X	
40.3.2.1.2 1 2	Stabilization		X	
40 3 2.1.2 2	Operating Modes		X	
40 3.2 1.2.3	Antenna Steering Modes		X	
40.3.2.1.2.3.1	GPC Acquisition, Passive Mode	X		2.4, 2.12, 2.13
40 3.2 1 2.3.1.1	Search Phase	X		2.4
40.3.2 1.2.3.1 2	Acquisition Phase	X		2.4, 2.12
40.3 2.1.2.3 1.3	Initial Track Phase	X		2.4, 2.13
40 3 2.1.2 3 1.4	Final Track Phase	X		2.4, 2.13
40.3.2.1.2.3.2	GPC Designate, Passive Mode (TBS)	X		<u>Not verified</u>



Table 6. EA-2 LRU (Cont'd)

Rockwell Specification MC 409-0025, Rev B		Req'd per Table 40-IX Acceptance Tests	N/A	Hughes Acceptance Test Procedure TP 32012-076
Paragraph Number	Paragraph Title			Paragraph Number
40.3.2.1.2 3.3	Autotrack, Passive Mode	X		2.12, 2.13, 2.4
40.3.2.1.2.3.3.1	Search Phase	X		2.4
40.3.2.1.2.3.3.2	Acquisition Phase	X		<u>Not verified</u>
40.3.2.1.2.3.3.3	Initial Track	X		2.13, 2.4
40.3.2.1.2.3.3.4	Final Track	X		2.13, 2.4
40.3.2.1.2.3.4	Manual, Passive Mode	X		2.4
40.3.2.1.2.3.5	GPC Acquisition, Active Mode	X		2.12, 2.13, 2.4
40.3.2.1.2.3.5.1	Search Phase	X		2.4
40.3.2.1.2.3.5.2	Acquisition Phase	X		2.12, 2.13, 2.4
40.3.2.1.2.3.5.3	Track Phase	X		2.13, 2.4
40.3.2.1.2.3.6	GPC Designate, Active Mode	X		2.12, 2.13, 2.4
40.3.2.1.2.3.7	Autotrack, Active Mode	X		2.12, 2.13, 2.4
40.3.2.1.2.3.8	Manual, Active Mode	X		2.12, 2.13, 2.4
40.3.2.1.2.4	Prob. of Detection & False Alarm Rate	X		2.5, 2.6
40.3.2.1.2.5	Parameter Measurement Accuracies	X		2.9, 2.10, 2.11
40.3.2.1.2.5.1	Parameter Meas. Accuracy Convergence Time	X		<u>Not verified</u>
40.3.2.1.2.5.2	Measurement Data Output Sample Rate	X		<u>Not verified</u>
40.3.2.1.2.6	Clutter Performance	X		<u>Not verified</u>

Table 6 EA-2 LRU (Cont'd)

Rockwell Specification MC 409-0025, Rev B		Req'd per Table 40-IX Acceptance Tests	N/A	Hughes Acceptance Test Procedure TP 32012-076
Paragraph Number	Paragraph Title			Paragraph Number
40.3 2.1.2.7	Sidelobe Detection Discrimination	X		2.8, 2.12
40.3.2.1.2.8	Automatic Gain Control	X		2.7
40.3.2.1.2.8.1	Search Gain Control	X		2.7
40.3.2.1.2.8.2	Track Gain Control	X		2.7
40.3.2.1.2.9	Received Signal Amplitude Estimation	X		2.7
40.3.2.1.2.10	Status Flag Output Command Logic	X		2.3
40.3.2.1.2.10.1	Angle Rate Data Valid	X		2.3
40.3.2.1.2.10.2	Angle Data Valid	X		2.3
40.3.2.1.2.10.3	Angle Track Enable	X		2.3
40.3.2.1.2.10.4	Generating Test Target	X		2.3
40.3.2.1.2.10.5	Operate	X		2.3
40.3.2.1.2.10.6	Range Data Valid	X		2.3
40.3.2.1.2.10.7	Range Rate Data Valid	X		2.3
40.3.2.1.2.10.8	Miniscan	X		2.3
40.3.2.1.2.10.9	Sidelobe	X		2.3
40.3.2.1.2.10.10	Track	X		2.3
40.3.2.1.2.11	Built-In Test	X		2.4
40.3.2.1.2.12	GSE Test Points (GSE Connectors)	X		Tested throughout ATP
40.3.2.1.2.13	Electrical Power Consumption	X		2.2

Table 7 Timing Synchronization Signals

Designated Ranges		Search	Acquisition	Track
nm1	ft			
> 18.9	> 114,912			
9.3 - 18.9	56,544 to 114,912	{ Passive GPC $R_D = 94,000$ ft { (¶2.4.4.2)	{ Passive GPC $R_D = 94,000$ ft { (¶2.4.4.5) (Partial tests)	{ Passive* $R_D = 100,000$ ft { (¶2.4.4.7)
7.2 - 9.3	43,776 to 56,544			
3.8 - 7.2	23,104 to 43,776			
1.9 - 3.8	11,552 to 23,104			
0.95 - 1.9	5,776 to 11,552			
0.42 - 0.95	2,554 to 5,776	{ Passive GPC $R_D = 4,000$ ft { (¶2.4.4.1)	{ Passive GPC $R_D = 4,000$ ft { (¶2.4.4.5) (Partial tests)	{ Passive* $R_D = 4,000$ ft { (¶2.4.4.6)
0.016 - 0.42	97 - 2,554			
		{ Passive Manual/Auto { (¶2.4.4.3) $R_T = 4,000$ ft  { Active $R_T = 4,000$ ft { (¶2.4.4.4)	{ Active $R_T = 4,000$ ft { (¶2.4.4.5) (Partial tests)	{ Active $R_T = 4,000$ ft { (¶2.4.4.6)  { Active $R_T = 1,000,000$ ft { (¶2.4.4.6)

\*GPC & auto mode same

$R_D$  = Range Designate;  $R_T$  = Range of Target; Paragraphs refer to Hughes TS 32012-076 (EA-2 ATP)

Table 8. Deployed Assembly Gates

Designated Ranges		Search	Acquisition	Track
nm	ft			
> 18.9	> 114,912	{ Passive GPC $R_D = 128,000$ ft { (¶2.4.3.8)		
9.3 - 18.9	56,544 to 114,912			
7.2 - 9.3	43,776 to 56,544			{ Passive* $R_D = 48,000$ ft { (¶2.4.3.16) w/pulse width override { Passive* $R_D = 48,000$ ft { (¶2.4.3.17) w/o pulse width override
3.8 - 7.2	23,104 to 43,776	{ Passive GPC $R_D = 28,000$ ft { (¶2.4.3.7)		{ Passive* $R_D = 28,000$ ft { (¶2.4.3.15)
1.9 - 3.8	11,552 to 23,104	{ Passive GPC $R_D = 18,000$ ft { (¶2.4.3.6)		{ Passive* $R_D = 18,000$ ft { (¶2.4.3.14)
0.95 - 1.9	5,776 to 11,552	{ Passive GPC $R_D = 8,000$ ft { (¶2.4.3.5)		{ Passive* $R_D = 8,000$ ft { (¶2.4.3.13)
0.42 - 0.95	2,554 to 5,776	{ Passive GPC $R_D = 4,000$ ft { (¶2.4.3.4)		{ Passive* $R_D = 4,000$ ft { (¶2.4.3.12)
0.016 - 0.42	97 - 2,554	{ Passive GPC $R_D = 1,000$ ft { (¶2.4.3.1)		{ Passive* $R_D = 1,000$ ft { (¶2.4.3.11)
		{ Passive Manual/Auto, { short range (¶2.4.3.3) { Passive Manual/Auto, { long range (¶2.4.3.9)		{ Active* (¶2.4.3.19) $R < 9.3$ nm { w/pulse width override { $R_T = 50,000$ ft
NOTE: All tests repeated (¶2.4.3.23)	for test mode		*GPC & auto mode same	{ Active* (¶2.4.3.20) $R < 9.3$ nm { w/o pulse width override { $R_T = 50,000$ ft

$R_D$  = Range Designate,  $R_T$  = Range of Target, Paragraphs refer to Hughes TS 32012-076 (EA-2 ATP)

Table 8. Deployed Assembly Gates (Cont'd)

Designated Ranges		Search	Acquisition	Track
nm <sub>1</sub>	ft			
		{ Active GPC/Manual/Auto { (¶2 4 3 10)		{ Active* (¶2.4.3.2.1) w/o pulse width override { R > 9.3 nm <sub>1</sub> R <sub>T</sub> = 88,000 ft
NOTE	All tests repeated for test mode (¶2 4.3.23)			
	*GPC & auto mode same			
	R <sub>D</sub> = Range Designate			
	R <sub>T</sub> = Range of Target			
	Paragraphs refer to Hughes TS 32012-076 (EA-2 ATP)			

Table 9. Acquisition Program Verification

Designated Ranges		Search	Acquisition	Track
nm	ft			
> 18.9	> 114,912			
9.3 - 18.9	56,114 to 114,912		{ Passive GPS Acq (¶2.12.9) R <sub>D</sub> = 98,000 ft	
7.2 - 9.3	43,544 to 56,544			{ Passive* GPC (¶2.13.3) R > 7.2 nm R <sub>T</sub> = 50,000 ft
3.8 - 7.2	23,104 to 43,776		{ Passive GPC Acq (¶2.12.6) R <sub>D</sub> = 28,000 ft	{ Passive* GPC (¶2.13.2) 3.8 nm < R < 7.2 nm R <sub>T</sub> = 30,000 ft
1.9 - 3.8	11,552 to 23,104		{ Passive GPC Acq (¶2.12.3) R <sub>D</sub> = 10,000 ft	
0.95 - 1.9	5,776 to 11,552			
0.42 - 0.95	2,554 - 5,776			{ Passive* GPC (¶2.13.1) R < 3.8 nm R <sub>T</sub> = 4,000 ft
0.016-0.042	97 - 2,554		{ Passive GPC Acq (¶2.12.12) R <sub>D</sub> = 2,000 ft	
			{ Active GPC Acq (¶2.12.16) R > 9.5 nm R <sub>T</sub> = 80,000 ft  { Active GPC Acq (¶2.12.19) R < 9.5 nm R <sub>T</sub> = 20,000 ft	{ Active GPC (¶2.13.5) R > 9.5 nm R <sub>T</sub> = 600,000 ft  { Active GPC (¶2.13.4) R < 9.5 nm R <sub>T</sub> = 40,000 ft
*GPC & auto mode same				

R<sub>D</sub> = Range Designate, R<sub>T</sub> = Range of Target, Paragraphs refer to Hughes TS 32012-076 (EA-2 ATP)

Table 10. False Alarm Rate

Designated Ranges		Search	Acquisition	Track
nmi	ft			
> 18.9	> 114,912			
9.3 - 18.9	56,544 to 114,912	{ Passive GPC $R_D = 98,000$ ft. { (Para. 2.5.3)		
7.2 - 9.3	43,776 to 56,544			
3.8 - 7.2	23,104 to 43,776	{ Passive GPC $R_D = 28,000$ ft. { (Para. 2.5.3)		
1.9 - 3.8	11,552 to 23,104	{ Passive GPC $R_D = 18,000$ ft. { (Para. 2.5.3)		
0.95 - 1.9	5,776 to 11,552	{ Passive GPC $R_D = 8,000$ ft. { (Para. 2.5.3)		
0.42 - 0.95	2,554 to 11,552	{ Passive GPC $P_D = 4,000$ ft. { (Para. 2.5.3)		
0.016 - 0.42	97 - 2,554	{ Passive GPC $R_D = 1,000$ ft. { (Para. 2.5.1)		
		{ Active $R_T = 1,000$ ft. { (Para. 2.5.2)  { Manual/Auto { (Para. 2.5.4)		

$R_D$  = Range Designate,  $R_T$  = Range of Target, Paragraphs refer to Hughes TS 32012-076 (EA-2 ATP)

Table 11 Summary of Untested EA-2 Rockwell Specification Paragraphs

Item Number	Paragraph Number	Paragraph Title
1	40 3.1 2 4 1.2 Output b. c d.	Controls and Status Discretes (EA-1A Interface) Lobing Enable Lobing Alpha/Beta Lobing Phase 0 - 180°
2	40 3.1 2.4 2.1 e. f. h. i.	Controls and Status Discretes (DA-A Interface) Radar Sum Enable Radar Difference Enable Transmitter Limiter AGC First IF Step AGC
3.	40 3.2.1 2 3 2	GPC Designate, Passive Mode (TBS)
4.	40.3.2 1.2.3.3.2	Acquisition Phase (Autotrack, Passive Mode)
5.	40.3.2.1.2.5.1	Parameter Measurement Accuracy Convergence Time
6	40 3 2 1 2.5.2	Measurement Data Output Sample Rate
7.	40.3 2.1.2 6	Clutter Performance



### 6.3.2 EA-2 Conclusions/Recommendations

The amount of testing performed on the ADL EA-2 is more than adequate to ensure that the ADL EA-2 will meet its mission of verifying Shuttle interfaces. The prerelease version of the EA-2 ATP is an excellent start towards producing a comprehensive ATP.

Axiomatix does recommend, however, that some functional tests be conducted as a function of bus voltage and that the testing oversights listed in Table 11 be addressed by modifying the EA-2 ATP.

## 7.0 EFFECTS OF CROSS-COUPLING ON THE STABILITY AND TRACKING PERFORMANCE OF $\alpha/\beta$ SERVO LOOPS

### 7.1 Introduction

The Ku-band Communication Autotrack system contains  $\alpha$  and  $\beta$  servo loops whose purpose is to acquire and track the difference azimuth and elevation error angles, respectively. Cross-coupling between the difference elevation and azimuth channels which feed these loops, originating from the monopulse feeds and comparator network, can cause stability problems during acquisition and tracking operations. Furthermore, even if stable operation is assured, the cross-coupling produces a degrading effect on each loop's tracking performance in noise.

This section discusses the potential stability problem caused by cross-coupling and derives a necessary but insufficient condition to ensure stability. In addition, using mean-square phase jitter as a measure of tracking performance, the degradation in this measure caused by cross-coupling is assessed in terms of such parameters as servo noise bandwidth and damping factor for all the loops, and the pair of cross-coupling gains.

We begin our analysis by considering the noise-free model of the pair of cross-coupled loops with the purpose of examining each loop's response to an input phase step. The behavior of the corresponding loop phase error responses as time approaches infinity is then an indication of system stability.

### 7.2 Noise-Free Model of Coupled Loops (Response to Phase Step Input)

Consider the noise-free model for the cross-coupled  $\alpha$  and  $\beta$  servo loops, as illustrated in Figure 4. Here  $\alpha$  and  $\beta$  denote the angular errors (in radians) for the two servo loops, and  $\epsilon_\alpha$  and  $\epsilon_\beta$  are, respectively, the corresponding  $\alpha$ -axis and  $\beta$ -axis voltage errors. The gains  $K_\alpha$  and  $K_\beta$  are equivalent to  $K_{SC} = K_{SC1}K_{SC2}$  in the Hughes servo configuration single-axis block diagram, where  $K_{SC1} = 117.3 \text{ V/rad}$  and  $1 \leq K_{SC2} \leq 15$ . Since Figure 4 is an equivalent block diagram for the linear region of behavior, then, in reality,  $K_{SC}$  represents the slope of the two tracking characteristics at the origin, i.e.,

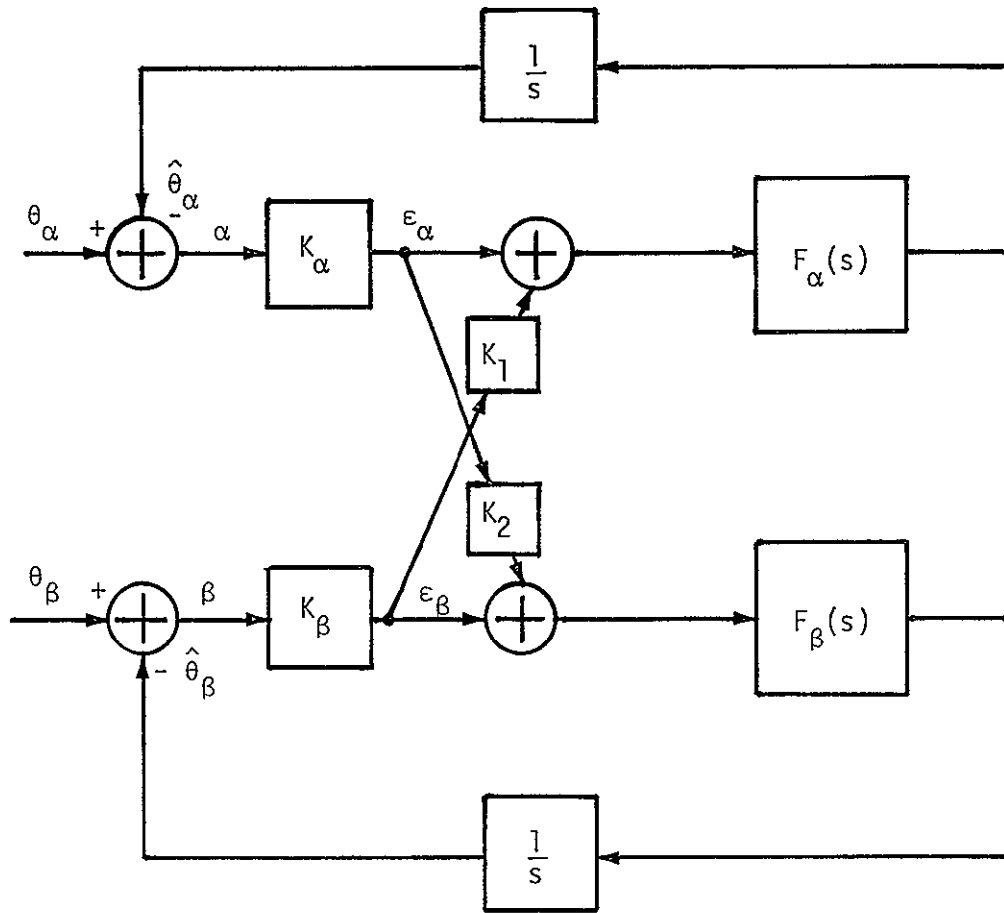


Figure 4 A Simple Block Diagram for the Cross-Coupled  $\alpha$  and  $\beta$  Servo Loops in the Absence of Noise

$$117.3 \leq \frac{d\varepsilon_\alpha}{d\alpha} \leq \underbrace{1759.5}_{(117.3)(15)} ; \quad 117.3 \leq \frac{d\varepsilon_\beta}{d\beta} \leq 1759.5 \quad (1)$$

we also have the equivalent relations

$$117.3\alpha \leq \varepsilon_\alpha \leq 1759.5\alpha ; \quad 117.3\beta \leq \varepsilon_\beta \leq 1759.5\beta \quad (2)$$

The blocks labeled  $K_1$  and  $K_2$  represent the normalized cross-coupling between the loops where, for the moment, we only restrict  $K_1$  and  $K_2$  so that each has a magnitude less than or equal to unity. The blocks marked  $1/s$  represent the transfer functions of the  $\alpha$ - and  $\beta$ -axis servo motors. Finally,  $F_\alpha(s)$  and  $F_\beta(s)$  represent the composite transfer functions of the various components and subloops which make up the rate stabilization loop for each axis. Later on, we shall go into the detail necessary to characterize  $F_\alpha(s)$  and  $F_\beta(s)$  in terms of the actual rate stabilization loop parameters. For the moment, we shall just treat  $F_\alpha(s)$  and  $F_\beta(s)$  as rational transfer functions in much the same manner as one characterizes a loop filter in a conventional phase-lock-loop.

By inspecting Figure 4, we can immediately write the following relations.

$$\varepsilon_\alpha = K_\alpha(\theta_\alpha - \hat{\theta}_\alpha) \quad , \quad \varepsilon_\beta = K_\beta(\theta_\beta - \hat{\theta}_\beta) \quad (3)$$

$$\hat{\theta}_\alpha = \frac{F_\alpha(s)}{s} (\varepsilon_\alpha + K_1 \varepsilon_\beta) \quad , \quad \hat{\theta}_\beta = \frac{F_\beta(s)}{s} (\varepsilon_\beta + K_2 \varepsilon_\alpha) \quad (4)$$

Combining (3) and (4) gives the pair of coupled equations

$$\begin{aligned} \varepsilon_\alpha (s + K_\alpha F_\alpha(s)) &= s K_\alpha \theta_\alpha - K_\alpha K_1 F_\alpha(s) \varepsilon_\beta \\ \varepsilon_\beta (s + K_\beta F_\beta(s)) &= s K_\beta \theta_\beta - K_\beta K_2 F_\beta(s) \varepsilon_\alpha \end{aligned} \quad (5)$$

Letting  $\theta_\alpha$  and  $\theta_\beta$  now correspond to step changes in phase, i.e.,

$$\theta_\alpha = \frac{\Theta_\alpha}{s} ; \quad \theta_\beta = \frac{\Theta_\beta}{s} \quad (6)$$

then substituting (6) into (5) and solving for  $\epsilon_\alpha$  and  $\epsilon_\beta$  yields, upon simplification,

$$\begin{aligned} \epsilon_\alpha &= \frac{K_\alpha [s + K_\beta F_\beta(s)] \Theta_\alpha}{[s + K_\alpha F_\alpha(s)] [s + K_\beta F_\beta(s)] - K_\alpha K_\beta K_1 K_2 F_\alpha(s) F_\beta(s)} \\ \epsilon_\beta &= \frac{K_\beta [s + K_\alpha F_\alpha(s)] \Theta_\beta}{[s + K_\beta F_\beta(s)] [s + K_\alpha F_\alpha(s)] - K_\alpha K_\beta K_1 K_2 F_\alpha(s) F_\beta(s)} \end{aligned} \quad (7)$$

Note that, for no cross-coupling, i.e.,  $K_1 = K_2 = 0$ , (7) reduces to

$$\begin{aligned} \epsilon_\alpha &= \frac{\Theta_\alpha}{s + K_\alpha F_\alpha(s)} = \left[ 1 - \frac{K_\alpha F_\alpha(s)}{s + K_\alpha F_\alpha(s)} \right] \left( \frac{\Theta_\alpha}{s} \right) \\ \epsilon_\beta &= \frac{\Theta_\beta}{s + K_\beta F_\beta(s)} = \left[ 1 - \frac{K_\beta F_\beta(s)}{s + K_\beta F_\beta(s)} \right] \left( \frac{\Theta_\beta}{s} \right) \end{aligned} \quad (8)$$

as it should. The results in (7) can be written in a more compact form by defining the closed-loop transfer functions in the absence of cross-coupling, i.e.,

$$\begin{aligned} H_\alpha(s) &= \frac{K_\alpha F_\alpha(s)}{s + K_\alpha F_\alpha(s)} \\ H_\beta(s) &= \frac{K_\beta F_\beta(s)}{s + K_\beta F_\beta(s)} \end{aligned} \quad (9)$$

Dividing the numerator and denominator of the right-hand side of (7) and using (9) gives the desired result, namely,

ORIGINAL PAGE IS  
OF POOR QUALITY

$$\begin{aligned} \epsilon_{\alpha}(s) &= \frac{\left[1 - H_{\alpha}(s)\right]\left(\frac{\Theta_{\alpha}}{s}\right) - K_1 H_{\alpha}(s)\left[1 - H_{\beta}(s)\right]\left(\frac{\Theta_{\beta}}{s}\right)}{1 - K_1 K_2 H_{\alpha}(s) H_{\beta}(s)} \\ \epsilon_{\beta}(s) &= \frac{\left[1 - H_{\beta}(s)\right]\left(\frac{\Theta_{\beta}}{s}\right) - K_2 H_{\beta}(s)\left[1 - H_{\alpha}(s)\right]\left(\frac{\Theta_{\alpha}}{s}\right)}{1 - K_1 K_2 H_{\alpha}(s) H_{\beta}(s)} \end{aligned} \quad (10)$$

To examine system stability, we consider the steady state ( $t \rightarrow \infty$ ) behavior of the angular error voltages in response to the step changes in phase of (6). Applying the final value theorem to (10), we observe that, if they exist, the limiting values of  $\epsilon_{\alpha}$  and  $\epsilon_{\beta}$  become

$$\lim_{t \rightarrow \infty} \epsilon_{\alpha}(t) = \lim_{s \rightarrow 0} s \epsilon_{\alpha}(s); \quad \lim_{t \rightarrow \infty} \epsilon_{\beta}(t) = \lim_{s \rightarrow 0} s \epsilon_{\beta}(s) \quad (11)$$

or

$$\begin{aligned} \lim_{t \rightarrow \infty} \epsilon_{\alpha}(t) &= \lim_{s \rightarrow 0} \frac{\left[1 - H_{\alpha}(s)\right] \Theta_{\alpha} - K_1 H_{\alpha}(s)\left[1 - H_{\beta}(s)\right] \Theta_{\beta}}{1 - K_1 K_2 H_{\alpha}(s) H_{\beta}(s)} \\ \lim_{t \rightarrow \infty} \epsilon_{\beta}(t) &= \lim_{s \rightarrow 0} \frac{\left[1 - H_{\beta}(s)\right] \Theta_{\beta} - K_2 H_{\beta}(s)\left[1 - H_{\alpha}(s)\right] \Theta_{\alpha}}{1 - K_1 K_2 H_{\alpha}(s) H_{\beta}(s)} \end{aligned} \quad (12)$$

Since, from (9),

$$\lim_{s \rightarrow 0} H_{\alpha}(s) = \lim_{s \rightarrow 0} H_{\beta}(s) = 1 \quad (13)$$

then, clearly, both  $\epsilon_{\alpha}(t)$  and  $\epsilon_{\beta}(t)$  will have limiting values of zero, i.e., a stable situation results in the steady state, if

$$1 - K_1 K_2 > 0 \quad (14)$$

or

$$\boxed{K_1 K_2 < 1} \quad (15)$$

Stated in words, (15) says that, for the pair of cross-coupled loops as modeled in Figure 4, a necessary (but insufficient) condition for each loop to acquire a phase input step is that the product of the relative cross-coupling gains be less than one. Note that this result has been obtained independent of the order of each of the uncoupled loops, i.e., it has not been necessary to restrict  $H_\alpha(s)$  and  $H_\beta(s)$  to obtain first- or second-order polynomials as denominators as would be the case for first- and second-order loops.

To say any more about loop stability, one must investigate the pole locations of  $\epsilon_\alpha(s)$  and  $\epsilon_\beta(s)$ , which requires investigation of the roots of the denominator  $1 - K_1 K_2 H_\alpha(s) H_\beta(s)$ . This, in turn, requires specifying the equivalent loop filters  $F_\alpha(s)$  and  $F_\beta(s)$ . Due to the complex form of the transfer functions which represent these filters (as we shall see later on), we shall not pursue the stability question any further. In the next section on tracking behavior in the presence of noise, however, it will be necessary to assume a particular functional form for  $F_\alpha(s)$  and  $F_\beta(s)$ . Since  $F_\alpha(s)$  and  $F_\beta(s)$  are, in general, the ratio of high-order polynomials (this will be seen later on), we shall assume that only the first-order terms are significant and, thus, model these filter transfer functions as

$$F_\alpha(s) = K_{F_\alpha} \frac{1 + s \tau_{2\alpha}}{1 + s \tau_{1\alpha}}, \quad F_\beta(s) = K_{F_\beta} \frac{1 + s \tau_{2\beta}}{1 + s \tau_{1\beta}} \quad (16)$$

Such a model is equivalent to assuming that each of the uncoupled loops act as a second-order servo. Even under this relatively simplistic model, we shall see that the specification of tracking behavior in terms of the mean-square angular error involves extremely complex algebraic manipulations as a result of the presence of cross-coupling. Nevertheless, we

shall pursue the results for this case, if only to give a qualitative indication of what might be expected if one were to consider higher order terms in  $F_\alpha(s)$  and  $F_\beta(s)$ .

### 7.3 Noise Model of Coupled Loops (Tracking Analysis)

Consider the noise model of the coupled  $\alpha$  and  $\beta$  servo loops, as illustrated in Figure 5. Here,  $K_{\alpha 1}$  and  $K_{\alpha 2}$  are identical to  $K_{sc1}$  and  $K_{sc2}$ , as previously defined. Similarly,  $K_{\beta 1}$  and  $K_{\beta 2}$  are identical to  $K_{sc1}$  and  $K_{sc2}$ . Furthermore,

$$K_\alpha = K_{\alpha 1} K_{\alpha 2} \quad ; \quad K_\beta = K_{\beta 1} K_{\beta 2} \quad (17)$$

Analogous to (3), we now have

$$\epsilon_\alpha = K_\alpha (\theta_\alpha - \hat{\theta}_\alpha) + K_{\alpha 2} N_\alpha \quad , \quad \epsilon_\beta = K_\beta (\theta_\beta - \hat{\theta}_\beta) + K_{\beta 2} N_\beta \quad (18)$$

whereas (4) still applies. Again combining (18) and (4) gives the pair of coupled equations

$$\begin{aligned} \epsilon_\alpha (s + K_\alpha F_\alpha(s)) &= s K_\alpha \theta_\alpha - K_\alpha K_1 F_\alpha(s) \epsilon_\beta + s K_{\alpha 2} N_\alpha \\ \epsilon_\beta (s + K_\beta F_\beta(s)) &= s K_\beta \theta_\beta - K_\beta K_2 F_\beta(s) \epsilon_\alpha + s K_{\beta 2} N_\beta \end{aligned} \quad (19)$$

Since we are interested here in the mean-square angular-tracking jitter due to noise, we may ignore the terms of (19) which involve  $\theta_\alpha$  and  $\theta_\beta$  and directly solve for  $\epsilon_\alpha$  and  $\epsilon_\beta$ . Doing so results, after some simplification, in a pair of equations analogous to (10), namely,

$$\begin{aligned} \epsilon_\alpha &= \frac{-K_1 K_{\beta 2} H_\alpha(s) [1 - H_\beta(s)] N_\beta + K_{\alpha 2} (1 - H_\alpha(s)) N_\alpha}{1 - K_1 K_2 H_\alpha(s) H_\beta(s)} \\ \epsilon_\beta &= \frac{-K_2 K_{\alpha 2} H_\beta(s) [1 - H_\alpha(s)] N_\alpha + K_{\beta 2} (1 - H_\beta(s)) N_\beta}{1 - K_1 K_2 H_\alpha(s) H_\beta(s)} \end{aligned} \quad (20)$$



ORIGINAL PAGE IS  
OF POOR QUALITY

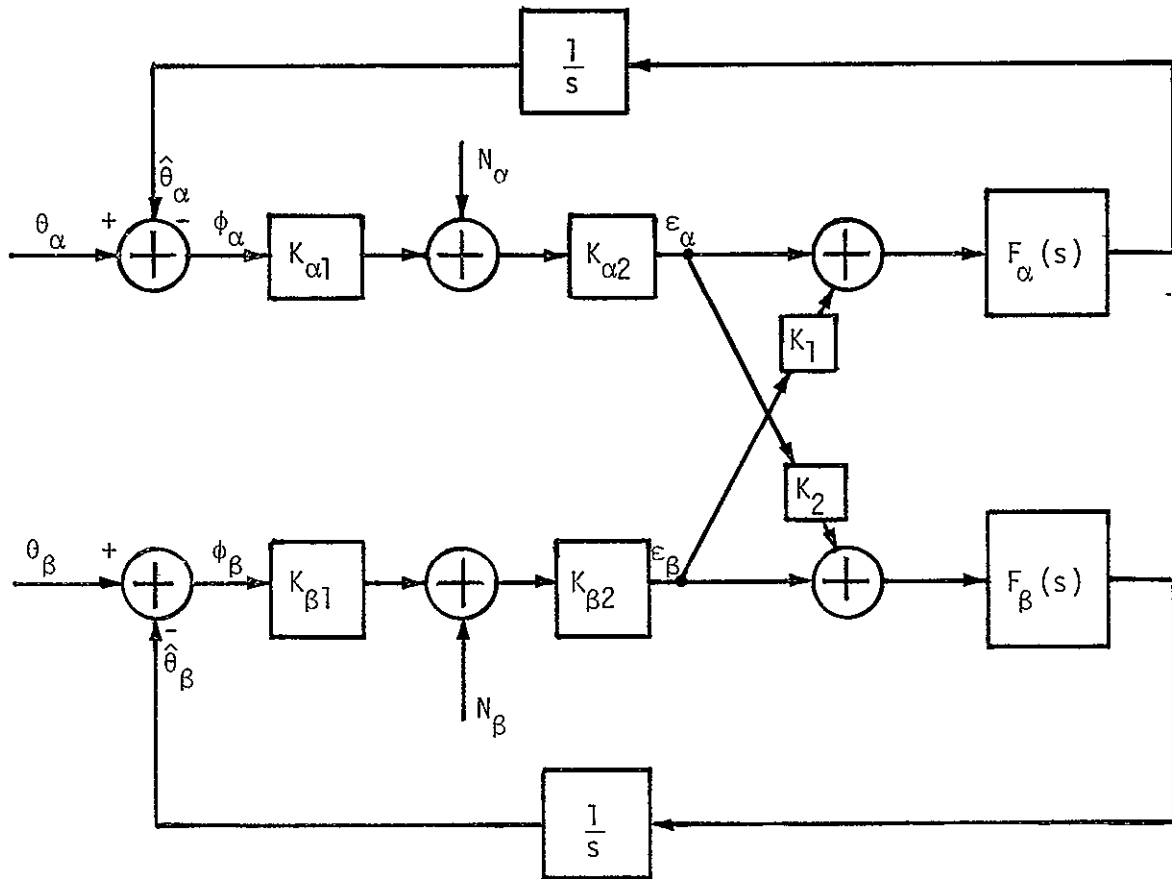


Figure 5 A Simple Block Diagram for the Cross-Coupled  $\alpha$  and  $\beta$  Servo Loops in the Presence of Noise

In the absence of cross-coupling (i.e.,  $K_1 = K_2 = 0$ ), (20) reduces to

$$\varepsilon_\alpha = K_{\alpha 2} (1 - H_\alpha(s)) N_\alpha \quad ; \quad \varepsilon_\beta = K_{\beta 2} (1 - H_\beta(s)) \quad (21)$$

as it should, that is, the noise sources are transformed by the out-of-band loop transfer functions insofar as their effect on the loop error voltage is concerned.

Actually, we are interested in the angular errors  $\phi_\alpha$  and  $\phi_\beta$  which, from Figure 5, are related to  $\varepsilon_\alpha$  and  $\varepsilon_\beta$  by

$$\phi_\alpha = \frac{\varepsilon_\alpha - K_{\alpha 2} N_\alpha}{K_\alpha} \quad ; \quad \phi_\beta = \frac{\varepsilon_\beta - K_{\beta 2} N_\beta}{K_\beta} \quad (22)$$

Substituting (20) into (22) and simplifying produced the desired results, namely,

$$\phi_\alpha = \frac{-\frac{K_1 K_{\beta 2}}{K_\alpha} H_\alpha(s) [1 - H_\beta(s)] N_\beta - \frac{1}{K_{\alpha 1}} H_\alpha(s) [1 - K_1 K_2 H_\beta(s)] N_\alpha}{1 - K_1 K_2 H_\alpha(s) H_\beta(s)}$$

$$\phi_\beta = \frac{-\frac{K_2 K_{\alpha 2}}{K_\beta} H_\beta(s) [1 - H_\alpha(s)] N_\alpha - \frac{1}{K_{\beta 1}} H_\beta(s) [1 - K_1 K_2 H_\alpha(s)] N_\beta}{1 - K_1 K_2 H_\alpha(s) H_\beta(s)} \quad (23)$$

We wish to compare the mean-square values of  $\phi_\alpha$  and  $\phi_\beta$  in (23) relative to the same values for  $K_1 = K_2 = 0$  so as to assess the degradation in mean-square phase jitter due to the cross-coupling effect. First setting  $K_1 = K_2 = 0$  in (23), we get\*

---

\* From here on, we shall consider the performance of the  $\alpha$ -channel only since, clearly, the equations have perfect symmetry with respect to  $\alpha$  and  $\beta$ .

$$\sigma_{\phi_0}^2 = \frac{(N_{0\alpha}/2)}{K_{\alpha 1}^2} \left[ \frac{1}{2\pi j} \int_{-j\infty}^{j\infty} |H_{\alpha}(s)|^2 ds \right] \triangleq \frac{N_{0\alpha} B_{L\alpha}}{K_{\alpha 1}^2} \triangleq \frac{1}{\rho_{\alpha}} \quad (24)$$

where  $B_{L\alpha}$  is the equivalent loop noise bandwidth of the  $\alpha$ -servo in the absence of cross-coupling and the zero subscript on  $\sigma_{\phi}^2$  denotes this case. Furthermore,  $N_{0\alpha}$  is the single-sided noise spectral density of the equivalent noise source  $N_{\alpha}(t)$ . In the presence of cross-coupling, we obtain from (23) the relation

$$\begin{aligned} \sigma_{\phi}^2 = & \frac{(N_{0\alpha}/2)K_1^2 K_{\beta 2}^2}{K_{\alpha}^2} \left[ \frac{1}{2\pi j} \int_{-j\infty}^{j\infty} \left| \frac{H_{\alpha}(s) [1 - H_{\beta}(s)]}{1 - K_1 K_2 H_{\alpha}(s) H_{\beta}(s)} \right|^2 ds \right] \\ & + \frac{(N_{0\alpha}/2)}{K_{\alpha 1}^2} \left[ \frac{1}{2\pi j} \int_{-j\infty}^{j\infty} \left| \frac{H_{\alpha}(s) [1 - K_1 K_2 H_{\beta}(s)]}{1 - K_1 K_2 H_{\alpha}(s) H_{\beta}(s)} \right|^2 ds \right] \end{aligned} \quad (25)$$

For the assumed loop filter transfer functions of (16), the closed-loop transfer functions of (9) can be written in the form

$$\begin{aligned} H_{\alpha}(s) &= \frac{1 + \left(\frac{r_{\alpha}+1}{4B_{L\alpha}}\right)s}{1 + \left(\frac{r_{\alpha}+1}{4B_{L\alpha}}\right)s + \frac{1}{r_{\alpha}}\left(\frac{r_{\alpha}+1}{4B_{L\alpha}}\right)^2 s^2} = \frac{1 + \tau_{2\alpha} s}{1 + \tau_{2\alpha} s + \frac{1}{r_{\alpha}} \tau_{2\alpha}^2 s^2} \\ H_{\beta}(s) &= \frac{1 + \left(\frac{r_{\beta}+1}{4B_{L\beta}}\right)s}{1 + \left(\frac{r_{\beta}+1}{4B_{L\beta}}\right)s + \frac{1}{r_{\beta}}\left(\frac{r_{\beta}+1}{4B_{L\beta}}\right)^2 s^2} = \frac{1 + \tau_{2\beta} s}{1 + \tau_{2\beta} s + \frac{1}{r_{\beta}} \tau_{2\beta}^2 s^2} \end{aligned} \quad (26)$$

where  $r_{\alpha} = 4\zeta_{\alpha}^2$  and  $r_{\beta} = 4\zeta_{\beta}^2$ , with  $\zeta_{\alpha}$  and  $\zeta_{\beta}$  the damping factors for the  $\alpha$  and  $\beta$  loops, respectively. Substituting (26) into the integrands of (25), we can express each of them as the ratio of two polynomials in  $s$ .

Thus, after much simplification, we obtain the following results:

$$\frac{H_{\alpha}(s) [1 - H_{\beta}(s)]}{1 - K_1 K_2 H_{\alpha}(s) H_{\beta}(s)} = \frac{a_0 + a_1 s + a_2 s^2 + a_3 s^3}{b_0 + b_1 s + b_2 s^2 + b_3 s^3 + b_4 s^4} \quad (27)$$

where

$$\begin{aligned} a_0 &= 0 \\ a_1 &= 0 \\ a_2 &= \frac{1}{r_{\beta}} \tau_{2\beta}^2 = \tau_{2\alpha}^2 \left( \frac{1}{r_{\beta}} \xi^2 \right) \\ a_3 &= \frac{1}{r_{\beta}} \tau_{2\beta}^2 \tau_{2\alpha} = \tau_{2\alpha}^3 \left( \frac{1}{r_{\beta}} \xi^2 \right) \\ b_0 &= \eta \\ b_1 &= (\tau_{2\alpha} + \tau_{2\beta}) \eta = \tau_{2\alpha} \eta (1 + \xi) \\ b_2 &= \frac{1}{r_{\alpha}} \tau_{2\alpha}^2 + \frac{1}{r_{\beta}} \tau_{2\beta}^2 + \eta \tau_{2\alpha} \tau_{2\beta} = \tau_{2\alpha}^2 \left( \frac{1}{r_{\alpha}} + \frac{1}{r_{\beta}} \xi^2 + \eta \xi \right) \\ b_3 &= \frac{1}{r_{\alpha}} \tau_{2\alpha}^2 \tau_{2\beta} + \frac{1}{r_{\beta}} \tau_{2\beta}^2 \tau_{2\alpha} = \tau_{2\alpha}^3 \left( \frac{1}{r_{\alpha}} \xi + \frac{1}{r_{\beta}} \xi^2 \right) \\ b_4 &= \left( \frac{1}{r_{\beta}} \tau_{2\beta}^2 \right) \left( \frac{1}{r_{\alpha}} \tau_{2\alpha}^2 \right) = \tau_{2\alpha}^4 \left( \frac{1}{r_{\alpha} r_{\beta}} \xi^2 \right) \end{aligned} \quad (28)$$

with

$$\begin{aligned} \eta &\triangleq 1 - K_1 K_2 \\ \xi &\triangleq \frac{\tau_{2\beta}}{\tau_{2\alpha}} = \frac{B_{L\alpha} (r_{\alpha} + 1)}{B_{L\beta} (r_{\beta} + 1)} \end{aligned} \quad (29)$$

Also,

$$\frac{H_{\alpha}(s) [1 - K_1 K_2 H_{\beta}(s)]}{1 - K_1 K_2 H_{\alpha}(s) H_{\beta}(s)} = \frac{c_0 + c_1 s + c_2 s^2 + c_3 s^3}{d_0 + d_1 s + d_2 s^2 + d_3 s^3 + d_4 s^4} \quad (30)$$

where

ORIGINAL PAGE IS  
OF POOR QUALITY

$$\begin{aligned}
 c_0 &= \eta \\
 c_1 &= (\tau_{2\alpha} + \tau_{2\beta})\eta = \tau_{2\alpha}\eta(1 + \xi) \\
 c_2 &= \frac{1}{r_\beta} \tau_{2\beta}^2 + \tau_{2\alpha} \tau_{2\beta}\eta = \tau_{2\alpha}^2 \left( \frac{1}{r_\beta} \xi^2 + \eta\xi \right) \\
 c_3 &= \frac{1}{r_\beta} \tau_{2\beta}^2 \tau_{2\alpha} = \tau_{2\alpha}^3 \left( \frac{1}{r_\beta} \xi^2 \right) \\
 d_0 &= \eta \\
 d_1 &= c_1 \\
 d_2 &= c_2 + \frac{1}{r_\alpha} \tau_{2\alpha}^2 = \tau_{2\alpha}^2 \left[ \frac{1}{r_\alpha} + \frac{1}{r_\beta} \xi^2 + \eta\xi \right] \\
 d_3 &= c_3 + \frac{1}{r_\alpha} \tau_{2\alpha}^3 \xi = \tau_{2\alpha}^3 \left[ \frac{1}{r_\alpha} \xi + \frac{1}{r_\beta} \xi^2 \right] \\
 d_4 &= \left( \frac{1}{r_\beta} \tau_{2\beta}^2 \right) \left( \frac{1}{r_\alpha} \tau_{2\alpha}^2 \right) = \tau_{2\alpha}^4 \left( \frac{1}{r_\alpha r_\beta} \xi^2 \right) \tag{31}
 \end{aligned}$$

Complex integrals of the type required in (25) have previously been evaluated [4]. In particular, since the denominator in both cases is a fourth-order polynomial, the following result applies

For

$$\begin{aligned}
 P(s) &= p_0 + p_1 s + p_2 s^2 + p_3 s^3 \\
 Q(s) &= q_0 + q_1 s + q_2 s^2 + q_3 s^3 + q_4 s^4 \tag{32}
 \end{aligned}$$

then

$$\begin{aligned}
 I_4 &\triangleq \frac{1}{2\pi j} \int_{-j\infty}^{j\infty} \frac{P(s) P(-s)}{Q(s) Q(-s)} ds = \frac{1}{2\pi j} \int_{-j\infty}^{j\infty} \left| \frac{P(s)}{Q(s)} \right|^2 ds \\
 &= \frac{p_3^2 (-q_0^2 q_3 + q_0 q_1 q_2) + (p_2^2 - 2 p_1 p_3) q_0 q_1 q_4}{2 q_0 q_4 (-q_0 q_3^2 - q_1^2 q_4 + q_1 q_2 q_3)} \\
 &\quad + \frac{(p_1^2 - 2 p_0 p_2) q_0 q_3 q_4 + p_0^2 (-q_1 q_4^2 + q_2 q_3 q_4)}{2 q_0 q_4 (-q_0 q_3^2 - q_1^2 q_4 + q_1 q_2 q_3)} \tag{33}
 \end{aligned}$$

Equating the coefficient sets  $\{p_i\}$  and  $\{q_i\}$  with either  $\{a_i\}$  and  $\{b_i\}$  or  $\{c_i\}$  and  $\{d_i\}$ , then (33) can be used to evaluate the two integrals required in (25). In particular, after considerable algebraic manipulation and simplification, we obtain the following results.

$$\begin{aligned} \frac{1}{2\pi j} \int_{-j\infty}^{j\infty} \left| \frac{H_\alpha(s) [1 - H_\beta(s)]}{1 - K_1 K_2 H_\alpha(s) H_\beta(s)} \right|^2 ds &\triangleq 2B_{L\beta} K_{\beta\alpha} \\ \frac{1}{2\pi j} \int_{-j\infty}^{j\infty} \left| \frac{H_\alpha(s) [1 - K_1 K_2 H_\beta(s)]}{1 - K_1 K_2 H_\alpha(s) H_\beta(s)} \right|^2 ds &\triangleq 2B_{L\alpha} K_{\alpha\alpha} \end{aligned} \quad (34)$$

where

$$\begin{aligned} K_{\beta\alpha} &= \frac{\xi^2 r_\alpha^2 r_\beta + \xi^3 (1+\xi) (\eta r_\alpha^3 r_\beta + \xi r_\alpha^2) + \xi^5 r_\alpha^3}{(r_\beta + 1) \left\{ r_\beta^2 + r_\alpha^2 \xi^4 + \eta \xi (1+\xi) (r_\alpha r_\beta^2 + r_\alpha^2 r_\beta \xi) + \xi r_\alpha r_\beta [(1+\xi^2)(1-\eta) - 2\eta \xi] \right\}} \\ &\quad \frac{r_\beta^2 (1+\eta r_\alpha) + r_\alpha^2 (1+r_\alpha) \xi^4 + \eta \xi (1+\xi) [r_\alpha r_\beta^2 (1+\eta r_\alpha) + r_\alpha^2 r_\beta (1+r_\alpha) \xi]}{+ \xi r_\alpha r_\beta [(1+r_\alpha - \xi)(1-\eta) - (1+r_\alpha) 2\eta \xi]} \\ K_{\alpha\alpha} &= \frac{r_\beta^2 (1+\eta r_\alpha) + r_\alpha^2 (1+r_\alpha) \xi^4 + \eta \xi (1+\xi) [r_\alpha r_\beta^2 (1+\eta r_\alpha) + r_\alpha^2 r_\beta (1+r_\alpha) \xi]}{(r_\alpha + 1) \left\{ r_\beta^2 + r_\alpha^2 \xi^4 + \eta \xi (1+\xi) (r_\alpha r_\beta^2 + r_\alpha^2 r_\beta \xi) + \xi r_\alpha r_\beta [(1+\xi^2)(1-\eta) - 2\eta \xi] \right\}} \end{aligned} \quad (35)$$

Note that, for  $\eta = 1$ , e.g.,  $K_2 = 0$ ,  $K_1 \neq 0$ , we have

$$K_{\alpha\alpha} = 1 \quad (36)$$

in accordance with (24) and

$$K_{\beta\alpha} = \frac{r_\alpha \xi^2}{r_\beta (r_\beta + 1)} \frac{[r_\beta + r_\alpha r_\beta \xi (1+\xi) + \xi^2 (1+\xi) + r_\alpha \xi^3]}{\left\{ \frac{r_\beta}{r_\alpha} + r_\beta \xi + \xi^2 (r_\alpha + r_\beta - 2) + r_\alpha \xi^3 + \frac{r_\alpha}{r_\beta} \xi^4 \right\}} \quad (37)$$

which resembles a result for two-way phase-coherent tracking systems (see [5], eq. (3-18)).

Finally, combining (25) with (34) and using (24) gives the mean-square phase jitter of the angular error in the  $\alpha$ -servo loop as

$$\sigma_{\phi}^2 = \left( \frac{K_1^2 K_{\beta}^2}{K_{\alpha}^2} \right) \rho_{\beta} + \frac{K_{\alpha\alpha}}{\rho_{\alpha}} \quad (38)$$

where, analogous to (24),

$$\rho_{\beta} \triangleq \frac{K_{\beta 1}^2}{N_{0\beta} B_{L\beta}} \quad (39)$$

is the  $\beta$ -servo loop SNR in the absence of cross-coupling.

$F_{\alpha}(s)$  and  $F_{\beta}(s)$  are currently being evaluated in terms of the rate stabilization loop parameters. Numerical results will be presented in a subsequent report.

## 8.0 AXIOMATIX COVERAGE OF THE DA ATP REVIEW MEETING

### 8.1 Introduction

As NASA is well aware, it has been difficult to relate the Rockwell Ku-band specification MC 409-0025, Rev. B, to the four Hughes acceptance test procedures (ATP's) because Hughes has written their own internal LRU specifications which differ significantly in format from the Rockwell document. To resolve this situation, a number of joint Axiomatix/Hughes/Rockwell meetings have been held over the past year in order to discuss and understand the EA-1, EA-2, SPA and DA ATP's.

Wayne McQuerry of Rockwell had previously reviewed the DA ATP and Hughes test specification 32012-042B in detail and generated 24 pages of comments, as shown in Appendix B. After Hughes studied the Rockwell comments, a series of four joint Axiomatix/Hughes/NASA/Rockwell meetings were held at Hughes

### 8.2 Findings

In the initial meeting, Mal Meredith of Hughes designated Paul Sterba, also of Hughes, to keep the meeting minutes and specifically record action items, action item responsibilities, closures and conclusions. Appendix C is the Hughes memorandum summarizing the four days of the DA ATP joint meetings.

To restate the meeting results as summarized on page 1 of Appendix C, each Rockwell comment was discussed in detail and the appropriate action taken. A total of 123 comments were presented by Rockwell (Appendix B), with the following dispositions:

1. Hughes accepts comments and no action required (5)
2. Rockwell withdrew comments (9)
3. Hughes will change DA ATS per comment (29)
4. Hughes action defined (59)
5. Hughes/Rockwell action defined (8)
6. Rockwell action defined (13)



The only open issue is the subject of system test equipment (STE) calibration which is involved in five of the eight Hughes/Rockwell actions (item 5) and 12 of the 13 Rockwell actions (item 6). Hughes contends that calibrating the STE (that is, having metrology certify the STE output signals) would be prohibitively expensive, yet Rockwell contends that Q.C. will not allow "uncalibrated" equipment to be connected to flight hardware. Basically, Rockwell is not insisting that the STE be "certified" by metrology but, rather, that the STE be affixed with Q.C. or equivalent seals and the STE configuration be controlled by the formal Hughes documentation process. At the present time, Rockwell and Hughes are still discussing how to resolve the STE calibration issue.

### 8 3 Conclusions/Recommendations

The four joint DA ATP meetings provided an opportunity for non-Hughes personnel to gain an understanding of the DA ATP and, at the same time, the meetings were an excellent start in correlating the Hughes DA ATP with the Rockwell requirements. The net results of these four meetings are a start in producing a DA ATP that all parties will have confidence in and an ATP which will ensure that quality flight hardware is being delivered.

An important outfall of the meetings, which will have an impact on other areas of the Ku-band project, is Mal Meredith of Hughes insisting that his personnel record the meeting minutes and document the action items, action item responsibilities, closures and conclusions. At the end of the meeting, a working document was produced so that each party knew what was required of it. The previous problems of everyone leaving the meeting "feeling good" but not remembering what was committed to or accomplished have been avoided, with Hughes becoming more disciplined.

As previously stated, Axiomatix feels that the DA ATP joint meetings are an excellent start towards correlating the DA ATP with the Rockwell requirements, but Axiomatix still feels that the process should be carried one step further. Both the DA ATP and the Rockwell DA specification are lengthy documents and, to ensure that there are no "holes" in the DA LRU testing, Axiomatix recommends that a correlation matrix be generated.

REFERENCES

1. "Shuttle Orbiter Ku-Band Radar/Communications System Design Evaluation," AXIOMATIX Report No. R8012-3, Final Report on NASA/JSC Contract NAS 9-15795, dated December 22, 1980.
2. SPA LRU Development Specification #DS 32012-011, Rev. A.
3. Preliminary System Specification #HS 237-2781, dated May 19, 1980.
4. W. W. Seifert, C. W. Steeg, Jr , Editors, Control Systems Engineering, McGraw-Hill Book Co., Inc., NY, NY, 1980, pp 945-955 (This portion was reprinted from a laboratory report by R. C. Booton, Jr , M. V. Mathews and W. W. Seifert, MIT, 1953).
5. W. C Lindsey and M. K. Simon, Telecommunication Systems Engineering, Prentice-Hall, Inc., Englewood Cliffs, NJ, 1973

APPENDIX A

HUGHES DEPLOYED ASSEMBLY ATP

AXIOMATIX MEMO DATED SEPTEMBER 11, 1980



9841 Airport Boulevard • Suite 912 • Los Angeles, California 90045 • Phone (213) 641 8600

File: Contract 16067 "A"

TO: Jim Kelly, EE3  
NASA Lyndon B. Johnson Space Center  
Tracking & Communications Development Division

FROM. R.G. Maronde

DATE. September 11, 1980

SUBJ: Hughes Deployed Assembly ATP

NASA has requested that Axiomatix review and comment upon Hughes test specification TS32012-Q42, Revision B, "Ku-Band Deployed Assembly (DA) Acceptance Test Specification with Appendices A,B,C,D,E,F." This acceptance test procedure (ATP) will be used by Hughes to demonstrate the DA LRU has been properly manufactured prior to delivery to Rockwell, whereas any qualification test procedure (QTP) will be used to verify the DA LRU design

In the past, when requested to review ATP's or QTP's, Axiomatix has constructed a test verification matrix. Axiomatix has always assumed the baseline LRU design document to be the respective Rockwell equipment specifications. Therefore, the Axiomatix test verification matrix has one axis being the Rockwell specification paragraphs and the other axis being the tests listed in the ATP or QTP. Any "holes" in the testing program are readily apparent since unverified specification paragraphs are highlighted.

During this initial review of TS32012-Q42, Axiomatix did not construct a test verification matrix. Instead, the ATP was carefully read, along with the six appendices. The procedure contained many tests, detailed test set-up diagrams and data sheets which at first appeared to be very satisfactory. However, after rereading the ATP, the major question remaining was: What exactly did the procedure test or verify? Since Rockwell specification MC409-0025, Revision B with changes, "Integrated

Communications and Radar Equipment, Ku-Band," is the baseline document, a cursory search was conducted to determine whether there was any correspondence between the Rockwell specification paragraphs and the tests outlined in the DA ATP.

Before discussing the findings, an important point needs to be made. Some of Rockwell's vendors have always constructed their ATP's or QTP's in almost the same format as the test verification matrix presented in the corresponding Rockwell equipment specification. Constructing an Axiomatrix test verification matrix, therefore, was straightforward because of the high degree of correlation between the Rockwell specification paragraphs and the ATP or QTP tests. The Axiomatrix test verification matrix uncovered a number of "holes" in the testing program mainly because the precise Rockwell specification paragraphs being tested were readily ascertained.

Hughes, on the other hand, for some reason does not use the Rockwell test verification matrices presented in the Revision B Ku-band specification as a guide when writing test procedures. The result is a number of tests that may be good tests in their own right but which nevertheless may not be relevant to demonstrating Rockwell specification compliance. For example, during the Ku-band system verification for the ADL LRU's, the tests were such that one test may have verified a number of specification paragraphs and another test may have not verified any paragraphs.

As previously mentioned, the Axiomatrix approach assumes the Rockwell specifications are the baseline documents. Therefore, since there is a low correlation in formats between the Rockwell Ku-band specification and the Hughes test procedures, constructing a test verification matrix is very time consuming. However, once constructed, these matrices in the past have shown an incredible number of "holes"

In the initial review of TS32012-Q42, there is no apparent correlation between the tests presented and the Rockwell Revision B paragraphs for the DA LRU. Axiomatrix could construct a test verification matrix to ascertain exactly to what extent the Hughes ATP tests the DA, but the matrix presents two problems. The first problem is that, because of the low Rockwell specification/Hughes ATP correlation factor, constructing the matrix will be very time-consuming.

The second problem is that a large amount of controversy will be created. Axiomatix, Hughes and Rockwell will all have their own interpretations as to whether a test completely verifies a specific Rockwell specification paragraph.

Axiomatix feels TS32012-042 in its present form is inadequate to demonstrate conformance to the Rockwell Revision B specification. It is recommended that Hughes change the ATP format to reflect a high degree of correlation with the Rockwell documents, which will result in minimizing any controversy

cc:

Jack Johnson, JSC  
Wayne McQuerry, Rockwell International

APPENDIX B

ROCKWELL COMMENTS ON HUGHES DA ATP TS 32012-042B

## Comments on TS32012-042B

These comments are divided into three parts as follows:

1. All sections of TS32012-042B except for the functional/performance tests per 3.2.3 through 3.2.4.25 and Appendices A through F.
2. Functional/performance tests per 3.2.3 through 3.2.4.25 and Appendices A through F.
3. Functional/performance requirements not addressed per 2 above.

Section 1 - All sections of TS32012-042B except for functional/performance tests.

Item Page Paragraph

1-1 2 2.

Change line 3 to read "...specifications and drawings listed...".

Delete last sentence.

Rationale: The ATP is a Type I document; drawings are Type II. Therefore, drawings cannot take precedence over the ATP.

1-2 20 and following:

Figures 3-1 through 3-9 except for 3-7. Descriptions of test set-up/test configuration are very general and, except the RF and IF inputs and outputs, it is impossible to identify inputs and outputs in terms of DA connector/pin and to determine the validity of these inputs/outputs for testing. Items of concern include those inputs/outputs where timing or polarity are critical and inputs/outputs drawing sufficient current to result in appreciable IR drop in the inter LRU cabling such as the following:

- a) Encoder drive
- b) Gyro spin motor excitation
- c) Gyro primary excitation
- d) (Possibly) positive and negative drivers ( $\pm 15$  VDC)

SIZE	CODE IDENT NO	DRAWING NO	
A	03953		
SCALE	REV	SHEET	OF



TS32012-042B Review - Section 1 Comments (cont.)

Item Page Paragraph

1-2 20 and following (cont.)

Other problems associated with incomplete definition of test set-up/test specimen configuration are identified in Section 2 comments. Revise figures and/or text to define test set-up/test configuration.

1-3 31 4.1.3

Change test to read as follows: "The sequence of tests shall be in the numerical order presented in this procedure except when the sequence is specifically defined elsewhere, e.g., Figure 3-11 or, in the case of functional/performance tests, the order of performing specific tests or measurements is identified as "optional" in the procedure. In event retest (other than merely repeating measurements just completed due to personnel error or test equipment malfunction where it is obvious that the error or malfunction could not overstress or otherwise damage the test specimen) or a modified testing sequence is required, testing shall be stopped and a Failure Report prepared. Testing shall be resumed as/if directed by disposition of the Failure Report."

1-4 33 4.2.2.1

Delete last sentence.

1-5 33 4.2.2.3

The post environmental monopulse phase verification test should be performed prior to the tests per 3.2.3 through 3.2.3.16.4.

1-6 34 4.2.4.3.2

What is purpose of "...in qual..."? Last sentence reads "...five 'limit'..." - Table 4-4 shows 8 limit values. Paragraph should be clarified.

	SIZE	CODE IDENT NO	DRAWING NO	
	A	03953		
	SCALE	REV	SHEET	OF

## TS32012-042B Review - Section 1 Comments (cont.)

Item	Page	Paragraph
1-7	35	4.2.4.4.9
	36	Table 4-2
<p>Exactly what functional tests are to be performed and when?; e.g., are tests performed per the "pre-vib" col. (Table 4-2) <u>before</u> each axis of vibration and per the "post vib" column <u>after</u> each axis of vibration? Clarify requirements.</p>		
1-8	35	4.2.4.4.5
		5.3.5.5.6
<p>Revise as required to reflect the following:</p>		
<p>a) Define test specimen configuration insofar as input commands, i.e., define state of signals such as sum and difference ch. enable, HSR Select, alpha-beta and 0-180 lobing, polarization, etc.</p>		
<p>b) Require verification that gimbal lock remains locked and transmitter remains off and that there is no intermittency or anomalous behavior of outputs monitored during vibration.</p>		
<p>c) Check difference channel as well as sum channel during vibration-- either input signal into J5A as well as J4A or use self test function. (Self test function is preferred.)</p>		
<p>d) Add the following outputs to the list monitored:</p>		
<p>Alpha Axis High</p>		
<p>Beta Axis High</p>		
<p>Operate Status</p>		
<p>Boom Stow Enable II</p>		
<p>± 15 VDC (positive and negative drivers)</p>		
<p>Data IF</p>		
<p>Track IF</p>		

- a) Define test specimen configuration insofar as input commands, i.e., define state of signals such as sum and difference ch. enable, HSR Select, alpha-beta and 0-180 lobing, polarization, etc.
- b) Require verification that gimbal lock remains locked and transmitter remains off and that there is no intermittency or anomalous behavior of outputs monitored during vibration.
- c) Check difference channel as well as sum channel during vibration-- either input signal into J5A as well as J4A or use self test function. (Self test function is preferred.)
- d) Add the following outputs to the list monitored:
  - Alpha Axis High
  - Beta Axis High
  - Operate Status
  - Boom Stow Enable II
  - ± 15 VDC (positive and negative drivers)
  - Data IF
  - Track IF

SIZE

A

CODE IDENT NO

03953

DRAWING NO

SCALE

REV

SHEET

OF

## TS32012-042B Review - Section 1 Comments (cont.)

Item Page Paragraph

1-8 (cont.) Temperature Sensors

DEA Heater Current - both

Diode Current - alpha-beta lobing = alpha

- e) Operating mode is Radar, ch. 3 throughout. MC calls for 1/2 time in radar, 1/2 time in comm. Radar mode only appears OK - MC change required.
- f) RF input is J4A only so check sum ch. receiver only. Should use self test function and check both receivers. Could input signal into J5A as well as J4A but this is an unnecessary complexity.
- g) Accept/reject criteria specified only for accelerometers, strain gages, bus current and DMA heater current and data sheets provide no entry for these items. Should verify the following during vibration and data sheets should provide entries for each:
- (1) Gimbal lock remains locked.
  - (2) Transmitter does not cause an even momentarily.
  - (3) No intermittent conditions or anomalous behavior for all inputs and outputs monitored.

1-9 33 4.2.1 or ?

Add requirement (either para 4.2.1 or elsewhere) for weight per MC409-0025, para 4.2.2.1.

1-10 46 4.2.5 thru 4.2.5.3

Temperatures are defined for ATVT. Thermal CDR has not been conducted. Thermal environments may be revised as a result of CDR.

1-11 49 4.2.5.4.2.9 Table 4-2 does not define post TV tests. Per 4.2.2.3 post TV tests consist of all tests defined in Section 3. Revise Table 4-2 to show post TV tests or change 4.2.5.4.2.9 to "... perform tests per 3.2.3 through 3.2.4.25 ..."

C-3	SIZE	CODE IDENT NO	DRAWING NO	
	A	03953		
SCALE	REV	SHEET	OF	

Item Page Paragraph

1-12 - -

No leakage test is performed. (Test per 3.2.3.2 is only a pressurization check.) A leak test in accordance with paragraph 4.2.2.5 of MC409-0025 is required after completion of environmental test.

1-13 - -- Text implies DA is OFF during "cool-down". ATVT is an operating test so DA is to be ON throughout test unless required to be OFF during latter of "cool-down" only to achieve test temperatures in a reasonable time. When functional testing is not in progress, alternate between radar and comm operating modes so that approximately half of test time is in each operating mode.

1-14 - -- Transmitter ON/Off not defined during ATVT. Transmitter is to be ON throughout test except when functional testing requires it to be OFF or during "cool-down" if DA has to be OFF.

1-15 - -- Add requirement to record temperatures, as indicated by DA temperature sensors, hourly during all testing except ATVT and every 15 minutes during ATVT. Add the necessary data sheets.

1-16 - -- Add requirement to monitor inputs and outputs during ATVT when functional testing is not in progress, including temperature transitions, and verify no intermittent conditions or anomalous behavior.

1-17 32 4.1.6 (c) Change tolerance for random vibration level from plus 3 dB, minus 1.5 dB to plus 1.0 dB, minus 3.0 dB.

1-18 31 4.1 Delete last sentence in first paragraph

1-19 32 4.1.4 Add sentence "whenever a Failure Report (Hughes Aircraft form 11873) is initiated, the Buyer shall be notified per PDRL RA 24."

SIZE	CODE IDENT NO	DRAWING NO	
A	03953		
SCALE	REV	SHEET	OF

## TS32012-042B REVIEW - SECTION 2 COMMENTS

Item	Page	Paragraph
2-1	5	<p>3.2.3.3.1-.1.6 Cannot verify lock motor drive signal level and polarity and loads for the <math>\pm 15</math> vdc outputs are compatible with EA-1. Either revise procedure, including data sheets to define these parameters or provide test equipment description/operating manuals or instructions and calibration requirements (as Type II data) which define these parameters.</p>
2-2	7	<p>3.2.3.3.3-.3.3 Power is radar standby (per 3.2.3.3.1.3) and gimbals are locked (per 3.2.3.3.1.6).</p> <p>Revise to define configuration for this test.</p>
2-3	7	<p>3.2.3.3.3-.3.3 Cannot verify inputs for gyro spin motor drive and gyro primary excitation and the load for gyro outputs are compatible with the requirements of EA-1 plus interconnecting wiring.</p> <p>Same as for item 2-1</p>
2-4	7	<p>3.2.3.3.3-3.3 The tolerance allowed (<math>\pm 3.7\%</math>) is considerably greater than the <math>\pm 1\%</math> used in presentations on servo performance and must be justified since this test represents the primary verification of this critical parameter after exposure to AVT and ATVT. It appears that the "justification" could be relatively simple and would consist of a statement similar to the following (either in TMO1A or the analysis report):</p> <p>"workmanship defects, component tolerance buildups/changes, etc. expected to be detected during acceptance testing (i.e., "aging", AVT, ATVT, etc.) and which could cause the scale factor to exceed design requirements (<math>\pm 1\%</math>) would normally result in changes exceeding the ATP allowed tolerance (<math>\pm 3.7\%</math>) because...</p> <p>In event the scale factor actually did exceed design requirements,</p>

## TS32012-042B Review- Section 2 Comments (cont'd.)

Item	Page	Paragraph
2-4	7	<p>but did not exceed the ATP allowed tolerances, system performance degradation would not exceed ... 1)</p> <p>NOTE: This test is considered a satisfactory test for verifying the scale factor during DA acceptance testing and there is no intent to require a more sophisticated test. However, since the allowed tolerances exceed those used (to date) in defining system performance capabilities, these differences must be justified and the justification documented.</p>
2-5	7	<p>3.2.3.3.4-.4.2 The configuration is inadequately defined (per procedure the DA gimbals are still locked and in "standby" power) and level and polarity of encoder drive signal cannot be checked for compatibility with EA-1 output levels and wire drop.</p> <p>See previous comments concerning this type of discrepancy.</p>
2-6	7	<p>3.2.3.3.4-.4.2 Add requirement for visual verification that antenna is approximately at the commanded position, i.e., verify the antenna is, approximately, at 0,0 when 0,0 is commanded, etc. The purpose of this addition is to screen out wiring/polarity errors that could result in the antenna being at <math>\alpha = 0^\circ</math>, <math>\beta = -30^\circ</math> but readouts showing <math>\alpha = 0^\circ</math>, <math>\beta = +30^\circ</math> and gross encoder "count" errors resulting in antenna being <math>0^\circ</math>, <math>60^\circ</math> and reading <math>0^\circ</math>, <math>30^\circ</math>. Figure 3-7 shows definition of + and - as well as alpha and beta.</p>
2-7	7	<p>3.2.3.3.5-5.2 The theory on which this test is based and how this measurement relates to items verified e.g., encoder accuracy/encoder, MIP position, encoder rf axis alignment, etc and the overall accuracy associated with the test are not obvious.</p>

## TS32012-042B Review - Section 2 Comments (cont'd.)

Item	Page	Paragraph
2-7 (Cont'd.)		Provide a description of test and an error analysis defining actual errors associated with items verified by this test. Can be either in TMO1A or a formally submitted report referenced in TMO1A.
2-8	8	<p>3.2.3.3.6-.6.4 No accept/reject criteria. Test proves little, if anything, about DA not covered by other tests. Instrumenting set up to provide essential information e. g., moments of inertia, motor torque scale factor, etc--would be very difficult and information required can be obtained by a relatively simple transfer function test.</p> <p>Retain main scan test--provides a "warm feeling". Delete miniscan unless this test can be revised to provide more useful information concerning DA performance capabilities.</p>
2-9	8	<p>3.2.3.3.7-.7.4</p> <p>(a) Configuration/inputs not adequately defined--see previous comments concerning this type problem</p> <p>(b) Scale factor tolerance (+ 4.9%) is greater than value used for servo analysis/ servo evaluation.</p> <p>Same comment as made per item 2-5 applies.</p> <p>(c) Add requirement to verify direction of travel as a function of motor drive polarity.</p> <p>Actually a part of (a) above.</p> <p>(d) The scale factor of 149 in-lbs/amp implies a shunt of 0.11114 ohms resistance.</p> <p>Does not seem reasonable--define test set-up.</p> <p>(e) Clarify procedures for determining friction from data. ESTL data shows 3.54 in.-lb. for alpha and 2.049 in.-lb. for beta; should show 17.68 in.-lb. for alpha and 5.96 in.-lb for beta.</p>
2-10	9	3.2.3.3.8 No comment.

## TS32012-042B Review-Section 2 Comments (Cont'd.)

Item	Page	Paragraph
2-11	10	<p>3.2.3.4.2-.2.9 Procedure (3.2.3.4.2.1) says "Enable radar standby and radar on." Implying both commands to the DA are set HIGH simultaneously and both are HIGH for all measurements. The data sheets indicate current measurements are made for both standby and on configurations. Furthermore, both commands should not be HIGH simultaneously.</p> <p>Clarify procedure</p>
2-12	10	<p>3.2.3.4.2-.2.9 Add upper limits for power consumption--both standby and radar ON. These limits, for 28 vdc input, shall be 132 watts for standby and 275 watts for radar ON per the most recent SE08A. NOTE: SE08A erroneously shows the power consumption as DEA power consumption. MC409-0025 will be revised to reflect these values.</p>
2-13	11	<p>3.2.3.4.3-.3.3 Additional information required to verify proper response to frequency select A, B, C signals and compatibility with EA-2.</p> <p>See previous comments on configuration.</p>
2-14	11	<p>3.2.3.4.4-.4.5 (a) Change to reflect that <u>average</u> power is being measured.</p> <p>(b) Accept/reject criteria for high power would allow DA to "pass" even though output was significantly degraded. Change to reflect the required DEA output of <math>46.1 \pm 1.3</math> dBm peak power output (reduced by duty cycle) and use actual coupler loss (carry forward data).</p> <p>(c) Tolerances of <math>\pm 3</math> dB for medium and low power appear to be unnecessary--Hughes has indicated compliance with the <math>\pm 2</math> dB requirements.</p> <p>Change to <math>\pm 2</math> dB.</p> <p>NOTE: If the hardware, as designed, will not comply with the <math>\pm 2</math> dB tolerance, Hughes should advise Rockwell and Rockwell will determine whether this requirement can be relaxed.</p>



## TS32012-042B Review - Section 2 Comments (Cont'd.)

2-14 (Cont'd.)

Item Page Paragraph

(d) What are the requirements (Hughes defined) for power output in the TWT by-pass mode?

DA LRU Spec requirements:  $7.55 \pm 1.45$  dBm Peak

Early version of DEA ATP:  $6.65 \pm 2.25$  dBm Peak

Present DA ATP (equivalent):  $6.7 \pm 5.0$  dBm Peak

Hughes determine what requirements are and advise Rockwell. Change ATP as/if required. Rockwell will change MC409-0025 accordingly.

(e) Add accept/reject criteria for power monitor output for High and medium power. Use power monitor calibration (carry forward data) and set limits to confirm  $46.1 \pm 1.3$  dBm peak output from DEA.

(f) Point for measurement not identified. Change procedure to specify J4A.

2-15 11 3.2.3.4.6 through 3.2.3.4.6.5 In several cases, as indicated below, requirements are confusing and text and data sheets do not seem to correlate.

Clarify procedures and requirements.

Examples of problems in reviewing this section are as follows:

(a) Paragraph 3.2.4.6.2 reads "...enable Comm A standby and Comm A on."

Which command is the DA to receive?

(b) Line 7 on data sheet calls for "verification", "Comm A ON."

How is this to be verified? Per (a) above have "enabled"

both standby and ON.

(c) Line 4 on data sheet--is equipment in STANDBY or ON?

(d) Nomenclature for beam select signals not per DA input signals.

Clarify when DA is receiving "wide beam select" and "wide beam transmit select" signals.

## TS32012-0423 Review - Section 2 Comments (Cont'd.)

Item Page Paragraph

2-15 (Cont'd) (e) Line 6 of data sheet has no entry in "requirement" column: should be

OFF or LOW apparently since the transmit enable signals appear later.

Also, are Transmit Enable KUA and Transmit Enable Comm A both low, as data sheet implies, or is Transmit Enable Comm A HIGH and Transmit Enable KUA LOW as text implies?

(f) No apparent data sheet entry for verifying Operate<sup>i</sup> Status signal is LOW when Transmit Enable Comm A is LOW and Transmit Enable KUA is HIGH.

(g) Line 10 of data sheet reads "Comm A-KUA", "Verification".

What is being verified? How?

(h) What is configuration for current measurement per line 11?

Is it as follows:

Comm A ON: HIGH

Transmit Enable Comm A: HIGH

Transmit Enable KUA: HIGH

Operate Status Signal: HIGH ( or ON)

(i) Apparently no data sheet entry covering DA response to Transmit Enable 30 deg. deploy signal HIGH--i.e., operate status signal should be HIGH or ON.

2-16 11 3.2.3.4.6-.6.5 Change entry in requirements column for standby and on power consumption (current measurements) from "Data" to the maximum allowed value. These limits, for 28 vdc input, shall be 132 watts for standby and 308 watts for Comm on, per the most recent SE08A.

NOTE: SE08A erroneously shows the power consumption on "DEA" power consumption. MC409-0025 will be revised to reflect these values.

## TS 32012-042B Review - Section 2 Comments (Cont'd.)

Item	Page	Paragraph
2-17	11	<p>3.2.3.4.8-. / ,</p> <p>(a) Definition of configuration is not clear</p> <p>See previous comments pertaining to definition of configuration</p> <p>(b) Add measurement of time from exciter gate trailing edge to RF pulse trailing edge. Same delay requirements apply; or verify transmitted pulse width is same as exciter gate pulse width <math>\pm 20</math> nsec for pulse width <math>\geq 2.7</math> microseconds and <math>\pm 10</math> nsec for pulse width = 122 nsec per DA LRU spec, Para. 3.2.1.2.1.1.9.</p> <p>(c) Difference between time delay, as measured at J4A, and the requirement, which is specified at the antenna output, and the justification for only measuring at J4A must be covered by analysis.</p>
2-18	12	<p>3.2.3.4.9-.9.2 Actual configuration of test specimen difficult to determine.</p> <p>See previous comments</p>
2-19	12	<p>3.2.3.4.10 through 3.2.3.4.11.2 Configuration and requirements incompletely defined.</p> <p>See previous comments pertaining to this. Examples of problems encountered in reviewing this section include the following:</p> <p>(a) What are the levels of the 156 MHz and 1875 MHz inputs?</p> <p>These were adjusted earlier in the procedure but this could have been performed hours (or days?) prior to this test.</p> <p>(b) Antenna select commands are not relatable to DA inputs. (See 2-15 (d).</p> <p>(c) How much (over what range) is the 1875 MHz signal swept?</p> <p>(d) Over what frequency band is flatness verified?</p> <p>(e) What does "Mode 6" and "Mode 7" mean in terms of DA inputs?</p>

Item	Page	Paragraph
2-20	12	3.2.3.4.10 through 3.2.3.4.11.2
		(a) Change requirements to sweep the 1875 MHz signal over sufficient range to determine transmit 3 dB bandwidth. Record the 3 dB bandwidth for information (data) only.
		(b) Change flatness requirement to 1 dB peak-to-peak (not <u>±</u> 1 dB) over <u>±</u> 112.5 MHz bandwidth.
		(c) Change power monitor requirement from "reference" to specific accept limits. These limits shall be equivalent to the DEA output requirements. Coupler/monitor calibration data (carry forward data) shall be used to verify compliance with requirements.
		(d) Change tolerance requirements for J4A and J5A measurements from <u>±</u> 3 dB to <u>±</u> 1.2 dB and use coupler calibration data to verify compliance.
2-21	13	3.2.3.4.12 through 3.2.3.4.12.10 This section must be revised to provide a more meaningful test. The test, as defined, does not verify a compatible interface with EA-2 for system self test purposes or provide an adequate check on performance of items not otherwise verified after exposure to test environments and during ATVT such as antenna difference channel circuitry, including the comparator, antenna sum channel circuitry, including the polarization switch, and rotating joints. All measurements, except for alpha-beta lobing current, state of the operate status signal and first LO frequency and amplitude, are identified either as "reference"--i.e., no accept/reject criteria--or the specified requirements are "applicable if measurable". The DA would "pass" the test with the comparator completely disconnected from the antenna difference channel elements and, if the requirements were applied literally, it would pass with the DEA signal source disconnected from the self test dipole.

Item Page Paragraph

2-21 13 (Cont'd.)

Requirements applicable to the self test function include radar IF modulation (magnitude and phase or polarity) as a function of the lobing signals as well as radar IF level as a function of self test attenuator signals or commands.

Because of tolerances allowed for the various parts of the self test circuitry/components, it probably will be necessary to use data acquired during the pre-environment test as a baseline, or reference, and define requirements for subsequent tests--i.e., post vibration, during and after ATVT and post environment testing -- in terms of allowed changes from this baseline. These tests (tests after the initial, pre-environment exposure) would verify that exposure to the test environment did not degrade, or change, performance of the items checked only by the "self test" test beyond acceptable limits.

The DA self test capability provides a simple, fast, check of the exciter, receiver, antenna sum and difference channel circuitry, etc., and should be utilized between environment tests and during ATVT to minimize test time.

2-22 14 3.2.3.4.13 through 3.2.3.4.13.7 Test requirements and configuration not clear in some cases.

See previous comments on this item

Examples of problems encountered in reviewing this section include the following:

(a) Para. 3.2.3.4.13.3 says "Measure track IF frequency...". Data sheet has only one entry. What is RF input frequency (at J5A) and what is status of Frequency select A, B and C?

Item 2-22 Paragraph 3.2.3.4.13.3 (Cont'd.)

(b) Para 3.2.3.4.13.3 (and others) says "Verify passband..." but no requirements identified. Data sheet shows " $X \pm 10$  MHz" (where "X" is nominal or center frequency for each channel) in requirement column. The only entries in the "test" and "re-test" columns for ESTL tests are "✓". Thus, presumably, the only item QC is to, or can, verify is that the input was swept over the required range--i, e., the test specimen would "pass" this test regardless of output.

(c) Para. 3.2.3.4.13.4 says Measure "...ripple modulation at the center frequency."

No definition of "ripple modulation at center frequency" is given.

No requirements (accept/reject criteria) shown.

No data sheet entries provided for this parameter.

What is QC supposed to verify?

(d) Are photographs of spectrum supposed to be made for 3.2.3.4.13.4 and 3.2.3.4.13.5?

Data sheet shows "passband (photos)" for 3.2.3.4.13.3 but there is no similar entry for 3.2.3.4.13.4 and 3.2.3.4.13.5.

ESTL data, both "test" and "retest" has photos for 3.2.3.4.13.4 and 3.2.3.4.13.5, but the photo for 3.2.3.4.13.4 in the "retest" data package submitted to Rockwell is unreadable ("white out")

and is out of sequence.

(e) ESTL data for noise level measurements inconsistent; data shows different channel levels of -30 dBm and -32 dBm for HSR= 1 and 0 respectively; gain data shows difference should be only 0.4dB. Data for sum channel is -34.5 dBm; noise figure and gain data show noise level should be approximately 2 dB higher than difference channel. Revise procedure as required to insure useful data. Add noise measurements for data and track IF's, comm freq. Make requirement dependent on measured gain to avoid problems associated with the allowed 8 dB gain variation allowed.

## TS32012-042B Review - Section 2 Comments (Cont'd.)

Item	Page	Paragraph
2-22 (Cont'd.)		<p>(e) Para. 3.2.3.4.13.5 Same as (a) above except dealing with Radar IF in lieu of Track IF.</p> <p>(f) Para. 3.2.3.4.13.5 says "Repeat...for each of two second IF bandwidths". Data sheet shows entries for 10 MHz and 3 MHz bandwidths. Bandwidth determined by state of the High Sample Rate Select command to DA. How is QC to verify state of this command?</p> <p>NOTE: Test equipment description/"operating manual" and calibration requirements are not controlled (Type I) documents.</p> <p>(g) Para. 3.2.3.4.13.7 says "... measure...and ripple modulation." There is no data sheet entry covering this item. What is QC supposed to verify?</p>
2-23	14	<p>3.2.3.4.13 through 3.2.3.4.13.7</p> <p>(a) Gain tolerances of <math>\pm 6.0</math> dB and <math>\pm 6.5</math> dB are 2 dB greater than the tolerances per the DA LRU specification.</p> <p>MC409-0025 is being revised to reflect the DA LRU spec requirements. If the <math>+ 6.0</math> and <math>\pm 6.5</math> dB tolerances are retained in the ATP, Comm and Radar system performances must reflect these tolerances and MC409-0025 will have to be revised again (after Hughes has submitted analysis showing performance requirements are met with these tolerances.)</p> <p>(b) Add a requirement to record the ratio of the difference channel gain to the sum channel gain, <u>including RF rotary joint losses</u> (SRU carry forward data), and to verify that this ratio is within the limits of <math>-2.2 \pm 1.9</math> dB when no AGC is applied.</p> <p>(c) Add requirements to verify the bandwidths and ripple of all three IF meet the requirements specified in DA LRU spec, Para. 3.1.2.4.14.1 through 3.1.2.4.14.3 and 3.2.1.2.2.14.</p>

## TS32012-042B Review - Section 2 Comments (Cont'd.)

Item Page Paragraph  
2-23 15 3.2.3.4.14 through 3.2.3.4.14.2

(a) The ATP does not reflect DA LRU Spec requirements as follows:

	DA LRU SPEC	ATP
TR Limeter AGC:	30 <u>±</u> 1 dB	30 <u>±</u> 1.5 dB
Step IF AGC:	30 <u>±</u> 2 dB	30 <u>±</u> 2.5 dB

MC409-0025 currently reflects DA LRU spec requirements.

Hughes define requirements and change ATP if required.

(MC409-0025 will be revised if the present ATP requirements are the "real" requirements.)

(b) For final (post environmental) test, measure response for both increasing and decreasing signal level.

(c) How is linear AGC slope to be determined?

Plot data and "eyeball" best straight line?

Use "least squares" mathematical computation??

Clarify procedure.

2-25 15 3.2.3.4.15 through 3.2.3.4.15.14

(a) S-Band Spur Rejection - Radar IF: The test requirements appear to be in excess of the requirements shown in the DA LRU Spec and MC409-0025.

Input, J4A:	+ 10 dBm
Coupler effects:	- 22 dB Nominal
Receiver Gain @ center Freq.	<u>+ 81 dB</u> Nominal
Expected IF output if	+ 69 dBm
Frequency = center Freq:	
Required output, ATP:	- 55 dBm max; ch 1, 10 MHz BW
Implied rejection reqmt.:	124 dB
Required rejection, DA LRU Spec:	45 dB minimum

Hughes explain rationale for test requirements.



## TS32012-042B Review - Section 2 Comments (Cont'd.)

Item	Page	Paragraph
2-25	15	3.2.3.4.15 through 3.2.3.4.15.14 (Cont'd.)

(b) Image frequency rejection - Radar IF: test requirements appear to be in excess of requirements per DA LRU Spec and MC409-0025.

Input, J4A:	+ 10 dBm	
Coupler effects:	- 22 dBm	Nominal
Receiver Gain (center freq.)	+ 81 dBm	Nominal
Expected IF level, Ctr. Freq. Input:	+ 69 dBm	
Required output, ATP	- 80 dBm max.	
Implied Rejection reqmt.	149 dB	
DA LRU Spec. reqmt.	70 dB	

Hughes explain rationale for test requirement

(c) S-Band Spur rejection and Comm Transmit Freq. rejection. Input is J4A only. Should be J5A for Track IF measurements and J4A for Data IF measurements. Track IF and Data IF tests, as defined, check sum channel recover only.

(d) Test access coupler characteristics: coupler characteristics are not defined. Must be defined at SRU level for the frequency band required for the test--carry forward data--and actual response used in determining rejection characteristics.

(e) Rejection requirements: in most cases requirements defined in terms of a maximum allowed IF signal level with an additional statement "or below noise level." Most data sheet entries for ESTL tests are simply "below noise level" or "BNL".

Change text and/or data sheets to require an entry showing rejection is greater than " X " dB when response is in the noise where "X" represents the minimum value that can be established due to noise level.

Item Page Paragraph  
 2-25 15 3.2.3.5.15 through 3.2.3.4.15.14 (Cont'd.)

(f) Comm transmit frequency rejection: rejection requirements must be justified. Minimum rejection implied is 103.5 dB for the track

IF test as follows:

Input, J4A:	+ 10 dBm
Coupler effects:	- 22 dB Nominal
Receiver Gain, sum input to track IF:	<u>+ 70.5 dB</u> Nominal
Expected IF, center frequency input:	58.5 dBm
Required output:	- 45.0 dBm Maximum
Implied rejection:	103.5 dB

Reflected power at receiver input is approx. 29.8 dBm as follows:

Rotary Joint VSWR, Sum ch:	1.35:1.0 Max.
Antenna sum ch. VSWR:	1.5:1.0 Max.

Nominal DEA output, comm narrow beam:	46.4 dBm = 43.65 watts
---------------------------------------	------------------------

Assuming nominal DEA output and a VSWR of 1.35:1.0 for the

DEA to rotary joint interface, the reflected power is:

$43.65 \text{ watts} \times 2.2\% = .96 \text{ watts} = 29.8 \text{ dBm}$ .

The received signal input to the DEA, assuming  $-126 \text{ dBw/m}^2$  power density and 37.1 dB<sub>i</sub> antenna gain, is approx. -103 dBm.

Thus the expected reflected power at the DEA input is approximately 133 dB above the expected received signal level. Also, the expected reflected power into the DEA is approximately 42 dB higher than the test signal used for this test.

(g) Comm transmit freq. rejection: add a test to measure track and data IF noise level (no RF input, J4A or J5A) with transmitter ON and with transmitter OFF and verify:

(1) no change in noise level between transmitter ON and transmitter OFF conditions

(2) no change in spurious outputs between the transmitter ON and transmitter OFF conditions for the band of  $647 \pm 150 \text{ MHz}$  (first IF filter band pass per DA LRU spec, Fig. 3.2.1.2-4.)

## TS32012-042B - Review - Section 2 Comments (Cont'd.)

Item	Page	Paragraph
1-25	15	<p>3.2.3.5.15 through 3.2.3.4.15.14 (Cont'd.)</p> <p>(h) Main bang leakage - radar: The DA LRU spec requirement is -40 dBm; the ATP requirement is 31 mv peak. It would appear the ATP requirements are considerably less stringent than the DA LRU spec requirements. Hughes justify/verify ATP is correct.</p> <p>(i) Configuration: clarification required i.e.,--What are DA inputs associated with "mode select switch on 8", "channel 6", etc.</p>
2-26	16	<p>3.2.3.4.16 through 3.2.3.4.16.3</p> <p>(a) Paragraph 3.2.3.4.16.3 calls for repeat of 3.2.3.4.16.1 and 3.2.3.4.16.2, but data sheets do not provide entries for a repeat of 3.2.3.4.16.1</p> <p>Correct data sheet.</p> <p>(b) Requirements (for measured times ) are different from DA LRU spec and tolerances are considerably greater than those in DA LRU spec.</p> <p>Hughes verify ATP requirements are correct--i.e., the values the system performance is based on and what EA-2 is "expecting". Hughes provide value for "TBD", 3.2.3.4.16.1.</p>
2-27	17	<p>3.2.4 through 3.2.4.25</p> <p>(a) Combination of text and data sheets seem to be an adequate definition of requirements for radar mode, linear polarization, channel 3 but are inadequate for other 4 frequencies and for circular polarization, Comm and radar.</p> <p>Revise data sheets, and text, if required, to clarify.</p>

## TS32012-042B Review- Section 2 Comments (Cont'd.)

Item	Page	Paragraph
2-27 (Cont'd.)		(b) Requirements for Comm (13.775 GHz, CP) and radar, active target mode (13.883 GHz, CP) are not adequately defined. Should be a maximum phase error of 30 degrees.  Clarify.
2-28	Appendix A	No comments
2-29	Appendix B	No comments
2-30	Appendix C	(a) Change requirement for comm transmit frequency (14.85 to 15.15) gain to 37.9 dBi minimum.  (DA LRU spec requirement.)  (b) Requirements for monopulse tracking scale factor for CP, beta axis is $0.5 \pm 0.1$ ; DA LRU spec requirement is $0.6 \pm 0.1$ .  Hughes verify ATP values are acceptable--i.e., the value used in comm and radar performance analysis and the value EA-1 and EA-2 are "expecting".  (c) Add the following self test dipole measurements:  (1) Sum channel coupling, antenna circularly polarized. (2) Difference channel coupling, alpha (3) Difference channel coupling, beta  (d) Narrow beam beamwidth requirements are less than the DA LRU spec calls for--Comm, radar active mode tgt.  Hughes verify ATP values acceptable, i. e., the values used, or to be used for Comm and radar system performance analysis.
2-31	Appendix D--	Add loss measurement for coax cable from DEA to self test dipole.
2-32	Appendix E	(a) Both High Scale (coarse) and Low Scale (fine) scale factors specified for rates of 10 degrees/second and greater.  Hughes verify no scale factor requirements for rates less than 10 degrees/second.  (b) Fine scale factor tolerance is $\pm 3\%$ .  Hughes verify this is acceptable.

## TS32012 -042B Review - Section 2 Comments (Cont'd.)

Item	Page	Paragraph
2-33	16	Appendix F

(a) Test access connector measurements per 4.4.4.7.1 and 4.4.7.3 specify  $-22 \pm 2$  dB. This is requirement for output at J4A and J5A per MC409-0025, Para. 30.3.2.1.2.3.2.3.c. Per Hughes drawing 3561604 the cable between the DEA and J4A or J5A is approximately 14 inches of RG142 B/U.

Add coax cables to DEA for this measurement or reduce DEA allowed coupling/loss to accommodate coax cable loss.

(b) Test access coupling measurements are made only at 15 GHz. Coupling data is also required for the frequency range from 12.48 GHz to 14 GHz.

Add measurement.

(c) Noise figure requirements per 4.4.4.8.8 (6.4 dB and 6.6 dB for sum and difference channels respectively) when the step IF AGC and Tr limiter AGC are applied are unrealistic and equipment does not comply

Revise requirements per DA LRU spec.

## 32012-042B Review - Section 3 Comments

## 3. Performance requirements/parameters not verified.

Performance requirements/parameters identified in this section are not verified by the ATP as written plus changes made to correct discrepancies identified in Sections 1 and 2 of these notes. Analysis showing that workmanship errors during fabrication and assembly, component tolerance build-ups, etc, that would result in the DA failing to perform as required, either initially or during and after exposure to the specified environments, will be detected (screened out) by inspection, inline tests or other tests performed during acceptance testing must be submitted by Hughes, and approved by Rockwell, or tests must be added to cover these items

3.1 The procedure, as written, calls for testing to be performed with nominal inputs. Review of the design and/or problems during development indicates the deployed assembly performance is, or may be, sensitive to variations allowed for certain inputs. The most critical inputs include the following:

- a) Encoder Driver
- b) Gyro Spin Motor Drive
- c) Gyro Primary Excitation
- d) 156 MHz reference
- e) 1875 MHz Exciter IF
- f) 28 vdc power

If tests are added to verify DA performance over the allowed range of inputs, these additional tests should be limited to measuring (verifying) selected, most sensitive, performance parameters for maximum and minimum values of the inputs and should be performed during ATVT at both temperature extremes.

3.2 Specific performance parameters not verified include the following:

- a) Transmitter - Comm operations
  - (1) Phase linearity
  - (2) Gain Slope
  - (3) AM to PM conversion
  - (4) Spurious outputs
  - (5) Broadband noise output
  - (6) IFM
  - (7) IAM
  - (8) Phase noise

## TS 32012-042B Review - Section 3 Comments (Cont'd.)

## 3.2 (Cont'd.)

- b) Receiver-Comm operations
  - (1) Gain Slope
  - (2) Phase linearity
  - (3) AM to PM conversion
  - (4) Intermodulation products
- c) Transmitter - radar operations
  - (1) Broadband noise outputs
  - (2) Spurious outputs
- d) Receiver - radar operation --see (b) above
- e) Antenna alignment - rf axes, rf axes to encoders.
- f) Alignment, mirror "cube" and antenna A axis.
- g) DA dynamic properties as applicable to antenna servo operations
- \*h) Antenna/gimbal moments of inertia (servo item)
- \*i) Motor torque scale factor (servo item)
- j) Heater power consumption
- k) Antenna gain, beamwidth, axial ratio, etc. after exposure to vibration and during exposure to a thermal vacuum environment.

\*These two servo related items ( h and i) can be covered by a simple transfer function test at the "cross over" frequency and at one frequency considerably less than the "cross over" frequency. Such a test would be performed in ambient laboratory environment (post environmental or final performance test) only and two or three gimbal positions should be sufficient.

APPENDIX C

ACTION ITEMS TO ADDRESS ROCKWELL COMMENTS ON

HUGHES DA ATP TS 32012-042B





ORIGINAL PAGE IS  
OF POOR QUALITY



INTERDEPARTMENTAL CORRESPONDENCE

TO	Distribution	cc	Data Bank (2)	DATE	28 April 1981
ORG				REF.	HS237-3343
SUBJECT	RI/HAC/NASA DA ATS Comment Review Meeting			FROM	<input checked="" type="checkbox"/> P. E. Sterba
				ORG	40-92-20
				BLDG	S13 MAIL STA D329
				LOC	SC EXT 59354

Reference: HS237-354-929 dated March 24, 1981, Subject: Purchase Order No. M7J3XMB-48139D, Ku-Band Deployed Assembly Acceptance Test Procedure with Appendices A, B, C, D, E and F (TM11-A).

Four joint Hughes/Rockwell/NASA meetings have been held to review Rockwell's comments to the DA Acceptance Test Specification (ATS) TS32012-042B contained in the above reference. Those attending these meetings are listed in table 1. Each comment was discussed and action items were defined to address the issues raised by the comments where appropriate. The defined action for each comment is given in table 2 and the corresponding notes.

A total of 123 comments were presented in the referenced document. No action is required for 14 of the comments. A summary of the disposition of these comments follow:

- 1) Hughes accepts comments and no action required - (5).
- 2) Rockwell withdrew comment - (9).
- 3) Hughes will change DA ATS per comment - (29).
- 4) Hughes action defined - (59).
- 5) Hughes/Rockwell action defined - (8).
- 6) Rockwell action defined - (13).

The subject of STE calibration is involved in 5 of the 8 Hughes/Rockwell actions and 12 of the 13 Rockwell actions.

P. E. Sterba

PES:10

Attachment

1 OF 13

TABLE 1: DA ATP MEETING ATTENDANCE

<u>Attendees</u>	<u>M E E T I N G S</u>			
	<u>4/9</u>	<u>4/10</u>	<u>4/16</u>	<u>4/20</u>
<u>Rockwell</u>				
W.S. Pope	X		X	
F.E. Cummings	X	X	X	
W.H. McQuerry	X	X	X	X
D. Potts	X	X	X	X
<u>Hughes</u>				
M. Meredith	X			
P.E. Sterba	X	X	X	X
K. Stern	X	X	X	X
W. Turner	X	X	X	
S. Kubo	X	X	X	
V. Karpenko	X	X	X	
T. DeGasperi	X			X
A. Hanson		X		
R. Chan	X			X
J. Riles			X	
<u>NASA/JSC</u>				
J. Kelley	X			
<u>Axiomatix</u>				
R.G. Maronde	X	X	X	

COMMENT ITEM NUMBER (REFERENCED DOCUMENT)	<u>A</u> ACTION KUBO REVISE ATS- PER COMMENT	<u>B</u> ACTION KUBO (SEE NOTE)	<u>C</u> ACTION HUGHES (SEE NOTE)	<u>D</u> ACTION ROCKWELL (SEE NOTE)	<u>E</u> NO ACTION COMMENT WITHDRAWN BY ROCKWELL	<u>F</u> NO ACTION HUGHES ACCEPTS COMMENT	<u>G</u>  NOTES  ORIGINAL PAGE IS OF POOR QUALITY
1-1	X						
1-2a				X			N1-8a
b				X			N1-8a
c				X			N1-8a
d				X			N1-8a
1-3		X					N1-3
1-4		X					N1-4
1-5		X					N1-5
1-6	X						
1-7	X						
1-8a		X		X			N1-8a
1-8 b, c	X						
1-8d		X					N1-8d
1-8e, f, g	X						
1-9	X						
1-10						X	
1-11	X						
1-12		X					N1-12
1-13	X						
1-14	X						
1-15		X					N1-15
1-16		X					N1-16
1-17				X			N1-17
1-18	X						
1-19					X		

COMMENT ITEM NUMBER (REFERENCED DOCUMENT)	A ACTION KUBO REVISE ATS PER COMMENT	B ACTION KUBO (SEE NOTE)	C ACTION HUGHES (SEE NOTE)	D ACTION ROCKWELL (SEE NOTE)	E NO ACTION COMMENT WITHDRAWN BY ROCKWELL	F NO ACTION HUGHES ACCEPTS COMMENT	G  NOTES  ORIGINAL PAGE IS OF POOR QUALITY
2-1				X			N1-8a
2-2		X					N2-2
2-3				X			N1-8a
2-4					X		
2-5		X					N2-5
2-6	X						
2-7			X				N2-7
2-8		X					N2-8
2-9a		X		X			N2-9a
b					X		N1-8a
c				X			N2-9d
d			X				N2-9e
e		X					
2-10						X	
2-11					X		
2-12		X					N2-12
2-13				X			N1-8a
2-14a	X						N2-14b
b		X					N2-14c
c			X				N2-14d
d			X				N2-14e
e		X					
f	X						
2-15a					X		N2-15b
b		X				X	N2-15c
c							N1-8a
d				X			N2-15b
e		X					N2-15b
f		X					N2-15b
g		X					N2-15b
h		X					N2-15i
i		X					
2-16		X					N2-12

COMMENT ITEM NUMBER (REFERENCED DOCUMENT)	A ACTION KUBO REVISE ATS PER COMMENT	B ACTION KUBO (SEE NOTE)	C ACTION HUGHES (SEE NOTE)	D ACTION ROCKWELL (SEE NOTE)	E NO ACTION COMMENT WITHDRAWN BY ROCKWELL	F NO ACTION HUGHES ACCEPTS COMMENT	G  NOTES ORIGINAL PAGE IS OF POOR QUALITY
2-17a b c		X	X	X			N1-8a N2-17b N2-7
2-18				X			N1-8a
2-19a b c d e		X X		X X			N1-8a N1-8a N2-19c N2-19d N1-8a
2-20a b c d		X X X X		X			N2-19c N2-19d N2-20c N2-14b
2-21		X					N2-21
2-22a b c d e1 e2 f g	X	X X X X X X		X			N2-22a N2-22b N2-22c N2-22c N2-22e (1) N2-22a N2-22d
2-23a b c	X	X	X X				N2-14b N2-23b
2-24a b c	X X				X		
2-25a b c d e f g h i	X X X X	X	X X X	X			In SCN 001 In SCN 001 N2-33b N2-25f N2-25g N2-25h N1-8a

COMMENT ITEM NUMBER (REFERENCED DOCUMENT)	A ACTION KUBO REVISE ATS PER COMMENT	B ACTION KUBO (SEE NOTE)	C ACTION HUGHES (SEE NOTE)	D ACTION ROCKWELL (SEE NOTE)	E NO ACTION COMMENT WITHDRAWN BY ROCKWELL	F NO ACTION HUGHES ACCEPTS COMMENT	G  NOTES  ORIGINAL PAGE IS OF POOR QUALITY
2-26a b	X		X				N2-26b
2-27a b	X X						
2-28						X	
2-29						X	
2-30a b c d	X		X X X				N2-30b N2-30c N2-30d
2-31						X	
2-32a b		X			X		N2-32a
2-33a b c		X	X X				N2-33a N2-33b N2-33c
3-1a b c d e f			X X X X X X				N3-1a N3-1a N3-1a N3-1a N3-1a N3-1a

6

COMMENT ITEM NUMBER (REFERENCED DOCUMENT)	<u>A</u> ACTION KUBO REVISE ATS PER COMMENT	<u>B</u> ACTION KUBO (SEE NOTE)	<u>C</u> ACTION HUGHES (SEE NOTE)	<u>D</u> ACTION ROCKWELL (SEE NOTE)	<u>E</u> NO ACTION COMMENT WITHDRAWN BY ROCKWELL	<u>F</u> NO ACTION HUGHES ACCEPTS COMMENT	<u>G</u>  NOTES ORIGINAL PAGE IS OF POOR QUALITY
3-2 a(1) (2) (3) (4) (5) (6) (7) (8)			X X X X X X X X				N3-2a (1) N3-2a (2) N3-2a (3) N3-2a (3) N3-2a (3) N3-2a (2) N3-2a (2) N3-2a (2)
3-2 b(1) (2) (3) (4)			X X X X				N3-2a (2) N3-2a (1) N3-2b (3) N3-2a (3)
3-2 c(1) (2)			X X				N3-2a (3) N3-2a (3) N3-2a (2)
3-2 d e f g h i j k	X	X X	X  X X  X		X		N3-2e N3-2e N3-2g N3-2g  N3-2g

NOTES:

- N 1-3. Revise DA ATS to add first sentence only of the comment. The rest of paragraph will not be added to the ATS.
- N 1-4. Revise DA ATS to remove second sentence in paragraph 4.2.2.1 of the ATS. Add a sentence which allows performing the thermal and vibration environmental tests in reverse order at REA's discretion.
- N 1-5. Revise inprocess test spec 32012-073 to measure phase and self test at the same time during testing of the Qualification Unit to confirm that self test is adequate to verify phase. If the results of the tests are positive, then Rockwell agrees to approve a change in the DA ATS to remove the monopulse test conducted on the slant range (approximately one week) and use the self test to verify monopulse phase.
- Change figure 3-11 to agree with paragraph 4.2.2.3 in the DA ATS.
- N 1-8a. Hughes - Write a short (one page or less) description of the Hughes approach to testing with special test equipment built specially for testing the deliverable equipment. Explain how Hughes has confidence that the outputs and performance of the special test equipment meet requirements without calibrating this equipment.
- Rockwell - Define specific outputs from the special test equipment which Hughes is required to verify by measurement prior to acceptance testing deliverable DA hardware.
- N 1-8d Revise the DA ATS to add continuous monitoring of the following signals during vibration tests.
- 1) The temperature sensor connected in series.
  - 2) Both heater currents.
  - 3) The alpha - beta lobing diode current.
  - 4) The second IF output using a diode.
- N 1-12 Review techniques for measuring leak rate at ambient or during thermal vacuum test to see if test can be added to verify leak requirement.



ORIGINAL PAGE IS  
OF POOR QUALITY

- N 1-15 Revise DA ATS per comment except temperature may be recorded every 30 minutes (instead of every 15 minutes) during ATVT.
- N 1-16 Revise DA ATS to list what inputs and outputs are to be monitored during ATVT.
- N 1-17 Determine acceptability of allowing spikes which exceed the random vibration tolerances listed in this comment during random vibration testing.
- N 2-2 Revise DA ATS to add procedure for redeploying the antenna prior to conducting the drift tests and define the configuration (state) of the hardware.
- N 2-5 Revise DA ATS to define hardware configuration during tests described in paragraph 3.2.3.3.3.1 of the ATS.
- N 2-7 Turner: Comply with comment by documenting required analysis in Development Test Report TM 012.
- N 2-8 Revise DA ATS to retain main scan and delete miniscan per comment.
- N 2-9a Hughes: Revise ATS to add operational steps to clarify procedure including configuration information.  
Rockwell: N1-8a
- N 2-9d Riles: Review paragraph 3.2.3.3.7.2 of DA ATS and explain test point scale factor value.
- N 2-9e Revise DA ATS to add words "stop to stop" to paragraph 3.2.3.3.7.2.
- N 2-12 Revise DA ATS to add power consumption limit values. Ron Chan is to provide these values to Kubo (for ATS) and System Engineering for update of SE08A.
- N 2-14b Revise DA ATS to add requirement for change in peak power output between measurements with a common test setup (same cable effects) to repeat within  $1.5 \pm$  db.  
System Engineering Mohler: Review test approach and determine if measurement error can be reduced to value consistent with hardware performance requirement.
- N 2-14c Hughes - Stern: Change DA Development Specification to increase peak power tolerances to  $\pm$  3db.
- N 2-14d Hughes - Stern: Determine correct value for power output in the TWT by-pass mode and write ECR to correct Development Specification and ATS.  
Rockwell: Revise MC409-0025 to reflect the value established by System Engineering
- N 2-14e Hughes. Revise DA ATS to add acceptance criteria for power monitor output at high power.  
Rockwell: Determine acceptability of two point calibration of monitor output.

**Suggested calibration technique: Feed Ku-Band variable power source into waveguide ahead of rotary joint and calibrate power monitor.**

- N 2-15b Revise DA ATS data sheet page 70 (3.2.3.4.6) to clarify operation.
- N 2-15c Information: Equipment mode is COMM A ON. **ORIGINAL PAGE IS OF POOR QUALITY**
- N 2-15i Add additional entry to data sheet.
- N 2-17b Revise DA ATS to add measurement of time from exciter gate trailing edge to RF pulse trailing edge.
- N 2-19c Revise DA ATS to define range of sweep to the 3db points.
- N 2-19d Revise DA ATS to add bandpass value.
- N 2-20c Hughes: Revise DA ATS to add power monitor acceptance limits to data sheet.  
Rockwell: N 1-8a
- N 2-21 Revise DA ATS to add acceptance levels for items listed in comments.
- N 2-22a Hughes - Revise DA ATS to define the hardware configuration during the track IF test.  
Rockwell - N1-8a
- N 2-22b Revise DA ATS that the bandwidth is defined as the 3db point.
- N 2-22c Revise DA ATS to delete the ripple requirement.
- N 2-22d Revise DA ATS data sheet to require photographs be taken
- N2-22e(1) Review comment with Hughes RF specialists and develop a response to the comment.
- N 2-23b Kubo: Determine the feasibility of measuring % AM per degree during initial phase adjustment on the slant range.  
System Engineering: Define % AM requirements.  
Note: Rockwell - McQuerry states that rotary joint test requirement can be deleted if % AM test is added.
- N 2-25f Receiver COMM frequency rejection measurement contained in DA ATS has been corrected by SCN 001.  
Kubo: Revise DA ATS to add test to measure transmitter isolation requirement specified in DA Development Specification.

N 2-25f (cont'd)

System Engineering - Stern: Review DA Development Specification and add transmitter isolation requirement if it is not specified (reference MC409-0025, par. 3.0.3.2.1.2.3.7q).

N 2-25g Revise DA ATS to satisfy comment

(1) and (2) respectively by the following action:

(1) Satisfy by photographs of spectrum analyzer output when measuring data and track IF.

(2) Accomplish by visual observation for an interval greater than 30 seconds.

N 2-25h System Engineering - Stern: Review ATS measurement value per comment and confirm ATS value is correct.

N 2-26b Kubo: Document how the tolerance for receiver gate to detected Radar IF measurement was determined.

Turner/Karpenko: Determine how performance requirements are going to be verified if test accuracy is insufficient to verify requirements to specified tolerance.

N 2-30b Turner/Karpenko: Submit an ECR to change the monopulse scale factor in the DA Development Specification from  $0.6 \pm 1$  to  $0.5 \pm 0.1$  which agrees with achievable DA antenna performance.

N 2-30c Hanson: Revise DA ATS Appendix C to add measurements requested by comment with note that they are for information only.

N 2-30d Turner/Karpenko: Submit ECR to DA Development Specification to change the narrow beam beamwidth to agree with the ATS.

N 2-32a Revise DA ATS Appendix E, paragraph 4.1.5.c by replacing the words "rates higher" with "rates lower".

N 2-33a DeGasperin: Revise the DEA ATS to comply with comment.

N 2-33b Previously requested coupler test data down to 12.48 GHz was provided by DeGasperin and accepted by McQuerry.

DeGasperin: Submit an ECR to Appendix F of the DA ATS to add measurement of coupling value for both couplers in the Radar Band (already measured in COMM transmit band).

DeGasperin: Generate analysis to define expected out of band (12.48 to 15.3 GHz) coupling value performance.

Turner/Karpenko: Document above DA analysis in Development Test Report TM 012.

N 2-33c Prepare an SCN to delete noise figure measurement for transmitter AGC per ECR 936524.

N 3-1a Turner: Collect existing development test data for inputs listed in comment and provide to Rockwell by April 30, 1981.

N3-2a(1) DeGasperin: Define justification for not measuring parameters during DEA acceptance testing (AT).

Turner: Define justification for not measuring parameters during DA AT. Document the DA and the DEA justification in Development Test Report TM 012.

N3-2a(2) System Engineering - Mohler: Define and document justification for not measuring parameter during AT.

N3-2a(3) DeGasperin: Define justification for not measuring parameter during DA AT.

Turner/Karpenko: Document above justification in Development Test Report TM 012.

N3-2b(3) System Engineering: N3-2a(2)

System Engineering: Define performance of parameters and add to DA Development Specification.

N3-2e Document technique of aligning RF antenna axis to the reference mirror "cube".

N3-2g Turner/Karpenko: Determine parameter performance by analysis and document in Development Test Report TM012.



### 1.3 Deployed Assembly

#### 1.3.1 Lien #03, Sum and Difference Phase Measurement

No action on Lien required; however, difference port on DEA should be properly terminated.

#### 1.3.2 Lien #11, Undervoltage Autorecovery Inoperative

Unit should be fixed or user should be made aware of limits on low-voltage operation.

### 1.4 SPA

#### 1.4.1 Lien #01, Frame Synchronization Word Error Tolerance

Frame synchronization will not occur if error is in the first four bits.

#### 1.4.2 Lien #02, 1.875 GHz Reference Signal Level

Signal level is low; verify ability to drive transmitter; fix if required.

#### 1.4.3 Lien #03, Phase/State Selection (QPSK/FM BB Generator IF)

Verify proper power split, adjust as required.

#### 1.4.4 Lien #05, Return Link Differential Phase, Gain K Factor Measurements

Perform required measurement.

#### 1.4.5 Lien #06, Block I Convolutional Encoder SRU with Inverter

Replace with Block II convolutional encoder with  $G_2$  inversion and midbit detector.

#### 1.4.6 Lien #07, FM Module Unmodified

Repair module to prevent oscillation.

#### 1.4.7 Lien #11, Management Handover

Verify compatibility of EA-1 and SPA interface without "encoded mode" bits.

- 2.0 LIENS FROM REFERENCE (2)
- 2.1 EA-1
  - 2.1.1 Lien #03, Data-Good Flag Incorrect  
Probable design anomaly; verify.
  - 2.1.2 Lien #15, Communication Signal Strength Indicator  
Probable ESTL-only problem; verify.
  - 2.1.3 Lien #27, Communication Track IF  
Should not be a problem since it is not tracking but should verify that there is no interaction with the data channel.
- 2.2 EA-2  
No liens appropriate to communications.
- 2.3 Deployed Electronic Assembly
  - 2.3.1 Lien #12, No Transmitter Output, Intermittent Output  
Fix race problem in LVPS/HVPS.
  - 2.3.2 Lien #19, Transmitter Turn-Off  
Fix DEA logic.
  - 2.3.3 Lien #20, Transmitter Noise  
Correct missing ground in ferrite switch.
- 2.4 SPA
  - 2.4.1 Lien #11, Unmodulated Carrier Offset  
Incorporate redesigned FM module.
  - 2.4.2 Lien #15, Spurious Noise on Unmodulated Carrier  
Bring up to specification.

2.4.3 Lien #18, FM VCO Redesign

See 2.4.1.

2.4.4 Lien #19, Reversed Capacitor

Fix to prevent breakdown.

2.5 Deployed Assembly (DMA)

No liens appropriate to communications.

3.0 DELIVERABLE SYSTEM TEST EQUIPMENT

Use of ADL DSTE to operate and maintain system in proposed activity must be established

Attachments: References (1) and (2) to addressee only





9841 Airport Boulevard • Suite 912 • Los Angeles, California 90045 • Phone (213) 641-8600

TECHNICAL MEMORANDUM NO. M8209-3

TO: J. Dodds

DATE: September 30, 1982

FROM: U. Cheng

FILE: NAS 9-16067"A"

SUBJECT: Effects of Cross Coupling on the Stability and Tracking Performance of Alpha and Beta Servo Loops

-----

## 1 0 INTRODUCTION

The Ku-Band Communication Autotrack System contains  $\alpha$  and  $\beta$  servo loops whose purpose is to acquire and track the difference azimuth and elevation error angles, respectively. Cross coupling between the difference elevation and azimuth channels which feed these loops, originating from the monopulse feeds and comparator network, has the potential to cause stability problems during acquisition and tracking operations. Furthermore, even if stable operation is assured, cross coupling produces a degrading effect on each loop's tracking performance in noise.

In this memo, we discuss the potential stability problem caused by cross coupling and derive a necessary but insufficient condition to ensure stability. In addition, using mean-squared phase jitter as a measure of tracking performance, the degradation in this measure caused by the cross coupling is assessed in terms of such parameters as the servo noise bandwidth and damping factor for each of the loops as well as the pair of cross-coupling gains.

We begin our analysis by considering the noise-free model of the pair of cross-coupled loops with the purpose of examining each loop's response to an input phase step. The behavior of the corresponding loop phase error responses as time approaches infinity is then an indication of the stability of the system.

## 2.0 NOISE-FREE MODEL OF CROSS-COUPLED LOOPS (RESPONSE TO PHASE-STEP INPUT)

Consider the noise-free model for the cross-coupled  $\alpha$  and  $\beta$  servo loops, as illustrated in Figure 1. Here  $\alpha$  and  $\beta$  denote the angular errors for the two servo loops and  $\epsilon_\alpha$  and  $\epsilon_\beta$  are, respectively, the corresponding  $\alpha$ -axis and  $\beta$ -axis voltage errors. The gains  $K_\alpha$  and  $K_\beta$  are equivalent to  $K_{SC} = K_{SC1}K_{SC2}$  in the HAC

ORIGINAL PAGE IS  
OF POOR QUALITY

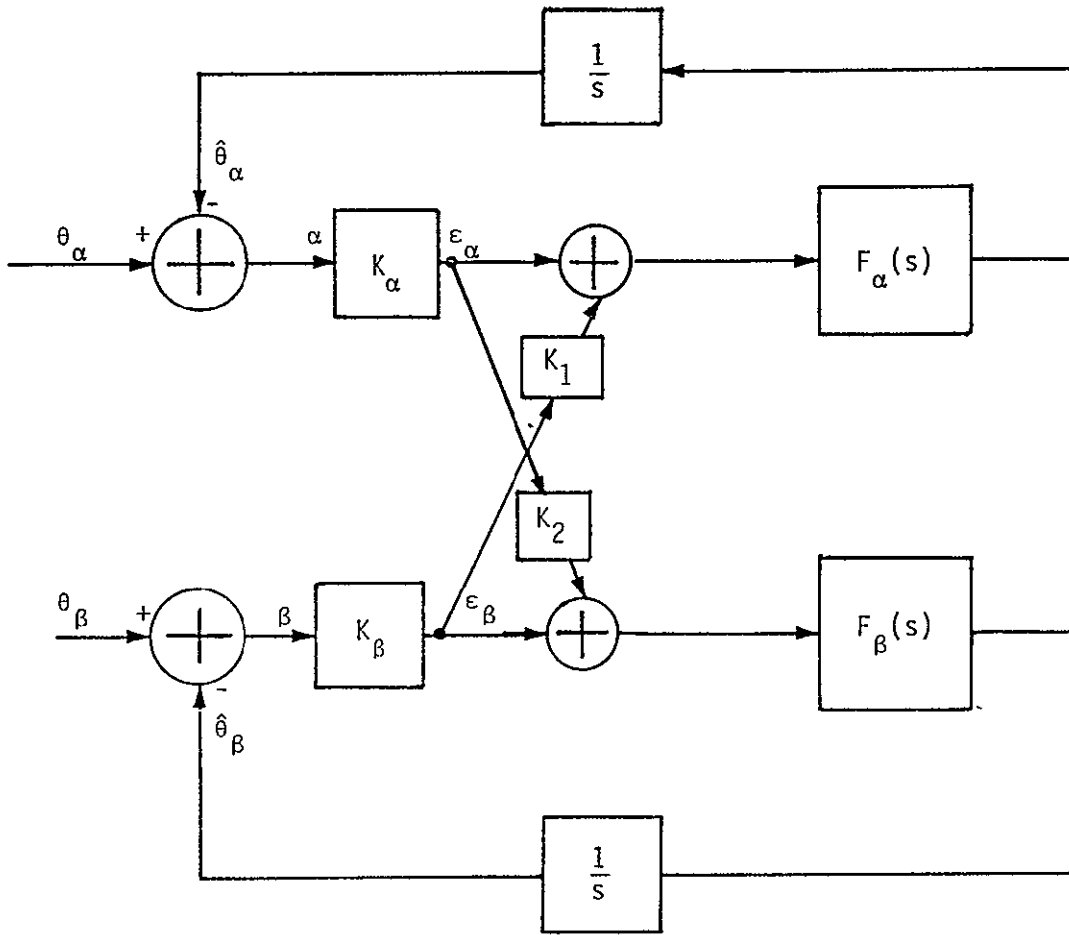


Figure 1 A Simple Block Diagram for the Cross-Coupled  $\alpha$  and  $\beta$  Servo Loops in the Absence of Noise

**ORIGINAL PAGE IS  
OF POOR QUALITY**

servo configuration single-axis block diagram where  $K_{SC} = 117 \text{ V/rad} = 2.047 \text{ V/deg}$  and  $1 \leq K_{SC2} \leq 15$ . Note that Figure 1 is an equivalent block diagram for the linear region of behavior

The blocks labeled  $K_1$  and  $K_2$  represent the normalized cross coupling between the loops where, for the moment, we restrict  $K_1$  and  $K_2$  to have a magnitude less than or equal to unity. The blocks marked  $1/s$  represent the transfer functions of the  $\alpha$ -axis and  $\beta$ -axis servo motors. Finally,  $F_\alpha(s)$  and  $F_\beta(s)$  represent the composite transfer functions of the various components and subloops that comprise the rate-stabilization loop for each axis. Later on, we shall discuss the detail required to characterize  $F_\alpha(s)$  and  $F_\beta(s)$  in terms of the actual rate-stabilization-loop parameters. But, for the moment, we shall treat  $F_\alpha(s)$  and  $F_\beta(s)$  as rational transfer functions in much the same manner as one characterizes a loop filter in a conventional phase-locked loop.

By inspecting Figure 1, we can immediately write the following relations

$$\epsilon_\alpha = K_\alpha(\theta_\alpha - \hat{\theta}_\alpha), \quad \epsilon_\beta = K_\beta(\theta_\beta - \hat{\theta}_\beta) \quad (1)$$

and

$$\hat{\theta}_\alpha = \frac{F_\alpha(s)}{s} (\epsilon_\alpha + K_1 \epsilon_\beta), \quad \hat{\theta}_\beta = \frac{F_\beta(s)}{s} (\epsilon_\beta + K_2 \epsilon_\alpha) \quad (2)$$

Combining (1) and (2) gives the pair of coupled equations

$$\begin{aligned} \epsilon_\alpha \left( \frac{1}{K_\alpha} + \frac{F_\alpha(s)}{s} \right) + \frac{K_1 F_\alpha(s)}{s} \epsilon_\beta &= \theta_\alpha \\ \epsilon_\alpha \left( \frac{K_2 F_\beta(s)}{s} \right) + \epsilon_\beta \left( \frac{1}{K_\beta} + \frac{F_\beta(s)}{s} \right) &= \theta_\beta \end{aligned} \quad (3)$$

After solving (3), we get

$$\begin{aligned} \epsilon_\alpha &= \frac{sK_\alpha(s + K_\beta F_\beta(s))\theta_\beta - sK_\alpha K_\beta K_1 F_\alpha(s)\theta_\beta}{(s + K_\alpha F_\alpha(s))(s + K_\beta F_\beta(s)) - K_\alpha K_\beta K_1 K_2 F_\alpha(s)F_\beta(s)} \\ \epsilon_\beta &= \frac{sK_\beta(s + K_\alpha F_\alpha(s))\theta_\beta - sK_\beta K_\alpha K_2 F_\beta(s)\theta_\alpha}{(s + K_\alpha F_\alpha(s))(s + K_\beta F_\beta(s)) - K_\alpha K_\beta K_1 K_2 F_\alpha(s)F_\beta(s)} \end{aligned} \quad (4)$$

Now letting  $\theta_\alpha$  and  $\theta_\beta$  correspond to step changes in phase, i.e.,

$$\theta_\alpha = \frac{\Theta_\alpha}{s}, \quad \theta_\beta = \frac{\Theta_\beta}{s} \quad (5)$$

then substituting (5) into (4) results in

$$\begin{aligned} \epsilon_\alpha &= \frac{K_\alpha (s + K_\beta F_\beta(s)) \theta_\alpha - K_\alpha K_\beta K_1 F_\alpha(s) \theta_\beta}{(s + K_\alpha F_\alpha(s))(s + K_\beta F_\beta(s)) - K_\alpha K_\beta K_1 K_2 F_\alpha(s) F_\beta(s)} \\ \epsilon_\beta &= \frac{K_\beta (s + K_\alpha F_\alpha(s)) \theta_\beta - K_\beta K_\alpha K_2 F_\beta(s) \theta_\alpha}{(s + K_\alpha F_\alpha(s))(s + K_\beta F_\beta(s)) - K_\alpha K_\beta K_1 K_2 F_\alpha(s) F_\beta(s)} \end{aligned} \quad (6)$$

Note that, for no cross coupling, i.e. ;  $K_1 = K_2 = 0$ , (6) reduces to

$$\epsilon_\alpha = \frac{K_\alpha \theta_\alpha}{s + K_\alpha F_\alpha(s)}, \quad \epsilon_\beta = \frac{K_\beta \theta_\beta}{s + K_\beta F_\beta(s)} \quad (7)$$

as it should. The results in (6) can be written in a more compact form by defining the closed-loop transfer functions in the absence of cross coupling, i.e.

$$H_\alpha(s) = \frac{K_\alpha F_\alpha(s)}{s + K_\alpha F_\alpha(s)}, \quad H_\beta(s) = \frac{K_\beta F_\beta(s)}{s + K_\beta F_\beta(s)} \quad (8)$$

Dividing the numerator and denominator of the right-hand side of (6) and using (8) gives the desired result, namely,

$$\begin{aligned} \epsilon_\alpha(s) &= \frac{K_\alpha (1 - H_\alpha(s)) \frac{\Theta_\alpha}{s} - K_1 K_\beta H_\alpha(s) (1 - H_\beta(s)) \frac{\Theta_\beta}{s}}{1 - K_1 K_2 H_\alpha(s) H_\beta(s)} \\ \epsilon_\beta(s) &= \frac{K_\beta (1 - H_\beta(s)) \frac{\Theta_\beta}{s} - K_2 K_\alpha H_\beta(s) (1 - H_\alpha(s)) \frac{\Theta_\alpha}{s}}{1 - K_1 K_2 H_\alpha(s) H_\beta(s)} \end{aligned} \quad (9)$$

In order to examine system stability, we consider the steady-state ( $t \rightarrow \infty$ ) behavior of the angular error voltages in response to the phase step changes of (5). Applying the final-value theorem to (9), we observe that, if they exist, the limiting values of  $\epsilon_\alpha$  and  $\epsilon_\beta$  become

$$\lim_{t \rightarrow \infty} \epsilon_\alpha(t) = \lim_{s \rightarrow 0} s \epsilon_\alpha(s) \quad ; \quad \lim_{t \rightarrow \infty} \epsilon_\beta(t) = \lim_{s \rightarrow 0} s \epsilon_\beta(s) \quad (10)$$

or

$$\lim_{t \rightarrow \infty} \epsilon_\alpha(t) = \lim_{s \rightarrow 0} \frac{K_\alpha(1 - H_\alpha(s)) \theta_\alpha - K_1 K_\beta H_\alpha(s)(1 - H_\beta(s)) \theta_\beta}{1 - K_1 K_2 H_\alpha(s) H_\beta(s)}$$

and

$$\lim_{t \rightarrow \infty} \epsilon_\beta(t) = \lim_{s \rightarrow 0} \frac{K_\beta(1 - H_\beta(s)) \theta_\beta - K_2 K_\alpha H_\beta(s)(1 - H_\alpha(s)) \theta_\alpha}{1 - K_1 K_2 H_\alpha(s) H_\beta(s)} \quad (11)$$

Since, from (8),

$$\lim_{s \rightarrow 0} H_\alpha(s) = \lim_{s \rightarrow 0} H_\beta(s) = 1$$

it is clear that both  $\epsilon_\alpha(t)$  and  $\epsilon_\beta(t)$  will then have limiting values of zero if  $K_1 K_2 \neq 1$ , however, when  $K_1 K_2 = 0$ , we know that the system is stable. Hence, it is believed that  $K_1 K_2 < 1$  is the condition required for each loop to be stable. Note that this result was obtained independent of the order of each of the uncoupled loops, i.e., it was unnecessary to restrict  $H_\alpha(s)$  and  $H_\beta(s)$  to have first-order or second-order polynomials as their denominators, as would be the case for the first-order and second-order loops.

Before further discussing loop stability, one must investigate the pole locations of  $\epsilon_\alpha(s)$  and  $\epsilon_\beta(s)$ , which requires investigating the roots of the denominator  $1 - K_1 K_2 H_\alpha(s) H_\beta(s)$ . This in turn requires specifying the equivalent loop filters  $F_\alpha(s)$  and  $F_\beta(s)$ .

For many cases,  $K_1 K_2 < 1$  is the necessary and sufficient condition for each loop to be stable. Let us consider two of these cases.

(1) We let

$$F_\alpha(s) = A \quad , \quad F_\beta(s) = B \quad (12)$$

Equation (4) then becomes

$$\begin{aligned}\epsilon_{\alpha} &= \frac{sK_{\alpha}(s+BK_{\beta})\theta_{\alpha} - K_1K_{\alpha}K_{\beta}sA\theta_{\beta}}{s^2 + (AK_{\alpha} + BK_{\beta})s + (1 - K_1K_2)ABK_{\alpha}K_{\beta}} \\ \epsilon_{\beta} &= \frac{sK_{\beta}(s+AK_{\alpha})\theta_{\beta} - K_2K_{\alpha}K_{\beta}sB\theta_{\alpha}}{s^2 + (AK_{\alpha} + BK_{\beta})s + (1 - K_1K_2)ABK_{\alpha}K_{\beta}}\end{aligned}\quad (13)$$

We can make two observations about the denominator of  $\epsilon_{\alpha}$ . First, since  $K_1$ ,  $K_2$ ,  $K_{\alpha}$ ,  $K_{\beta}$ ,  $A$  and  $B$  are positive, one has

$$(AK_{\alpha} + BK_{\beta})^2 - 4(1 - K_1K_2)ABK_{\alpha}K_{\beta} = (AK_{\alpha} - BK_{\beta})^2 + 4ABK_{\alpha}K_{\beta} > 0 \quad (14)$$

Hence, both of these two roots are real. Secondly, both roots are negative only if  $K_1K_2 < 1$ .

(2) We let

$$F_{\alpha}(s) = 1 + \frac{A}{s}, \quad F_{\beta}(s) = 1 + \frac{B}{s} \quad (15)$$

Equation (4) then becomes

$$\begin{aligned}\epsilon_{\alpha} &= \frac{s^2K_{\alpha}(s^2 + sK_{\beta} + BK_{\beta})\theta_{\alpha} - K_1K_{\beta}(sK_{\alpha} + AK_{\alpha})s^2\theta_{\beta}}{(s^2 + sK_{\alpha} + AK_{\alpha})(s^2 + sK_{\beta} + BK_{\beta}) - K_1K_2(sK_{\alpha} + AK_{\alpha})(sK_{\beta} + BK_{\beta})} \\ \epsilon_{\beta} &= \frac{s^2K_{\beta}(s^2 + sK_{\alpha} + AK_{\alpha})\theta_{\beta} - K_2K_{\alpha}(sK_{\beta} + BK_{\beta})s^2\theta_{\alpha}}{(s^2 + sK_{\alpha} + AK_{\alpha})(s^2 + sK_{\beta} + BK_{\beta}) - K_1K_2(sK_{\alpha} + AK_{\alpha})(sK_{\beta} + BK_{\beta})}\end{aligned}\quad (16)$$

When  $A=B$ , the denominator of  $\epsilon_{\alpha}$  can be factorized as follows

$$(s^2 + sK_{\alpha} + AK_{\alpha})(s^2 + sK_{\beta} + BK_{\beta}) - K_1K_2(sK_{\alpha} + AK_{\alpha})(sK_{\beta} + BK_{\beta}) = (s^2 + E_1(s+A))(s^2 + E_2(s+A)) \quad (17)$$

where

$$E_1 = \frac{(K_{\alpha} + K_{\beta}) - \sqrt{(K_{\beta} - K_{\alpha})^2 + 4K_1K_2K_{\alpha}K_{\beta}}}{2} \quad (18)$$

and

ORIGINAL PAGE IS  
OF POOR QUALITY

$$E_2 = \frac{(K_\alpha + K_\beta) + \sqrt{(K_\beta - K_\alpha)^2 + 4 K_1 K_2 K_\alpha K_\beta}}{2} \quad (19)$$

Hence, all roots will have negative real parts only if  $E_1 > 0$ ; however, this can be true only if  $K_1 K_2 < 1$ .

### 3.0 NOISE MODEL OF CROSS-COUPLED LOOPS (TRACKING ANALYSIS)

Consider the noise model of the cross-coupled  $\alpha$  and  $\beta$  servo loops, as illustrated in Figure 2. Here  $K_{\alpha 1}$  and  $K_{\alpha 2}$  are identical to  $K_{SC1}$  and  $K_{SC2}$ , as previously defined. Similarly,  $K_{\beta 1}$  and  $K_{\beta 2}$  are identical to  $K_{SC1}$  and  $K_{SC2}$ . Furthermore,

$$K_\alpha = K_{\alpha 1} K_{\alpha 2}, \quad K_\beta = K_{\beta 1} K_{\beta 2} \quad (20)$$

Analogous to (1), we now have

$$\epsilon_\alpha = K_\alpha (\theta_\alpha - \hat{\theta}_\alpha) + K_{\alpha 2} N_\alpha, \quad \epsilon_\beta = K_\beta (\theta_\beta - \hat{\theta}_\beta) + K_{\beta 2} N_\beta \quad (21)$$

whereas (2) still applies. Again combining (21) and (2) gives the pair of coupled equations

$$\begin{aligned} \epsilon_\alpha \left( \frac{F_\alpha(s)}{s} + \frac{1}{K_\alpha} \right) + \epsilon_\beta \left( \frac{F_\alpha(s)}{s} K_1 \right) &= \theta_\alpha + \frac{N_\alpha}{K_{\alpha 1}} \\ \epsilon_\beta \left( \frac{F_\beta(s)}{s} K_2 \right) + \left( \frac{F_\beta(s)}{s} + \frac{1}{K_\beta} \right) \epsilon_\beta &= \theta_\beta + \frac{N_\beta}{K_{\beta 1}} \end{aligned} \quad (22)$$

Since we are interested in the mean-square angular-tracking jitter due to noise, we may ignore the terms in (22) that involve  $\theta_\alpha$  and  $\theta_\beta$  and solve directly for  $\epsilon_\alpha$  and  $\epsilon_\beta$ . After some simplification, this results in a pair of equations analogous to (4), namely,

ORIGINAL PAGE IS  
OF POOR QUALITY

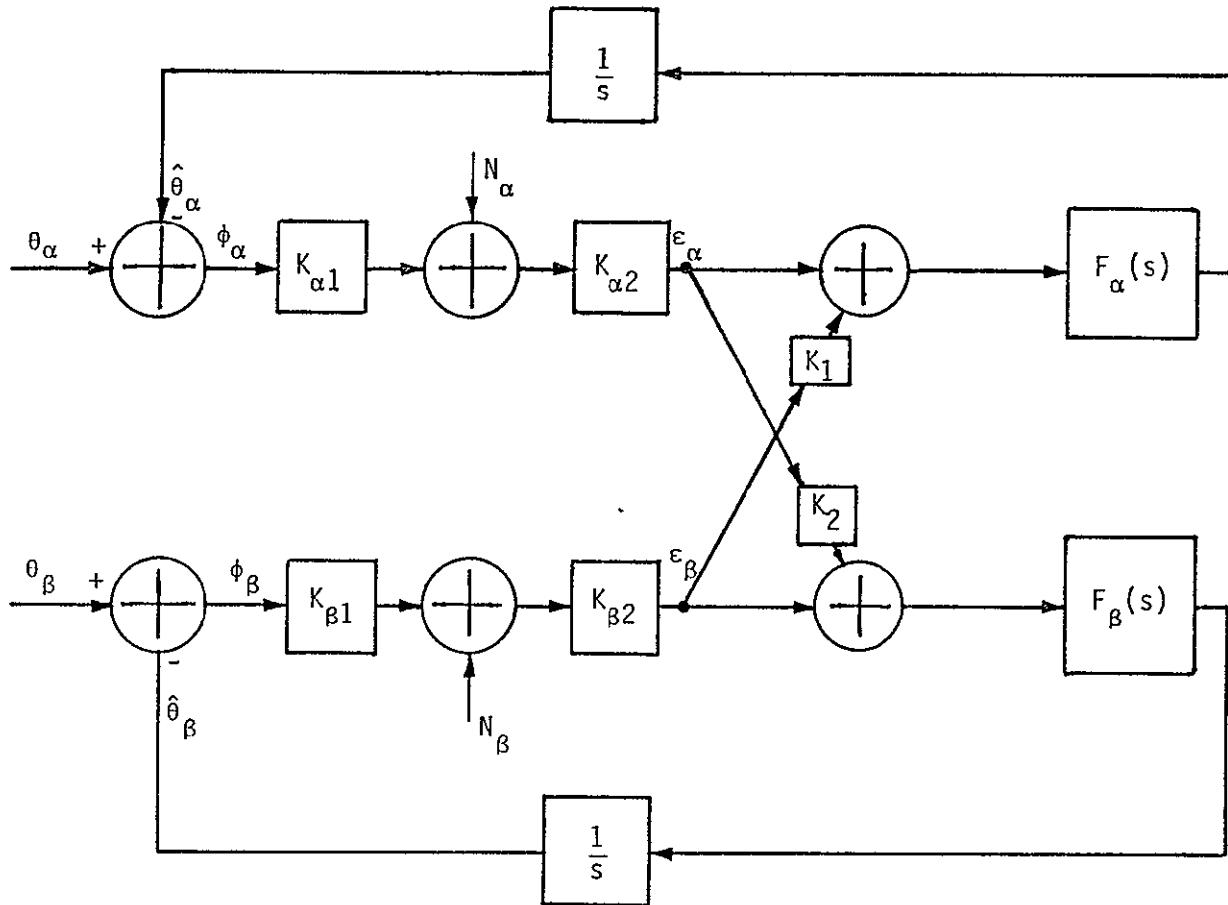


Figure 2 A Simple Block Diagram for the Cross-Coupled  $\alpha$  and  $\beta$  Servo Loops in the Presence of Noise



$$\begin{aligned}\epsilon_{\alpha} &= \frac{sK_{\alpha}(s+K_{\beta}F_{\beta}(s))\frac{N_{\alpha}}{K_{\alpha 1}} - sK_{\alpha}K_{\beta}K_1F_{\alpha}(s)\frac{N_{\beta}}{K_{\beta 1}}}{(s+K_{\alpha}F_{\alpha}(s))(s+K_{\beta}F_{\beta}(s)) - K_{\alpha}K_{\beta}K_1K_2F_{\alpha}(s)F_{\beta}(s)} \\ \epsilon_{\beta} &= \frac{sK_{\beta}(s+K_{\alpha}F_{\alpha}(s))\frac{N_{\beta}}{K_{\beta 1}} - sK_{\alpha}K_{\beta}K_2F_{\beta}(s)\frac{N_{\alpha}}{K_{\alpha 1}}}{(s+K_{\alpha}F_{\alpha}(s))(s+K_{\beta}F_{\beta}(s)) - K_{\alpha}K_{\beta}K_1K_2F_{\alpha}(s)F_{\beta}(s)}\end{aligned}\quad (23)$$

In the absence of cross coupling (i.e.,  $K_1 = K_2 = 0$ ), (23) reduces to

$$\epsilon_{\alpha} = K_{\alpha 2}(1 - H_{\alpha}(s))N_{\alpha} ; \epsilon_{\beta} = K_{\beta 2}(1 - H_{\beta}(s))N_{\beta} \quad (24)$$

as it should, i.e., the noise sources are transformed by the out-of-band loop transfer functions insofar as their effect on the loop error voltage is concerned.

Actually, we are interested in the angular error voltages  $\phi_{\alpha}$  and  $\phi_{\beta}$  which, from Figure 2, are related to  $\epsilon_{\alpha}$  and  $\epsilon_{\beta}$  by

$$\phi_{\alpha} = \frac{\epsilon_{\alpha} - K_{\alpha 2}N_{\alpha}}{K_{\alpha}} , \quad \phi_{\beta} = \frac{\epsilon_{\beta} - K_{\beta 2}N_{\beta}}{K_{\beta}} \quad (25)$$

Substituting (23) into (25) and simplifying produces the desired results.

$$\begin{aligned}\phi_{\alpha} &= \frac{\frac{H_{\alpha}(s)}{K_{\alpha 1}}(1 - K_1K_2H_{\beta}(s))N_{\alpha} - \frac{K_1K_{\beta 2}}{K_{\alpha}}H_{\alpha}(s)(1 - H_{\beta}(s))N_{\beta}}{1 - K_1K_2H_{\alpha}(s)H_{\beta}(s)}} \\ \phi_{\beta} &= \frac{-\frac{K_2K_{\alpha 2}}{K_{\beta}}H_{\beta}(s)(1 - H_{\alpha}(s))N_{\alpha} + \frac{H_{\beta}(s)}{K_{\beta 1}}(1 - K_1K_2H_{\alpha}(s))N_{\beta}}{1 - K_1K_2H_{\alpha}(s)H_{\beta}(s)}\end{aligned}\quad (26)$$

We now wish to compare the mean-square values of  $\phi_{\alpha}$  and  $\phi_{\beta}$  in (26) relative to the same values for  $K_1 = K_2 = 0$  so as to assess the degradation in mean-square phase jitter due to the cross-coupling effect. First, setting  $K_1 = K_2 = 0$  in (26), we get

$$\sigma_{\phi_{\alpha 0}}^2 = \frac{1}{K_{\alpha 1}^2} \frac{N_{0\alpha}}{2} \left( \frac{1}{2\pi j} \int_{-j\infty}^{j\infty} |H_{\alpha}(s)|^2 ds \right) \triangleq \frac{N_{0\alpha} B_{L\alpha}}{K_{\alpha 1}^2} \triangleq \frac{1}{\rho_{\alpha}} \quad (27)$$

where  $B_{L\alpha}$  is the equivalent loop noise bandwidth of the  $\alpha$ -servo in the absence of cross coupling and the zero subscript on  $\sigma_{\phi_{\alpha 0}}^2$  denotes this case. Furthermore,  $N_{0\alpha}$  is the single-sided noise spectral density of the equivalent noise source  $N_{\alpha}(t)$ .

In the presence of cross coupling, we obtain from (26) the relation

$$\begin{aligned} \sigma_{\phi_{\alpha}}^2 = & \frac{K_1^2 K_{\beta 2}^2 N_{0\beta}}{K_{\alpha}^2} \left( \frac{1}{2\pi j} \int_{-j\infty}^{j\infty} \left| \frac{H_{\alpha}(s)(1-H_{\beta}(s))}{1-K_1 K_2 H_{\alpha}(s) H_{\beta}(s)} \right|^2 ds \right) \\ & + \frac{1}{K_{\alpha 1}^2} \frac{N_{0\alpha}}{2} \left( \frac{1}{2\pi j} \int_{-j\infty}^{j\infty} \left| \frac{H_{\alpha}(s)(1-K_1 K_2 H_{\beta}(s))}{1-K_1 K_2 H_{\alpha}(s) H_{\beta}(s)} \right|^2 ds \right) \end{aligned} \quad (28)$$

For the assumed loop-filter transfer functions

$$F_{\alpha}(s) = K_{F_{\alpha}} \quad , \quad F_{\beta}(s) = K_{F_{\beta}} \quad (29)$$

The closed-loop transfer function of (8) can be written in the form

$$H_{\alpha}(s) = \frac{1}{1 + \frac{s}{K_{\alpha} K_{F_{\alpha}}}} \quad , \quad H_{\beta}(s) = \frac{1}{1 + \frac{s}{K_{\beta} K_{F_{\beta}}}} \quad (30)$$

Substituting (30) into the integrands of (28), we can get

$$\sigma_{\phi_{\alpha}}^2 = \frac{N_{0\alpha}}{4K_{\alpha 1}^2} \frac{1}{K_{\alpha} K_{F_{\alpha}} + K_{\beta} K_{F_{\beta}}} \left( (1-K_1 K_2) K_{\alpha} K_{F_{\alpha}} K_{\beta} K_{F_{\beta}} + (K_{\alpha} K_{F_{\alpha}})^2 \right) + \frac{N_{0\beta} (K_1 K_{\beta 2} K_{F_{\alpha}})^2}{4(K_{\alpha} K_{F_{\alpha}} + K_{\beta} K_{F_{\beta}})} \quad (31)$$

Defining

$$\frac{1}{2\pi j} \int_{-j\infty}^{j\infty} \left| \frac{H_\alpha(s)(1-H_\beta(s))}{1-K_1K_2H_\alpha(s)H_\beta(s)} \right|^2 ds \triangleq 2B_{L\beta}K_{\beta\alpha}$$

and

$$\frac{1}{2\pi j} \int_{-j\infty}^{j\infty} \left| \frac{H_\alpha(s)(1-K_1K_2H_\beta(s))}{1-K_1K_2H_\alpha(s)H_\beta(s)} \right|^2 ds \triangleq 2B_{L\alpha}K_{\alpha\alpha} \quad (32)$$

and noting that

$$B_{L\alpha} = \frac{K_\alpha K_{F\alpha}}{4}, \quad B_{L\beta} = \frac{K_\beta K_{F\beta}}{4} \quad (33)$$

we end up with

$$K_{\alpha\alpha} = \frac{1}{K_\alpha K_{F\alpha} + K_\beta K_{F\beta}} \left( (1-K_1K_2) K_\beta K_{F\beta} + K_\alpha K_{F\alpha} \right)$$

$$K_{\beta\alpha} = \frac{K_\alpha K_{F\alpha}}{K_\alpha K_{F\alpha} + K_\beta K_{F\beta}} \frac{K_\alpha K_{F\alpha}}{K_\beta K_{F\beta}} \quad (34)$$

and (31) can be written as

$$\sigma_{\phi_\alpha}^2 = \frac{K_{\alpha\alpha}}{\rho_\alpha} + \left( \frac{K_1^2 K_\beta^2}{K_\alpha^2} \right) \frac{K_{\beta\alpha}}{\rho_\beta} \quad (35)$$

Note that, for  $K_1K_2 = 0$ , we have

$$K_{\alpha\alpha} = 1 \quad (36)$$

We also note that, in (35),  $\rho_\beta$  is defined as

$$\rho_\beta = \frac{K_{\beta 1}^2}{N_{0\beta} B_{L\beta}} \quad (37)$$

where (37) is analogous to (27).

4.0 EVALUATION OF  $F_\alpha(s)$  AND  $F_\beta(s)$  IN TERMS OF RATE STABILIZATION LOOP PARAMETERS

Analogous to the mathematical model in Figure 2, Figure 3 is a simplified block diagram of the  $\alpha$ -axis servo loop alone. Thus, the equivalent loop filter  $F_\alpha(s)$  in Figure 2 is the product of the gains  $K_4$  and 0.92 and the transfer function  $H_{RS}(s)$  of the rate-stabilization loop whose block diagram is illustrated in Figure 4. Letting  $F_{RS}(s)$  denote the transfer function loop-shaping filter (See Figure 5 and Table 1) and  $H_{RSA}(s)$  denote the transfer function of the rate sensor assembly (see Figure 6), then

$$F_\alpha(s) = 0.92 K_4 H_{RS}(s) = \frac{F_{RS}(s) G_{MD}(s) K_{TM} \cos \beta}{(1 + T_R s) J(\beta) s + 1.745 \times 10^{-2} H_{RSA} F_{RS} G_{MD}(s) K_{TM} \cos \beta} \quad (38)$$

Now, from Figure 6, we see that

$$H_{RSA}(s) \triangleq \frac{x_2(s)}{x_3(s)} = \frac{10.05 K_{SG} K_G K_C (1 + T_G s) (1 + T_5 s)}{K_G s^2 (1 + T_g s) (1 + T_4 s)^4 + K_{SG} K_C (1 + T_G s) (1 + T_5 s)} = \frac{\sum_{i=0}^2 h_1^{(1)} s^i}{\sum_{i=0}^7 h_1^{(2)} s^i} \quad (39)$$

where

$$\begin{aligned} h_0^{(1)} &= 7.992 \times 10^6 \\ h_1^{(1)} &= 7.992 \times 10^6 T_G + 7.992 \times 10^4 \\ h_2^{(1)} &= 7.992 \times 10^4 T_G \end{aligned} \quad (40)$$

$$\begin{aligned} h_0^{(2)} &= 1.698 \times 10^5 \\ h_1^{(2)} &= 1.698 \times 10^5 T_G + 1.698 \times 10^3 \\ h_2^{(2)} &= 1.698 \times 10^3 T_G + 4.864 \end{aligned} \quad (41)$$

From Figure 5, we see that

$$F_{RS}(s) \triangleq \frac{x_5(s)}{x_4(s)} = F_1 F_2 K_B \left[ \frac{K_{CA} (1 + T_{LA} s)}{1 + T_{CA} s} \right] \left( G_{NL1} G_{NL2} K_L + \frac{K_{1A} K_{XA}}{s} \right) = F_1 F_2 K_B \frac{\sum_{i=0}^8 h_1^{(3)} s^i}{\sum_{i=0}^8 h_1^{(4)} s^i} \quad (42)$$

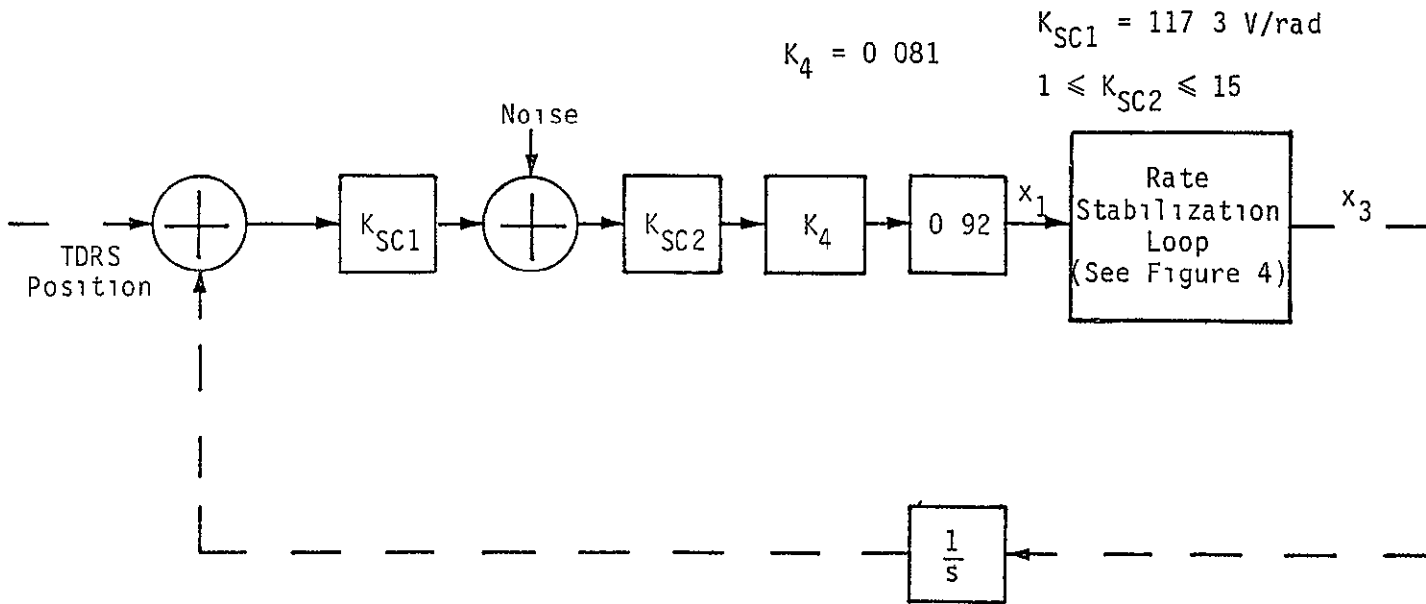


Figure 3 Simplified Block Diagram of the  $\alpha$ -Axis Servo Loop

ORIGINAL PAGE IS  
OF POOR QUALITY

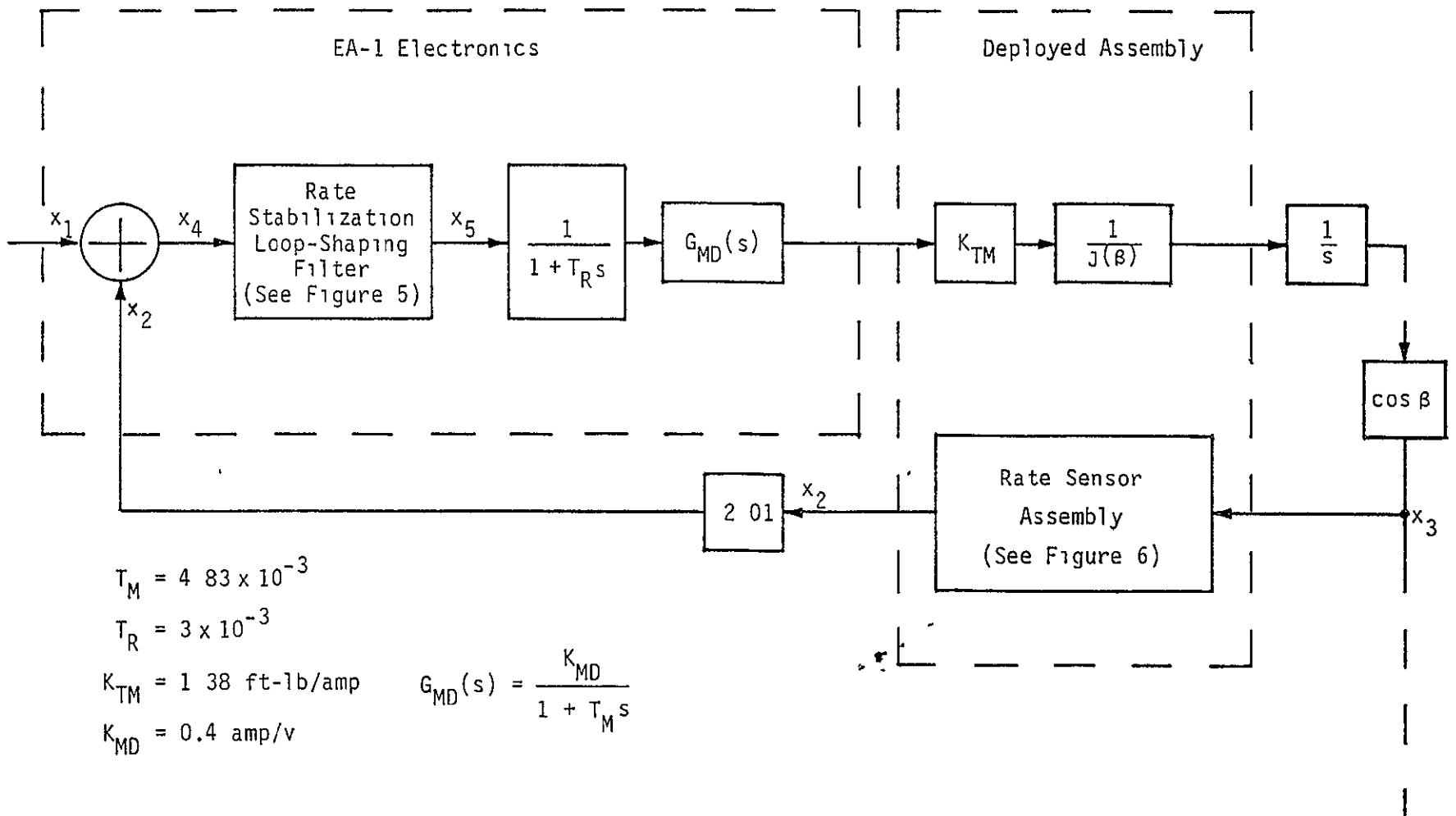
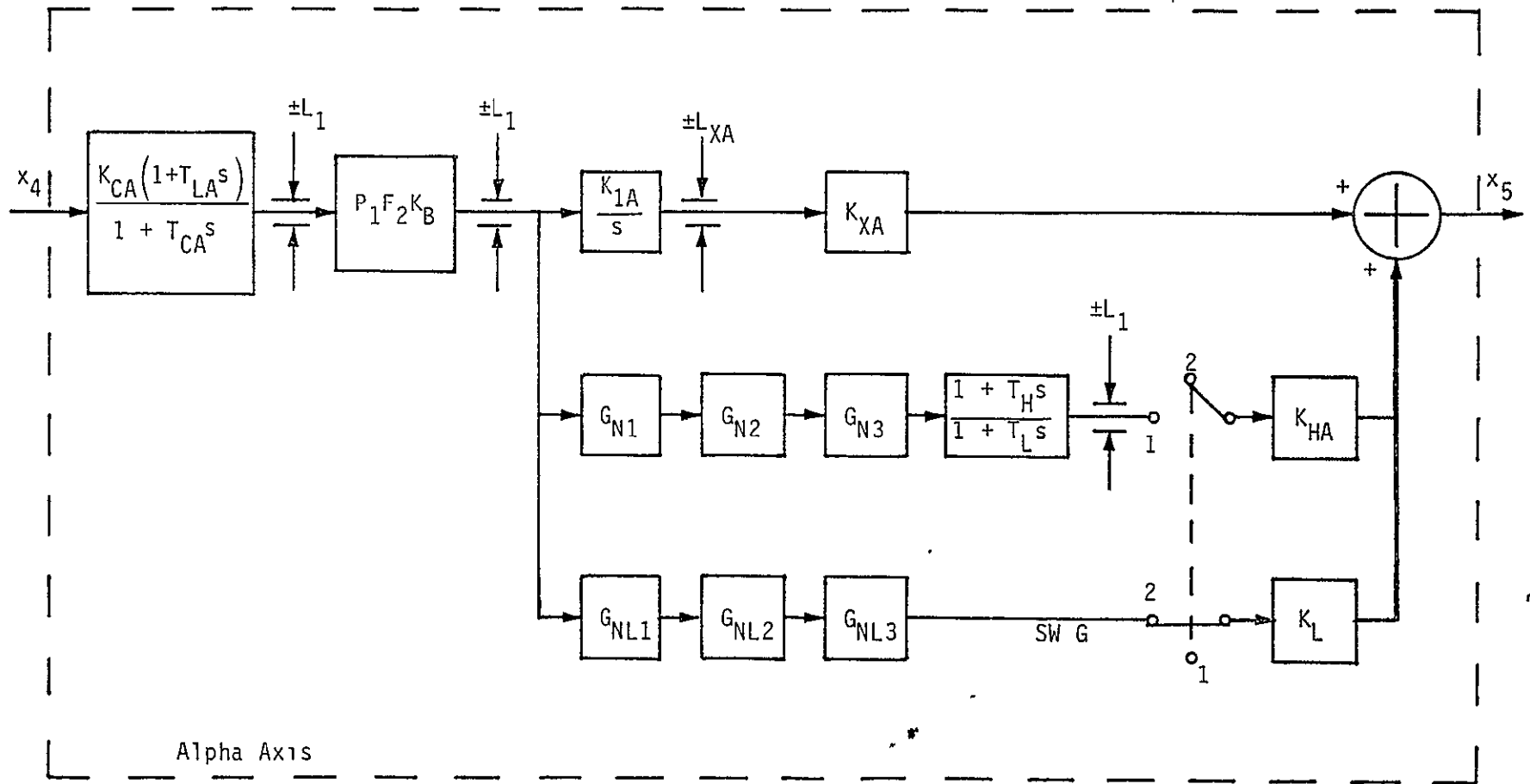


Figure 4 Rate-Stabilization-Loop Block Diagram



Alpha Axis

$$K_{CA} = 18.87 \pm 1.5\%$$

$$T_{LA} = 0.4200 \text{ s} \pm 1.5\%$$

$$T_{CA} = 4.194 \text{ s} \pm 1.5\%$$

$$K_{LA} = 1.212 \pm 1.5\%$$

Figure 5 The Rate-Stabilization Loop-Shaping Filter for the  $\alpha$ -Axis

Table 1. Parameter Values for the Rate-Stabilization Loop-Shaping Filter

$\frac{G_N \left[ \left( \frac{s}{\omega_N} \right)^2 + 2 \frac{\zeta_N}{\omega_N} s + 1 \right] (sZ + 1)}{\left[ \left( \frac{s}{\omega_D} \right)^2 + 2 \frac{\zeta_D}{\omega_D} s + 1 \right] (sP + 1)}$							
Symbol	$K_N$	$\omega_N/2\pi$	$\zeta_N$	$\omega_D/2\pi$	$\zeta_D$	Z	P
	±1.5%	Hz ± 2.25%	±1.5%	Hz ± 2.25%	±1.5%	MS±2 25%	MS±2.25%
$G_{N1}$	0.9757	13.02	0.9647	8.955	0.9783	23.92	23.58
$G_{N2}$	1.025	13.05	0.7064	8.967	0.7082	17.29	17.23
$G_{N3}$	0.9537	12.99	0.2579	8.995	0.2581	6.283	6.32
$G_{NL1}$	0.8457	15.40	0.7066	4.344	0.7023	14.48	14.61
$G_{NL2}$	1.000	26.97	0.0698	26.95	0.7062	0.8254	0.8240

Bandwidth	Gyro Output Used	$K_{XA}$ ±1.5%	$L_{XA} K_{XA}$ V ± 10%	$K_B$ ±1.5%	$K_{HA}$ ±1.5%	$K_L$ ±1.5%
Low	Fine	0.7331	10.08	0.2272	0	0.4434
High	Fine	0.7331	10.08	1.000	0.2104	0
Low	Coarse	3.675	10.08	0.2272	0	2.206
High	Coarse	3.675	10.06	1.000	1.050	0



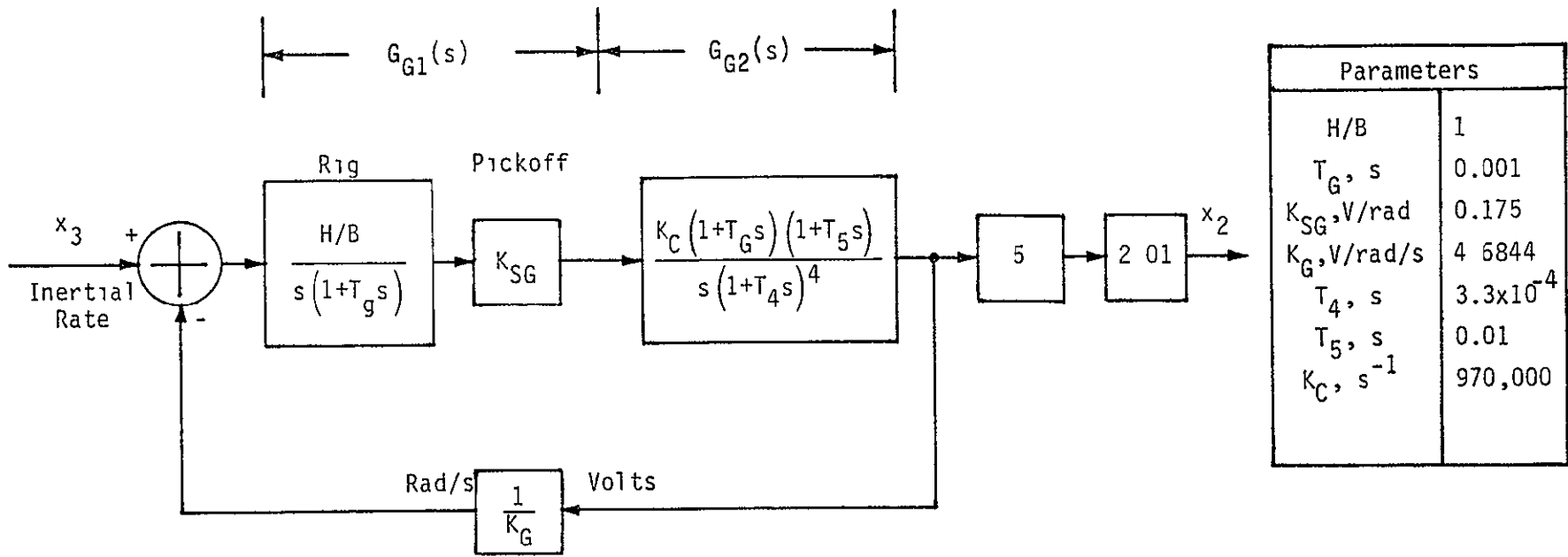


Figure 6 The Rate Sensor Assembly

ORIGINAL PAGE IS  
OF POOR QUALITY

where

ORIGINAL PAGE IS  
OF POOR QUALITY

$$\begin{aligned} h_0^{(3)} &= 24.25 K_{xA} \\ h_1^{(3)} &= 10.56 K_{xA} + 16.20 \\ h_2^{(3)} &= 1.893 \times 10^{-1} K_{xA} + 7.054 \end{aligned} \quad (43)$$

and

$$\begin{aligned} h_0^{(4)} &= 0 \\ h_1^{(4)} &= 1.060 \\ h_2^{(4)} &= 4.463 \end{aligned} \quad (44)$$

Combining (38), (39) and (42), we have

$$\begin{aligned} F_\alpha(s) &= \frac{0.92 K_4 F_1 F_2 K_B \left( \sum_{i=0}^8 h_i^{(3)} s^i \right) \left( \sum_{i=0}^7 h_i^{(2)} s^i \right) K_{MD} K_{TM} \cos \beta}{(1 + T_R s)(1 + T_M s) J(\beta) s \left( \sum_{i=0}^7 h_i^{(2)} s^i \right) \left( \sum_{i=0}^8 h_i^{(4)} s^i \right)} \\ &+ F_1 F_2 K_B 1.745 \times 10^{-2} \left( \sum_{i=0}^2 h_i^{(1)} s^i \right) \left( \sum_{i=0}^8 h_i^{(3)} s^i \right) K_{MD} K_{TM} \cos \beta \end{aligned} \quad (45)$$

If both the numerator and denominator of  $H_{RS}(s)$  retain only up to the first-order terms in  $s$ , we have

$$F_\alpha(s) \approx \frac{0.92 K_4 (h_0^{(2)} + h_1^{(2)} s)}{1.745 \times 10^{-2} (h_0^{(1)} + h_1^{(1)} s)} \quad (46)$$

$$F_\alpha(s) = 1.120 K_4 \quad (47)$$

Equation (46) is the result simply because the first term in the denominator of (45) begins with the second-order terms in  $s$ . Equation (47) results when we substitute (40) and (41) into (46).

Note that the only differences between the  $\alpha$ -axis and  $\beta$ -axis servo loops are the rate-stabilization loop-shaping filter and the moment of inertia. But neither of them appear in (46). Hence, as long as only the first-order term is retained, we have

$$F_{\beta}(s) = F_{\alpha}(s) = 1.120 K_4 \quad (48)$$

Substituting (47) and (48) into (31) with  $K_{SC1} = 2.047$  V/deg and  $K_4 = 0.0810$ , we end up with

$$\sigma_{\phi_{\alpha}}^2 = 5.537 \times 10^{-3} K_{SC2} \left( (2 - K_1 K_2) N_{0\alpha} + K_1^2 N_{0\beta} \right) \quad (49)$$

ORIGINAL PAGE IS  
OF POOR QUALITY



9841 Airport Boulevard • Suite 912 • Los Angeles, California 90045 • Phone (213) 641-8600

TECHNICAL MEMORANDUM NO. M8209-3

TO: J. Dodds

DATE: September 30, 1982

FROM: U. Cheng

FILE: NAS 9-16067"A"

SUBJECT. Effects of Cross Coupling on the Stability and Tracking Performance  
of Alpha and Beta Servo Loops

-----

## 1.0 INTRODUCTION

The Ku-Band Communication Autotrack System contains  $\alpha$  and  $\beta$  servo loops whose purpose is to acquire and track the difference azimuth and elevation error angles, respectively. Cross coupling between the difference elevation and azimuth channels which feed these loops, originating from the monopulse feeds and comparator network, has the potential to cause stability problems during acquisition and tracking operations. Furthermore, even if stable operation is assured, cross coupling produces a degrading effect on each loop's tracking performance in noise.

In this memo, we discuss the potential stability problem caused by cross coupling and derive a necessary but insufficient condition to ensure stability. In addition, using mean-squared phase jitter as a measure of tracking performance, the degradation in this measure caused by the cross coupling is assessed in terms of such parameters as the servo noise bandwidth and damping factor for each of the loops as well as the pair of cross-coupling gains.

We begin our analysis by considering the noise-free model of the pair of cross-coupled loops with the purpose of examining each loop's response to an input phase step. The behavior of the corresponding loop phase error responses as time approaches infinity is then an indication of the stability of the system.

## 2.0 NOISE-FREE MODEL OF CROSS-COUPLED LOOPS (RESPONSE TO PHASE-STEP INPUT)

Consider the noise-free model for the cross-coupled  $\alpha$  and  $\beta$  servo loops, as illustrated in Figure 1. Here  $\alpha$  and  $\beta$  denote the angular errors for the two servo loops and  $\epsilon_\alpha$  and  $\epsilon_\beta$  are, respectively, the corresponding  $\alpha$ -axis and  $\beta$ -axis voltage errors. The gains  $K_\alpha$  and  $K_\beta$  are equivalent to  $K_{SC} = K_{SC1}K_{SC2}$  in the HAC

ORIGINAL PAGE IS  
OF POOR QUALITY

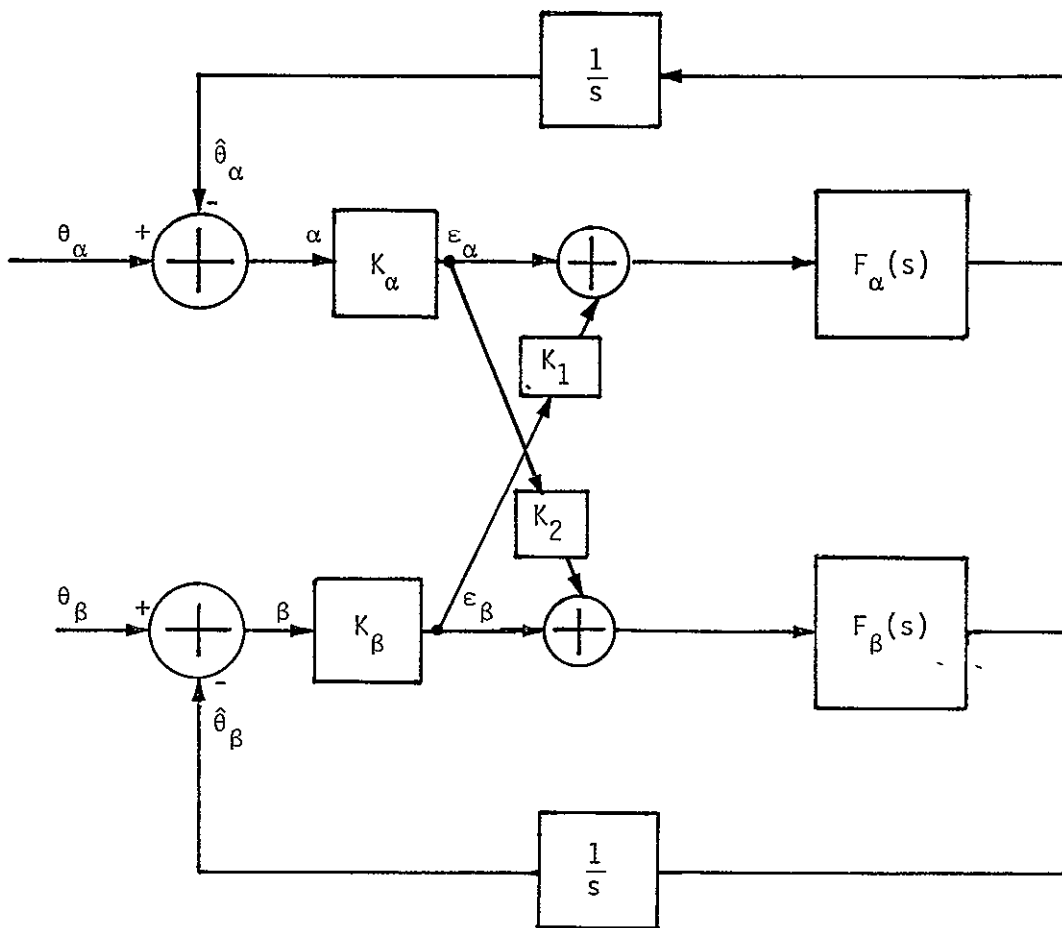


Figure 1 A Simple Block Diagram for the Cross-Coupled  $\alpha$  and  $\beta$  Servo Loops in the Absence of Noise

servo configuration single-axis block diagram where  $K_{SC}=117 \text{ V/rad} = 2.047 \text{ V/deg}$  and  $1 \leq K_{SC2} \leq 15$ . Note that Figure 1 is an equivalent block diagram for the linear region of behavior.

The blocks labeled  $K_1$  and  $K_2$  represent the normalized cross coupling between the loops where, for the moment, we restrict  $K_1$  and  $K_2$  to have a magnitude less than or equal to unity. The blocks marked  $1/s$  represent the transfer functions of the  $\alpha$ -axis and  $\beta$ -axis servo motors. Finally,  $F_\alpha(s)$  and  $F_\beta(s)$  represent the composite transfer functions of the various components and subloops that comprise the rate-stabilization loop for each axis. Later on, we shall discuss the detail required to characterize  $F_\alpha(s)$  and  $F_\beta(s)$  in terms of the actual rate-stabilization-loop parameters. But, for the moment, we shall treat  $F_\alpha(s)$  and  $F_\beta(s)$  as rational transfer functions in much the same manner as one characterizes a loop filter in a conventional phase-locked loop

By inspecting Figure 1, we can immediately write the following relations.

$$\epsilon_\alpha = K_\alpha(\theta_\alpha - \hat{\theta}_\alpha), \quad \epsilon_\beta = K_\beta(\theta_\beta - \hat{\theta}_\beta) \quad (1)$$

and

$$\hat{\theta}_\alpha = \frac{F_\alpha(s)}{s} (\epsilon_\alpha + K_1 \epsilon_\beta), \quad \hat{\theta}_\beta = \frac{F_\beta(s)}{s} (\epsilon_\beta + K_2 \epsilon_\alpha) \quad (2)$$

Combining (1) and (2) gives the pair of coupled equations

$$\begin{aligned} \epsilon_\alpha \left( \frac{1}{K_\alpha} + \frac{F_\alpha(s)}{s} \right) + \frac{K_1 F_\alpha(s)}{s} \epsilon_\beta &= \theta_\alpha \\ \epsilon_\alpha \left( \frac{K_2 F_\beta(s)}{s} \right) + \epsilon_\beta \left( \frac{1}{K_\beta} + \frac{F_\beta(s)}{s} \right) &= \theta_\beta \end{aligned} \quad (3)$$

After solving (3), we get

$$\begin{aligned} \epsilon_\alpha &= \frac{sK_\alpha(s + K_\beta F_\beta(s))\theta_\beta - sK_\alpha K_\beta K_1 F_\alpha(s)\theta_\beta}{(s + K_\alpha F_\alpha(s))(s + K_\beta F_\beta(s)) - K_\alpha K_\beta K_1 K_2 F_\alpha(s)F_\beta(s)} \\ \epsilon_\beta &= \frac{sK_\beta(s + K_\alpha F_\alpha(s))\theta_\beta - sK_\beta K_\alpha K_2 F_\beta(s)\theta_\alpha}{(s + K_\alpha F_\alpha(s))(s + K_\beta F_\beta(s)) - K_\alpha K_\beta K_1 K_2 F_\alpha(s)F_\beta(s)} \end{aligned} \quad (4)$$

Now letting  $\theta_\alpha$  and  $\theta_\beta$  correspond to step changes in phase, i.e.,

$$\theta_\alpha = \frac{\theta_\alpha}{s} \quad ; \quad \theta_\beta = \frac{\theta_\beta}{s} \quad (5)$$

then substituting (5) into (4) results in

$$\begin{aligned} \epsilon_\alpha &= \frac{K_\alpha (s + K_\beta F_\beta(s)) \theta_\alpha - K_\alpha K_\beta K_1 F_\alpha(s) \theta_\beta}{(s + K_\alpha F_\alpha(s))(s + K_\beta F_\beta(s)) - K_\alpha K_\beta K_1 K_2 F_\alpha(s) F_\beta(s)} \\ \epsilon_\beta &= \frac{K_\beta (s + K_\alpha F_\alpha(s)) \theta_\beta - K_\beta K_\alpha K_2 F_\beta(s) \theta_\alpha}{(s + K_\alpha F_\alpha(s))(s + K_\beta F_\beta(s)) - K_\alpha K_\beta K_1 K_2 F_\alpha(s) F_\beta(s)} \end{aligned} \quad (6)$$

Note that, for no cross coupling, i.e.,  $K_1 = K_2 = 0$ , (6) reduces to

$$\epsilon_\alpha = \frac{K_\alpha \theta_\alpha}{s + K_\alpha F_\alpha(s)} \quad , \quad \epsilon_\beta = \frac{K_\beta \theta_\beta}{s + K_\beta F_\beta(s)} \quad (7)$$

as it should. The results in (6) can be written in a more compact form by defining the closed-loop transfer functions in the absence of cross coupling, i.e.,

$$H_\alpha(s) = \frac{K_\alpha F_\alpha(s)}{s + K_\alpha F_\alpha(s)} \quad ; \quad H_\beta(s) = \frac{K_\beta F_\beta(s)}{s + K_\beta F_\beta(s)} \quad (8)$$

Dividing the numerator and denominator of the right-hand side of (6) and using (8) gives the desired result, namely,

$$\begin{aligned} \epsilon_\alpha(s) &= \frac{K_\alpha (1 - H_\alpha(s)) \frac{\theta_\alpha}{s} - K_1 K_\beta H_\alpha(s) (1 - H_\beta(s)) \frac{\theta_\beta}{s}}{1 - K_1 K_2 H_\alpha(s) H_\beta(s)} \\ \epsilon_\beta(s) &= \frac{K_\beta (1 - H_\beta(s)) \frac{\theta_\beta}{s} - K_2 K_\alpha H_\beta(s) (1 - H_\alpha(s)) \frac{\theta_\alpha}{s}}{1 - K_1 K_2 H_\alpha(s) H_\beta(s)} \end{aligned} \quad (9)$$

In order to examine system stability, we consider the steady-state ( $t \rightarrow \infty$ ) behavior of the angular error voltages in response to the phase step changes of (5). Applying the final-value theorem to (9), we observe that, if they exist, the limiting values of  $\epsilon_\alpha$  and  $\epsilon_\beta$  become

$$\lim_{t \rightarrow \infty} \epsilon_\alpha(t) = \lim_{s \rightarrow 0} s \epsilon_\alpha(s) \quad ; \quad \lim_{t \rightarrow \infty} \epsilon_\beta(t) = \lim_{s \rightarrow 0} s \epsilon_\beta(s) \quad (10)$$

or

$$\lim_{t \rightarrow \infty} \epsilon_\alpha(t) = \lim_{s \rightarrow 0} \frac{K_\alpha(1 - H_\alpha(s)) \theta_\alpha - K_1 K_\beta H_\alpha(s)(1 - H_\beta(s)) \theta_\beta}{1 - K_1 K_2 H_\alpha(s) H_\beta(s)}$$

and

$$\lim_{t \rightarrow \infty} \epsilon_\beta(t) = \lim_{s \rightarrow 0} \frac{K_\beta(1 - H_\beta(s)) \theta_\beta - K_2 K_\alpha H_\beta(s)(1 - H_\alpha(s)) \theta_\alpha}{1 - K_1 K_2 H_\alpha(s) H_\beta(s)} \quad (11)$$

Since, from (8),

$$\lim_{s \rightarrow 0} H_\alpha(s) = \lim_{s \rightarrow 0} H_\beta(s) = 1$$

it is clear that both  $\epsilon_\alpha(t)$  and  $\epsilon_\beta(t)$  will then have limiting values of zero if  $K_1 K_2 \neq 1$ ; however, when  $K_1 K_2 = 0$ , we know that the system is stable. Hence, it is believed that  $K_1 K_2 < 1$  is the condition required for each loop to be stable. Note that this result was obtained independent of the order of each of the uncoupled loops, i.e., it was unnecessary to restrict  $H_\alpha(s)$  and  $H_\beta(s)$  to have first-order or second-order polynomials as their denominators, as would be the case for the first-order and second-order loops.

Before further discussing loop stability, one must investigate the pole locations of  $\epsilon_\alpha(s)$  and  $\epsilon_\beta(s)$ , which requires investigating the roots of the denominator  $1 - K_1 K_2 H_\alpha(s) H_\beta(s)$ . This in turn requires specifying the equivalent loop filters  $F_\alpha(s)$  and  $F_\beta(s)$ .

For many cases,  $K_1 K_2 < 1$  is the necessary and sufficient condition for each loop to be stable. Let us consider two of these cases.

(1) We let

$$F_\alpha(s) = A \quad ; \quad F_\beta(s) = B \quad (12)$$



Equation (4) then becomes

$$\begin{aligned}\epsilon_{\alpha} &= \frac{sK_{\alpha}(s+BK_{\beta})\theta_{\alpha} - K_1K_{\alpha}K_{\beta}sA\theta_{\beta}}{s^2 + (AK_{\alpha} + BK_{\beta})s + (1 - K_1K_2)ABK_{\alpha}K_{\beta}} \\ \epsilon_{\beta} &= \frac{sK_{\beta}(s+AK_{\alpha})\theta_{\beta} - K_2K_{\alpha}K_{\beta}sB\theta_{\alpha}}{s^2 + (AK_{\alpha} + BK_{\beta})s + (1 - K_1K_2)ABK_{\alpha}K_{\beta}}\end{aligned}\quad (13)$$

We can make two observations about the denominator of  $\epsilon_{\alpha}$ . First, since  $K_1$ ,  $K_2$ ,  $K_{\alpha}$ ,  $K_{\beta}$ ,  $A$  and  $B$  are positive, one has

$$(AK_{\alpha} + BK_{\beta})^2 - 4(1 - K_1K_2)ABK_{\alpha}K_{\beta} = (AK_{\alpha} - BK_{\beta})^2 + 4ABK_{\alpha}K_{\beta} > 0 \quad (14)$$

Hence, both of these two roots are real. Secondly, both roots are negative only if  $K_1K_2 < 1$ .

(2) We let

$$F_{\alpha}(s) = 1 + \frac{A}{s}, \quad F_{\beta}(s) = 1 + \frac{B}{s} \quad (15)$$

Equation (4) then becomes

$$\begin{aligned}\epsilon_{\alpha} &= \frac{s^2K_{\alpha}(s^2 + sK_{\beta} + BK_{\beta})\theta_{\alpha} - K_1K_{\beta}(sK_{\alpha} + AK_{\alpha})s^2\theta_{\beta}}{(s^2 + sK_{\alpha} + AK_{\alpha})(s^2 + sK_{\beta} + BK_{\beta}) - K_1K_2(sK_{\alpha} + AK_{\alpha})(sK_{\beta} + BK_{\beta})} \\ \epsilon_{\beta} &= \frac{s^2K_{\beta}(s^2 + sK_{\alpha} + AK_{\alpha})\theta_{\beta} - K_2K_{\alpha}(sK_{\beta} + BK_{\beta})s^2\theta_{\alpha}}{(s^2 + sK_{\alpha} + AK_{\alpha})(s^2 + sK_{\beta} + BK_{\beta}) - K_1K_2(sK_{\alpha} + AK_{\alpha})(sK_{\beta} + BK_{\beta})}\end{aligned}\quad (16)$$

When  $A=B$ , the denominator of  $\epsilon_{\alpha}$  can be factorized as follows.

$$(s^2 + sK_{\alpha} + AK_{\alpha})(s^2 + sK_{\beta} + BK_{\beta}) - K_1K_2(sK_{\alpha} + AK_{\alpha})(sK_{\beta} + BK_{\beta}) = (s^2 + E_1(s+A))(s^2 + E_2(s+A)) \quad (17)$$

where

$$E_1 = \frac{(K_{\alpha} + K_{\beta}) - \sqrt{(K_{\beta} - K_{\alpha})^2 + 4K_1K_2K_{\alpha}K_{\beta}}}{2} \quad (18)$$

and

$$E_2 = \frac{(K_\alpha + K_\beta) + \sqrt{(K_\beta - K_\alpha)^2 + 4K_1K_2K_\alpha K_\beta}}{2} \quad (19)$$

Hence, all roots will have negative real parts only if  $E_1 > 0$ ; however, this can be true only if  $K_1K_2 < 1$ .

### 3.0 NOISE MODEL OF CROSS-COUPLED LOOPS (TRACKING ANALYSIS)

Consider the noise model of the cross-coupled  $\alpha$  and  $\beta$  servo loops, as illustrated in Figure 2. Here  $K_{\alpha 1}$  and  $K_{\alpha 2}$  are identical to  $K_{SC1}$  and  $K_{SC2}$ , as previously defined. Similarly,  $K_{\beta 1}$  and  $K_{\beta 2}$  are identical to  $K_{SC1}$  and  $K_{SC2}$ . Furthermore,

$$K_\alpha = K_{\alpha 1} K_{\alpha 2} \quad ; \quad K_\beta = K_{\beta 1} K_{\beta 2} \quad (20)$$

Analogous to (1), we now have

$$\epsilon_\alpha = K_\alpha(\theta_\alpha - \hat{\theta}_\alpha) + K_{\alpha 2} N_\alpha \quad , \quad \epsilon_\beta = K_\beta(\theta_\beta - \hat{\theta}_\beta) + K_{\beta 2} N_\beta \quad (21)$$

whereas (2) still applies. Again combining (21) and (2) gives the pair of coupled equations

$$\begin{aligned} \epsilon_\alpha \left( \frac{F_\alpha(s)}{s} + \frac{1}{K_\alpha} \right) + \epsilon_\beta \left( \frac{F_\alpha(s)}{s} K_1 \right) &= \theta_\alpha + \frac{N_\alpha}{K_{\alpha 1}} \\ \epsilon_\beta \left( \frac{F_\beta(s)}{s} K_2 \right) + \left( \frac{F_\beta(s)}{s} + \frac{1}{K_\beta} \right) \epsilon_\beta &= \theta_\beta + \frac{N_\beta}{K_{\beta 1}} \end{aligned} \quad (22)$$

Since we are interested in the mean-square angular-tracking jitter due to noise, we may ignore the terms in (22) that involve  $\theta_\alpha$  and  $\theta_\beta$  and solve directly for  $\epsilon_\alpha$  and  $\epsilon_\beta$ . After some simplification, this results in a pair of equations analogous to (4), namely,

ORIGINAL PAGE IS  
OF POOR QUALITY

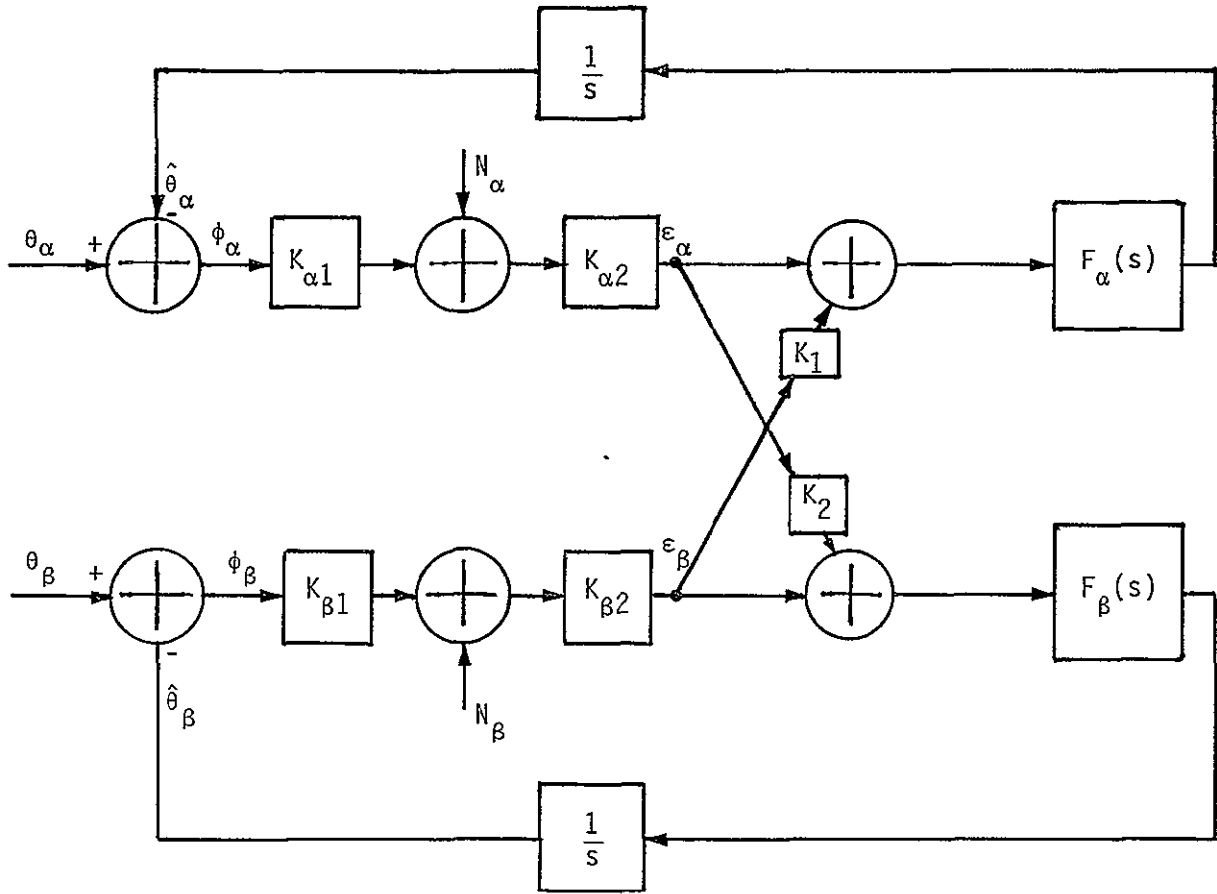


Figure 2 A Simple Block Diagram for the Cross-Coupled  $\alpha$  and  $\beta$  Servo Loops in the Presence of Noise

$$\begin{aligned}\epsilon_{\alpha} &= \frac{sK_{\alpha}(s+K_{\beta}F_{\beta}(s))\frac{N_{\alpha}}{K_{\alpha 1}} - sK_{\alpha}K_{\beta}K_1F_{\alpha}(s)\frac{N_{\beta}}{K_{\beta 1}}}{(s+K_{\alpha}F_{\alpha}(s))(s+K_{\beta}F_{\beta}(s)) - K_{\alpha}K_{\beta}K_1K_2F_{\alpha}(s)F_{\beta}(s)} \\ \epsilon_{\beta} &= \frac{sK_{\beta}(s+K_{\alpha}F_{\alpha}(s))\frac{N_{\beta}}{K_{\beta 1}} - sK_{\alpha}K_{\beta}K_2F_{\beta}(s)\frac{N_{\alpha}}{K_{\alpha 1}}}{(s+K_{\alpha}F_{\alpha}(s))(s+K_{\beta}F_{\beta}(s)) - K_{\alpha}K_{\beta}K_1K_2F_{\alpha}(s)F_{\beta}(s)}\end{aligned}\quad (23)$$

In the absence of cross coupling (i.e.,  $K_1 = K_2 = 0$ ), (23) reduces to

$$\epsilon_{\alpha} = K_{\alpha 2}(1 - H_{\alpha}(s))N_{\alpha} ; \epsilon_{\beta} = K_{\beta 2}(1 - H_{\beta}(s))N_{\beta} \quad (24)$$

as it should, i.e., the noise sources are transformed by the out-of-band loop transfer functions insofar as their effect on the loop error voltage is concerned.

Actually, we are interested in the angular-error voltages  $\phi_{\alpha}$  and  $\phi_{\beta}$  which, from Figure 2, are related to  $\epsilon_{\alpha}$  and  $\epsilon_{\beta}$  by

$$\phi_{\alpha} = \frac{\epsilon_{\alpha} - K_{\alpha 2}N_{\alpha}}{K_{\alpha}} , \quad \phi_{\beta} = \frac{\epsilon_{\beta} - K_{\beta 2}N_{\beta}}{K_{\beta}} \quad (25)$$

Substituting (23) into (25) and simplifying produces the desired results

$$\begin{aligned}\phi_{\alpha} &= \frac{\frac{H_{\alpha}(s)}{K_{\alpha 1}}(1 - K_1K_2H_{\beta}(s))N_{\alpha} - \frac{K_1K_{\beta 2}}{K_{\alpha}}H_{\alpha}(s)(1 - H_{\beta}(s))N_{\beta}}{1 - K_1K_2H_{\alpha}(s)H_{\beta}(s)}} \\ \phi_{\beta} &= \frac{-\frac{K_2K_{\alpha 2}}{K_{\beta}}H_{\beta}(s)(1 - H_{\alpha}(s))N_{\alpha} + \frac{H_{\beta}(s)}{K_{\beta 1}}(1 - K_1K_2H_{\alpha}(s))N_{\beta}}{1 - K_1K_2H_{\alpha}(s)H_{\beta}(s)}\end{aligned}\quad (26)$$

We now wish to compare the mean-square values of  $\phi_{\alpha}$  and  $\phi_{\beta}$  in (26) relative to the same values for  $K_1 = K_2 = 0$  so as to access the degradation in mean-square phase jitter due to the cross-coupling effect. First, setting  $K_1 = K_2 = 0$  in (26), we get

$$\sigma_{\phi_{\alpha 0}}^2 = \frac{1}{K_{\alpha 1}^2} \frac{N_{0\alpha}}{2} \left( \frac{1}{2\pi j} \int_{-j\infty}^{j\infty} |H_{\alpha}(s)|^2 ds \right) \triangleq \frac{N_{0\alpha} B_{L\alpha}}{K_{\alpha 1}^2} \triangleq \frac{1}{\rho_{\alpha}} \quad (27)$$

where  $B_{L\alpha}$  is the equivalent loop noise bandwidth of the  $\alpha$ -servo in the absence of cross coupling and the zero subscript on  $\sigma_{\phi_{\alpha 0}}^2$  denotes this case. Furthermore,  $N_{0\alpha}$  is the single-sided noise spectral density of the equivalent noise source  $N_{\alpha}(t)$ .

In the presence of cross coupling, we obtain from (26) the relation

$$\begin{aligned} \sigma_{\phi_{\alpha}}^2 = & \frac{K_1^2 K_{\beta 2}^2 N_{0\beta}}{K_{\alpha}^2} \left( \frac{1}{2\pi j} \int_{-j\infty}^{j\infty} \left| \frac{H_{\alpha}(s)(1-H_{\beta}(s))}{1-K_1 K_2 H_{\alpha}(s) H_{\beta}(s)} \right|^2 ds \right) \\ & + \frac{1}{K_{\alpha 1}^2} \frac{N_{0\alpha}}{2} \left( \frac{1}{2\pi j} \int_{-j\infty}^{j\infty} \left| \frac{H_{\alpha}(s)(1-K_1 K_2 H_{\beta}(s))}{1-K_1 K_2 H_{\alpha}(s) H_{\beta}(s)} \right|^2 ds \right) \end{aligned} \quad (28)$$

For the assumed loop-filter transfer functions

$$F_{\alpha}(s) = K_{F_{\alpha}} \quad ; \quad F_{\beta}(s) = K_{F_{\beta}} \quad (29)$$

The closed-loop transfer function of (8) can be written in the form

$$H_{\alpha}(s) = \frac{1}{1 + \frac{s}{K_{\alpha} K_{F_{\alpha}}}} \quad , \quad H_{\beta}(s) = \frac{1}{1 + \frac{s}{K_{\beta} K_{F_{\beta}}}} \quad (30)$$

Substituting (30) into the integrands of (28), we can get

$$\sigma_{\phi_{\alpha}}^2 = \frac{N_{0\alpha}}{4K_{\alpha 1}^2} \frac{1}{K_{\alpha} K_{F_{\alpha}} + K_{\beta} K_{F_{\beta}}} \left( (1-K_1 K_2) K_{\alpha} K_{F_{\alpha}} K_{\beta} K_{F_{\beta}} + (K_{\alpha} K_{F_{\alpha}})^2 \right) + \frac{N_{0\beta} (K_1 K_{\beta 2} K_{F_{\alpha}})^2}{4(K_{\alpha} K_{F_{\alpha}} + K_{\beta} K_{F_{\beta}})} \quad (31)$$

Defining

$$\frac{1}{2\pi j} \int_{-j\infty}^{j\infty} \left| \frac{H_\alpha(s)(1-H_\beta(s))}{1-K_1K_2H_\alpha(s)H_\beta(s)} \right|^2 ds \triangleq 2B_{L\beta}K_{\beta\alpha}$$

and

$$\frac{1}{2\pi j} \int_{-j\infty}^{j\infty} \left| \frac{H_\alpha(s)(1-K_1K_2H_\beta(s))}{1-K_1K_2H_\alpha(s)H_\beta(s)} \right|^2 ds \triangleq 2B_{L\alpha}K_{\alpha\alpha} \quad (32)$$

and noting that

$$B_{L\alpha} = \frac{K_\alpha K_{F\alpha}}{4}, \quad B_{L\beta} = \frac{K_\beta K_{F\beta}}{4} \quad (33)$$

we end up with

$$K_{\alpha\alpha} = \frac{1}{K_\alpha K_{F\alpha} + K_\beta K_{F\beta}} \left( (1-K_1K_2) K_\beta K_{F\beta} + K_\alpha K_{F\alpha} \right)$$

$$K_{\beta\alpha} = \frac{K_\alpha K_{F\alpha}}{K_\alpha K_{F\alpha} + K_\beta K_{F\beta}} \frac{K_\alpha K_{F\alpha}}{K_\beta K_{F\beta}} \quad (34)$$

and (31) can be written as

$$\sigma_{\phi_\alpha}^2 = \frac{K_{\alpha\alpha}}{\rho_\alpha} + \left( \frac{K_1^2 K_\beta^2}{K_\alpha^2} \right) \frac{K_{\beta\alpha}}{\rho_\beta} \quad (35)$$

Note that, for  $K_1K_2=0$ , we have

$$K_{\alpha\alpha} = 1 \quad (36)$$

We also note that, in (35),  $\rho_\beta$  is defined as

$$\rho_\beta = \frac{K_{\beta 1}^2}{N_{0\beta} B_{L\beta}} \quad (37)$$

where (37) is analogous to (27).

4.0 EVALUATION OF  $F_\alpha(s)$  AND  $F_\beta(s)$  IN TERMS OF RATE STABILIZATION LOOP PARAMETERS

Analogous to the mathematical model in Figure 2, Figure 3 is a simplified block diagram of the  $\alpha$ -axis servo loop alone. Thus, the equivalent loop filter  $F_\alpha(s)$  in Figure 2 is the product of the gains  $K_4$  and 0.92 and the transfer function  $H_{RS}(s)$  of the rate-stabilization loop whose block diagram is illustrated in Figure 4. Letting  $F_{RS}(s)$  denote the transfer function loop-shaping filter (See Figure 5 and Table 1) and  $H_{RSA}(s)$  denote the transfer function of the rate sensor assembly (see Figure 6), then

$$F_\alpha(s) = 0.92 K_4 H_{RS}(s) = \frac{F_{RS}(s) G_{MD}(s) K_{TM} \cos \beta}{(1 + T_R s) J(\beta) s + 1.745 \times 10^{-2} H_{RSA} F_{RS} G_{MD}(s) K_{TM} \cos \beta} \quad (38)$$

Now, from Figure 6, we see that

$$H_{RSA}(s) \triangleq \frac{x_2(s)}{x_3(s)} = \frac{10.05 K_{SG} K_G K_C (1+T_G s) (1+T_5 s)}{K_G s^2 (1+T_g s)(1+T_4 s)^4 + K_{SG} K_C (1+T_G s)(1+T_5 s)} = \frac{\sum_{i=0}^2 h_i^{(1)} s^i}{\sum_{i=0}^7 h_i^{(2)} s^i} \quad (39)$$

where

$$\begin{aligned} h_0^{(1)} &= 7.992 \times 10^6 \\ h_1^{(1)} &= 7.992 \times 10^6 T_G + 7.992 \times 10^4 \\ h_2^{(1)} &= 7.992 \times 10^4 T_G \end{aligned} \quad (40)$$

$$\begin{aligned} h_0^{(2)} &= 1.698 \times 10^5 \\ h_1^{(2)} &= 1.698 \times 10^5 T_G + 1.698 \times 10^3 \\ h_2^{(2)} &= 1.698 \times 10^3 T_G + 4.864 \end{aligned} \quad (41)$$

From Figure 5, we see that

$$F_{RS}(s) \triangleq \frac{x_5(s)}{x_4(s)} = F_1 F_2 K_B \left[ \frac{K_{CA} (1+T_{LA} s)}{1+T_{CA} s} \right] \left( G_{NL1} G_{NL2} K_L + \frac{K_{1A} K_{XA}}{s} \right) = F_1 F_2 K_B \frac{\sum_{i=0}^8 h_i^{(3)} s^i}{\sum_{i=0}^8 h_i^{(4)} s^i} \quad (42)$$

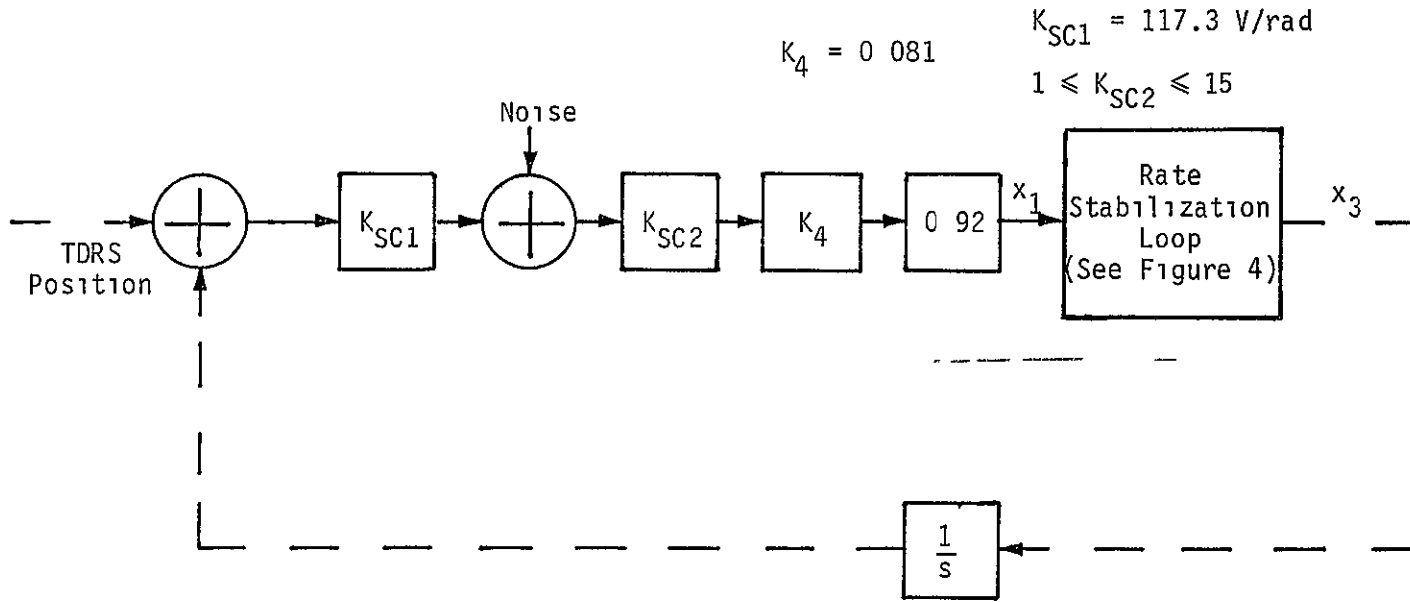
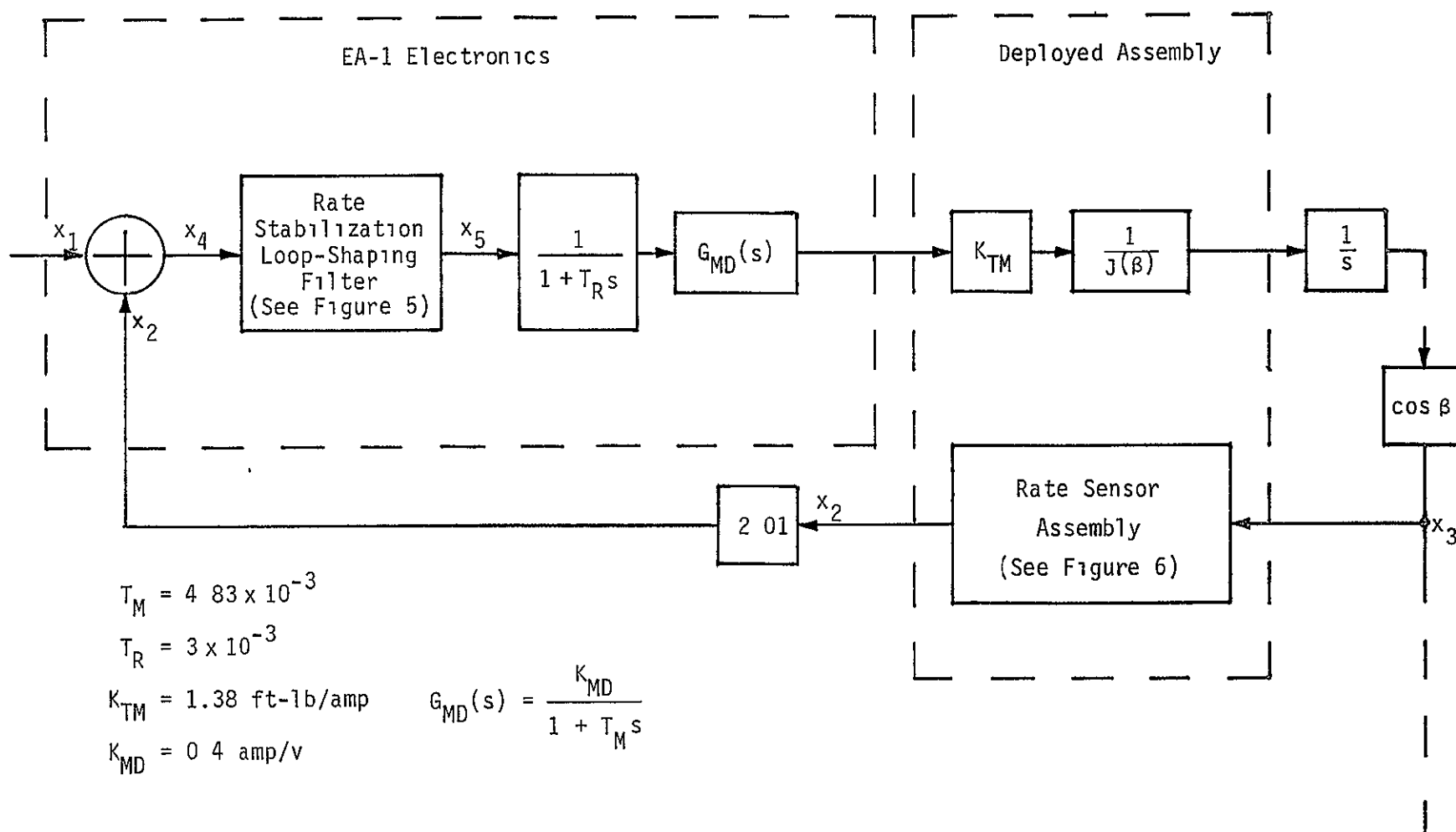


Figure 3 Simplified Block Diagram of the  $\alpha$ -Axis Servo Loop

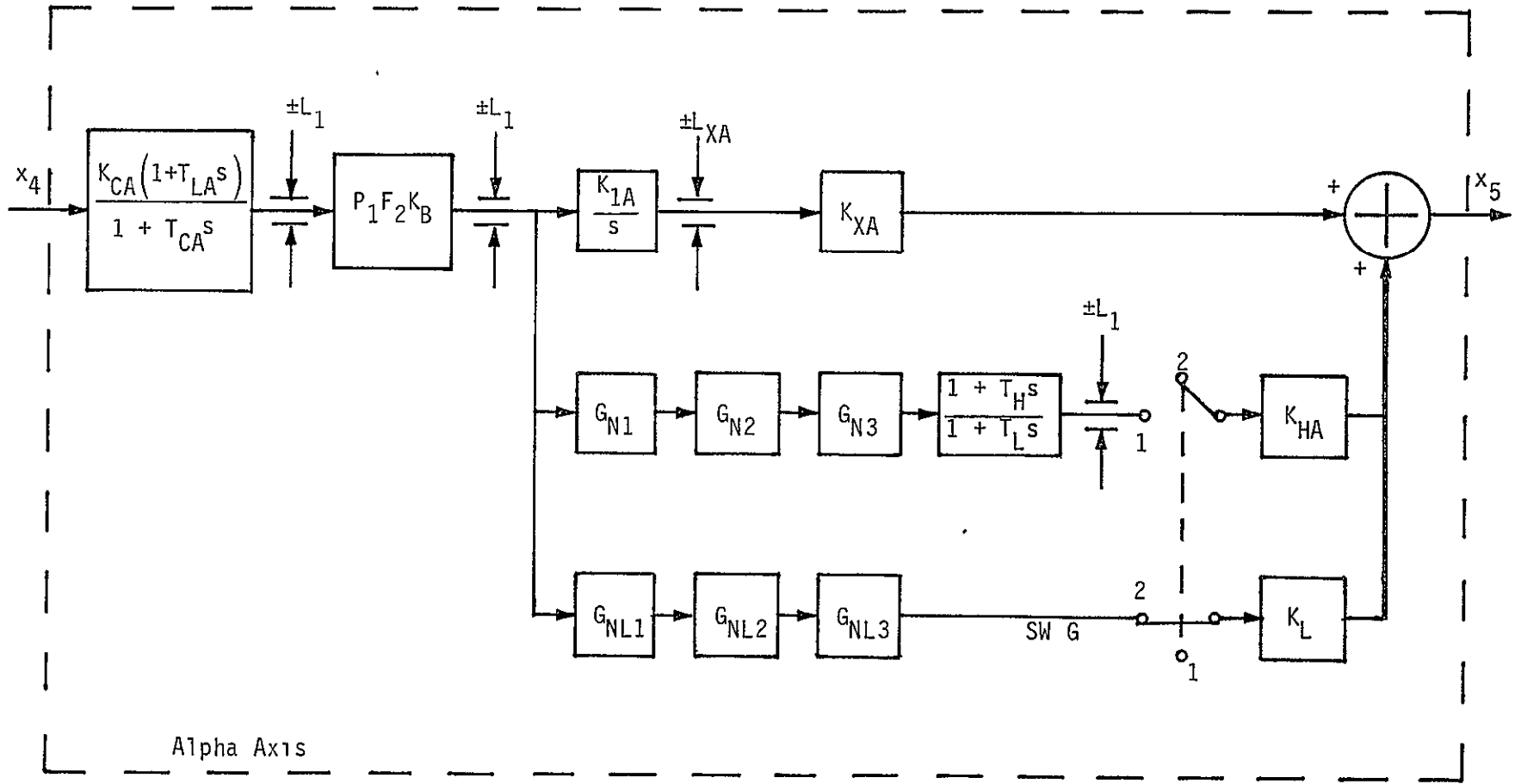
ORIGINAL PAGE IS  
OF POOR QUALITY





ORIGINAL PAGE IS  
OF POOR QUALITY

Figure 4 Rate-Stabilization-Loop Block Diagram



Alpha Axis

$$K_{CA} = 18.87 \pm 1.5\%$$

$$T_{LA} = 0.4200 \text{ s} \pm 1.5\%$$

$$T_{CA} = 4.194 \text{ s} \pm 1.5\%$$

$$K_{LA} = 1.212 \pm 1.5\%$$

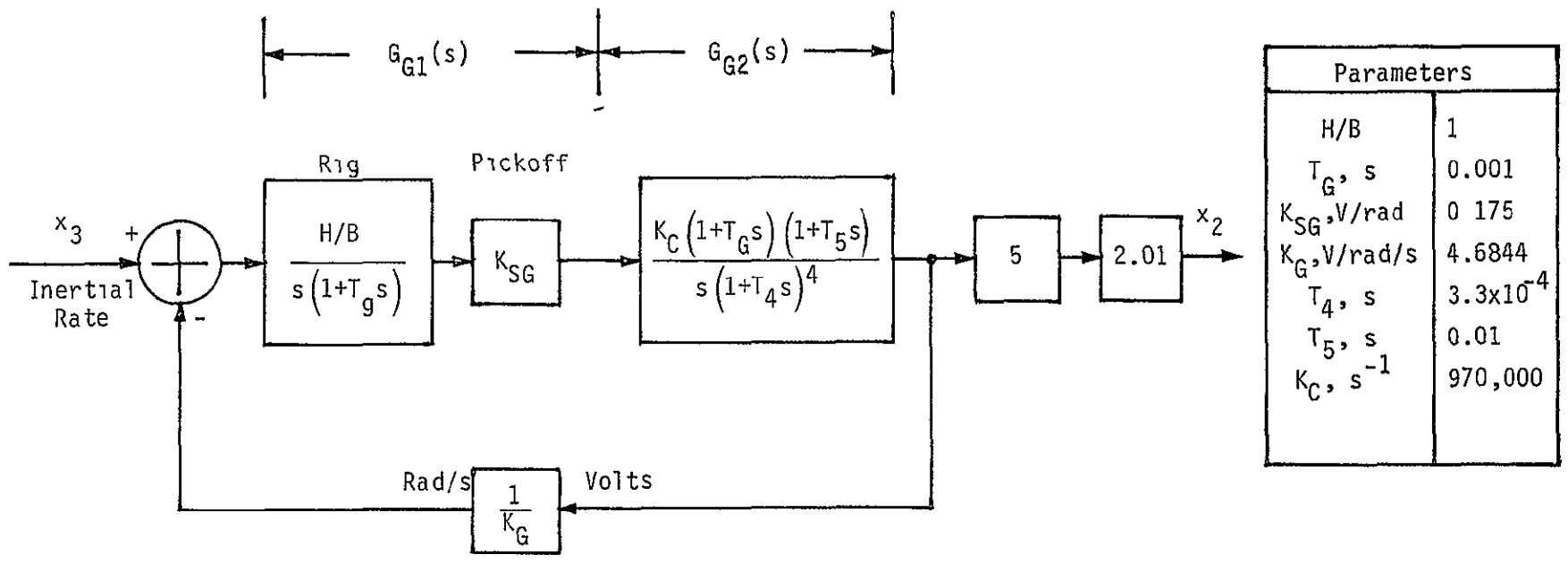
Figure 5 The Rate-Stabilization Loop-Shaping Filter for the  $\alpha$ -Axis

Table 1. Parameter Values for the Rate-Stabilization Loop-Shaping Filter

$$G_N \frac{\left[ \left( \frac{s}{\omega_N} \right)^2 + 2 \frac{\zeta_N}{\omega_N} s + 1 \right] (sZ + 1)}{\left[ \left( \frac{s}{\omega_D} \right)^2 + 2 \frac{\zeta_D}{\omega_D} s + 1 \right] (sP + 1)}$$

Symbol	$K_N$	$\omega_N/2\pi$	$\zeta_N$	$\omega_D/2\pi$	$\zeta_D$	Z	P
	$\pm 1.5\%$	Hz $\pm 2.25\%$	$\pm 1.5\%$	Hz $\pm 2.25\%$	$\pm 1.5\%$	MS $\pm 2.25\%$	MS $\pm 2.25\%$
$G_{N1}$	0.9757	13.02	0.9647	8.955	0.9783	23.92	23.58
$G_{N2}$	1.025	13.05	0.7064	8.967	0.7082	17.29	17.23
$G_{N3}$	0.9537	12.99	0.2579	8.995	0.2581	6.283	6.32
$G_{NL1}$	0.8457	15.40	0.7066	4.344	0.7023	14.48	14.61
$G_{NL2}$	1.000	26.97	0.0698	26.95	0.7062	0.8254	0.8240

Bandwidth	Gyro Output Used	$K_{XA}$ $\pm 1.5\%$	$L_{XA} K_{XA}$ V $\pm 10\%$	$K_B$ $\pm 1.5\%$	$K_{HA}$ $\pm 1.5\%$	$K_L$ $\pm 1.5\%$
Low	Fine	0.7331	10.08	0.2272	0	0.4434
High	Fine	0.7331	10.08	1.000	0.2104	0
Low	Coarse	3.675	10.08	0.2272	0	2.206
High	Coarse	3.675	10.06	1.000	1.050	0



Parameters	
H/B	1
$T_G, s$	0.001
$K_{SG}, V/rad$	0.175
$K_G, V/rad/s$	4.6844
$T_4, s$	$3.3 \times 10^{-4}$
$T_5, s$	0.01
$K_C, s^{-1}$	970,000

Figure 6 The Rate Sensor Assembly

ORIGINAL PAGE IS  
OF POOR QUALITY

where

$$\begin{aligned} h_0^{(3)} &= 24.25 K_{xA} \\ h_1^{(3)} &= 10.56 K_{xA} + 16.20 \\ h_2^{(3)} &= 1.893 \times 10^{-1} K_{xA} + 7.054 \end{aligned} \quad (43)$$

and

$$\begin{aligned} h_0^{(4)} &= 0 \\ h_1^{(4)} &= 1.060 \\ h_2^{(4)} &= 4.463 \end{aligned} \quad (44)$$

Combining (38), (39) and (42), we have

$$\begin{aligned} F_\alpha(s) &= \frac{0.92 K_4 F_1 F_2 K_B \left( \sum_{i=0}^8 h_1^{(3)} s^i \right) \left( \sum_{i=0}^7 h_1^{(2)} s^i \right) K_{MD} K_{TM} \cos \beta}{(1 + T_R s)(1 + T_M s) J(\beta) s \left( \sum_{i=0}^7 h_1^{(2)} s^i \right) \left( \sum_{i=0}^8 h_1^{(4)} s^i \right)} \\ &+ F_1 F_2 K_B 1.745 \times 10^{-2} \left( \sum_{i=0}^2 h_1^{(1)} s^i \right) \left( \sum_{i=0}^8 h_1^{(3)} s^i \right) K_{MD} K_{TM} \cos \beta \end{aligned} \quad (45)$$

If both the numerator and denominator of  $H_{RS}(s)$  retain only up to the first-order terms in  $s$ , we have

$$F_\alpha(s) \approx \frac{0.92 K_4 (h_0^{(2)} + h_1^{(2)} s)}{1.745 \times 10^{-2} (h_0^{(1)} + h_1^{(1)} s)} \quad (46)$$

$$F_\alpha(s) = 1.120 K_4 \quad (47)$$

Equation (46) is the result simply because the first term in the denominator of (45) begins with the second-order terms in  $s$ . Equation (47) results when we substitute (40) and (41) into (46).

Note that the only differences between the  $\alpha$ -axis and  $\beta$ -axis servo loops are the rate-stabilization loop-shaping filter and the moment of inertia. But neither of them appear in (46). Hence, as long as only the first-order term is retained, we have

$$F_{\beta}(s) = F_{\alpha}(s) = 1.120 K_4 \quad (48)$$

Substituting (47) and (48) into (31) with  $K_{SC1} = 2.047$  V/deg and  $K_4 = 0.0810$ , we end up with

$$\sigma_{\phi_{\alpha}}^2 = 5.537 \times 10^{-3} K_{SC2} \left( (2 - K_1 K_2) N_{0\alpha} + K_1^2 N_{0\beta} \right) \quad (49)$$

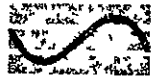
#### 4.0 S-BAND HARDWARE INVESTIGATIONS

The S-band hardware investigations centered on determining the reason for false lock of the TRW (the S-band hardware vendor) Spread-Spectrum Processor (SSP) in the spread mode with high-signal strengths. In addition, the impact of increased S-band forward-link doppler rates was investigated.

Analyses, documented in this section, indicated that the reason for the SSP false lock could be a fractional chip offset between the direct and the reference code channels. As a result, TRW modified the circuit to eliminate the fractional-chip offset. Unfortunately, this modification did not solve the problem. Since one of the SSP's did not false lock, AXIOMATIX tends to believe that the false-lock phenomenon may not be entirely intrinsic to a noncoherent tau-dither code loop, but may be related to some unknown vagaries of the particular components and circuit board used. At least, it causes AXIOMATIX to be concerned about the possibility of some SSP's false locking at less than 20 dB above threshold. As a result of these "post-fix" analyses and considerations, AXIOMATIX concluded that additional laboratory measurements on the SSP hardware are needed before an understanding of the false-lock phenomenon can be obtained. On a practical basis, none of the SSP's have false locked at the expected signal strengths from the TDRSS. Therefore, the problem has not been investigated further.

The analysis of the impact of increased S-band doppler rates showed that the S-band system performance was degraded negligibly. This analysis follows.

PRECEDING PAGE BLANK NOT FILMED



# Axiomatix

9841 Airport Boulevard • Suite 912 • Los Angeles, California 90045 • Phone (213) 641 8600

TECHNICAL MEMORANDUM NO. M8201-2

TO. P. Nilsen

DATE. January 11, 1982

FROM: J. Holmes

COPIES: 16067"A" Distribution

SUBJECT. Impact of the Increased S-Band  
Forward Link Doppler Rates

-----

## 1.0 SUMMARY

Based upon considering the effect of increased doppler rates upon the carrier demodulator, the code-tracking loop and the PN code acquisition circuitry, it is concluded that no problems will be encountered because of the increased forward link doppler rate and that the receiver sensitivity will not be affected.

The increased doppler rate still implies a negligible steady-state tracking error for both the carrier loop and the PN code loop. Furthermore, during a dwell time (during code acquisition), the code will slip a negligible amount during integration.

Because the static phase induced by the dynamics is negligible, the data detection loss is also negligible ( $< 0.1$  dB).

## 2.0 ANALYSIS

In this memo, we will briefly address the concerns of Sid Novosad concerning the effect of the increased doppler rate on the forward S-band link

### 2.1 Costas Loop Demodulator

The Costas loop demodulator in the TDRS mode must now tolerate a maximum carrier doppler rate of  $-165$  Hz/s [1]. The specification value is  $\pm 80$  Hz/s. Since the same Costas loop is used for both STDN and TDRS primary modes [2] and the maximum doppler rate is  $\pm 5000$  Hz/s in the STDN modes, it would appear that no problem exists.



As a verification, the static phase error associated with  $\ddot{f} = 165 \text{ Hz/s}$  is given by

$$\phi_{ss} = \frac{\dot{\omega}}{\omega_n^2} = \frac{(2\pi)(165)}{(370)^2} = 0.43^\circ \quad (1)$$

which is quite negligible. The value of  $\omega_n$  (370 rad/s) is obtained from the loop bandwidth  $B_L = 200 \text{ Hz}$  by the relationship

$$\omega_n = \frac{2 B_L}{\left(\zeta + \frac{1}{4\zeta}\right)} \quad (2)$$

where  $\zeta$  is the loop damping factor of a second-order phase-locked-loop and is assumed to be 0.707. Clearly, static phase offsets of  $0.4^\circ$  are entirely negligible. Carrier loop threshold will not change measurably when the static phase error goes from about  $0.2^\circ$  when  $\dot{f} = 80 \text{ Hz/s}$  to about  $0.4^\circ$  when  $\dot{f} = 165 \text{ Hz/s}$ .

## 2.2 Despreader Loop Tracking

Since the code-tracking loop has to tolerate the higher dynamic level, it is of interest to determine the value of the static phase error in tracking.

For a 10-Hz, one-sided code loop noise bandwidth, we have  $\omega_n = 18.86 \text{ rad/s}$  so that, using  $T = 0.88 \text{ chips/s}$ , we have [3]

$$\frac{\epsilon_{ss}}{T_c} = \frac{T}{\omega_n^2} = \frac{0.88}{(18.86)^2} = 0.0025 \text{ chips} \quad (3)$$

which again is a trivial amount and will not affect the threshold of the code loop.

During code acquisition, it is possible that the received code will slip during a dwell time (547  $\mu\text{s}$ ) relative to the transmitted code, which could degrade the code detectability.

The amount of code slippage is given by

$$\Delta c = (\text{code doppler rate}) \times (\text{dwell time}) = 0.88 \times 547 \times 10^{-6}$$

or

$$\Delta c = 4.8 \times 10^{-4} \text{ chips} \quad (4)$$

which again is a trivial amount that would not affect the detectability.

### 2.3 Data Detection

The data detection degradation due to imperfect carrier demodulation is approximately given by

$$L = 10 \log \{ \cos^2 \phi_{SS} \} \text{ dB}$$

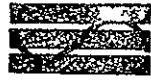
When  $\phi_{SS} = 0.43^\circ$ , we have

$$L = -0.0006 \text{ dB}$$

which is totally negligible.

### References

1. F. N. Barnes and F. E. Volentine, Lockheed memo of December 8, 1981.
2. R. Phillips (TRW S-band system engineer), private communications.
3. J. K. Holmes, Coherent Spread Spectrum Systems, text to be published by Wiley Interscience in January 1982.



# Axiomatix

9841 Airport Boulevard • Suite 912 • Los Angeles, California 90045 • Phone (213) 641 8600

TECHNICAL MEMORANDUM NO. M8201-4

TO: File DATE: January 22, 1982  
FROM: P. Nilsen COPIES: 16067"A" Distribution  
SUBJECT: Addendum to "Impact of the  
Increased S-Band Forward Link  
Doppler Rate," Memo No. M8201-1

-----

## 1.0 INTRODUCTION

The purpose of this memorandum is to extend the results of the subject memorandum to cover a doppler rate of 5000 Hz/s. In general, it can be expected that operation of the transponder at this rate, but in the TDRS mode, will provide acceptable performance. This is because, in the STDN mode, the transponder is designed to operate at the 5000 Hz/s rate and the Costas loop utilizes the same circuitry in both modes. The common circuitry feature was confirmed by examination of the transponder block diagrams and consultation with TRW (Bob Phillips).

The pertinent performance parameters that were calculated for 165 Hz/s are given below for 5000 Hz/s. In each case, the parameters are within an acceptable value, although they may be at the limit of the level of acceptability.

## 2.0 ANALYSIS

### 2.1 Costas Loop Static Phase Error

$$\phi_{ss} = \frac{(2\pi)(5000)}{(370)^2} = 13^\circ$$

This will cause some increase in carrier loop threshold and a decrease in the mean time to loss of lock but, since these dynamics occur during short ranges, no problem is expected.

## 2.2 Despreader Loop Tracking

$$\text{Loop static error} = \frac{0.88}{(18.86)^2} \left( \frac{5000}{165} \right) = 0.08 \text{ chips} \\ \text{(negligible)}$$

$$\text{Code slippage} = 0.88 \times 547 \times 10^{-6} \times \left( \frac{5000}{165} \right) \\ = 1.45 \times 10^{-2} \text{ chips (negligible)}$$

## 2.3 Data Detection

$$L \approx 10 \log \{ \cos^2 13^\circ \} \\ \approx 0.22 \text{ dB}$$

A loss of 0.22 dB is negligible considering the short range that exists during the 5000 Hz/s rate.

INVESTIGATION OF THE PN CODE FALSE-LOCK PROBLEM  
IN THE S-BAND SPREAD SPECTRUM PROCESSOR

Interim Report

Contract No. NAS 9-16067, Exhibit A

Technical Monitor: W. Teasdale

Prepared for

NASA Lyndon B. Johnson Space Center  
Houston, Texas 77058

Prepared by

Peter W. Nilsen  
Marvin K. Simon

Axiomatix  
9841 Airport Blvd., Suite 912  
Los Angeles, California 90045

Axiomatix Report No. R8111-1  
November 3, 1981

## 1.0 . INTRODUCTION AND SUMMARY

This report presents a discussion of Axiomatix's investigation of the false-lock problem in the S-band Spread Spectrum Processor (SSP). This phenomenon was observed by TRW during testing and has been documented by TRW [1,2,3]. The phenomena consists of three related problems. First, the code loop-lock detector incorrectly indicates lock. Second, the code loop tracks at a false-lock point, i.e., not at the true correlation point. Third, while false-lock tracking, the code loop oscillates at an 11-Hz rate  $\pm 0.3$  chips about the nominal tracking point.

The first phenomenon described above was analyzed by TRW and Axiomatix [1]. Axiomatix agreed with TRW, and the analysis is given in Section 2 of this report. Axiomatix also concurred with the fix recommended by TRW. It was thought that this fix--the elimination of fractional local code chip offset between direct and reference channels--would stop all three of the problems described above. Unfortunately, this fix did not work. Axiomatix then conducted an exhaustive investigation of the available test data taken during the Colorado Electronics (CE) tests which concluded that the fix did not work. Based on this data, Axiomatix could not reach any conclusion regarding the cause of the false-lock phenomenon.

The failure of the fix and the fact that SSP's currently are to be delivered with this false-lock problem existing prompts the question as to the advisability of Acceptance Test Procedure (ATP) false-lock testing (not currently part of the ATP). This issue is discussed in Section 4 of this report. In summary, Axiomatix feels that, in light of the probable additional cost of adding to the ATP, it cannot make a recommendation without additional information gained through analysis of the Shuttle launch S-band link or additional laboratory hardware testing

## 2.0 AN EVALUATION OF THE S-BAND SHUTTLE DESPREADER PN CODE FALSE-LOCK PROBLEM PRIOR TO ATTEMPTED FIX

### 2.1 Introduction

Laboratory measurements performed on the S-band Spread Spectrum Processor (SSP) have demonstrated its capability of false locking to an incorrect code phase under certain operating conditions. A theoretical explanation for the occurrence of this phenomenon during PN code acquisition was presented in [1]. The two items of concern there were the mechanism which caused the false-lock problem and the input signal power level (relative to threshold) at which it occurred. Briefly stated, the false-lock acquisition phenomenon was attributed to the cusp-like nature of the power spectral density of the despread PN code as a function of the relative timing offset (at least one chip) between the received PN code signal and the locally generated PN code replica. In particular, when the signal-to-noise ratio (SNR) was sufficiently high that the cusp peak (maximum power output of the acquisition (direct) channel) exceeded the power output of the referenced (tracking) channel (which is proportional to the average over the cusp-like spectral density), then the post-detection integrator would tend to go positive with increasing time, thus causing the detection threshold to be exceeded. An analysis of this phenomenon, including the effects of the noncoherent AGC which precedes the desreader, revealed that false lock would occur at 27 dB above threshold ( $C/N_0 = 48$  dB-Hz) for the low data rate (210-kHz predetection filter bandwidth) mode and about 25 dB above threshold ( $C/N_0 = 51$  dB-Hz) for the high data rate (480-kHz predetection filter bandwidth) mode.

Having thus identified the means and conditions by which the desreader would false lock during code acquisition, the next question to be answered was: would the code lock detector accept the synchronized PN code as a valid lock condition and, if so, would the PN tracking loop then proceed to track under these false lock conditions?

Indeed, this aspect of the false-lock problem was the more elusive to explain, and a complete understanding of its causes and effects became clear only after examining experimental measurements made on an operational despreader at Colorado Electronics (CE). These findings were reported in [2] along with a supporting analysis. The principal outcome of this investigation was that the combination of a low-frequency ( $\approx 11$  Hz) oscillation of the code loop of  $\pm 3/8$  chip about its nominal synchronization position with a noninteger ( $\approx 4.3$  chips) delay difference between the direct and reference channel epochs was capable of sustaining a false-lock condition in lock detection and tracking. An explanation for the fractional (0.3 chips) time skew in terms of the existing SSP hardware was given in [3].

Also discussed in [2] were suggestions for eliminating the false-lock problem attributed to the fractional offset between direct and reference channel codes. After considering several possibilities, some of which required no hardware changes, it was decided that the most practical solution, although requiring some simple modifications to the circuits [3], would be to correct the fractional offset to near zero.

The questions which naturally arise next are whether or not zero is indeed the "best" fractional offset for the observed tracking oscillation of  $\pm 3/8$  of a chip and how sensitive is the false lock problem to variations about this best offset value, i.e., what kind of tolerance must be imposed on the circuits once they have been modified? The word "best," as used above, refers to the least tendency to false lock. The measure used to describe this will be the same as that used in [2], namely, a comparison between the mean direct channel-to-mean reference channel voltage ratio in false lock to the same ratio in true lock at threshold conditions.

## 2.2 Computation of the Mean-Direct-Channel-to-Mean-Reference-Channel Voltage Ratio as a Function of Fractional Offset

We begin by recalling from [2] the expression for the cusp-like power spectral density of the product of the received PN code and the local PN code replica (near  $f = 0$ ):



$$S(f,x) = PT_c \left[ x^2 + 1 - x^2 \right] ; 0 \leq x \leq 1$$

$$S(f,x \pm N) = S(f,x) ; N \text{ any integer} \quad (1)$$

where P is the baseband signal power in watts,  $T_c$  is the PN code chip interval in seconds, and x is the chip timing error (normalized by  $T_c$ ) reduced modulo-one chip. The relations in (1) hold provided that the actual (unnormalized) timing error is greater than one chip. If we assume, as in [2] that, after a lock detection hit, the direct-channel code timing falls from the cusp peak to the valley, then, for a code loop oscillation of  $\pm 3/8$  chips, this timing will bounce between  $x_1 = 1/2 - 3/8 = 1/8$  and  $x_2 = 1/2 + 3/8 = 7/8$ . Furthermore, if the code loop spends approximately equal time at these two positions, i.e., the 11-Hz oscillation is assumed symmetrical, then, in the false lock mode, the signal component of the average voltage out of the direct channel is given by

$$\bar{e}_D \Big|_{\text{signal}} = \frac{1}{2} \left[ S\left(f, \frac{1}{8}\right) + S\left(f, \frac{7}{8}\right) \right] B = PT_c B \left[ \left(\frac{1}{8}\right)^2 + \left(\frac{7}{8}\right)^2 \right] = \frac{25}{32} PT_c B \quad (2)$$

where B is the noise bandwidth of the predetection filter.

Now assuming that the reference channel is delayed relative to the direct channel by  $N + \delta$ , when N is integer and  $\delta$  is an arbitrary fraction (in the Colorado Electronics test,  $\delta = 0.3$ ), in the false lock mode, the signal component of the average voltage out of the reference channel is then given by\*

$$\bar{e}_R \Big|_{\text{signal}} = \frac{1}{2} \left[ S\left(f, \frac{1}{8} + \delta\right) + S\left(f, \frac{7}{8} + \delta\right) \right] B \triangleq PT_c B \eta(\delta) \quad (3)$$

Using both the definition and periodic property of  $S(f,x)$  as given in (1), then, as  $\delta$  varies between zero and one, the parameter  $\eta(\delta)$  is evaluated as

---

\* Notice that, since the SSP is no longer in its search mode, the reference channel does not average over the cusp-like spectral density. Rather, it behaves like the direct channel in that it oscillates between two fixed-code positions.

$$\eta(\delta) = \begin{cases} \frac{1}{2} \left[ \left( \frac{1}{8} - \delta \right)^2 + \left( \frac{7}{8} + \delta \right)^2 \right] + \frac{1}{2} \left[ \left( \frac{1}{8} + \delta \right)^2 + \left( \frac{7}{8} - \delta \right)^2 \right]; & 0 \leq \delta \leq \frac{1}{8} \\ \frac{1}{2} \left[ \left( \delta - \frac{1}{8} \right)^2 + \left( \frac{9}{8} - \delta \right)^2 \right] + \frac{1}{2} \left[ \left( \frac{1}{8} + \delta \right)^2 + \left( \frac{7}{8} - \delta \right)^2 \right]; & \frac{1}{8} \leq \delta \leq \frac{7}{8} \\ \frac{1}{2} \left[ \left( \delta - \frac{1}{8} \right)^2 + \left( \frac{9}{8} - \delta \right)^2 \right] + \frac{1}{2} \left[ \left( \delta - \frac{7}{8} \right)^2 + \left( \frac{15}{8} - \delta \right)^2 \right]; & \frac{7}{8} \leq \delta \leq 1 \end{cases} \quad (4)$$

Figure 1 is a plot of  $\eta$  versus  $\delta$ , as given by (4). Actually, since  $\eta$  is a symmetrical function of  $\delta$  around  $\delta = 0.5$ , we have alternately drawn the plot for  $\delta$  in the range  $(-0.5, 0.5)$ . This is equivalent to defining  $\eta(-\delta) = \eta(1-\delta)$ . We have also marked with an x the point on the curve corresponding to  $\delta = 0.3$ . We note from this curve that the maximum value of  $\eta$  occurs for  $\delta = 1/8$ . In fact, for

$$0 < \delta < \frac{\sqrt{2}-1}{2\sqrt{2}} \quad (5)$$

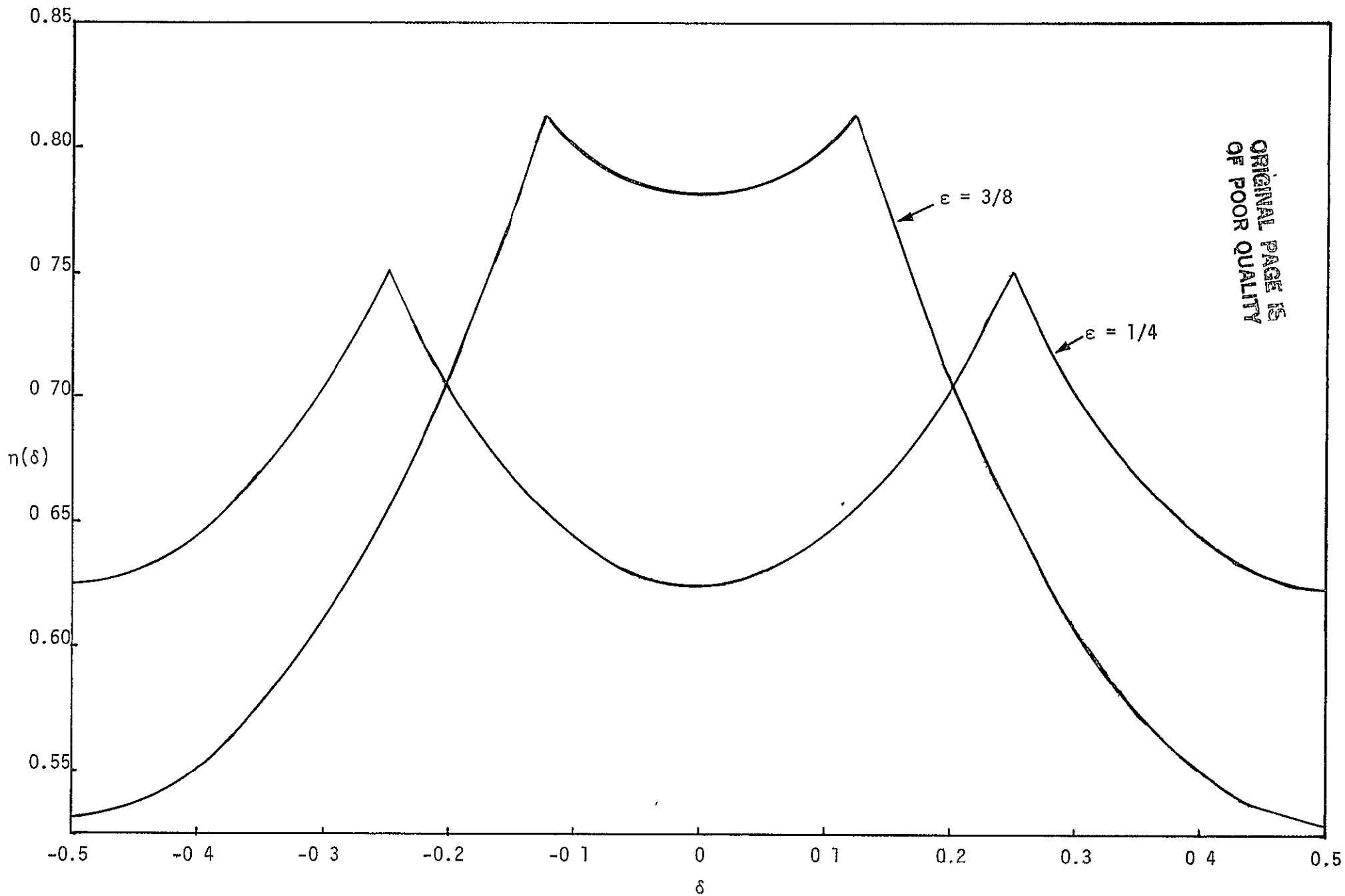
$\eta$  exceeds its value corresponding to  $\delta = 0$ . This latter result can be obtained by first simplifying (4) to

$$\eta(\delta) = \begin{cases} \frac{25}{32} + 2\delta^2 & ; & 0 \leq \delta \leq \frac{1}{8} \\ \frac{33}{32} - 2\delta + 2\delta^2 & ; & \frac{1}{8} \leq \delta \leq \frac{7}{8} \\ \frac{89}{32} - 4\delta + 2\delta^2 & , & \frac{7}{8} \leq \delta \leq 1 \end{cases} \quad (6)$$

then solving the equation

$$\frac{33}{32} - 2\delta + 2\delta^2 = \frac{25}{32} \quad (7)$$

for  $\delta$ .



ORIGINAL PAGE IS  
OF POOR QUALITY

Figure 1 A Plot of  $\eta(\delta)$  versus  $\delta$

Using (2) and (3), the total mean-direct-channel-to-total-mean-reference-channel voltage ratio in false lock is

$$\frac{\bar{e}_D}{\bar{e}_R} = \frac{N_0 B + \frac{25}{32} P T_c B}{N_0 B + P T_c B \eta(\delta)} = \frac{1 + \frac{25}{32} B T_c \gamma}{1 + \eta(\delta) B T_c \gamma} \quad (8)$$

where

$$\gamma \triangleq \frac{P}{N_0 B} \quad (9)$$

is the SNR in the predetection filter bandwidth. Clearly, whenever  $\delta$  satisfies (5), we will have  $\bar{e}_D/\bar{e}_R < 1$ , and the despreader will be less sensitive to false lock than if the fractional time offset were corrected to zero. In fact, for  $0 \leq \delta \leq 1/8$ , the ratio  $\bar{e}_D/\bar{e}_R$  is relatively insensitive to variations in  $\delta$ . Beyond  $\delta = 1/8$ ,  $\bar{e}_D/\bar{e}_R$  is a much more sensitive function of  $\delta$  since, from Figure 1,  $\eta$  falls off rapidly.

In the true-lock mode, we have

$$\frac{\bar{e}_D}{\bar{e}_R} = \frac{1 + \gamma_0 (0.75)^2}{1 + \frac{2}{3} B T_c \gamma_0} \quad (10)$$

where  $\gamma_0$  is the threshold SNR in the predetection filter bandwidth, the factor (0.75) accounts for the power loss corresponding to a 1/4 chip (worst-case for a 1/2-chip search increment) offset from the true PN code synchronization position, and the factor of 2/3 represents the average of  $S(f,x)$  of (1) over  $x$ , i.e.,

$$\int_0^1 [x^2 + (1-x)^2] dx = \frac{2}{3} \quad (11)$$

as occurs in the reference channel. In the high data rate mode, we have

$$\begin{aligned} 10 \log_{10} \gamma_0 &= 10 \log_{10} P_0/N_0 - 10 \log_{10} B \\ &= 51 - 10 \log_{10} (480 \times 10^3) = -5.812 \text{ dB} \end{aligned} \quad (12)$$

or

$$\gamma_0 = 0.262 \quad (13)$$

Also,

$$BT_c = \frac{B}{T_c} = \frac{480 \times 10^3}{11 \times 10^6} = 0.0436 \quad (14)$$

Thus, substituting (13) and (14) into (10) gives

$$\left. \frac{\bar{e}_D}{\bar{e}_R} \right|_{\substack{\text{true} \\ \text{lock}}} = 1.15 \quad (15)$$

Since false lock occurs about 25 dB above threshold [1], then  $\gamma = -5.812 + 25 = 19.188$  dB, or  $\gamma = 83.2$ . Thus, from (14) and (8),

$$\left. \frac{\bar{e}_D}{\bar{e}_R} \right|_{\substack{\text{false} \\ \text{lock}}} = \frac{3.836}{1 + 3.63 \eta(\delta)} \quad (16)$$

where  $\eta(\delta)$  is given by (6). Figure 2 plots

$$\left. \frac{\bar{e}_D}{\bar{e}_R} \right|_{\text{false lock}}$$

versus  $\delta$ .

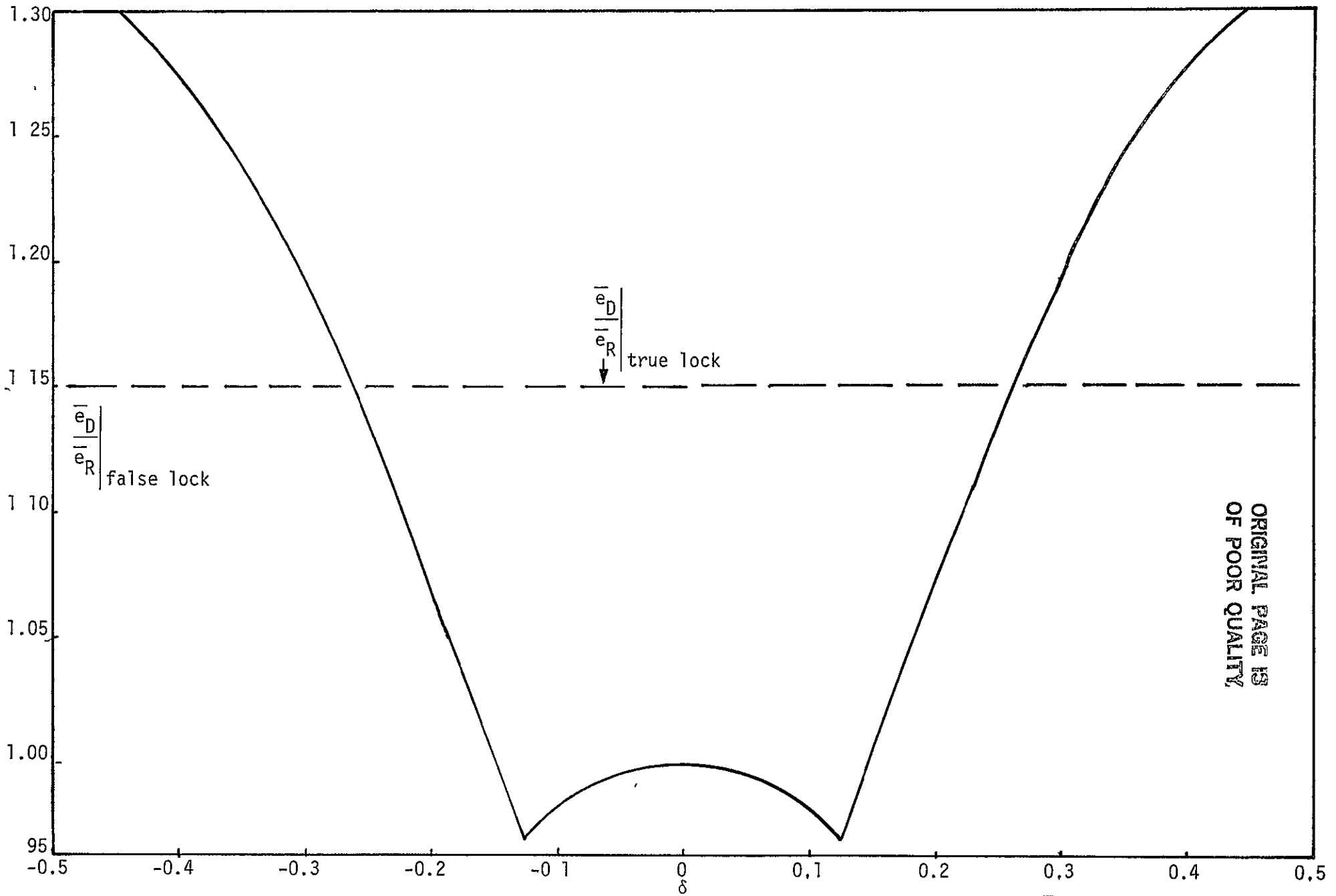


Figure 2. A Plot of  $\frac{|e_D|}{|e_R|}$  versus  $\delta$  ( $\epsilon = 3/8$ )

All of the foregoing assumed that, if the fractional timing offset  $\delta$  were other than 0.3 chips (the measured value in the CE test), then the PN tracking loop would still oscillate between  $+3/8$  and  $-3/8$  chips about its nominal value. Another possibility is that this oscillatory value of  $\pm 3/8$  chips will change from unit to unit and may even be related to  $\delta$ . If we let  $\pm\varepsilon$  denote the oscillation correlation values for the PN tracking loop, then (4) generalizes to

$$\eta(\delta) = \begin{cases} \frac{1}{2} \left[ \left( \frac{1}{2} - \varepsilon - \delta \right)^2 + \left( \frac{1}{2} + \varepsilon + \delta \right)^2 \right] + \frac{1}{2} \left[ \left( \frac{1}{2} - \varepsilon + \delta \right)^2 + \left( \frac{1}{2} + \varepsilon - \delta \right)^2 \right]; & 0 \leq \delta \leq \frac{1}{2} - \varepsilon \\ \frac{1}{2} \left[ \left( \delta - \frac{1}{2} + \varepsilon \right)^2 + \left( \frac{3}{2} - \varepsilon - \delta \right)^2 \right] + \frac{1}{2} \left[ \left( \delta + \frac{1}{2} - \varepsilon \right)^2 + \left( \frac{1}{2} + \varepsilon - \delta \right)^2 \right]; & \frac{1}{2} - \varepsilon \leq \delta \leq \frac{1}{2} + \varepsilon \\ \frac{1}{2} \left[ \left( \delta - \frac{1}{2} + \varepsilon \right)^2 + \left( \frac{3}{2} - \varepsilon - \delta \right)^2 \right] + \frac{1}{2} \left[ \left( \delta - \frac{1}{2} - \varepsilon \right)^2 + \left( \frac{3}{2} + \varepsilon - \delta \right)^2 \right]; & \frac{1}{2} + \varepsilon \leq \delta \leq 1 \end{cases} \quad (17)$$

which reduces to (4) when  $\varepsilon = 3/8$ . A simpler version of (17), which is analogous (6)

$$\eta(\delta) = \begin{cases} \frac{1}{2} + 2\varepsilon^2 + 2\delta^2 & , 0 \leq \delta \leq \frac{1}{2} - \varepsilon \\ 2\varepsilon^2 - 2\varepsilon + \frac{3}{2} - 2\delta + 2\delta^2 & ; \frac{1}{2} - \varepsilon \leq \delta \leq \frac{1}{2} + \varepsilon \\ 2\varepsilon^2 + \frac{5}{2} - 4\delta + 2\delta^2 & , \frac{1}{2} + \varepsilon \leq \delta \leq 1 \end{cases} \quad (18)$$

Superimposed on the previous result in Figure 1 is a plot of  $\eta(\delta)$  versus  $\delta$ , as computed from (18) for  $\varepsilon = 1/4$ . Here we see that the variation of  $\eta(\delta)$  with  $\delta$  is a much more sensitive function. Figure 3 shows the corresponding result for

$$\left. \frac{\bar{e}_D}{\bar{e}_R} \right|_{\text{false lock}}$$

as computed from

$$\left. \frac{\bar{e}_D}{\bar{e}_R} \right|_{\text{false lock}} = \frac{1 + 3.63 \eta(0)}{1 + 3.63 \eta(\delta)} \quad (19)$$

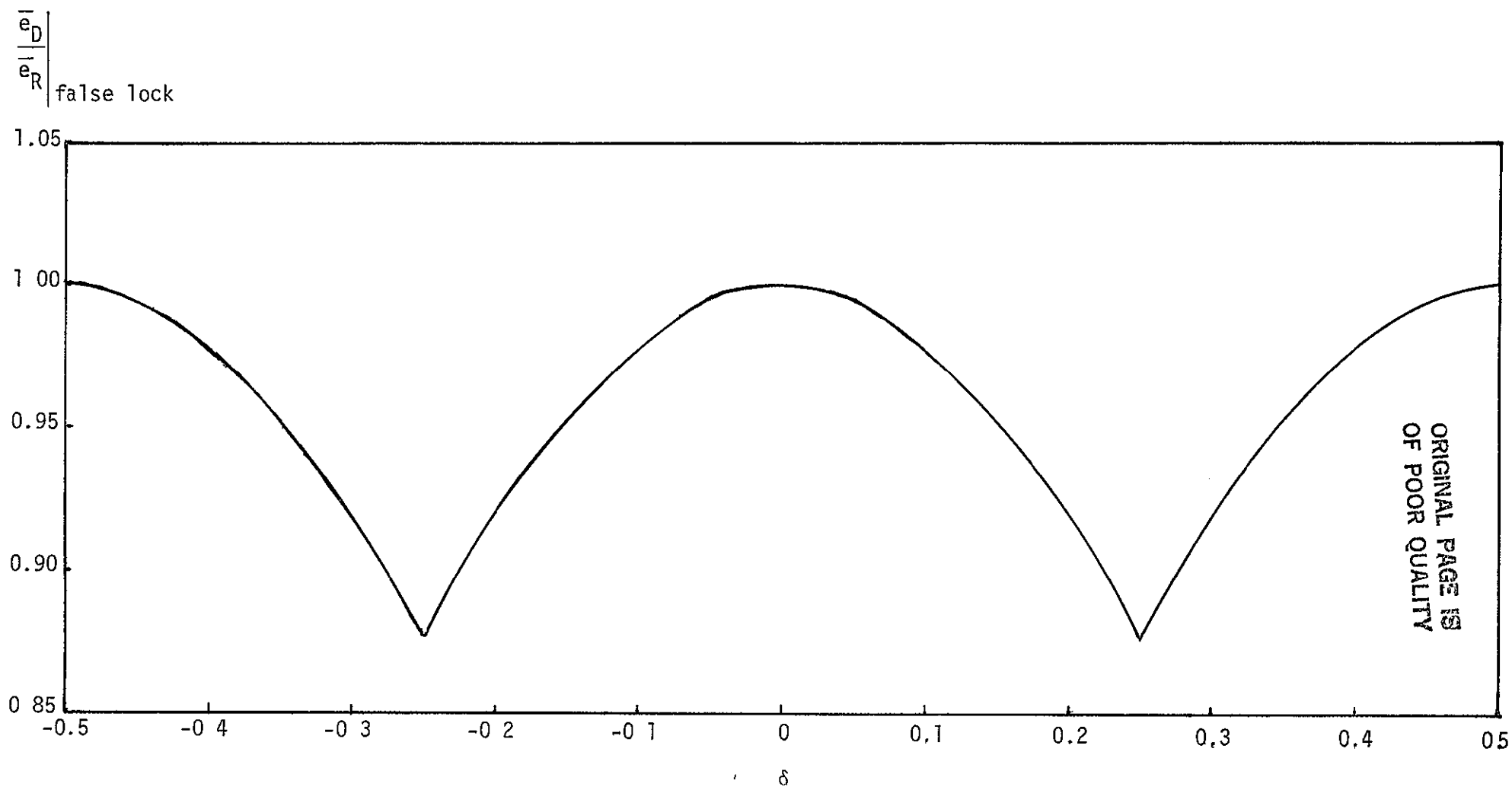


Figure 3 A Plot of  $\frac{\bar{e}_D}{\bar{e}_R} \Big|_{\text{false lock}}$  versus  $\delta$  ( $\epsilon = 1/4$ )



which, for  $\epsilon = 1/4$ , becomes

$$\left. \frac{\bar{e}_D}{\bar{e}_R} \right|_{\text{false lock}} = \frac{3.269}{1 + 3.63 \eta(\delta)} \quad (20)$$

### 3.0 EVALUATION OF FALSE-LOCK PROBLEM AFTER ATTEMPTED FIX

The fix to the SSP false lock suggested by TRW and concurred with by AXIOMATIX was tested at CE. Unfortunately, the fix (elimination of fractional chip offset between reference channel and direct-channel codes) did not cure the false-lock problem. As a consequence, AXIOMATIX made an intensive effort to determine the cause of the problem. Actually, the problem can be divided into three parts:

- (1) False indication of lock by the lock detector
- (2) Code-loop tracking at a false lock point
- (3) Code-loop oscillation (nominally 11 Hz rate,  $\pm 0.3$  chips about the false-lock point).

The first part of the problem is the one addressed by TRW and Section 2 of this report [1]. The second and third parts of the problem were addressed by a team effort of tracking-loop experts Marvin Simon, Jack Holmes, and Peter Nilsen. This team analyzed the data from the CE tests of the SSP in which the "fix" was incorporated. The team also postulated and analyzed several potential mechanisms for false-lock tracking and code-loop oscillation. However, none of the postulated mechanisms would sustain a discriminator-tracking characteristic. These attempts at understanding the false-lock phenomena are now summarized.

- (1) Analyzed the expected or predicted values of direct and reference channel outputs for the conditions of "in lock," "no lock," and "false-lock "
- (2) Analyzed the PN correlation process and the number of chips actually averaged as a result of the memory time of the circuits.

(3) Evaluated the mean and standard deviation for the partial correlation that takes place in the two channels.

(4) Developed an explanation and rationale for the conclusion that removal of the PRN or high-reference channel bias would eliminate the false-lock phenomenon.

(5) Formulated a new approach to avoid false lock based upon a slight modification of the hardware. This approach uses the AGC to control the gain of the reference channel.

(6) Considered the generation of a discriminator-tracking curve from the correlation side peaks as a means of sustaining false-lock tracking but found that this did not work.

(7) Investigated the possibility of large partial-correlation side peaks resulting in a discriminator function but found this not to work because of the rapid time variation of the amplitude of these peaks.

(8) Noted a cross coupling between reference and direct channels in the CE test data. This coupling is not explained by theory and could be related to the false-lock phenomena.

In addition to the efforts described above, Axiomatix also contacted Bob Phillips of TRW, who conducted the CE tests. Bob was most cooperative in discussing the observations he made during the tests. Unfortunately, this additional information still did not provide the explanation for the phenomena. However, two things Bob said are worth noting here. One is that, of the three SSP's tested for false lock, two false locked and one did not. Second, changing the 11-Hz code loop dither frequency slightly caused the 11-Hz code loop oscillation to cease. This latter fact should be pursued if further investigation is called for. Another observation which might be a potential lead for further investigation is that there was a much greater occurrence of false locks in the high data rate mode than in the low data rate mode. The fact that one of the SSP's did not false lock tends to lead Axiomatix to believe that the phenomenon may not be entirely intrinsic to a noncoherent  $\tau$ -dither code loop, but may be related to some unknown vagaries of the particular components and circuit board used. At least, it causes Axiomatix to be concerned about the possibility of some SSP's false locking at less than 20 dB above threshold.

As a result of these "post-fix" analyses and considerations, Axiomatix concluded that additional laboratory measurements on the SSP hardware are required before an understanding of the false lock can be obtained.

#### 4.0 RECOMMENDATIONS

Two courses of action concerning the SSP false-lock problem are possible at this point. One is to ignore the phenomenon and rely on operational procedures to avoid false lock; the second is to fix the problem. An attempt has already been made to fix the problem and failed, as discussed elsewhere in this report. Another fix has been suggested by Axiomatix as a result of its investigations of the phenomenon. This fix, control of the reference channel gain by the AGC, is more of the nature of a "bandaid" fix since it does not really directly address the root cause of the false lock. Unfortunately, in order to determine the root cause of the problem, additional laboratory tests and measurements on the SSP hardware would be required.

If the SSP is flown "as is," the question of whether or not to require additional ATP testing, i.e., false-lock testing, must be answered. The answer to this question depends on the possible range of signal level values over which the SSP will false lock and the expected signal levels during the Shuttle mission (specifically, during launch and ascent). Crucial to this issue is the probability of losing lock and the subsequent reacquisition requirement. Such analyses are also required to determine the effectiveness of operational fixes. Furthermore, these analyses are necessary to determine "pass/fail" criteria for false-lock ATP testing.

Axiomatix recognizes the cost implications of the testing and analyses discussed above. However, when making the decision on these matters, it is important to keep in mind that, although it is felt that signal levels on the order of 20 dB above threshold are required for false lock, without ATP false-lock testing, it will not be known if this is true of all SSP's.

In summary, Axiomatix does not feel that it has sufficient information, either as a result of analyses or hardware measurements, to make a recommendation concerning false-lock testing and/or modifying the SSP's to eliminate the problem. However, if so directed by NASA, Axiomatix is prepared to perform the analyses and/or participate in further SSP hardware investigations.

C-4

REFERENCES

1. J. K. Holmes, "S-Band Shuttle Desreader False Lock of the PN Code," TRW Interoffice Correspondence SCTE-50-80-510, May 30, 1980.
2. J. K. Holmes and M. Y. Huang, "S-Band Shuttle Desreader PN Code False Lock Investigation at Colorado Electronics." TRW Interoffice Correspondence SCTE-50-80-514, #80-7327.01-039, August 26, 1980.
3. W. D. Nations, "Spread Spectrum Processor (Shuttle) Timing Problem," TRW Interoffice Correspondence #80-7327.02-001, July 25, 1980.

## 5.0 SHUTTLE/CENTAUR COMMUNICATION SYSTEM ENGINEERING INVESTIGATIONS

The second major effort under Task 15 involved the Shuttle/Centaur communication-system engineering investigations. These investigations became part of Task 15 as the Centaur communication system progressed further into the hardware development stages. These investigations occurred from October 1, 1982 to September 30, 1983.

The majority of investigations are documented in Axiomatix Report No. R8310-4, "Shuttle/Centaur Communication System Engineering Investigations, Final Report for Contract No. NAS 9-16067, Exhibit A," dated October 20, 1983. The final report focusses on the following areas: (1) generation of the hard-line ICD, (2) recommendation of a test technique to verify data bit-jitter performance, (3) investigation of the BER requirement allocation to DCU memory as impacted by cosmic-ray hits, (4) evaluation of potential RFI to the Shuttle due to intermods from multiple transmitters operating simultaneously, (5) evaluation of the impact on data loss due to antenna-switching transients, (6) evaluation of antenna-switching techniques to minimize data loss, (7) communication system requirements evaluation via design review and panel meeting participation, (8) communication system LRU requirements evaluation via design reviews and panel meeting participation, and (9) generation of parameter values for Goddard simulation of the Centaur/TDRSS link.

In addition to the evaluations of data loss due to antenna-switching transients documented in the final report, Axiomatix Technical Memo No. M8310-2, "Probability of Loss of Lock During a 5-ms Centaur Carrier-Loop Dropout," dated October 18, 1983, considers the effects of the Centaur antenna-switching transients on the TDRSS ground Costas-loop carrier demodulation. Based on thermal-noise considerations during the antenna transient-induced dropout (~ 5 ms) and since a small doppler shift exists between the two transmit antennas, it was concluded that, under disadvantageous phasing conditions, the Costas-loop demodulator could lose lock for the full 5-ms dropout time. In addition, it would take about 9.5 ms to reacquire with probability near one. On the other hand, under favorable conditions, noise, antenna-switching and doppler effects would cause only a small phase perturbation without loss of lock and with almost no effect on the data.

It was also concluded that a good portion of a minor frame could be lost (data inverted) using NRZ-L under unfavorable antenna-switching conditions. However, NRZ-S or NRZ-M would greatly minimize data loss. It is recommended that NRZ-S or NRZ-M be used if possible--not NRZ-L!

SHUTTLE/CENTAUR COMMUNICATION SYSTEM  
ENGINEERING INVESTIGATIONS

FINAL REPORT

Contract No. NAS9-16067, Exhibit A

Prepared for

NASA Lyndon B. Johnson Space Center  
Houston, Texas 77058

Prepared by

Axiomatix  
9841 Airport Blvd., Suite 912  
Los Angeles, California 90045

Axiomatix Report No. R8310-4  
October 20, 1983

## TABLE OF CONTENTS

- 1.0 INTRODUCTION
- 2.0 SUMMARY
- 3.0 TECHNICAL OUTPUTS
  - 1. Centaur Telemetry Data Bit-Jitter Measurement Techniques
  - 2. A Technique to Minimize Antenna-Switching Transient Effects the Centaur Vehicle
  - 3. Viewgraph Presentations
- 4.0 ORBITER-VEHICLE/CENTAUR HARDLINE ICD



## 1.0 INTRODUCTION

This final report documents the work performed by Axiomatix on the communication system engineering support for the Centaur/Shuttle vehicle. The work focussed on the following areas:

1. Writing a hardline ICD
2. Recommendation of a test technique to verify data bit-jitter performance
3. Investigation of the BER requirement allocation to DCU memory as impacted by cosmic-ray hits
4. Evaluation of potential RFI to the Shuttle due to intermods from multiple transmitters operating simultaneously
5. Evaluation of the impact of antenna-switching transients on the data loss
6. Evaluation of antenna-switching techniques to minimize the data loss
7. Communication system requirements evaluation via design review and panel meeting participation
8. Communication system LRU requirements evaluation via design review and panel meeting participation
9. Generation of parameter values for Goddard simulation of the Centaur/TDRSS link.

Axiomatix outputs on each of the above activities were written reports and memoranda, panel meeting presentations, RID's submitted at design reviews, and Section 5 of ICD-2-1F001. All of the written reports, memos and briefing charts are contained in Section 3 of this report. Section 5 of ICD-2-1F001, the "hardline ICD," is given in Section 4, while Section 2 contains a brief summary of the results of the analyses and design investigations.

## 2.0 SUMMARY

The following briefly summarizes the findings of the analysis and design investigations conducted by AXIOMATIX. Greater detail is provided in Section 3 or the panel meeting presentations.

Title	Summary
Bit Jitter Test Technique	A technique using off-the-shelf commercial test equipment is described.
Allocation of BER Due To Cosmic-Ray Upset of DCU Memory	Showed an increase in BER and recommended the use of hardened memory
Evaluation of RFI From Intermods	Reviewed RF emissions with Art Rubins of JSC; he concluded that there was no problem
Impact of Antenna Switching	Showed that significant data can be lost in light potential TDRSS high-dynamics demod dropout and reacquisition
Evaluation of Antenna-Switching Techniques	Recommended different switching point in spin cycle; also recommended ferrite-latching switch to reduce switching transient time

3.0 TECHNICAL OUTPUTS

CENTAUR TELEMETRY DATA  
BIT-JITTER MEASUREMENT TECHNIQUES

Interim Report

Contract NAS 9-16067"A"

Prepared for  
NASA Lyndon B. Johnson Space Center  
Houston, Texas 77058

Prepared by  
S. Udalov  
Dr. K. T. Woo

AXIOMATIX  
9841 Airport Blvd., Suite 912  
Los Angeles, California 90045

AXIOMATIX Report No. R8309-2  
September 30, 1983

## 1.0 INTRODUCTION AND OVERVIEW

A test setup for measuring bit-jitter characteristics of the data stream outputted by the Digital Computer Unit (DCU)/Pulse-Code Modulation Telemetry System, a part of the Centaur Integrated Support System (CISS), is described in this report. The telemetry data stream developed by the DCU is applied to the Space Shuttle Orbiter avionics via either a hardware or an RF link during the initial phases of the Centaur vehicle launch. During subsequent phases of the launch when the Centaur vehicle is outside the 10-nm radio communication range to the Orbiter, the telemetry stream outputted by the DCU is transmitted via an S-band link to the Tracking and Data-Relay Satellite System (TDRSS).

Because the Orbiter avionics interfaces of the DCU are not specified in terms of bit jitter, the primary driver for testing DCU bit-jitter characteristics is compliance with the TDRSS specifications. Bit-jitter specifications for the TDRSS link are quite comprehensive in terms of the parameters to be measured. Consequently, this report describes the techniques and test setup configurations which are specifically designed to test compliance with the TDRSS bit-jitter specifications.

Section 2 of this report contains the specifications, as defined for bit-jitter compliance of the TDRSS users. Section 3 defines the test setup that provides for the bit-jitter measurements which are compatible with the specifications listed in Section 2. Section 4 describes interfaces of the DCU to which the bit-jitter test setup can be connected. Section 5 describes the software which may be required to analyze the measured bit-jitter spectrum in terms of TDRSS requirements. Appendices A and B contain the support data and specifications pertaining to the commercial test equipment recommended for the test setup.

## 2.0 BIT-JITTER SPECIFICATIONS

Salient characteristics of the TDRSS bit-jitter constraint includes subdividing the latter into two categories: (1) bit-jitter specification for bit-slip rate (BSR) and, (2) bit-jitter specification for bit-error rate (BER). Bit-jitter measurement for compliance within these two categories is defined analytically in terms of pertinent equations and corresponding weighting functions. Furthermore, of particular importance is a specification, applicable to both of the above categories, which describes discrete-frequency-type bit jitter. The latter requirement dictates that compliance with the bit-jitter specification be performed in terms of spectral analysis of the bit-jitter component of the DCU output signal.

Defined below are the bit-jitter specifications for BSR and BER in terms of the discrete components (i.e.; the line spectrum) as well as the random jitter components.

### 2.1 Bit-Jitter Specification for BSR Control

The allowable BSR-defined bit jitter, expressed in radians, is specified according to the formula:

$$\sigma_B = \underbrace{\sum_1^{\text{Summed to } R_s/2} \beta_1 \sqrt{W_s(f_1)}}_{\text{Discrete frequency bit-jitter term}} + \underbrace{\sqrt{\int_0^{R_s/2} S_j(f) W_n(f) df}}_{\text{Random bit-jitter term}} \leq A \quad (2-1)$$

where.

$\sigma_B$  = data bit jitter in radians

$\beta_1$  = amplitude, in radians, of the  $i$ th spurious term at frequency  $f_1$   
(summation from zero frequency to  $R_s/2$ )

$R_s$  = telemetry symbol rate

$W_s(f_1)$  = weighting function as given in Figure 2.1

$S_j(f)$  = random bit-jitter spectrum

$W_n(f)$  = weighting function as given in Figure 2.1.

The maximum permitted value of A is a function of the type of service provided by the TDRSS. The values are given below:

Specification Values of A versus Type of Service

All uncoded services	A = 1.5	} Radians
Single-access (SA), rate 1/2 coded	A = 0.9	
S-band single-access (SSA), rate 1/3	A = 0.6	
Multiple-access (MA)	A = 0.6	

Equation (2-1) states that the total allowable data-bit jitter for BSR control consists of two components, as follows: (1) one consisting of discrete lines and (2) a continuous-spectrum random component defined by the phase spectrum  $S_J(f)$ . This implies that, for any given telemetry system such as the DCU, a detailed spectrum characteristic of the data bit jitter must be obtained, and the weighting functions  $W_S(f_i)$  and  $W_n(f)$  must be applied to determine compliance with the total allowable data-bit jitter A. Figure 2.1 defines  $W_S(f_i)$  and  $W_n(f)$  as well as the appropriate constants in terms of the service provided by the TDRSS system.

2.2 Bit-Jitter Specification for BER Control

Similar to the previously defined BSR specification, the TDRSS user must meet a bit-jitter specification that is driven by the requirement to keep the jitter-induced BER at a level which is acceptable to the TDRSS link. This BER-related bit jitter is specified in terms of percentage of the bit time. The specification is as follows.

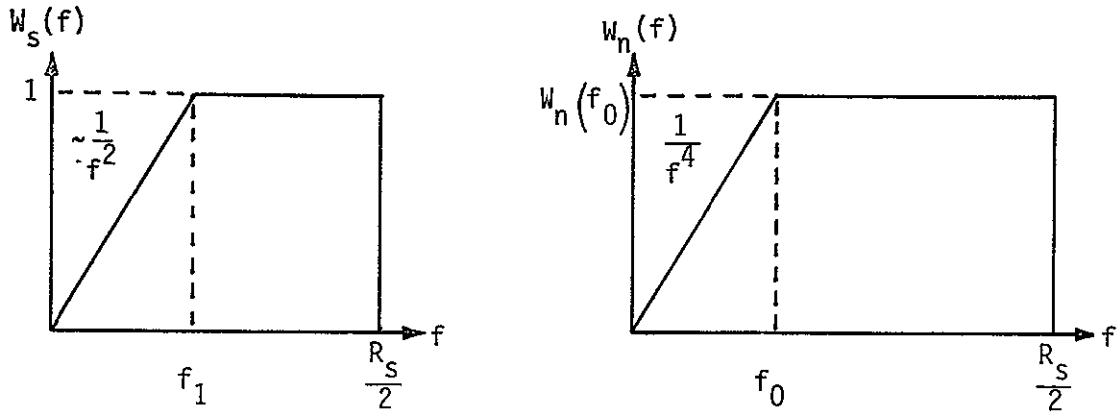
$$A \geq \sigma_B = \sqrt{\int_{0.01 \text{ Hz}}^{R_S/2} S_J(f) W_\Delta(f) df} + \sqrt{C_2 \left[ \sum_i \beta_1 \sqrt{W_L(f_i)} \right]^2 + C_1 \int_{0.01 \text{ Hz}}^{R_S/2} S_J(f) W_L(f) df} \quad (2-2)$$

where:

$\sigma_B$  = bit jitter expressed in percent of bit time

$S_J(f)$  = bit-jitter spectrum determined by random-bit-duration jitter

Weighting Functions



Pertinent Constants

Services	$W_s(f)$	$W_n(f)$	
	$f_1$	$f_0$	$W_n(f_0)$
All uncoded	$1.3 \times 10^{-3} \times R_s$	$2.2 \times 10^{-3} \times R_s$	15.0
SA, $R = 1/2$ , Coded	$3.0 \times 10^{-4} \times R_s$	$5.2 \times 10^{-4} \times R_s$	7.7
SSA, $R = 1/3$ , Coded	$2.7 \times 10^{-4} \times R_s$	$4.7 \times 10^{-4} \times R_s$	5.0
Multiple Access	$2.7 \times 10^{-4} \times R_s$	$4.7 \times 10^{-4} \times R_s$	5.0

Figure 2.1 BSR Specification Data-Bit Jitter Weighting Functions and Pertinent Constants as Function of Service



$W_{\Delta}(f)$  = weighting function shown in Figure 2.2

$\beta_i$  = amplitude, in radians, of the  $i$ th frequency spurious term

$W_L(f_i)$  = weighting function shown in Figure 2.2

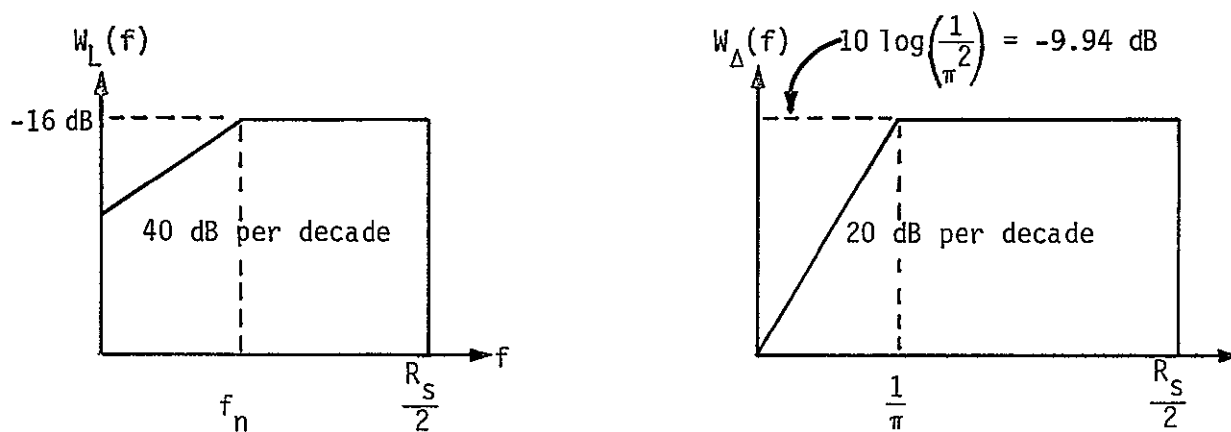
$C_1$  and  $C_2$  = constants defined in Table 2.1.

Figure 2.2 shows the weighting functions included in (2-2). The appropriate numerical values are also given in Figure 2.2.

Table 2.1. Specifications and Constants for BER Jitter Specification as a Function of Service

Service	A(% of Bit Time)	$C_1$	$C_2(\text{rad}^{-2})$
All uncoded, NRZ	7.0	11.5	0.30
All uncoded, biphase	3.5	11.5	0.30
All coded, NRZ	8.5	16.23	0.37
All coded, biphase	4.2	16.23	0.37

ORIGINAL PAGE IS  
OF POOR QUALITY



Services	$f_n/R_s$
All uncoded, NRZ	$2 \times 10^{-3}$
All uncoded, biphase	$2 \times 10^{-3}$
All coded, NRZ	$4.2 \times 10^{-4}$
All coded, biphase	$4.2 \times 10^{-4}$

Figure 2.2 BER Specification Data-Bit Jitter Weighting Function and Pertinent Constants as Function of Service

### 3.0 BIT-JITTER MEASUREMENT TEST-CONFIGURATION DESCRIPTION

#### 3.1 Test Configuration Description

The proposed test configuration specifically addresses the task of determining the data-bit jitter from the spectral characteristics of the jitter. It accomplishes this task in the following two-step procedure:

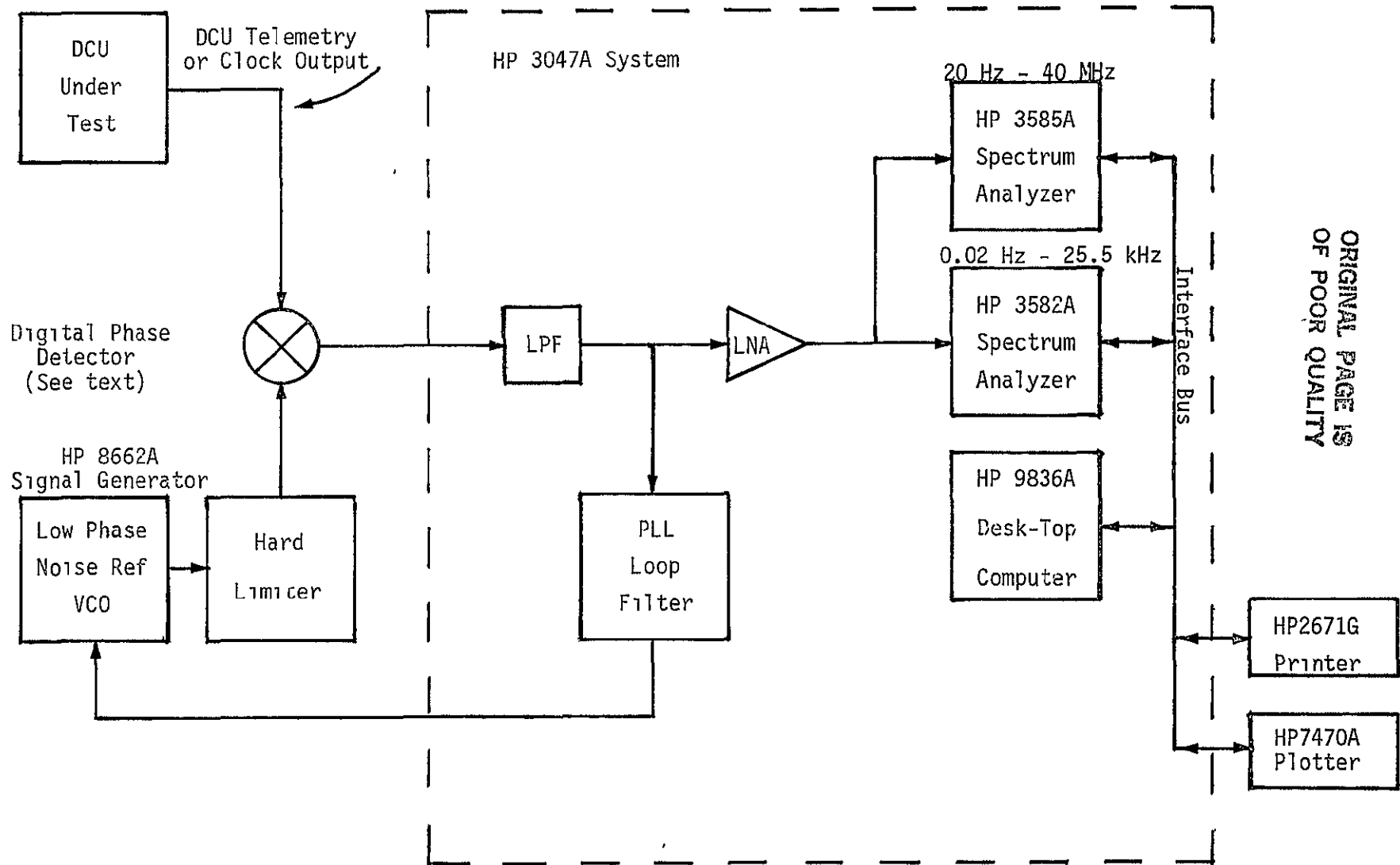
(1) Measure phase noise and spurious phase modulation components of the DCU data or clock output

(2) Obtain data-bit jitter by computing weighted sums on discrete spurs and weighted/integrated phase noise for BSR and BER considerations.

Figure 3.1 show the block diagram for the proposed test configuration. As can be seen from it, the key element of the test setup is the HP3047A spectrum analyzer system. As illustrated in this figure, the bit-jitter information is generated by comparing an output signal of the DCU with a reference signal of the same frequency. The output signal of the DCU may be either the telemetry data stream or a clock signal associated with the telemetry stream. In the data case, the DCU must be programmed such that a continuous string of alternating "ones" and "zeroes" is developed. If the clock signal is used instead of actual telemetry data bits, one must be reasonably certain that the clock signal jitter is representative of the data stream jitter.

The output of the phase detector is applied via a phase-lock-loop (PLL) filter to a low-phase-noise reference VCO. The PLL is then completed by hard-limiting the VCO output signal, then applying this signal to the second input terminal of the phase detector. The phase error appearing at the output of the phase detector thus consists of two components: (1) the component which is due to misalignment of the DCU and the reference signal and, (2) that which is due solely to bit jitter (or clock jitter) of the signal emerging from the DCU.

The first component is utilized by the PLL to lock the VCO to the exact frequency and the average phase of the signal outputted by the DCU. The second component (i.e., that due to jitter, both discrete-line-type (spurs) and continuous-spectrum type, is subjected to spectrum analysis by the HP3582A and HP3585A spectrum analyzers. The output of these two spectrum analyzers is applied to the HP9836A desk-top computer which performs the necessary system calibration corrections to yield an accurate readout of the phase-noise spectrum. Table 3.1 summarizes the salient features of the HP3047A spectrum-analyzer system.



ORIGINAL PAGE IS  
OF POOR QUALITY

Figure 3 1. Phase-Noise Measurement Test Configuration

Table 3.1. HP3047A Phase-Noise-Measurement Capabilities

1. Measures phase-noise from 0.01 Hz to 40 MHz
  - a.  $\pm 2$ -dB accuracy (from 0.02 Hz to 40 MHz)
  - b. Spurious measured to  $\pm 2$  dB
  - c.  $\mathcal{L}(f)$  measurement normalized to 1 Hz bandwidth
  
2. Automated-calibration procedure with the HP9836A desk-top computer software
  - a. Automatically establish the PLL
  - b. Characterize the PLL
  - c. Performs calculations for calibrated phase-noise measurement.

Of particular importance to bit-jitter testing is the automated calibration software included in the 3047A spectrum-analyzer system. Specifically, this software will operate as follows:

- (1) Establish input-carrier level (in dB) relative to spectrum analyzer readings over the frequency range of interest
- (2) Calibrate external phase detector (or a mixer) gain slope
- (3) Characterize VCO (in HP8662A signal generator) gain curve
- (4) Measure PLL closed-loop transfer function
- (5) Calibrate spectrum analyzer noise bandwidth at each IF frequency setting
- (6) Measure  $\mathcal{L}(f)$  by averaging multiple RMS voltage readings normalized by spectrum-analyzer noise bandwidth
- (7) Normalize  $\mathcal{L}(f)$  measurements by PLL transfer function measured
- (8) Plot or print output.

Utilization of the automatic-calibration feature is a great advantage for "taking out" the PLL frequency-response effect (i.e., loop bandwidth characteristics) from the measured jitter spectrum. With a conventional bit-jitter analyzer which typically examines the jitter noise outside the bit-synchronizer data-transition tracking loop, the frequency response of the latter usually distorts the observed jitter noise. The loop-response compensation provided by the automatic-calibration procedure of the HP3047A system results in a bit-jitter noise spectrum measurement which is a true representation of the spectrum characteristics of the jitter.

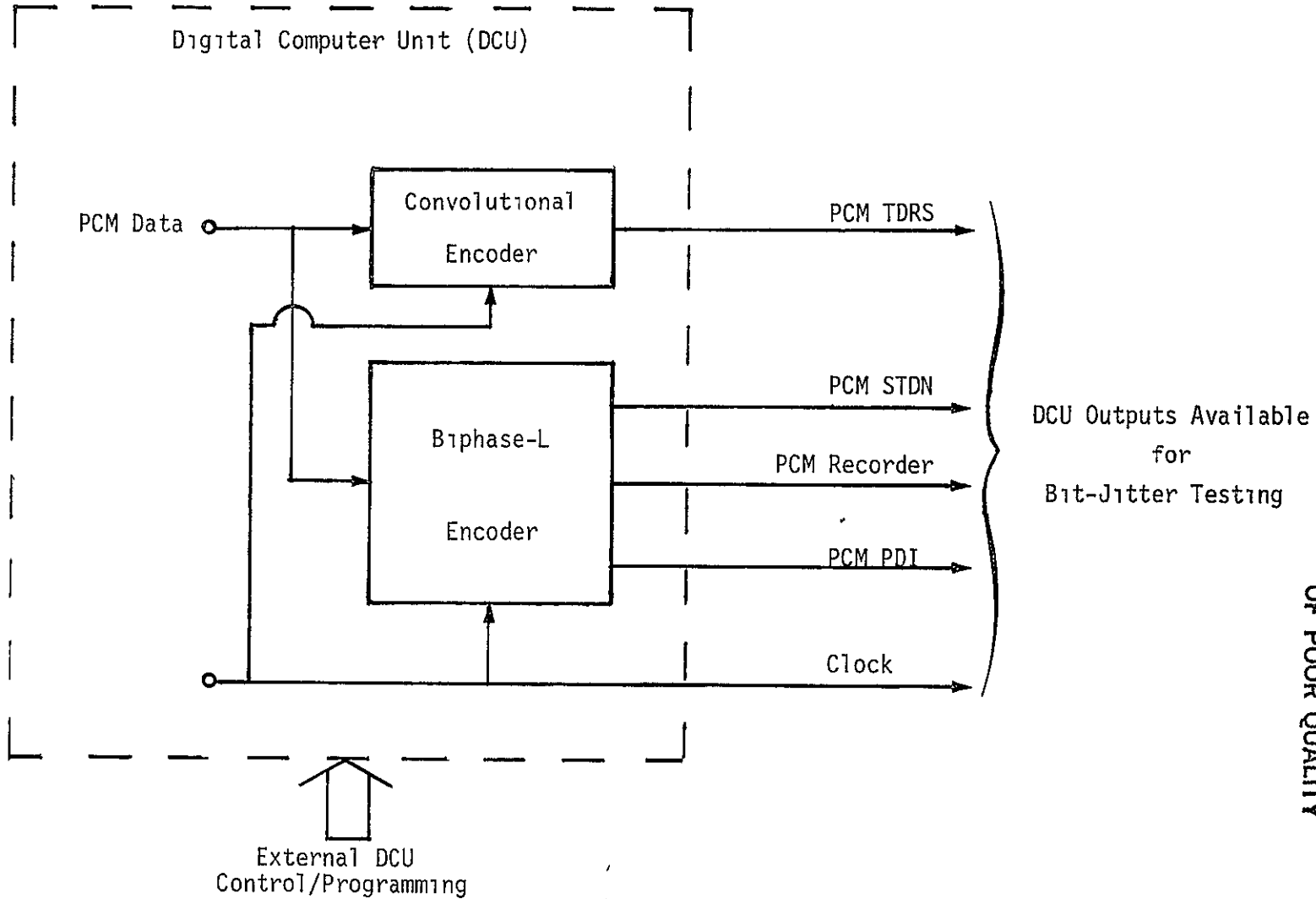
#### 4.0 DIGITAL COMPUTER UNIT INTERFACES

Figure 4.1 shows the digital computer unit (DCU) output interface lines which are available for bit-jitter testing. The line for which the bit-jitter specification applies is the PCM TDRS line. Other lines, such as PCM STDN, PCM recorder and PCM PDI, can also be used provided that the DCU design is such that the bit jitter on these lines is identical to that on the PCM TDRS line. Furthermore, the clock signal can also be used with the same restriction, namely, that the jitter on the clock is identical to that on the TDRS line.

Usually, the digital equipment design is such that all output lines are clocked with the same signal; consequently, it is a reasonably sure assumption that all of the PCM telemetry output lines of the DCU will have identical bit-jitter characteristics. Thus, although the TDRS line has to be measured for specified bit jitter, a good possibility exists that other output lines can be used for this measurement if, for some reason, it is not feasible to use the TDRS line for the tests. The most important constraint on the output signal format tested for bit jitter is that it is a square wave to which the reference signal can be locked, as shown in Figure 3.1. Thus, it is mandatory that the DCU be commanded to generate this type of output data. Specifically, such a capability is required of the TDRS line emerging from the convolutional encoder.

Fortunately, the specification [1] for the convolutional encoder is such that either an all-ONES or all-ZEROS data input to the encoder will produce an alternating symbol sequence of high/low states, i.e., a square wave with period equal to the data-bit period. Thus, the DCU must be commanded to produce such a condition. Furthermore, the biphase-L encoding of the PCM STDN, PCM recorder and PCM PDI data streams also facilitates outputting the square-wave signal at these output lines. Again, all that is required is to command the DCU externally for an input of either an all-ONES or all-ZEROS input to the biphase-L encoder.

The remaining question concerns the effect of the frame synchronization word on the spectral characteristics of the DCU output data streams programmed for the square-wave output. The best way to eliminate the synchronization pattern effect is to command the DCU to "wipe out" this pattern. If this is impossible, one must analyze the effect of the synchronization pattern on the phase-spectral characteristics of the measured output signal. Ideally, the synchronization pattern periodically included in the square-wave pattern should not produce any responses which may be interpreted as bit-jitter spurs. If this is



ORIGINAL PAGE IS  
OF POOR QUALITY

\*Note External controls should be set to provide a pattern of alternating ones and zeros (i.e., a square wave) at DCU outputs tested for bit jitter.

Figure 4.1. DCU Outputs for Bit-Jitter Testing



not the case, then the test setup for bit-jitter spectral analysis, such as that shown in Figure 3.1, should be carefully calibrated to "notch out" these responses. Use of the programmable desk-top computer in conjunction with spectral analysis should facilitate such "notching out" performed in software.

## 5.0 ADDITIONAL SOFTWARE REQUIREMENTS

The 3047A spectrum analyzer system has software available to calibrate the system and to perform the required spectral analysis. However, showing that the DCU bit jitter meets the specifications requires additional processing of the measured spectrum. This processing, which can be done with the desk-top computer, will require the following additional software:

- (1) Software to collect spurious levels and respective frequencies
- (2) Software to obtain continuous phase noise spectrum from subtracting discrete spurs from total  $\mathcal{L}(f)$  measurements.

Furthermore, additional software is required to:

- (3) Perform weighted sum on spurs for BSR and BER data bit-jitter calculations
- (4) Perform weighted phase-noise integration for BSR and BER data bit-jitter calculations.

All this additional software should be developed as part of the DCU bit-jitter testing procedure.

## REFERENCES

1. - Shuttle/Centaur Functional Requirements Document (Preliminary), Document No. SC113-1, Revision--Basic, General Dynamics/Convair Division, San Diego, California, 5 March 1963.

APPENDIX A

PHASE ERROR DETECTOR IMPLEMENTATION TECHNIQUES

This appendix describes various techniques which can be used to implement a phase detector. Such a phase detector is required for a phase-locked loop (PLL) used for detecting the phase noise of the tested signal. Figure A.1 shows a PLL setup for measuring either the phase noise or jitter, as the case may be. As shown in this figure, the input signal is phase compared with a reference signal (spectrally "clean"). The phase error developed in the phase detector is used to lock the phase and frequency of the reference VCO to the input signal. Once such lock is established and the reference VCO is tracking the input signal perfectly, the output of the phase detector contains only the random phase (or jitter components) component of the input signal.

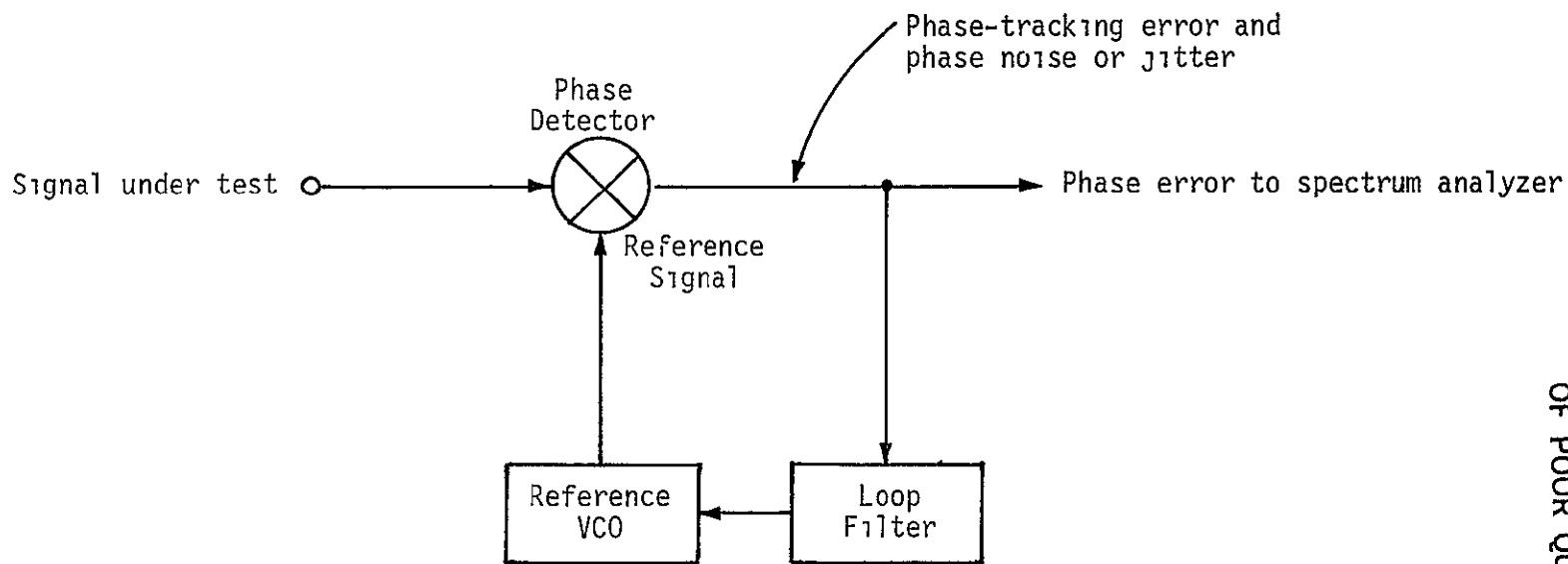
Depending on the type of signal used, the phase detector may be either digital or analog. Implementations of these detectors are described below.

A.1 DIGITAL PHASE DETECTORS

(1) Exclusive-OR Logic Gate Phase Detector

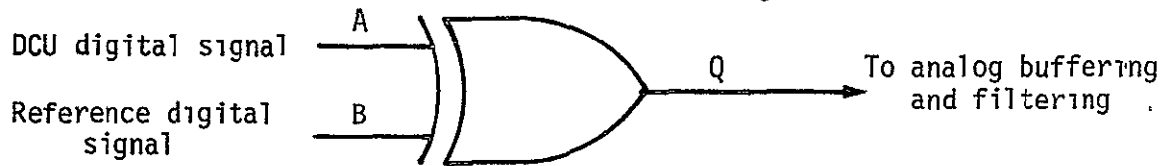
One of the simplest devices for implementing a digital phase detector is via an exclusive-OR logic gate. The operation of such a detector is explained in Figure A.2(a) of the exclusive-OR (EXOR) gate connection. Inputs A and B are  $T^2L$  (or other logic level) digital signals. Digital output Q is also of the same logic level. It is applied, via analog buffering and lowpass (LP) filtering to the loop filter of the PLL. Part (b) of Figure A.2 shows the output signal for a  $45^\circ$  shift between inputs A and B. In turn, part (c) shows the output signal for the  $90^\circ$  relative phase shift between A and B. This is typically the desired condition for tracking. At this condition, one of the tracking points, such as that shown in part (d) is established by the PLL implementation. Any shift from this "zero-error" reference condition, such as in part (b), changes the error voltage, thus resulting in a correction from the VCO.

It must be noted that the waveforms shown in Figure A.2 are based on perfectly symmetrical square waves at inputs A and B to the EXOR gate. If the duty cycle of one of these waveforms is not 50%, such as may be the case when the clock output of the DCU is used as one of the signals, the phase detector characteristic will not be symmetrical, as shown in part (d). Instead, one of the slopes of the up/down ramp shown in (d) will be steeper than the other.

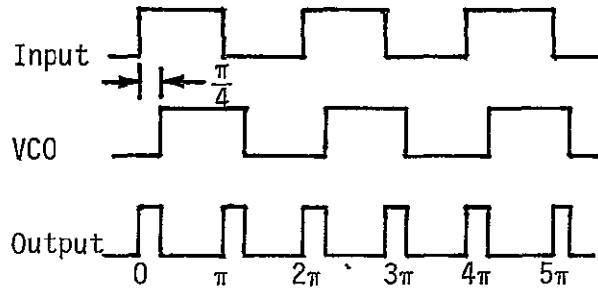


ORIGINAL PAGE IS  
OF POOR QUALITY

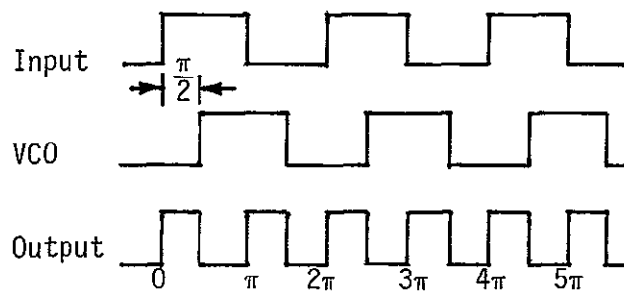
Figure A.1. Phase-Locked-Loop (PLL) used for Detecting Phase Noise (or Jitter) of Test Signal



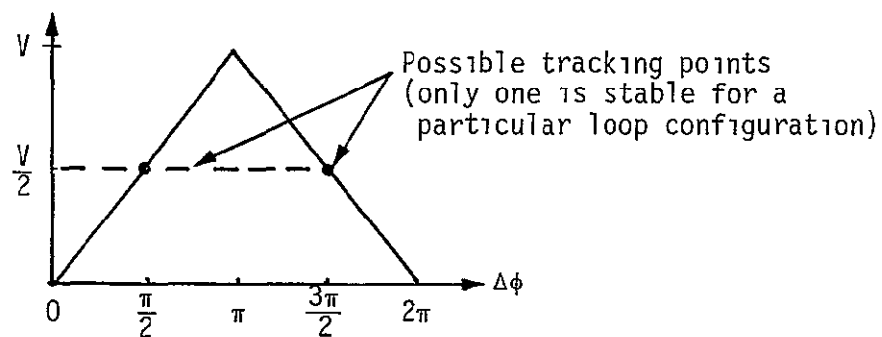
(a) Exclusive-OR Logic Gate



(b) Input signal leads VCO signal by  $\pi/4$ , or  $45^\circ$



(c) Input signal leads VCO signal by  $\pi/2$ , or  $90^\circ$



(d) Exclusive-OR Phase-Detector Input/Output Characteristic

Figure A.2. Exclusive-OR Logic Gate as a Digital Phase Detector

This in turn will change the gain of the PLL used to track the input signal. With the HP 3047A system\*, however, this is not a problem because the automatic calibration should take care of this. Except for the jitter per se, the only important requirement is that the duty cycle does not change during the spectral measurement.

### (2) Edge-Triggered Phase Detector

Another type of digital phase detector is the edge-triggered one. Figure A.3 shows how a simple R-S flip-flop can be used as a phase detector. The input/output waveforms, as well as the phase-detector characteristic of such a detector, are also shown. As can be seen in part (b) of this figure, the edge-triggered detector is particularly useful for short-duration signals, i.e., those having a low duty cycle. Also, from Figure A.3(c), it is evident that the tracking range of an edge-triggered phase detector is twice the range of the EXOR gate detector. Thus, the edge-triggered detector has better capture, tracking and locking characteristics as compared to the EXOR detector.

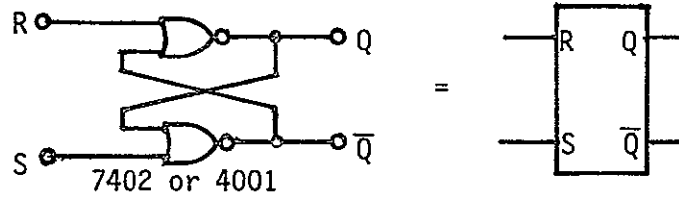
### (3) Motorola MC4044 Phase Detector

A digital-phase detector which is superior to both EXOR and the edge-triggered detector is the Motorola MC4044 integrated circuit. Figure A.4 shows the various details pertaining to the operation of this circuit. As can be seen from this figure, the MC4044 consists of two phase detectors. Phase detector 1 is used for developing the phase error, while phase detector 2 can be used to indicate the condition when the two signals are in lock.

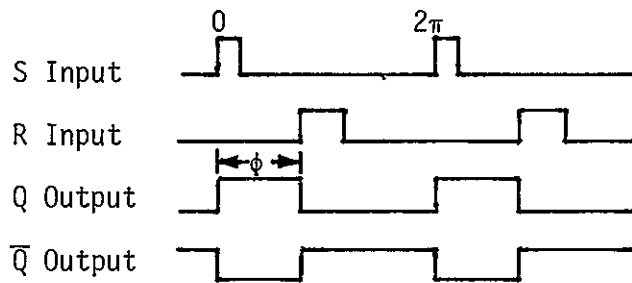
The important feature of MC4044 is that it has a phase characteristic that extends over  $4\pi$  radians, i.e., twice the range of the edge-triggered detector. Furthermore, the advantage of MC4044 as compared to other detectors is its insensitivity to harmonics of the input signal. Also, MC4044 does not have the duty-cycle problems and limitations of the aforementioned digital detectors. Because of these advantages, MC4044 is a good digital phase detector to use for PLL implementations.

---

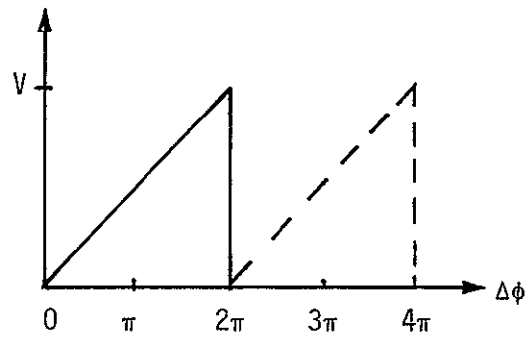
\* Such as that proposed by AXIOMATIX for bit-jitter measurement.



(a) R-S Flip-Flop as an Edge-Triggered Phase Detector



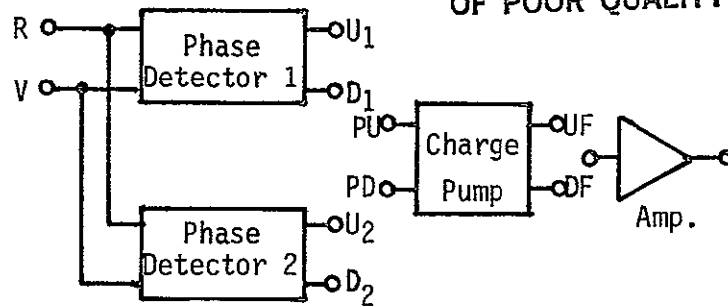
(b) Input/Output Waveforms for the R-S Flip-Flop, Edge-Triggered Phase Detector



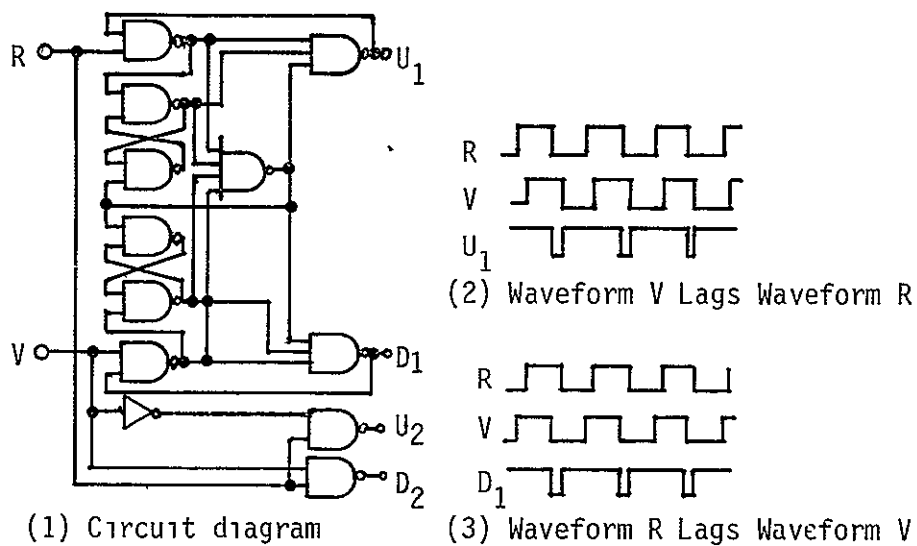
(c) Edge-Triggered Phase-Detector Input/Output Characteristic

Figure A.3. Edge-Triggered Phase Detector Implemented with an R-S Flip-Flop

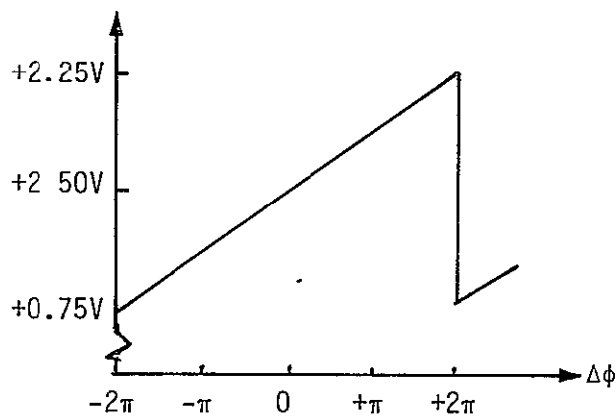
ORIGINAL PAGE IS  
OF POOR QUALITY



(a) Block Diagram of the MC4044 Phase Detector



(b) Circuit Diagram and Input/Output Waveforms for the MC4044 Phase Detector



(c) MC4044 Input/Output Characteristic for Phase Detector No. 1

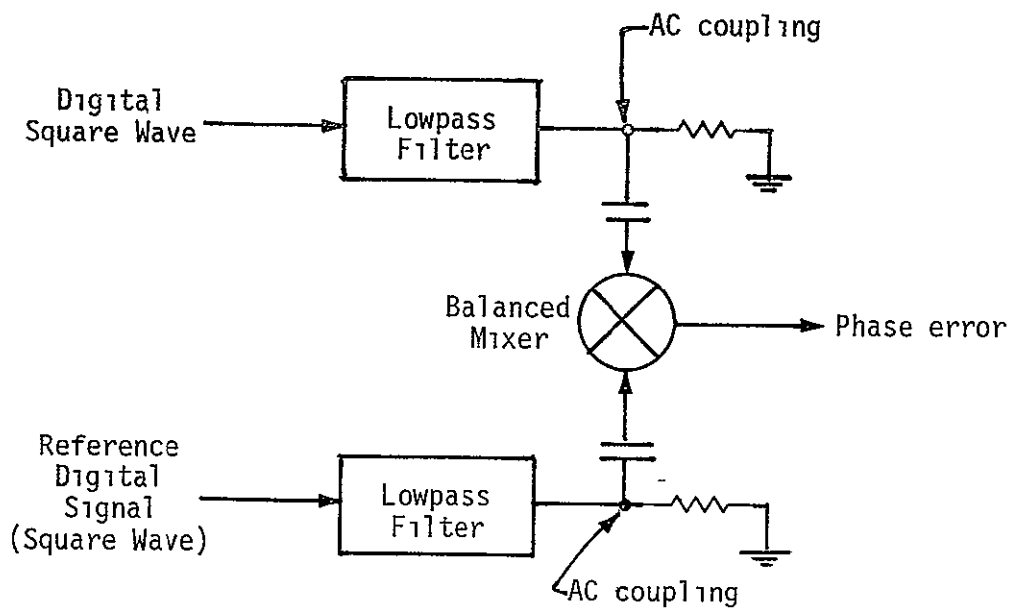
Figure A.4. Motorola MC4044 Digital Phase Detector

## A.2 ANALOG PHASE DETECTORS

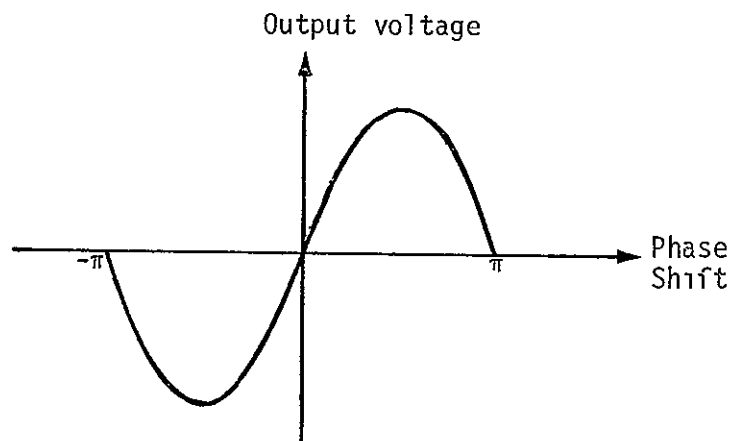
It is important to note that the digital phase detectors described in the preceding paragraphs provide input/output characteristics that are not bipolar, i.e., they have some DC level which is used as a tracking-reference point. For the case where digital signals are used, yet it is desirable to have a zero voltage as a reference-tracking point, a balanced mixer can be used, as shown in Figure A.5. Here the lowpass filters remove the higher harmonics of the square waves (both reference and tracked inputs) and the resulting sinusoidal signal (fundamentals) are AC coupled to the mixer points. The resulting phase-error characteristic is sinusoidal in shape and provides a zero-voltage reference point for phase tracking. The advantage of such a phase-error characteristic is that no DC offset is required to compensate for the non-zero DC-error response of a digital phase detector.



ORIGINAL PAGE IS  
OF POOR QUALITY



(a) Balanced Mixer as a Phase Detector



(b) Phase-Error Characteristics

Figure A.5. Analog Mixer Phase-Detector Configuration and Phase-Error Characteristic

APPENDIX B

HEWLETT PACKARD SPECTRUM ANALYSIS SYSTEM 3047A

# Provides Three Measurement Modes for Complete Answers to Your Frequency

ORIGINAL PAGE IS OF POOR QUALITY

## Direct Spectrum Mode

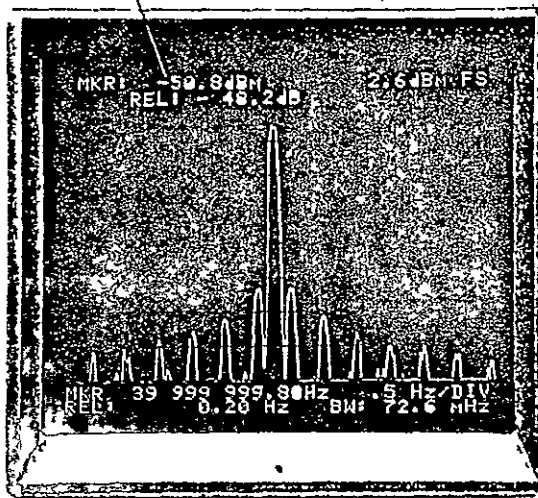
0.02 Hz Resolution to 40 MHz with FFT Analysis Speed

In the Direct Spectrum Mode the system hardware is used as a down converter to bring 19 kHz to 40 MHz signals into the frequency range of the 3582A Real Time Spectrum Analyzer. This allows the very high resolution and measurement speed of the Real Time Spectrum Analyzer to be used up to 40 MHz. In this mode the system is capable of resolution bandwidths as narrow as 0.02 Hz and is one to two orders of magnitude faster than a swept spectrum analyzer. The system provides these measurements over the wide dynamic range of 70 dB, calibrated in both frequency and amplitude.

Calibrated Results, Accurate to  $\pm 0.9$  dB

Make Measurements With the Analyzer Display or Save as Printed or Plotted Copy

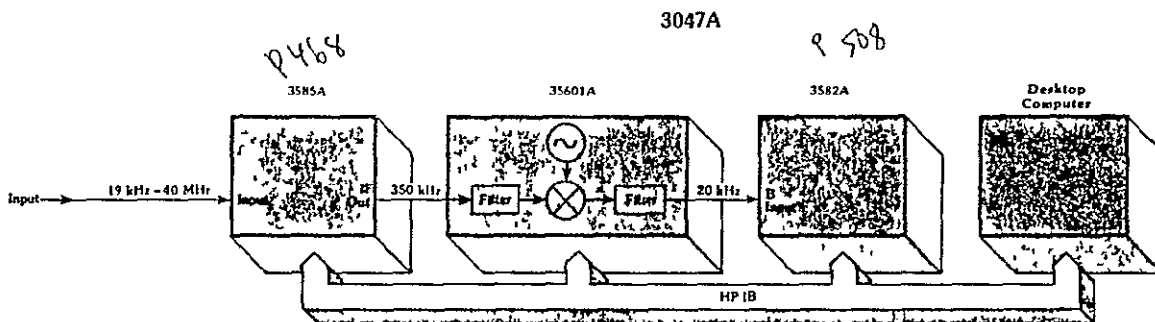
70 dB Dynamic Range



\*MKR -48.8 dBm  
 \*REL -45.9 dBm

2.2 dBm FS

MKR 40.00000058 Hz  
 REL 0.20 Hz  
 BW 72.6 MHz  
 5 Hz/DIV



# Frequency Stability Analysis Problems.

## Noise Sideband Mode

Amplitude and Phase Noise Measurements  
from 0.02 Hz to 25 kHz away from  
Carriers 20 Hz to 40 MHz

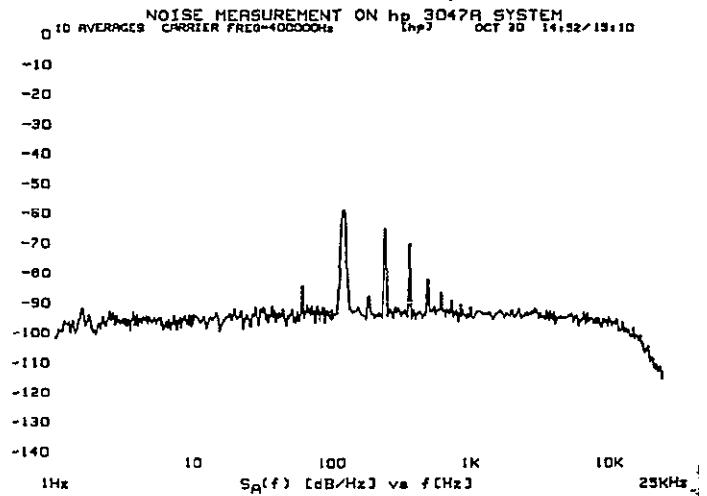
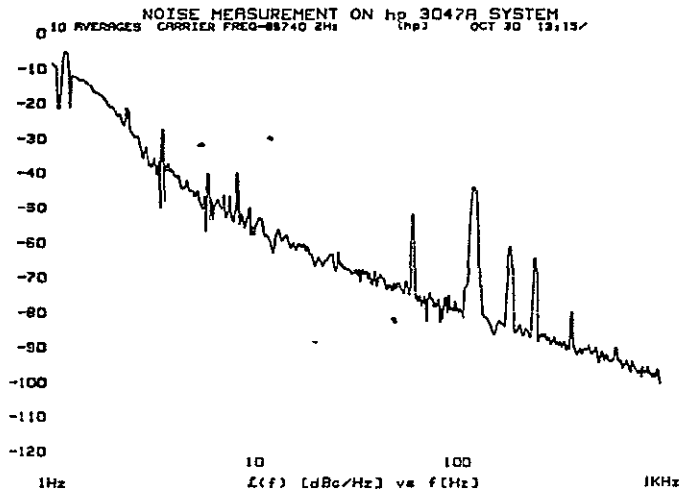
ORIGINAL PAGE IS  
OF POOR QUALITY

While the 3047A can measure very high quality sources in the Phase Noise Mode, moderate performance sources can be measured more easily in the Noise Sideband Mode. In this mode the system measures both AM and PM noise without additional hardware. The system software connects the 3047A input to the 3585A and the output of the analyzer is fed into an internal phase detector. The output of the detector is connected to the 3582A Analyzer and the phase noise measured over the 0.02 Hz to 25 kHz range. In addition, a second detector is provided which outputs the AM noise of the signal to the second channel of the 3582A Analyzer.

Sources with noise greater than the 3585A Spectrum Analyzer's local oscillators are very easy to measure with the 3047A in this mode. The source under test is just connected to the 3047A and the measurement is run. There is no need for a high quality reference or for a frequency discriminator.

Phase Noise

Amplitude Noise



# The 3047A Spectrum Analyzer System

ORIGINAL PAGE IS  
OF POOR QUALITY

## Phase Noise Mode

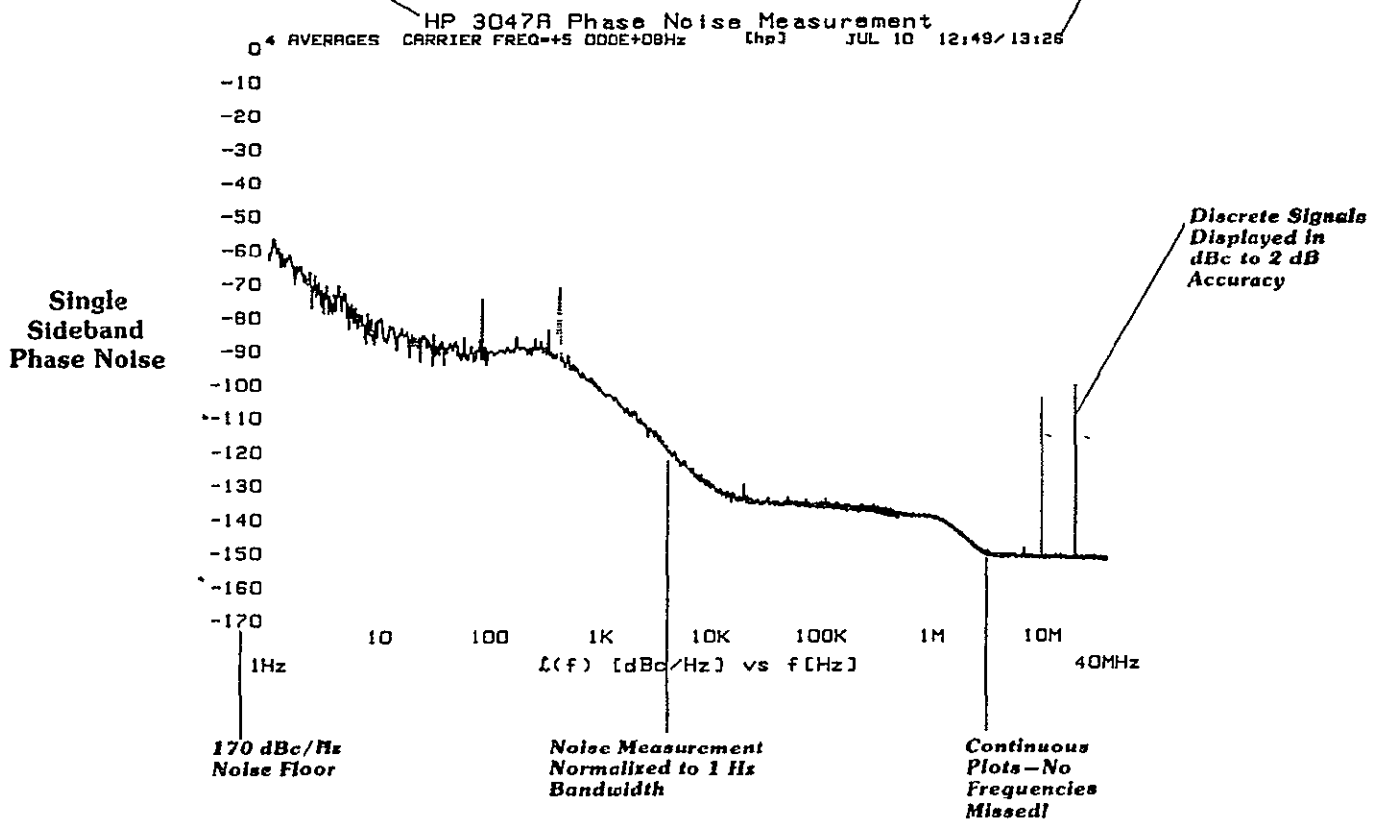
The Ultimate Performance in Phase Noise Measurements

Measure 0.02 Hz to 40 MHz away from  
5 MHz to 18 GHz Carriers  
including measurements on.

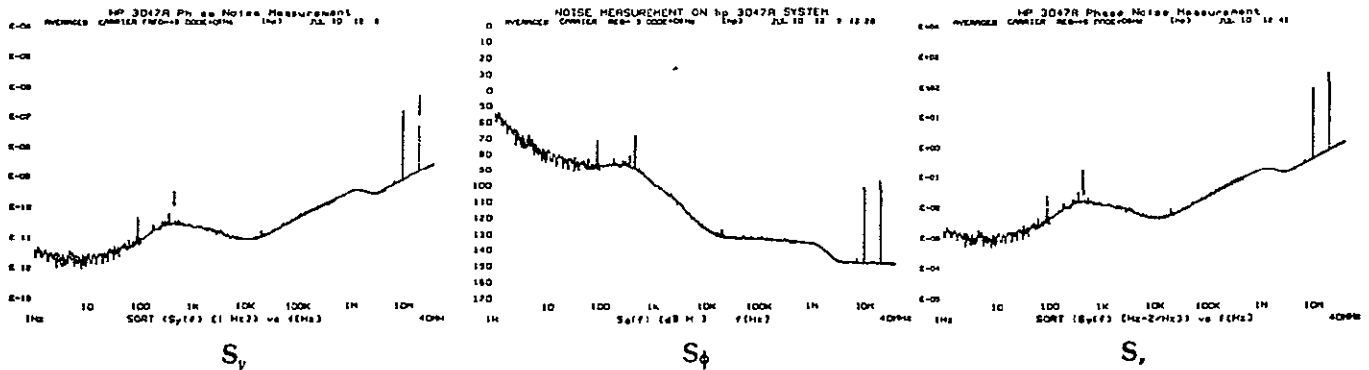
- Oscillators
- Frequency Standards
- Amplifiers
- Frequency Multipliers & Dividers

User Annotation of  
Up to 58 Characters

Dated Plots  
With Measurement  
Start/Stop Time



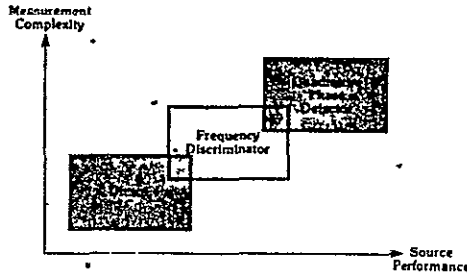
Or, if you prefer, measurements can be presented as  $S_v$ ,  $S_\phi$  or  $S_f$ .



# Phase Noise Operating Mode

## Phase Noise Measurements

When used with the 3047A, the term phase noise includes all forms of frequency and phase instabilities. Frequency and phase noise as well as undesired modulation like power-line phase modulation and phase jitter are included in the term and can be measured by the 3047A Spectrum Analyzer System.



The complexity of phase noise measurements increases with increasing source performance. For relatively noisy sources, the noise can be measured directly on an existing spectrum analyzer. However, for many sources this measurement is not sensitive enough. If the spectrum analyzer is preceded by a frequency discriminator or phase detector, the system sensitivity can be increased at the cost of additional measurement hardware. The Phase Noise Measurement Mode of the 3047A is designed to reduce the difficulty of making accurate phase noise measurements with either the frequency discriminator or quadrature phase detector techniques.

Discrete Signals  
Displayed in dBc



Noise Measurement  
Normalized to 1 Hz  
Bandwidth

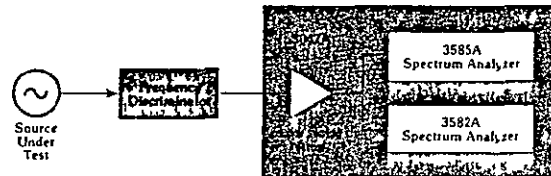


No matter which of the above techniques are used, phase noise measurements are always made with respect to a 1 Hertz bandwidth. To measure the entire spectrum in a 1 Hertz bandwidth would take an excessive amount of time so, as is common practice, the 3047A measures the phase noise in wider bandwidths as the frequencies are further removed from the carrier (Close to the carrier, bandwidths much less than 1 Hertz must be used.) From these measurements, the system normalizes the noise to a 1 Hertz bandwidth and plots this result. However, if a discrete tone is measured (coherent phase modulation or a "bright line"), then the measurement should not be corrected for the measurement bandwidth as the level of the tone is independent of the measurement bandwidth. The 3047A detects the presence of discrete signals in the spectrum and does not normalize their amplitude, plotting these signals with a dotted line to show this fact.

This is just one example of the system software detecting and correcting possible measurement errors. The desktop computer monitors all measurements to detect conditions that would effect the accuracy of the results. For instance, in the phase quadrature measurement mode the software can detect if the two sources have injection locked or if the phase lock loop comes out of lock. Either of these conditions invalidates any measurement so the measurement is stopped and the software gives an error message to the operator. Under other possible error conditions the measurement may be valid, but with reduced accuracy. In these cases the software stops the program, warning the operator about the reduced accuracy but allows him to continue the test if desired.

## Frequency Discriminator Method

Phase noise measurements with a frequency discriminator are the easiest to understand. Any variations in the carrier frequency or phase are changed into voltage variations by the discriminator. These voltage variations are then analyzed by the 3047A System. The system software can present the measurement as frequency ( $S_v(f)$  or  $S_y(f)$ ) or phase noise ( $S_\phi(f)$  or  $L(f)$ ). However, frequency discriminators with adequate sensitivity to measure state-of-the-art sources are inherently narrow band devices. Since the system covers the extremely wide frequency range of 5 MHz to 18 GHz, it is not feasible to include a frequency discriminator or even a set of discriminators in the system to measure sources over this entire range. Instead, the capability of making calibrated measurements with a customer supplied frequency discriminator is included in the 3047A System. To calibrate the system, the user can provide a known level of phase modulation or add in a signal of known level and the 3047A software will properly calibrate the system to give results accurate to  $\pm 2$  dB.

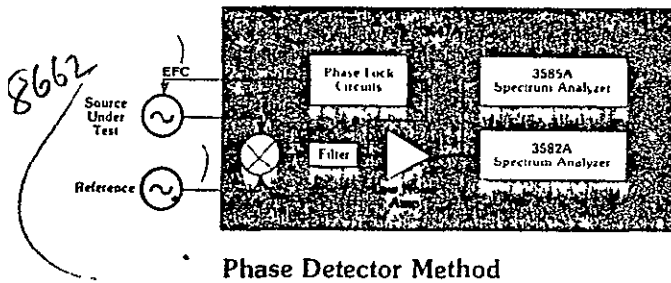


### Phase Detector Method

As mentioned above, phase noise can also be measured with a phase detector. A common way to make a low noise phase detector is to use a double balanced mixer. If two signals of the same frequency and 90° out of phase are applied to the mixer, the output will contain a low frequency signal whose amplitude represents the phase noise of the sources. This signal can be amplified and analyzed by a low frequency spectrum analyzer to give the noise as a function of frequency away from the carrier frequency. As in the frequency discriminator measurements, the system software can present this phase noise measurement as phase noise  $L(f)$  or  $S_o(f)$  or frequency noise  $(S_s(f))$  or  $S_v(f)$ .

This quadrature phase detector method has the advantage of using an inherently wideband mixer as the phase detector. Therefore, only the two detectors provided are needed to cover the 5MHz to 18 GHz frequency range of the 3047A and this frequency range can be easily extended either higher or lower in frequency by adding appropriate mixers and filters. For instance, millimeter wave sources could be measured using a mixer mounted in a waveguide as the phase detector. Because the system software can measure the sensitivity of this external detector, the measurement results are fully calibrated.

Another advantage of the quadrature phase detector method is that it inherently rejects AM noise whereas most frequency discriminator circuits do not. AM noise is usually less than the phase noise but in cases where this is not true, this is an important advantage.



This phase detector system depends on the 90° phase relation between two sources. Unless the sources are extremely stable, they will not stay 90° out of phase for any length of time. A solution to this problem is to lock one of the sources to the other with a phase-lock loop. The loop provides a tuning voltage to one of the sources to maintain the two sources at the same frequency and, on the average, 90° out of phase. For frequencies relatively far from the carrier, the phase-lock loop does not affect the signal to the analyzer. For lower frequencies, the phase lock loop causes the controlled source to follow the phase variations of the other source. This causes the voltage to the analyzer to represent the frequency noise at low frequencies and phase noise at higher frequencies.

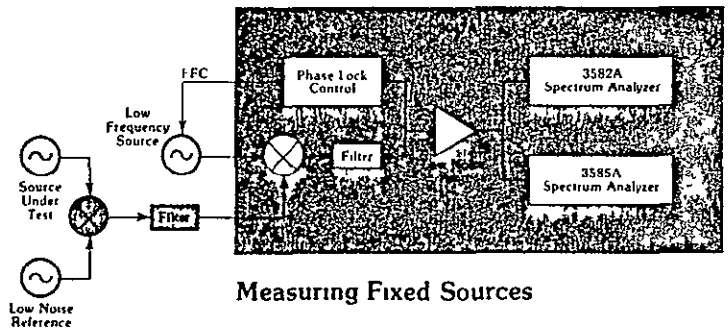
To avoid this difficulty, previous techniques restricted the loop bandwidth to much less than the lowest frequency to be measured. These techniques work well with very quiet sources like crystal oscillators, but a narrow bandwidth loop cannot track the variations in a noisy source. Therefore, these techniques have not previously been used to measure phase noise close to noisy signals.

The 3047A's unique approach solves this tradeoff by adding the computing power of a Desktop Computer. The system software measures the transfer function of the phase lock loop before the phase noise measurement and uses this information to correct for the effects of the phase-lock loop on the voltage to the analyzer. This means that the loop bandwidth can now be chosen to be wide enough to keep a noisy source in lock and yet measurements can still be made as close as 0.2 Hz from the carrier.

Since the phase noise measured by the quadrature phase detector method is the sum of the noise of the reference and the source-under-test, it requires that the reference source be of at least equal phase noise performance to the source-under-test. This can be done when measuring sources with good phase noise performance by adding a high quality frequency synthesizer like the HP 8662A to the system as a reference. Its large frequency range is ideal for testing a wide variety of sources. However, if the test calls for measuring a truly state-of-the-art source, no frequency synthesizer will have sufficient performance. Then the only way to make the measurement is to use a second source, identical to the source-under-test as a reference. Since a frequency discriminator does not have sufficient sensitivity to make this measurement, this is often the only way to measure very low phase noise sources. When attempting to improve low noise source designs, the 3047A offers the three source comparison software (described in the next section) which separates out the noise contribution of each source.

An additional requirement of the quadrature phase detector method is that one of the sources must have electronic frequency control. Many sources are designed with this capability or it can be easily added. In the few cases where this is not practical, a third tunable source can be added to the system to complete the phase-lock loop as shown in the figure below.

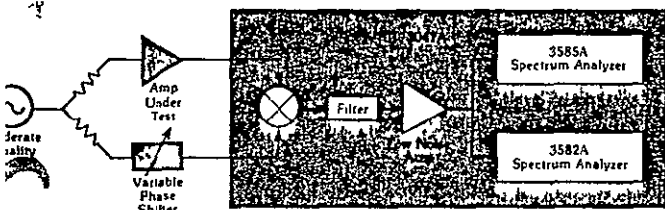
One such case occurs when measuring frequencies in the gigahertz region where low phase noise sources are often only available at fixed frequencies (e.g. a low noise multiplied crystal oscillator). If such a low noise source is mixed with the source-under test, a low frequency signal is generated. This signal can then be measured by the 3047A against a tunable low frequency reference.



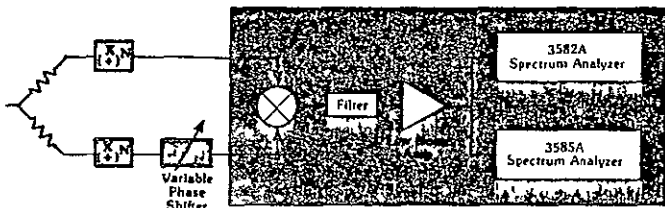
In addition to measuring LC, YIG, Crystal, SAW, and other sources as shown above, the 3047A Spectrum Analyzer System can be used to measure the phase noise of frequency standards, amplifiers, frequency dividers and multipliers

## Measuring Amplifiers, Frequency Dividers and Multipliers

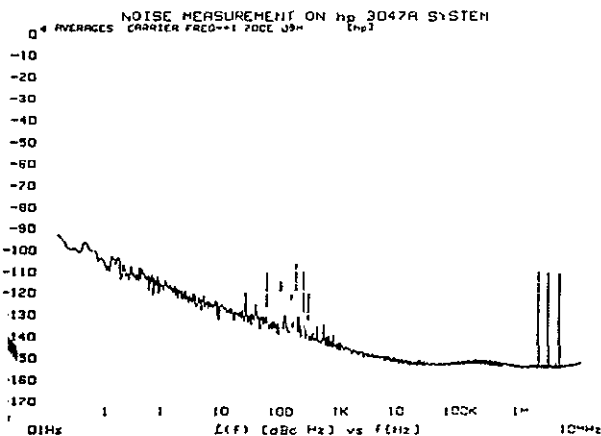
The phase noise performance of amplifiers, frequency multipliers and dividers used can often limit system performance. The 3047A can easily measure these components with the addition of a source at the desired stimulus frequency. Only a moderate quality source is needed since its phase noise is applied to both 3047A inputs and is canceled.



Measuring Amplifier Noise



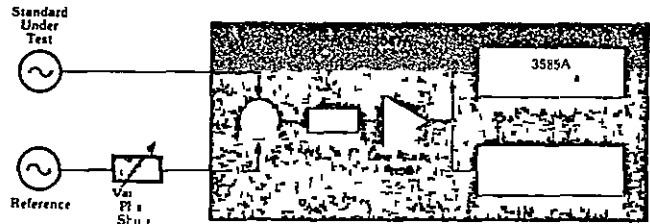
Measuring Multiplier or Divider Noise



Amplifier Phase Noise

## Measuring Frequency Standards

Because two frequency standards will be at the same frequency, there is no need to complete the phase-lock loop used above with other sources. To insure that the two standards are 90° apart, a phase shifter should be added and adjusted until the meter on the 3047A reads zero. Because of the inherent stability of the frequency standards, phase quadrature can be maintained throughout the measurement.



Measuring Frequency Standards

As in measuring oscillators, the phase noise plot will be the sum of the noise of both standards. If the reference frequency standard's phase noise is not known, then its effects cannot be removed in a single measurement. However, if a third frequency standard is available, the phase noise of each standard can be determined using the 3 oscillator comparison software described next.

## Three Source Comparison Measurements

To make phase noise measurements on state-of-the-art sources, you must normally compare two sources in phase quadrature. (Generally, the frequency discriminator method will not yield an adequate noise floor due to the limited sensitivity of the discriminator.) However, when two sources are compared, the resulting noise measurement is the sum of the noise of both sources. Two assumptions have been made in the past to deal with this problem. First, if the noise of the reference source is known, it can be subtracted from the measurement. Second, if the sources are nominally identical, 3 dB is subtracted from the curve under the assumption that the noise contributions are equal. This is often not the case when the noise source is device dependent, e.g., flicker noise in transistors or quartz crystal resonators.

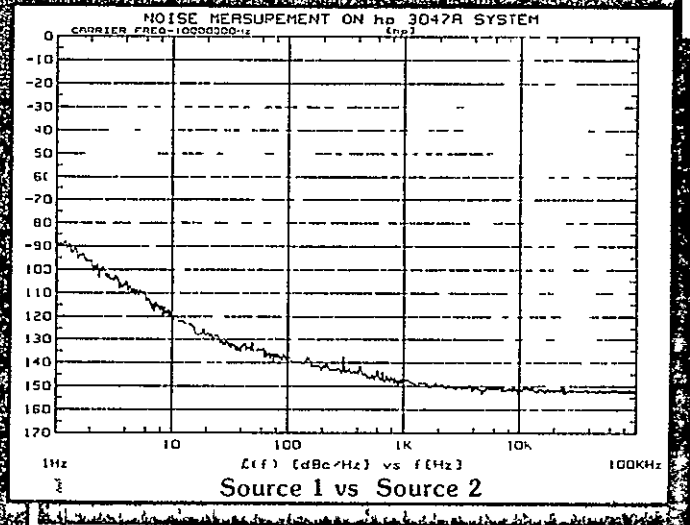
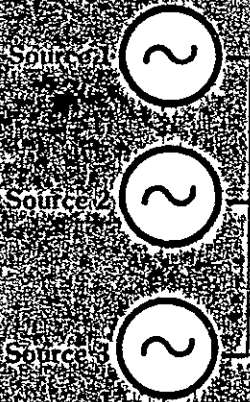


**ORIGINAL PAGE IS  
OF POOR QUALITY.**

There is, however, a third alternative which has been implemented in the 3047A System. If three sources are compared pair-wise in three separate measurements, the absolute noise level of each source can be determined by solving three simultaneous linear equations at

each measurement frequency. While this would be a tedious calculation if done by the operator, the powerful computational capability of the 3047A's Desktop Computer easily makes this calculation at all the measurement frequencies of the system.

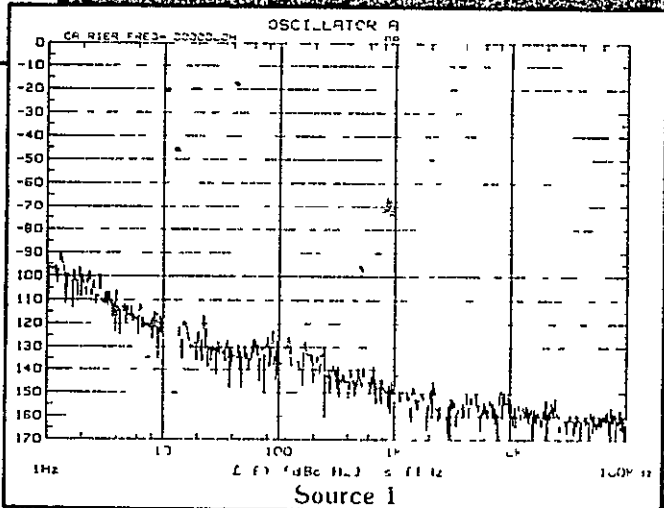
**Three Source Comparison Measurement**



Source 2 vs Source 3

Source 1 vs Source 3

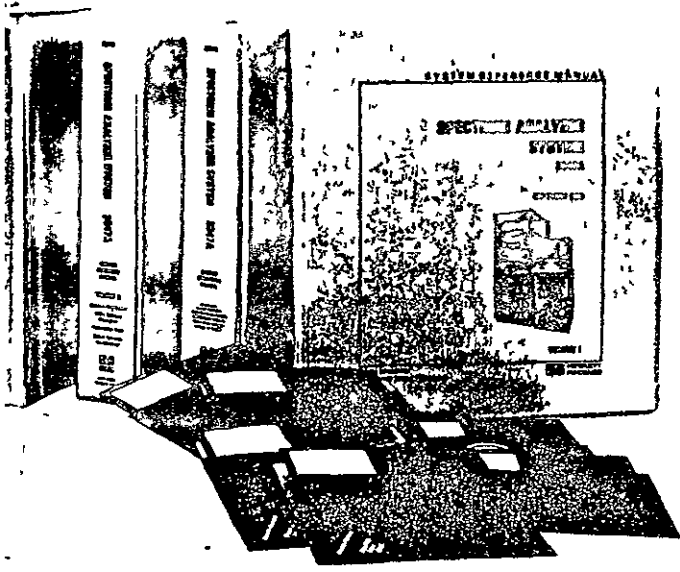
Three Source  
Comparison  
Software



Source 1

Source 2

Source 3



## Specifications

### Phase Noise Measurement Mode

#### Phase Detector Inputs

#### Frequency

Carrier Frequency Range 5 MHz to 18 GHz in two ranges

	Frequency Range	Return Loss	Isolation
Low Frequency Inputs	5 MHz to 1.6 GHz	5 dB (3.5 VSWR)	15 dB
High Frequency Inputs (may be deleted with Option 110)	1.2 GHz to 18 GHz	5 dB (3.5 VSWR)	15 dB

(The frequency range can be extended with customer supplied mixer or frequency discriminator)

#### Offset Frequency Range

0.2 Hz to 40 MHz for carriers from 95 MHz to 18 GHz  
0.2 Hz to 1 MHz for carriers from 5 MHz to 95 MHz

#### Amplitude

	5 MHz - 1.6 GHz	1.2 GHz - 18 GHz		
	L input	R input	L input	R input
Maximum Signal Level (dBm)	+23	+23	+10	+10
Minimum Signal	+15	-5	+7	+0

### System Library

The 3047A System Library consists of all operation and service manuals for the instruments in the system as well as all the manuals for the Desktop Computer.

In addition, the following system reference materials are included: an installation manual, which contains all necessary information for system installation and checkout, an operating manual, to aid in setting up and running the actual measurements, and a two volume reference guide, which includes software flowcharts and gives suggestions on how to change the test configuration to avoid errors detected by the system.

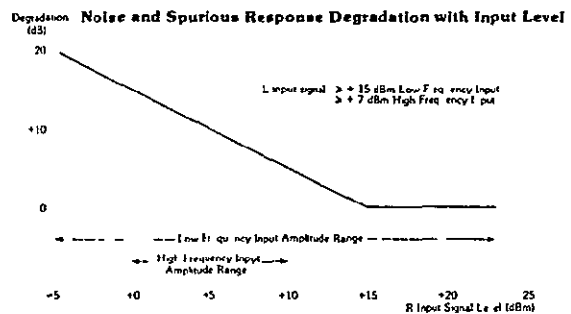
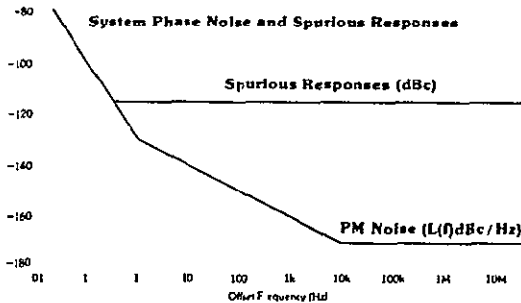
### System Installation and Training

To help you quickly get good measurements, system installation and training at your site are included with the 3047A system. A trained HP customer engineer will come to your site, install the system and verify that it is operating correctly. In addition, an HP System Engineer will come to your site and give a one day course on how to make measurements with the system.

### System Warranty \*

A complete warranty program covers the HP 3047A system hardware for 90 days (U.S. and Canada) following the system installation date. During this period, HP will diagnose system failures at your site and provide appropriate repairs. (Controller repairs will normally be completed on site, instruments may require return to an HP service center.)

\*Outside the U.S. and Canada, the warranty for the HP 3047A is determined by local HP policy. Contact your local HP Sales and Service Office for more information.

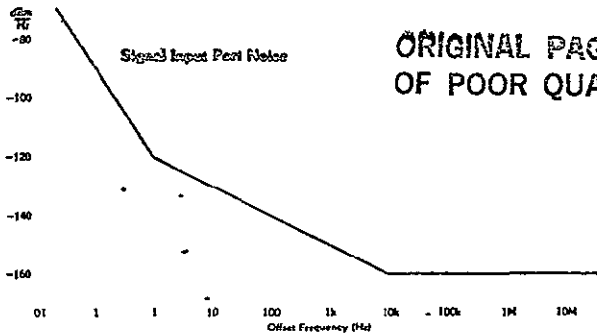


To determine system noise and spurious response levels find the dB degradation at the signal input level from the lower graph and add to upper curves. For example if a +15 dBm signal is applied to the Low Frequency L Input and a +5 dBm signal to the R Input the degradation is +10. Therefore the system spurious signals are 105 dBc at all offset frequencies and the system noise curve is raised 10 dB giving a noise floor at large offset frequencies of 160 dBc/Hz.

#### Accuracy

± 2 dB	± 4 dB	
0.2 Hz	1 MHz	40 MHz

**Signal Input Port** (for use with external phase detector or frequency discriminator)  
 Frequency Range 0.02 Hz to 40.1 MHz  
 Input Impedance 50Ω, Return Loss 9.5 dB (2.1 VSWR)  
 Max Amplitude 1 Volt peak  
 Spurious Responses < -100 dBm



Accuracy External phase detector measurements or frequency discriminator measurements calibrated with ± 1 dB accurate signals

± 2 dB ± 4 dB  
 0.02 Hz 1 MHz 40 MHz

**Control Voltage Output**

Voltage Range ± 10V  
 Current ± 20 mA max  
 Impedance 50Ω

**Measurement Restrictions**

In addition to the above stated limitations on the amplitude and frequency of the sources which can be measured in this mode, the following restrictions also apply

Source Return Loss 9.5 dB (2.1 VSWR)  
 Source Harmonic Distortion < -30 dB (or the source may output a square wave)

If either of these conditions are violated, the accuracy of the system measurement will be reduced

Also, the tuning range of the source which is controlled by the phase lock loop must be commensurate with the noise level of both sources. If the tuning range is too narrow, the source will not be able to track the noise and the loop will fall out of lock. Because any measurements made under this condition are invalid, the 3047A detects this condition and halts the measurement. If the tuning range of the controlled source is too large, the source will be extremely sensitive to noise on the control line and this will increase the effective noise of the reference oscillator.

For instance, if we wish to use a fundamental crystal oscillator as the reference source, it will not be possible to measure LC oscillators with the system. The crystal oscillator has a tuning range of a few tenths of Hertz whereas the LC oscillator will drift well out of this tuning range.

**Noise Sideband Mode**

**Frequency**

Carrier Frequency Range 20 Hz to 40.095 MHz  
 Offset Frequency Range

Carrier Freq	Offset Freq
95 kHz to 40 MHz	0.02 Hz to 25 kHz
9.5 kHz to 95 kHz	0.02 Hz to 1 kHz
950 Hz to 9.5 kHz	0.02 Hz to 100 Hz
95 Hz to 950 Hz	0.02 Hz to 10 Hz
20 Hz to 95 Hz	0.02 Hz to 1 Hz

Carrier Signal Level +30 dBm to -60 dBm

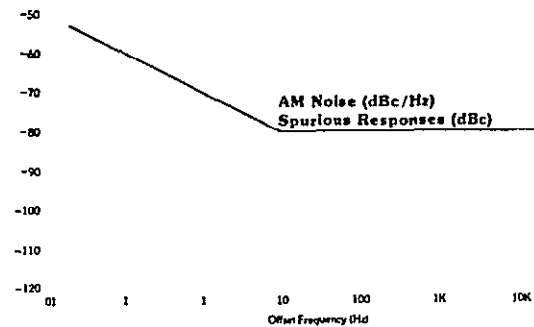
Input Impedance 50Ω

Phase and Amplitude Accuracy

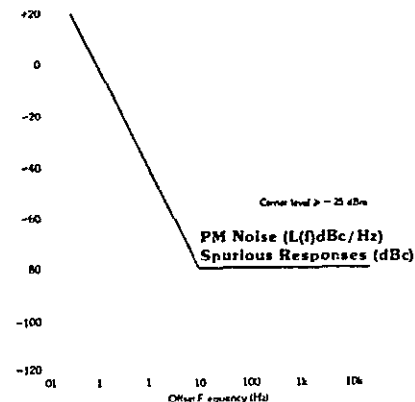
From 0.02 Hz to 1/2 maximum offset frequency ± 1.5 dB

From 1/2 maximum to maximum offset frequency ± 3 dB

**AM Analysis**



**PM Analysis**



**Measurement Restrictions**

Tracking Range ± 150 Hz (The system is capable of tracking up to 150 Hz of carrier drift during the measurements)

Amplitude variations must be less than ± 5 dB during measurements

# Direct Spectrum Measurement Mode

## Frequency

Center Frequency Range 20 kHz to 40 095 MHz  
 Frequency Span 5 Hz to 10 kHz  
 Center Frequency Accuracy  $\pm$  ( 1ppm/month + 0 1 Hz)  
 Center Frequency Resolution 1 Hz  
 Filter Passband Shape

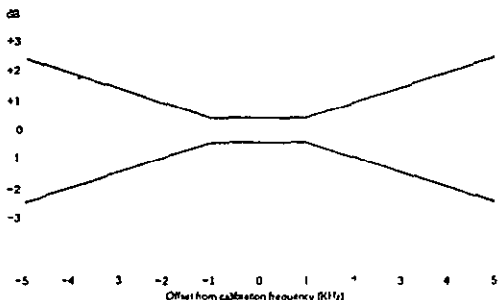
	Flat Top	Hanning	Uniform
3 dB bandwidth	(1 4 $\pm$ 0 1)% of Span	(0 58 $\pm$ 0 05)% of Span	(0 35 $\pm$ 0 02)% of Span
Shape Factor 60 dB bandwidth 3 dB bandwidth	2 6 $\pm$ 0 1	9 1 $\pm$ 0 2	716 $\pm$ 2'

Frequency Span	Time Record Length (N $\Delta$ t)	Calculated Point Spacing ( $\Delta$ f)
5 Hz	50 sec	02 Hz
10 Hz	25 sec	04 Hz
25 Hz	10 sec	1 Hz
50 Hz	5 sec	2 Hz
100 Hz	2 5 sec	4 Hz
250 Hz	1 sec	1 Hz
500 Hz	500 msec	2 Hz
1 kHz	250 msec	4 Hz
2 5 kHz	100 msec	10 Hz
5 kHz	50 msec	20 Hz
10 kHz	25 msec	40 Hz

The Flat Top Passband Shape provides optimum amplitude accuracy. The Uniform Passband Shape is optimized for use with transients and the Hanning Passband Shape provides an amplitude/frequency resolution compromise and is used for general noise measurements.

## Amplitude

Measurement Range + 30 dBm to - 130 dBm noise floor  
 Input Impedance 50 $\Omega$   
 Display Modes 10 dB/division or 2 dB/division  
 Dynamic Range > 70 dB (except 3rd order inter-modulation distortion, < - 40 dB)  
 Amplitude Accuracy  $\pm$  0 9 dB at reference level and center frequency  
 Filter Accuracy  
 Flat Top Filter +0 -0 1 dB  
 Hanning Filter +0, -1 5 dB  
 Uniform Filter +0, -4 0 dB  
 Frequency Response



Amplitude Linearity  $\pm$  0 2 dB  $\pm$  0 02% of full scale  
 Overall accuracy is the sum of the accuracy at the reference level and center frequency, the filter accuracy, frequency response and amplitude linearity  
 Resolution  $\pm$  0 1 dB with the marker

## Marker

Resolution 4% of span, 0 1 dB  
 Marker Units dBm, dBV, relative or absolute amplitude and frequency, RMS noise density (in 1 Hz BW)

## Average Modes

RMS for each calculated frequency point the displayed amplitude is

$$\sqrt{\frac{1}{N} \sum A_i^2(f)} \text{ and the phase is } \frac{1}{N} \sum \phi_i(f)$$

Peak For each calculated frequency point the displayed amplitude is MAX  $A_i(f)$  and the phase is the corresponding value for the retained amplitude point

Number of Averages 4 to 256 in a binary sequence plus exponential. Exponential in the RMS mode gives a running average with new spectral data weighted 1/4 and the previous result by 3/4. Exponential in the peak mode gives a continuous peak hold operation.

## General Information

**Size:** The system instruments are mounted in a 142 cm (56 inch) rack. Outside dimensions approximately 163 x 76 x 70 cm (64 x 30 x 27) inches.

The Desktop Computer sits separate from the instrument rack. Outside dimensions approximately 45 x 66 x 43 cm (18 x 26 x 17) inches.

**Weight:** Net Rack 227 Kg (500 lbs)  
 Computer 36 Kg (80 lbs)  
 Shipping 400 Kg (900 lbs)

**Power Requirements:** 700 VA  
 48 66 Hz  
 100 V, 110 V, 220 V, 240 V  
 Line Operation Options  $\pm$  10%

**Warm up Time.** System will meet full specifications 20 minutes after turn on.

## Operating Environment:

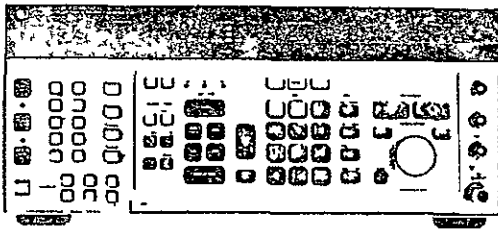
Temperature Range 0°C to 55°C

General Considerations The 3047A Spectrum Analyzer has been designed to have a low susceptibility to RFI and mechanical vibration. However, a great deal of care must be exercised in making measurements in high RFI or mechanical vibration environments as spurious signals may be induced directly in the source-under-test, in the test fixture, or in the system itself. If a problem is suspected, the system can be tested for noise floor and spurious responses using the test fixture and software provided.

EMI 9836A based 3047A systems satisfy Level B of VDE specification 0871.

For complete information on these products, consult their respective data sheets

## HP 8662A/8663A Synthesized Signal Generators



HP 8663A

The HP 8662A and 8663A Synthesized Signal Generators offer superior spectral purity, frequency resolution and stability over a wide frequency range. Covering 10 kHz to 1280 MHz (to 2560 MHz with the 8663A), they are the ideal reference sources for many phase noise measurements.

### Abbreviated Specifications

**Frequency Range:** 10 kHz to 1280 MHz (8662A) or 100kHz to 2560 MHz (8663A)

**Frequency Resolution:** 0.1 Hz to 640 MHz, 0.2 Hz to 1280 MHz, 0.4 Hz to 2560 MHz

**Output Level Range:** -139.9 to +13 dBm (8662A) or +16 dBm (8663A)

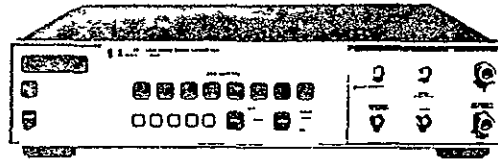
**Spectral Purity:** (SSB phase noise in 1 Hz BW,  $320 < F_c < 640$  MHz)

Offset from carrier	10	100	1K	10K	100K	Hz
residual, CW/AM modes	-100	-112	-121	-131	-132	dBc/Hz
typ absolute	-90	-110	-123	-136	-136	dBc/Hz

(absolute noise includes the phase noise contributed by the synthesizer's internal 10 MHz reference oscillator)

**Modulation:** complete AM and FM capabilities. External FM input may be DC coupled for phase locked loop operation.

## HP 11729A/B Low Noise Downconverter



HP 11729A/B

The 11729A/B Low Noise Downconverter facilitates phase noise measurements on microwave sources to 18 GHz. A low noise mixing process translates input signals to the band 5-1280 MHz for input to the HP 3047A's quadrature phase detector. In this frequency range, the HP 8662A and 8663A are both suitable reference sources yielding accurate, sensitive phase noise measurements.

Input frequency range extends to 18 GHz in bands of 1280 or 2560 MHz depending on residual noise requirements. Model 11729A is the single band version, model 11729B provides multiband operation and complete HP IB control.

### Abbreviated Specifications

**Test Signal Input:**

5 MHz to 18 GHz, depending on options chosen  
+6 dBm min to +18 dBm max

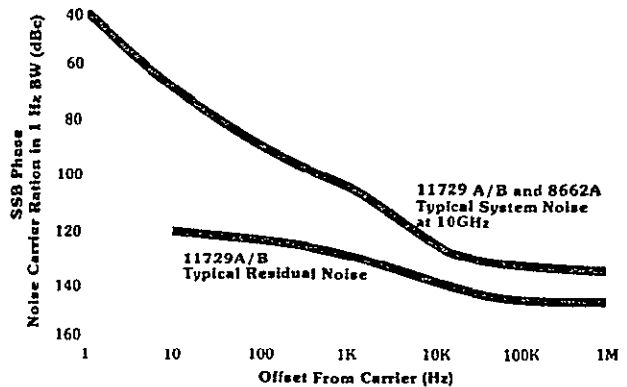
**RF Source Input:**

Requires HP 8662A or 8663A with options HO3 and H12

**RF Output:**

5 MHz to 1280 MHz at +7dBm minimum

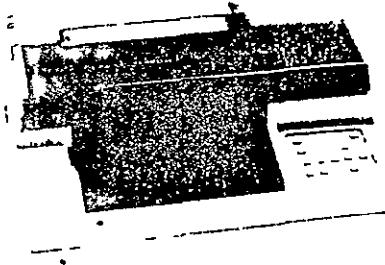
**Residual Noise:**



Typical 11729A/B residual noise and system noise at 10 GHz

## 9872C/T and 7470A Graphics Plotters

The addition of an HP-IB graphics plotter makes it easy to record HP 3047A system measurements for analysis, documentation and presentation. The multi color report quality graphics are ready for publication when drawn on paper and for group presentations when drawn on overhead transparency film. Recommended plotters include the 8 pen 9872C/T and the 2 pen 7470A.



HP 7470A Graphics Plotter

## 2671G Graphics Printer

This quiet thermal printer provides hard copies of system generated text and graphics. With high resolution dot matrix graphics and full alphanumeric capabilities, the 2671G reproduces plots and listings from the 9836A CRT at the touch of a single key.

ORIGINAL PAGE IS  
OF POOR QUALITY

## 3047A Spectrum Analyzer System consists of:

---

**HP 3585A** 20 Hz - 40 MHz Spectrum Analyzer

**HP 3582A** 0.2 Hz - 25 kHz Dynamic Signal Analyzer

### Spectrum Analyzer Interface

**Rack cabinet** 142 cm (56 inches) tall with all required RF power and HP-IB cabling, RFI filtering and sliding shelf

**Desktop Computer** configured as follows

#### 9836A Based Systems

HP 9836A Desktop Computer  
HP 98601A Option 655 BASIC 2.0 (ROM based)  
(2 ea) HP 98256A 256 Kbyte memory expansion module

#### 9845B Series 100 Based Systems

HP 9845B Option 175 Standard Performance Desktop  
Computer  
HP 98034B HP-IB Interface  
HP 98035A Option 001 Real Time Clock

#### 9845B Series 200 Based Systems

HP 9845B Option 275 High Performance Desktop  
Computer  
HP 98034B HP-IB Interface  
HP 98035A Option 001 Real Time Clock

### Also included

system installation and checkout at your site  
operator training at your site  
two complete sets of data cartridges or flexible discs containing all system software  
full set of manuals including  
System Installation Manual  
System Operator's Manual  
System Reference Manual  
Controller Manuals  
Operating and Service Manuals for all instruments

For more information call your local HP Sales Office or nearest Regional Office • Eastern (201) 265-5000 • Midwestern (312) 255-9800 • Southern (404) 955-1500 • Western (213) 970-7500 • Canadian (416) 678-9130. Ask the operator for instrument sales. Or write: Hewlett-Packard, 1501 Page Mill Road, Palo Alto, CA 94304. In Europe: Hewlett-Packard SA, 7 rue du Bois du Lon, P.O. Box CH 1217 Meyrin 2, CH 1255 Switzerland. In Japan: Hewlett-Packard Ltd., 29-21 Takaido Higashi 3-chome, Sugnamiku, Tokyo 168.

Printed in U.S.A.

Data Subject to Change

5952-5106



9841 Airport Boulevard • Suite 912 • Los Angeles, California 90045 • Phone (213) 641 8600

TECHNICAL MEMORANDUM NO. M8305-1

TO: P. Nilsen

DATE: May 10, 1983

FROM: R. Iwasaki

COPIES: NAS9-16067"A"

SUBJECT: A Technique to Minimize Antenna-Switching Transient Effects  
for the Centaur Vehicle

-----

The antenna-switching transients on the Centaur vehicle pose some serious problems that may interfere with the transmission of telemetry during the high-spin-rate mode prior to payload separation. However, it may be possible to minimize the data loss, even with the existing antenna-switching technique presently envisioned. "Simple" modifications of the ground-based receiver are proposed that may circumvent the problem.

The General Dynamics memorandum from P. Lathrop to B. Shiba, dated May 2, 1983, discusses the problem thoroughly. This proposal is an extension of the author's analysis and attempts to define means for (1) minimizing the signal fade from an interference null, (2) detecting and compensating for the possible  $\pm 180^\circ$  phase shift resulting from the antenna switching and, (3) transmitting a "flag" to indicate antenna switching to reconstruct the data stream.

The first problem to be dealt with is the signal fade resulting from the destructive interference from two radiating elements spaced widely apart during the 5-ms "make-before-break" switching procedure. Using the polar antenna patterns in the General Dynamics memo, Figure 1 shows the interference lobes for both antennas, Figure 2 shows a representative antenna pattern, and Figure 3 shows an overlay of the two opposite antenna patterns plus the interference region superimposed, where constructive and destructive interference occurs. Note that the signal during the switching period may either increase or decrease in this region, depending on the position of the interference lobes which are spaced  $1.36^\circ$  apart. The 5-ms switching transient constitutes only  $0.14^\circ$  at 4.7 RPM, so the "array" pattern of both antennas radiating can indeed be in the null condition such that signal fading occurs, with subsequent data loss.

ORIGINAL PAGE IS  
OF POOR QUALITY

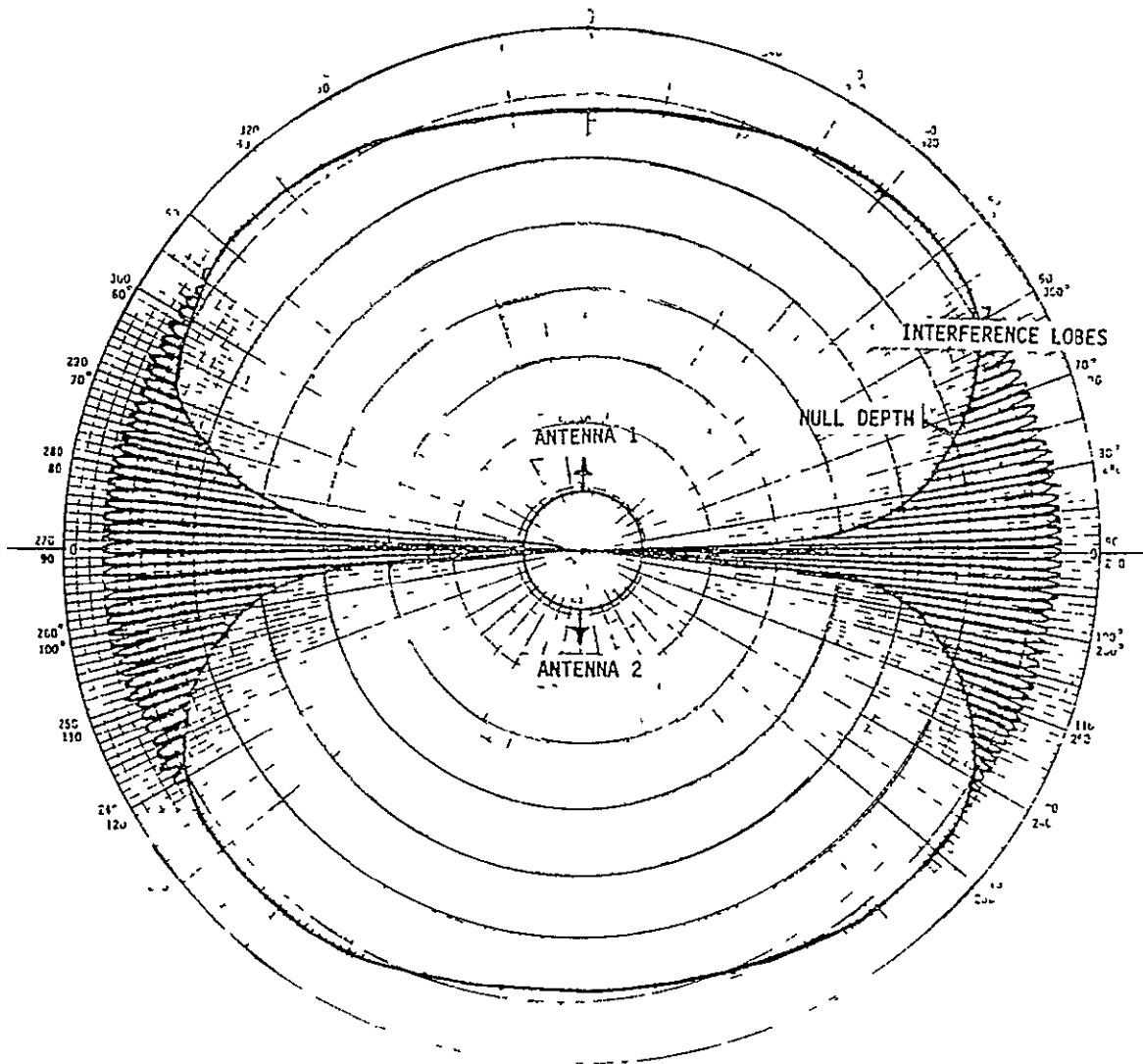


Figure 1. Combined Antenna Pattern Showing the Interference Lobes During the Antenna-Switching Transient when Both Antennas Radiate



ORIGINAL PAGE IS  
OF POOR QUALITY

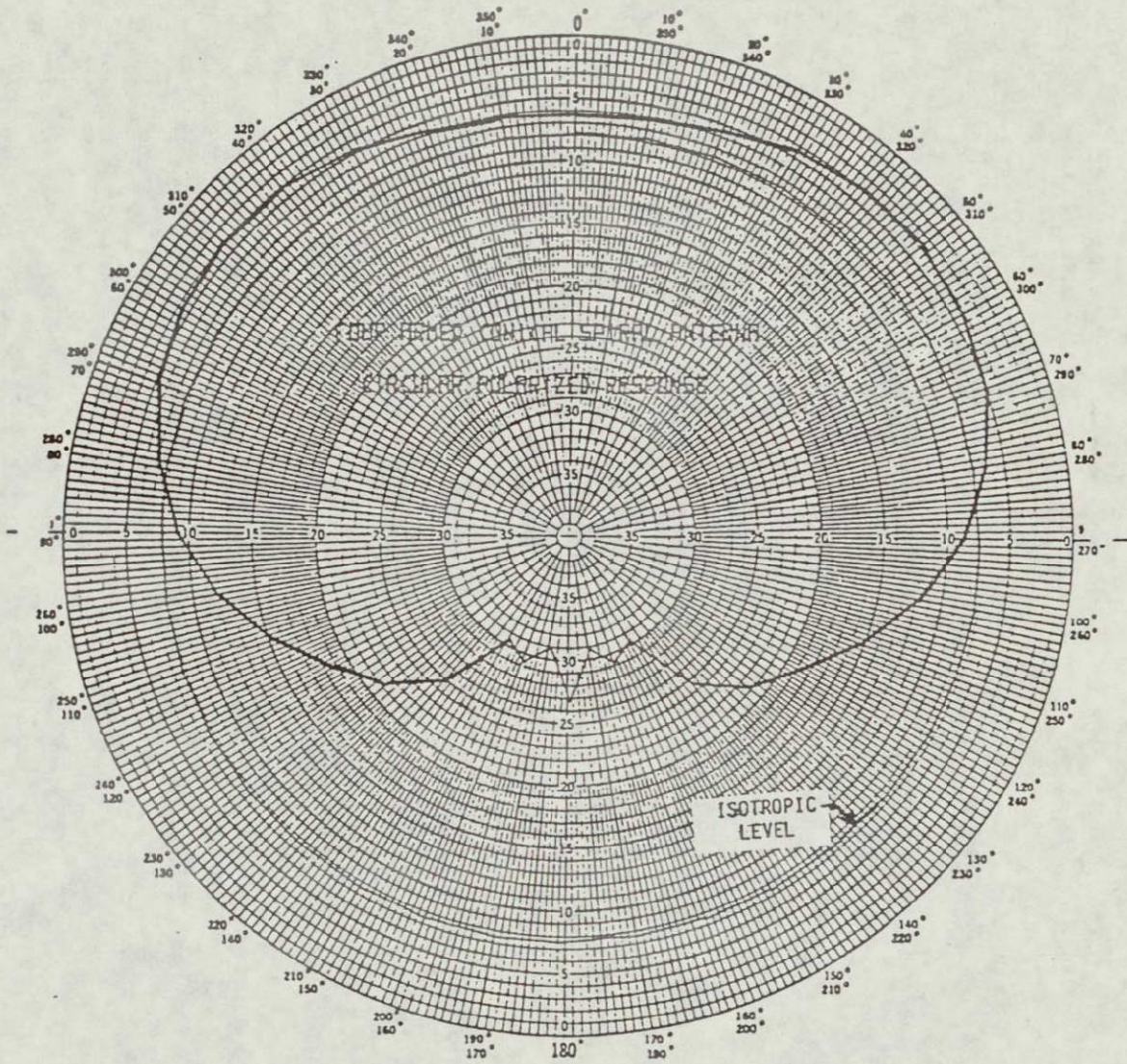


Figure 2. Assumed Antenna Pattern Used for Antenna-Switching Transient Analysis

ORIGINAL PAGE IS  
OF POOR QUALITY

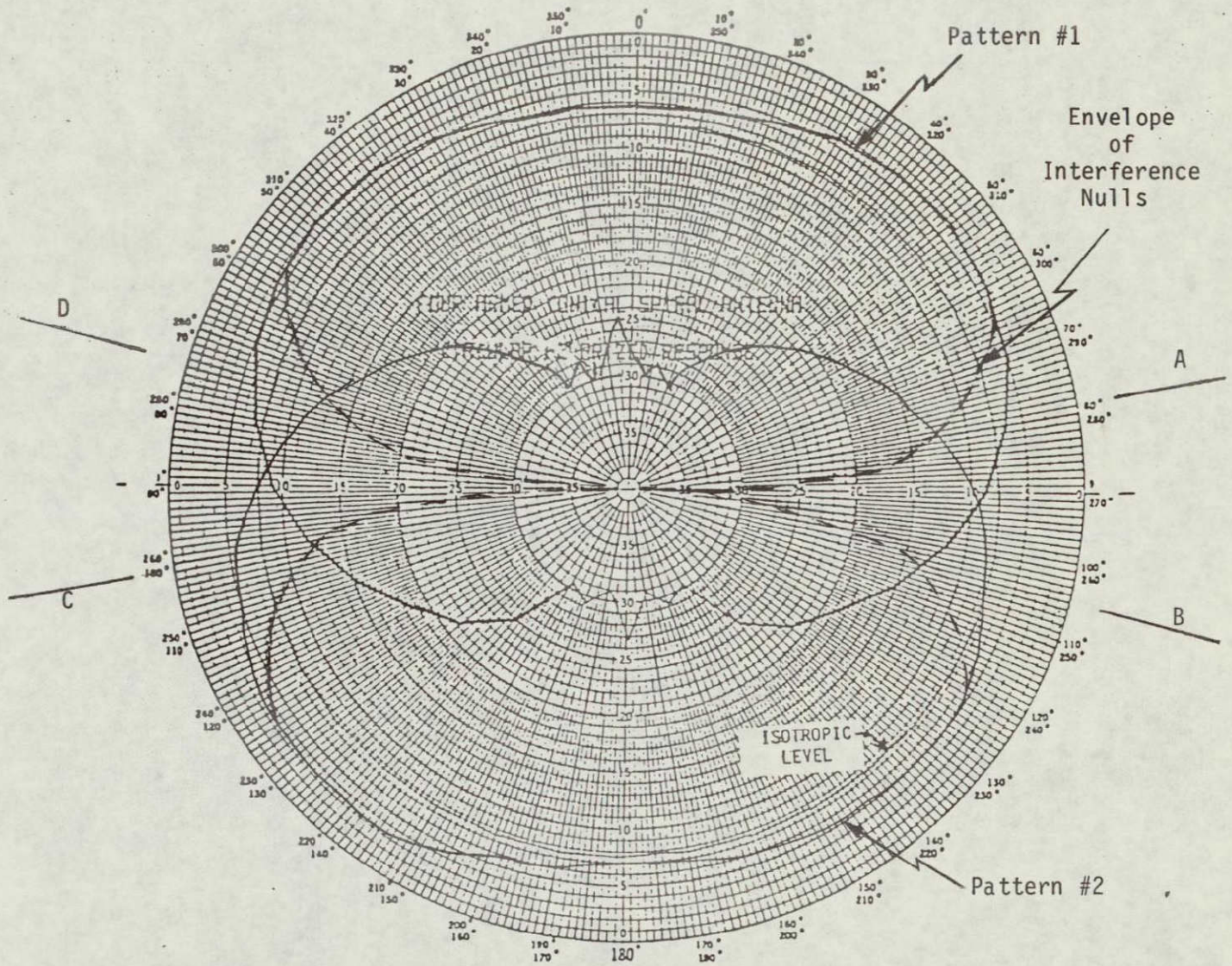


Figure 3. Assumed Superimposed Antenna Patterns Used for Antenna-Switching Transient Analysis Including the Envelope of Interference Nulls

In order to minimize this fading effect, it is proposed that the antennas be switched at a position where the null magnitude is the same as the radiation pattern of the opposite antenna such that the signal level will be at least constant (or, more probably, greater). There are four positions per revolution where this condition occurs, as indicated by the letters A, B, C and D in Figure 3. The imposition of this requirement maintains a minimum signal level of operation established by the worst-case interference null which, by definition, is the back lobe pattern of the opposite antenna that will be transmitting during the other half of the revolution. Obviously, it is desirable to have the highest gain possible in order to increase the minimum signal level, and this should be a consideration when specifying the desired antenna pattern, which can be adjusted appropriately.

The next problem is to cope with the phase-shift transient, which may be as large as  $\pm 180^\circ$ . The key to this part of the transient-compensation technique is that the magnitude of the received signal is a direct indication of the phase transient. For example, if the signal level is high (i.e., higher than prior to switching), then the interference pattern is constructive and the phase of the other antenna matches (or is in synchronization with) the first antenna. On the other hand, if there is an abrupt drop in signal at the switching point, the interference is obviously destructive and  $\pm 180^\circ$  apart, which requires that the data polarity must be inverted in order to compensate and correct the phase imbalance.

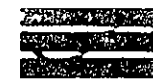
The concept proposed to maintain the communication link is either to sense this abrupt drop in signal level, signifying the phase shift, or record the incoming data stream which provides a buffer for subsequent signal processing. Once recorded, the pertinent data can be retrieved by data manipulation, especially when the antenna-switching instant is well known.

There are many possible phase-shift values resulting from the antenna switching but, since the minimum null depth indicating the  $\pm 180^\circ$  phase-shift condition is equated to the back lobe of the other antenna, this information can be utilized to ascertain the degree of phase-shift occurring. For example, if the signal level is higher (i.e., +1.6 dBc, as in the GD report), constructive interference is occurring and the phases of the two radiation patterns are in synchronism. On the other hand, if the signal level remains constant during and after switching, the  $\pm 180^\circ$  phase offset exists and provisions must be made to correct the data by inversion to reconstruct the data stream. Any point in

between these two extremes must be evaluated to determine if corrective procedures must be included, but the fact that the data utilizes BPSK modulation greatly simplifies this decision.

The last point to be discussed is the transmission of a signal to pinpoint the exact switching instant such that it can be used to reconstruct the data if it is indeed determined that a  $\pm 180^\circ$  phase inversion occurred. Once this switch point is known, the data being recorded can be readily manipulated simply by analyzing the signal strength level and correcting the phase accordingly.

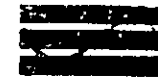
Axiomatix realizes that this technique will impact the TDRS ground equipment, which may not be acceptable; however, it does offer the possibility of recovering data that might otherwise be lost. This technique could be of considerable value in the event of a catastrophic failure, where telemetry is essential.



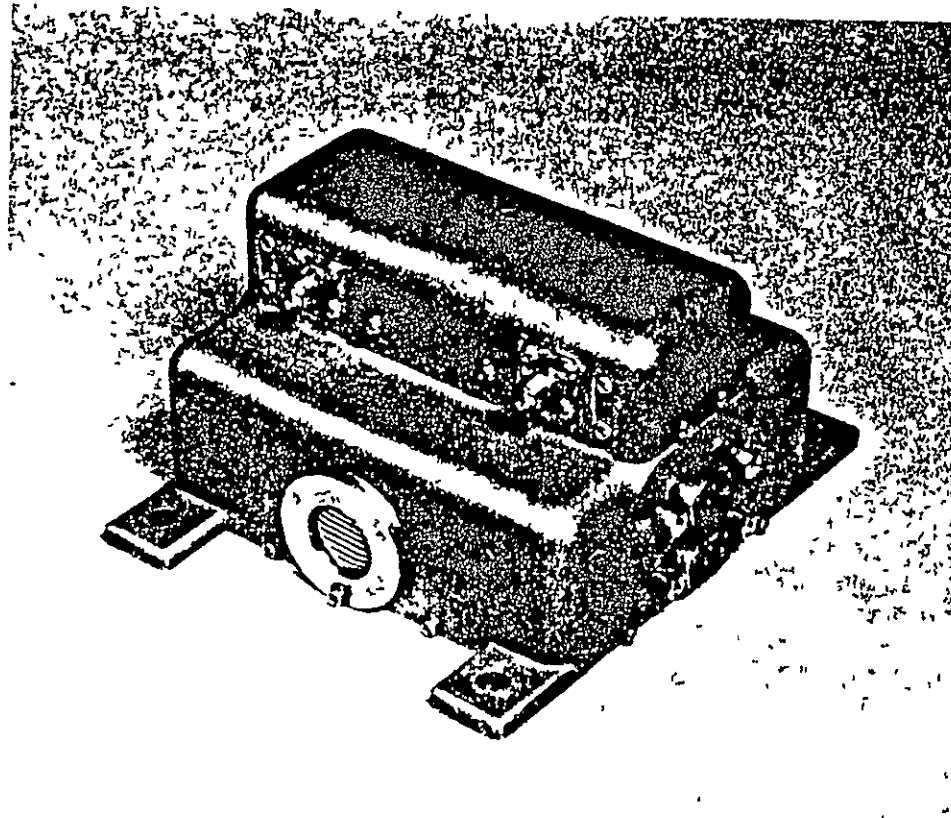
- ELECTROMECHANICAL SWITCH
  - 5 ms "MAKE-BEFORE-BREAK"
  - $(5 \times 10^{-3}) (16 \times 10^3) = 80 \text{ BITS}$
  
- LATCHING CIRCULATOR (SIMILAR TO THAT USED ON SPACE TELESCOPE)
  - 150  $\mu$ s SWITCHING
  - $(0.15 \times 10^{-3}) (16 \times 10^3) = 2.4 \text{ BITS}$
  
- SUBSTANTIALLY DECREASES THE POSSIBILITY OF DEMODULATOR AND DECODER SYNCHRONIZATION LOSSES
  
- INTERFERENCE LOBES STILL EXIST DURING TRANSITION
  - POSSIBLE GRADUAL TRANSITION OF POWER DIVISION

ORIGINAL PAGE IS  
OF POOR QUALITY

DPDT REDUNDANCY S-BAND LATCHING SWITCH  
FOR SATELLITE APPLICATIONS



Axiomatix



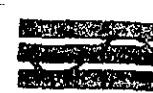
ORIGINAL PAGE IS  
OF POOR QUALITY

FREQUENCY	2 GHz
LOSS	0.5 dB MAXIMUM
ISOLATION	20 dB MINIMUM
MTBF	$5 \times 10^5$ HOURS MINIMUM

USEFUL LIFE (ORBITAL) 5 YEARS MINIMUM

FULL REDUNDANCY--SINGLE-POINT FAILURE PROOF

TWO-JUNCTION L-BAND SWITCHING ASSEMBLY  
MODEL 212-2

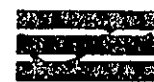


Axiomatix

THIS UNIT IS BEING DEVELOPED FOR THE SPACE TELESCOPE PROGRAM..

CONFIGURATION	TWO INTERNALLY CONNECTED LATCHING CIRCUITS
FREQUENCY	2100 MHz
BANDWIDTH	100 MHz
ISOLATION	20 dB PER JUNCTION
INSERTION LOSS	0.4 dB PER JUNCTION
VSWR	1.2:1 MAXIMUM
RF CONNECTORS	SMA FEMALE
SWITCHING TIME	200 $\mu$ s MAXIMUM (150 MICROSECONDS; TYPICAL)
SWITCHING RATE.	100 Hz MAXIMUM
DC SUPPLY	24 TO 34 V DC
OPERATING TEMPERATURE	-18 TO +60°C
COMMAND REQUIREMENTS	UNIT WILL TRIGGER ON LEADING EDGE OF SQUARE-WAVE PULSE OF A DURATION OF 20ms WITH AN AMPLITUDE OF 21 TO 29V
SIZE (EXCLUDING CONNECTORS)	4" x 3.5" x 2.5"
WEIGHT	1,200 GRAMS
SPECIAL FEATURE	REDUNDANT DRIVER

ORIGINAL PAGE IS  
OF POOR QUALITY

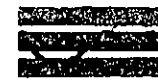


- MAJOR FRAME SYNCHRONIZATION ESTABLISHES PHASE REFERENCE
- MAJOR FRAME-TIMING SEQUENCE KNOWN BY PROCESSOR
- ANTENNA SWITCHING PRIOR TO MAJOR FRAME SYNCHRONIZATION DESIRABLE
- AT 4 7 RPM, SPIN RATE APPROXIMATELY  $30^\circ/s$
- MAJOR FRAME SYNCHRONIZATION OCCURS APPROXIMATELY EVERY SECOND
- TWO  $30^\circ$  ANTENNA-SWITCHING REGIONS PER REVOLUTION

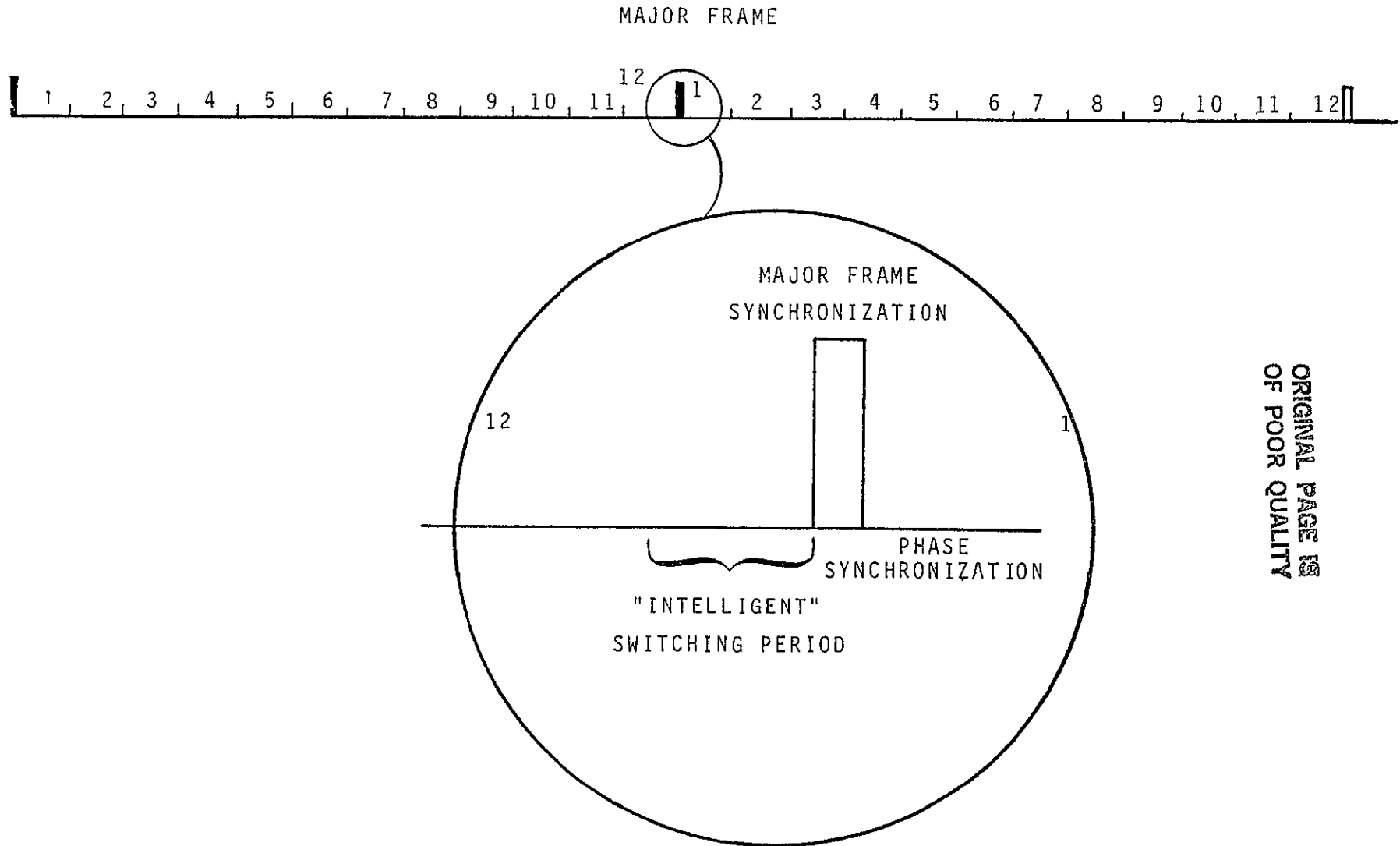
ORIGINAL PAGE IS  
OF POOR QUALITY



"INTELLIGENT" SWITCHING  
USING MAJOR FRAME SYNCHRONIZATION



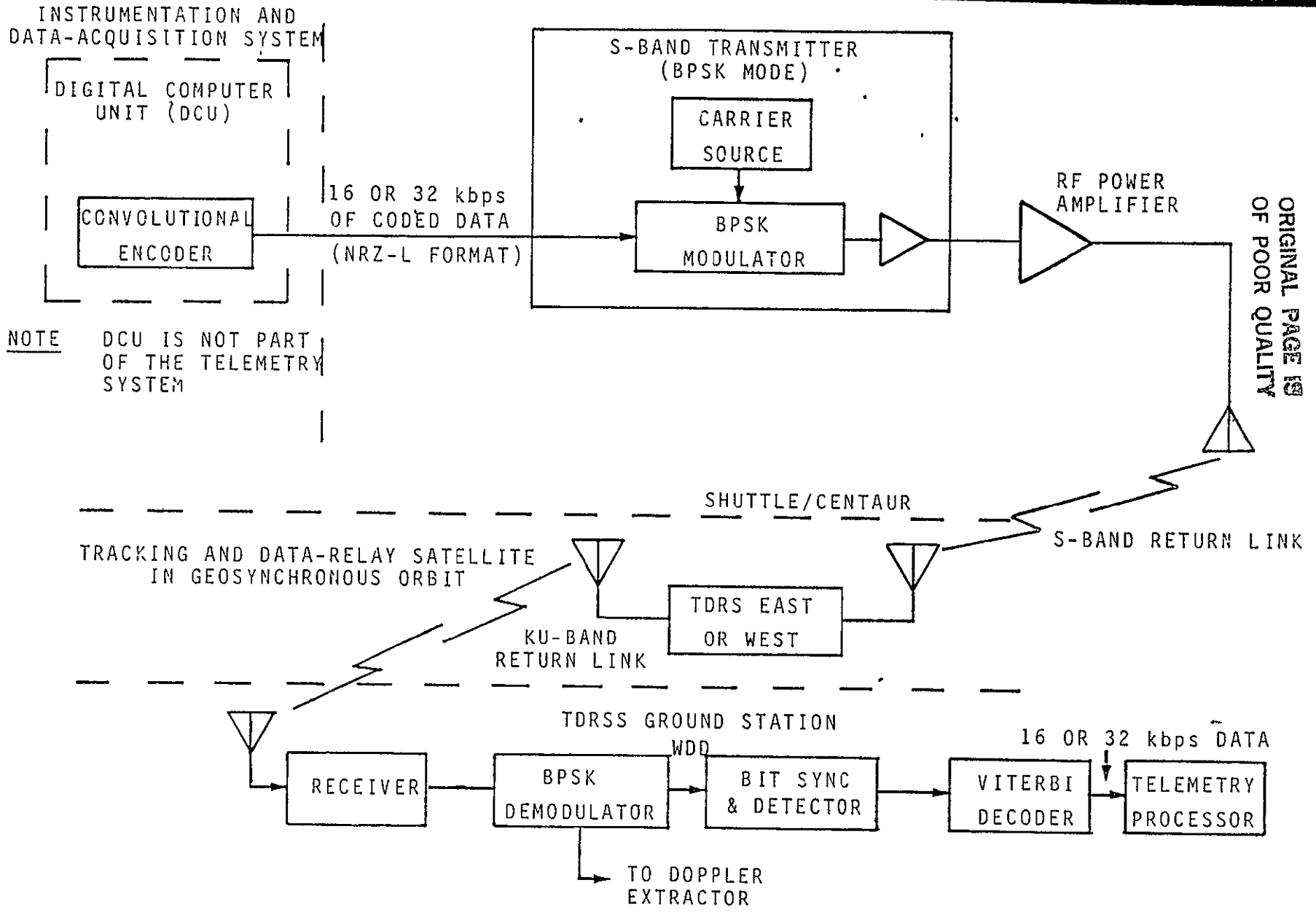
Axiomatix



ORIGINAL PAGE IS  
OF POOR QUALITY

- SYNCHRONIZATION CONTROL LOOPS REQUIRE "ADEQUATE" SIGNAL LEVELS AT ALL TIMES DURING SPIN
- PURPOSE IS TO MAINTAIN "ADEQUATE" SIGNAL LEVELS
- SIGNAL DROPOUT OCCURS BY DESTRUCTIVE INTERFERENCE OF BOTH ANTENNAS DURING SWITCHING
- MAGNITUDE OF MAXIMUM DESTRUCTIVE INTERFERENCE OR NULL VARIES ABOUT THE SPACECRAFT
- NULL ENVELOPE DESCRIBES MINIMUM SIGNAL LEVEL
- OMNIDIRECTIONAL ANTENNAS HAVE SUBSTANTIAL BACKLOBES
- FOUR REGIONS ABOUT SPACECRAFT DEFINE APPROXIMATELY EQUAL NULL-ENVELOPE AND BACKLOBE SIGNAL LEVELS
- ANTENNA SWITCHING IN THESE FOUR REGIONS DEFINES MINIMUM SIGNAL LEVEL EXPECTED
- ALSO, A PROBABILITY THAT CONSTRUCTIVE INTERFERENCE OCCURS, ACTUALLY INCREASING SIGNAL LEVEL

ORIGINAL PAGE IS  
OF POOR QUALITY

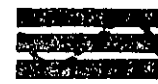


CENTAUR DATA LOSS ANALYSIS

PETER NILSEN

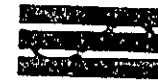
AXIOMATIX

AUGUST 4, 1983



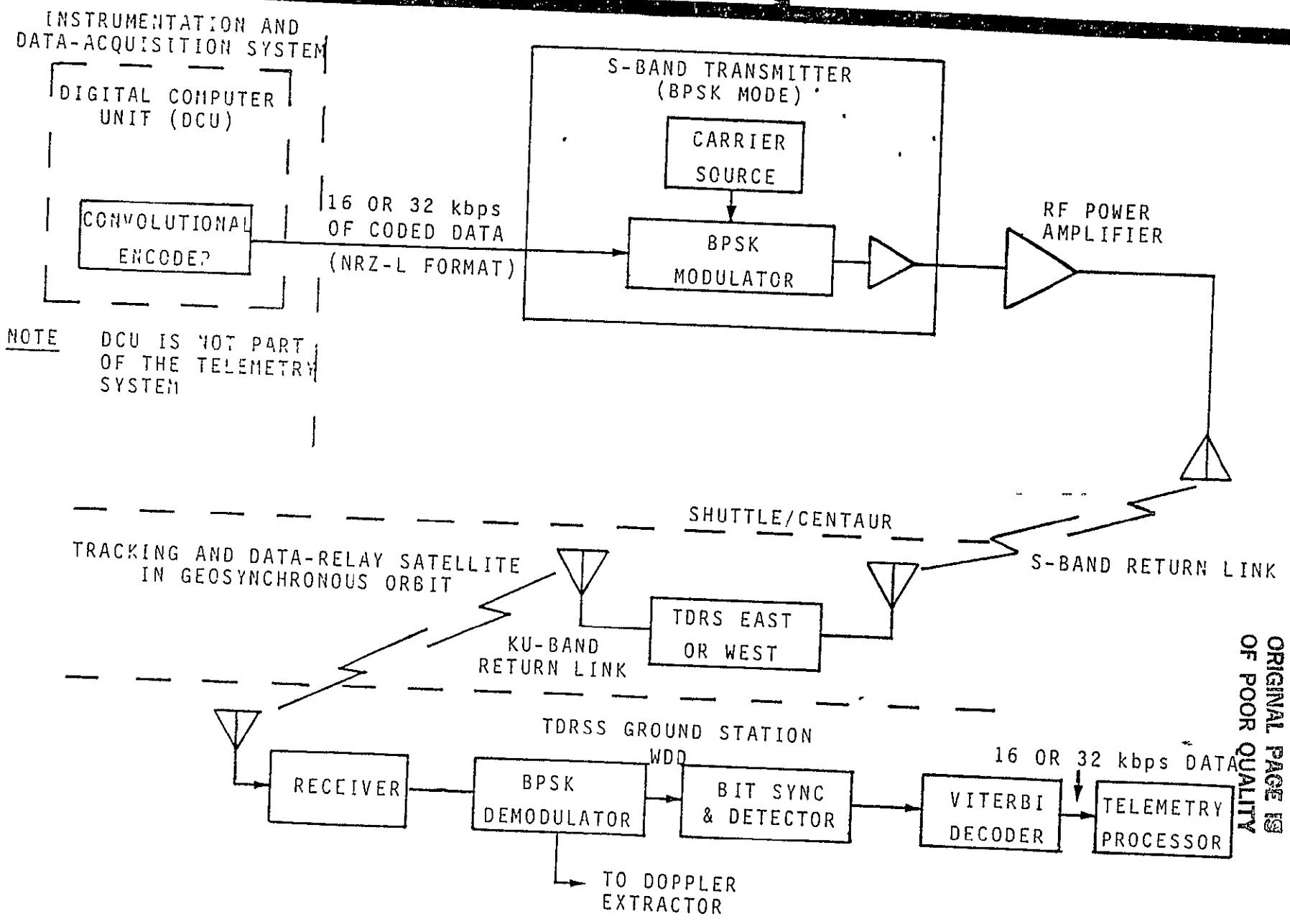
- DURING HIGH-SPEED SPIN-UP AND PRIOR TO S/C SEPARATION, TELEMETRY DATA WILL BE LOST DUE TO ANTENNA-SWITCHING TRANSIENTS
  - RATE ANTENNA SWITCH EVERY ~6 s (4.7 RPM)
  - SWITCHING-TRANSIENT DURATION 5 ms
  - SPIN DURATION ~1.5 min
  - LINK VARIATION DEEP FADES TO BELOW TRACKING THRESHOLD ARE PROBABLE AS WELL AS 180° PHASE SHIFTS
  - PRESENT PLAN CENTAUR WILL STORE CRITICAL NAV DATA IN MEMORY FOR READOUT AFTER DESPIN
  
- IT IS NECESSARY TO QUANTIFY DATA LOSS
  - TDRSS GROUND TERMINAL EQUIPMENT PERFORMANCE GREATLY IMPACTS AMOUNT OF DATA LOSS
  - SOME INFORMATION HAS INDICATED THAT, WITH THE PRESENT DESIGN, UP TO THREE TO FOUR SECONDS OF DATA PER ANTENNA-SWITCHING TRANSIENT CAN BE LOST

ORIGINAL PAGE IS  
OF POOR QUALITY



- SOLUTION APPROACH
  - ANALYZE AND INVESTIGATE ALL PERTINENT COMMUNICATION LINK PROCESSING ELEMENTS
    - WDD
    - VITERBI DECODER
  - ANALYZE AND INVESTIGATE ANTENNA SWITCHING SYSTEM TO SEE IF SWITCHING-CAUSED FADES CAN BE MINIMIZED

ORIGINAL PAGE IS  
OF POOR QUALITY



NOTE DCU IS NOT PART OF THE TELEMETRY SYSTEM

ORIGINAL PAGE IS OF POOR QUALITY

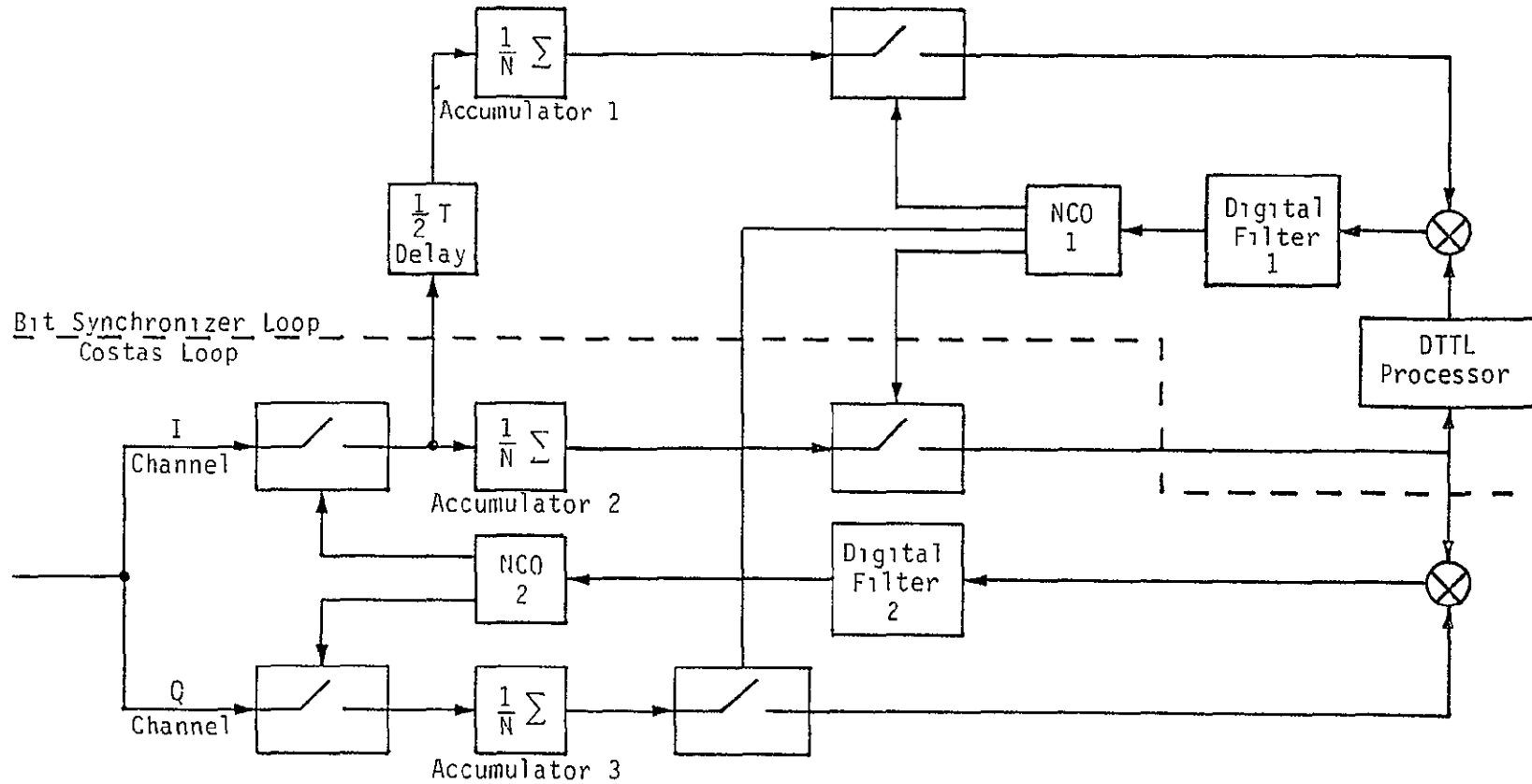


- WDD LOSS OF PHASE COHERENCE ANALYSIS
- DATA DEMODULATION/DECODING PROBLEMS ANALYSIS AND INVESTIGATIONS

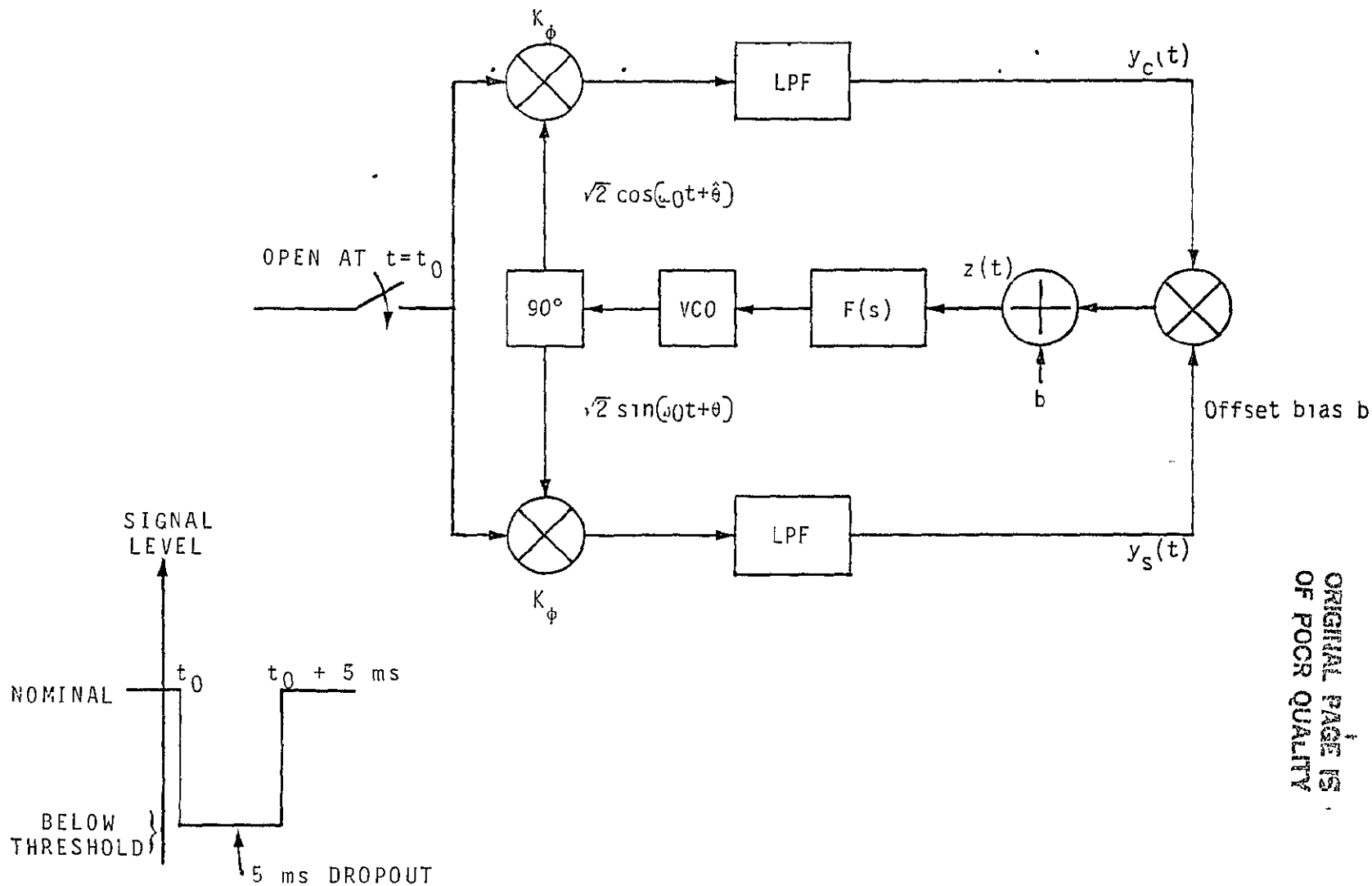
ORIGINAL PAGE IS  
OF POOR QUALITY



WIDE DYNAMICS DEMODULATOR CARRIER-TRACKING LOOP  
FUNCTIONAL BLOCK DIAGRAM



ORIGINAL PAGE IS  
OF POOR QUALITY



ORIGINAL PAGE IS  
OF POOR QUALITY

- PROBABILITY OF LOSING LOCK DUE TO NOISE DURING DROPOUT IS SMALL (FIRST-ORDER LOOP MODEL)

T(ms)	$P_{LL}$
2.5	0 999999792
5.0	0 9999978
10 0	0 999947
25 0	0 9983

- PARAMETERS FOR ANALYSIS

- $B_L = 420$  Hz (SECOND-ORDER LOOP)
- $R_b = 32$
- $SNR_{EFF} = 14$  dB

- CONCLUSION

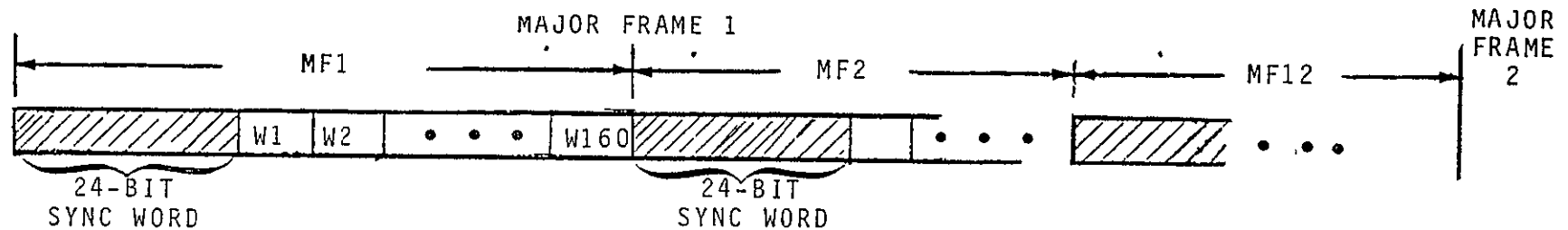
- LOSS OF PHASE COHERENCE DUE TO 5-ms DROPOUT NOT LIKELY

ORIGINAL PAGE IS  
OF POOR QUALITY

- ANTENNA-INDUCED PHASE SHIFT OF  $\sim 180^\circ$  CAN CAUSE PHASE INVERSION OF DATA
  
- 5 ms DROPOUT CAN CAUSE UP TO A 250-BIT LOSS DUE TO THE VITERBI CODER SEARCH
  - FROM HARRIS VIA STI
  
- 2 5 ms DROPOUT CAN CAUSE THE WDD TO REACQUIRE, WHICH CAN TAKE FROM ONE-HALF TO FOUR SECONDS
  - FROM HARRIS VIA STI

ORIGINAL PAGE IS  
OF POOR QUALITY

● FRAME STRUCTURE

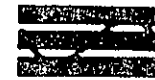


- 160 WORDS PER MINOR FRAME
- 12 MINOR FRAMES PER MAJOR FRAME
- EIGHT BITS PER WORD
- DUE TO ANTENNA-SWITCHING, A PHASE INVERSION CAN CAUSE DATA INVERSION
- PHASE FLIPPING WILL CAUSE THE LOSS OF A MINOR FRAME
- THE DOPPLER SHIFT BETWEEN ANTENNAS IS NOT A PROBLEM
- THE FOLLOWING MINOR FRAME WILL ALLOW DATA INVERSION
- CONCLUSION WILL LOSE A PORTION OF A MINOR FRAME OF DATA

ORIGINAL PAGE IS  
OF POOR QUALITY

- 5 ms DROPOUT
  - CAN CAUSE UP TO 500 SYMBOLS (250 BITS) DATA LOSS DUE TO RESYNCHRONIZATION TIME REQUIRED BY DECODER
  - NO EASY FIX TO THIS PROBLEM
  
- 2.5 ms DROPOUT
  - CAN CAUSE WDD TO ENTER REACQ MODE, TAKING ONE-HALF TO FOUR SECONDS
  - POSSIBILITY OF NARROWING LOCK DETECTOR FILTER BW TO RIDE OVER 2.5 TO 5 ms DROPOUTS
  - THIS IS THE GREATEST POTENTIAL SOURCE OF DATA LOSS  
--RECOMMEND AXIOMATIX BE PUT IN CONTACT WITH HARRIS

ORIGINAL PAGE IS  
OF POOR QUALITY



- INVESTIGATED FEASIBILITY OF CHANGING SOFTWARE OR HARDWARE TO IMPLEMENT DPSK
  - NOT FEASIBLE
  
- REVIEWED HARRIS WDD SPECIFICATIONS
  - REVIEWED HARRIS' SPECIFICATIONS ON TDRSS SSAR WDD
  - ONLY ISSUE RELATED TO LOSS OF LOCK WAS
    - LOSS OF PN AND CARRIER LOCK SHALL HAVE MEDIAN REACQUIRE TIME OF  $\leq 20$  s AS DESIGN GOAL (pp 61, PIPF SPEC, DECEMBER 20, 1983)
  
- RECOMMEND TELEPHONE CONFERENCE WITH HARRIS ON OPERATION OF LOCK DETECTOR IN WPD RECEIVER TO DETERMINE IF IT CAN BE MODIFIED TO RIDE OVER  $2\frac{1}{2}$  - 5 ms DROPOUTS

ORIGINAL PAGE IS  
OF POOR QUALITY

- ART RUBINS INDICATES MID-SEPTEMBER DATE FOR COMPUTER RUN
  - HAS INDICATED THAT ANNEX TO PIP IS REQUIRED
  
- HIS PRELIMINARY (UNOFFICIAL) APPRAISAL OF FREQUENCIES IS THAT THERE IS NO PROBLEM
  - RECOMMENDS SHUTTLE 2217 5 TRANSMIT
  
- RECOMMENDS NOT USING FM TRANSMITTER ON UPPER HEMI DURING MISSION
  - BASED ON SPA'S AND IUS

ORIGINAL PAGE IS  
OF POOR QUALITY



RESULTS OF COSMIC-RAY/DCU MEMORY STUDY

BY

AXIOMATIX

AUGUST 4, 1983

ORIGINAL PAGE IS  
OF POOR QUALITY

● ACTION ITEM

- DETERMINE THE EFFECT OF COSMIC RAYS ON CENTAUR'S DCU TELEMETRY BUFFER RAM (16 k, 4X H6514 CMOS RAM)

● SPECIFICS

- ESTABLISH BER CONTRIBUTION DUE TO RANDOM BIT FLIPS CAUSED BY HIGH-ENERGY PARTICLES

● FINDINGS

- RANDOM BIT FLIPS MAKE ONLY A NEGLIGIBLE CONTRIBUTION ( $\approx 10^{-9}$ ) TO TELEMETRY BIT RATE OF  $10^{-5}$
- LATCH-UPS, HOWEVER, CAUSE PERMANENT DAMAGE WHICH MAY AFFECT THE PERFORMANCE OF THE TELEMETRY LINK

● RECOMMENDATION

- USE RADIATION-HARDENED RAM TO REDUCE THE PROBABILITY OF SEVERE TELEMETRY-LINK DEGRADATION

● SINGLE-EVENT UPSETS (SEU) IN SEMICONDUCTOR MEMORIES ARE OF TWO TYPES:

- BIT FLIPS
  - SOFT ERRORS
  - DEVICE CAN BE WRITTEN OVER
  
- LATCH-UPS
  - LARGE CURRENTS ARE DRAWN
  - DEVICE BURNOUT RESULTS

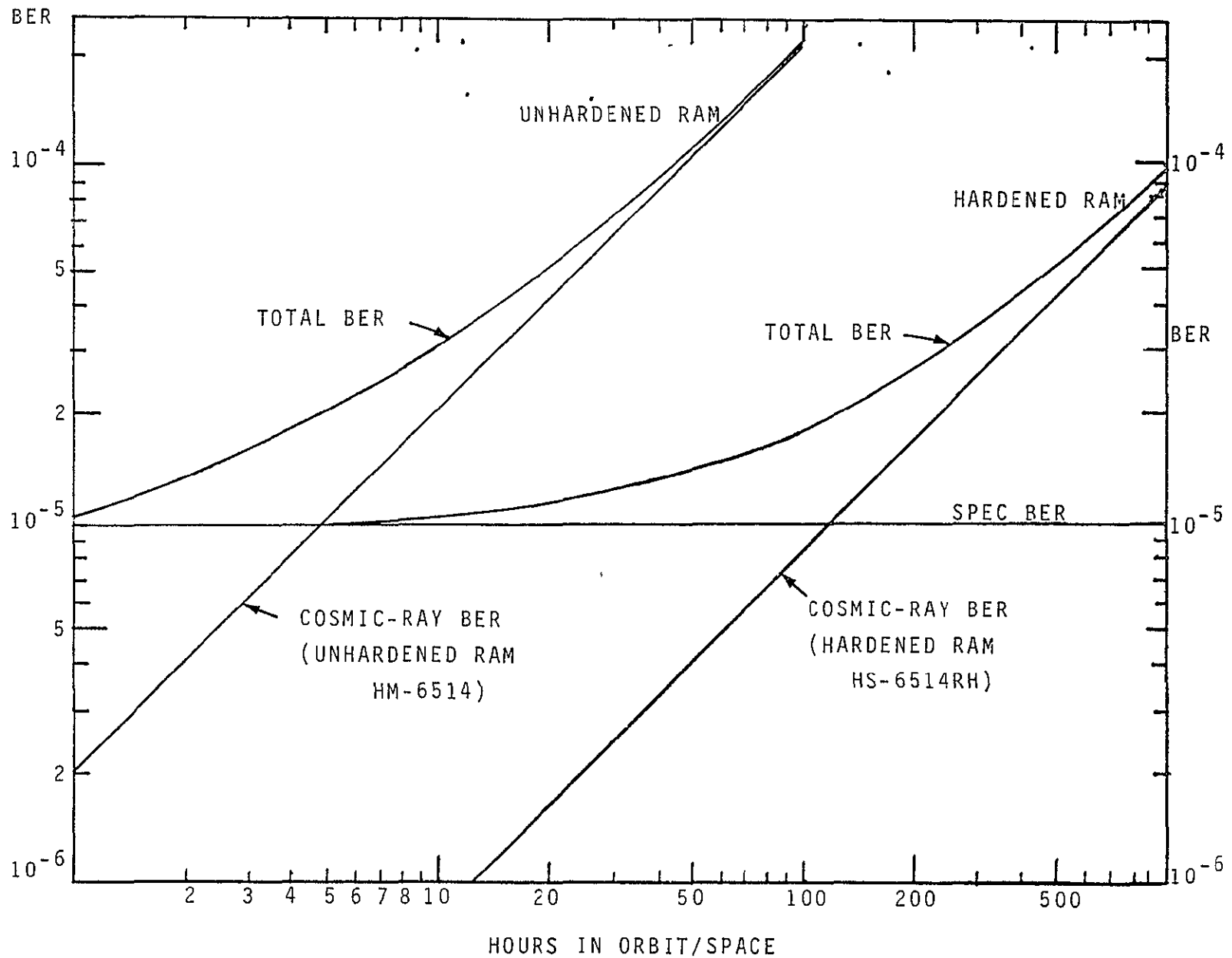
● RELATIVE FREQUENCY OF OCCURENCE OF SEU'S FOR CMOS RAM\* (WORST CASE)

<u>SEU</u>	<u>UNHARDENED</u>	<u>HARDENED</u>	
BIT FLIPS	$10^{-4}$	$4 \times 10^{-6}$	} EVENTS/BIT/DAY
LATCH-UPS	$10^{-4} - 10^{-6}$	$4 \times 10^{-6}$ TO $4 \times 10^{-8}$	

ORIGINAL PAGE IS  
OF POOR QUALITY

---

\*HM-6508, HM-6504 AND HM-6514 FAMILY BY HARRIS SEMICONDUCTOR DIVISION



ORIGINAL PAGE IS  
OF POOR QUALITY

- BIT-FLIP ERROR RATE (COSMIC-RAY UPSETS)

$$R_e \left( \frac{\text{ERRORS}}{\text{SEC}} \right) = R_u \left( \frac{\text{ERRORS}}{\text{DAY-BIT}} \right) \times \frac{1}{86,400} \left( \frac{\text{DAYS}}{\text{SEC}} \right) \times \text{RAM SIZE (BITS)}$$

- UNHARDENED RAM

$$R_e = 10^{-4} \left( \frac{\text{ERRORS}}{\text{DAY-BIT}} \right) \times \frac{1}{86,400} \left( \frac{\text{DAYS}}{\text{SEC}} \right) \times (16 \times 10^4) \text{ (BITS)} = \underline{\underline{1.852 \times 10^{-5} \text{ ERRORS/S}}}$$

EQUIVALENT BER FOR COSMIC-RAY BIT FLIPS

$$\text{BER}_{\text{CR}} = \frac{1.852 \times 10^{-5} \text{ ERRORS/S}}{1.6 \times 10^{-4} \text{ BITS/S}} = \underline{\underline{1.158 \times 10^{-9} \text{ ERRORS/BIT}}}$$

RELATIVE RATES  $1.158 \times 10^{-9} \ll 10^{-5}$   
(BIT FLIPS) (LINK SPEC)

- CONCLUSION

COSMIC RATE NOT A DRIVER FOR HARDENED RAM REQUIREMENT

ORIGINAL PAGE IS  
OF POOR QUALITY

C E N T A U R   P A N E L   M E E T I N G

AXIOMATIX/GENERAL DYNAMICS/NASA

MARCH 24, 1983

- FREQUENCY STABILITY FOR PSP/DCU INTERFACE
  - RESOLVED BY SPECIFICATION CHANGE TO 0.04% OF DATA RATE
  
- BIT JITTER MEASUREMENT TECHNIQUE
  - SEE PRESENTATION FOR STATUS
  
- ERROR RATE ALLOCATION FOR DCU RAM
  - SEE PRESENTATION FOR STATUS

ORIGINAL PAGE IS  
OF POOR QUALITY

ORIGINAL SPECIFICATION (DCU/PCM TELMETRY SYSTEM PDR DATA, DECEMBER 1982)--TELEDYNE SPEC.

- BIT JITTER (¶ 3.6 9 4 3 2)--THE TIME DISPLACEMENT OF A BIT START IN AN INTERVAL OF 320 BITS RELATIVE TO THE NOMINAL START TIMES ESTABLISHED BY AN AVERAGE OVER THE PRECEDING INTERVAL OF 400 BITS SHALL NOT EXCEED 0.5% OF THE BIT PERIOD. BIT JITTER REFERS TO THE SYMBOL JITTER RATE WHEN THE DATA IS CODED.
- BIT JITTER RATE (¶ 3 6 9 4 3.3)--THE PEAK BIT CLOCK FREQUENCY JITTER RATE (SINUSOIDAL OR 3σ RANDOM) SHALL NOT EXCEED 0 5% OF THE BIT CLOCK FREQUENCY. BIT JITTER RATE REFERS TO THE SYMBOL JITTER RATE WHEN THE DATA IS CODED.

REPLACED BY

- TDRSS USER GUIDE, REVISION 4 (PAGES I-2,3, DCN 004)

NOTE PAYLOAD DATA INTERLEAVER (PDI) HAS NO BIT JITTER SPECIFICATION. THUS, BIT JITTER PERFORMANCE IS DICTATED BY TDRS LINK OPERATION

ORIGINAL PAGE IS  
OF POOR QUALITY



- TDRSS USERS' GUIDE, REVISION 4, DEFINES BIT JITTER FOR THE FOLLOWING TWO REQUIREMENTS

1 BIT ERROR RATE (BER)

2. BIT SLIP RATE (BSR)

ORIGINAL PAGE IS  
OF POOR QUALITY

APPROACHES IN ORDER OF PREFERENCE

- 1 FIND COMMERCIALLY AVAILABLE OFF-THE-SHELF EQUIPMENT AND USE IT  
"AS IS"
  
- 2 PURCHASE OFF-THE-SHELF EQUIPMENT AND MODIFY IT TO DO THE JOB
  
- 3 DESIGN AND BUILD A BIT JITTER TESTER

ORIGINAL PAGE IS  
OF POOR QUALITY

COMPANIES CONTACTED REGARDING BIT-JITTER TEST EQUIPMENT

	<u>APPLICABLE EQUIPMENT</u>
HEWLETT PACKARD	YES
TAU-TRON	NO
AYDIN MONITOR	NO
DATA CHECK CORPORATION	YES
HEKIMIAN LABORATORIES	YES*
DECOM SYSTEMS INC.	NO
ACROMATICS	NO
FAIRCHILD WESTON SYSTEMS, INC	YES

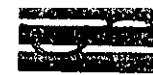
ORIGINAL PAGE IS  
OF POOR QUALITY

\* DISCONTINUED

EQUIPMENT APPLICABLE TO BIT JITTER TESTING

<u>MANUFACTURER</u>	<u>MODEL/FUNCTION</u>	<u>COMMENTS</u>
HEWLETT PACKARD	3785A JITTER RECEIVER	<ol style="list-style-type: none"> <li>1 DESIGNED FOR 2048 Kbps AND UP</li> <li>2 REQUIRES RECLOCKING OF DATA STREAM WITH A HIGHER CLOCK</li> </ol>
HEWLETT PACKARD	5370A UNIVERSAL TIME-INTERVAL COUNTER	<ol style="list-style-type: none"> <li>1. OPERATES DIRECTLY ON THE TIME-DOMAIN STRUCTURE OF PCM DATA TRANSITIONS</li> <li>2 MAY REQUIRE ADDITIONAL EQUIPMENT TO PROVIDE FREQUENCY ANALYSIS OF JITTER</li> </ol>
FAIRCHILD WESTON SYSTEMS, INC	EMR MODEL 721 TELEMETRY BIT-ERROR RATE DETECTOR	<ol style="list-style-type: none"> <li>1. HAS OUTPUT SIGNAL PROPORTIONAL TO BIT JITTER</li> <li>2. MAY REQUIRE ADDITIONAL EQUIPMENT TO PROVIDE FREQUENCY ANALYSIS OF JITTER</li> </ol>
DATA CHECK CORP	8300 A-W FLUTTER METER	<ol style="list-style-type: none"> <li>1 PROVIDES DIRECT READOUT OF PERCENT JITTER</li> <li>2 BUILT-IN FREQUENCY-ANALYSIS CAPABILITY</li> <li>3. REQUIRES CHANGE OF INTERNAL CRYSTAL REFERENCE TO EXTERNAL CLOCK INPUT</li> </ol>

ORIGINAL PAGE IS OF POOR QUALITY



- CENTAUR TELEMETRY LINK BER IS SPECIFIED AT  $10^{-5}$
- DCU'S TELEMETRY BUFFER USES SEMICONDUCTOR DEVICES FOR RAM
- SEMICONDUCTOR DEVICES ARE SUBJECT TO SINGLE-EVENT UPSETS (SEU'S) DUE TO COSMIC RAY EXPOSURE
- SEU'S CAUSE BIT FLIPS IN SEMICONDUCTOR RAM'S

ACTION ITEM ESTIMATE BER VALUE DUE TO SEU'S IN CENTAUR TELEMETRY BUFFER RAM

NOTE PRESENT ALLOCATION IS  $10^{-9}$  (GENERAL DYNAMICS' ESTIMATE)

ORIGINAL PAGE IS  
OF POOR QUALITY

ACTION ITEM STATUS REPORT

- SEMICONDUCTOR MANUFACTURERS (HARRIS, MOTOROLA, INTEL, ETC.) WERE CONTACTED REGARDING COSMIC RAY EFFECTS
- MANUFACTURERS ARE AWARE OF NUCLEAR-BLAST-HARDENING PROGRAMS, BUT COULD NOT SUPPLY INFORMATION ON COSMIC RAY EFFECTS
- JET PROPULSION LABORATORIES (JPL) WAS CONTACTED AND PERTINENT INFORMATION RECEIVED\*
- AXIOMATIX IS EVALUATING THE JPL DATA AND WILL FOLLOW UP WITH RELATED REFERENCE MATERIAL

\* JPL REPORT TITLED "SINGLE-EVENT UPSET (SEU) OF SEMICONDUCTOR DEVICES--A SUMMARY OF JPL TEST DATA" (JUNE 1982)

ORIGINAL PAGE IS  
OF POOR QUALITY

• ERROR RATE CONTRIBUTION (ESTIMATE) DUE TO SEU'S

- COSMIC RAY HIT RATE = 1 HIT/SECOND/cm<sup>2</sup>
- HIT RATE OF RAM AREA = RAM AREA x HIT RATE  
= 0.01 cm<sup>2</sup> x 1 = 0.01 HITS/SECOND

<u>SYMBOL RATE (KSPS)</u>	<u>LINK ERRORS/SEC. BER = 10<sup>-5</sup></u>	<u>COSMIC RAY HIT CONTRIBUTION</u>	<u>COSMIC RAY EFFECTIVE BER</u>
32	0.32	$\frac{0.01}{0.32} = 3.1 \times 10^{-2}$	$3.1 \times 10^{-2} \times 10^{-5} = \underline{3.1 \times 10^{-7}}$
64	0.64	$\frac{0.01}{0.64} = 1.6 \times 10^{-2}$	$1.6 \times 10^{-2} \times 10^{-5} = \underline{1.6 \times 10^{-7}}$

• OTHER FACTORS TO CONSIDER

- ACTUAL AREA OF RAM
- ENERGY DISTRIBUTION OF COSMIC RAYS

ORIGINAL PAGE IS OF POOR QUALITY

SOURCE NAME	CENTER FREQUENCY	MAXIMUM EIRP	MODULATION	MODULATION INDEX	MAXIMUM SYMBOL RATE
CENTAUR	2267.5	11.4 dBW	BPSK DATA DIRECT OR BPSK BY 1.024-MHz SUBCARRIER	90°	64 KSPS
	OR 2272.5			90°	64 KSPS
SSO	2287.5	17.6 dBW	BPSK	90°	384 KSPS
	OR 2217.5				
TDRSS	2106.4	4.4 dBW	BPSK	90°	3 MCPS
	OR 2041.9				
GALILEO	2295.0	75.0 dBW	PM	80°	57.6 KSPS
	OR 2296.481481				
	8415.000000	93.0 dBW	PM	67.6°	286.8 KSPS
	OR 8420.432097				

ORIGINAL PAGE IS  
OF POOR QUALITY

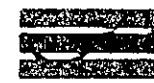
WHEN GALILEO S&X ARE TRANSMITTED SIMULTANEOUSLY, X SYMBOL RATE IS LIMITED TO 1200 SPS.





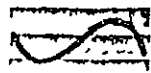
- RECOMMENDATIONS FROM LAST PANEL MEETING HAVE BEEN INCORPORATED
  
- MAJOR CHANGE
  - REMOVE PROGRAM-SPECIFIC PARAGRAPHS FROM MAIN BODY AND PUT THEM IN THE APPENDIX
  
  - APPENDIX IS PRESENTLY TBD
  
- COPIES AVAILABLE FOR DISTRIBUTION TO PANEL MEMBERS, JSC, LeRC, GDC

ORIGINAL PAGE IS  
OF POOR QUALITY



- TDRSS SELF-INTERFERENCE
  - REVIEWED STI REPORT
    - "AN ASSESSMENT OF THE IMPACT OF TDRSS SELF-INTERFERENCE ON COMMUNICATION PERFORMANCE," 9/10/82 (CLASSIFIED)
  - CONCLUSION NO SELF-INTERFERENCE DUE TO FREQUENCY SEPARATION
  
- INTERMOD ANALYSIS DUE TO MULTIPLE RF SOURCES
  - SSO, TDRSS, CENTAUR, GALILEO (S&X)
  - SUBMITTED DATA TO ART RUBINS FOR COMPUTER PROGRAM RUN

ORIGINAL PAGE IS  
OF POOR QUALITY



# Axiomatix

9841 Airport Boulevard • Suite 912 • Los Angeles, California 90045 • Phone:(213) 641 8600

November 5, 1982

Mr. Bob Godfrey  
NASA Goddard Space Flight Center  
Code 831.1  
Bldg. 12, Room 11232  
Greenbelt, Maryland 20771

ORIGINAL PAGE IS  
OF POOR QUALITY

Dear Bob

Enclosed please find the preliminary pertinent data for the Centaur telemetry system for the Galileo mission. As discussed at last weeks Centaur Panel meeting, this data is being supplied for the purpose of initiating a preliminary CLASS run. Since a released spec for the Centaur telemetry system was not available, this data must be considered preliminary.

I have also enclosed a sketch showing the approximate location of the antenna on the vehicle as well as some very preliminary antenna patterns. This information, combined with the roll rate information in table 1 should be helpful in determining signal amplitude modulation due to antenna motion.

At this moment I am still working on obtaining a range and range rate (to TDRSS) profile. Mr. Tom Jawoski of GSFC is helping me in this matter. Please call if I can be of assistance in interpreting the enclosed information.

Yours truly,

Peter Nilsen

Enclosures

Table 1  
Antenna Patterns  
Sketch of Antenna location

cc Mr. John MacLeod, NASA Johnson Space Center  
Mr. Heinz Weimer, NASA Lewis Research Center  
Dr. Walter Braun, Lincoln  
Mr. Mike Roberts, General Dynamics

TABLE 1: Summary of Preliminary Centaur (Galileo Mission) Telemetry System Characteristics

Minimum EIRP (16KBPS) (32KBPS)	:+11.4 dBW (assumes -1.5 dB ant gain) +14.4 dBW (assumes +1.5 dB ant gain)
Carrier Frequency (Primary) (Secondary)	2272.5 MHz $\pm$ .003% <i>2,270 / &gt;</i> 2267.5 MHz $\pm$ .003%
Data Format	.Rate 1/2 convolutionally encoded, B1 $\phi$ -L
Carrier Modulation	.B1-phase shift keyed ( $\pm 90^\circ$ )
Data Rate	.16 KBPS 32 KBPS
Transmitter Bandwidth	2.048 MHz <BW <TBS
Antenna Pattern	See Figures 1 & 2
Antenna Switching Transient Duration	.3 milliseconds

User Constraints

Data Asymmetry (peak)	$\pm 3\%$
Data Rise Time	$\leq 5\%$ of symbol duration
Data Bit Jitter	TBS
BPSK Phase Imbalance	$\pm 6^\circ$
Gain Imbalance	$\pm 25$ dB
Phase Nonlinearity,	$\pm 3^\circ$ over $\pm 150$ KHz
Gain Flatness	+ 3dB over $\pm 150$ KHz
Gain slope (peak)	$\pm .1$ dB/MHz over $\pm 150$ KHz
AM/PM	$\leq 12$ deg/dB
Frequency Stability (peak)	$\pm 3 \times 10^{-9}$ over 1 second $\pm 1 \times 10^{-7}$ over 5 hours $\pm 3 \times 10^{-7}$ over 1 year
Incidental AM	The RSS of all amplitude modulations $\leq 5\%$

Composite Spurious Outputs  
 within  $\pm 2$  x channel BW  $\geq 29.8$  dBc  
 outside  $\pm 2$  x channel BW  $\geq$  TBD  
 Phase Noise  
     1-10Hz 5° Rms  
     10-100Hz 1° Rms  
     100-1000Hz 1° Rms  
     1000-128KHz 1° Rms

ORIGINAL PAGE IS  
 OF POOR QUALITY

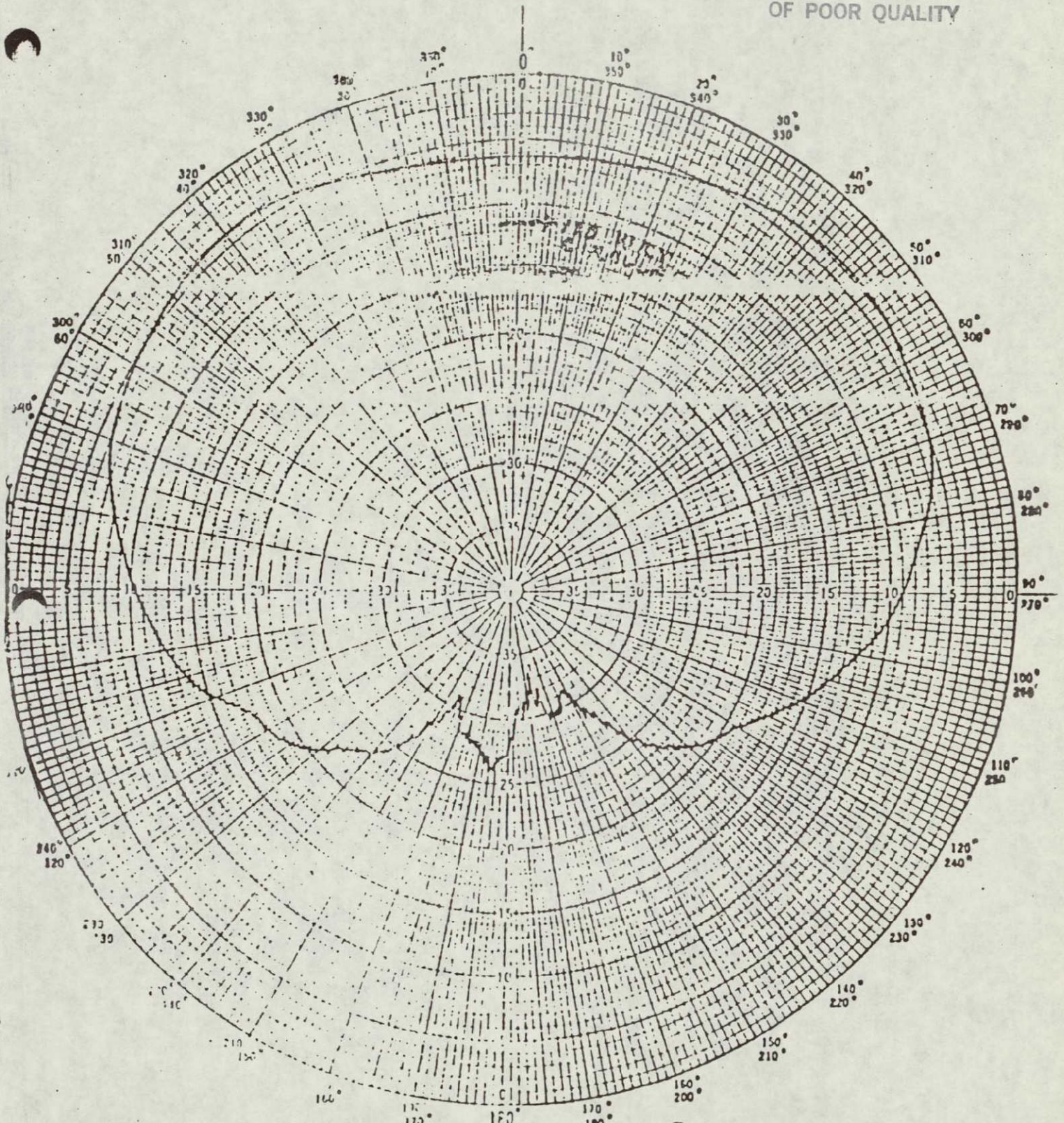
Centaur Vehicle Events  
(Galileo Mission)

<u>Event</u>	<u>Time*</u>
Separation from SSO	5.31:25
Activate RF Link to TDRSS W(16KBPS)	5 45:05
Reorient Centaur to Burn Altitude	5 59.49
Switch to 32 KBPS	6 01 05
TDRSS E, Signal Lock on	6 16 00
Start Centaur Burn (Powered Flight)	6:17 49
Centaur MECO (End Powered Flight)	6 27:31
Switch to 16 KBPS Format	6 27 31
Begin 1/2 RPM Roll	6.28.01
Increase Roll to 1.0 RPM	7.00 30
Separate S/C	7.03 51
Reorient to Retro Vector	7 08.52
Deflection Maneuver	7 10.22
Deflection Maneuver	7 11 12
Terminate Centaur Operations	7 17 37

\* Time is relative to Orbiter Launch at 0 00 00

Centaur Vehicle Dynamics  
(Galileo Mission)

Range Profile to TDRSS . TBD  
Range Rate Profile to TDRSS . TBD

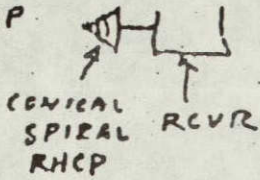


Handwritten text: *100 WATT*

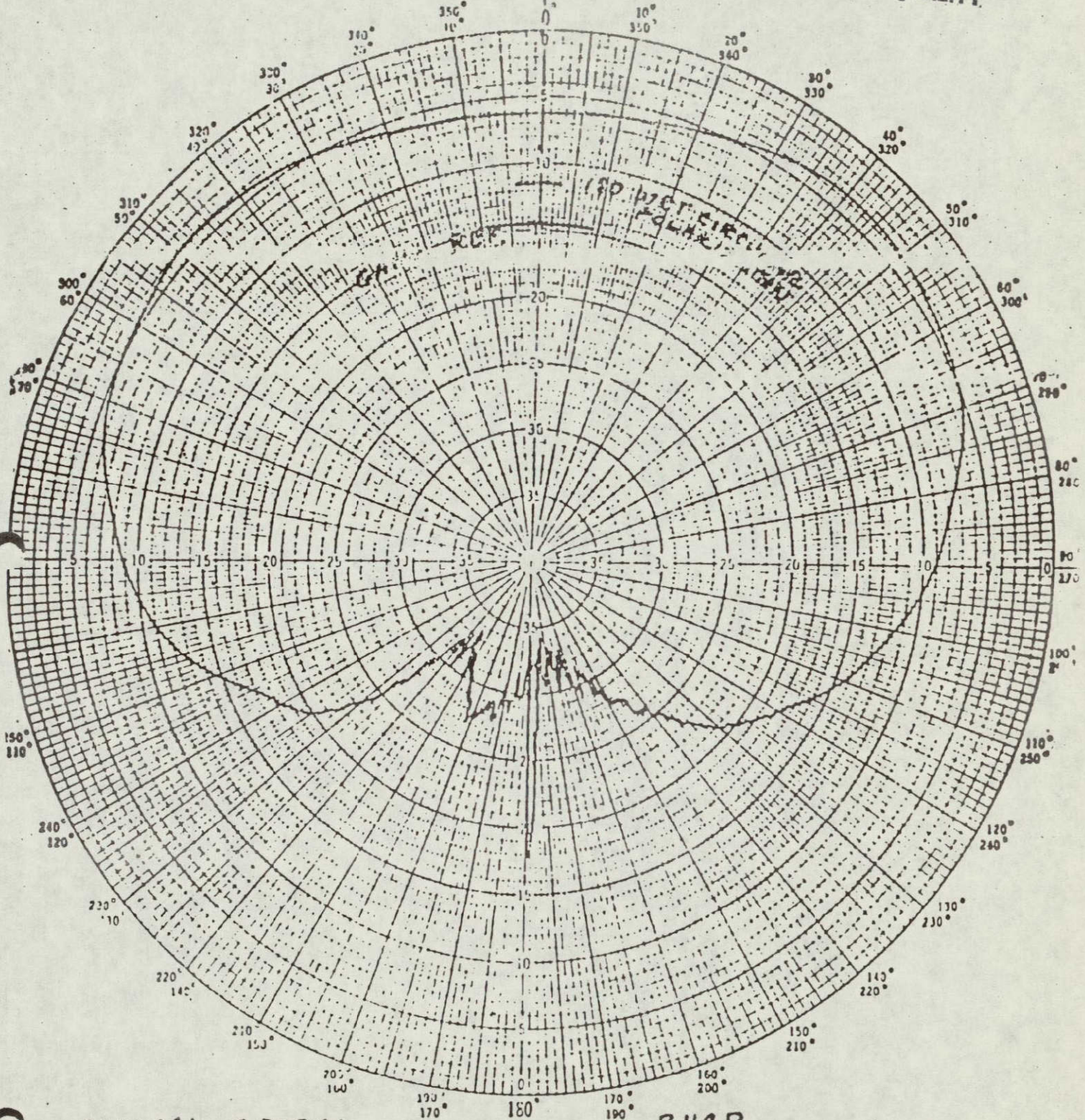
TYPE CONICAL SPIRAL  
 Q: 2.05:1 SCALE 200 MHz  
 FREQUENCY \_\_\_\_\_  
 CREATOR \_\_\_\_\_ DATE \_\_\_\_\_  
 NO. \_\_\_\_\_ FILE NO. \_\_\_\_\_

POLARIZATION RH-P VARIABLE ANGLE \_\_\_\_\_  
 PATTERN PLANE EQ (YAW) GROUND PLANE \_\_\_\_\_  
 AIRCRAFT PATTERN PLANE \_\_\_\_\_  
 PITCH ( ) | ROLL ( ) | YAW ( )

RHCP



ORIGINAL PAGE IS OF POOR QUALITY



CONICAL SPIRAL

POLARIZATION RHCP VARIABLE ANGLE \_\_\_\_\_

PATTERN PLANE E @ (PITCH) GROUND PLANE \_\_\_\_\_

AIRCRAFT PATTERN PLANE \_\_\_\_\_

SCALE 2.05:1 SCALE FREQUENCY 2250 MHz

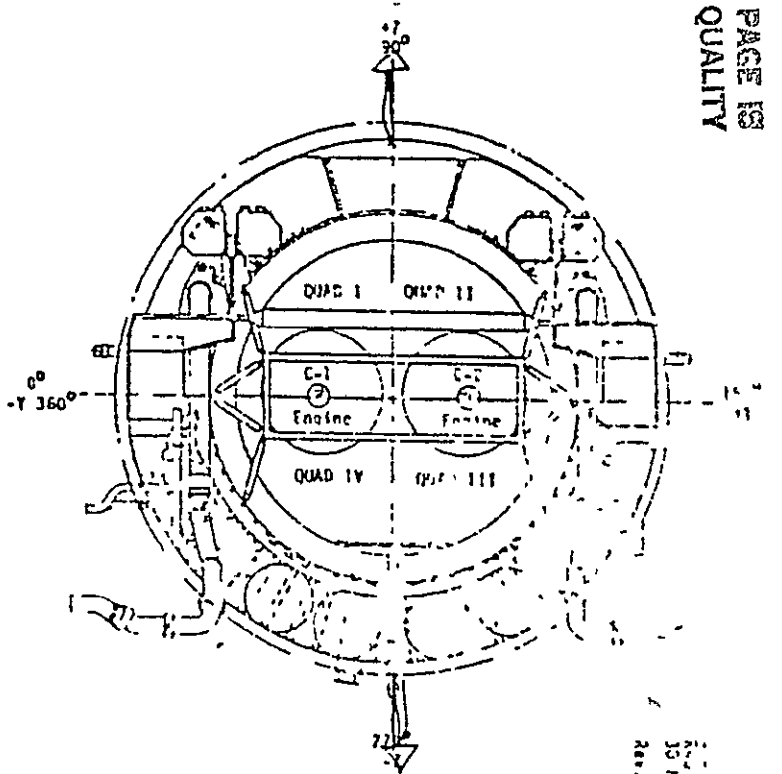
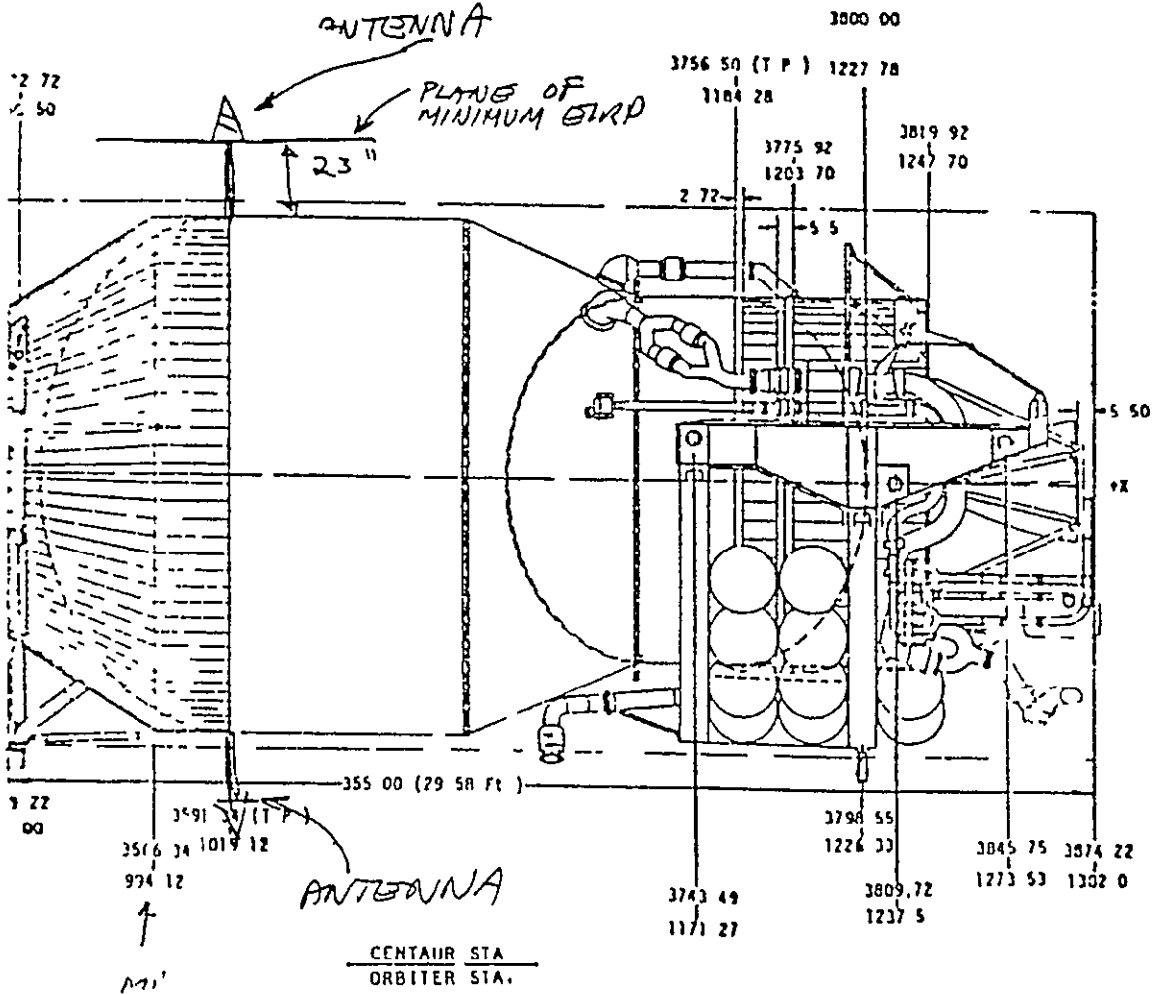
PITCH : 1 ROLL : 1 YAW

DATE \_\_\_\_\_

FILE NO \_\_\_\_\_



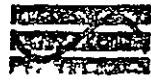




Rev. 02 - 14 October 1962

ORIGINAL PAGE IS  
OF POOR QUALITY

CALL BOB GODFREY 344-9160 FOR PICK UP



Axiomatix

9841 Airport Boulevard • Suite 912 • Los Angeles, California 90045 • Phone (213) 641 8600

December 8, 1982

Mr Bob Godfrey  
NASA Goddard Space Flight Center  
Code 831.1  
Bldg. 12, Room N232  
Greenbelt, Maryland 20771

Dear Bob:

Attached is an update on the Centaur parameters that I just received from GDC. Please reflect these in your CLASS run. Also, the CLASS run should include the effects of interference from the Shuttle's S-Band TDRSS link. The pertinent parameters for this link are:

FREQUENCY • 2287.5 MHz

EIRP : 17.7 dBw

SYMBOL RATE 576 ksps

MODULATION . BPSK

Please call if I can be of assistance

Yours truly,

Peter Nilsen

Attachment

PN.sp

ORIGINAL PAGE IS  
OF POOR QUALITY

Summary of Preliminary Centaur Telemetry System Characteristics for Transmissions to TDRSS

**Data Rate:** 16 Kbps or 32 Kbps, varies during the mission

**Minimum EIRP:** + 11.4 dBW (16 Kbps)  
+ 14.4 dBW (32 Kbps)

**Data Format:** Rate 1/2 convolutionally encoded, NRZ-L

**Carrier Frequency** (Primary) 2272.5 MHz  $\pm$  0.003%  
(Secondary) 2267.5 MHz  $\pm$  0.003%  
Selection of operating frequency made prior to launch

**TDRSS return link service:** S-band single access, data Group 2, BPSK modulation

**Antenna polarization:** Right hand circular

**Antenna switching action:** Make before break RF switch  
(Phase and amplitude transients are not controlled during switching)

**Antenna switching transient duration:** 3 milliseconds maximum

**Antenna switching rate** (Varies during the mission)  
1 switch/5 minutes or  
1 switch/ 1 minute or  
1 switch/ 30 seconds or  
1 switch/ 10 seconds or  
1 switch/ 6 seconds (ISPM mission only)

**Maximum RF emissions:** 0 dBc within  $F_c \pm 1.2$  MHz  
-60 dBc outside  $F_c \pm 12.1$  MHz  
falling 18 dB/octave between  
 $F_c \pm 1.2$  MHz and  $F_c \pm 12.1$  MHz

Preliminary Centaur TDRSS User Constraint Values

<u>Parameter</u>	<u>Centaur Limit</u>	<u>User Constraint</u>
Data Asymmetry (peak)	3%	3%
Data Rise Time	5% of symbol time	5% of symbol time
Data Bit Jitter (weighted):		
For BER requirements	0.52 radians	0.52 radians
For BSR requirements	0.60 radians	0.60 radians
BPSK Phase Imbalance	6.8 degrees	6.0 degrees
Gain Imbalance	0.05 dB	0.25 dB
Phase Nonlinearity (peak)	3 degrees over $\pm 75$ KHz	3 degrees over $\pm 3.5$ MH
Gain Flatness (peak)	0.05 dB over $\pm 75$ KHz	0.3 dB over $\pm 3.5$ MI
Gain Slope	0.1 dB/MHz over $\pm 75$ KHz	0.1 dB/MHz over $\pm 3.5$ MHz
M/PM	15 degrees/dB	12 degrees/dB
Frequency Stability (peak)	$\pm 3 \times 10^{-9}$ over 1 second $\pm 1 \times 10^{-7}$ over 5 hours $\pm 3 \times 10^{-7}$ over 1 year	$\pm 3 \times 10^{-9}$ over 1 sec. $\pm 1 \times 10^{-7}$ over 5 hours $\pm 3 \times 10^{-7}$ over 1 year
Incidental AM (peak)	1.5%	5%
Untracked Spurious PM (Note 1)	2° RMS	2° RMS
Untracked Phase Noise (Note 1)	3° RMS	3° RMS
3 dB Bandwidth (minimum)	2.3 MHz	128 KHz

Note 1: The untracked phase noise and untracked spurious PM values are for operation with a 2nd order carrier tracking loop with a one-sided bandwidth of 2.3% of the symbol rate (i.e. - 735 Hz for the 16 Kbps data rate, and 1470 Hz for the 32 Kbps data rate.)

4.0 ORBITER-VEHICLE/CENTAUR HARDLINE ICD

C-3

Electrical and electronic interfaces are defined in this section for each test, checkout, and Launch functional operation or family of operations required to be accomplished through the interfaces between the Orbiter Vehicle and the CCE. The functional, performance, and design requirements are defined according to the primary subsystem through which the function is accomplished on the Space Shuttle Vehicle. Interface performance and design requirements are uniquely defined for the individual functions or family of functions and the physical provisions identified by reference to the interface number and mating part identification.

### 5.1 General Requirements

The following general requirements and constraints are applicable to all Electrical/Electronic interface functions unless otherwise stipulated for a specific function.

#### 5.1.1 Electromagnetic Compatibility

##### 5.1.1.1 CCE EMI Test Requirements

The individual CCE subsystems/equipments shall meet the EMI requirements as specified in MF0004-002B.

The RSO3 test level shall be 2v/m from 14 KHz to 10 GHz except at S-Band (1.7 GHz to 2.3) GHz, the test level shall be 25 v/m and at Ku-Band (13 GHz to 15 GHz) the test level shall be 10 v/m.

##### 5.1.1.2 Ku-Band Radar Beam

If the Ku-Band radar main beam intersects the Centaur during erection or deployment from the payload bay, exposure levels could reach 200 v/m.

##### 5.1.1.3 Bonding

###### 5.1.1.3.1 Subsystem and System

The CCE subsystem/equipment and the CCE integrated system shall be bonded in accordance with MIL-B-5087.

###### 5.1.1.3.1.1 CISS to Orbiter

The CCE shall be bonded to the Orbiter as shown in Fig 3.3-8 of ICD-2-AF002.

###### 5.1.1.3.1.2 CISS to Deployment Adapter (Centaur Responsibility)

The CISS to deployment adapter bonding shall meet MIL-B-5087, Class R requirements.

## INTERFACE CONTROL DOCUMENT

ORBITER-VEHICLE/CENTAUR	SIZE	ICD NO	REV	SHEET <u>107</u>
	A	ICD-2-1F001	NC	OF _____

5.1.1.3.1.3 The Deployment Adapter to Centaur (Centaur Responsibility)

The Deployment adapter to the Centaur shall be RF bonded in accordance with MIL-B-5087, Class R requirements.

5.1.1.3.2 Payload Attach Fittings

The active and passive payload attach fittings are non-conductive; therefore, they do not provide a bond between the CCE and the Orbiter.

5.1.1.4 Static Charge Protection

All CCE metallic and non-metallic surfaces shall be bonded in accordance with MIL-B-5087 to prevent static charge build up.

5.1.1.5 Explosive Devices

All explosive devices used on the CCE shall meet the requirements of the Space Shuttle Pyrotechnic Specification, JSC 08060, the Air Force Eastern Test Range Safety Manual Volume 1, AFETRM 127-1 and the Western Test Range Safety Manual, SAMTEC 127-1.

5.1.1.6 EMC Circuit Classification

CCE power and signal circuits which interface with the Orbiter shall meet the EMC classification requirements of Table 5.1-1 at the CCE/Orbiter interface.

5.1.1.7 Circuit Isolation Requirements

CCE circuits which interface with the Orbiter shall meet the signal and power isolation requirements of Paragraph 3.4.10.1 of MF0004-002B. Coaxial circuits must meet the isolation requirement. If these requirement conflict with specific isolation requirements in this ICD the latter requirement shall be applicable.

5.1.1.8 Lightning Protection

Lightning protection shall be provided in accordance with induced field levels as defined in JSC-07636. Lightning protection of new electrical equipment shall be accomplished by satisfying the pulse voltage requirement in Paragraph 5.1.1.9.

ORIGINAL PAGE IS  
OF POOR QUALITY

INTERFACE CONTROL DOCUMENT

ORBITER-VEHICLE/CENTAUR	SIZE	ICD NO	REV	SHEET
	A		ICD-2-1F001	NC

Where is asterisk

ORIGINAL PAGE IS  
OF POOR QUALITY

5.1.1.9 Pulse Voltage Requirement

The equipment shall be designed to withstand a pulse voltage transient applied during normal operating conditions without sustaining damage, malfunction, or upset. Power circuits and signal circuits that reference vehicle structure ground at both terminations shall be designed to withstand a common mode (applied from line to structure ground) 500\* volt square pulse using a source impedance of one (1) ohm or less for 50 microseconds. All other signal circuits shall be designed to withstand a common mode (applied from line to structure ground) 500\* volt square pulse using a source impedance of one (1) ohm or less for 5 microseconds.

Note: The 500 volt pulse amplitude may be reduced after the wiring is defined and voltage levels determined.

5.1.2 Circuit Protection

Circuit malfunction protection shall be provided to prevent failure propagation through the Orbiter Vehicle/Centaur interfaces. The specific circuits requiring protection, location of circuit protection function relative to interface and protection circuit interfaces defined herein.

5.1.3 Electrical Interface Tabulations

Electrical interface functional, performance, and design criteria are defined by use of electrical interface tabulations. Table 5.1-2 identifies the CCE to Orbiter services at the port CISS interface (OC-11); Table 5.1-3 identifies the CCE to Orbiter services at the starboard CISS interface (OC-12), Table 5.1-4 identifies the CCE to Orbiter T-0 umbilical services at the port CISS interfaces (OC-11); and Table 5.1-5 identifies the CCE to Orbiter T-0 umbilical services at the starboard CISS interface (OC-12). The content of the electrical interface tabulation is defined as follows.

5.1.3.1 Connector Identification

Interface electrical connectors are identified by corresponding "J-No." and "P-No." and the respective part numbers. The connector identification numbers are used in conjunction with the interface number and figure reference to cross index to the physical interface definition given in Section 3.0.

5.1.3.2 Interface Number

The interface identification as defined in paragraph 1.2, for the physical interface through which the particular interface functions are implemented.

5.1.3.3 Reference Figure Numbers

A direct reference to the applicable figure is section 3.0 which defines the physical interface provisions for the given electrical connector.

INTERFACE CONTROL DOCUMENT

ORBITER-VEHICLE/CENTAUR	SIZE A	ICD NO ICD-2-1F001	REV NC	SHEET 09 OF
-------------------------	-----------	-----------------------	-----------	----------------



5.1.3.4 Pin Identification

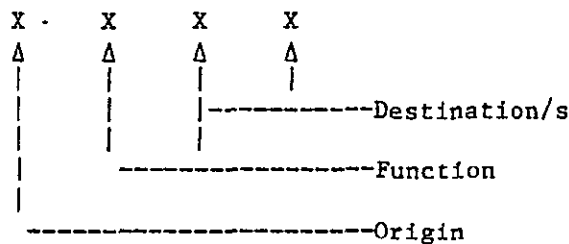
The individual contact within the mating connector halves through which the electrical function is transmitted. The pin identification letter is the same as the pin designation on the connector halves.

5.1.3.5 Function

The descriptive title of the functional operation(s) which the interface is designed to fulfill.

5.1.3.6 Origin/Command or Response

Definition of the Signal source and if it is a command or response.



Origin & Destination

- O - Orbiter
- G - Ground Support Equipment
- L - Launch Processing System
- P - Centaur Element

Function

- C - Command
- R - Response
- S - Source

5.1 3.7 Orbiter Wire Gage AWG

AWG wire size used on the Orbiter Vehicle side of the interface

5.1.3.8 Centaur Wire Gage AWG

AWG wire size used on the CCE side of the interface.

5.1.3.9 Connector (Conn) Pin Gage AWG

AWG size of contact used in both halves of the interface connector.

5.1.3.10 Voltage (Volt LVL)

The voltage or voltage range and tolerances thereon required to be delivered at the 'design to' interface to fulfill the functional requirement.

INTERFACE CONTROL DOCUMENT

ORBITER-VEHICLE/CENTAUR	SIZE	ICD NO	REV	SHEET
	A		NC	110
		ICD-2-1FOOL	OF	

5.1.3.11 Load

The circuit design load or load range and tolerances thereon defined by parameters appropriate to the imposed load (current, impedance, etc.) required to fulfill the functional requirements.

5.1.3.12 Description

The wire type required from both sides of the interface according to the following codes:

- SC = Single Conductor
- TP-X = Twisted Pair  
(wire twisted with wire)
- TT-X, Y = Twisted triplet  
(wire twisted with wire X and Y)
- TQ-X, Y, Z = Twisted quadruplet  
wires twisted together
- T6 = Six wires twisted together
- TSP = Twisted shielded pair
- TST = Three wires twisted together and shielded
- TSQ = Four wires twisted together and shielded
- X(s) = Indicated pin used for shield
- T5C = Twisted five conductor
- TS5C = Twisted shielded five conductor

5.1.3.13 Circuit Classification (CKT CLAS)

The Electromagnetic Interference (EMI) circuit classification according to codes and design criteria defined in SD73-SH-0216, Space Shuttle Electromagnetic Effects Control Plan.

5.1.3.14 Ground Location (GND LCT)

The required location of electrical ground in terms of Orbiter Vehicle or Centaur ground. The codes listed below indicate the location of circuit return or shield ground to structure.

- GND - Single Point Ground in Centaur
- ORB - Single Point Ground in ORB
- MPG - Grounded at each end and at each intermediate opportunity.
- BAL - Differential circuit not grounded at either end. Part of a balanced circuit.
- FL - Floating (transformer coupled). Not referenced to structure.

INTERFACE CONTROL DOCUMENT

ORBITER-VEHICLE/CENTAUR	SIZE A	ICD NO ICD-2-1F001	REV NC	SHEET III OF
-------------------------	-----------	-----------------------	-----------	-----------------

5.1.3.15 Circuit Protection (CKT PTCT)

The circuit protection required to prevent failure propagation through the interface as defined by parameters appropriate to the type of protection (min. voltage, max. voltage, limit current, time, or any combination thereof). Circuit protection shall be provided on the "origin" side of the interface unless otherwise noted.

The codes listed below indicate the circuit protection provided on the origin side of the interface.

- OA - Protected by Orbiter current limiting electronics
- OB - Protected by Orbiter power controller
- OC - Protected by Orbiter fuse
- OD - Protected by Orbiter voltage drop resistor
- QE - Protected by Orbiter relay
- GA - Protected by GSE current limiting electronics
- GND - Protected by LPS/GSE
- OP - Protected by Centaur current limiting electronics

5.1.3.16 T-0 Connector and Pin Number

Identifies the Orbiter T-0 umbilical termination of the Orbiter wiring for reference only. Applicable to Tables 5.1-3 and 5.1-4 only.

5.1.3.17 Cable Resistance

Provides the maximum wire resistance @ 200°F, from the CISS interface connector pin to the referenced T-0 umbilical connector pin. Applicable to Tables 5.1-3 and 5.1-4 only.

5.1.3.18 Notes

Notations of other specific requirements limitation or conditions applicable to the definition of the individual interface function.

5.1.4 Connector Deadfacing

Electrical deadfacing of interfacing connectors when mating or demating shall comply with JSCM-8080, Standard 69, except that connectors which mechanically demate in flight will not require deenergizing of signals prior to demating if the current on any single circuit does not exceed 500 milliamperes at the time of demate. Either the demated connector retained in the Orbiter cargo bay shall be the socket (female) side of the connector, or all power shall be removed from the connector prior to the entry phase of the flight.

INTERFACE CONTROL DOCUMENT

ORBITER-VEHICLE/CENTAUR	SIZE	ICD NO	REV	SHEET
	A	ICD-2-1F001	NC	12 OF

5.2 Orbiter DC Power Requirements & Allocations

The Orbiter supplies 28 VDC power to the Orbiter-CCE interface:

Characteristics of 28 VDC power are defined in Table 5.2-1.

Utilization of DC power is defined in Table 5.2-2.

5.2.1 Orbiter-Centaur DC Power Interfaces

Orbiter-CCE DC power interface is identified in Figure 3.2-3 by Interface Number and J Number.

5.3 Orbiter AC Power Requirements & Allocations

The Orbiter shall provide three redundant sources of three phase AC power (115 VAC, 400 Hz, nominal) to the CCE. The primary AC power will be provided from Orbiter AC bus 1 and AC bus 3; backup power is provided by AC bus 2.

The primary AC power (busses 1 and 3) may be manually switched on and off to the CCE interface from the aft F/D during the Shuttle mission. However, the backup power (AC bus 2) will be present at the interface throughout the mission.

Characteristics are defined in Table 5.3-1.

Utilization of AC power is defined in Table 5.3-2.

5.3.1 Orbiter-CCE AC Power Interfaces

Orbiter-CCE AC power interfaces are identified in Figure 3.2-3 by Interface Number and J Number.

Functional interface data for AC power is defined by J number and Pin Number in Table 5.1-2.

5.4 Instrumentation Data Links.

The Orbiter shall provide the capability to acquire and transmit analog and discrete measurements and selected data from four PCM digital data streams (CISS, Centaur, and two S/C) from the CCE to the ground. The Orbiter shall also provide the capability to record digital data from two PCM data streams (CISS & Centaur). Telemetry data flow is shown in Figure 5.4-1.

During prelaunch checkout, three additional PCM streams (CISS, Centaur and Spacecraft) will be hardwired from the CCE, through the Orbiter, to the Ground Support Equipment.

INTERFACE CONTROL DOCUMENT

ORBITER-VEHICLE/CENTAUR	SIZE A	ICD NO ICD-2-1F001	REV NC	SHEET 113 OF
-------------------------	-----------	-----------------------	-----------	-----------------

During the final countdown and ascent mission phases the CCE will provide six data streams (max. 64 kbps each) to the Orbiter and the Orbiter will select and interleave 6.4 kbps (max) of data from four of the six PCM streams and transmit this information to the ground for real-time systems evaluation. In addition, two of the six CCE data streams shall be recorded by the Orbiter for transmission to the ground after achieving orbit. Each data stream to recorder and Orbiter telemetry system shall be isolated from each other at the Orbiter interface.

During on-orbit operations, prior to Centaur stage deployment, the Orbiter will select, interleave, and transmit a maximum of 64 kbps of the CCE data. The Orbiter shall continue to record one of the CCE data streams for delayed transmission to the ground. After Centaur stage deployment, only one PCM stream (CISS) will continue to be supplied via hardline and one PCM stream (Centaur) directly to the Orbiter via RF link. The data from both of these streams will be interleaved with the Orbiter operational PCM data for transmission to the ground. The characteristics for the telemetry link from detached Centaur to the Shuttle Orbiter are defined in ICD-2-1F002 Shuttle-Centaur/Orbiter RF Communications and Tracking.

5.4.1 Payload Data Interleaver Interface.

The Orbiter shall provide for the acquisition of asynchronous PCM data via the Payload Data Interleaver (PDI) from the four (1 CISS, 1 Centaur stage, and 2 spacecraft) CCE channels and from the Payload Signal Processor for the deployed Centaur. The PDI has a maximum composite throughput on-orbit of 64 kbps. However, ascent downlink CCE data shall be limited to that specified in paragraph 5.4.1.3.1.1. See Figure 5 4-1 for payload data interleaver data flow.

5.4.1.1 PDI Input Data Format Characteristics.

The PDI shall accept data streams originating from the CISS, CENTAUR and CENTAUR PAYLOAD. Each data format is defined as a format containing master frames and minor frames. Every minor frame shall be identified by a minor frame sync pattern which occurs once each minor frame, and shall be the same for all minor frames. A master frame shall contain minor frames. Additionally, every minor frame contains an eight bit minor frame count word or a minor frame sync word. The start of the master frame shall be identified as the minor frame which contains the master frame sync word or initial value of the minor frame count word.

5.4.1.1.1 CISS Data Format Characteristics.

The PDI shall accept one data stream from the CISS via the CISS interface. The CISS data format characteristics shall be as shown in Table 5.4-1.

ORIGINAL PAGE IS  
OF POOR QUALITY

INTERFACE CONTROL DOCUMENT

ORBITER-VEHICLE/CENTAUR	SIZE A	ICD NO ICD-2-1F001	REV NC	SHEET 114 OF
-------------------------	-----------	-----------------------	-----------	-----------------

5.4.1.1.2 Centaur Data Format Characteristics.

The PDI shall accept one data stream from the Centaur via the CISS interface. The Centaur data format characteristics shall be as shown in Table 5.4-2.

5.4.1.1.3 Centaur Payload Data Format Characteristics.

The PDI shall accept two redundant data streams from the Centaur payload via the CISS interface. The general capabilities of the PDI to accommodate these data streams is defined in Table 5.4.3. The format characteristics of the data streams will be different for different missions as defined in Appendix I.

5.4.1.1.4 Detached Centaur Data Format Characteristics.

In the detached mode, the Centaur will transmit a data stream via an RF link to the Orbiter Payload Signal Processor (PSP) via the Payload Interrogator while, at the same time, the CISS (5.4.1.1.1) will also transmit a data stream via hardline (paragraph 5.4) to the PDI. Refer to ICD-2-1F002 for definitions of the RF link, data and format characteristics.

*what's this? clarify*

5.4.1.2 PDI Electrical Interface Characteristics

5.4.1.2.1 CCE/PDI Data Electrical Interface Characteristics.

The electrical interface characteristics of each of the CCE data streams interfacing with the Orbiter PDI shall be as shown in Table 5.4-4.

*needs more clarification 5.4 does not say much about H/L per se.*

5.4.1.2.2 CCE/PDI Clock Electrical Interface Characteristics.

The electrical interface characteristics of each of the Centaur Payload clocks interfacing with the Orbiter PDI shall be as shown in Table 5.4-5.

5.4.1.2.3 Grounding and Shielding.

Grounding and shielding for the PDI Data and clock interfaces shall be as shown in Figure 5.4-2.

5.4.1.3 Orbiter PCM TLM Downlink Service.

Throughputting Payload data to the ground via the Orbiter's PCM TLM downlink is implemented via the PDI's Toggle Buffer for individual Master Frames. Before individual Master Frames can be transferred to the PDI's Toggle Buffer, recognition by the PDI of two successive valid Master Frame Sync patterns must first occur. When this has happened, Toggle Buffer storage for each Master Frame shall proceed as follows

INTERFACE CONTROL DOCUMENT

ORBITER-VEHICLE/CENTAUR	SIZE A	ICD NO ICD-2-1F001	REV NC	SHEET 115 OF
-------------------------	-----------	-----------------------	-----------	-----------------

- a. The Time Homogenous Data Set (THDS) within the PDI's Toggle Buffer shall, in part, consist of a Payload Master Frame either in total or a subset thereof. Those Payload Master Frame words to be downlinked shall be partitioned into 16 bit groups (two consecutive or nonconsecutive eight bit Master Frame words) for storage within each Toggle Buffer location.
- b. The remainder of the THDS shall consist of three additional 16 bit Status Words appended to the Master Frame words by the PDI as shown in Figure 5.4-3.

5.4.1.3.1 CCE and Detached Centaur PCM Downlink Measurements.

Measurements and their format locations for CISS, attached Centaur, detached Centaur and Centaur Payload, required for PCM downlink are identified in Section 6.0 Software.

5.4.1.3.1.1 CCE Ascent Downlink Data.

Total combined CISS, Centaur and Centaur Payload downlink data shall be limited to 6.4 KBPS during the ascent phase.

5.4.1.3.1.2 CCE On Orbit Downlink Data.

Total combined CISS, Centaur and Centaur Payload downlink PCM data shall be limited to 64 KBPS during on orbit pre-deployment checkout.

5.4.1.3.1.3 Detached Centaur PCM Downlink Data.

The Payload Signal Processor (PSP) receives Centaur telemetry data via the Payload Interrogator and routes the telemetry data to the PDI. Total data on this link is limited to 16 KBPS. When interleaved with the CISS Data, total combined CISS and detached Centaur downlink PCM data shall be limited to 64 KBPS.

5.4.1.4 Orbiter GPC Software Service.

Transferring individual payload measurements to the Orbiter's GPC Software Services is implemented via the PDI's Data Ram. Before individual measurements within the Master Frame can be transferred to the PDI's Data RAM, recognition of two successive valid Master Frame Sync patterns must first occur. When this has happened, Data RAM storage for each Payload measurement shall proceed as follows:

- a. Each Master Frame eight bit word associated with a Payload measurement that is required to be processed by the Orbiter's GPC Software Services shall be stored within a separate Data RAM byte address.

INTERFACE CONTROL DOCUMENT

ORBITER-VEHICLE/CENTAUR	SIZE	ICD NO	REV	SHEET
	A	ICD-2-1F001	NC	16
			OF	

ORIGINAL PAGE IS  
OF POOR QUALITY

- b. A multisyllable Payload measurement shall have its constituent eight bit bytes independently stored within a separate Data RAM byte address whenever its word position within the Master Frame is processed.
- c. Maintaining the time homogeneity for both individual multisyllable Payload measurements and Payload measurement word sets cannot be guaranteed.

5.4.1.4.1 Format Locations.

Measurements and their format locations for CISS, attached Centaur, detached Centaur and Centaur Payload required for GPC software service are identified in Section 6.0 Software.

5.4.2 CCE PCM Recording.

(B) 5.2.3

The Orbiter shall provide the capability to record biphas-level digital data from two sources. Additionally the Orbiter operational recorders will record all data included in the PCM downlink data stream. Payload recorder data flow is shown in Figure 5.4-1.

5.4.2.1 CISS PCM Recording.

(u) 5.2.3(a)

The Orbiter shall provide the capability to record biphas-level digital data from the CISS for a minimum period of 13 hours and 52 minutes. The electrical interface characteristics at the Orbiter/CISS interface shall be as shown in Table 5.4-6.

5.4.2.2 Centaur PCM Recording.

(u) 5.2.3(b)

The Orbiter shall provide the capability to record biphas-level digital data from the Centaur for a minimum period of 64 minutes. The electrical interface characteristics at the Orbiter interface shall be as shown in Table 5.4-6.

5.4.2.3 Grounding and Shielding.

Grounding and shielding for the CCE data recording shall be as shown in Figure 5.4-4.

5.4.2.4 Centaur Payload PCM Recording.

No direct recording capability will be provided for the recording of Centaur Payload PCM data. However, those parameters in the PCM data downlink will be recorded on the operational recorder

5.4.2.5 Recorder Playback.

In flight playback of CCE digital data is via the Orbiter KU-Band transmitter to ground. Playback of data to GSE is via the Orbiter T-O umbilical.

INTERFACE CONTROL DOCUMENT

ORBITER-VEHICLE/CENTAUR

SIZE ICD NO

A

ICD-2-1F001

REV

NC

SHEET 117

OF



5.4.3 Multiplexer/Demultiplexer (MDM) Signal Acquisition Interface.

The MDM signal acquisition interface is defined in Paragraph 5.5.5, "Systems Management Processing".

5.5 Command, Control, and Display Interfaces

The Orbiter shall provide the capability for three command paths from the Payload Signal Processor (PSP) to the CISS interface in addition to high level discrete commands from flight critical MDM's. Command data flow is shown in Figure 5.5.1.

- Control functions will be provided using the standard switch panel and display capability will be provided using the Orbiter systems management function.

5.5.1 Payload Signal Processor

- A single path shall be provided from a single PSP to the CISS interface for the purpose of providing command data to the CISS/Centaur during the attached Centaur mode. Redundant command data paths from redundant PSP's shall be provided to the CISS interface for the purpose of providing command data to the Centaur payload while operating in the attached mode. Command data can be provided by only one path at a time.

5.5.1.1 CISS/Centaur Command Data Output

A single (non-redundant) command path shall be provided as shown in Figure 5.5-1 from a single PSP to the CISS interface for the purpose of providing command data to the CISS/Centaur while operating in the attached mode. The command data output shall have the characteristics shown in Table 5.5-1. The command data format shall be as shown in Figure 5.5-2.

5.5.1.2 Centaur Payload Command Data Output

- A dual redundant command path shall be provided as shown in Figure 5.5-1 from two PSP's to the CISS interface for the purpose of providing command data to the Centaur payload while operating in the attached mode. Only one of the two PSP's may be active at a time. The command data output for either PSP shall have the characteristics shown in Table 5.5-1. The command data format shall be as shown in Appendix I.

INTERFACE CONTROL DOCUMENT

ORBITER-VEHICLE/CENTAUR	SIZE A	ICD NO ICD-2-1F001	REV NC	SHEET <u>118</u> OF <u>    </u>
-------------------------	-----------	-----------------------	-----------	------------------------------------

5.5.1.3 Idle Pattern Generation

The PSP can output an unmodulated or modulated 16 KHz subcarrier to allow the CISS/Centaur or payload to maintain command receiver lock. The idle pattern modulation consists of alternating "ones" and "zeros". The rate of the idle pattern is the same as the last "real" command data transmission, and always begins with a logic "one". The idle pattern begins in the first bit period following the last bit of the last "real" command data word transmission if the idle pattern enable bit in the previous PSP configuration word has been set. Likewise, the idle pattern will end with the last bit period prior to transmission of the first bit of the next "real" command message. The idle pattern can only be output on one active command channel at a time.

5.5.1.4 Grounding and Shielding

Grounding and shielding for the PSP/CISS interfaces shall be as shown in Figure 5.5-4.

5.5.2 Flight Critical MDM's

The Orbiter will provide four high level discrete output (DOH) commands from each flight AFT MDM to CCE to initiate and terminate the CCE propellant dump sequence in event of mission abort. During the ascent mission phase, the commands shall be automatically initiated by the Orbiter General Purpose Computer (GPC) redundant set (RS) or by the Backup Flight System (BFS) GPC, through Flight Critical MDM's. The commands required and sequence of initiation are shown in Table 5.5-2.

The electrical characteristics of the circuits are shown in Table 5.5-3.

5.5.2.1 MDM Grounding and Shielding

Grounding and shielding for MDM's are shown in Figure 5.5-5.

5.5.3 Standard Switch Panel

Both halves of one standard switch panel (SSP) will be provided at the aft flight deck for on-orbit control of CCE functions.

The SSD switch interface is shown in Figure 5.5-7. Characteristics of the switches and talkbacks are shown in Table 5.5-4.

5.5.4 Caution and Warning Electronics Assembly (CWEA)

The Orbiter shall provide five circuits for inputs to the "Payload Warning" CWEA indicator at the CISS interface. All five inputs are combined at the CWEA. The CCE will utilize only one of the P/L caution circuits, the four remaining circuits shall have the signal and return shorted together (less than 2.0 ohm resistance) on the CCE side of the CISS interface.

INTERFACE CONTROL DOCUMENT

ORBITER-VEHICLE/CENTAUR	SIZE A	ICD NO ICD-2-1F001	REV NC	SHEET 119 OF
-------------------------	-----------	-----------------------	-----------	-----------------

The electrical characteristics of the CCE warning signals are shown in Table 5.5-5.

5.5.5

Systems Management Processing

The Orbiter will provide fault detection and annunciation of the CCE parameters listed in Table 5.5-6. The Orbiter shall provide data channels for the acquisition of these data parameters through MDM's which are under control of the on-board computers. MDM signal transfer capabilities at the Orbiter/CISS interface are:

- a. 7 low level differential analog inputs (AID)
- b. 4 high level discrete inputs (DIH)

5.5.5.1

Low Level Differential Analog Inputs (AID)

The electrical interface characteristics of the MDM low level differential analog inputs at the Orbiter/CISS interface shall be as shown in Table 5.5-7.

5.5.5.2

High Level Discrete Input (DIH)

The electrical interface characteristics of the MDM high-level discrete input signals from the CISS, at the Orbiter/CISS interface shall be as shown in Table 5.5-8

5.5.5.3

Grounding and Shielding

Grounding and shielding for MDM's is shown in Figure 5.5-5.

6.0

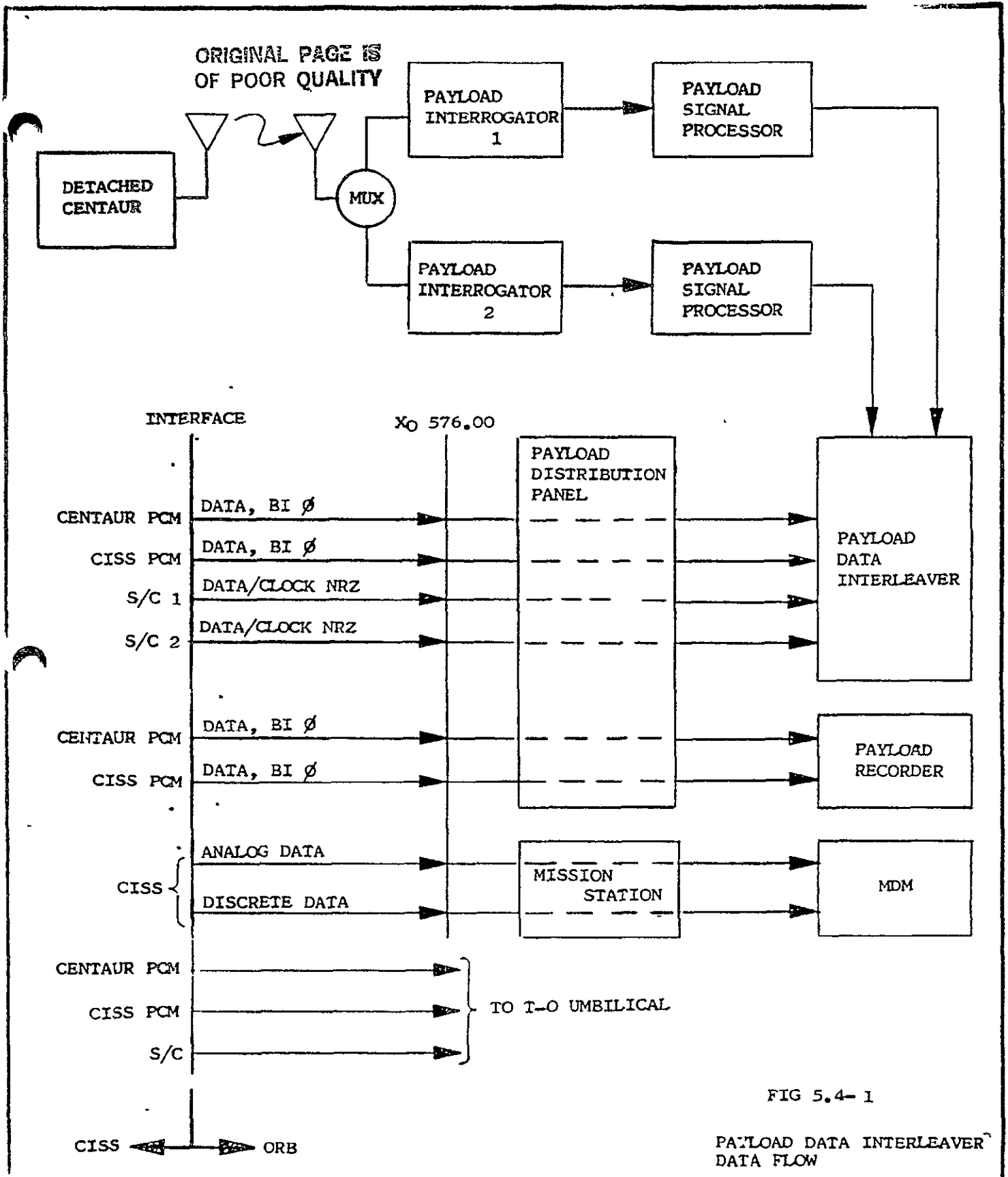
Software

*what is supposed to be here?*

ORIGINAL PAGE IS  
OF POOR QUALITY

INTERFACE CONTROL DOCUMENT

ORBITER-VEHICLE/CENTAUR	SIZE A	ICD NO ICD-2-1F001	REV NC	SHEET 120 OF
-------------------------	-----------	-----------------------	-----------	-----------------



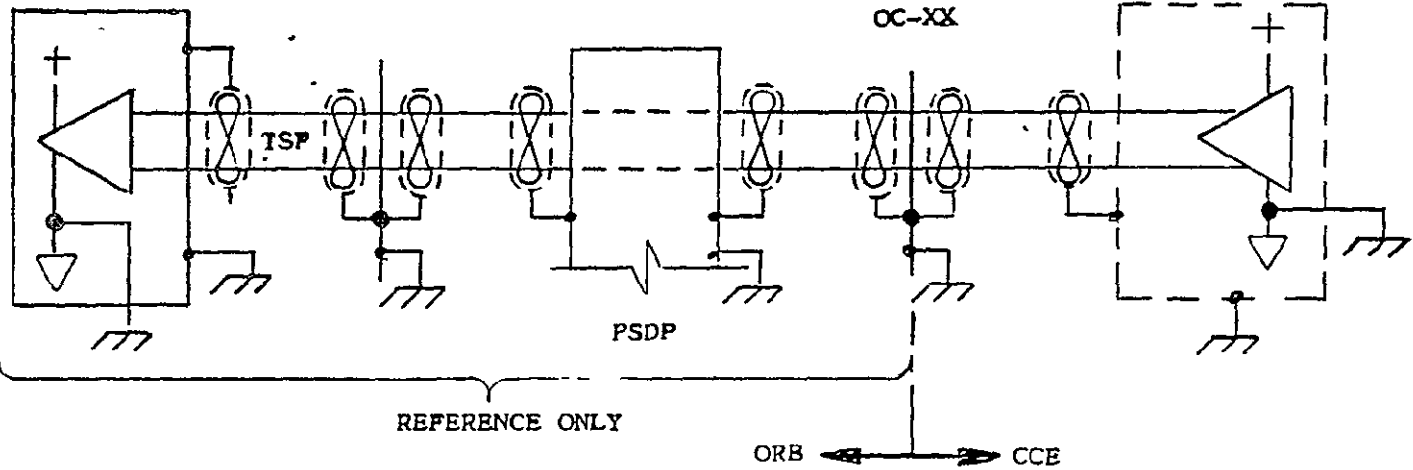
**INTERFACE CONTROL DOCUMENT**

ORBITER-VEHICLE/CENTAUR	SIZE <b>A</b>	ICD NO. ICD-2-1F001	REV NC	SHEET <u>121</u> OF <u>    </u>
-------------------------	------------------	------------------------	-----------	------------------------------------

ORIGINAL PAGE IS  
OF POOR QUALITY

PAYLOAD DATA  
INTERLEAVER

TYPICAL DRIVER




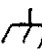
- NOTES: 1.  DEFINES SECONDARY POWER GROUND  
2.  DEFINES STRUCTURE GROUND

FIG 5.4-2

PAYLOAD DATA INTERLEAVER GROUNDING AND  
SHIELDING INTERFACE DATA & CLOCK

INTERFACE CONTROL DOCUMENT

ORBITER VEHICLE/CENTAUR

SIZE  
A

ICD NO  
ICD-2-1FC01

REV  
NC

SHEET 22  
OF

INTERFACE CONTROL DOCUMENT

STATUS  
WD 1

STATUS  
WD 2

STATUS  
WD 3

FRAME DATA SET STATUS WORDS

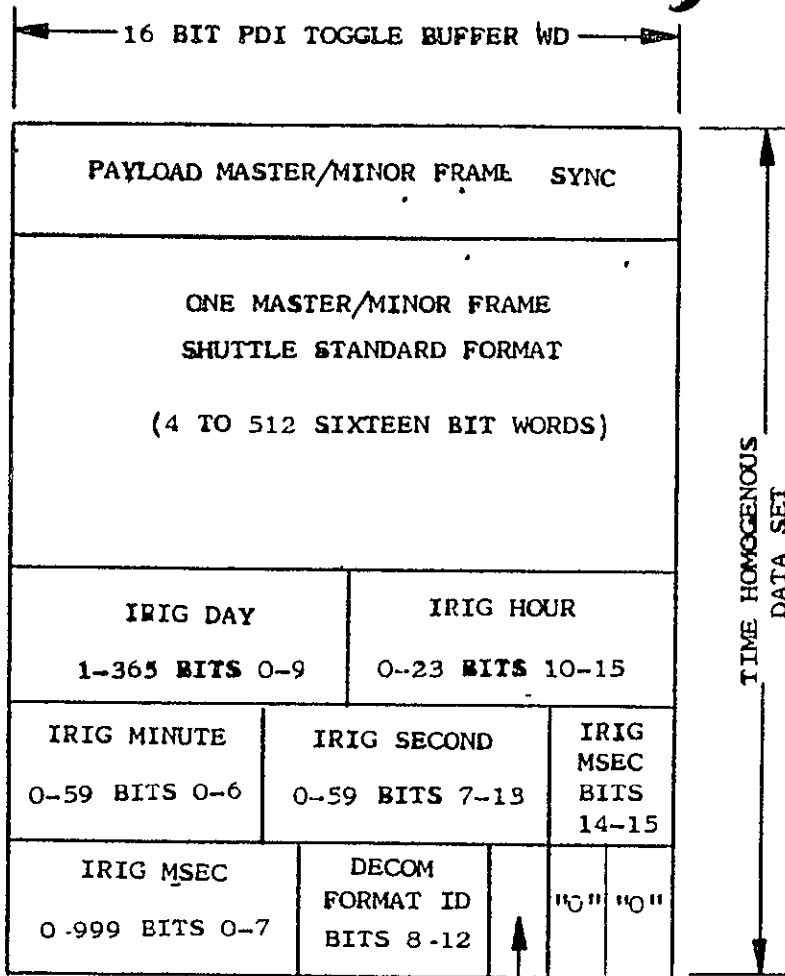


FIGURE 5.4-3

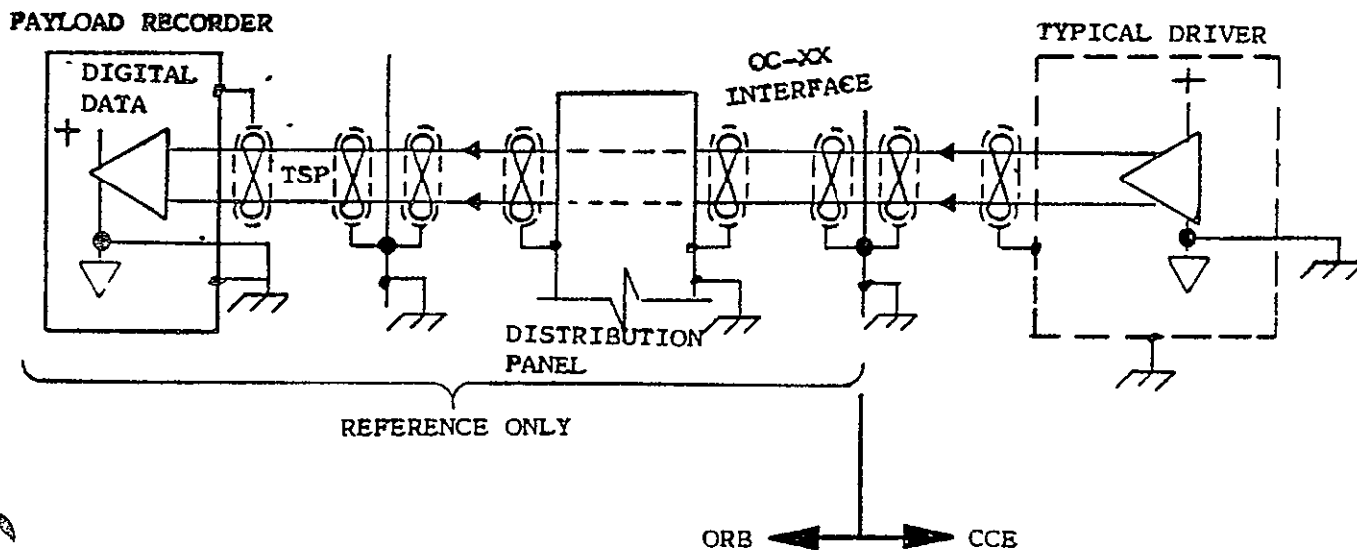
NOTES:

1. IRIG DAY, HOUR, MINUTE, AND SECOND ARE BCD CODED, MSB FIRST IRIG MSEC IS BINARY CODED, MSB FIRST.

"1" - IN TOLERANCE  
"0" - OUT OF TOLERANCE, BUT STILL IN LOCK

ORIGINAL PAGE IS  
OF POOR QUALITY

ORIGINAL PAGE IS  
OF POOR QUALITY



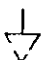
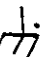
- NOTES:
1.  DEFINES SECONDARY POWER GROUND
  2.  DEFINES STRUCTURE GROUND

FIG. 5.4-4

DATA RECORDER GROUNDING AND SHIELDING

INTERFACE CONTROL DOCUMENT

ORBITER-VEHICLE/CENTAUR

SIZE  
A

ICD NO  
ICD-21FO01

REV  
NC

SHEET 124  
OF

REVISIONS			
LTR	DESCRIPTION	DATE	APPROVED

ORIGINAL PAGE IS  
OF POOR QUALITY

NOTES:

1. DIFFERENTIAL PHASE SKEW = (LEADING EDGE PHASE SHIFT - TRAILING EDGE PHASE SHIFT)
2. WHERE: LEADING/TRAILING EDGE PHASE SHIFT IS THE TIME DIFFERENTIAL BETWEEN THE 50% POINTS OF ASSOCIATED AMPLITUDE TRANSITIONS OF THE TWO DIFFERENTIAL INPUTS.

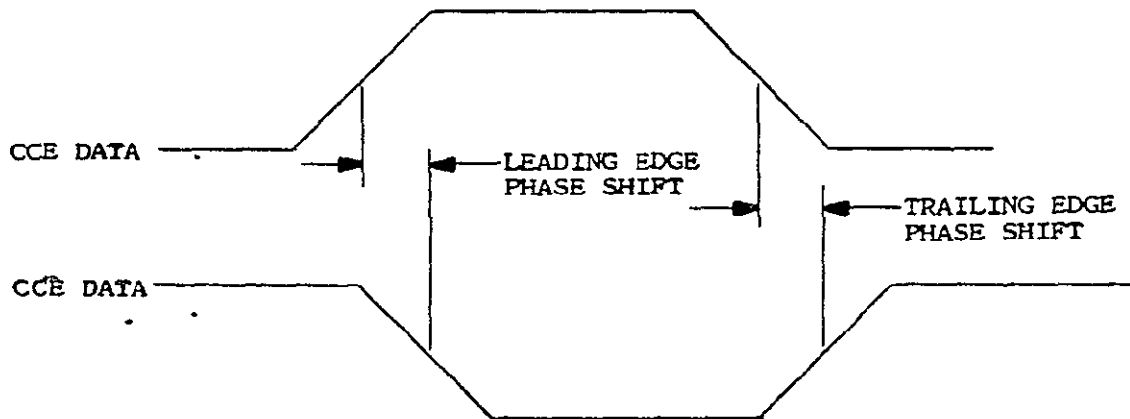


FIG.5.4-5

DIFFERENTIAL PHASE SKEW

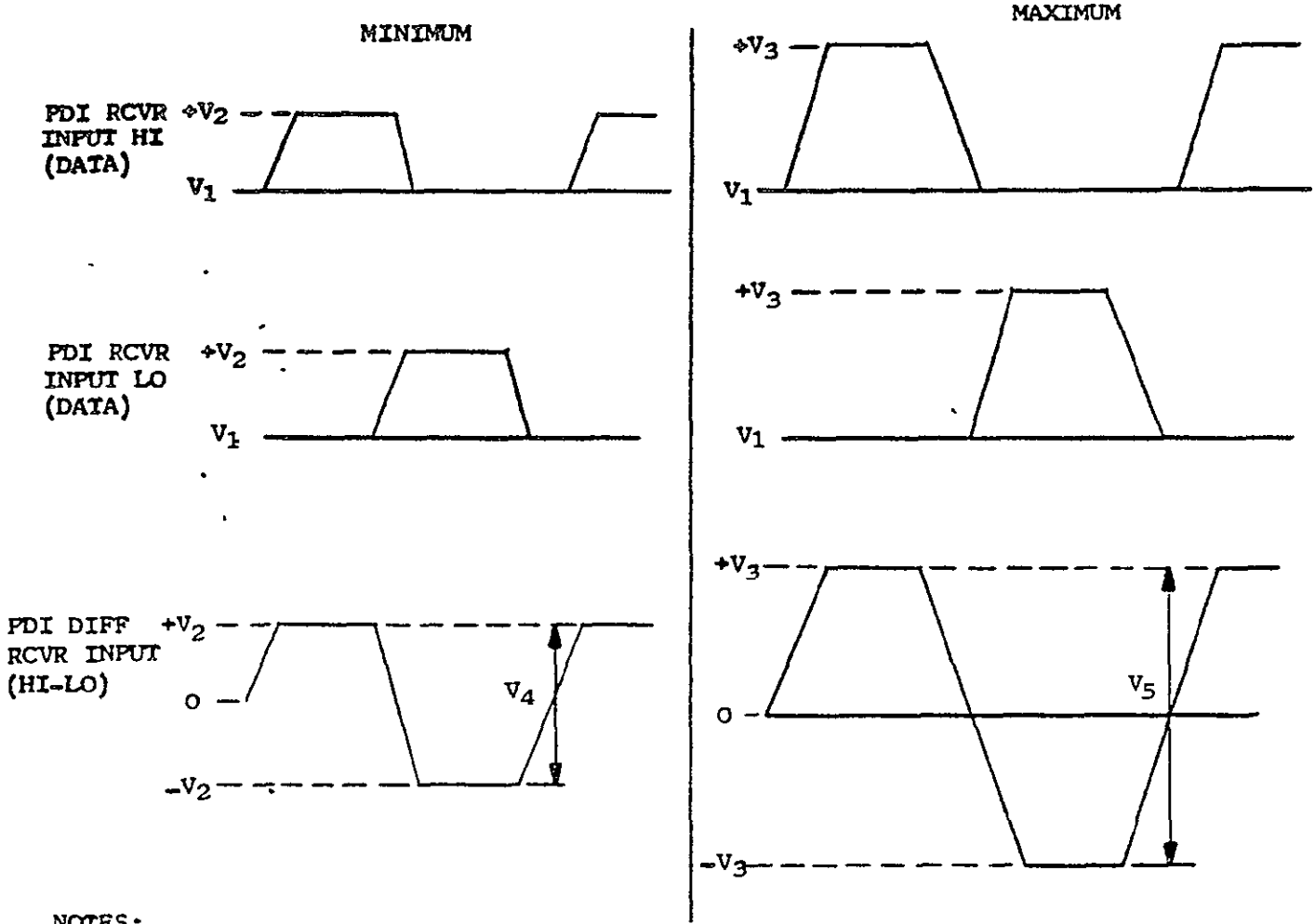
INTERFACE CONTROL DOCUMENT

ORBITER-VEHICLE/CENTAUR	SIZE A	ICD NO ICD-2-1Pool	REV N/A	SHEET OF
				29



ORIGINAL PAGE IS  
OF POOR QUALITY

REVISIONS			
LTR	DESCRIPTION	DATE	APPROVED



NOTES:

- $V_1$  = SIGNAL GROUND
- $V_2$  = 1.25 VOLTS LINE TO SIG. GND.
- $V_3$  = 4.5 VOLTS TO SIG. GND.
- $V_4$  = 2.5 VOLTS P-P LINE TO LINE DIFFERENTIAL BALANCED
- $V_5$  = 9.0 VOLTS P-P LINE TO LINE DIFFERENTIAL BALANCED

FIG.5.4-6

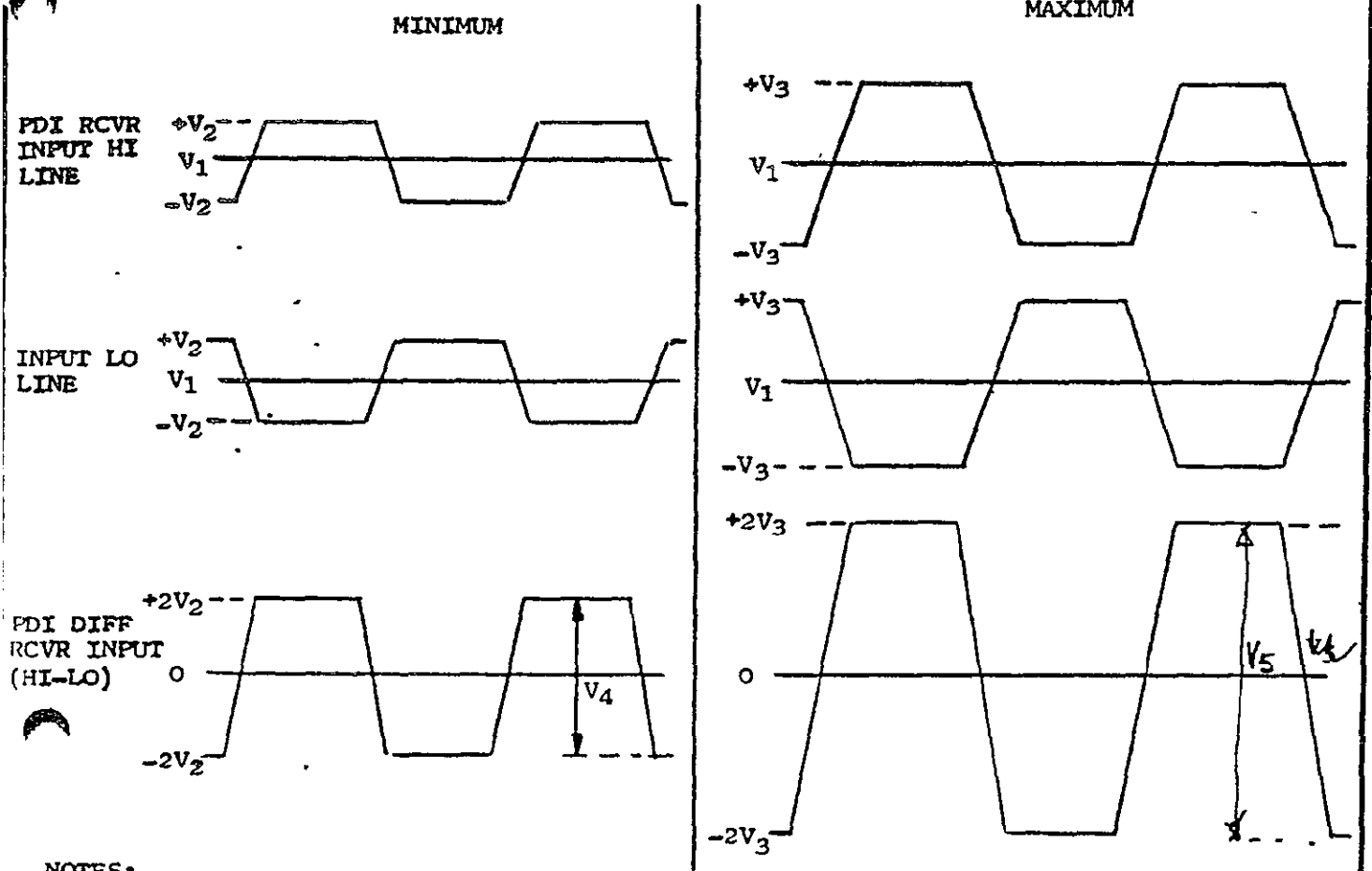
DATA/DATA-DIFFERENTIAL TRANSMISSION

INTERFACE CONTROL DOCUMENT

ORBITER-VEHICLE/CENTAUR	SIZE <b>A</b>	ICD NO ICD-2-1FO01	REV N/C	SHEET OF <u>26</u>
-------------------------	------------------	-----------------------	------------	-----------------------

ORIGINAL PAGE IS  
OF POOR QUALITY

REVISIONS			
LTR	DESCRIPTION	DATE	APPROVED



NOTES:

- $V_1$  - SIGNAL GROUND
- $V_2$  - 0.625 VOLTS LINE TO SIGNAL GROUND
- $V_3$  - 2.25 VOLTS LINE TO SIGNAL GROUND
- $V_4$  - 2.5 VOLTS P-P DIFFERENTIAL LINE-TO-LINE BALANCED
- $V_5$  - 9.0 VOLTS P-P DIFFERENTIAL LINE-TO-LINE BALANCED

FIG. 5.4-7

BI-POLAR LINE-DIFFERENTIAL TRANSMISSION

INTERFACE CONTROL DOCUMENT

ORBITER-VEHICLE/CENTAUR	SIZE <b>A</b>	ICD NO. ICD-2-1F001	REV N/C	SHEET <u>127</u> OF <u>  </u>
-------------------------	------------------	------------------------	------------	----------------------------------

ORIGINAL PAGE IS  
OF POOR QUALITY

REVISIONS			
LTR	DESCRIPTION	DATE	APPROVED

NOTES:

- 1 THE RISING EDGE OF EACH CLOCK SIGNAL SHALL BE COINCIDENT WITH THE STARTING EDGE OF THE CORRESPONDING DATA BIT PERIOD WITHIN PLUS OR MINUS 10 PERCENT OF THE CLOCK MAXIMUM.

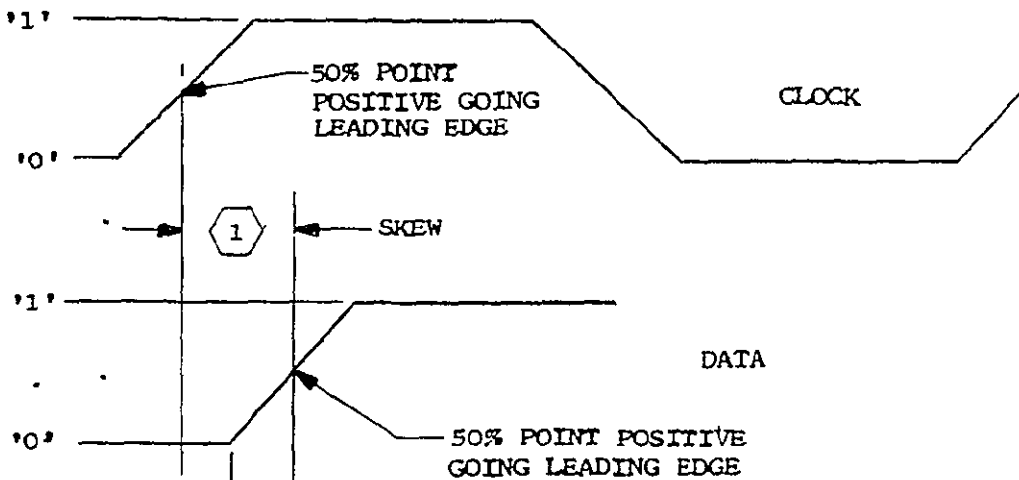


FIG. 5.4-8  
SKEW

INTERFACE CONTROL DOCUMENT

ORBITER-VEHICLE/CENTAUR	SIZE A	ICD NO. ICD-2-1F001	REV N/C	SHEET 178 OF
-------------------------	-----------	------------------------	------------	-----------------

ORIGINAL PAGE 13  
OF POOR QUALITY

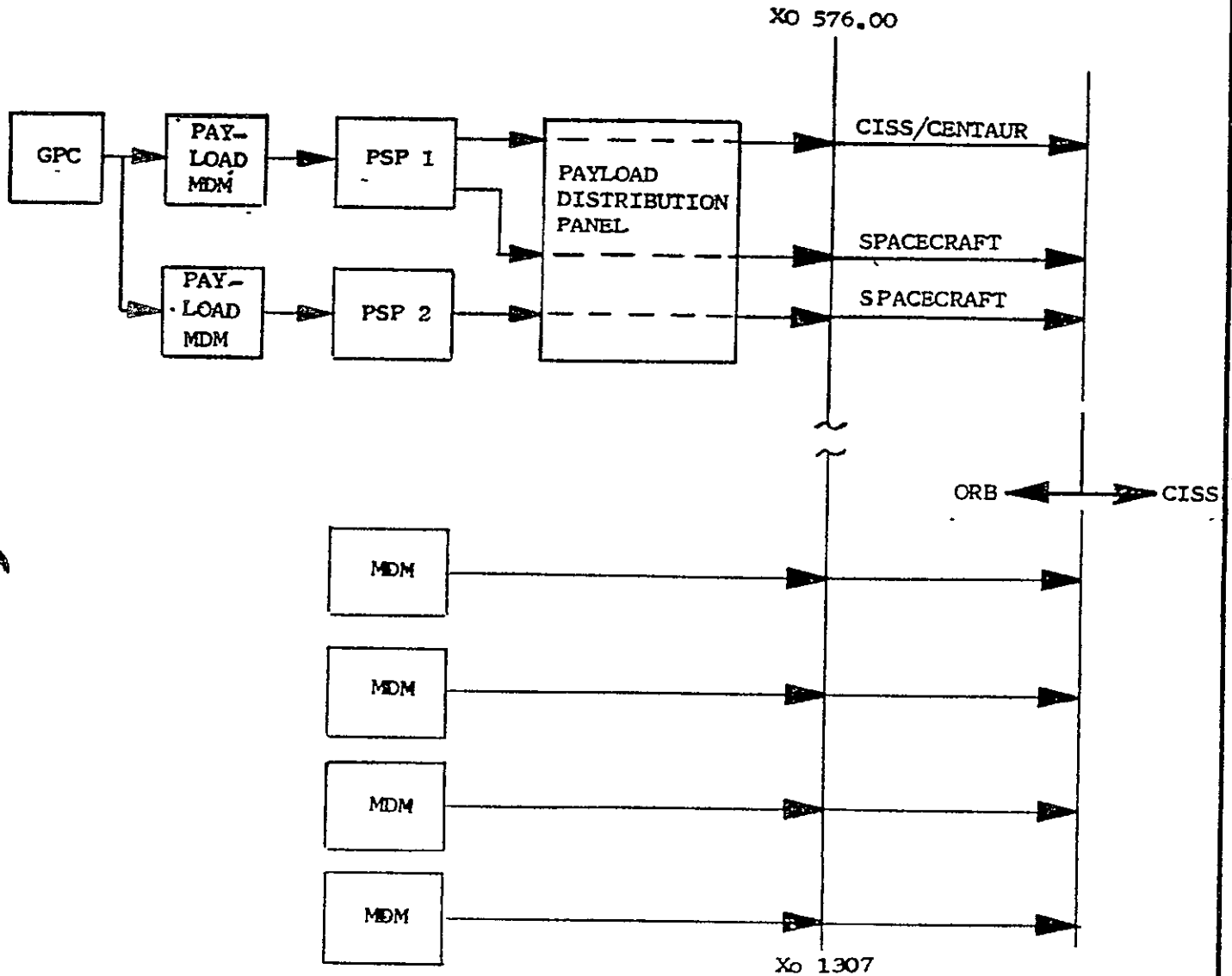


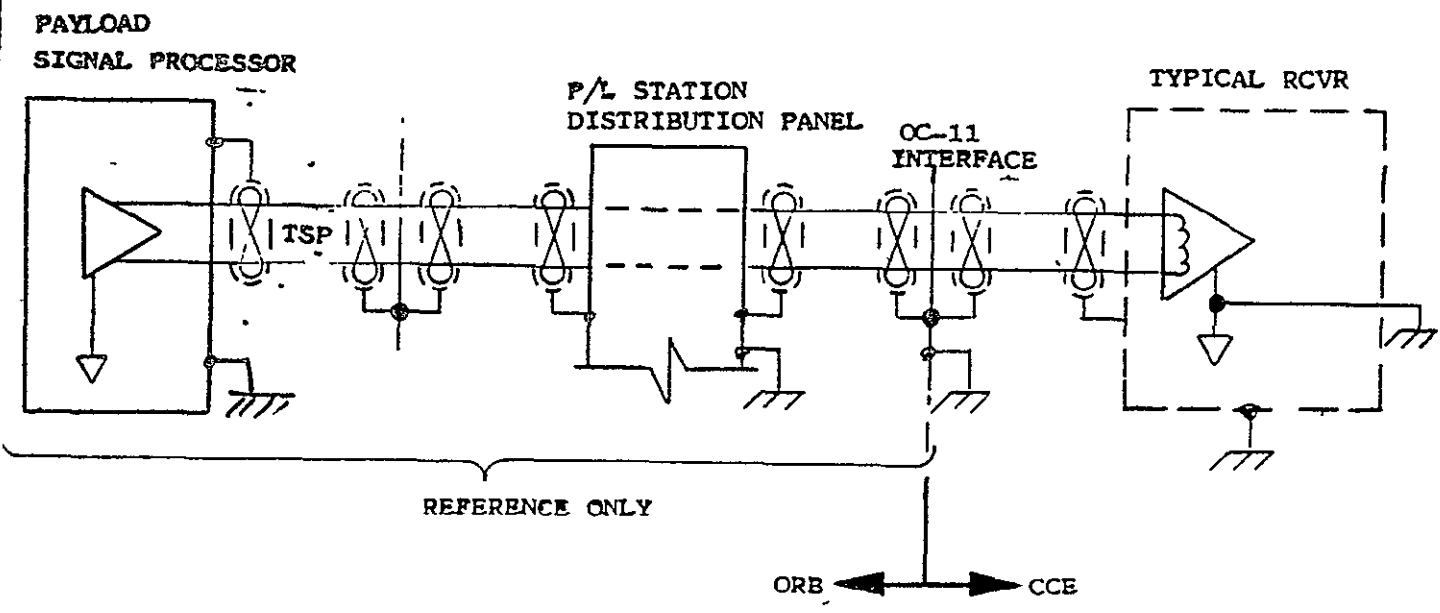
FIG 5.3-1,

MDM AND PAYLOAD SIGNAL PROCESSOR  
COMMAND DATA FLOW

INTERFACE CONTROL DOCUMENT

ORBITER-VEHICLE/CENTAUR	SIZE <b>A</b>	ICD NO. ICD-2-1F001	REV NC	SHEET <u>129</u> OF _____
-------------------------	------------------	------------------------	-----------	------------------------------

ORIGINAL PAGE IS  
OF POOR QUALITY





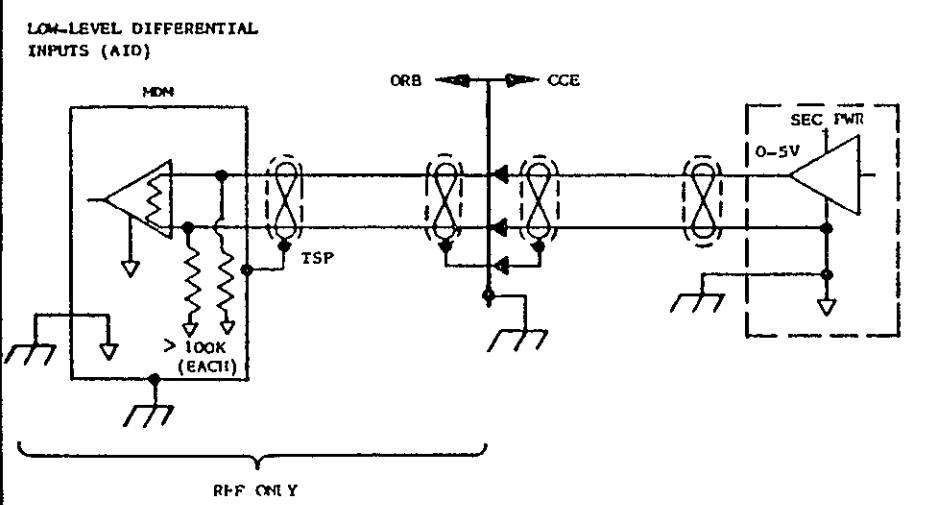
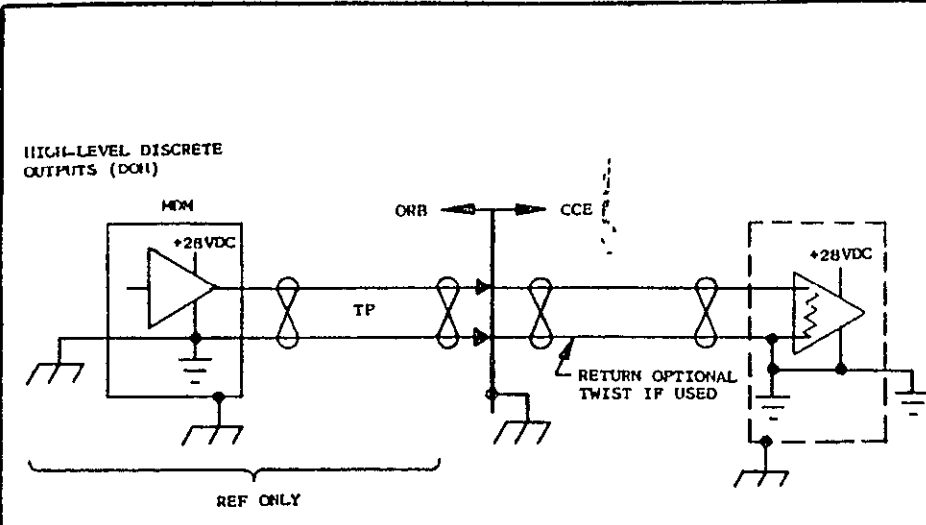
- NOTES:
1.  DEFINES SECONDARY POWER GROUND.
  2.  DEFINES STRUCTURE GROUND.

FIG 5.5-4

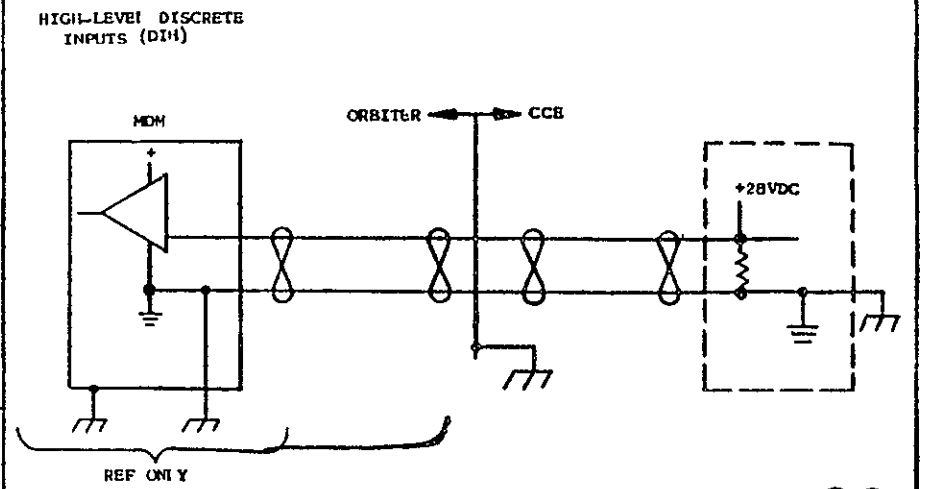
PAYLOAD SIGNAL PROCESSOR GROUNDING  
AND SHIELDING

INTERFACE CONTROL DOCUMENT

ORBITER-VEHICLE/CENTAUR	SIZE <b>A</b>	ICD NO ICD-2-1F001	REV NC	SHEET <u>130</u> OF _____
-------------------------	------------------	-----------------------	-----------	------------------------------



REVISIONS			
LTR	DESCRIPTION	DATE	APPROVED



- NOTES:
1. DEFINES SECONDARY POWER GROUND.
  2. DEFINES STRUCTURE GROUND.
  3. STRUCTURE OR CHASSIS GROUND.

ORIGINAL PAGE IS OF POOR QUALITY

FIG 5.5-5

MDM INTERFACE GROUNDING AND SHIELDING

INTERFACE CONTROL DOCUMENT			
SIZE	ICD NO	REV	SHEET
B	ICD-2-1F001		13/

REVISIONS			
LTR	DESCRIPTION	DATE	APPROVED

ORIGINAL PAGE IS  
OF POOR QUALITY

NOTES:

1.  $t_{MAX}$ -MAXIMUM SYMBOL PERIOD
2.  $t_{MIN}$ -MINIMUM SYMBOL PERIOD
3.  $t_{AVE}$ -IS THE AVERAGE SYMBOL PERIOD
4.  $T_o$  - IS THE OBSERVATION TIME
5. ASYMMETRY DOES NOT ACCUMULATE (i.e.,  $t_{AVE} + = \frac{1}{R}$  WERE R IS THE DATA RATE)

$$\text{ASYMMETRY \%} = \frac{t_{MAX} - t_{MIN}}{t_{MAX} + t_{MIN}} \times 100\%$$

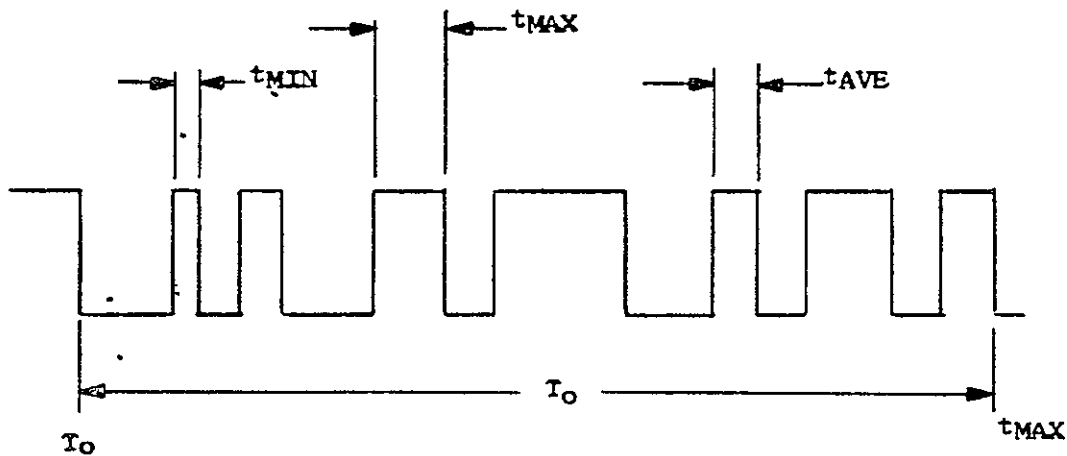


FIG. 5.5-6

DIGITAL DATA ASYMMETRY

INTERFACE CONTROL DOCUMENT

ORBITER-VEHICLE/CENTAUR	SIZE A	ICD NO ICD-2-1FO01	REV N/C	SHEET OF
				132 

LTR

REVISIONS DESCRIPTION

LTR

REVISIONS DESCRIPTION

## GENERAL NOTES

1. THIS TABLE DOES NOT DESCRIBE THOSE WIRE TYPES WHICH ARE PERMITTED TO USE STRUCTURE FOR THE CIRCUIT RETURN.

2 WHERE THE CAPACITANCE PER FOOT IS CRITICAL, CONTROLLED IMPEDANCE WIRING SHOULD BE USED. SERIAL DIGITAL I/O, DATA BUS, VIDEO AND CLOCK CIRCUITS OPERATING BELOW 1.024 MHz WILL REQUIRE SPECIAL SHIELDED - TWISTED - PAIR CABLES (NOM 71 OHM). RF CIRCUITS, INCLUDING CLOCK CIRCUITS OPERATING AT 1.024 OR ABOVE, WILL USE COAXIAL CABLE.

3 WHERE A CIRCUIT IS BALANCED BY A TRANSFORMER, DIFFERENTIAL, OR OPTICAL ISOLATION, THE SHIELD SHALL BE MULTIPPOINT GROUNDED TO STRUCTURE.

4 DISTANCE BETWEEN SHIELD GROUNDS SHALL NOT EXCEED 18 METERS.

PRECEDING PAGE BLANK NOT FILMED

ORIGINAL PAGE IS  
OF POOR QUALITY

TABLE 5.1-1  
SHEET 1 OF 2

CIRCUIT EMC CLASSIFICATION

## INTERFACE CONTROL DOCUMENT

ICD NO	REV	SHEET
ICD-2-1F001	HC	134



Freq. of Rise and/or Fall Time	Source Impedance (ohms)	Load Impedance (ohms)	Voltage or Sensitivity	Circuit Class.	Wire Type Required	Shield Grounding Reqs.
Analog, Alternating or Direct Current	< 100	100-600K, 0-200 0-200	< 6v > 6v to < 40v > 40v	ML HO EO	TWS TW TW	SPG $\Delta$ NONE NONE
	$\leq$ 2.5K	100-600K > 600K	< 100mv	ML	TWS TWDS	SPG $\Delta$ SPG $\Delta$
	< 100	> 200 > 200 > 200	> 100mv to < 6v > 6v to < 40v > 40v	ML HO EO	TWS TW TW	SPG $\Delta$ NONE NONE
< 50 KHz or Rise & Fall Time > 10 Micro Seconds	< 100	> 10K 0-200 0-200	< 6v > 6v to < 40v > 40v	ML HO EO	TWS TW TW	SPG $\Delta$ NONE NONE
	< 2.5K	100-600K > 600K	< 100mv	ML	TWS TWDS	SPG $\Delta$ SPG $\Delta$
	$\geq$ 200	> 200 > 200 > 200	> 100mv to < 6v > 6v to < 40v > 40v	ML HO EO	TWS TW TW	SPG $\Delta$ NONE NONE
> 50 KHz or Rise & Fall Time < 10 Microsec	ALL	ALL	< 100mv > 100mv to < 6v	RF RF	TWDS $\Delta$ TWS $\Delta$	MPG MPG
		< 1000 > 1000	> 6v	RF	TWS $\Delta$ TWDS	HPG MPG
> 1 024 MHz	ALL	ALL	ALL	RF RF	COAX TWS	HPG MPG $\Delta$
TV VIDEO	ALL	ALL	ALL	RF RF	COAX TWS	HPG MPG $\Delta$

## SYMBOLS USED

KHz - Kiloherztz  
 mv - Millivolts  
 SPG - Single Point Ground  
 MPG - Multiple Point Ground  
 TW - TWISTED  
 TWDS - Twisted Double Shielded  
 RF - Radio Frequency

TWS - Twisted Shielded  
 AF - Audio Frequency  
 < - Less than  
 $\leq$  - Less than or equal to  
 > - Greater than  
 $\geq$  - Greater than or equal to

 TABLE 5.1-1  
 SHEET 2 OF 2

CIRCUIT EMC CLASSIFICATION

## INTERFACE CONTROL DOCUMENT

ICD NO

ICD-2-1P001

REV NO

SHEET

135

LTR REVISIONS DESCRIPTION

LTR REVISIONS DESCRIPTION

ORIGINAL PAGE IS  
OF POOR QUALITY

ORIGINAL PAGE IS  
OF POOR QUALITY

TABLE 5.1-2  
SHEET 1 OF 2

ELECTRICAL CONNECTOR I/F  
ORB-CISS L.H. OC-11

INTERFACE CONTROL DOCUMENT		
ICD NO	REV NC	SHEET
ICD-2-1F001		136

LTR

REVISIONS DESCRIPTION

LTR

REVISIONS DESCRIPTION

PIN NO.	ORB WIRE GAGE AWG	CISS WIRE GAGE AWG	CONN PIN GAGE AWG	FUNCTION	ORIG CMD OR RESP	VOLT LVL.	LOAD	CKT PICT	GND LCT	CKT CLAS	DESCRIPTION

ORIGINAL PAGE IS  
OF POOR QUALITY

INTERFACE NO OC-11

ORBITER CONNECTOR GND CONNECTOR  
CISS CONNECTOR

TABLE 5.1-2  
SHEET 2 OF 2

ELECTRICAL CONNECTOR I/F  
ORB-CISS L.H. OC-11

## INTERFACE CONTROL DOCUMENT

ICD NO	REV	SHEET
ICD-2-1F001	NC	137

PRECEDING PAGE BLANK NOT FILMED

LTR				REVISIONS DESCRIPTION				LTR				REVISIONS DESCRIPTION			
PIN NO	ORB WIRE GAGE AWG	CISS WIRE GAGE AWG	CONN PIN GAGE AWG	FUNCTION	ORIG CHD OR RESP	VOLT LVL	LOAD	CKT PTCT	GND LCT	CKT CLAS	DESCRIPTION				
ORIGINAL PAGE IS OF POOR QUALITY															

INTERFACE NO OC-12

ORBITER CONNECTOR  
CISS CONNECTOR

GND CONNECTOR

TABLE 5.1-3  
SHEET 2 OF 2

ELECTRICAL CONNECTOR I/P  
ORB-CISS R.H. OC-12

INTERFACE CONTROL DOCUMENT			
ICD NO	ICD-2-1F001	REV NC	SHEET 139

PRECEDING PAGE BLANK NOT FILMED

FIN NO	ORB WIRE CAGE ANG	CISS WIRE CAGE ANG	CONN PIN CAGE ANG	FUNCTION	ORIG CHD OR RESP	VOLT IVL	LOAD	CKT PILL	CHD ICI	CKT CLAS	DESCRIPTION

ORIGINAL PAGE IS OF POOR QUALITY

INTERFACE NO OC-11

ELECTRICAL CONNECTOR INTERFACE ORB-CISS I.II OC-11  
(10 I-0)  
VEHICLE CONNECTOR GND CONNECTOR

TABLE 5.1-4  
SHEET 2 OF 2

INTERFACE CONTROL DOCUMENT		
ICD NO	REV NO	SHEET
ICD-2-1F001		141

PRECEDING PAGE BLANK NOT FILMED

LTR				REVISIONS DESCRIPTION				LTR				REVISIONS DESCRIPTION			
PIN NO.	ORB WIRE CAGE AWG	CISS WIRE CAGE AWG	CONN PIN CAGE AWG	FUNCTION	ORIG CHD OR RESP	VOLT LVL	LOAD	CKT PTGT	GND LCT	CKT CLAS	DESCRIPTION				
ORIGINAL PAGE IS OF POOR QUALITY															
INTERFACE NO. OC-12				ORBITER CONNECTOR CISS CONNECTOR				GND CONNECTOR				TABLE 5.1-5 SHEET 2 OF 2  ELECTRICAL CONNECTOR I/P ORB-CISS R.H. OC-12 (10 TO)			

INTERFACE CONTROL DOCUMENT			
ICD NO	ICD-2-1F001	REV	SHEET
		193	193

28VDC ELECTRICAL POWER CHARACTERISTICS AT OC-12 INTERFACE

STEADY STATE VOLTAGE 27.0V TO 32.0V

TRANSIENT SURGE VOLTAGE LIMITS

- NORMAL AS SPECIFIED IN FIG. 1
- ABNORMAL AS SPECIFIED IN FIG. 2

RIPPLE VOLTAGE

- MAX RIPPLE COMPONENT 0.9V PEAK TO PEAK
- TOTAL BROADBAND RIPPLE 1.6V PEAK TO PEAK

RIPPLE VOLTAGE-FREQUENCY CHARACTERISTICS

AS SPECIFIED IN FIG. 3

VOLTAGE SPIKE

- 2 TIMES LINE VOLTAGE MAX OR 100V WHICHEVER IS LESS

• NORMAL AND ABNORMAL SWITCHING CONDITIONS ARE DEFINED AS FOLLOWS:

- a) NORMAL OPERATION OF THE ELECTRIC SYSTEM IS ALL THE FUNCTIONAL OPERATIONS REQUIRED FOR SHUTTLE OPERATION. THESE OPERATIONS OCCUR AT ANY GIVEN INSTANT AND ANY NUMBER OF TIMES DURING GROUND OPERATIONS, LAUNCH PREPARATION, ASCENT, ON-ORBIT, AND LANDING. EXAMPLES OF SUCH OPERATIONS ARE SWITCHING OF UTILIZATION EQUIPMENT LOADS AND BUS SWITCHING.
- b) ABNORMAL OPERATION OF THE ELECTRIC SYSTEM IS THE UNEXPECTED LOSS OF CONTROL OF THE ELECTRIC SYSTEM. THE INITIATING ACTION OF THE ABNORMAL OPERATION IS UNCONTROLLED AND THE EXACT MOMENT OF OCCURRENCE IS NOT ANTICIPATED. HOWEVER, RECOVERY FROM THIS OPERATION IS A CONTROLLED ACTION. AN EXAMPLE OF AN ABNORMAL OPERATION IS THE FAULTING OF ELECTRIC POWER TO STRUCTURE AND ITS SUBSEQUENT CLEARING BY FAULT PROTECTIVE DEVICES.

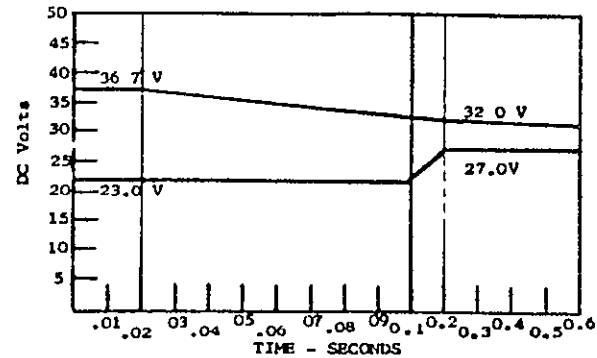


FIG. 1 Transient Surge of DC Voltage Step Function Local Limits During Normal Equipment Switching Conditions

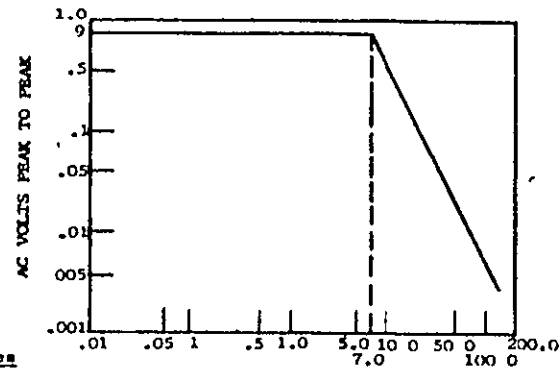


FIG. 3 Frequency Characteristics of Ripple Voltage in 28 Volt Electrical System

Coordinates	
F-KHz	V-Volts
0.01	0.9
7.0	0.9
150.0	0.0021

REVISIONS			
LTR	DESCRIPTION	DATE	APPROVED

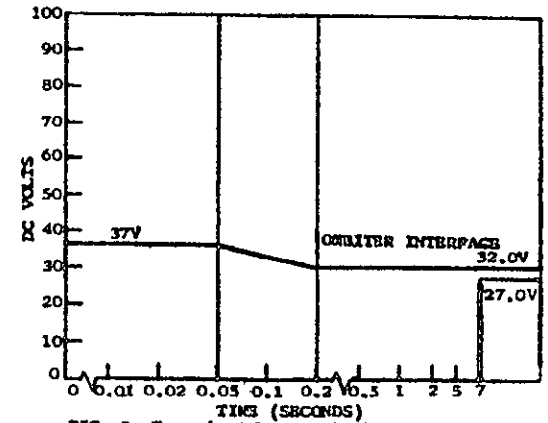


FIG. 2 Transient Surge of DC Voltage Step Function Local Limits During Abnormal Switching Conditions

TABLE 5 2-1  
28V DC POWER

INTERFACE CONTROL DOCUMENT			
SIZE	ICD NO	REV	SHEET
B	ICD-2-1F001	1C	144

ORIGINAL PAGE IS OF POOR QUALITY

CONDITION	CONTINUOUS WATTS	③
PRE LAUNCH	3.2KW	① ②
ASCENT	3.2KW	① ②
ON-ORBIT	4.0KW	
DESCENT	3.2KW	① ②
POST LANDING	3.2KW	① ②

ORIGINAL PAGE IS  
OF POOR QUALITY

NOTES:

- ① WITH ALL THREE ORBITER FUEL CELL POWER PLANTS (FCP) AND MAIN DC BUSES OPERATIONAL. FOLLOWING A FCP OR MAIN DC BUS FAILURE, THE ORBITER MAY REMOVE ALL PRIMARY DC POWER FROM THE CCE INTERFACE.
- ② ASSUMES THAT ORBITER FCP'S HAVE EXPENDED LESS THAN 75% OF THEIR PROJECTED OPERATIONAL LIFE.
- ③ IN ADDITION TO THE PRIMARY DC POWER ALLOCATED TO THE CISS INTERFACE IN THIS TABLE, THE ORBITER HAS ALLOCATED APPROXIMATELY 800 WATTS OF CONTINUOUS POWER TO THE SPACECRAFT RTG COOLING PACKAGE LOCATED IN THE CARGO BAY (300W FROM MN DC BUS A, 300 W FROM MN DC BUS B, AND ADDITIONAL POWER AS ALLOCATED PER TABLE 5.3-2).

TABLE 5.2-2

PRIMARY DC POWER UTILIZATION

INTERFACE CONTROL DOCUMENT

ORBITER-VEHICLE/CENTAUR	SIZE	ICD NO	REV	SHEET
	A	ICD-2-1F001	NC	195 OF



AC POWER CHARACTERISTICS 0C-12

3 PHASE, 4 WIRE WYE CONNECTED.

NOMINAL VOLTAGE: 115/200 (VRMS).

FREQUENCY: 400Hz ± 7 Hz

FREQUENCY MODULATION: ± 1 Hz OF MEAN FREQUENCY

PHASE DISPLACEMENT: WITHIN 120 DEGREE  
LIMITS ± 2 DEGREES

PHASE SEQUENCING: ~~ABC~~ A, B, C

CREST FACTOR: 1.41 ± 0.15

TOTAL HARMONIC CONTENT: 5% OF RMS

INDIVIDUAL HARMONIC CONTENT: 4% OF RMS

VOLTAGE MODULATION: 3.5V MAX PEAK TO VALLEY  
STEADY STATE! DIFFERENTIAL FOR 1 SECOND MIN.

TRANSIENT VOLTAGE SURGE: AS SPECIFIED IN  
FIG'S 1, 2 & 3

REVISIONS			
LTR	DESCRIPTION	DATE	APPROVE

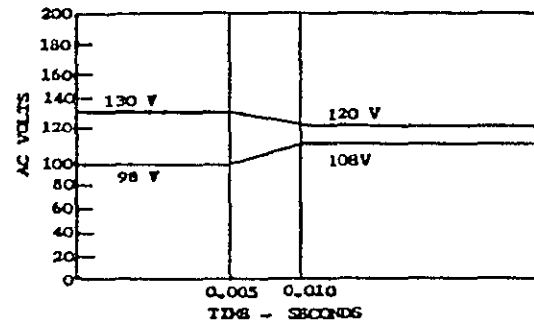


FIG. 1 TRANSIENT AC VOLTAGE STEP FUNCTION LOCK LIMITS DURING NORMAL SWITCHING CONDITIONS

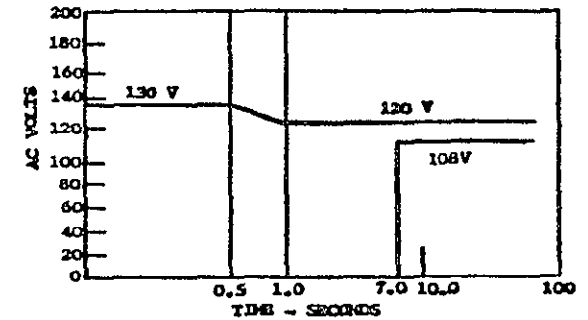


FIG. 2 TRANSIENT SURGE AC VOLTAGE STEP FUNCTION LOCK LIMITS DURING ABNORMAL SWITCHING CONDITIONS

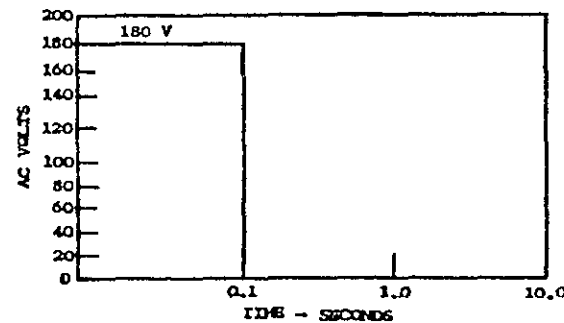


FIG. 3 TRANSIENT SURGE AC VOLTAGE STEP FUNCTION LOCK LIMITS DURING EMERGENCY SWITCHING CONDITIONS

TABLE 5.3-1

AC POWER

INTERFACE CONTROL DOCUMENT			
SIZE	ICD NO	REV	SHEET
B	ICD-3-1P00R	NC	196

ORIGINAL PAGE IS  
OF POOR QUALITY

CONDITION	CONTINUOUS WATTS (RMS)/PHASE	TRANSIENT WATTS (RMS)/PHASE
PRE LAUNCH	0	0
ASCENT	0	0
ON-ORBIT	25	75 (MAXIMUM)
DESCENT	0	0
POST LANDING	0	0

- 200 WATTS FROM EITHER AC BUS 3 (PRIMARY) OR AC BUS 2 (BACKUP) IS ALLOCATED FOR RTG COOLING PACKAGE LOCATED IN ORBITER CARGO BAY.

ORIGINAL PAGE IS  
OF POOR QUALITY

TABLE 5.3-2

AC POWER UTILIZATION

INTERFACE CONTROL DOCUMENT

ORBITER-VEHICLE/CENTAUR	SIZE	ICD NO	REV	SHEET
	A	ICD-2-1F001	NO	OF 147

Parameter	Dimension	CISS Characteristics	Notes
Bit rate	KBPS	64	ORIGINAL PAGE IS OF POOR QUALITY
Code		Bi0-L	
Word Length	Bits	TBD	
Minor Frame Length	Words	TBD	
Minor Frame Rate	Frames/Sec	TBD	
Master Frame Length	Minor Frames	TBD	
Minor Frame Sync		TBD	
Master Frame Sync		TBD	
Format Sample Rates		TBD	

TABLE 5.4-1

PAYLOAD DATA INTERLEAVER INPUT DATA  
FORMAT CHARACTERISTICS-CISS

INTERFACE CONTROL DOCUMENT

ORBITER-VEHICLE/CENTAUR	SIZE	ICD NO	REV	SHEET
	A		ICD-2-1F001	NC

Parameter	Dimension	CENTAUR Characteristics	Notes
Bit rate	KBPS	64	ORIGINAL PAGE IS OF POOR QUALITY
Code		Bi0-L	
Word Length	Bits	TBD	
Minor Frame Length	Words	TBD	
Minor Frame Rate	Frames/Sec	TBD	
Master Frame Length	Minor Frames	TBD	
Minor Frame Sync		TBD	
Master Frame Sync		TBD	
Format Sample Rates		TBD	

TABLE 5.4-2

PAYLOAD DATA INTERLEAVER  
INPUT DATA FORMAT  
CHARACTERISTICS-CENTAUR

INTERFACE CONTROL DOCUMENT

ORBITER-VEHICLE/CENTAUR	SIZE	ICD NO ICD-2-1F001	REV	SHEET 149
	A		NC	OF

Parameter	Dimension	Characteristics	Payload Characteristic	Notes
Bit rate	KBPS	10 BPS to 64 KBPS	See Appendix I for Payload Characteristics	ORIGINAL PAGE IS OF POOR QUALITY
Code		NRZ-L, M or S Bi Ø -L, M or S		
Word Length	Bits	8 or multiples of 8		
Minor Frame Length	Words	8 to 1024 (8-bit words)		
Minor Frame Rate	Frames/Sec	200 Max		
Master Frame Length	Minor Frames	2-256		
Minor Frame Sync		8, 16, 24 or 32 bits any pattern. Contiguous locations in first or last word(s) of every minor frame		
Master Frame Sync		8, 16, 24 or 32 bits any pattern Contiguous locations in first or last word every master frame or 8 bit minor frame counter		
Format Sample Rates		One equal to minor frame rate. Six equal to interger submultiple of Minor Frame Rate including one equal to master frame rate		

TABLE 5.4-3

PAYLOAD DATA INTERLEAVER  
INPUT DATA FORMAT  
CHARACTERISTICS-CENTAUR  
PAYLOAD

INTERFACE CONTROL DOCUMENT

ORBITER-VEHICLE/CENTAUR	SIZE	ICD NO	REV	SHEET
	A	ICD-2-1F001	NC	150 OF

NOTES:

- 1 Relative position of B10-L mid bit transition at interface
- 2 Any bit or clock transition point occurs in time at the 50% pk-pk amplitude point.
- 3 The PDI shall set an error flag within its BITE Status Register whenever the Payload bit rate exceeds  $\pm 3.25\%$  of its specified center frequency.
- 4 CCE Signal Differential Phase skew, as defined here, shall consist of the absolute value of the difference between the Leading Edge Phase Shift and the Trailing Edge Phase Shift (refer to Figure 5.4-5) and is independent of Payload amplitude level.  
  
CCE Signal Phase Shift is the time differential between the 50% points of associated amplitude transitions of the two CCE differential inputs.
- 5 Volts over frequency spectrum from DC to 100 KHz.
- 6 All parameters referenced to CISS interface

ORIGINAL PAGE IS  
OF POOR QUALITY

TABLE 5.4-4  
SHEET 1 of 3

PDI DATA INPUT/CCE TO  
ORBITER ELECTRICAL INTERFACE  
CHARACTERISTICS

INTERFACE CONTROL DOCUMENT

ORBITER-VEHICLE/CENTAUR	SIZE A	ICD NO ICD-2-1F001	REV NC	SHEET 151 OF
-------------------------	-----------	-----------------------	-----------	-----------------

Parameter	Dimension	Characteristics Orbiter/CCE Interface	Notes
Signal Type		Differential-Balanced	Refer to Figures 5.4-6 and 5.4-7
Amplitude	Volts pk-pk	Min: 2.5 Max: 9.0	Measured line-to-line at CISS interface $\triangle$
Duty Cycle	Percent	50 $\pm$ 3	$\triangle$ $\triangle$
Bit-Rate Accuracy	Percent	$\pm$ 3.25	$\triangle$
Stability		< 1 part in 10 <sup>5</sup> over 60 sec period	
Waveform Distortion		Overshoot and undershoot less than 20% of peak amplitude level	
Noise	Millivolts	100 pk-pk, differential line-to-line, DC to 100 KHz	CCS transmitting, not transmitting, or failed
Cable		2 conductor twisted, shielded, jacketed controlled impedance	Rockwell design standard MP572-0328-0002 (Orbiter)
Cable Impedance	Ohm	75 $\pm$ 5	Characteristic Impedance
Cable Capacitance	Picofarads	2900 max	Capacitance across differential line pair from CISS interface to PDI (18 to 23 pF/ft)
Load Impedance	Ohm	74 min 91 max	DC resistance line-to-line at interface includes cable resistance

ORIGINAL PAGE IS  
OF POOR QUALITY

TABLE 5.4-4  
SHEET 2 of 3

PDI DATA INPUT/CCE TO  
ORBITER ELECTRICAL INTERFACE  
CHARACTERISTICS

INTERFACE CONTROL DOCUMENT

ORBITER-VEHICLE/CENTAUR	SIZE A	ICD NO ICD-2-1F001	REV NC	SHEET OF
-------------------------	-----------	-----------------------	-----------	-------------

52

Parameter	Dimension	Characteristics Orbiter/CCE Interface	Notes
Cable Resistance	Ohm	4.4 per conductor max	Based on 126 foot cable length from CISS interface to PDI input
Cable Length	Feet	126 (max)	From CISS interface to PDI input
Rise/Fall Time	Microsec	1 (max)	
Skew-Differential Phase	Nanosecond	$\leq 127$	⚠️ 4
Common Mode	Volt	+3 pk-pk continuous or -60 pk-pk for 10 $\mu$ sec for damage level	⚠️ 5 + 3 volts from EMI, negligible from CCE or PDI.

ORIGINAL PAGE IS  
OF POOR QUALITY

TABLE 5.4-4  
SHEET 3 of 3

PDI DATA INPUT/CCE TO  
ORBITER ELECTRICAL INTERFACE  
CHARACTERISTICS

INTERFACE CONTROL DOCUMENT

ORBITER-VEHICLE/CENTAUR	SIZE	ICD NO	REV	SHEET
	A	ICD-2-1F001	NC	153 OF



NOTES:

1

Any bit or clock transition point occurs in time at the 50% pk-pk amplitude point.

2

The PDI shall set an error flag within its BITE Status Register whenever the Payload bit rate exceeds  $\pm 3.25\%$  of its specified center frequency.

3

Volts across frequency spectrum from DC to 100 KHz.

4. All parameters referenced to CISS interface

ORIGINAL PAGE IS  
OF POOR QUALITY

TABLE 5.4-5  
SHEET 1 of 3

PDI CLOCK INPUT/CCE TO ORBITER  
ELECTRICAL INTERFACE  
CHARACTERISTICS

INTERFACE CONTROL DOCUMENT

ORBITER-VEHICLE/CENTAUR	SIZE A	ICD NO ICD-2-1F001	REV NC	SHEET OF 154
-------------------------	-----------	-----------------------	-----------	-----------------

Parameter	Dimension	Characteristics Orbiter/CCE Interface	Notes
Signal Type	N/A	Differential-Balanced	Refer to Figures 5.4-6 and 5.4-7
Amplitude	Volts pk-pk	Min: 2.5 Max: 9.0	Measured line-to-line
Duty Cycle	Percent	50 $\pm$ 5	NRZ bit rate clock $\triangle$ 1
Skew - Data to Clock (NRZ)	N/A	Max: + 10% of clock period	Bit rate clock to NRZ bit start (1). See Figure 5.4-8
Stability	N/A	< 1 part in 10 <sup>5</sup> over 60 sec period	
Clock Accuracy	Percent	+ 3.25	$\triangle$ 2
Waveform Distortion	N/A	Overshoot and undershoot less than 20% of peak amplitude level	
Noise	Millivolts	100 pk-pk, differential line-to-line, DC to 100 KHz	CCE transmitting, not transmitting, or failed
Cable	N/A	2 conductor twisted, shielded, jacketed, controlled impedance	Rockwell design standard MP572-0328-0002 (Orbiter)
Cable Impedance	Ohm	75 $\pm$ 5	Characteristic Impedance
Cable Capacitance	Picofarads	2900 max	Capacitance across differential line pair from CISS interface to PDI (18 to 23 pf/ft)


ORIGINAL PAGE IS  
OF POOR QUALITY

TABLE 5.4-5  
SHEET 2 of 3

PDI CLOCK INPUT/CCE TO ORBITER  
ELECTRICAL INTERFACE  
CHARACTERISTICS

## INTERFACE CONTROL DOCUMENT

ORBITER-VEHICLE/CENTAUR	SIZE A	ICD NO ICD-2-1F001	REV NC	SHEET OF
				155

Parameter	Dimension	Characteristics Orbiter/CCE Interface	Notes
Load Impedance	Ohm	74 min 91 max	DC resistance line-to-line at interface includes cable resistance
Cable Resistance	Ohm	4.4 per conductor (max)	Based on 126 ft. cable length
Cable Length	Feet	126 max	From CISS interface to PDI input
Rise/Fall Time	N/A	Max: Refer to Differential Phase Skew	RT/FT are independent of bit rate and data code type (BiØ or NRZ)
Skew-Differential Phase	Nanosecond to Millisecond depending on bit rate	Maximum value shall be the same as that specified for associated NRZ data	
Common Mode	Volt	Max +3 pk-pk continuous or +60 pk-pk for 10 µ sec for damage level	+ 3V from EMI, negligible from payload or PDI 

ORIGINAL PAGE IS  
OF POOR QUALITY

TABLE 5.4-5  
SHEET 3 of 3

PDI CLOCK INPUT/CCE TO ORBITER  
ELECTRICAL INTERFACE  
CHARACTERISTICS

## INTERFACE CONTROL DOCUMENT

ORBITER-VEHICLE/CENTAUR	SIZE	ICD NO	REV	SHEET
	A	ICD-2-1F001	NC	156 OF

NOTES:

- ① Referenced to Signal Ground
- ② Based on 126-ft cable length from CISS interface to payload recorder input
- ③ TI SN55114, or equivalent
- ④ All parameters referenced to CISS interface

ORIGINAL PAGE IS  
OF POOR QUALITY

TABLE 5.4-6  
SHEET 1 of 2

DIGITAL DATA RECORDING ELECTRICAL  
INTERFACE CHARACTERISTICS

INTERFACE CONTROL DOCUMENT

ORBITER-VEHICLE/CENTAUR	SIZE A	ICD NO ICD-2-1F001	REV NC	SHEET 157 OF _____
-------------------------	-----------	-----------------------	-----------	-----------------------

Parameter	Dimension	Characteristics Orbiter/CCE Interface	Notes
Bit Rate	kbps	64	
Signal Type		Differential	
Data Type		Bi $\phi$ -L	
Rise & Fall Time	Percent Bit Cell Time (BCT)	10 Max	
Signal Amplitude	V, P-P	3.5 Min 9 Max	2
Jitter & Assymetry	Percent of BCT	$\pm 2$	
Input Impedance (Recorder)	Ohms, L-L	75 $\pm$ 10%	
Source Impedance CCE	Ohms, L-L	TTI Compatible 3	
Common-mode Rejection	Volts	$\pm 15$	1
Cable Type		Twisted Shielded Pair	RI design std MP572-0328-0002 (Orbiter)
Cable Impedance (Orbiter)	Ohms	75 $\pm$ 5	
Cable Resistance (Orbiter)	Ohms	4.4 per conductor (max)	
Cable Capacitance (Orbiter)	PICO Farads	2900 Max	18 to 23 pf per foot

ORIGINAL PAGE IS  
OF POOR QUALITY

TABLE 5.4-6  
SHEET 2 of 2

DIGITAL DATA RECORDING ELECTRICAL  
INTERFACE CHARACTERISTICS

## INTERFACE CONTROL DOCUMENT

ORBITER-VEHICLE/CENTAUR

SIZE  
A

ICD NO  
ICD-2-1F001

REV  
NC

SHEET 158  
OF

NOTES:

- 1. Based on MTU accuracy and stability
- 2. Based on 126 foot cable length from PSP output to CISS interface
- 3. All parameters referenced to CISS interface
- 4. Data rate for CISS/CENTAUR is 2000 BPS  $\pm$  0.001 percent. Data rate for payload is defined in Appendix I. Accuracy is based on MTU accuracy and stability.

ORIGINAL PAGE IS  
OF POOR QUALITY

TABLE 5.5-1  
SHEET 1 of 3

PSP COMMAND DATA OUTPUT,  
ELECTRICAL INTERFACE  
CHARACTERISTICS

INTERFACE CONTROL DOCUMENT

ORBITER-VEHICLE/CENTAUR	SIZE A	ICD NO ICD-2-1F001	REV NC	SHEET 159 OF
-------------------------	-----------	-----------------------	-----------	--------------------

Parameter	Dimension	Value	Notes
Subcarrier Frequency	KHz	16 + 0.001% (24hr) △	Sine wave
Subcarrier Harmonic Distortion	Percent	Less than 2% of the power in the subcarrier	Total harmonic distortion
Subcarrier Frequency Stability		< 10 <sup>-7</sup> of the sub-carrier frequency over a 10 second period (short term) △	
Subcarrier Modulation		PSK	
Data Rate	bps	4 △	
Data Rate Stability		10 <sup>-7</sup> over a 10 second period (short term) △	
Data Types		NRZ-L	
Frequency-to-Bit Rate Ratio		Multiple of data rate	Data waveform shall conform to S/C zero crossings within ± 10 degrees
Data Transition		Data shall alter S/C phase by ± 90° ± 10%	
Amplitude	Volts p-p	3.2 to 4.4, line-to-line into minimum specified load impedance	Voltage at CISS interface includes orbiter cable losses
Phase Jitter	Percent of bit period	3 max	

ORIGINAL PAGE IS  
OF POOR QUALITY

TABLE 5.5-1  
SHEET 2 of 3

PSP COMMAND DATA OUTPUT,  
ELECTRICAL INTERFACE  
CHARACTERISTICS

INTERFACE CONTROL DOCUMENT

ORBITER-VEHICLE/CENTAUR	SIZE	ICD NO	REV	SHEET
	A	ICD-2-1F001	NC	160
			OF	

Parameter	Dimension	Value	Notes
Data Asymetry	Percent of bit period	2 max over a 300 bit period	See Fig 5.5-6
Channel-to-Channel Isolation	dB	40 min	Between-channel isolation when each channel is terminated with 75 ohms
Source Impedance	Ohms	< 15	
Load Impedance	Ohms	68 min 1000 max	
Output Type		Differential	
Load Termination		Differential, Direct Coupled	
Offset	Volts	0.0 ± 0.5 either line-to-ground	
Cable Type		Twisted Shielded Pair	RI design standard MP572-0328-0002 (ORBITER)
Cable Impedance (Orbiter)	Ohms	75 ± 5 @ 1 MHZ 200 @ 16 KHZ	
Cable Capacitance (Orbiter)	Picofarads	1900 max $\triangle$ <sub>2</sub>	18 to 23 pF per foot
Cable Resistance (Orbiter)	Ohms	4.4 maximum per conductor $\triangle$ <sub>2</sub>	
Cable Length (Orbiter)	Feet	126 (max)	From PSP to CISS interface

ORIGINAL PAGE IS  
OF POOR QUALITY

TABLE 5.5-1  
SHEET 3 of 3

PSP COMMAND DATA OUTPUT,  
ELECTRICAL INTERFACE  
CHARACTERISTICS

INTERFACE CONTROL DOCUMENT

ORBITER-VEHICLE/CENTAUR	SIZE	ICD NO	REV	SHEET <u>161</u>
	A		ICD-2-1F001	NC OF _____



NOTES:

1

REFERENCE 28-VOLT POWER RETURN

2

ALL PARAMETERS REFERENCED TO GISS INTERFACE

ORIGINAL PAGE IS  
OF POOR QUALITY

PRECEDING PAGE BLANK NOT FILMED

162, 163

TABLE 5.5-3  
SHEET 1 of 3

HIGH-LEVEL DISCRETE OUTPUT  
(DOH)/ORBITER-TO-PAYLOAD  
ELECTRICAL INTERFACE  
CHARACTERISTICS

INTERFACE CONTROL DOCUMENT

ORBITER-VEHICLE/CENTAUR	SIZE A	ICD NO ICD-2-1F001	REV NC	SHEET 164 OF _____
-------------------------	-----------	-----------------------	-----------	-----------------------

Parameter	Dimension	Characteristics Orbiter/CCIS Interface	Notes
Type		Single-Ended Discrete	
Code		Step Level	
Discrete- False ("0")	Min Volt Max Volt	0 3	⚠
Discrete- True ("1")	Min Volt Max Volt	19.5 32	⚠
Ripple & Noise	Max Millivolt	0.9 V p-p Single Freq. 1.6 V p-p Broadband	
Rise/Fall Time	Min Microsec Max Microsec	10 100	
Transfer		Direct Coupled	

ORIGINAL PAGE IS  
OF POOR QUALITY.

TABLE 5.5-3  
SHEET 2 of 3

HIGH-LEVEL DISCRETE OUTPUT  
(DOH)/ORBITER-TO-PAYLOAD  
ELECTRICAL INTERFACE  
CHARACTERISTICS

### INTERFACE CONTROL DOCUMENT

ORBITER-VEHICLE/CENTAUR	SIZE <b>A</b>	ICD NO ICD-2-1F001	REV NC	SHEET <b>165</b> OF
-------------------------	------------------	-----------------------	-----------	------------------------

Parameter	Dimension	Characteristics Orbiter/CCIS Interface	Notes
Source Impedance (Orbiter)	Ohm Ohm	0 450	
Load Impedance Min (CCE)	Ohm	3.2K	
Max	Ohm	10K	
Capacitance Max	Pico-Farad	3500	CCE 1500 Max
Pwr-Off Impedance Min	Ohm	10K (+8VDC)	CCE 3K Min
Current Drive	Milliamp	10 (Logic "1")	
Current Sink	Milliamp	NA	
Overvoltage Protection Max	Volt	+ 32	
Fault Voltage Mission Max	Volt	+ 32	
Fault Current Limitation	Milliamp	20	

ORIGINAL PAGE IS  
OF POOR QUALITY

TABLE 5.5-3  
SHEET 3 of 3

HIGH-LEVEL DISCRETE OUTPUT  
(DOH)/ORBITER-TO-PAYLOAD  
ELECTRICAL INTERFACE  
CHARACTERISTICS

INTERFACE CONTROL DOCUMENT

ORBITER-VEHICLE/CENTAUR	SIZE A	ICD NO ICD-2-1F001	REV NC	SHEET OF 166
-------------------------	-----------	-----------------------	-----------	-----------------

NOTES:

1

Full ON indication given (up or down) for greater than 18 VDC applied.  
Full OFF indication given (center position) for zero volts applied.

2

Full ON indication given for greater than 18 VDC applied.  
Full OFF indication given for 5 VDC applied.

ORIGINAL PAGE IS  
OF POOR QUALITY



TABLE 5.5-4  
SHEET 1 of 2

SSP STATUS INDICATORS AND  
SWITCH ELECTRICAL CHARACTERISTICS

INTERFACE CONTROL DOCUMENT

ORBITER-VEHICLE/CENTAUR	SIZE	ICD NO	REV	SHEET <u>167</u>
	<u>A</u>		ICD-2-1F001	NC

SSP STATUS INDICATORS

Indicator Identification	Type	VDC	Input Impedence Kilohms
DS1, DS2, DS13, DS14	3 position 	28 VDC	53 ±5
DS3 to DS12, DS15 to DS24	2 position 	28 VDC	28 ±3

SWITCH ELECTRICAL CHARACTERISTICS

ORIGINAL PAGE IS  
OF POOR QUALITY

Switch Identification	No of Poles	No of Pos.	Operations	Volt Rating	Amp Rating
S1, S2, S5, S9, S13 S14, S17, S21	2	3	momentary ON maintained OFF momentary ON	32 VDC	5
S10, S22	2	2	maintained ON maintained ON	32 VDC	5
S3, S4, S6, S7, S8, S11, S15, S16, S18, S19, S20, S23	2	2	maintained ON maintained ON	32 VDC	5
S12, S24	2	3	maintained ON maintained OFF maintained ON	32 VDC	5

TABLE 5.5-4  
SHEET 2 of 2

SSP STATUS INDICATORS AND  
SWITCH ELECTRICAL CHARACTERISTICS

INTERFACE CONTROL DOCUMENT

ORBITER-VEHICLE/CENTAUR	SIZE <b>A</b>	ICD NO ICD-2-1F001	REV NC	SHEET <u>168</u> OF <u>    </u>
-------------------------	------------------	-----------------------	-----------	------------------------------------

NOTES:

1

SOURCE IMPEDANCE 100 OHMS MAXIMUM WITH 10 OHMS MAXIMUM UNBALANCE FOR 0.5% RMS ONE SIGMA OF FULLSCALE ENCODING ACCURACY.

2

THE MEASUREMENT ACCURACY SHALL BE WITHIN .50% (1 SIGMA FULL SCALE). THE ACCURACY IS DIRECTLY AFFECTED BY INPUT NOISE WITHIN THE FILTER PASSBAND OR SIGNALS CHANGING DURING THE AID CONVERSION TIME.

3. ALL PARAMETERS REFERENCED TO CISS INTERFACE

ORIGINAL PAGE IS  
OF POOR QUALITY

PRECEDING PAGE BLANK NOT FILMED

169 - 172

TABLE 5.5-7  
SHEET 1 of 3

LOW LEVEL DIFFERENTIAL ANALOG  
INPUT (AID), CISS TO ORBITER,  
ELECTRICAL  
INTERFACE CHARACTERISTICS

INTERFACE CONTROL DOCUMENT

ORBITER-VEHICLE/CENTAUR	SIZE	ICD NO	REV	SHEET
	A		ICD-2-1F001	NC

Parameter	Dimension	Characteristics ORB/CISS Interface	Notes
Type		Differential Analog	Direct Coupled
Analog Range			
Min	Volt	-5.0	△ <sub>2</sub>
Max	Volt	+5.0	
Source Impedance			
Min (CCE)	Ohm	0	△ <sub>1</sub>
Max	Ohm	100	
Load Impedance			
Min (Orbiter)	Ohm	500K	> 100K power off
Max	Ohm	NA	
Capacitance			
Max	Pico-Farad	5000	
Pwr-Off Impedance			
Min	Ohm	100K	
Input Filter 3db Bandwidth	Hertz	DC to 40 ± 10%	
Roll-off Rate			
Min	dB/Octave	6	
CMRR	dB	60 (within Bandwidth)	
Accuracy	Percent	+ 0.5	△ <sub>1</sub> With 10 Ohms Maximum Unbalance
Frequency	Hertz	See Filter Bandwidth	

ORIGINAL PAGE IS  
OF POOR QUALITY

TABLE 5.5-7  
SHEET 2 of 3

LOW LEVEL DIFFERENTIAL ANALOG  
INPUT (AID), CISS TO ORBITER,  
ELECTRICAL  
INTERFACE CHARACTERISTICS

INTERFACE CONTROL DOCUMENT

ORBITER-VEHICLE/CENTAUR	SIZE	ICD NO	REV	SHEET
	A	ICD-2-1F001	NC	174
			OF	

Parameter	Dimension	Characteristics ORB/CISS Interface	Notes
Current Sink	Milliamp	0.024	At 5.0 volts
Overvoltage Protection Max	Volt	+ 32	
Fault Voltage Emission Max	Volt	+ 15	
Fault Current Limitation Max	Milliamp	1	
Cable		TSP-ML	

ORIGINAL PAGE IS  
OF POOR QUALITY

TABLE 5.5-7  
SHEET 3 of 3

LOW LEVEL DIFFERENTIAL ANALOG  
INPUT (AID), CISS TO ORBITER,  
ELECTRICAL  
INTERFACE CHARACTERISTICS

### INTERFACE CONTROL DOCUMENT

ORBITER-VEHICLE/CENTAUR	SIZE	ICD NO	REV	SHEET
	A	ICD-2-1F001	NC	175
				OF



NOTES:

1. ALL PARAMETERS REFERENCED TO CISS INTERFACE

ORIGINAL PAGE IS  
OF POOR QUALITY

TABLE 5.5-8  
SHEET 1 of 3

HIGH-LEVEL DISCRETE INPUT (DIH)  
CCE TO ORBITER-ELECTRICAL  
INTERFACE CHARACTERISTICS

INTERFACE CONTROL DOCUMENT

ORBITER-VEHICLE/CENTAUR	SIZE A	ICD NO ICD-2-1F001	REV NC	SHEET 176 OF _____
-------------------------	-----------	-----------------------	-----------	-----------------------

Parameter	Dimension	Characteristics ORB/CISS Interface	Notes
Type		Single-Ended Discrete	
Code		Threshold Decision	
Discrete- False ("0")	Min Max Volt Volt	0 6	An open circuit input results in a "FALSE" indication.
Discrete- True ("1")	Min Max Volt Volt	10 32	
Ripple & Noise	Max Millivolt	600	
Rise/Fall Time	Min Max Microsec Microsec	10 100	
Input Filter 3db Bandwidth	Hertz	DC TO 1K $\pm$ 12%	(Low-Pass Filter)
Roll-off Rate	Min dB/Octave	6	
Transfer		Direct Coupled	

ORIGINAL PAGE IS  
OF POOR QUALITY

TABLE 5.5-8  
SHEET 2 of 3

HIGH-LEVEL DISCRETE INPUT (DIH)  
CCE TO ORBITER-ELECTRICAL  
INTERFACE CHARACTERISTICS

### INTERFACE CONTROL DOCUMENT

ORBITER-VEHICLE/CENTAUR

SIZE  
A

ICD NO  
ICD-2-1F001

REV  
NC

SHEET 177  
OF

Parameter	Dimension	Characteristics ORB/CISS Interface	Notes
Source Min Impedance (CCE)	Ohm	0	
	Ohm	1K	
Load Min Impedance (Orbiter) Max	Ohm	245K	
	Ohm	357K	
Capacitance Max	Pico-Farad	5000	
Pwr-Off Min Input Impedance Min	Ohm	245K	
	Ohm	357K	
Current Sink Max	Milliamp	0.13	At 32 volts
Over-voltage Protection Max	Volt	+ 32	
Fault Voltage Mission Max	Volt	+ 32	
Fault Current Limitation Max	Microamp	320	

ORIGINAL PAGE IS  
OF POOR QUALITY

TABLE 5.5-8  
SHEET 3 of 3

HIGH-LEVEL DISCRETE INPUT (DIH)  
CCE TO ORBITER-ELECTRICAL  
INTERFACE CHARACTERISTICS

### INTERFACE CONTROL DOCUMENT

ORBITER-VEHICLE/CENTAUR	SIZE <b>A</b>	ICD NO ICD-2-1F001	REV NC	SHEET OF <u>178</u>
-------------------------	------------------	-----------------------	-----------	------------------------

APPENDIX I

100.0 Payload Command and Data Format Characteristics

This appendix defines the format characteristics for Centaur Payload Telemetry and Command data.

100.1 Centaur Payload Telemetry Data Format Characteristics

Format characteristics for the Centaur Payload telemetry data which interferes with the orbiter Payload Data interleaver are defined in Table A.

100.2 Centaur Payload Command Data Format Characteristics

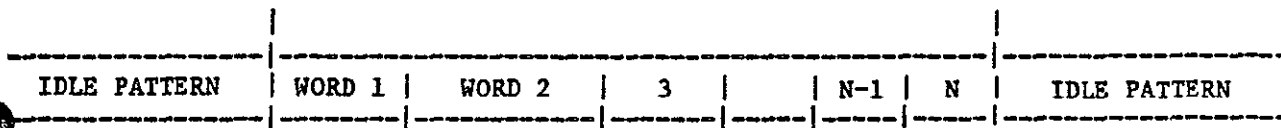
Format characteristics for the Centaur Payload command data requirements are defined in Figure A.

ORIGINAL PAGE IS  
OF POOR QUALITY

APPENDIX I

INTERFACE CONTROL DOCUMENT

ORBITER-VEHICLE/CENTAUR	SIZE A	ICD NO ICD-2-1F001	REV NC	SHEET 179 OF
-------------------------	-----------	-----------------------	-----------	-----------------



- . IDLE PATTERN IS 101010 .. - MINIMUM OF 132 BITS PRECEEDING EACH MESSAGE
- . ALL WORDS ARE 16 BITS. THERE ARE NO START OR STOP BITS BETWEEN WORDS.
- . WORD 1 IS A FIXED SYNCHRONIZATION PATTERN, REGARDLESS OF THE MESSAGE TYPE. THE SPECIFIC PATTERN IS TBD.
- . WORD 2 DEFINES THE MESSAGE TYPE (I.E., COMMAND OR NAVIGATION UPDATE) AND MESSAGE LENGTH (NUMBER OF WORDS).
- . WORD N IS A CHECKSUM OF THE PREVIOUS WORDS FOR ERROR DETECTION PURPOSES. THERE IS NO ERROR CORRECTION CAPABILITY.
- . THE TOTAL MESSAGE LENGTH IS VARIABLE.

ORIGINAL PAGE IS  
OF POOR QUALITY

APPENDIX I  
FIGURE A

CENTAUR PAYLOAD COMMAND FORMAT

INTERFACE CONTROL DOCUMENT

ORBITER-VEHICLE/CENTAUR	SIZE	ICD NO	REV	SHEET 180
	A	ICD-2-1F001	NC	OF

Parameter	Dimension	Gallileo Payload Characteristic	ISPM Payload Characteristic	Remarks
Bit Rate	<del>4800</del>	1.2 <i>Kbps</i>	15.625 <i>Bps</i>	
Code		NRZ-L	BIQ-L	
Word Length	Bits	TBD	TBD	
Minor Frame Length	Words	TBD	TBD	
Minor Frame Rate	Frames/Sec	TBD	TBD	
Master Frame Length	Minor Frame	TBD	TBD	
Minor Frame Sync		TBD	TBD	
Master Frame Sync		TBD	TBD	
Format Sample Rates		TBD	TBD	

ORIGINAL PAGE IS  
OF POOR QUALITY

APPENDIX I  
TABLE A

PAYLOAD DATA FORMAT  
INPUT DATA FORMAT  
CHARACTERISTICS-CENTAUR  
PAYLOAD

INTERFACE CONTROL DOCUMENT

ORBITER-VEHICLE/CENTAUR	SIZE	ICD NO	REV	SHEET
	A	ICD-2-1F001	NC	181

LIST OF ACRONYMS AND ABBREVIATIONS

CCE	Centaur Cargo Element
CISS	Centaur Integrated System Structure
CKT	Circuit
CONN	Connector
CU	Control Unit
CMD	Command
DIM	Dimension
ECLSS	Environmental Life Support System
ET	External Tank
FSS	Fixed Service Structure
GDC	General Dynamics Corporation
GH <sub>2</sub>	Gaseous Hydrogen
GN <sub>2</sub>	Gaseous Nitrogen
GND	Ground
GO <sub>2</sub>	Gaseous Oxygen
GSE	Ground Support Equipment
He	Helium
I/F	Interface
JSC	Johnson Space Center
KSC	Kennedy Space Center
LCT	Location
LeRC	Lewis Research Center
LO <sub>2</sub>	Liquid Oxygen
LP <sup>2</sup>	Launch Platform
LRU	Line Replacement Unit
MDM	Multiplexer/Demultiplexer
MPS	Main Propulsion System
MSFC	Marshall Space Flight Center
NASA	National Aeronautics & Space Administration
OCV	Orbiter Centaur Vehicle
OLS	Orbiter Landing Station
OPF	Orbiter Processing Facility
ORB	Orbiter
PCM	Pulse Code Modulation
PDI	Payload Data Interleaver
PGHM	Payload Ground Handling Mechanism
P/L	Payload
PV&D	Purge Vent & Drain
QD	Quick Disconnect

ORIGINAL PAGE IS  
OF POOR QUALITY

INTERFACE CONTROL DOCUMENT

ORBITER VEHICLE/CENTAUR	SIZE	ICD NO.	REV	SHEET
	A	ICD-2--1F001	NC	182
			OF	

LIST OF ACRONYMS AND ABBREVIATIONS (Cont'd)

RI	Rockwell International
RSS	Rotating Service Structure
RTG	Radioisotope Thermo-electric Generator
SRB	Solid Rocket Booster
TBD	To be Determined
TBS	To be Supplied
T-0	Time Minus Zero
UMB	Umbilical

ORIGINAL PAGE IS  
OF POOR QUALITY

INTERFACE CONTROL DOCUMENT

ORBITER VEHICLE/CENTAUR	SIZE <b>A</b>	ICD NO ICD-2-1F001	REV NC	SHEET <u>183</u> OF _____
-------------------------	------------------	-----------------------	-----------	------------------------------





## 2.0 SWITCHING MODEL

In this memorandum, we consider the probability of losing lock due to a signal dropout for a 5-ms period. Basically, the dropout occurs when the second Centaur antenna is switched on before the first has been disconnected. Consequently, the sum signal is transmitted to the TDRSS and relayed to the ground. Since the two signals can be either additive or subtractive, it is possible to obtain a null or an enhancement of the sum signal.

We consider two sources of loss of lock due to the dropout: (1) the effect of this loop noise when the signal is absent; (2) the doppler shift of the signal after the antenna is switched. First, we consider the effects of thermal noise during the 5-ms dropout.

Figure 1 [1] illustrates the null depth curve which corresponds to destructive as well as constructive signal combining. Note that, with the estimated angle of switching at  $90^\circ \pm 5^\circ$  ( $10^\circ$  angular region), about seven deep nulls appear. Since, at a maximum spin rate of 4.7 RPM, a 5-ms duration occurs for about  $0.15^\circ$  and the interference lobes are about  $1.36^\circ$  [1] wide, we conclude that the assumption of a complete fade (loss of signal) is certainly possible and is a worst-case (WC) model.

ORIGINAL PAGE IS  
OF POOR QUALITY

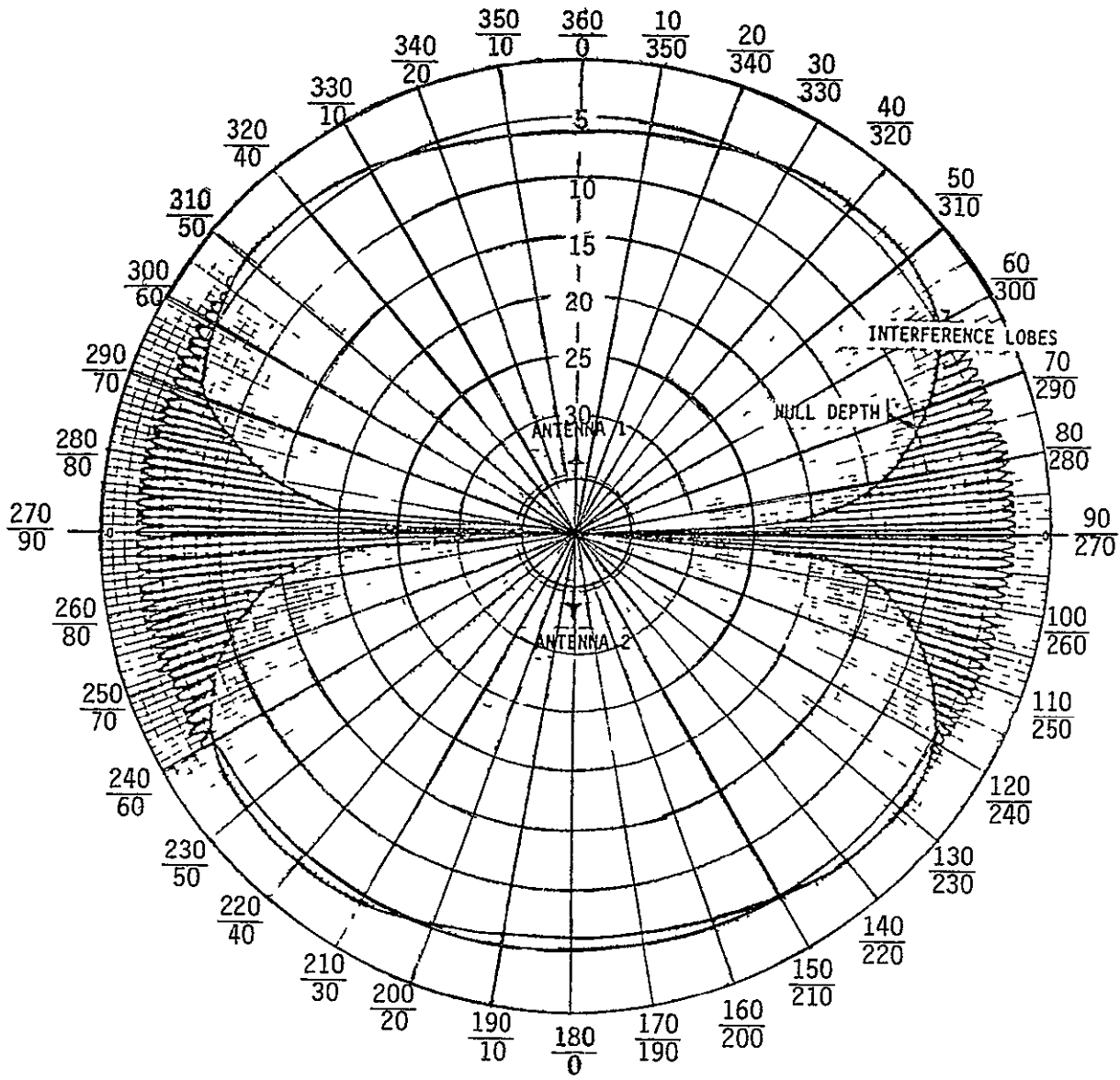


Figure 1. Combined Antenna Pattern Showing the Interface Lobes During The Antenna-Switching Transient When Both Antennas Radiate

## 3.0 STOCHASTIC DIFFERENTIAL EQUATION MODEL OF CARRIER LOOP (COSTAS LOOP)

The actual Costas loop used in the TDRSS ground station with the wide dynamic demodulator (WDD) is a digital integrate-and-dump arm filter, a second-order Costas loop, as shown in Figure 2. For ease of analysis, however, a first-order ordinary Costas loop will be analyzed. The model is illustrated in Figure 3.

Let the received signal be represented by

$$y(t) = \sqrt{2A} d(t) \sin(\omega_0 t + \theta(t)) + n(t) \quad (1)$$

where the noise process  $n(t)$  can be represented by its inphase and quadrature components by

$$n(t) = \sqrt{2} n_c(t) \cos(\omega_0 t + \theta_0) + \sqrt{2} n_s(t) \sin(\omega_0 t + \theta_0) \quad (2)$$

Signals  $y_c(t)$  and  $y_s(t)$  are given by

$$y_c(t) = K_\phi \left( A \bar{d}(t) \sin\phi + \tilde{n}_c(t) \cos\phi + \tilde{n}_s(t) \sin\phi \right) \quad (3)$$

and

$$y_s = K_\phi \left( A \bar{d}(t) \cos\phi - \tilde{n}_c(t) \sin\phi + \tilde{n}_s(t) \cos\phi \right) \quad (4)$$

where

$$\phi = \theta - \theta_0, \quad \text{the phase error} \quad (5)$$

and

$$\bar{d}(t) = \text{filtered version of } d(t), \quad \tilde{n}(t) = \text{filtered version of } n(t) \quad (6)$$

Hence, error-control signal  $z(t)$  becomes

$$z(t) = K_\phi^2 \left[ \frac{A^2}{2} (\bar{d})^2 \sin 2\phi + A \bar{d}(t) \tilde{n}_s(t) \sin 2\phi + \left[ \frac{(\tilde{n}_s)^2}{2} - \frac{(\tilde{n}_c)^2}{2} \right] \sin 2\phi \right. \\ \left. + (A \bar{d}(t) + \tilde{n}_s) \tilde{n}_c \cos 2\phi \right] + b \quad (7)$$

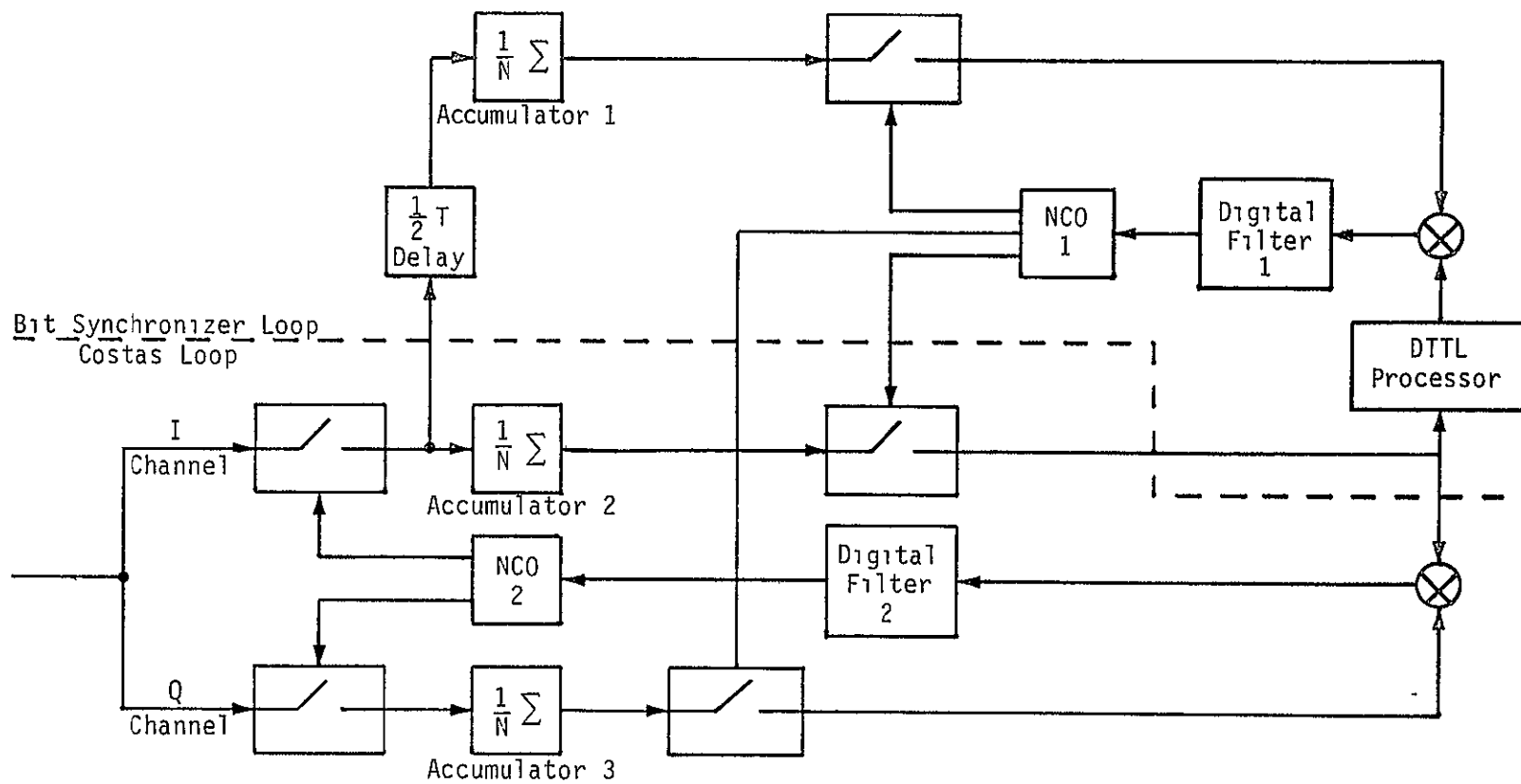
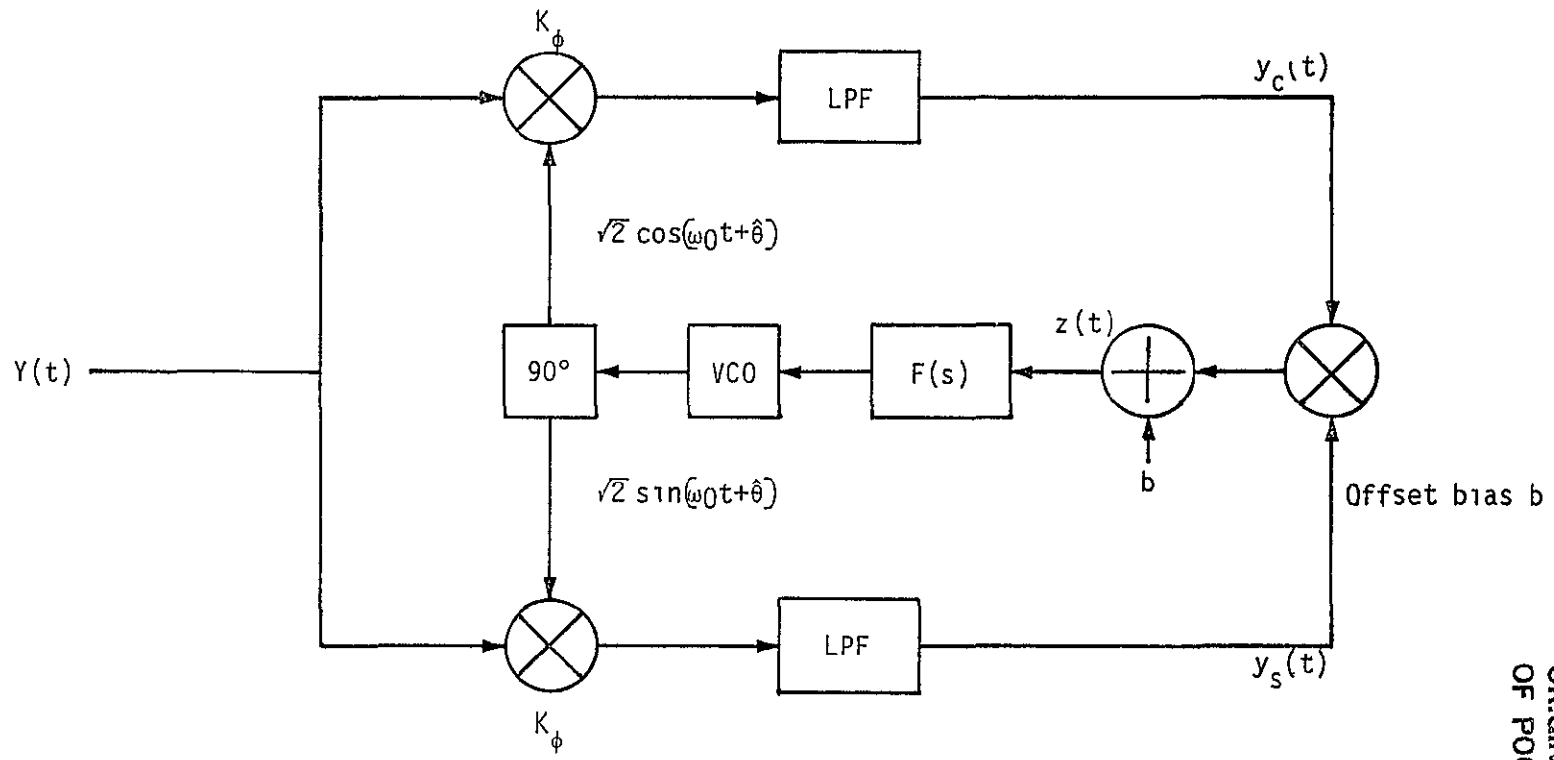


Figure 2. Wide-Dynamic Demodulator Carrier-Tracking-Loop Block Diagram



ORIGINAL PAGE IS  
OF POOR QUALITY

Figure 3. Ordinary Costas-Loop Model of the Wide-Dynamic Demodulator

where  $b$  is a model of any bias due to the multipliers, etc. The VCO phase estimate is given by

$$\hat{\theta} = \frac{K_{VCO} F(s)}{s} z(t) \quad (8)$$

where  $s$  is the Heaviside operator. The stochastic differential equation in  $\phi(t)$  follows from (5), (7) and (8), and is

$$\begin{aligned} F(s) \frac{\alpha K A^2}{2} \sin 2\phi + \dot{\phi} = \dot{\theta} - AKF(s) \left[ \tilde{d}(t) \tilde{n}_s(t) \sin 2\phi \right] - F(s) \left[ \frac{\tilde{n}_s^2 - \tilde{n}_c^2}{2} \right] K \sin 2\phi \\ - KF(s) (A \tilde{d}(t) + \tilde{n}_s) \tilde{n}_c \cos 2\phi - \frac{F(s) Kb}{K_\phi^2} \end{aligned} \quad (9)$$

where  $\alpha$  is the filtering loss of the data stream  $d(t)$  through the lowpass arm filters and  $K = K_\phi^2 K_{VCO}$ :

When the signal is gone,  $A = 0$ , so that (9) becomes

$$\dot{\phi} = \dot{\theta} - KF(s) \left( \frac{\tilde{n}_s^2 - \tilde{n}_c^2}{2} \right) \sin 2\phi - KF(s) \left[ \tilde{n}_s \tilde{n}_c \cos 2\phi \right] - \frac{KF(s)b}{K_\phi^2} \quad (10)$$

If we define the noise term by  $N(t)$ , then

$$N(t) = \frac{\tilde{n}_s^2 - \tilde{n}_c^2}{2} \sin 2\phi + \tilde{n}_s \tilde{n}_c \cos \phi \quad (11)$$

Since  $\tilde{n}_s$  is statistically independent of  $\tilde{n}_c$ , we deduce that

$$E[N(t)|\phi] = 0 \quad (12)$$

After some algebra, evaluating  $E[N(t)N(t+\tau)|\phi]$  produces

$$E[N(t)N(t+\tau)|\phi] = R_{\tilde{n}_s}^2(\tau) \quad (13)$$

We assume that: (1) the AGC has a large rise-time time constant compared to the dropout time; (2) it does not change from that value during the dropout.

The resulting stochastic differential equation is given by

$$\dot{\phi} = \dot{\theta} - KF(s) N(t) - \frac{KF(s)b}{K_{\phi}^2} \quad (14)$$

Since, for ease of analysis, we have decided to make our initial estimate based on a first-order PLL, we let  $F(s) = 1$ , then obtain

$$\dot{\phi} = \dot{\theta} - KN(t) - \frac{Kb}{K_{\phi}^2} \quad (15)$$



## 4.0 DERIVATION OF PROBABILITY OF SLIPPING WITH SIGNAL ABSENT

As long as the phase error remains within our (to be specified) limits  $\pm\theta_L$ , the probability density function obeys the Fokker-Plank equation, which is specified below for a first-order loop. We assume that the AGC does not respond significantly during the dropout time, so the effective noise spectral density is constant with time.

$$\frac{\partial p(\phi, t)}{\partial t} = \frac{\partial}{\partial \phi} \left[ A_1(\phi) p(\phi, t) \right] + \frac{1}{2} \frac{\partial^2}{\partial \phi^2} \left[ A_2(\phi) p(\phi, t) \right] \quad (16)$$

$$A_1(\phi) = \lim_{\Delta t \rightarrow 0} \left\{ \frac{E[\Delta\phi | \phi]}{\Delta t} \right\} \quad (17)$$

$$A_2(\phi) = \lim_{\Delta t \rightarrow 0} \left\{ \frac{E[(\Delta\phi)^2 | \phi]}{\Delta t} \right\} \quad (18)$$

Using (14), we obtain

$$\Delta\phi = \theta(t+\Delta t) - \theta(t) - K \int_t^{t+\Delta t} n(u) du - \frac{Kb}{K_\phi} \Delta t \quad (19)$$

so that

$$A_1(\phi) = \dot{\theta} - \frac{Kb}{K_\phi} \quad (20)$$

Now considering  $A_2(\phi)$ , we have,

$$E[\Delta\phi^2 | \phi] = \left( \theta(t+\Delta t) - \theta(t) - \frac{Kb\Delta t}{K_\phi} \right)^2 + EK^2 \int_t^{t+\Delta t} \int_t^{t+\Delta t} n(u)n(v) dudv \quad (21)$$

If  $\dot{\theta} = \Delta\omega$ , then,

$$A_2(\phi) = K^2 \frac{N_0}{2} \quad (22)$$

Hence, the Fokker-Planck equation becomes

$$\frac{\partial p(\phi, t)}{\partial t} = -\left(\dot{\phi} - \frac{Kb}{K_\phi}\right) \frac{\partial p(\phi, t)}{\partial \phi} + \frac{N_0' K^2}{4} \frac{\partial^2 p(\phi, t)}{\partial \phi^2} \quad (23)$$

We want to find the probability of not slipping (diffusing) to either boundary  $\phi_L$  or  $-\phi_L$  given that  $\phi(t) = \phi_0$  when  $t = 0$ . Darling and Siegert [2] have shown that the probability density  $P_{\phi_L}(t|\phi_0)$  of first crossing the boundaries  $\pm\phi_L$  can be found from the following discussion. Given the Fokker-Planck equation (23), the Laplace transform of  $P_{\phi_L}(t|\phi_0)$  which is denoted by  $\hat{P}(s|\phi_0)$  satisfies

$$\hat{P}(s|\phi_0) = \frac{v(\phi_0)[u(b) - u(-b)] - u(\phi_0)[v(b) - v(-b)]}{u(b)v(-b) - u(-b)v(b)} \quad (24)$$

where  $u(\phi)$  and  $v(\phi)$  are any two linearly independent solutions of the ordinary differential equation

$$\frac{K^2 N_0'}{4} \frac{d^2 y}{d\phi^2} - \left(\dot{\phi} - \frac{Kb}{K_\phi}\right) \frac{dy}{d\phi} - sy = 0 \quad (25)$$

Hence, in order to solve the slip-time probability density, we must solve an ordinary differential equation, then take the inverse Laplace transform of  $\hat{P}(s|\phi_0)$ .

Note that the probability that the phase process  $\phi(t)$  has not passed the level  $\pm\phi_L$  up to time  $T$  is given by the integral

$$P(\phi_L|\phi_0) = 1 - \int_0^T P(t|\phi_0) dt \quad (26)$$

Considering the solution to (25), let

$$y(\phi) = e^{a\phi} \quad (27)$$

We then have

$$\frac{K^2 N_0'}{4} a^2 e^{a\phi} - \left( \dot{\phi} - \frac{Kb}{K_\phi^2} \right) a e^{a\phi} - s e^{a\phi} = 0 \quad (28)$$

Hence, the two independent solutions are

$$u(\phi) = e^{\Delta\omega/2D + 1/2D \sqrt{(\Delta\omega)^2 + 4DS}} \quad (29)$$

and

$$v(\phi) = e^{\Delta\omega/2D - 1/2D \sqrt{(\Delta\omega)^2 + 4DS}} \quad (30)$$

where

$$D = \frac{K^2 N_0'}{4} \quad (31)$$

and

$$\Delta\omega = \dot{\phi} - \frac{Kb}{K^2} \quad (32)$$

It is not hard to show that the Laplace transform of the probability of crossing one of the thresholds is given by

$$\hat{P}(s|\phi_0) = \frac{e^{r(\phi_0+\phi_L)} \sinh[\lambda(\phi_L-\phi_0)] + e^{r(\phi_0-\phi_L)} \sinh[\lambda(\phi_L+\phi_0)]}{\sinh(2\phi_L)} \quad (33)$$

where

$$r = \Delta\omega/2D, \quad \lambda = 1/2D \sqrt{(\Delta\omega)^2 + 4DS} \quad (34)$$

Inverting (34) yields [3]

$$P(t|\theta_0) = \frac{\pi D}{\phi_L^2} e^{-\Delta\omega\phi_L/2D} \sum_{m=1}^{\infty} m \exp \left\{ \left[ -\frac{D\pi^2 m^2}{4\phi_L^2} + \frac{(\Delta\omega)^2}{4D} \right] t \right\} g_m \quad (35)$$

ORIGINAL PAGE IS  
OF POOR QUALITY

where

$$g_m = \begin{cases} (-1)^{\frac{m-1}{2}} \cosh \left[ \frac{\Delta\omega\phi_L}{2D} \right] \cos \left[ \frac{\pi m \phi_0}{2\phi_L} \right] & m \text{ odd} \\ (-1)^{\frac{m-1}{2} - 1} \sinh \left[ \frac{\Delta\omega\phi_0}{2D} \right] \sin \left[ \frac{\pi m \phi_0}{2\phi_L} \right] & m \text{ even} \end{cases} \quad (36)$$

The probability that  $\phi(t)$  has not passed through  $\pm\phi_L$  at time  $T$  is given by

$$P(\phi_L | \phi_0) = 1 - \int_0^T P(t | \phi_0) dt \quad (37)$$

so that our basic result is given by

$$P(\phi_L | \phi_0) = \frac{\pi D}{\phi_L^2} \exp \left\{ -\frac{\Delta\omega\phi_L}{2D} \right\} \sum_{m=1}^{\infty} \frac{mg_m}{\frac{D\pi^2 m^2}{4\phi_L^2} + \frac{(\Delta\omega)^2}{4D}} \exp \left\{ -\left[ \frac{D\pi^2 m^2}{4\phi_L^2} + \frac{(\Delta\omega)^2}{4D} \right] T \right\} \quad (38)$$

Equation (38) follows from (35) and (36) since

$$\frac{\pi D}{\phi_L^2} \exp \left\{ \frac{-\Delta\omega\phi_L}{2D} \right\} \sum_{m=1}^{\infty} \frac{mg_m}{\left[ \frac{D\pi^2 m^2}{4\phi_L^2} + \frac{(\Delta\omega)^2}{4D} \right]} = 1 \quad (39)$$

5.0 NUMERICAL EVALUATION OF  $P(t, \phi_0)$  FOR CENTAUR DUE TO NOISE

Since actual information on the wide dynamic demodulator (WDD) is limited, both facts and assumptions will be used to evaluate the probability of slipping a cycle. Since the actual implementation of the Costas loop is done digitally, it is expected that DC offsets will be very small, hence, using results from the first-order loop is reasonable (and can be solved). The parameters are:

$$\begin{aligned} R_b &= 32,000 \text{ bits/second} & \phi_0 &\approx 0 \text{ assumption} \\ B_L &= 420 \text{ Hz (second order)} & \phi_L &= \pi \text{ (condition for a possible slip)} \\ A^2/N_0 &= 7.3 \text{ dB} + 10 \log(32,000) & & \\ &= 52.4 \text{ dB (assumption)} & \Delta\omega &\approx 0 \text{ assumption} \end{aligned}$$

Now we must estimate what the value  $D$  is given by. From (31), note that  $D = K^2 N_0' / 4$ . For a first-order Costas loop,  $B_L = AK/4$  and  $\text{SNR} = A^2/4N_0'B$  so that

$$D = \frac{B_L}{\text{SNR}'} \quad (40)$$

where  $B_L$  is the one-sided closed-loop bandwidth and  $\text{SNR}'$  is the effective loop SNR when the signal is present. The effective SNR is defined by

$$\text{SNR}' = \frac{A^2}{4N_0' B_L} = \frac{1}{4\theta_\phi^2} = \frac{1}{\sigma_\phi^2} \quad (41)$$

with  $\sigma_\phi^2$  being the effective linearized tracking-error variance. For the linearized tracking error, we have from [4] that

$$\sigma_\phi^2 = \frac{4N_0' B_L}{P} \left[ 1 + \frac{N_0}{2PT} \right] \quad (42)$$

Evaluating using (42) yields

$$\text{SNR}' = 13.75 \text{ dB (23.7)} \quad (43)$$

Simplifying (38) and (36) to the case where  $\phi_0 = 0$  and  $\Delta\omega = 0$  yields

$$P(\phi_L | 0) = \frac{4}{\pi} \sum_{n=1}^{\infty} \frac{(-1)^{n-1}}{(2n-1)} e^{-\left[ \frac{\pi^2 (2n-1)^2 B_L T}{4 \phi_L^2 \text{SNR}'} \right]} \quad (44)$$

Evaluating (44) for the case where  $\phi_L = \pi$  yields the results listed in Table 1.

Table 1. Probability of Slipping 1/2-Cycle in Specified Time

T (seconds)	$P(\phi_L   0)$
0.0025	0.999999792
0.005	0.9999978
0.01	0.999947
0.025	0.9983

Thus, we see that it is very unlikely to slip one-half cycle which, by itself would probably cause a transient loss of lock. In fact, we can evaluate (38) by letting  $\phi_L = 0.5$  radians ( $\sim 29^\circ$ ) and  $T = 0.005$  second, with the result that  $P(\phi_L | 0) = 0.9952$  and therefore conclude that, due to thermal noise during the 5-ms dropout, the main concern is the phase shift during both make and break. The analysis neglected any offsets that might be present in the loop since no estimates were available.

Now we address the effects of doppler on loss of lock.

## 6.0 EFFECTS OF DOPPLER ON LOSS OF LOCK

In this section, we determine the doppler shift between the two Centaur antennas which are separated by 18 feet. Since the Centaur is rotating at a maximum of 4.7 RPM, the doppler difference between antennas is given by

$$\Delta f = \frac{d\dot{\theta}}{c} f \quad (45)$$

where  $d$  is the distance between antennas (18' or 5.5 m),  $\dot{\theta}$  is the angular rate (m/s),  $c$  is the speed of light (m/s), and  $f$  is the carrier frequency of 2272.5 MHz. Evaluating (45), we obtain  $\Delta f = 20.45$  Hz, which can be either plus or minus algebraically. Using some results of P. Nilsen [4, Chapter 4], we see that, after  $4B_L^{-1}$  seconds, the probability of reacquisition using a second-order loop with  $\Delta f = 20.5$  Hz and  $B_L = 420$  Hz is approximately unity. The duration of  $4B_L^{-1}$  seconds or 9.5 ms is the time it takes to acquire when a doppler shift causes a frequency error of about 21 Hz during the dropout. During much of the 9.5-ms period, the signal is not in frequency error but has a decreasing error. Hence, we assume that approximately one-half of the time is equivalent to a dropout and the other half has degraded BER performance.

In conclusion, the total effective drop-out time is 9.75 ms, and the loop will reacquire with probability  $\approx$  unity in 14.5 ms.

## 7.0 EFFECTS OF LOSS OF LOCK ON THE DATA

Since the Centaur/TDRSS link utilizes NRZ-L (PSK) modulation--not NRZ-M or NRZ-S modulation--a phase reversal by the Costas loop when it reacquires (after the dropout) will not cause a serious problem in the Viterbi decoder since the code is transparent but will, in all probability, cause a frame of data to be lost. The reason this occurs is that, with NRZ-L data, a frame synchronization word must be correlated against the received data in order to determine whether or not the data polarity is flipped. Hence, if the dropout occurs in the middle of a minor frame, half of the bits would be inverted, regardless of whether or not the correlator determined that the frame should be inverted. In adverse cases, it could be greater than half a frame.

We conclude that at least half of the bits decoded in a minor frame could be incorrectly decoded (inverted) if NRZ-L is used and if the Costas loop suffered phase inversion during antenna switching. However, if NRZ-M or NRZ-S (differential encoding) were used, probably only a few bits would be lost if the Costas loop suffered only phase inversion, thus, either NRZ-M or NRZ-S if be a much better choice of data format.

When a dropout occurs under adverse phasing conditions, at least 160 bits will be decoded randomly

### References

1. P. Lathrop, "Preliminary Analysis of Shuttle/Centaur Telemetry Signal Transients During Antenna Switching " General Dynamics Memo #6070-83-66, May 2, 1983.
2. D. A. Darling and A. J. F. Siegert, "The First Passage Problem for a Continuous Markov Process, Annals of Math Statistics, Vol. 24, 1953, pp. 624-639.
3. U. Timor, "On the Behavior of a Phase-Locked Loop During a Temporary Loss of Signal," JPL SPS #37-61, Volume III.
4. J. K. Holmes, Coherent Spread Spectrum Systems, Chapter 5, Wiley Interscience, 1982.
5. S. M. Novosad, Shuttle/Centaur-TDRSS RF Interfaces, NASA/Johnson Space Center, Memorandum No. EE8-2/83-014, February 15, 1983.